Analysing and modelling the effects of galactic cosmic rays on the Earth's atmosphere over daily timescales

Benjamin A. Laken

July 2010

Department of Geography,

University of Sussex Falmer,

Brighton, BN1 9QJ, UK

A thesis submitted for the degree of Doctor of Philosophy

To illuminate a cloudy day

Abstract

In recent years, a range of detailed palaeoclimatic reconstructions have shown indications of a connection between changes in solar activity and Earth's climate. However, a process that may explain such a relationship has yet to be reliably demonstrated. One proposed mechanism concerns the theoretical link between the solar-modulated galactic cosmic ray (GCR) flux and Earth's cloud cover. Several microphysical pathways have been suggested which could account for this relationship, including (*i*) changes in the concentration of cloud condensation nuclei by an ion-mediated growth of aerosol particles, and (*ii*) the accumulation of charge at cloud boundaries predicted to influence the ability of cloud droplets to grow by scavenging processes.

This work uses an original epoch-superpositional (composite) methodology to present new indications of statistically significant relationships between the rate of GCR flux (measured from neutron monitor sites across the globe) and changes in the rate of numerous large-scale atmospheric parameters (derived from satellite, reanalysis and weather station datasets) over daily timescales. Attempts are made to reproduce the observed anomalous atmospheric responses within a general circulation model. The results strongly suggest that some of the observed anomalies may be causally related to cloud changes and, furthermore, provide some support for possible links between the GCR flux, cloud anomalies and atmospheric responses. This relationship appears to be sensitive to changes in the rate of GCR flux and is also likely constrained by internal conditions.

Acknowledgements

First and foremost, I would like to thank my two supervisors Dr Dominic Kniveton and Dr Michael Frogley for their constant support, advice and comments on all things scientific and otherwise. Their unwavering encouragement and guidance over the last few years has made this work not only possible but also enjoyable.

I would also like to thank the numerous people who have given helpful and supportive academic correspondences and comments over the last few years, including: Professor Lois Steanman Clarke, Dr Charlie Williams, Sir Arnold Wolfendale, Professor William Rossow, Professor Giles Harrison, Dr Julian Murton, Miss Mary-Beth Kitzel, Mr Christopher Smith, Mr Jerome Curroy and numerous anonymous reviewers. Also, a special thank you to Mr James Crawford and Miss Nicola Broodbank, for doing their best to keep me relatively sane over the last few years.

Finally, I am eternally thankful for my parents, whose love and support has made this work possible. Thanks for all the proof reading Dad.

Table of Contents

List of Figures

List of Tables

List of Equations

List of Abbreviations

ACRIM	Active Cavity Radiometer Irradiance Monitor
AGD	Antarctic GCR Decrease (referring to the name of a sample)
AI	Antarctic Increase (referring to the name of a sample)
BHN	Binary Homogenous Nucleation
B_y	North-South component of the IMF
B_z	East-West component of the IMF
CN	Condensation Nuclei
CCN	Cloud Condensation Nuclei
CERN	Organisation Européenne pour la Recherche Nucléaire
CFC	Chlorofluorocarbon
CLOUD	CERN's Cosmics Leaving Outdoor Droplets Experiment
DF	Diffuse Fraction
DMS	Dimethylsulfide
DMSP	Dimethylsulfoniopropionate
ECMWF	European Centre for Medium range Weather Forecasting
EUV	Extreme Ultraviolet
FD	Forbush Decrease
FORTRAN	Formula Translation language
fu	Flux Unit (1 *fu* = 10^{-22} W m^{-2} Hz^{-1})
GCM	General Circulation Model
GCR	Galactic Cosmic Ray
GEC	Global Electric Circuit
GI	Global Increase (referring to the name of a sample)
GLE	Ground Level Enhancement
GPH	Geopotential Height
HadAM3	Atmosphere only model from the UKMO

HCS	Heliospheric Current Sheet
IFN	Ice Forming Nuclei
IMF	Interplanetary Magnetic Field
IPCC	Intergovernmental Panel on Climate Change
IR	Infrared
IRD	Ice Rafted Debris
ISCCP	International Satellite Cloud Climatology Project
J_z	Vertical Conduction Current
LCC	Low Cloud Cover (>680 mb)
LCF	Liquid Cloud Fraction
LIA	Little Ice Age
LW	Longwave
MC	Monte Carlo
MG II	Magnesium II chromospheric absorption feature of solar UV spectrum
MLCD	Mid-Latitude Cloud Decrease (referring to a GCM experiment)
MLD	Middle Latitude Decrease (referring to the name of a sample)
MODIS	Moderate Resolution Imaging Spectrometer
MWP	Medieval Warm Period
NCAR	National Centre for Atmospheric Research
NASA	National Aeronautics and Space Administration
NCEP	National Centres for Environmental Research
NGDC	National Geophysical Data Centre
NOAA	National Oceanographic and Atmospheric Administration
PCI	Polar cloud increase (referring to a GCM experiment)
PDF	Probability Density Function
PG	Potential Gradient
PMOD	Physikalisch-Meteorologisches Observatorium Davos
PSC	Polar Stratospheric Cloud
PV	Polar Vortex

PW	Precipitable Water content
Q-Q	Quantile-Quantile
RB	Rayleigh-Bérnard convection
SBS	Reference to Svensmark et al., 2009
SEP	Solar Energetic Particle
SNR	Signal-to-Noise Ratio
SPIDR	NASA's Space Physics Interactive Data Resource
SW	Shortwave
THN	Ternary Homogenous Nucleation
TK	Reference to Todd and Kniveton (2001, 2004)
TOMS	NASA's Total Ozone Measuring Spectrometer
TSI	Total Solar Irradiance
UGMAP	UK Universities Global Atmospheric Modelling Programme
UKMO	United Kingdom Meteorological Office
UM	Unified Model
UV	Ultraviolet
V_i	Ionospheric potential
WBF	Wegener-Bergeron-Findeisen

Chapter 1 An introduction to solar–terrestrial studies

1.1 Introduction

The primary aim of this thesis is to examine the effect of solar activity upon the climate system. The mean state of the climate system is subject to long-term variations which are the result of both internal and external forcing agents. Internal forcing agents include phenomena such as continental drift, volcanism and greenhouse gases, while external forcing agents include meteorite impacts, orbital variations and long-term changes in total solar irradiance (TSI). Although variations in TSI appear to be an important factor influencing climate change over decadal timescales (e.g. Usoskin et al., 2005; Camp and Tung, 2007), a number of recent palaeoclimatic reconstruction studies have proposed the existence of a relationship between small variations in solar activity and the climate system which cannot adequately be explained by irradiance variations alone (Foukal et al., 2004). Instead, an additional forcing mechanism that is capable of amplifying the effect of small changes in solar activity may be required to account for the presence of the solar–climate relationships suggested by palaeoclimatic reconstruction studies (Bond et al., 2001; Neff et al., 2001). Several such mechanisms have been proposed:

(1) Variations in the ultraviolet (UV) spectrum which influence both (i) stratospheric ozone production (Haigh, 1996), and (ii) the production of sulphate aerosol species over clean marine environments (Kniveton et al., 2003).

(2) The variation of atmospheric ionisation by a solar modulation of the Galactic Cosmic Ray (GCR) flux which may theoretically influence cloud properties via two distinct microphysical pathways (via a direct effect on aerosol growth (a.k.a. the clean-air effect) and/or an effect on the accumulation of electrical charge at cloud boundaries (a.k.a. the near-cloud effect)). It has been proposed that variations in the GCR flux may ultimately result in an anticorrelation between solar activity and Earth's albedo, governed by changes in cloudiness (Svensmark and Friis-Christensen, 1997). Additionally, it has been proposed that the GCR flux may also influence the terrestrial climate via a reaction pathway involving the modulation of halogenated compounds and Ozone destruction in the stratosphere (Lu, 2010).

Of the proposed mechanisms linking solar activity and climate, a GCR-based relationship is of particular note, as the GCR flux arriving at the Earth is strongly modulated by several factors,

including the solar wind, Earth's geomagnetic field and our local galactic environment. These factors vary over periods ranging from hourly timescales to billions of years. Due to this wide ranging temporal variability, a hypothetical link between the GCR flux and Earth's atmosphere may potentially account for climatological variations across a large range of timescales (Veizer, 2005; Kirkby, 2007): investigation of this important possibility will therefore be the primary focus of this study.

1.2 A brief history of solar–terrestrial studies

Of the proposed irradiance, UV and GCR-based theories, the purported relationship between cloud cover and the GCR flux is the most contentious. This theory has resulted in vigorous debate in the scientific literature in recent years. The GCR–cloud hypothesis has become regarded as highly controversial due to the claims by some researchers that it provides an alternative sun-driven explanation for recent climate change (Friis-Christensen and Lassen, 1991; Svensmark and Friis-Christensen, 1997; Svensmark, 2007). However, despite the recent interest in the field, notions of a link between solar activity and climate are not new; the idea was first proposed more than 200 years ago by the Astronomer Royal, William Herschel, who observed a correlation between the numbers of sunspots and the price of wheat (Herschel, 1801). Since this initial finding, many studies have observed a statistical connection between solar activity and climate over a range of timescales. In recent years, detailed palaeoclimatic reconstructions have provided good evidence of a centennial solar influence on climate which is difficult to refute. For example, the oxygen isotope signature of stalagmite growth in a cave in Oman over the Holocene period reveals decadal to centennial oscillations between wet and dry conditions; these oscillations strongly correlate with cosmogenic isotope records (Neff et al., 2001; Fleitmann et al., 2003). Similar associations between cosmogenic isotopes (e.g. ^{14}C) and monsoon intensity have also been identified in the Asian monsoon, where a high resolution record of monsoon variability over the past 9 ka demonstrates an apparent correlation between monsoon intensity and changes in ^{14}C (which may or may not also be correlated to solar irradiance changes) (Wang et al., 2005). This relationship includes eight distinct weakening events, each lasting around one to five centuries, and is broadly coincident with long-term fluctuations in solar activity.

The association between cosmogenic isotopes and decadal to centennial variations in the Indian monsoon has been linked to a displacement of the inter-tropical convergence zone (ITCZ). Southerly shifts in the ICTZ appear to correlate with periods of increased cosmogenic isotope

production (indicating a decreased period of solar activity) and a decrease in monsoon rainfall (Neff et al., 2001). Quaternary sedimentary records from Africa appear to confirm this pattern of variability; they demonstrate a low latitude decadal/centennial oscillation between wet and dry periods over southern Africa as a result of southerly shifts in the ICTZ (Garcin et al., 2007). Palaeoclimatic evidence drawn from sediment deposits also appear to show that Antarctic climate variability over the Holocene may be strongly linked to solar cycles over both centennial (Leventer et al., 1996) and decadal timescales (Costa et al., 2007).

Perhaps the most tantalising evidence of a solar-terrestrial linkage over the Holocene period comes from the examination of North Atlantic oceanic sediment cores; these cores often reveal layers of rock debris, which appear with a regular periodicity incorporated within the fine-grained oceanic sediment (Bond et al., 1997). The debris was originally carried into the North Atlantic as entrained material, frozen into vast numbers of icebergs, which originated north of Iceland. These iceberg 'armadas' periodically discharged in to the North Atlantic and deposited their debris on the ocean floor upon melting (Bond et al., 2001). The layers of ice-rafted debris (IRD), known as Heinrich layers (Heinrich, 1988), appear approximately every 1470 ±500 years, extending back throughout at least the last glacial. Throughout this period, climatic conditions shifted regularly and significantly, however, the rafting events continued with an uninterrupted periodicity and may have occurred simultaneously from disparate ice sheets (Grousset et al., 2000; Bond and Lotti, 1995). This suggests the operation of a pervasive external forcing mechanism, unrelated to internal climate processes. In support of this notion, variations in cosmogenic isotopes demonstrate a close relationship to the appearance of IRD in the stratigraphy; however, it is important to note there are many alternative 'internal mechanism' theories which have been proposed to account for IRDs, such as, MacAyeal's 'binge-purge' hypothesis (MacAyeal, 1993).

Over centennial timescales, the sun undergoes periods of extremes of high or low activity (known as grand maximums and grand minimums respectively). Palaeoclimatological reconstructions suggest that temperature anomalies across Europe may be positively correlated to such periods of solar activity (Dahl-Jensen et al., 1998; Moberg et al., 2005). For example, the Medieval solar grand maximum (1100–1250 A.D.) corresponds to the Medieval Warm Period (MWP) (Jirikowic and Pallé, 1994), while the Maunder solar grand minimum (1645–1715 A.D.) corresponds to the Little Ice Age (LIA) (Eddy, 1976). The spatial extent of the climate anomalies associated with the MWP/LIA is highly debated; a reconstruction of temperature over the Holocene period (based on a range of proxy data) appears to indicate that the MWP/LIA may have only been a regional phenomena (Mann et al., 1999). However, it has been argued that the sensitivity of most Holocene temperature proxies (such as those used in the reconstructions of Mann *et al*. [1999]) may be too low to successfully detect global temperature

variability associated with the MWP/LIA (which may have been less than ~1 °C). To account for this, two temperature proxies (mountain snowline fluctuations and borehole thermometry), which have a relatively high degree of precision (around 0.5 °C) should be favoured above alternative proxies (such as tree rings, coral and flora/faunal records). The mountain snowline and borehole thermometry proxy records both demonstrate a pattern of temperature change over the Holocene which is consistent with the occurrence of a global MWP/LIA (Broecker, 2001). There is also further evidence from a range of sources which suggests that the climate fluctuations associated with the MWP/LIA may have been global in their extent (Soon and Baliunas, 2003), including: the advance of glaciers in the Venezuelan Andes (Polissar et al., 2006); sea surface temperature changes and droughts in Mexico's Yucatan peninsula (Hodell et al., 2005); the occurrence of abnormally cold and wet periods in south-western China (Chen et al., 2005); abnormal changes in lake levels across Africa (Russell and Johnson, 2005); and, abrupt changes in the extent of the Indian monsoon (Gupta et al., 2003). Considered together, the results of these studies implies that the LIA and MWP experienced across Europe may have been the most well documented (or strongest) part of a regionally widespread climatic responses to changes in solar activity, which may suggest a simultaneous influence of solar input influencing monsoon and polar front regions.

Despite the evidence from palaeoclimatic studies, our current level of understanding of a physical solar–climate linkage is relatively poor. Consequently, such studies merely provide a tantalising indication of a possible connection, hinting that developing a further understanding of a solar–climate link may be a crucial aspect in improving our current level of understanding of natural climate variability, upon which anthropogenic climate change is superimposed.

1.3 Controversy, politics and recent studies

Some recent studies, which utilise satellite-based atmospheric datasets, have claimed to identify a correlation between low altitude cloudiness and the GCR flux operating over decadal timescales (Svensmark and Friis-Christensen, 1997; Marsh and Svensmark, 2000). Proponents of this theory have reasoned that, as solar activity has approximately doubled over the last century (Solanki et al., 2004) and the GCR flux has undergone a corresponding long-term decrease over this period, this may have resulted in a long-term reduction in low-level cloud amounts and may have consequently increased global surface temperatures in recent years. Such a relationship implies that recent anomalous climate change may be predominately attributable to solar activity and not anthropogenic emissions (Svensmark, 2007). However, such

conclusions are highly controversial and have been heavily criticised on a number of fundamental issues, which will be considered in the following chapter.

Despite the overwhelming evidence supporting anthropogenic climate change coupled with the scientific ambiguities behind solar–climate interactions, the political importance of climate issues is such that in the popular media and public forums detractors of policies to mitigate human emissions have often attempted to dissuade public opinion by presenting arguments of a solar driven climate. Consequently, such theories have become inseparably associated with anthropogenic climate change scepticism and, as a result, the majority of scientists view solar–terrestrial studies (and in particular a GCR–cloud link) as an unattractive field of study for fear of appearing to support a viewpoint which runs contrary to scientific consensus. Ultimately, a lack of evidence coupled with the political controversy has polarised much of the scientific community against notions of solar–terrestrial climate linkage (particularly via GCR connected pathways). This situation is unfortunate, as palaeoclimatic evidence indicates that this field of study may provide important advances to our understanding of natural climate variability.

1.4 Key research question and purpose of investigation

The core question this thesis essentially seeks to address is: *'*to what extent are small variations in solar activity able to influence Earth's climate?' While there is good palaeoclimatic data to support the existence of a relationship between solar activity and climate, similar evidence from modern climatological datasets is relatively sparse (Gray et al., 2005). It is crucial to determine if a relationship between solar activity and the climate system exists and how it operates, as, demonstrating such a process may ultimately lead to an improved understanding of natural climate variability. Crucially, if a quantifiable response between solar activity and climate can be established and incorporated in to climate models, our ability to predict future climate change may be improved. Enhancing the accuracy of climate predictions is of vital importance, as models are a critical tool in developing climate change mitigation strategies, yet they currently have many shortcomings (Gleckler et al., 2008). Furthermore, it is also possible that the identification of a link between the GCR flux and clouds may possibly result in the eventual establishment of a new branch of physical science concerning the interactions between atmospheric electricity and cloud microphysics and potentially offer new insights into atmospheric processes.

1.5 Aim and objectives

Aims

To assess the existence and nature of a daily timescale relationship between the GCR flux and Earth's climate using a combination of remotely sensed atmospheric datasets and General Circulation Model (GCM) experiments.

Objectives

(1) To test for the existence of a relationship between clouds and the GCR flux using a methodological approach based on the epoch-superpositional (composite) sampling techniques of past daily timescale GCR climate studies.

(2) If a relationship between clouds and the GCR flux is identified then it will be essential to determine:

(A) If the observed clouds changes are capable of forcing significant atmospheric changes.

(B) If it is possible to reproduce the observed effects in a GCM.

1.6 Structure of the thesis

This thesis will be organised as follows:

Chapter 2 **Detailed background**. Provides a detailed review of the theories and background science behind solar–terrestrial linkages.

Chapter 3 **Methods and datasets**. Presents a general description of the datasets and data handling techniques employed in this study.

Chapter 4 **Forbush Decreases**. Re-analyses the impacts of the rare high magnitude daily timescale disturbances in solar activity known as Forbush Decrease (FD) events on cloud cover.

Chapter 5 **Cloud based sampling**. Provides an analysis of the relationship between cloud changes and solar activity using a novel sampling technique.

Chapter 6 **Atmospheric analysis**. Discusses and analyses the atmospheric impacts of samples discussed in chapters 4 and 5.

Chapter 7 **Climate model experiments**. Describes and analyses several GCM experiments designed to simulate the cloud change scenarios observed in chapter 5. A comparison of the resulting modelled atmospheric anomalies against observations is presented, along with an evaluation of the ability of the GCM to replicate the observed circulatory and cloud conditions.

Chapter 8 **Discussion and concluding remarks**. A discussion of the overall findings and the extent to which they fulfilled the primary aim of the thesis is presented, along with a broad overview of the wider significance of the findings in the context of the ongoing academic discussion concerning the field of study. Limitations and possible directions for future work are also discussed.

Chapter 2 The science behind solar–terrestrial linkages

2.1 Introduction

The primary reason for a low confidence in the role of solar forcing on Earth's climate is due to a lack of a widely accepted physical mechanism to account for such a relationship (Gray et al., 2005). Several mechanisms have been proposed, the theoretical and empirical evidence behind them will now be discussed in an attempt to provide an overview of the field of solar–terrestrial physics and a contextual framework for this thesis.

2.2 Solar irradiance variations

In the past it had been assumed that the Sun was able to influence Earth's climate directly, simply through changes in total solar irradiance (TSI) resulting from sunspot blocking, facular-emission and network emission in the Sun's photosphere (Hoyt and Schatten, 1993). It is not possible to precisely measure TSI variations over a solar cycle at the Earth's surface; consequently, the extent to which TSI varies through time was not known until the arrival of satellite-based instrumentation in 1987. Such measurements reliably showed that TSI varies by approximately 0.1 % over the course of an 11-year solar cycle (this is equal to a top of the atmosphere [TOA] radiative forcing of approximately 0.90 Wm^{-2}) (Willson et al., 1981; Lean, 1987; Haigh, 2003). Studies attempting to calculate the effects of such decadal TSI changes on global surface temperatures have arrived at a range of results, from around 0.1 K (Douglass and Clader, 2002; Lean, 2005; Scafetta and West, 2005) to ~0.2 K (Coughlin and Tung, 2004; Camp and Tung, 2007). Observational evidence appears to support the higher (~0.2 K) estimates (Labitzke et al., 2002; Haigh, 2003; Loon et al., 2004). The spatial pattern of the temperature changes resulting from decadal TSI oscillations (relative from solar minimum to solar maximum) indicates that the effects of TSI variations are largest over high latitude regions (Tung and Camp, 2008). The authors suggest this is due to a range of positive feedback processes, involving ice-albedo, cloud, water vapour and lapse rate feedback mechanisms over such regions. However, despite these claims, a decadal temperature variation of the appropriate magnitude has yet to be simulated by climate models via forcing changes in the TSI alone.

Although the time period covered by the satellites only extends back four decades, it is possible to reconstruct centennial timescale irradiance variations by calibrating the proxy records of solar activity against modern satellite measurements. From such calibrated reconstructions it has been found that since 1750, changes in TSI may have only contributed a radiative forcing of approximately 0.12[+0.06 -0.30] W m^{-2} to global temperature changes (IPCC, 2007). However, differing results have been suggested: a model study by Krivova et al. (2007) which reconstructs TSI variations back to 1700 using geomagnetic indexes suggests that TSI may have had a significantly larger impact on the climate, calculating an increase of approximately 1.3[+0.2 -0.4] W m^{-2} since the Maunder minimum (Krivova et al., 2007).

Longer reconstructions spanning 11.4 ka indicate that the current levels of solar activity are unusually high compared to the rest of the Holocene period. The last time that the sun was in a comparable state of activity was around 8 ka ago; indications suggest that the sun may only spend around 10 % of its time in such an active state (Solanki et al., 2004). It has been proposed that this anomalously active state may have contributed to climate variability during the last century, although it appears that since the 1970s, TSI changes cannot account for more than 30 % of the observed climate variations (Solanki and Krivova, 2003).

It is difficult to determine recent decadal TSI trends, as there exist no continuous measurements over the last 30 years; instead, TSI data must be reconstructed from various satellite datasets. There are two primary reconstructions of TSI, namely, the ACRIM (Willson and Mordvinov, 2003) and PMOD (Lee et al., 1995) composites (ACRIM and PMOD are abbreviations of the Active Cavity Radiometer Irradiance Monitor and the Physikalisch-Meteorologisches Observatorium Davos respectively). The primary difference between the composites stem from adjustments made to the Nimbus 7 HF data made in the PMOD composite (Lockwood and Fröhlich, 2008). The (unadjusted) ACRIM composite finds that TSI has increased by around 0.05 % over the last two solar cycles (producing a radiative forcing of 0.1 W m^{-2}), whereas the PMOD composite shows a cooling of similar magnitude over the same time period (Willson and Mordvinov, 2003). The uncertainty in TSI trends is significant, as it may call in to question the reliability of long-term irradiance reconstruction studies, as such reconstructions are calibrated against the satellite data. It appears likely that the PMOD composite is the most accurate, as studies have demonstrated an agreement between the PMOD composite, the Earth Radiation Budget Experiment (ERBE) data (Lee et al., 1995; Fröhlich, 2006), the PMOD composite and magnetograms (Wenzler et al., 2006). These findings suggest the ACRIM data is in error, and that TSI may have undergone a slight decrease over the last 30 years.

Overall, although uncertainties in the nature of TSI variability still exist, the evidence appears to suggest that over long timescales, TSI changes may be an important factor influencing climate

change. However, over shorter timescales irradiance changes may be too small to account for many of the observed solar-terrestrial linkages discussed in chapter 1 without invoking a wide range of feedback processes, the existence of which is unsupported by model studies (Tung and Camp, 2008).

2.3 Variations in UV radiation

Although TSI only varies by around 0.1 % over an 11-year solar cycle, changes in the absolute amount of radiation, and what height it is absorbed in the atmosphere are far greater, varying by as much as 10 % in the 150–300 nm range and by more than 50 % at shorter-wavelengths near 121.6 nm (at the Ly-α emission line) (Floyd et al., 2003). Overall, wavelengths shorter than 400nm (the UV range) constitute approximately 32–60 % of the TSI variability which occurs over an 11-year solar cycle (Haigh, 1996; Floyd et al., 2002; Krivova et al., 2006). UV variability may have important influences on the climate: emissions in the Ly-α UV range play a crucial role in upper stratosphere and mesosphere chemistry via several important photochemical pathways. Specifically, radiation at these wavelengths ionise nitric oxide, influencing electron density distribution and stimulating the dissociation of water vapour, thereby resulting in the production of chemically active OH(x) hydroxyl free radicals which catalyse recombination of oxygen to O_3 and O_2 species, leading to a thinner ozone layer than if the hydroxyl was not present (Krivova et al., 2009).

In the stratosphere, the photochemical dissociation of oxygen by UV radiation is the primary process responsible for forming ozone molecules. The chemical reactions which recombine O_2 to O_3 and vice versa occur rapidly in equilibrium; resulting in an absorption of radiation and a consequent generation of heat (Wallace and Hobbs, 1977). The majority of ozone formation takes place at low latitudes in the upper stratosphere. The UV radiation drives the photolyzation of oxygen molecules, which combine to form stratospheric ozone. Although the majority of ozone production occurs at low latitudes, ozone is distributed ubiquitously throughout the mid- to high latitude stratosphere due to meridional transport by stratospheric winds (Haigh, 2007). Under specific latitude and altitude conditions, stratospheric ozone exists in a dynamic equilibrium. The rate of photolyzation of oxygen molecules which form ozone and the rate of photodissociation of ozone by the absorption of UV radiation are equal; this equilibrium shields the surface of Earth from UV radiation. Decadal variations in UV emissions modify this equilibrium (Vallero, 2008). Such variations may potentially alter the thermodynamic structure

of the stratosphere; these changes are coupled to tropospheric dynamics, and consequently influence Earth's climate (Haigh, 1996; Shindell et al., 1999).

GCMs that take in to account the changes in upper stratospheric ozone over the course of the solar cycle, successfully demonstrate the coupling between the stratosphere and troposphere resulting from UV variations. Such models have been able to reproduce many of the observed climate features seen to occur in association with the solar cycle including circulatory changes which originate from the stratosphere and penetrate into the troposphere (Shindell et al., 1999). GCMs have been successful in reproducing observed general patterns of climate variability associated with solar activity such as: changes in geopotential heights, and changes in stratospheric zonal winds which alter the propagation of planetary scale waves (Shindell et al., 1999). Such circulatory changes result from a solar-maximum associated warming of the summer stratosphere. This causes a strengthening of easterly winds, enabling them to penetrate in to the equatorial upper troposphere, thereby producing a pole-wards shift in the subtropical westerly jet stream. In turn, this forces a pole-ward shift in the descending portions of the Hadley circulatory cells, and shifts in the loci of mid-latitude storm-tracks (Haigh, 1996; Haigh and Blackburn, 2006). However, it is noted that the changes simulated by the GCMs are generally smaller than those observed in reality. Although it is highly likely that a combination of both UV and TSI variations influence Earth's climate, these mechanisms may be unable to fully account for some of the observed solar–climate linkages.

In addition to the ozone interactions, it has also been suggested that UV variations may affect the climate via an effect on dimethylsulphide (DMS) production. DMS is a key component of the sulphur cycle and its oxidation provides the primary source of cloud condensation nuclei (CCN) over clean marine environments. DMS itself is produced by the breakdown of planktonic algae through various pathways (such as physical turbulence via wave action and mechanical break-up by grazing zooplankton). The breakdown of phytoplankton releases dimethylsulphoniopropionate (DMSP), the precursor molecule of DMS (Kniveton et al., 2003). The DMSP is converted by marine bacteria to sulphur and DMS; due to its volatile nature, the DMS then readily evaporates in to the atmosphere.

It has been suggested that the relationship between algae, DMS and CCN form a negative feedback cycle, whereby and increase in irradiance increases the growth of phytoplankton. In turn, this increases the atmospheric DMS concentration, leading to higher concentrations of CCN and hence more clouds, resulting in a decrease in shortwave (SW) radiation reaching the oceans (Charlson et al., 1987). UV radiation influences these processes in several distinct ways:

(1) It results in DNA damage to phytoplankton and zooplankton (Lindell et al., 1995).

(2) It reduced the production of DMSP from phytoplankton (Hefu and Kirst, 1997).

(3) It reduces the removal of DMSP from ocean water by bacterial organisms (Slezak et al., 2001).

(4) It enhances the rate of photolysis of DMS to other molecules (Hatton, 2002).

Overall, UV radiation appears to be anticorrelated to DMS concentrations. This suggests that in addition to the stratospheric ozone modulating effects of oscillations in UV radiation, UV changes may also possibly result in alterations in cloud formation over clean marine environments (Kniveton et al., 2003).

2.4 Background to the galactic cosmic ray flux

The Earth is constantly exposed to high-energy particles travelling at relativistic (near-light) speeds; these particles are ubiquitous throughout our galaxy. The particles (termed Galactic Cosmic Rays [GCRs]) are thought to originate from high energy astrophysical environments such as supernovae remnants (Berezhko, 2008). Of the GCR flux which reaches Earth 98 % is comprised of protons and 2 % of electrons. Of the proton component, around 87 % are individual protons, while 12 % are helium nuclei (alpha particles); the remaining 1 % are assorted species of heavier nuclei (Simpson, 1983). GCR particles range in energy levels from 1.0 MeV–1000.0 TeV ($1 \times 10^6 - 1000 \times 10^{12}$ electron volts), however particles with energy levels between 0.1–15.0 GeV ($0.1 - 15 \times 10^6$ electron volts) carry around 60 % of all the total energy of the GCR spectrum and make up approximately 95 % of the total flux (Stozhkov, 2003).

In addition to radiation, the Sun also emits charged particles and magnetic fields; together these make up the solar wind. As the solar wind leaves the Sun it is travelling around several million kilometres per hour, although it slows with increasing distance from the Sun, as pressure from the interstellar medium increases. The solar wind ceases altogether as pressure from the interstellar medium eventually balances the pressure of the solar wind (this point is known as the heliopause and occurs at around 100 AU [Astronomical Unit]). The region within the heliopause is known as the heliosphere; within this region the density, velocity, strength and three dimensional structure of the magnetic field emanating from the Sun (known as the Interplanetary Magnetic Field (IMF)) and the Heliospheric Current Sheet (HCS) varies over the course of a solar cycle. The IMF is able to deflect GCRs with energy levels <10 GeV (Gleeson

and Axford, 1968): as the majority of the GCR flux possesses energy levels below 15 GeV, the GCR flux reaching Earth is strongly susceptible to modulation by the solar wind. As a result, the GCR flux within the local solar system demonstrates a strong anticorrelation to solar activity, with the GCR flux arriving at Earth varying by approximately 15 % over the course of an 11-year solar cycle (Carslaw et al., 2002).

GCRs interact with Earth's atmosphere at all levels, the maximum level of interaction is ~15 km (this is termed the Pfotzer maximum [Bazilevskaya and Svirzhevskaya, 1998]); they collide with molecules in Earth's atmosphere and split their atomic nuclei. This process, termed spallation, produces a series of secondary charged-particles made up of pi-mesons (pions), which further collide with other atmospheric molecules producing muons and neutrinos. If the initial impetus is large enough, these secondary particles may be capable of generating a cascade of charged particles (known as a particle shower), which may penetrate to sea level. The majority of the particles produced by spallation are extremely unstable and decay before they reach the troposphere; as a result, the majority of remaining particles within the troposphere are comprised of muons. Muons loose energy by ionisation and are responsible for virtually all atmospheric ionisation away from terrestrial sources of radiation and electrically active clouds (termed the fair weather region) (Kirkby, 2007). Ultimately, the anti-correlation between solar activity and the GCR flux provides an indirect pathway linking small changes in solar activity to variations in tropospheric ionisation.

In addition to the heliospheric modulation of the GCR flux, the Earth's magnetosphere also influences incoming GCRs. Generally, the Earth's geomagnetic shielding is strongest at low latitudes and altitudes, although in reality it does not vary quite so uniformly, as the magnetic poles of the Earth are offset from the geographically 'true' poles by some distance. As a result, the Earth's magnetic field is not positioned symmetrically over the Earth, and so magnetic field strength varies in intensity to a small degree along the same latitudinal zone (figure 2.1). Furthermore, the structure of Earth's magnetic field is also complicated by its interactions with the solar wind, which act to deform the field by compressing its sunward-facing side towards the Earth and extending the opposing side. Due to this interaction, the amount of magnetic shielding at a specific location varies with the time of day, Earth's orbital position, and the space weather conditions (Smart et al., 2008). The magnetosphere itself also undergoes fundamental changes as the geomagnetic poles drift over decadal timescales (Courtillot et al., 2007). The entire geomagnetic field fluctuates in strength by tens of percent over millennial timescales (geomagnetic excursions), and periodically undergoes complete geomagnetic reversals. While a consideration of such intricate variations and deformations of the magnetosphere are beyond the scope of this thesis, it is important to appreciate the non-uniform

nature of GCR related ionisation and how the terrestrial GCR flux is a function of both external and internal influences.

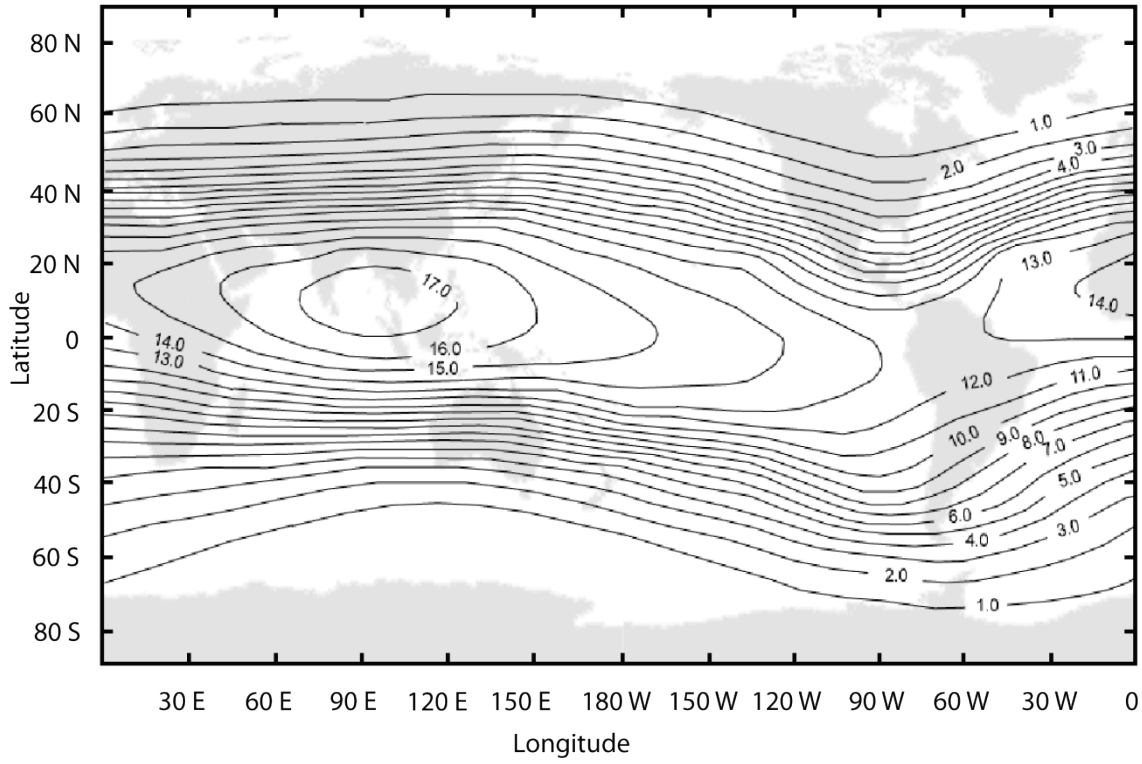

Figure 2.1 Geomagnetic cut-off rigidity

Geomagnetic shielding effect, indicating the minimum energy level (cut-off rigidity) an incident GCR must possess to penetrate at a given location (units in GeV). Figure sourced from http://bit.ly/d877IE (accessed 07/04/2010).

For the purposes of this work, the magnetospheric influence on GCR flux can be considered as a shielding of low latitudes from the relatively low energy (and most abundant) GCRs, deflecting them to higher latitudes. As a result, average ion production rates in the troposphere range with latitude and altitude from around 2 $cm^{-3}s^{-1}$ at ground level, to 10 $cm^{-3}s^{-1}$ at 5 km and 20–50 $cm^{-3}s^{-1}$ at 15 km. It is important to note that the component of the GCR spectrum most susceptible to diversion to high latitudes by the magnetosphere is also the part most susceptible to modulation by the heliosphere. Consequently, during the course of a solar cycle high latitude ionisation rates vary by approximately 20–25 % in the upper troposphere and 5–10 % in the lower troposphere, whereas at low latitudes the ionisation rate only varies by around 4–7 % in the upper troposphere and 3–5 % in the lower troposphere (Yu, 2002). The positive ions and free electrons created by the GCRs quickly interact with atmospheric molecules to form complex positive and negative cluster ions known as small ions. The average ion pair concentrations in the atmosphere vary from around 200–500 cm^{-3} at ground level to

approximately 1000–3000 cm^{-3} in the lower stratosphere (Ermakov et al., 1997; Carslaw et al., 2002).

2.4.1 Ionisation and tropospheric aerosols

Dickinson (1975) first suggested that atmospheric ionisation may potentially play some role in cloud formation, via an influence on the development of aerosols necessary for the growth of clouds. Since Dickinson's initial suggestion several decades ago, two primary theories of GCR–cloud interactions have developed. The first is known as the clean air effect (a.k.a. the direct effect) and refers to a process whereby atmospheric ionisation may influence the formation and growth of aerosol particles, ultimately affecting the number of aerosols which reach CCN sizes (approximately 0.1 μm) (Carslaw et al., 2002).

Unless otherwise explicitly specified, the term aerosol will hereafter refer to sulphate aerosols (as these are predicted to be the primary nucleating agents of the free troposphere). Aerosol particles are constantly being removed from the atmosphere through various processes such as wet and dry sedimentation, photolytic reactions, self coagulation and cloud droplet scavenging. Consequently, the typical lifespan of an aerosol particle ranges from around 6 hours to several weeks. As a result, they do not persist long enough to accumulate in large concentrations and so the rate of formation of new aerosol particles largely controls the ambient concentration of tropospheric aerosols (Rogers and Yau, 1989; Carslaw et al., 2002; Laakso, 2002; Tinsley and Yu, 2004; Kirkby, 2002).

Due to the difficulties in observing sub-nanometre scale processes, the genesis of new (ultrafine [≤3 nm diameter]) aerosol particles is still poorly understood, despite decades of research, it is unknown exactly how new aerosol particles form (Yu and Turco, 2000). It is thought that nucleation of trace condensable vapours of gases such as H_2SO_4 in the atmosphere may be an important source of new ultrafine aerosol particles as such gases are often observed prior to the detection of ultrafine aerosols. Many observations of ultrafine aerosols have been made over the last decade; these indicate that the typical aerosol growth rates can vary with air temperature and condensable vapour concentrations. Rates of aerosol growth have been observed to range from approximately 1–20 nm hr^{-1} (at mid-latitude regions) to 0.1 nm hr^{-1} (at polar latitudes). Aerosol formation rates are found to be approximately 0.01–10 particles cm^{-3} s^{-1} in the boundary layer (although for costal environments and industrial plumes, formation rates may be as large as 10^4–10^5 particles cm^{-3} s^{-1}) (Weber et al., 1998; Kulmala et al., 2004; Kirkby, 2007).

Current theoretical models attempting to explain the formation of new ultrafine aerosols appear to largely underestimate rates of particle production. Traditional models of aerosol formation are based around neutrally charged nucleation theories, such as binary homogenous nucleation

theory (BHN) and ternary homogenous nucleation (THN) theory. Based on such classical BHN models, aerosol nucleation rates at low tropospheric levels are predicted to be far lower than observations suggest, by a factor of around 10^{10} (Jaecker-Voirol and Mirabel, 1989). However, models which include the speculative effects of charge on aerosol formation and growth (known as ion mediated nucleation (IMN)) are able to predict formation rates far greater than neutrally charged nucleation models allow. Consequently, it is proposed that IMN may potentially account for some of the discrepancies between observations and traditional nucleation mechanisms (Clarke et al., 1998).

IMN operates by encouraging the condensation of polar non-water molecules (such as H_2SO_4), accompanied by a fraction of water molecules on to small ions by electrostatic attraction and enhanced particle coagulation, resulting in a rapid and large increase in ultrafine aerosol growth rates. In nature, large and sudden increases in tropospheric ultrafine aerosol concentrations have been observed; these are known as nucleation bursts. Theories of ultrafine aerosol nucleation, which do not invoke the electrostatic growth processes of IMN, are unable to account for the existence of such nucleation bursts (Horrak et al., 1998). IMN models, however, have been shown to successfully simulate nucleation events where traditional models have failed (Yu and Turco, 2008). In addition, the simulation of ion clusters in jet contrails provides further evidence of the existence of IMN processes, as IMN models are able to successfully describe the evolution of chemiions (negative aerosol cluster ions) in aircraft plumes (Kiendler and Arnold, 2002).

Model studies by Yu and Turco (2008) have identified two key parameters which control aerosol nucleation: (1) sulphuric acid vapour concentration, (2) air temperature, and (3) background aerosol concentration. Secondary parameters are also found to be important, including: the ionisation rate, relative humidity, and condensation sinks. Models suggest that variations in the ionisation rate, resulting from changes in the GCR flux, can exert an influence over tropospheric aerosol production. This effect may be most pronounced in the marine boundary layer, where there is minimal pollution and a low availability of ions. It is postulated that the low ion concentrations in such environments may act as a limiting factor on nucleation processes (Yu and Turco, 2001).

As aerosol production is a function of several variables, a change in ionisation may result in differing impacts to aerosol production at different locations. It has been predicted that the sign of change resulting from an increase in ionisation may be altitude dependant (Yu, 2002). This would result in an increase in particle production in low tropospheric levels (>680 mb), but a decrease in production at high tropospheric levels (<440 mb), whereas the nucleation change at mid-tropospheric levels (440–680 mb) is predicted to be negligible. The altitude dependence of

the sign of change is largely a function of the distribution of sulphuric acid vapour in the troposphere versus the abundance of tropospheric ions. In the lower troposphere, sulphuric acid vapour concentrations are relatively high, whereas ionisation rates are relatively low, consequently, nucleation is limited by the ionisation rate; therefore, an increase in the GCR flux is predicted to result in an increase in nucleation production at low tropospheric levels. Conversely, in the upper troposphere, the ionisation rate is relatively high while sulphuric acid vapour concentrations are relatively low; thus, particle formation is limited by sulphuric acid vapour and not by the ionisation rate (Yu, 2002). Model studies by different groups estimating the importance of IMN on aerosol production suggest that IMN may be an important process over several areas, for example: Boy et al. (2008) have estimated that over boreal forest environments IMN may contribute as much as 15 % of the new particle formation for particles between diameters of 3–10 nm in the mixing layer, while Kazil et al. (2006) studied the formation of aerosols in the troposphere over ocean regions and found indications that the strongest aerosol production occurred at high tropospheric levels over regions with frequent convective activity, but that the net impacts of these effects were small (less than those resulting from changes in irradiance over a solar cycle).

Ultimately, a link between the GCR flux and CCN concentrations may indirectly influence clouds, as the abundance of CCN determines cloud properties such as droplet concentration, albedo and cloud lifetimes. Variations in the CCN concentrations may also be indirectly capable of influencing cloud longevity by controlling the ability of a cloud to precipitate. Precipitation requires the formation of large cloud droplets (with radii of around 50 μm); high CCN concentrations produce small cloud droplets (with droplet radii of around 10 μm) which inhibits the development of precipitation in low-level stratus clouds and consequently increases cloud lifetimes. As a secondary effect, this process may also increase the amount of cloud water available, thereby influencing storm systems by controlling the amount of latent heat available to the system (Rogers and Yau, 1989; Carslaw et al., 2002; Tinsley and Yu, 2004).

Observational evidence of a relationship between increases in atmospheric ionisation and the concentration of tropospheric sulphate and nitrate aerosols have been presented by Mironova et al. (2008). The authors demonstrated that following an extreme solar energetic particle (SEP) event, statistically significant increases in aerosol concentrations were observed over high magnetic latitudes (Mironova et al., 2008); these results provide a good indication that variations in ionisation may be linked to changes in aerosol concentrations. In addition, good observational evidence of IMN was also found by a sophisticated long-term (decadal) aerosol monitoring study (Kulmala et al., 2009); the work appears to indicate IMN may indeed encourage the formation and development of new aerosol particles, although the authors conclude that GCR-induced ionisation may only influence around 10 % of the ultrafine aerosol

population. Furthermore, evidence of IMN bursts in the Earth's atmosphere have also been presented by other studies over a range of environments, including boreal forests and urban centres (e.g. Kulmala et al., 2004; Maso et al., 2005; Iida et al., 2008). A preliminary experimental study by Svensmark et al. (2007) showed indications that the production of new aerosol particles is proportional to negative ion densities. They concluded that their results demonstrated that ions are capable of generating a build-up of small, thermodynamically stable ultrafine aerosol clusters, which may ultimately influence the number of aerosols which grow to CCN sizes (Svensmark et al., 2007). The initial findings of Svensmark et al. (2007) have recently been added to by the pilot study of the CERN Proton Synchrotron in preparation for the Cosmics Leaving Outdoor Droplets (CLOUD) experiment. Preliminary CLOUD experiments suggest that ion-induced nucleation and ion-ion recombination contribute to the formation of neutral clusters and provide sources of new tropospheric aerosol particles with formation rates similar to those observed in nature (Duplissy et al., 2010).

Despite the observational and experimental evidence, however, it is still unclear to what extent variations in IMN may be capable of altering global CCN concentrations and ultimately cloud cover (Carslaw, 2009). A recent model study by Pierce and Adams (2009) using a GCM with the inclusion of aerosol microphysics predicts that, although IMN may influence tropospheric aerosol production, its overall impact on cloud physics is likely to be two orders of magnitude too small to account for observed cloud cover changes. The authors predict that resulting changes in global CCN concentrations between solar minimum and maximum may be less than 0.1 %, which equates to a radiative forcing of only 0.005 W m^2. Consequently, the authors conclude that the effect of IMN on CCN may be unable to account for observed solar–terrestrial relationships (Pierce and Adams, 2009). Similar conclusions regarding the importance of IMN on CCN concentrations have also been drawn by other model-based studies (e.g. Pierce and Adams, 2007; Spracklen et al., 2008).

2.4.2 The Global Electric Circuit

The second mechanism whereby changes in the GCR flux may influence cloud is known as the near cloud effect (a.k.a the indirect effect). This theory is based on the relationship between the GCR flux and the Global Electric Circuit (GEC). To properly explain how this may impact cloud formation requires a brief explanation of the GEC itself.

The GEC was first proposed by Lord Kelvin, who suggested that the Earth's surface and ionosphere together could act as a spherical capacitor. We now know that the ionosphere receives and transmits current generated by electrified clouds at low latitudes (Harrison, 2004). There are four quasi-direct current sources of charge generation which charge the ionosphere: thunderstorms, non-thunderstorm electrified clouds, a dynamo interaction between the solar wind and the magnetosphere, and the dynamo influence of atmospheric tides within Earth's thermosphere (Roble, 1991; Bering et al., 1999).

The most significant source of current (by a factor of 3) in the GEC is from thunderstorms (Roble, 1991), while the second most significant source is electrically active (non-thunderstorm) clouds. Large positive electric potentials are generated above thunderstorms and other electrically active clouds; if the thunderstorms are large enough, the currents that flow upwards from the tops of such clouds may be capable of penetrating into the ionosphere (this current is known as the Wilson current, after C.T.R. Wilson, who first hypothesised that thunderstorms may provide the principle source of current generation in the GEC (Wilson, 1920). The majority of these charge generating clouds are distributed at low latitudes. When averaged, the net upward charge generated from their cloud tops is approximately 1,000 A (this current is known to vary by around ±20 %). The upward current flows in to the highly conductive ionosphere, where it generates a diurnally varying ionospheric potential difference (V_i), with a daily average of roughly 250 kV. Due to the high conductivity of the ionosphere, this charge is equally distributed from the equator to approximately (50°N/S). At higher latitudes, there is an additional charge input from the interactions between the Earth's magnetosphere and the IMF; this results in an additional dawn to dusk potential change of around 40–100 kV (Siingh et al., 2006).

The flow of current in the GEC is uninterrupted as the low latitude generation of current is continual. On average, around 200 thunderstorms are active at one time (Williams, 1996). These mainly occur over the tropics during late afternoon (resulting in the diurnal variation of V_i) and cover around 10 % of the Earth's surface at any one instant (Markson, 1978). The V_i produces a vertical current density (J_z) of approximately 1–6 pA m^{-2}, which flows through all fair weather regions (the remaining 90 % of the Earth which is not undergoing thunderstorm activity); the return time of the GEC is around 2–10 minutes. The J_z results in a weak electrification at the boundaries of stratiform clouds (Harrison and Carslaw, 2003). Resistance of the atmospheric column in fair weather regions is on average approximately 300 ohms; however, the resistance at a given location varies greatly. It is principally determined by the surface altitude and the GCR flux. Thus, variations in the GCR flux affect both the upward current and the vertical return current. The J_z demonstrates variations on multiple temporal and spatial scales in association with solar activity, the GCR flux, internal changes in the GEC, and local variations

in natural and anthropogenic aerosol loading (although, the largest variations in J_z are a function of geographical location) (Hays and Roble, 1979; Rycroft et al., 2000; Harrison, 2004; Tinsley and Zhou, 2006; Tinsley et al., 2007).

2.4.3 The near-cloud effect

Variations in the GCR flux may be one of several inputs capable of modulating the vertical current density flowing from the ionosphere to the Earth's surface, which may alter the current density passing through clouds thereby influencing their properties; this process may indirectly link cloud microphysics to changes in solar activity via the GEC (Tinsley, 2008).

Microphysically, this process is the result of the build-up of elemental charges on particles and droplets at the boundaries of clouds and the effect this charge has on the scavenging and subsequent development of the clouds. Small ions within clouds are efficiently scavenged by droplets, resulting in decreased electrical conductivity by a factor of around 3–30 times relative to the surrounding cloud-free air (Griffiths et al., 1974). When the J_z encounters the conductivity gradient at the boundaries of stratiform clouds, it results in the formation of gradients in the electrical field and an accumulation of space charge density (the electric field generated is proportional to the current density, and inversely proportional to the conductivity). The charge generated attaches to cloud droplets and aerosol particles, producing highly charged droplets (of around 100 e) at both the upper and lower boundaries of the cloud. The sign of charge at the top and bottom cloud boundaries are opposing; the lifetime of charge on the particles at these boundaries is approximately 15 minutes (Tinsley et al., 2000; Tinsley et al., 2007). The presence of elemental charge at stratified cloud tops has been established by both aircraft (Beard et al., 2004) and balloon measurements (Nicoll and Harrison, 2009).

There are two potential effects resulting from the charging of droplets and aerosols at cloud boundaries:

(1) An influence on the ice content of clouds. When charged droplets evaporate they leave behind highly charged, coated evaporation nuclei, which may be scavenged by falling cloud droplets more effectively than uncharged particles as a result of an image charge induced on to the cloud droplets; this processes is termed electroscavenging. Some of the electroscavenged particles will be ice forming nuclei (IFN). These are nuclei species capable of forming ice crystals by contact ice nucleation (Tinsley et al., 2001). Field measurements show that the tops of clouds often contain a significant amount of liquid water below freezing point; water can

remain supercooled in a liquid state in clouds between -40 to 0 °C as water requires a suitable nucleating surface for ice crystals to form. Since IFN are relatively scarce in the troposphere, an increase in the rate of scavenging may greatly increase the IFN content of such supercooled clouds. The presence of ice crystals in a water saturated cloud will result in the rapid growth of the ice crystals and encourage the development of precipitation via the Wegener-Bergeron-Findeisen (WBF) mechanism. The WBF mechanism operates through the difference in vapour pressures between ice and water; water saturated clouds have a high supersaturation relative to ice and as a result fuel the rapid growth of ice by diffusion and deposition. This process continues as long as liquid cloud droplets are available to evaporate and maintain the vapour pressure at equilibrium relative to water (Rogers and Yau, 1989; Tinsley 2000; Tinsley et al., 2000).

(2) Modification of cloud microphysics via the alteration of the growth of liquid phase cloud droplets, controlled by the coalescence of aerosol particles and cloud droplets. Experiments indicate that charged raindrops approximately 0.5 mm in diameter are around 100 times more efficient at scavenging aerosols compared with neutral raindrops of the same size. This is predicted to occur even in weakly electrified cloud layers. If only one particle is charged then the collision efficiency is enhanced by electroscavenging. However, if both particles are charged, then the influence may be either attractive or repulsive (depending on the sign of both charges). For aerosols colliding with large cloud droplets (>10 μm), the influence of increasing same sign charge is to increase collision efficiency (by up to an order of magnitude for 100 e charged droplets). Conversely, for aerosols or small droplets (<4 μm), an increase in same sign charge results in a strong suppression of collision efficiency (by up to several orders of magnitude for 100 e charged particles); this is termed electroprotection and acts to inhibit coagulation otherwise caused by Brownian diffusion or phoretic forces (Tinsley et al., 2006).

2.4.4 Some potential mesoscale GEC–cloud processes

It has been suggested that electroscavenging and ice formation in clouds may influence the development of mid-latitude cyclones (Tinsley and Heelis, 1993). In regions of baroclinic instability, the layer clouds associated with the warm front of cyclones may be sensitive to enhanced ice production through electroscavenging (Tinsley and Deen, 1991). As the warm front advances and the layer cloud becomes forced to rise above the surrounding cold air-mass to greater altitudes, cloud top temperatures fall between 0–15 °C and the cloud becomes supercooled. An increase in J_z will result in an increase in space charge accumulation at the

boundaries of the layer cloud, thereby increasing the elementary charging on particles at the cloud boundaries. This may in turn result in increased ice formation in the supercooled cloud top through enhanced IFN scavenging. The consequent ice particle growth through the WBF mechanism may then increase precipitation in clouds at lower tropospheric levels of the frontal system through a seeder-feeder process, whereby ice particles generated in high level clouds fall through lower level clouds and continue their growth through vapour deposition processes previously discussed (Rutledge and Hobbs, 1983). Increased precipitation will result in an increase in the latent heat released into the cyclonic storms, producing enhanced updrafts and storm vorticity (Tinsley, 2008). Observations of mid-latitude cyclone variations following both energetic particle events (Tinsley and Deen, 1991; Veretenenko and Thejil, 2004) and the 11-year solar cycle (Veretenenko et al., 2005; Veretenenko et al., 2007) have been identified which support notions of a GCR-related influence on cyclone properties.

In addition, for thin layer clouds where transfers of latent heat are not important, changes in cloud lifetime and optical depth may have significant impacts on the balance between incoming SW radiation and outgoing LW radiation, influencing tropospheric thermodynamics. Furthermore, if such GEC influences on clouds were to display meridional gradients (relating to the high variation in atmospheric ionisation at high latitudes relative to low latitudes) there may be a significant impact on baroclinic gradients, which may as a result influence mid-latitude cyclonic intensity (Tinsley, 2008). It has also been suggested that polar environments may be highly sensitive to GEC-related cloud responses and that radiative balance changes may influence the katabatic wind regime over Antarctica and Greenland (Troshichev and Janzhura, 2004). The katabatic wind regime is crucial to the tropospheric circulation patterns over the Antarctic continent and any modification to the strength of the wind may have significant impacts on the strength of the circumpolar vortex and, by extension, climate over the southern hemisphere (Parish and Bromwich, 1991; Thompson and Solomon, 2002; Troshichev et al., 2005; Tinsley, 2008).

2.4.5 Studies of relationships between the GCR flux and cloud cover

In 1997, Henrick Svensmark and Eigil Friis-Christensen published work which suggested the total cloud cover on Earth between 1983–1994 varied closely in phase with the terrestrial GCR flux (as measured from Climax Colorado neutron monitor (Simpson, 1957)) (figure 2.2). The authors concluded that this observation was evidence of a causal relationship between the GCR flux and Earth's climate (Svensmark and Friis-Christensen, 1997). In an update to these initial findings, Svensmark further suggested that the Earth's air temperature closely followed the decadal variations in the GCR flux as a result of a GCR–cloud relationship and also argued that

no other relationship between solar activity and climate (such as those related to TSI, UV, and IMF variations) was able to account for these observations (Svensmark, 1998). However, despite these claims, subsequent studies found that the observed correlation between cloud cover and the GCR flux over the 1983–1994 period was only limited to low-level clouds (Marsh and Svensmark, 2000; Pallé and Butler, 2000). As more time passed and further cloud data became available, even the GCR–low cloud relationship began to break down; between 1991–1994, cloud cover began to lag changes in the GCR flux by around six months (Laut, 2003) (figure 2.3). Such a lag cannot be resolved by the response time of either the direct (ion–aerosol) or indirect (near-cloud) GEC pathways (which operate on the order of days and minutes respectively) (Yu and Turco, 2000; Tinsley, 2008). Finally, after 1994, the correlation between low-cloud and the GCR flux disappeared altogether (Laut, 2003). In response to these findings, Svensmark and his team have argued that the temporal breakdown of the correlation between low-cloud cover and the GCR flux after 1994 is an artefact resulting from calibration issues related to the International Satellite Cloud Climatology Project (ISCCP) itself (Marsh and Svensmark, 2003), however, these claims are disputed (Rossow, 2010).

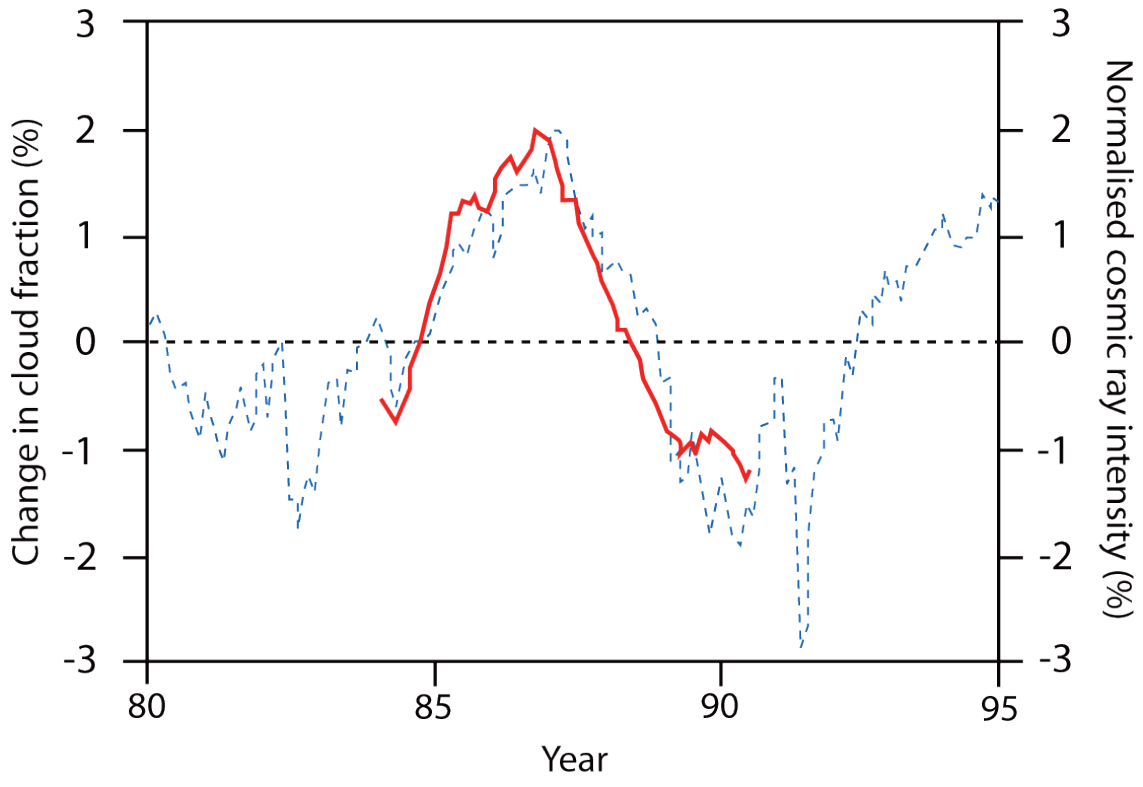

Figure 2.2 Long-term GCR–cloud relationship (from Svensmark and Friis-Christensen 1997)

A 12-month running average of ISCCP C2 monthly cloud cover (red line) from geostationary satellite data over ocean areas only and normalised monthly mean cosmic ray intensity from Climax Colorado neutron monitor (blue dashed line). Figure reproduced from Svensmark and Friis-Christensen (1997), Fig. 2, pp. 1228.

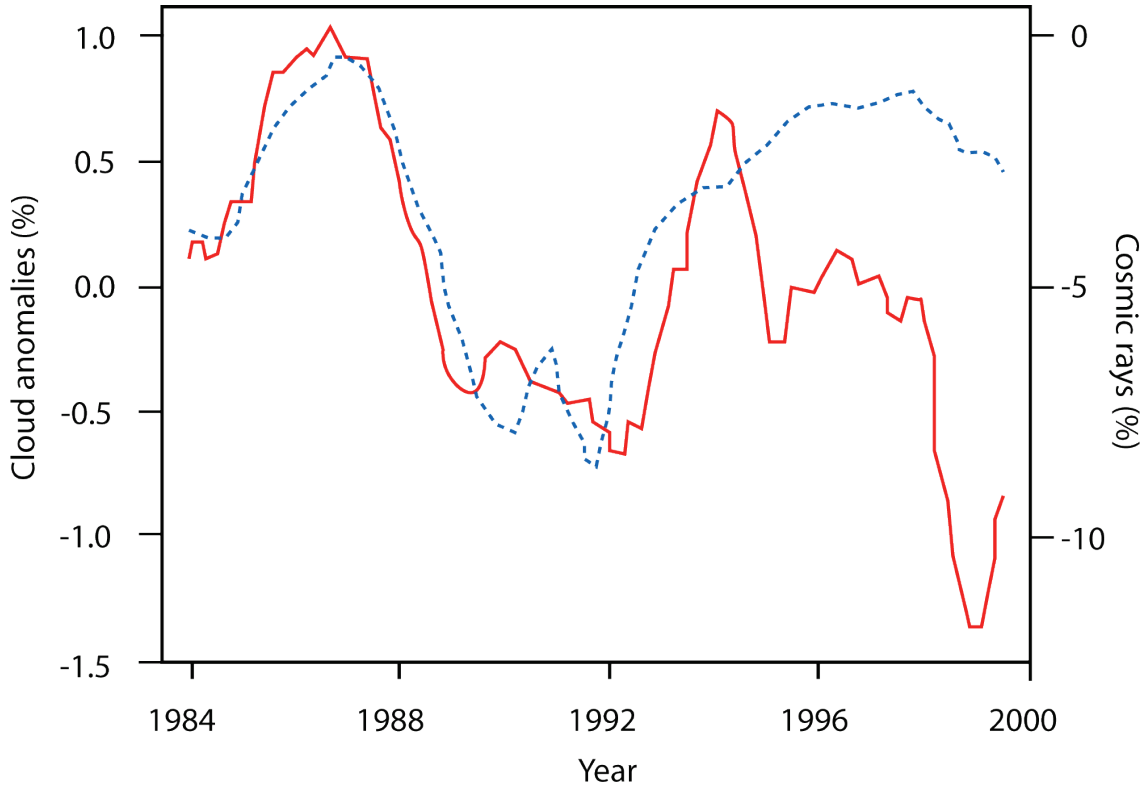

Figure 2.3 Long-term GCR–low cloud relationship (from Laut 2003)

Smoothed low-cloud cover (blue line) and cosmic ray flux from Huancayo, Peru (red line). Figure reproduced from Laut (2003), Fig. 2, pp. 804.

The GCR–cloud link proposed by Svensmark and Friis-Christensen has also been criticised on several other issues: (1) it has been asserted that long-term climate periodicities (such as the El Niño oscillation) may have contributed to the observed cloud trends (Farrar, 2000); (2) the detected long-term cloud trends may be subject to errors resulting from satellite artefacts (Evan et al., 2007); (3) it has also been asserted that the original figures from Svensmark and Friis-Christensen (1997) were presented in such a way that markers were superimposed on to the graph to intentionally mislead readers by obscuring the data content (Laut, 2003). Reanalysis of the original data made by Kristjánsson and Kristiansen (2000) finds that the obscured data did not contribute to the observed GCR–cloud relationship as implied by Svensmark and Friis-Christensen (1997). Kristjánsson and Kristiansen (2000) argue that the data Svensmark and Friis-Christensen intentionally obscured would otherwise have weakened their argument (Kristjánsson and Kristiansen, 2000).

In addition to Svensmark's decadal studies there have been other attempts to discern a long-term relationship between cloud and the GCR flux. Measurements of solar radiation taken from sites across the UK since 1947 have been compiled and used to infer daily cloud cover values

(Harrison and Stephenson, 2006); these workers used the ratio of diffuse to total solar radiation to calculate the diffuse fraction (DF). Comparing the DF to the GCR flux (measured at Climax Colorado neutron monitor [for which data are available between 1951–2000]), Harrison and Stephenson find, that on days of high neutron counts, the probability of an overcast day increases by approximately 20 % and the DF increases by around 2 %. Conversely, during rare high magnitude decreases (of ≥3 %) in the GCR flux (known as Forbush Decrease [FD] events (Forbush, 1993)), small but statistically significant decreases were found to occur in the DF. These observations led the authors to conclude that changes in the DF are causally related to the GCR flux and, although over daily timescales this effect is small, over the longer-term the aggregate influence of this relationship may have a significant impact on climate (Harrison and Stephenson, 2006).

Similar work analysing the long-term records of sunshine hours measured at sites across Ireland (1881–1998) has been carried out by Pallé and Butler (2001). The authors found that since records began there has been a gradual decrease in sunshine hours, implying an increase in cloud amounts over the last century. It was proposed that this trend may indicate a gradual increase in water vapour content of the troposphere, resulting from an increase in mean air temperatures over the period (conforming to the Clausius-Clapeyron relation). Pallé and Butler (2001) also report a correlation between sunshine hours and the length of the sunspot cycle. However, unlike Harrison and Stephenson (2006), they found no reliable relationship between sunshine hours and the GCR flux between 1951–1998 (using the Climax Colorado neutron monitor dataset) with either the overall GCR flux or FD events (Pallé and Butler, 2001).

Over recent years, shorter (daily) timescale satellite based studies have been used to test for the presence of a GCR–cloud relationship. These studies are able to overcome many of the issues which plagued their longer term (annual/decadal) counterparts. They are based around a composite (epoch-superpositional) approach, focused around the occurrence of FD events. A detailed investigation of these events and the findings of past FD-based composite studies will be given in chapter 4.

2.4.6 Clouds: importance and recent trends

Over the last century there has been a long-term decline in the GCR flux arriving at the Earth due to increasing levels of solar activity (Lockwood et al., 1999). If cloud changes are linked to solar activity by the previously described processes, then there may be significant potential for

an underlying trend in solar-related climate variations over the last century (Svensmark, 2000). The presence of a relationship between the GCR flux and Earth's cloud cover to even a small degree would be hugely important. Clouds have an enormous impact on Earth's radiation budget as they reflect incoming solar shortwave (SW) radiation and absorb/re-emit outgoing terrestrial longwave (LW) radiation. Individually, the radiative impact of a single cloud depends on its specific properties, including morphology, droplet size, droplet concentration, water phase/content and altitude. Results from the Earth Radiation Budget Experiment (ERBE) have demonstrated that, overall, clouds reduce the absorbed solar radiation by -48 Wm^{-2}, while simultaneously enhancing the greenhouse effect by 30 Wm^{-2}, giving a net-cooling effect of -18 Wm^{-2}. This cooling effect is largest over the mid-latitude and high latitude oceans, whereas, in low latitude regions LW and SW forcings are approximately balanced (Ramanathan and Inamdar, 2006). Consequently, Earth's climate is highly sensitive to even small changes in long-term cloud amounts.

The question whether there are long-term trends present in Earth's cloud cover is very difficult to answer. The only truly effective means of measuring global scale cloud systems are from satellite-based platforms such as the International Satellite Cloud Climatology Project (ISCCP) (Rossow et al., 1996), yet such datasets have major limitations. ISCCP provides an 8-times daily, global measurement of cloud cover over a 2.5° latitude/longitude grid, beginning in 1983. The data are constructed from both polar-orbiting and geostationary satellites. ISCCP uses a threshold method of identifying cloud, relying on the assumption that clouds are brighter and colder than their underlying surface. Consequently, dark warm pixels are identified as clear sky, whereas bright cold pixels are identified as cloudy. Numerous statistical tests which establish pixel radiances through space and time are performed to establish cloudy/clear sky radiance levels at each location (Rossow et al., 1993). It has been noted, however, that cloud detections may be problematic over high latitude ice-covered regions (Todd and Kniveton, 2004); in addition, the ISCCP dataset is also limited by obstructed views of low-level cloud (due to the top-down perspective of satellite views) (Norris, 2000).

Studies based on ISCCP data have reported evidence of a long-term decline in global cloud cover between 1987 and 2000 (Pallé et al., 2004b; Hatzianastassiou et al., 2005; Pinker et al., 2005). However, these findings have not been supported by either alternate satellite data or ground based measurements. Alternate satellite measurements from the High Resolution Infrared Radiometer Sounder (HIRS) and the Advanced Very High Resolution Radiometer (AVHRR) projects both indicate a slight increase in cloud amounts over recent decades (Jacobwitz et al., 2003; Wylie et al., 2005). On the other hand, long-term ground-based measurements show a small annual increase at Syowa station, Antarctica, over the past 50 years (of around 0.014 % yr^{-1}) (Yamanouchi and Shudou, 2007) and a small increase in cloud cover

over the last century at Armagh, Ireland (Butler et al., 2008). These observations appear to contradict those of the ISCCP dataset and several authors have demonstrated good evidence to suggest why such trends may be present in the ISCCP data.

For example, Norris (2000) showed regions of temporally correlated cloud anomalies within the ISCCP data which closely corresponds to the geostationary viewing footprint of Meteosat data (which is incorporated in to the ISCCP dataset). Norris suggests that the attempts to account for instrument degradation and miscalibration between datasets have not been fully successful and have consequently resulted in inhomogeneities in the data partly responsible for producing spurious trends (figure 2.4). Furthermore, Norris (2000) suggests that Marsh and Svensmark (2000) have mistakenly correlated these false trends to the GCR flux.

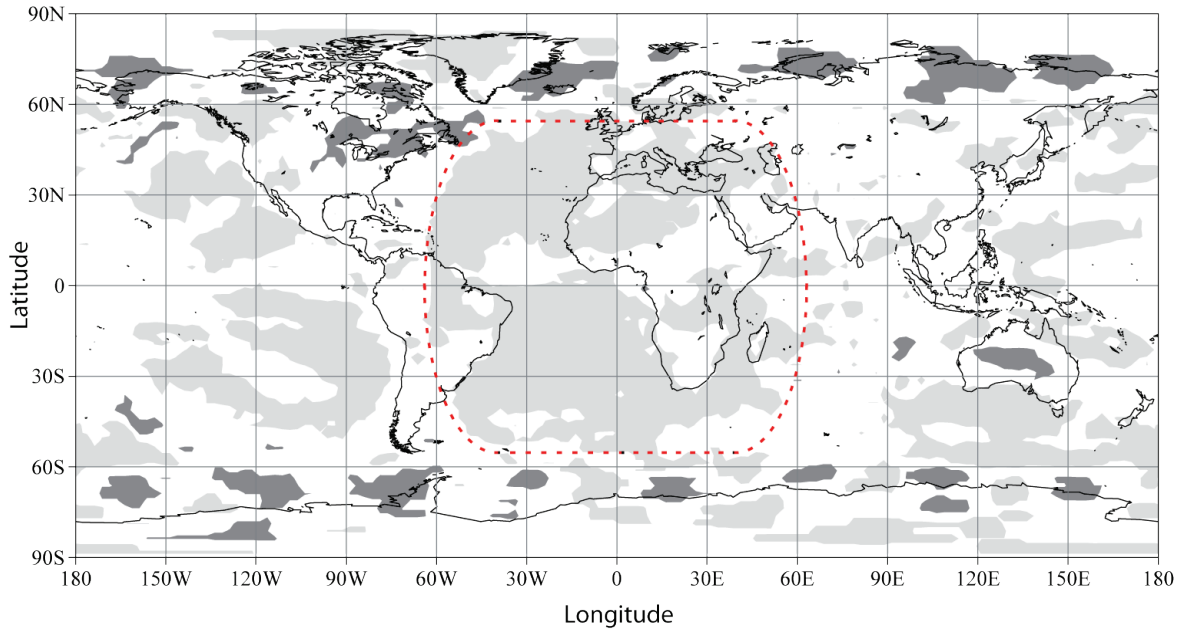

Figure 2.4 ISCCP long-term correlation anomalies

Correlation of ISCCP D-series grid box time series with ISCCP time series. Light grey shading indicates correlations above 0.4, dark grey indicates correlations below -0.4. Red dotted line shows approximate footprint of Meteosat. Sourced from Norris (2000), Figure 2, pp. 378.

Secondly, Campbell (2004) demonstrated the existence of 'seams' in the ISCCP data, supporting the findings of Norris (2000). Based on these observations, Campbell suggested that more cloud is erroneously detected as the viewing angle of the satellites increases. This finding has important implications for the detection of long-term trends, because as the ISCCP project has progressed, increasing numbers of satellites have been added to the dataset. This resulted in a long-term decrease in the average viewing angle, reducing the amount of spurious cloud

detection and therefore giving the appearance of a long-term cloud decrease (Pallé, 2005; Evan et al., 2007). After applying a correction to account for the induced viewing angle error, Campbell noted that the long-term cloud decrease was largely reduced and suggested that the remaining decrease may potentially be explained by the presence of still further errors related to satellite calibration issues (Campbell, 2004; 2006).

Finally, a discontinuity in the amount of cloud detected after October 2001 appears to have occurred, following the replacement of the NOAA 14 Advanced Very High Resolution Radiometer (AVHRR) by the NOAA 16 AVHRR satellite (Campbell, 2006; Knapp, 2008).

2.5 The GCR flux and stratospheric ozone depletion

In addition to the proposed connection between tropospheric cloud cover and the GCR flux, a relationship between the GCR flux and stratospheric ozone depletion (hereafter referred to as the GCR–ozone hypothesis) has also been proposed (Lu and Madley, 1999). This may provide a new mechanism to explain the formation of ozone holes in the polar stratosphere (Lu, 2010). This link was first suggested after a series of laboratory experiments which suggested that, following electron-dissociation, free-electrons may be absorbed on to polar surfaces (such as ice crystals) and react with halogenated molecules ultimately leading to the enhanced formation of ozone-depleting compounds (Lu and Madley, 1999; Lu and Sanche, 2001). Specifically, it is theorised that electrons produced by GCR ionisation are captured on the surface of polar stratospheric cloud (PSC) crystals (which are comprised of water, ice or nitric acid/ice) and the absorbed electron then converts inactive halogenated compounds (also absorbed by the PSC) such as chlorofluorocarbons (CFCs) or HCl molecules in to photoreactive $Cl_{2(g)}$ species, which release chlorine atoms that then destroy ozone (Lu, 2010). Model studies have suggested that this mechanism may have only a limited impact on stratospheric ozone (Müller, 2003), although direct measurements from satellite, balloons and ground stations suggest otherwise. These indicate that ozone loss is strongly correlated to latitudinal/altitudinal variations in GCR driven ionisation and this relationship extends over full two solar cycles-worth of NASA's Total Ozone Measuring Spectrometer (TOMS) satellite data (Lu and Sanche, 2001; Lu, 2009). The GCR–ozone hypothesis is also given support by the experimental and theoretical analysis of several other investigators (e.g. Fabrikant, 2007; Tachikawa and Abe, 2007). Lu (2010) suggests that the GCR–ozone relationship has resulted in an 11-year cyclic variation of ozone loss and stratospheric cooling between 1956 and 2008; Lu also proposes that the concentrations of CFCs in the stratosphere may play a dominant role in global surface temperature change, which has

been underestimated by the IPCC. Lu (2010) suggests that, due to the importance of stratospheric CFC concentrations, the GCR–ozone relationship may be responsible for producing a weak, but detectable, decadal oscillation in surface temperatures.

2.6 Solar modulation of extra-terrestrial dust

Finally, there is evidence of one additional solar–terrestrial pathway. Spectral analysis of tree rings taken from several sites located in the Arctic circle suggest that periodicities of approximately 20-22, 30-33 and 80-90 years are detectable in the dendochronology of Fennoscandian and Kola sites (Kasatkina et al., 2006). It was proposed that the periodicities may be linked to oscillations in stardust flux within the solar system during solar cycles. The authors suggested that this relationship may modulate the amount of extra-planetary material entering Earth's atmosphere, periodically altering atmospheric transparency and as a result the growth of the trees.

Observations of interplanetary dust variations have been made by the Ulysses probe. Measurements indicate that dust levels inside the solar system underwent significant variations during the last solar maximum, suggesting that solar cycles may be related to the modulation of interplanetary dust concentrations. Ulysses measurements show that the interstellar dust stream present in the inner solar system may be influenced by several factors: (1) the solar radiation pressure force; (2) gravitational focusing; and, (3) the interaction of charged dust grains with IMF (Krüger and Grün, 2008). In 1996 a significant decrease in interstellar dust flux (from 1.5×10^{-4} m^{-2} s^{-1} to 0.5×10^{-4} m^{-2} s^{-1}) was observed. This decrease appears to have been the result of a combination of increased filtering of small (<0.2 μm) dust grains by enhanced IMF variations, and increased filtration by solar radiation pressure of 0.4 μm grains within heliocentric distances of 4 AU (Grün et al., 1994; Landgraf et al., 1999). This suggests that changes in the IMF may indeed be linked to large changes in interplanetary dust concentrations. However, the evidence for a link between interplanetary dust and the Earth's climate is tenuous. The relationship proposed by Kasatkina and Shumilov (2006) is weakened by several factors:

(1) The lack of detection of an 11-year Schwabe cycle. This is the strongest solar oscillation and its lack of detection implies the observations do not relate to solar cycles.

(2) The detected periodicities are only present at 2 out of 3 sample sites. Northern Siberian tree rings do not demonstrate similar growth patterns, suggesting that the observed periodicities are not regional in their extent.

(3) A separate dendochronology study, using the Sitka spruce trees (*Picea sitchensis*) from northern England, similarly finds indications of a consistent multi-decadal correlation between tree ring growth and solar activity between 1961 and 2005 (Dengel et al., 2009). However, unlike Kasatkina and Shumilov (2006), the authors conclude that their findings suggest the existence of a relationship between the GCR flux and cloud cover. The authors speculate that a GCR–cloud relationship is able to influence tree growth by influencing the diffuse component of solar radiation, thereby modulating the photosynthetic activity of canopy level trees (Dengel et al., 2009).

Thus, although it is likely that interplanetary dust is modulated by solar cycles, there has been no robust evidence yet demonstrated that this modulation is capable of influencing the Earth's climate.

2.7 General summary

A range of mechanisms have been proposed linking solar activity to Earth's climate, involving a range of processes including interactions between the IMF and Earth's ionosphere, changes in TSI and solar UV output, variations in interplanetary dust concentrations and changes in the GCR flux. Of these mechanisms, those pertaining to a link between the GCR flux and cloud cover are of particular interest. This proposed relationship is highly controversial, as it has been suggested that a correlation between the GCR flux and cloud cover may potentially account for a significant portion of anomalous 20th century warming. However, such claims have been thoroughly dissected and it can be concluded that this possibility is highly unlikely, as the observed correlation between clouds and climate was found to discontinue after the 1990's. Despite this, it is still possible that the GCR flux may modulate Earth's cloud cover to a small degree; recent experimental and model evidence appears to support notions of a microphysical pathway between the GCR flux and clouds via either a direct ion-aerosol effect, or an indirect GEC based effect, implying that a relationship between the GCR flux and cloud cover may yet be found. The identification of a small relationship between the GCR flux and cloud cover would be highly significant, as the GCR flux on Earth varies by ~10 % over differing timescales; this would suggest that a GCR–cloud relationship may have significant implications to climate over long timescales. Consequently, gaining a deeper understanding of GCR–cloud processes may further our understanding of natural climate variability and provide explanations for the diverse range of observations of solar-terrestrial linkages suggested by palaeoclimatic reconstructions.

Chapter 3 Methods and datasets

3.1 Introduction to datasets and methods

The purpose of this chapter is to provide an overview to the datasets, data handling methods and statistical tests which will be used throughout this thesis. The chapter will first introduce the relevant datasets and explain why they have been selected and then a brief description and justification of the data handling techniques and statistical techniques employed throughout this work will be given.

3.2 Datasets

This thesis will utilise a range of space weather and atmospheric datasets (listed in table 3.1). The former are derived from either ground-based or space-based monitoring platforms, obtained from NOAA's Space Physics Interactive Data Resource (SPIDR) (accessible from http://gcmd.nasa.gov/records/NOAA-SPIDR.html), while the latter (atmospheric) datasets come from a range of sources (detailed below).

The International Satellite Cloud Climatology Project (ISCCP). Consists of cloud data based on radiance measurements taken from a suite of weather satellites in geostationary and polar orbits providing global coverage at a 2.5°x2.5° horizontal resolution at 3-hour time intervals (further information is available at http://isccp.giss.nasa.gov/) (Rossow et al., 1996). This thesis will use IR retrieved, daily averaged measurements of cloud cover at a range of pressure levels between 10–1,000 mb. ISCCP will be the preferred source of cloud data used in this work due to its consistent spatial coverage and extensive temporal range.

Moderate Resolution Imaging Spectroradiometer (MODIS). Cloud fraction and liquid cloud fraction data taken from the TERRA (EOS AM) polar orbiting satellite. MODIS has a 1°x1° horizontal resolution and provides partial global coverage over a 24-hour period (further information is available from http://modis.gsfc.nasa.gov/index.php). MODIS will not be widely utilised in this thesis due to its limited temporal range and only partial global coverage over a 24-hour period. The dataset will primarily be used in chapter 4 to reproduce the results of a past study to investigate purported relationships between the GCR flux and atmospheric responses.

National Centres for Environmental Research (NCEP)/National Centre for Atmospheric Research (NCAR) Reanalysis II. Reanalysis data are produced by a state of the art analysis/forecast system based on the assimilation of observations from a range of sources (including land surface, ship, rawinsonde, piloted-balloon (pibal), aircraft, satellites and other data sources) to produce a 2.1°x2.1° horizontal resolution dataset, available over a range of temporal scales and vertical levels (available from http://www.esrl.noaa.gov/psd/data/gridded/) (Kalnaya et al., 1996). The NCEP/NCAR reanalysis data will be extensively employed due to its comparable spatio-temporal coverage to the ISCCP data, making it an excellent dataset with which to perform a comparative analysis. The choice to use the NCEP/NCAR reanalysis data over other similar datasets (such as those of the ERA40 project) was made based on observations of the NCEP/NCAR and ERA40 reanalysis datasets responses to variations in the solar activity, which showed that the ERA40 reanalysis demonstrates a substantially muted response to changes in solar irradiance compared to equivalent NCEP reanalysis data (Gleisner et al., 2005).

Automatic Weather Station (AWS) data from Antarctica. The Antarctic Automatic Weather Station project provides real time meteorological observations from robotic monitoring sites across Antarctica. This study will use data from Dome C and Dome C II stations, located on the Antarctic plateau at 74.50°S, 123.00°E, 3,280 m asl (Dome C) and 75.121°S, 123.374°E, 3,250 m asl (Dome C II) (further information regarding the AWS data are available from http://amrc.ssec.wisc.edu/aws.html). This dataset will be used to verify reanalysis observations over the Antarctic plateau which are known to be notoriously problematic over high latitude regions (Kanamitsu et al., 1997).

10.7cm radio flux (F10.7). Dataset comprises absolute daily solar radio flux, measured at wavelengths of 10.7 cm (2.8 GHz), near the peak of solar radio emission. The values are a proxy for extreme UV activity, which is important for heating Earth's thermosphere. Data is shown in flux units (*fu*) [1 *fu* = 10^{-22} W m^{-2} Hz^{-1}]. Data has been adjusted to account for the varying distance between the Sun and Earth over the course of a year, recorded at Pentiction Ottawa radio observatory in Canada at local noon.

Galactic Cosmic Ray (GCR) flux. Daily averaged cosmic ray data from several neutron monitor sites located across the globe (see table 3.2 for list of sites, locations and data source) (measured units: counts). Data are adjusted for changes in barometric pressure at each monitoring station.

Interplanetary Magnetic Field (IMF). A geocentric solar magnetospheric (GSM) based measurement of magnetic field strength in three axis in space (units measured in nanoteslas [nT]) with an *x*-axis directed along the line from the centre of the Earth to the centre of the Sun,

a *z*-axis directed along Earth's magnetic dipole (north=positive) on to the plane perpendicular to the *x*-axis, and the *y*-axis is defined as the cross product of the x-axis and magnetic dipole axis. The IMF OMNI data are obtained from NOOA's SPIDR archive (further details are available at http://www.ysn.ru/ipm/omni_descr.htm).

Ultraviolet (UV) emissions. The MG II core-to-wing ratio is a measurement of the amplitude of chromospheric Mg II ion emission at 280 nm. This parameter has a strong correlation with solar UV and EUV (150–400 mb) activity and provides a reliable indication of variations in solar activity. Data are based on daily observations recorded from polar orbiting NOAA satellites and scaled to the original NOAA TIROS NOAA9 measurements (Viereck and Puga, 1999).

Parameter	Source	Resolution		Data range	Coverage (%)
		Spatial (degrees)	Temporal		
Infrared cloud cover	ISCCP D1	2.5 x 2.5	daily	1985 - 2006	94.2
Total cloud fraction Liquid cloud fraction	MODIS (TERRA)	1 x 1	daily	2000 - 2009	98.4
Air temperature Pressure Geopotential height Vertical velocity Meridional/Zonal wind Precipitiation	NCEP/NCAR Reanalysis	2.5 x 2.5	daily	1953 - 2006	100
Interplanetary magnetic field (north/south and east/west)	GSM OMNI	NA	daily	1985 - 2006	85.1
F10.7	10.7cm radio flux	NA	daily	1989 - 2006	52.9
Ultraviolet irradiance	MG II core to wing ratio	NA	daily	1985 - 2006	93.1
Galactic Cosmic Ray flux	Neutron counts (various monitors)	NA	daily	1953 - 2006	Varies with monitor
Antarctic air temperature Antarctic pressure	Automatic weather station from Dome C, Antarctica	NA	daily	1985 - 2006	99.8

Table 3.1 Description of datasets parameter

Table listing basic information about the resolution, sources and coverage of the atmospheric and space weather datasets used throughout this thesis.

Neutron monitors	Location	Altitude (m asl)	Cut-off rigidity (GeV)	Data range	Coverage (%)
Alma Ata-B	43.2°N, 76.6°E	3340	6.61	1973 - 2006	83.6
Apatity	67.57°N, 33.39°E	181	0.65	1961 - 2007	99.3
Climax	39.37°N, -106.18°W	3400	2.99	1953 - 2006	97.6
Inuvik	68.4°N, 133.7°W	21	0.17	1964 - 2006	85.2
Kiel	54.30°N, 10.10°W	54	2.36	1957 - 2006	98.6
Magadan	60.04°N, 151.05°E	220	2.09	1971 - 2006	96.7
Mcmurdo	77.9°S, 166.6°E	48	0.00	1960 - 2006	99.9
Moscow	55.47°N, 37.32°E	200	2.43	1958 - 2006	99.6
Newark	39.7°N, 75.7°W	50	2.09	1978 - 2006	81.4
South Pole	90°S, --	2820	0.09	1964 - 2005	100
Thule	76.5°N, 68.7°W	26	0.00	1957 - 2006	99.6

Table 3.2 Neutron monitor details

List of various neutron monitors used in this thesis. All neutron monitor data was obtained from NOAA's SPIDR archive, in 4096 format (adjusted for barometric pressure variations).

3.3 Data handling and statistical techniques

Although more specific data handling and statistical techniques will be discussed as and when appropriate throughout the thesis, certain practices will remain consistent, including (1) the use of rates of change; (2) the use of epoch-superpositional (composite) samples; (3) statistical significance testing using the Students T-test.

3.3.1 Rates of change

All values will be calculated as rates of change rather than absolute values. Primarily, this approach is adopted because it is speculated that GCR-enhanced cloud formation may be distinguishable from natural cloud variability by the rapidity of the cloud changes. This hypothesis is based on models and observations which suggest that electrically enhanced aerosol/cloud droplet growth processes are more efficient and rapid than growth under non-charged conditions (Yu and Turco, 2000; Tinsley and Yu, 2004; Svensmark et al., 2007; Duplissy et al., 2010). There are also secondary benefits to using rates of change rather than absolute values, including the normalisation of the samples to account for the wide range of differing initial conditions present in the composite. In addition, the use of rates of change

results in a normal distribution of the samples, enabling the use of parametric statistical tests; if absolute values were considered, this would not be possible (as, for example, the GCR flux would demonstrate a bimodal distribution due to the solar cycle).

The daily rates of change are calculated by means of the equation below (Eqn. 3.1), using a three-day averaging period which maintains a fixed relative position beginning five days prior to each date calculated. The two-day gap between the averaging period and the key date has been selected to minimise autocorrelation within the data; autocorrelation testing indicated this to be the optimum time period for both GCR and cloud datasets (figure 3.1). Although similar methodologies are common among studies concerning the daily timescale analysis of solar–terrestrial connections, this approach has been adapted specifically from the work of Todd and Kniveton (2000; 2004) and has since been utilised in Laken and Kniveton (2010).

$$Daily\,rate = x - \left(\frac{\sum\big((x-5)+(x-4)+(x-3)\big)}{3}\right)$$

Equation 3.1 Daily rate formulae

Equation to calculate the daily rate of change, where x is a value corresponding to a specific day, i.e. if x equals average cloud cover on 06/01/1985, then x-5 equals average cloud cover on 01/01/1985 (calculated units: unit day^{-1}).

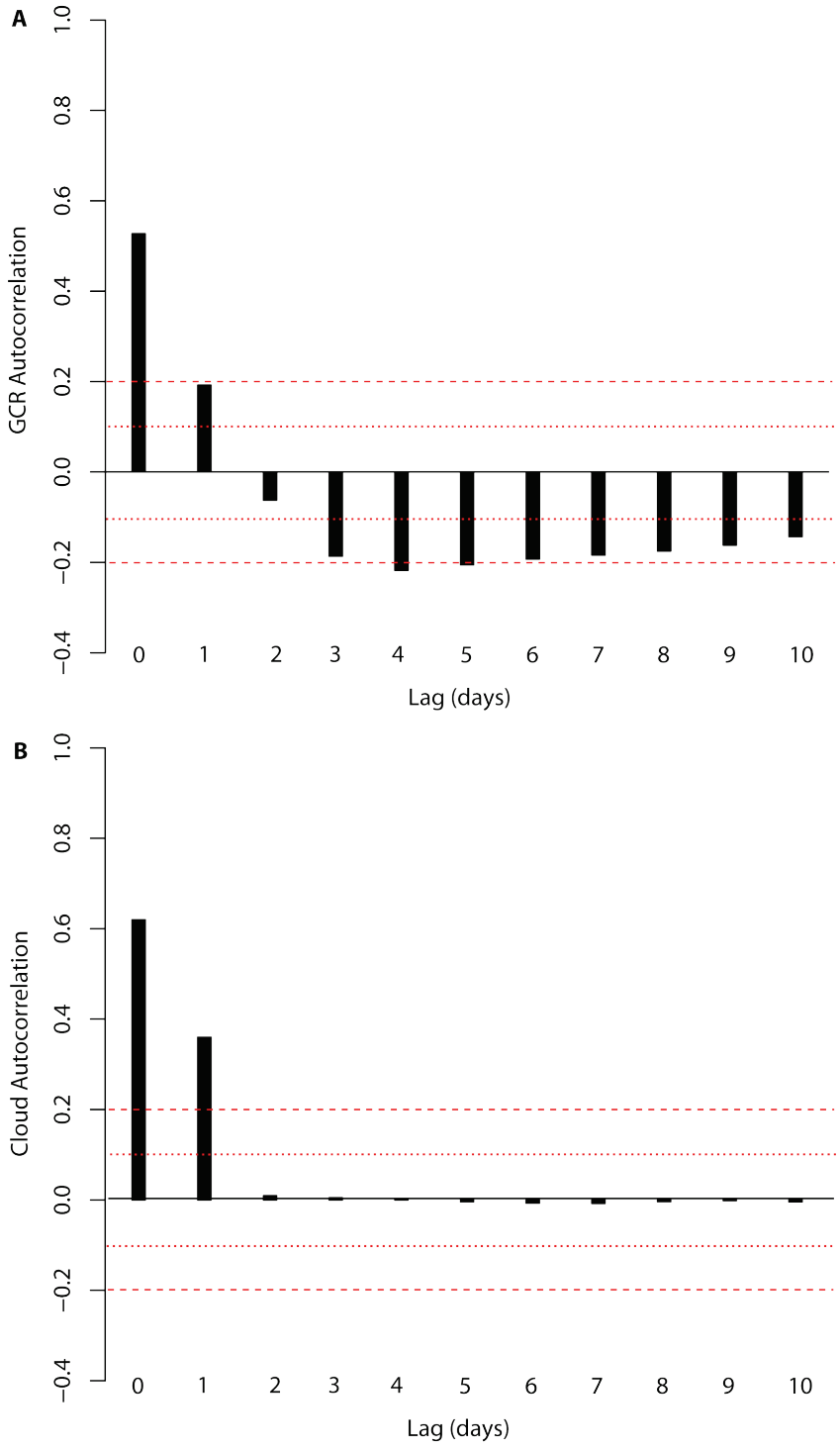

Figure 3.1 Rate of GCR flux and cloud autocorrelation

Correlogram of **A)** the daily averaged rate of GCR flux time series, where the *x*-axis shows the incrementally increasing gap between a three-day averaging period and a key date (i.e. 0 day gap = day *x* - (average (day *x* -1) + (day *x* -2) + (day *x* -3))), and the *y*-axis shows the measure of correlation, and **B**) ISCCP globally-averaged IR retrieved cloud cover (1,000–10 mb). Correlation values = -0.06 and 0.009 (respectively) with a 2-day gap. Dashed and dotted red lines indicate correlation values of 0.2 and 0.1 respectively.

3.3.2 Composite samples

When the use of epoch-superpositional (composite) samples is employed, key dates will be selected on the basis of criteria specified at the time. However, there will be a common procedure for the treatment of composite samples:

(a) After the list of key dates have been compiled, data are retrieved for a period of 20 days prior to, and 3 days following, each date.

(b) The difference between conditions prior to, during and after the key day is established by applying Eqn. 3.1 to calculate the normalised rate of change occurring over the composite period.

(c) The changes of various atmospheric and space weather parameters are then statistically examined from a variety of spatio-temporal perspectives to test if any significant changes over the composite periods are occurring.

This methodology has several important benefits over long-term correlation studies. These include: an ability to isolate small signals from noisy datasets; providing a method of separating out the influences of various space weather parameters (since over short term (daily) timescales the effects of various parameters are distinguishable from one another); and also preventing interference from either long-term instrumental errors, or long-term climate periodicities (such as El Niño/La Niña), from influencing the results. However, it should also be noted the usefulness of composite-based approaches can be unduly influenced by small sample sizes, and poor data quality.

3.3.3 Sample distribution

To determine the appropriate statistical test to apply to the composites, the nature of the sample distribution must be determined. Normal quantile-quantile (Q-Q) plots can graphically demonstrate the distribution of a population, comparing it to a theoretically perfect normal distribution; representative examples of these plots are presented for a range of datasets (figure 3.2). Although only a subsample of the total datasets is presented, the normalcy demonstrated by these samples is representative of all datasets used. Results of the Shaprio-Wilks test, a quantitative measure which provides evidence of non-normality, is also presented in table 3.4 (Shapiro and Wilk, 1965). Normalcy is accepted/rejected under the Shapiro-Wilks test if the W-value is large/small and the probability (P) value is less/greater than 0.05 (at the 0.95 level

confidence interval). Interpretation of the Q-Q plots and Shapiro-Wilks tests indicates that the data can be considered to be normally distributed. Interestingly, the largest departures from this distribution appear to be from the rate of GCR flux and the MG II index. The rate of GCR flux undergoes high magnitude variations (referred to as Forbush Decreases (FDs) and Ground Level Enhancements (GLEs)) and the presence of these events is the source of the departure from normalcy. Unless otherwise stated, therefore, FDs and GLEs will be removed from the composites, thereby allowing an analysis of the comparatively low magnitude standard GCR variability (which demonstrates a more normal distribution (as indicated by the W statistic shown in table 3.3)). The MG II index of UV and EUV solar activity shows the lowest W statistic (of 0.432), indicating that the sample is not normally distributed. The data have a modal value of 0.0 which can be attributed to the low resolution of the index; the index is accurate to 4 decimal places. However, it is found that for the majority of the sample there is no detectable change in the rate of MG II change over daily timescales, resulting in the non-normal distribution. Under periods of changing solar activity, space weather parameters tend to vary roughly in tandem and so it is unlikely that composite samples (which highlight changes in solar activity) will be greatly influenced by the occurrence of zero values. These results indicate that the use of parametric statistical tests is appropriate for all datasets except the MG II index, to which the non-parametric Mann-Whitney U test will be applied.

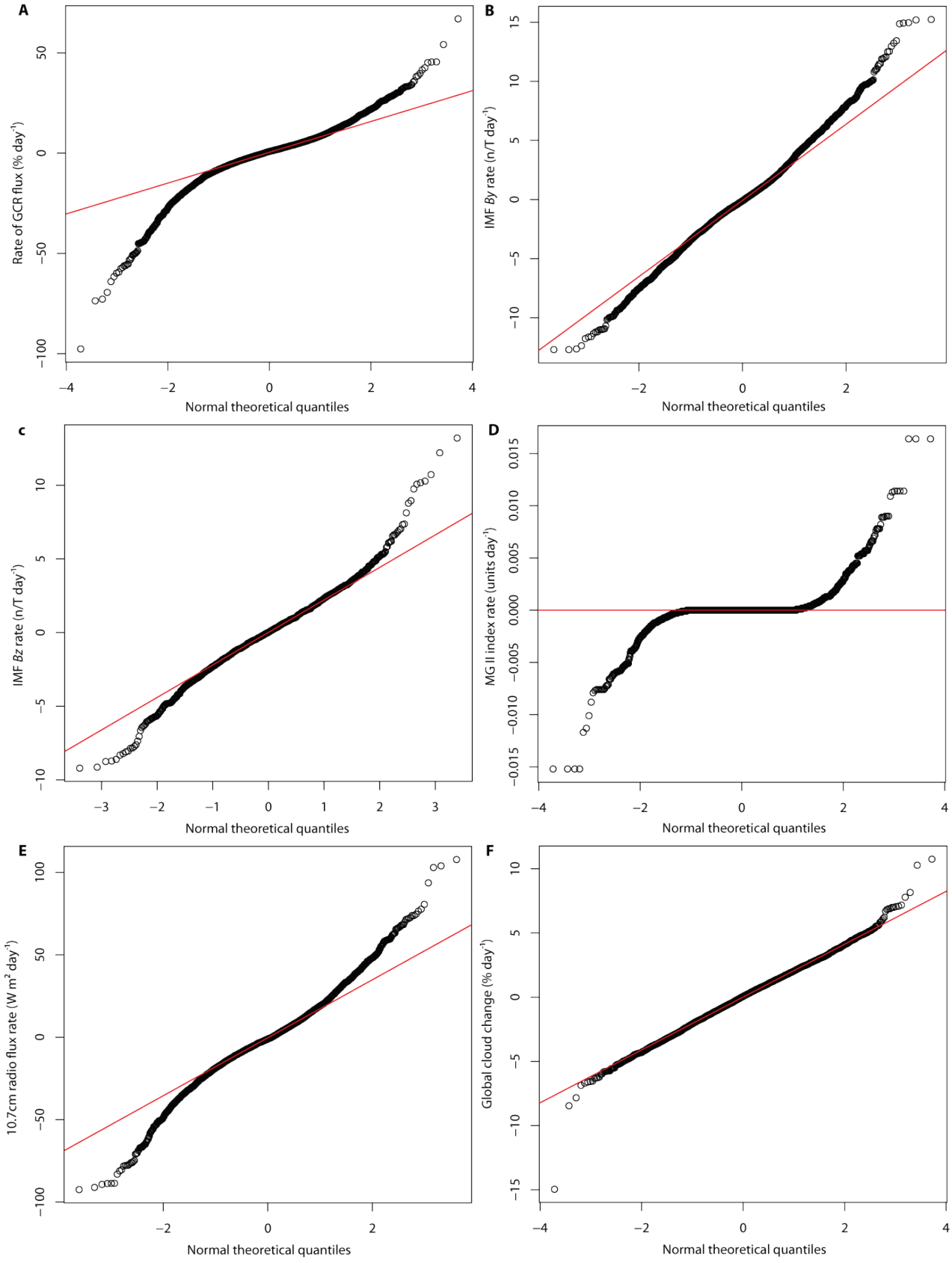

Figure continued overleaf...

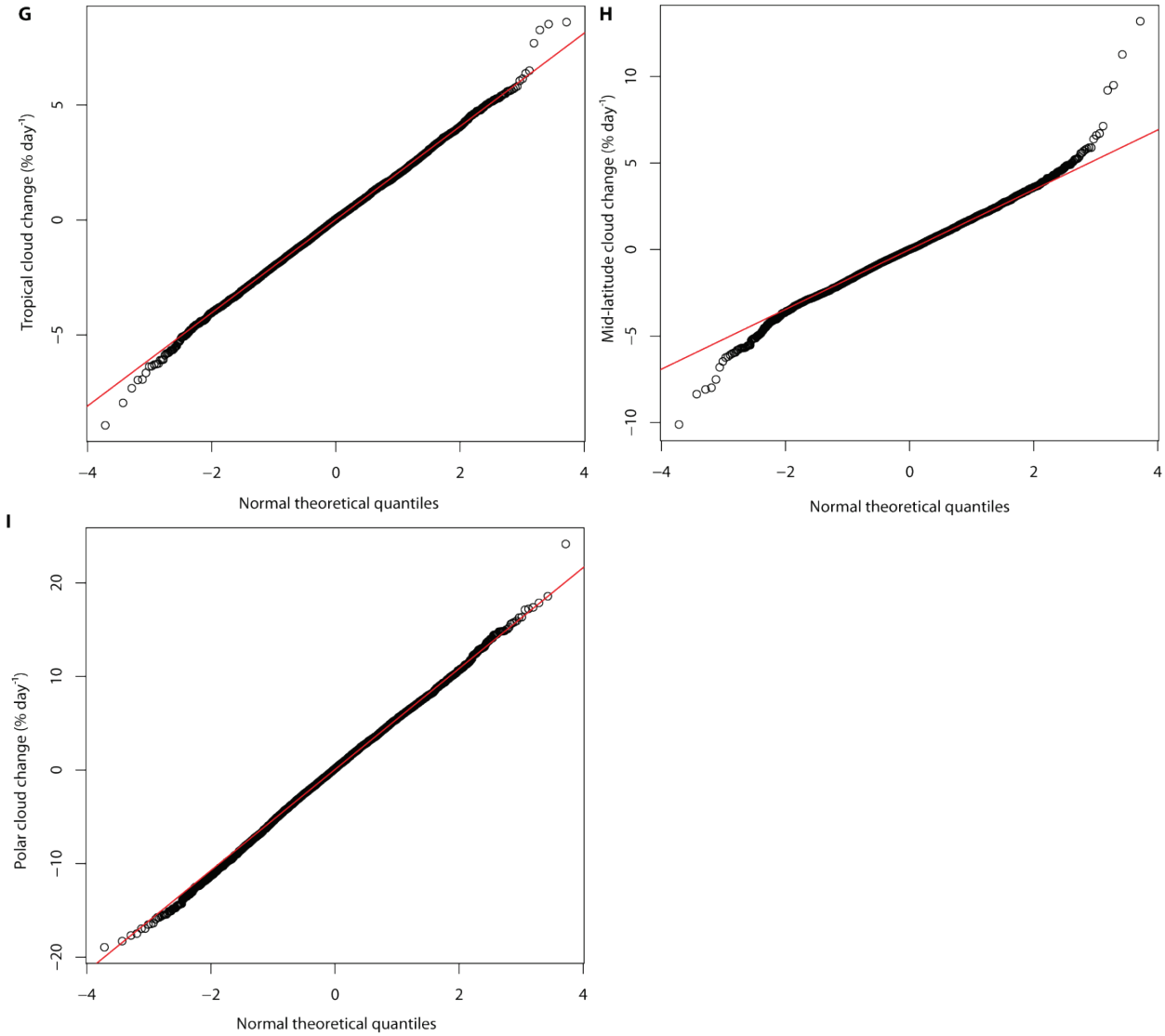

Figure 3.2 Normal Q-Q plots

Normal Q-Q plots illustrating typical representative sample distributions (circular markers) against an equivalent theoretically perfect normal distribution (red line). The rate changes of various datasets are shown: **A)** GCR flux measured from Climax Colorado, values are shown as a % change normalised against variation over an 11-year solar cycle; **B–C)** IMF B_y/B_z rates; **D)** MG II index of UV and EUV activity; **E)** 10.7 cm radio flux; **F–I)** ISCCP D1 IR retrieved cloud change between 1,000–10 mb over the globe (90°N–90°S) tropics (30°N–30°S) mid-latitudes (60°–30°N/S) and polar (90°–60°N/S) regions.

Parameter	W value	P value
GCR rate	0.8578	2.20E-16
GCR rate**	0.9224	2.20E+16
IMF *By* rate	0.9929	1.30E-12
IMF *Bz* rate	0.9789	1.10E-13
10.7 cm radio flux rate	0.9768	2.20E-16
MG II index rate	0.4327	2.20E-16
10-1,000 mb Globe cloud rate	0.9958	7.70E-11
10-1,000 mb Tropics cloud rate	0.9992	0.0215
10-1,000 mb Mid-latitude cloud rate	0.9908	2.20E-16
10-1,000 mb Pole cloud rate	0.999	0.00546

Table 3.3 Shaprio-Wilks test of normalcy

Results of the Shapiro-Wilks test of normalcy for a range of datasets. W value indicates Shapiro-Wilks statistic (where large values indicate normal distribution and small values indicate non-normal distribution). P-value shows probability level (where less than 0.05 indicates statistical significance at a 0.95 level confidence interval). Two GCR rates are presented for comparative purposes; the GCR rate** has high magnitude FDs/GLEs removed.

3.3.4 T-tests and Monte Carlo simulations

With the exception of the MG II index, the datasets have been shown to demonstrate a normal distribution and therefore allow for the use of parametric statistical tools. A two-tailed Students T-test (assuming paired samples and unequal variance) is selected as the primary method of analysis, as this work will require the comparison of key dates against averaging periods, and the T-test is particularly suited to comparing populations of roughly equal sample size in this manner. Essentially, the T-test will compare the sample distribution of a composite of key dates against the distribution of an averaging period to determine if there are differences between the distributions of two populations which lie outside the realms of standard variability (quantified by significance levels).

Critical T-values for determining significance (at the 0.95 level) are calculated for area-averaged atmospheric samples and space weather data by the use of brute force Monte Carlo (MC) simulations; samples of 130 random observations are constructed from each dataset, and a T-test performed. This procedure is repeated 1,000 times and the resulting distribution of the T-values are plotted (figure 3.3). The T-values occurring at the 0.975 percentiles are extracted, and this value is assigned as the criteria for the critical T-value (±) to accept statistical significance at the two-tailed 0.95 confidence level. A range of MC-simulated critical T-values

are shown in table 3.4 as examples; the FORTRAN software developed to calculate these values is presented in Appendix 1.

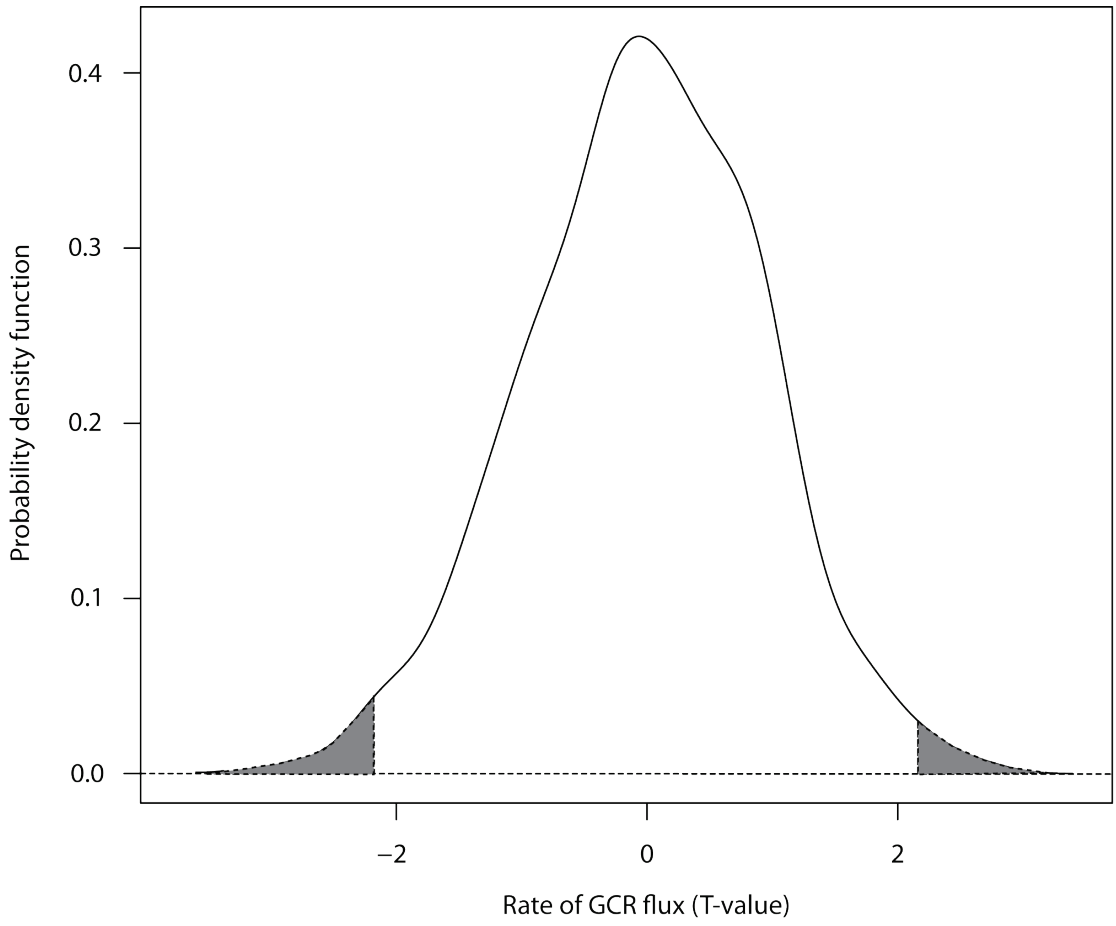

Figure 3.3 Monte Carlo simulated rate of GCR flux T-values

Kernel density estimation of rate of GCR flux Student's T-values, based on 1,000 random samples (each comprised of 100 data points) (kernel bandwidth = 0.2142). Grey shaded distribution tail cover the 0.975 interval, indicating a statistically significant T-value at the two-tailed 0.95 significance level (according to MC simulations) is 2.1.

Parameter	0.95 MC Critical T-value
GCR rate	2.11617
IMF B*y* rate	2.51999
IMF B*z* rate	2.7241
10.7 cm radio flux rate	1.87198
MG II index rate	2.25482
10-1,000 mb Globe cloud rate	2.53095
10-1,000 mb Tropics cloud rate	2.40315
10-1,000 mb Mid-latitude cloud rate	2.52353
10-1,000 mb Pole cloud rate	2.49494

Table 3.4 Table of Monte Carlo simulated critical T-values

Examples of MC simulated critical T-values produced by the software presented in Appendix 1.

3.4 General summary

This chapter has outlined the primary datasets and data handling techniques which will be used throughout this thesis, as well as justifying their selection. In addition, the chapter has also outlined the primary statistical procedures which will be used for significance testing and described the rationale behind their selection.

Chapter 4 High magnitude variations in the GCR flux and cloud cover

4.1 Introduction

In an attempt to test the validity of a possible GCR–cloud link a range of studies have focused on the onset of unique high magnitude low frequency decreases in the GCR flux known as Forbush decrease (FD) events. These events result from magnetohydrodynamic disturbances in the solar wind created by solar coronal mass ejections (Kirkby, 2007) and have been explicitly defined as a decline in neutron counts of greater than 3 % at the Earth's surface as recorded by the neutron monitor at Mount Washington, USA (39.23°N, 76.41°W) (Todd and Kniveton, 2004).

This chapter will re-examine the results of several FD-based composite studies (Todd and Kniveton, 2001, 2004; Kristjánsson et al., 2008; Svensmark et al., 2009) and attempt to expand upon their findings by refining and extending their methodologies. Although FD-based superposed epoch analyses have several limitations (which mainly stem from small sample sizes) they provide an excellent starting point from which to begin a daily timescale analysis of the impacts of GCR variations on cloud cover.

4.1.1 The advantages and findings of FD-based studies

Superposed epoch analysis of FD events provides a unique opportunity to assess the influences of large (decadal magnitude) GCR variations on the Earth's atmosphere over daily timescales. This analytical approach possesses a number of significant advantages over longer timescale approaches, for example:

(1) The ability to separate cloud changes from internal periodicities (e.g. El Niño); this is something decadal studies are unable to achieve (Farrar, 2000).

(2) At a daily timescale resolution it is possible to distinguish variations in the GCR flux from co-temporal variations in solar irradiance, UV wavelengths and the interplanetary magnetic field (IMF).

(3) A composite approach minimises the impact of artificial errors related to long-term instrumental issues contributing to any detected cloud variations in a daily timescale composite; such errors may have potentially affected the results of decadal cloud studies reducing their reliability (Evan et al., 2007).

(4) The magnitude of the GCR variations associated with FD events is comparable to that of GCR variations experienced over a decadal solar cycle; consequently the impacts of FD events on clouds may provide a good indication of the extent to which GCR are able to influence cloud changes over decadal timescales.

Despite the noted advantages of FD-based composite analysis, the findings of past studies have not provided conclusive evidence of a relationship between GCR variations and cloud cover changes. Instead, past studies have demonstrated a wide range of conflicting results: some have found indications of statistically significant cloud decreases occurring over high latitude regions following FD events (Pudovkin and Veretenenko, 1995; Veretenenko and Pudovkin, 1997; Todd and Kniveton 2004), while others have found no statistically significant relationship at high latitudes (Lam and Rodger, 2002) or over southern hemisphere ocean regions (Kristjánsson et al., 2008). Some studies have even indicated increases in cloud following the onset of FD events (Wang et al., 2006; Troshichev et al., 2008). Due to this wide range of conflicting results the level of confidence we can place in the validity of a GCR–cloud link based on the results of FD studies is highly limited.

4.2 An unusual FD study

The findings of a recent study by Svensmark et al. (2009) (hereafter referred to as SBS) differs notably from other similar studies. Generally, FD studies have either failed to identify a coherent relationship between GCR and cloud cover or have identified a statistically significant but highly localised relationship at high latitude regions. In contrast to this, SBS claimed to show evidence of a globally significant variation in several atmospheric parameters following the onset of FD events, detectable in both the MODIS and ISCCP datasets. SBS claim the changes they observe provide good evidence of a widespread and significant relationship between cloud cover and the GCR flux. Based upon this and other work the authors suggest that solar activity is a primary driver of natural climate variability and a potential cause of the climatic anomalies of recent decades (Svensmark, 2007). Due to the enormous importance of issues relating to climate change it is essential to examine such claims in detail. Consequently,

the findings of SBS will now be carefully re-examined before a broader analysis of the importance of FD events is considered.

4.2.1 A coherent and global response to FD events?

The primary findings of SBS are based around an analysis of only five FD onset events selected from a total of 26 events occurring between 1987 and 2007. These five events were selected on the basis of two criteria:

(1) For each chosen event there needed to be data coverage in all datasets over a period of -15 days to 20 days around each event.

(2) The FD events selected needed to be the largest ranked decreases out of the sample.

The actual rank of the 5 decreases in relation to the full list of 26 dates selected by SBS was 1st, 3rd, 4th, 6th and 7th due to a lack of data coverage during several the 2nd and 5th event. Using these events, SBS composited several atmospheric datasets including the MODIS liquid cloud fraction (hereafter referred to as LCF) and the ISCCP low cloud cover (hereafter referred to as LCC). Interestingly SBS reported that these parameters gave very similar time profiles, appearing to demonstrate a coherent global decrease in LCC and LCF at an approximately 6 day time lag following the onset of FD events (figure 4.1 displays the LCC and LCF changes as they appeared in SBS). They concluded that these findings provided good evidence of a global scale link between solar activity, clouds and Earth's atmosphere operating via a GCR related modulation of aerosol formation. A re-analysis of the ISCCP LCC and MODIS LCF occurring over these events will now follow to test the validity of these claims.

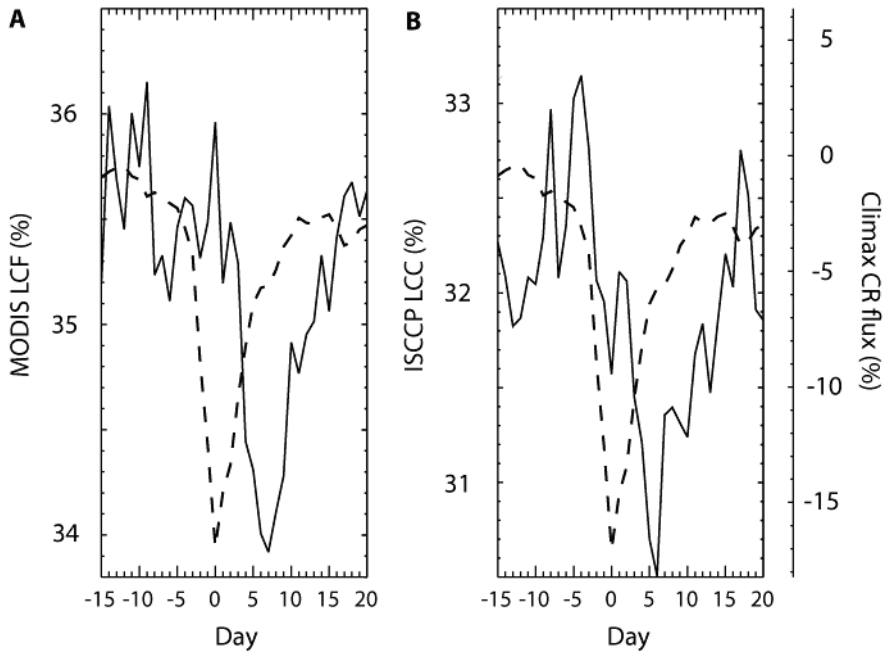

Figure 4.1 MODIS and ISCCP changes presented by SBS

A) Average global MODIS detected LCF and **B**) Average ocean area ISCCP detected LCC. Both parameters are compared against normalised GCR variations measured at Climax Colorado neutron monitor (indicated by the dashed line). Changes displayed are a composite of 5 FD onset events. Figure adapted directly from SBS, figure 1, pp. 2.

4.2.2 Re-analysing the temporal profile of liquid cloud fraction changes

The average MODIS LCF values during the 5 key SBS dates have been re-calculated and presented in figure 4.2 for an extended time period (±40 days either side of the key dates). The LCF values are calculated as an equal area weighted daily average value and a simple linear fit has been applied to the data. The data have also been separated into ocean and land regions; this is because if a mechanistic relationship between aerosols and GCR exists and is responsible for a GCR–LCF interaction as SBS claim, then there may be appreciable differences in the response between land and ocean regions due to the differing sources and abundances of aerosols over these environments.

Figure 4.2 shows that a decrease in the LCF does occur following the key date of the sample over both ocean and land regions as SBS claim. In both instances, these decreases reach a maximum around day 6 of the composite. Although the amplitude of the decrease appears to be comparable between the ocean and land regions (approximately -1 %) the ocean decrease is far more prolonged, LCF values do not return to day 0 levels for approximately 15 days over ocean regions, whereas, the LCF recovery over land regions occurs more rapidly after the FD event.

Despite this agreement to SBS's results, it is clear that the day 6 SBS decreases are not the largest magnitude changes observed over the composite period. However, by plotting the LCF data over a shorter time period (identical to the time interval presented by SBS), the detected LCF changes become comparable to those demonstrated by SBS (figure 4.3). The selective time period presented in these graphs along with the skewed axis gives a misleading sense that the LCF decreases are abnormally large, when it is clear from figure 4.2, that the LCF decreases are not unusual.

The downward sloping linear fit of figure 4.2B suggests that the oceanic LCF change is occurring during a longer term decrease. This change may provide an explanation for the extensive recovery time of the oceanic LCF previously noted. A 10-day running mean is plotted in order to better observe long-term trends underlying the LCF data (figure 4.4A). Additionally, using the running mean, anomalous LCF variations are also calculated, by subtracting the daily average LCF from the running mean (figure 4.4B). The 10-day running mean confirms the notion that the LCF data are underpinned by several long-term (approximately 20-day) decreases and partial recoveries; one of these decreases peaks on day 6, coinciding with the peak GCR–cloud change date claimed by SBS. Anomalous LCF changes are evident around day 6 of the composite as SBS suggest, however, the magnitude of the anomaly is unremarkable and anomalies of similar and greater magnitude are found to be common over the composite period.

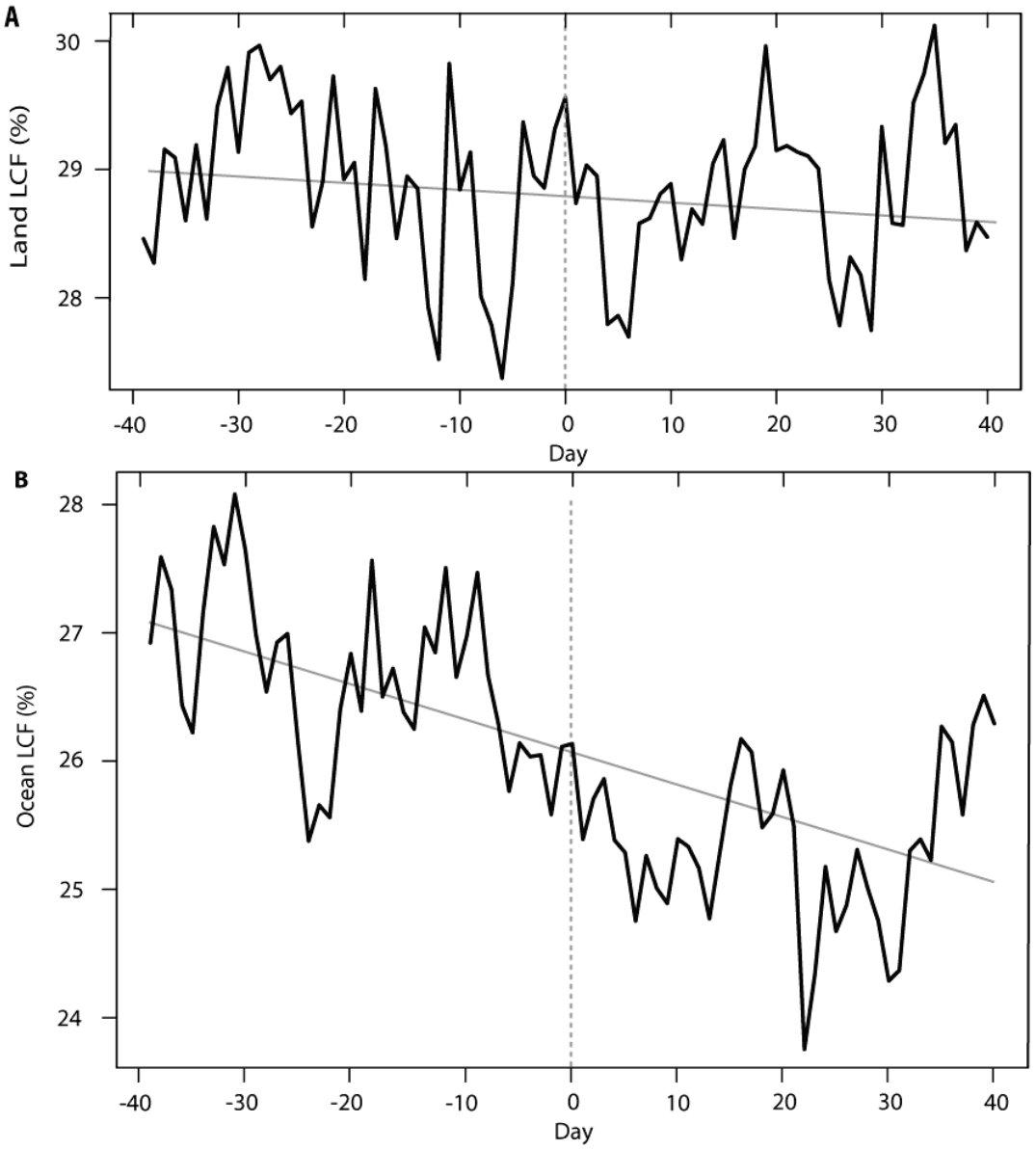

Figure 4.2 MODIS LCF: Land and ocean regions

A) Daily average LCF values over land-covered regions, and **B)** daily average LCF values over ocean regions. Vertical dashed line indicates key date (FD onset event). Line of best fit is also displayed (grey solid line). Values are based on a composite of the 5 SBS key events.

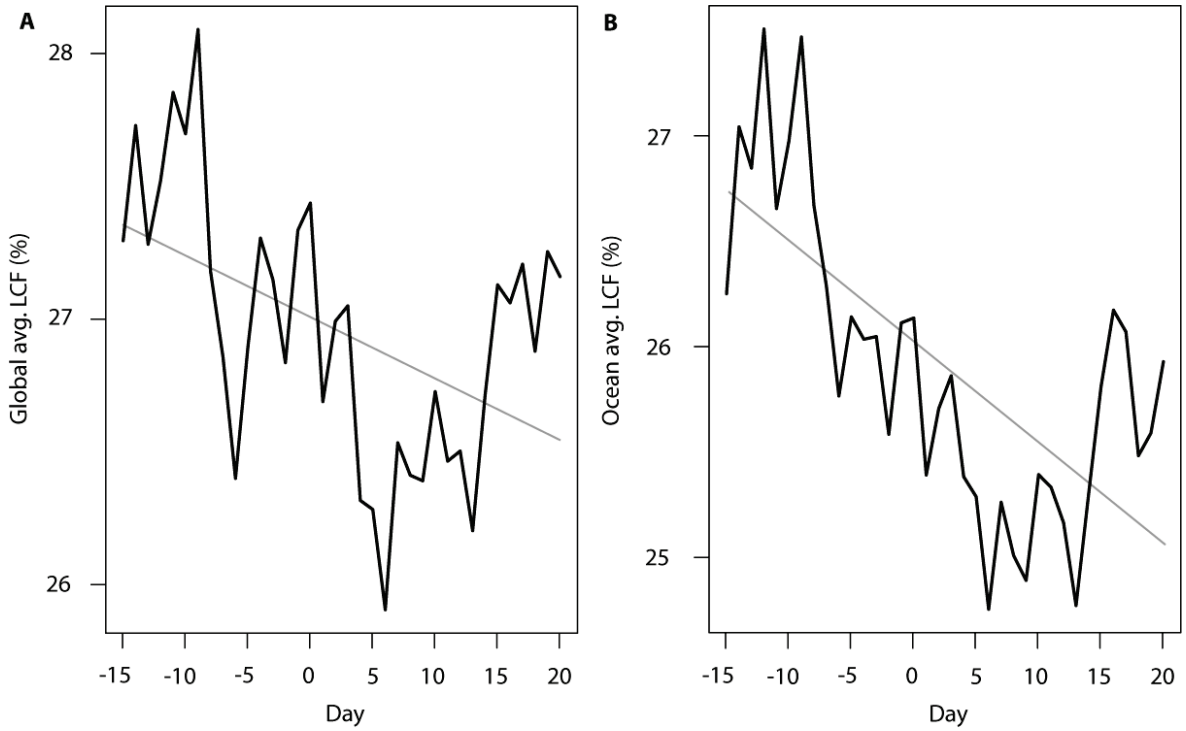

Figure 4.3 LCF values in SBS style

A) Globally-averaged LCF (ocean and land) and **B)** ocean area only LCF values. The graphs are modified to present similar dimensions to those of SBS. Lines of best fit are also shown (solid grey lines).

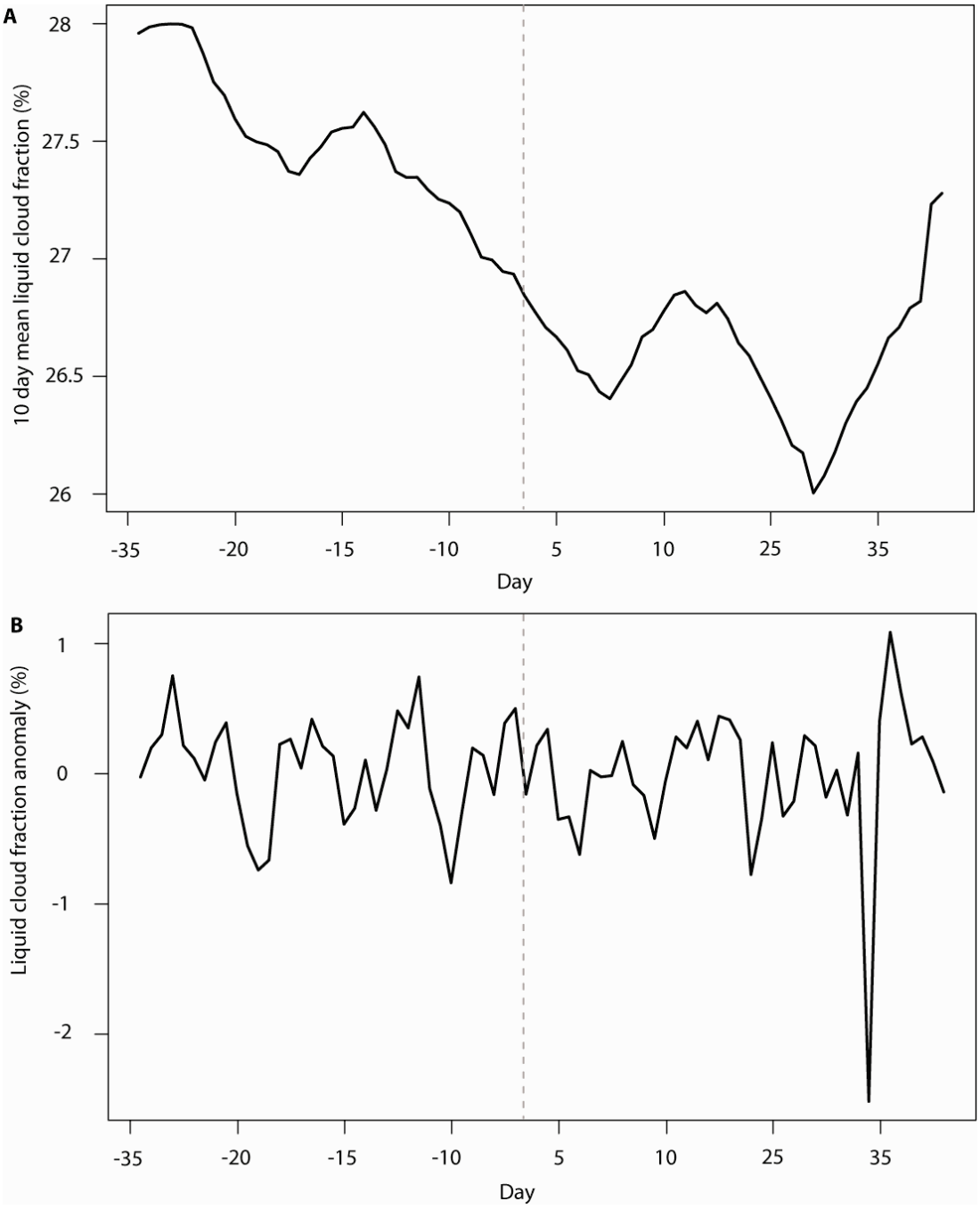

Figure 4.4 LCF long-term trends and anomalies

A) Global (ocean and land area) daily average LCF values taken over a 10-day running mean. **B**) Global LCF anomaly, calculated from subtracting the daily average global LCF value from the 10-day running mean. Vertical dashed line indicates key (FD onset) date.

4.2.3 Analysis of individual liquid cloud fraction changes

One of the primary benefits of a composite analysis approach is the ability to identify small signals present in atmospheric datasets. Individual observations in a composite should not necessarily be expected to demonstrate similar changes over the sample period, as the background noise of atmospheric datasets is often greater than any underlying signal. However, SBS explicitly state that '*the effects [of GCR] on clouds and aerosols are not dominated by any single event among the 5 averaged [observations]*' (Svensmark et al., 2009, p.2). Contrary to these claims, a plot of the individual LCF variations occurring over the 5 key events shows that there is no coherence between the changes occurring; the average LCF decrease following the key date (identified in figures 4.2–4.3) appears to be the result of a single event (19/01/2005) (Figure 4.5): this observation contradicts the assertions made by SBS.

Furthermore, the event which is largely responsible for the mean LCF decrease (19/01/2005) has problematic complications to consider, which are not discussed by SBS. Figure 4.6 shows the cosmic ray intensity recorded by the Lomnický Štít neutron monitor (49.20°N, 20.22°E, 2634 m asl) together with average LCF over ocean regions for the time interval of ±12 days centred around 17/01/2005 (two days before the key event of 19/01/2005). During this period, the GCR flux actually shows two separate FD events, occurring on the 18/01/2005 and 22/01/2005, in addition, a SEP event occurs between these FD events on the 20/01/2005 (Flueckiger et al., 2005). Any reduction in atmospheric ionisation occurring as result of the FD events may be negated over high latitude regions due to the effects of the SEP event (Usoskin et al., 2009). The LCF changes observed during the 19/01/2005 event appear to occur from the key date onwards (until around day 5). If one were to assume the global LCF value is influenced by FD in the manner described by SBS then it is surprising to find a uni-directional and consistent decrease during complex and multi-staged ionisation changes occurring over this period. Considering that this event is responsible for the majority of the LCF decrease observed by SBS this finding challenges the validity of their conclusions.

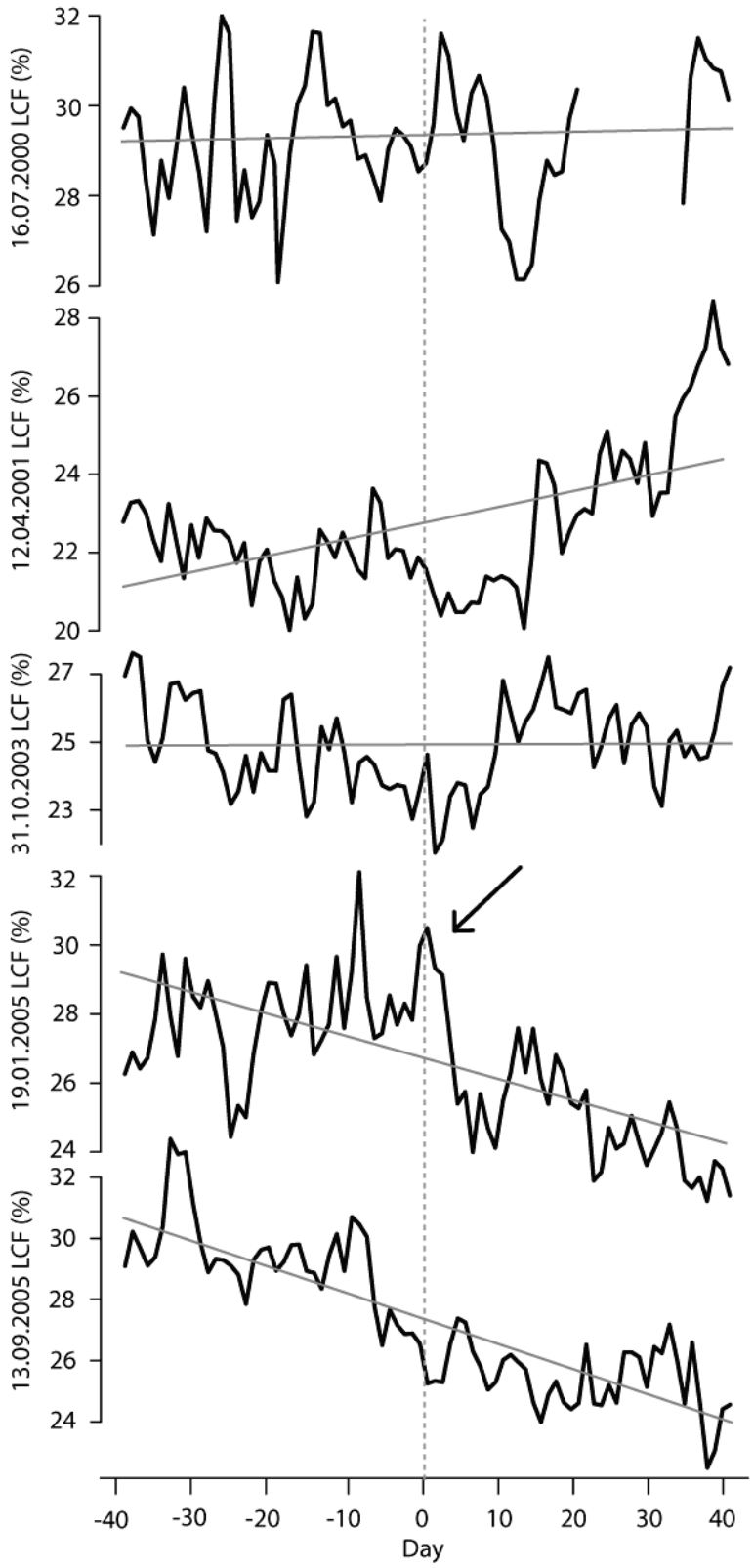

Figure 4.5 Individual daily average global area LCF

The 5 individual events of SBS are displayed in descending chronological order (dates are stated on the *y*-axis). A line of best fit for each data series are also displayed (solid grey line). Vertical dashed line indicates key date of the composite (FD onset date). Arrow indicates most 'responsive' date in accordance with the claims of SBS.

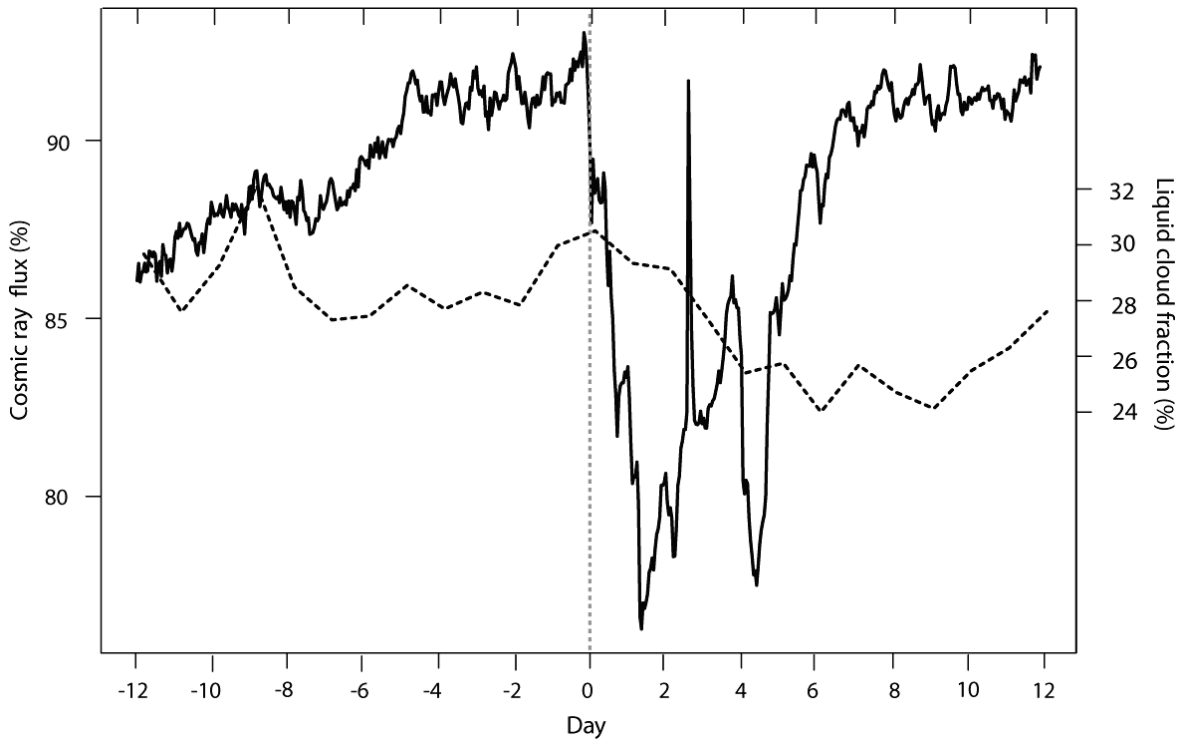

Figure 4.6 Cosmic ray and LCF variations on 19/01/2005

Hourly neutron monitor data from Lomnický Štít (49.20°N, 20.22°E) neutron monitor (solid black line) over a ±12 day period around the 17/01/2005 during the onset of the associated FD event (two days prior to the date selected by SBS as the key day). The daily average ocean area LCF (black dashed line) is also displayed. Vertical grey dashed line indicates the onset of the FD event.

4.2.4 An important note regarding SBS's treatment of ISCCP data

SBS state in their paper that the ISCCP D1 data used to calculate the LCC covers the ocean regions only. However, not explicitly stated is the fact that the SBS data do not cover the entire globe; instead, SBS only use data covering the subtropics/tropic regions between 40°N to 40°S. This detail only became apparent through personal correspondence with the authors and is now available as a formal note, accessible on request from the authors; this note is presented in its original form in Appendix 3. The restriction of the ISCCP data in this way is counterintuitive to the claims by SBS that their data demonstrate a 'global' signal. A full (90°N–90°S) analysis of the ISCCP LCC changes occurring during the 5 SBS events will now be given.

4.2.5 Re-analysing the temporal profile of low cloud cover changes

The LCC parameter was constructed from three separate ISCCP D1 variables:

(1) The total number of pixels.

(2) Number of cloudy pixels 680 mb < PC <= 800 mb.

(3) Number of cloudy pixels 800 mb < PC <= 1000 mb.

The numbers of pixels on each of the two separate pressure levels are added together, and this value is divided by the total number of pixels to produces LCC. For reference LCC variations reported by SBS has been shown in figure 4.1B. The LCC values are calculated for an extended composite period (identical to that described in section 4.2.2) and these changes are then separated into both ocean and land regions (figure 4.7).

Figure 4.7 demonstrates that there is a very different response between land and ocean regions. While ocean regions do indeed show a decline in LCC as described by SBS, over land regions the decrease is far less prominent and only begins around 3 days after the FD onset date. Presenting the data in a similar format to that of SBS (i.e. a shorter time period of -15 to 20 days, with an enlarged *x*-axis) the ocean area LCC changes appear to be similar to those reported by SBS (figure 4.8). However, the decrease is less confined; it appears that the supposedly arbitrary latitudinal restriction (40°N–40°S) placed on the data by SBS, had the serendipitous effect of producing a stronger and more uni-directional change over the composite period.

A 10-day running mean of the LCC data designed to show longer-term variations, suggests that the anomalous decrease identified by SBS are occurring during a relatively longer term period of LCC decrease (figure 4.9A). This implies that the LCC decrease is, at the very least, being enhanced by relatively longer-term variations. LCC anomalies calculated by subtracting the daily average from the 10-day running mean show that, while the anomalous decrease is large (approximately -1.5 %) (figure 4.9B), the value is by no means unique; approximately 5 decreases of comparable magnitude are found to occur over the observation period.

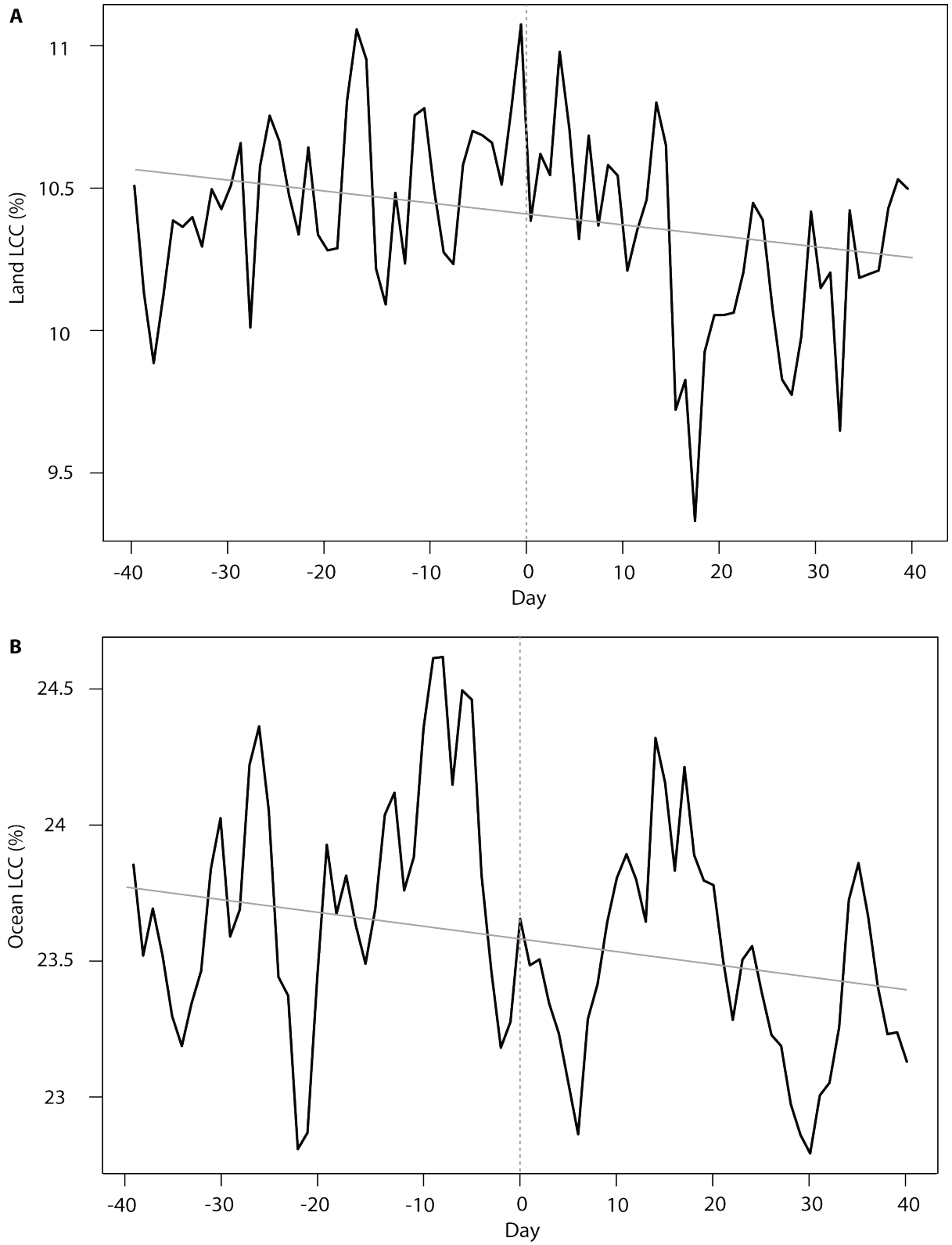

Figure 4.7 ISCCP LCC: Land and ocean regions

A) Daily average LCC values over land regions and **B)** daily average LCC values over ocean regions. Vertical dashed line indicates key (FD onset) event. Line of best fit is also displayed (grey solid line). Values are based on a composite of the 5 SBS key events.

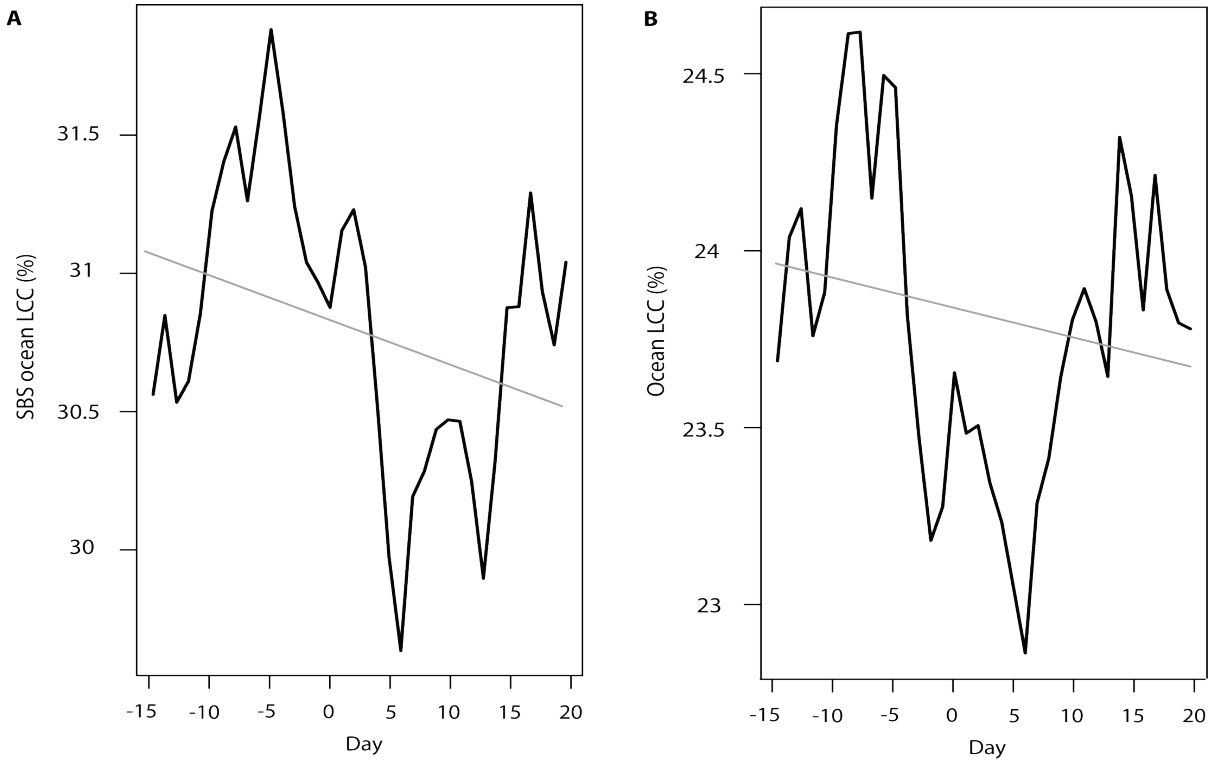

Figure 4.8 LCC ocean data in SBS style

A) Ocean area data over the SBS restricted area of 40°N to 40°S. **B)** Ocean area LCF values over the whole globe. The graphs have been modified to present similar dimensions to that presented by SBS. Line of best fit is also shown (solid grey line).

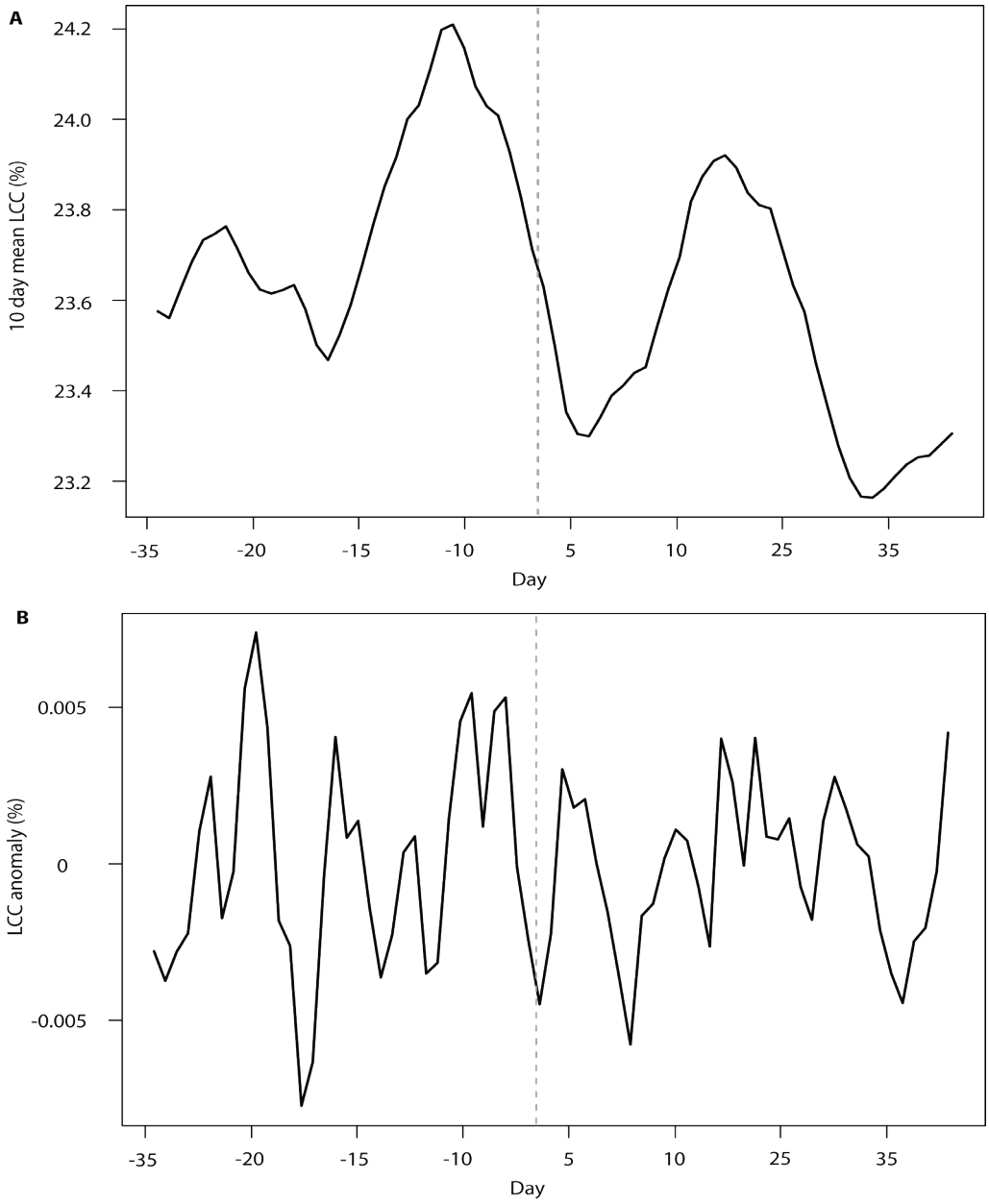

Figure 4.9 LCC long-term trends and anomalies

A) Ocean area LCC values taken over a 10-day running mean. **B)** Anomalous ocean area LCC values, calculated from subtracting the daily average ocean area LCC value from the 10-day running mean. Vertical dashed line indicates key (FD onset) date.

4.2.6 Individual LCC changes

As with the MODIS LCF, LCC values during the 5 key events are again presented on an individual basis (figure 4.16). Before these data are discussed it should again be stated that over a composite sample the individual events should not necessarily be expected to display agreement. A lack of agreement does not necessarily invalidate a composite sample; but SBS have explicitly stated that across their chosen 5 events no one observation is contributing disproportionately to the average. However, contrary to this claim, figure 4.10 shows that the patterns of individual LCC change demonstrate a widely differing response.

Relatively large decreases appear to follow the FD onset date on 3 out of 5 events (specifically, on the events of 16/07/2000, 31/10/2003 and 19/01/2005). Of those 3 events, only two (3/10/2003 and 19/01/2005) show decreases which appear to adhere to the changes proposed by SBS (specifically, these dates show an approximately 6 day decrease beginning after the FD onset event). Overall, the individual LCC changes broadly differ from the MODIS LCF data, suggesting that any apparent agreement between the two datasets is superficial. Consequently, the conclusion drawn by SBS that the ISCCP and MODIS datasets show a consistent response supporting a GCR-modulated cloud change is not supported by these findings.

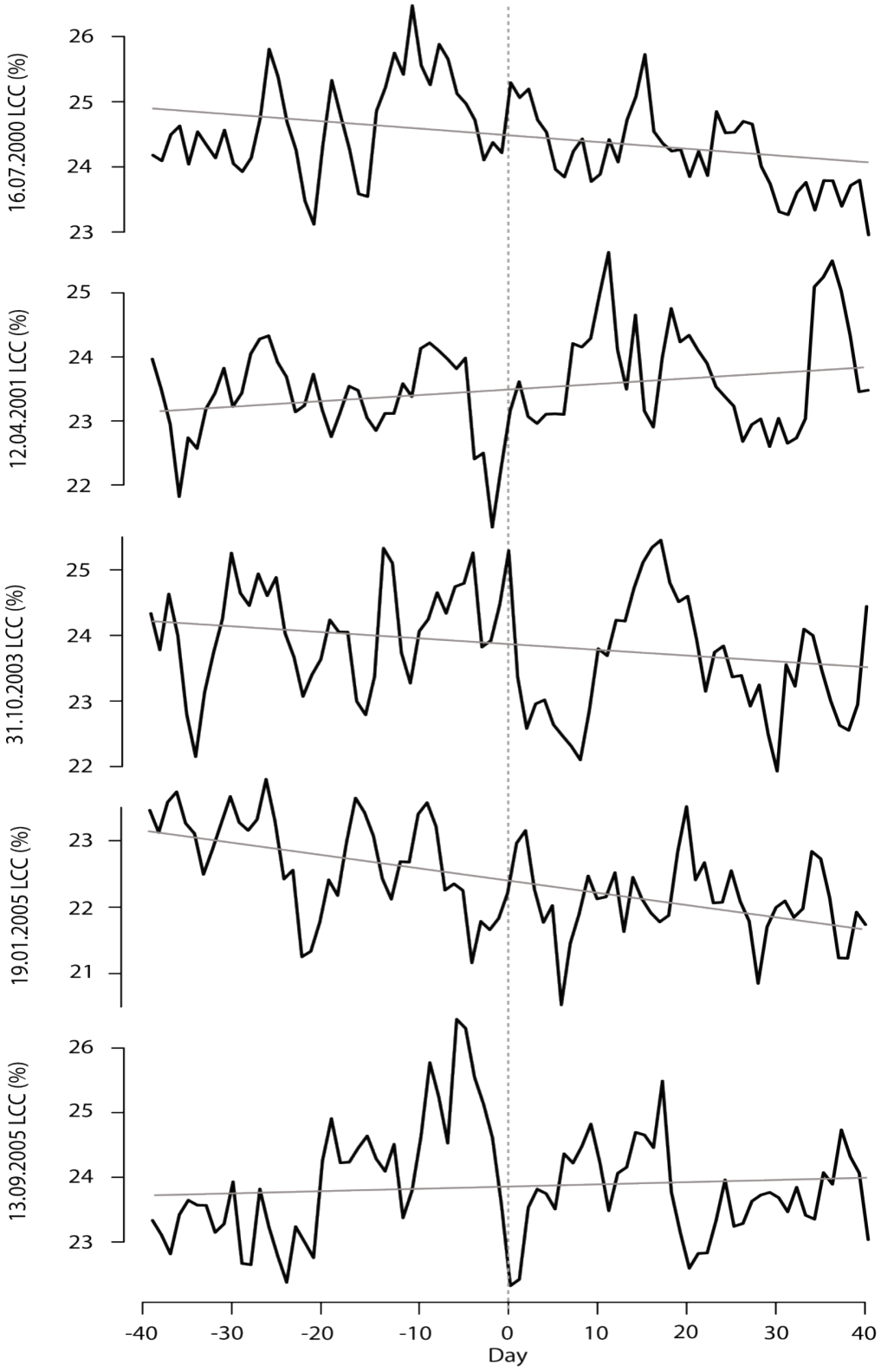

Figure 4.10 Individual daily average ocean area LCC

The individual 5 SBS events are displayed in descending chronological order (dates are stated on the *y*-axis). A line of best fit for each data series is also displayed (solid grey line). Vertical dashed line indicates key date of the composite (FD onset date).

4.2.7 Aerosol microphysics of the detected cloud anomalies

As discussed in section 2.4, the GCR flux may potentially influence cloud microphysics via either IMN or by a GEC related mechanism. SBS claim that the cloud changes they observe are the result of an IMN effect, whereby, GCR decreases alter the growth rate of ultrafine particles to CCN sizes over a period of 6 days. SBS state that approximately 5 days after the FD onset date, the amount of aerosols detected by AERONET at 340 nm and 440 nm wavelengths undergoes a rapid decline. They suggest that this decline may result specifically from either a decrease in the abundance of ultrafine aerosol particles, or an enhancement of the scavenging of smaller particles by larger aerosol particles themselves.

No other FD-based study has found indications of an IMN effect occurring after such long time delay, for example: indirect measurements of cloud changes using DF variations suggest a small but immediate (same day) response to FD events (Harrison and Stephenson, 2006). While direct measurements of changes in various atmospheric parameters (including cloud, precipitation, temperature and pressure) occurring during composites of FD events show a 1–2 day response time (Veretenenko and Pudovkin, 1995; Egrova et al, 2000; Todd and Kniveton, 2001, 2004). A review of evidence considering theoretical, observational and laboratory studies of IMN pathways suggests that a response time between 6 hours to several days is plausible (Kazil et al., 2008; Rycroft et al., 2008). No observational precedents or theoretical support can be found to verify the validity of a 6-day lag time as proposed by SBS.

Furthermore, it is difficult to reconcile the notion that IMN could be effective enough to result in a globally detectable cloud response following FD events, as it has been widely suggested the modulation of CCN concentrations in the troposphere by GCR changes may be a highly ineffective process (Pierce and Adams, 2009; Kulmala et al., 2010). It has been argued that CCN concentrations are relatively insensitive to GCR variations, as only a limited amount of ultrafine particles ever grow to CCN sizes, regardless of nucleation rate. This is because during the time it takes for ultrafine particles to grow to CCN sizes, pre-existing aerosols deplete the ambient ultrafine particle numbers through coagulation processes (Carslaw, 2009).

4.2.8 Conclusions on the findings of SBS

SBS claim to have identified a relationship between decreased in the GCR flux and decreases in both the LCF over the globe and LCC over the oceans. The authors propose that this relationship results from an ion-aerosol effect, and that it provides a strong indication that GCR variations drive climate by modulating the cloud cover over the globe. The authors even go so

far as to conclude "*so marked is the response to relatively small variations in the total ionisation, we suspect that a large fraction of Earth's clouds could be controlled by ionisation*" (Svensmark et al., 2009, pp.4). However, after re-examining the data, the claims of SBS are found to be unsupported on a number of issues:

(1) SBS suggest that the decrease in LCF and LCC is abnormally large. However, upon considering the data over an extended time period both datasets show that anomalous decreases of similar and greater magnitude are common.

(2) SBS state that the cloud changes are occurring across all 5 FD events. However, an individual analysis of both the LCF and LCC variations occurring over the key events demonstrated a poor agreement between the samples, with only one or two events contributing to the observed decrease.

(3) The most responsive event selected by SBS (19/01/2005) is actually comprised of two separate FD events and a GLE. The LCC/LCF changes occurring during this complex event to not appear to in any way reflect this situation, suggesting that the global LCC/LCF changes are insensitive to these variations.

(3) SBS claim that the MODIS and ISCCP datasets show complementary changes. However, they are comparing two distinct cloud properties at two different spatial domains (global MODIS LCF, to ocean area ISCCP LCC restricted to 40°N–40°S). Their claim of a comparable change between these datasets breaks down when ISCCP is considered over a global area (at either ocean or land covered regions).

(4) The physical mechanism suggested by SBS linking the cloud decreases to FD events is a reduction in global CCN concentration as a result of decreased IMN. However, the suggestion of a 6-day time lag between GCR decreases and CCN reductions are physically unsupported by theoretical or observational evidence.

An analysis of the ISCCP detected cloud changes occurring during events selected by SBS has also been carried out by Calogovic et al. (2010). They performed a detailed correlation analysis between atmospheric ionisation changes and cloud changes at 3 different altitudes (for high >6.5 km, middle 3.2–6.5 km and low clouds <3.2 km) at 3 hour time intervals with a 0 to 10 day lag time. From this study, the authors concluded that: (1) there exists no significant global (ISCCP) cloud/ionisation correlation during the dates selected by SBS, (2) nor did they find any regional correlation to atmospheric ionisation variations regardless of the time lag and, (3) both cloud changes showed no statistically significant difference before or after the FD events (Calogovic et al., 2010). These conclusions confirm the findings presented here, strongly indicating that SBS did not detect a globally significant cloud response related to FD events.

4.3 Results of past FD studies

Generally, FD-based studies have demonstrated widely conflicting results: some have found indications of significant decreases in cloud at high latitudes (Pudovkin and Vertenenko, 1995; Todd and Kniveton, 2001, 2004; Solovyev and Kozlov, 2009; Laken and Kniveton, 2010), while others have failed to identify any significant cloud changes (Pallé and Butler, 2001; Lam and Rodger, 2002; Kristjánsson et al., 2008), or have even found indications of significant increases in cloud (Wang et al., 2006). There are several possible explanations for the lack of agreement between FD studies:

(1) FD events may be unrelated to cloud cover changes.

(2) FD events may merely be a proxy indicator for periods when other solar parameters (such as the IMF) are influencing cloud cover.

(3) FD events may only poorly define periods when GCRs are influencing cloud cover and as a result, composites based upon FD events may be producing relatively weak observations of a GCR–cloud relationship.

(4) If a GCR–cloud relationship is constrained by precursor conditions (e.g. if certain conditions are needed for a GCR-related mechanism to operate) then a small composite sample based on quasi-random (FD) events may be unlikely to identify a significant relationship (as it has no capacity to account for such conditions).

With respect to the third possibility, there has been some recent effort to determine the usefulness of FD onset dates as a basis for composite analysis studies. Using satellite measurements of cloud, Todd and Kniveton (2004) (hereafter TK04) demonstrated the occurrence of statistically significant zonal mean cloud decreases over high tropospheric (10–180 mb) levels during austral winter over parts of the Antarctic plateau; these changes were observed immediately following the onset of FD events. Troshichev et al. (2008) reassessed several of the dates selected by TK04 and suggested that FD onset dates were only poorly defined indicators of GCR change, arguing that between various studies onset dates can differ by as much as 5 days. After realigning the key dates of their composite to reflect the maximal GCR decrease rather than the FD onset date, they observed increases in cloud cover over regions of Antarctica (although it should be noted that these results cover only a limited period and were based on visual assessments of cloud from several Antarctic stations). The results hint that it may be more appropriate to consider the date of maximal decrease in the GCR flux over the FD period rather than the FD onset date itself. By isolating the maximal GCR decrease occurring over past FD events it should potentially increase the detectibly of a GCR–cloud signal (if one is present).

4.3.1 FD composite construction

In order to construct an adjusted composite, 47 FD onset dates (occurring between 1988 and 2006) were sourced from two past studies (Todd and Kniveton, 2004; Kristjánsson et al., 2008). The dates were then adjusted to align the key date of the composite to the date of maximal rate of GCR decrease occurring in closest proximity to the FD onset date. During the FD analysis, measurements of GCR variations are taken from the McMurdo neutron monitor data in order to provide a precise indication of variations in the GCR flux over Antarctica. It is to this dataset that the maximal GCR decrease alignment is performed (it is important to note that neutron data from varying sites can demonstrate a difference in the maximal decrease key date due to the differing geomagnetic latitudes of the neutron monitors).

Similar to the methodology of TK04 and Kristjánsson et al. (2008), any key date which falls within a three day (±) range of a SEP event is excluded from the composite. This is necessary as it has been speculated that during SEP events, increases in atmospheric ionisation may act to oppose any decreases in atmospheric ionisation resulting from a reduced GCR flux over high latitude regions (Pudovkin and Veretenenko, 1995). Data regarding the timing of SEP event were obtained from the NOAA space environment services centres web page on SEP events affecting the Earth environment (Kristjánsson et al., 2008). This treatment resulted in the exclusion of 15 SEP events coincident dates from the composite, leaving a sample size of n = 32; the full list of dates (including the dates sourced from original studies) are displayed in table 4.1.

Event	Original	Adjusted	Event	Original	Adjusted
1	20/02/1988	21/02/1988	28	29/11/2000	29/11/2000**
2	20/07/1988	18/07/1988	29	12/04/2001	12/04/2001**
3	11/02/1989	13/02/1989	30	29/04/2001	29/04/2001**
4	19/08/1989	20/08/1989	31	28/08/2001	28/08/2001
5	28/08/1989	28/08/1989	32	26/09/2001	26/09/2001**
6	18/09/1989	19/09/1989	33	25/11/2001	25/11/2001**
7	17/05/1990	20/05/1990	34	30/07/2002	30/07/2002
8	12/03/1991	10/03/1991	35	19/11/2002	19/11/2002
9	24/04/1991	26/04/1991	36	31/05/2003	31/05/2003**
10	18/08/1991	19/08/1991	37	23/06/2003	23/06/2003
11	07/11/1991	29/10/1991**	38	31/10/2003	31/10/2003**
12	25/02/1992	27/02/1992	39	24/11/2003	18/11/2003**
13	08/09/1992	10/09/1992	40	10/01/2004	11/01/2004
14	19/02/1993	24/02/1993	41	25/01/2004	22/01/2004
15	22/10/1993	26/10/1993	42	27/07/2004	27/07/2004**
16	16/04/1994	17/04/1994	43	10/11/2004	10/11/2004**
17	17/06/1994	20/06/1994	44	19/01/2005	19/01/2005**
18	03/04/1998	09/04/1998	45	16/05/2005	09/05/2005
19	12/01/1999	14/01/1999	46	17/07/2005	17/07/2005**
20	07/10/1999	15/10/1999	47	13/09/2005	11/09/2005**
21	06/12/1999	03/12/1999			
22	04/02/2000	07/02/2000			
23	01/05/2000	03/05/2000			
24	20/05/2000	24/05/2000			
25	09/07/2000	04/07/2000			
26	16/07/2000	16/07/2000**			
27	18/09/2000	18/09/2000			

Table 4.1 Original and adjusted dates

A list of the original dates sourced from TK04 and Kristjánsson et al. (2008) and the adjusted dates (aligned to maximal GCR decrease). SEP event coincident dates are indicated by markers (**).

4.3.2 FD composite results: GCR variations, F10.7 and space weather

A comparison between changes in the mean rate of GCR flux during the original (FD onset) dates (of TK04 and Kristjánsson et al., 2008) and the adjusted FD dates initially suggests that a similar pattern and magnitude of GCR change is found across both samples (figure 4.11). Although the sample means appear fairly similar, an examination of the GCR changes occurring over the individual events shows that the original sample demonstrates a considerable range of variability not present in the adjusted sample (figure 4.12). This is further illustrated by box plots, which indicate that the adjusted FD sample has isolated a far more statistically significant and confined GCR decrease than was obtained by the use of FD onset dates (figure 4.13). This suggests that composites based around FD onset events may have not properly isolated a GCR decrease associated with FD events and may have consequently failed to capture an accurate representation of GCR related cloud changes during FD periods.

With regards to solar activity variations occurring during the adjusted FD composite, no statistically significant change in the rate of F10.7 or UV variations are observed (figure 4.14). However, an increase in F10.7 is observed around day -3 of the sample (figure 4.14A) and a non decrease in UV activity is seen on the key date (figure 4.14B).

Large variations in the IMF B_y component are identified during the composite period. The B_y component undergoes a large negative (westwards) increase around day -7, followed by a large positive (eastwards) increase which reaches a statistically significant peak on day -3, before again undergoing negative changes which peak on day 1. A less pronounced, but comparable sequence of variations is also evident in the B_z component (figure 4.15). This pattern of change indicates that large disturbances in the IMF are occurring; such changes likely signify the passage of coronal mass ejections which are producing the FD events. It should be noted that the IMF, UV and F10.7 datasets have a limited coverage over the sample period; restricting the confidence that can be placed in these results (coverage of the datasets is detailed in table 4.2).

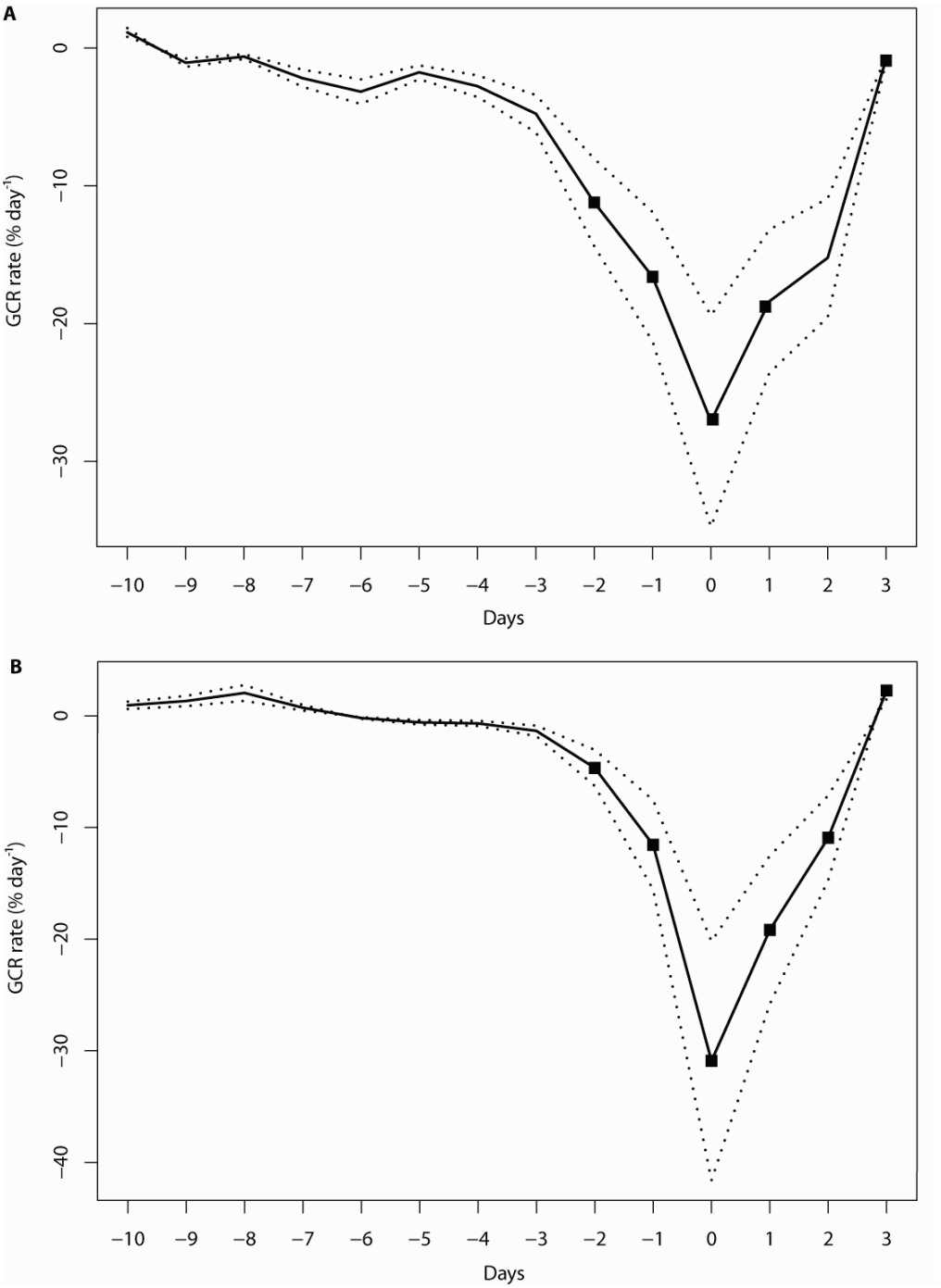

Figure 4.11 Original and adjusted FD samples mean rate of GCR flux

The mean daily neutron count measured at McMurdo over the **A)** original FD sample and, **B)** adjusted FD sample. The 0.95 confidence interval is displayed (dotted line), days of statistically significant change are indicated by markers. GCR variations are normalised against the peak to peak variations of the 11-year solar cycle.

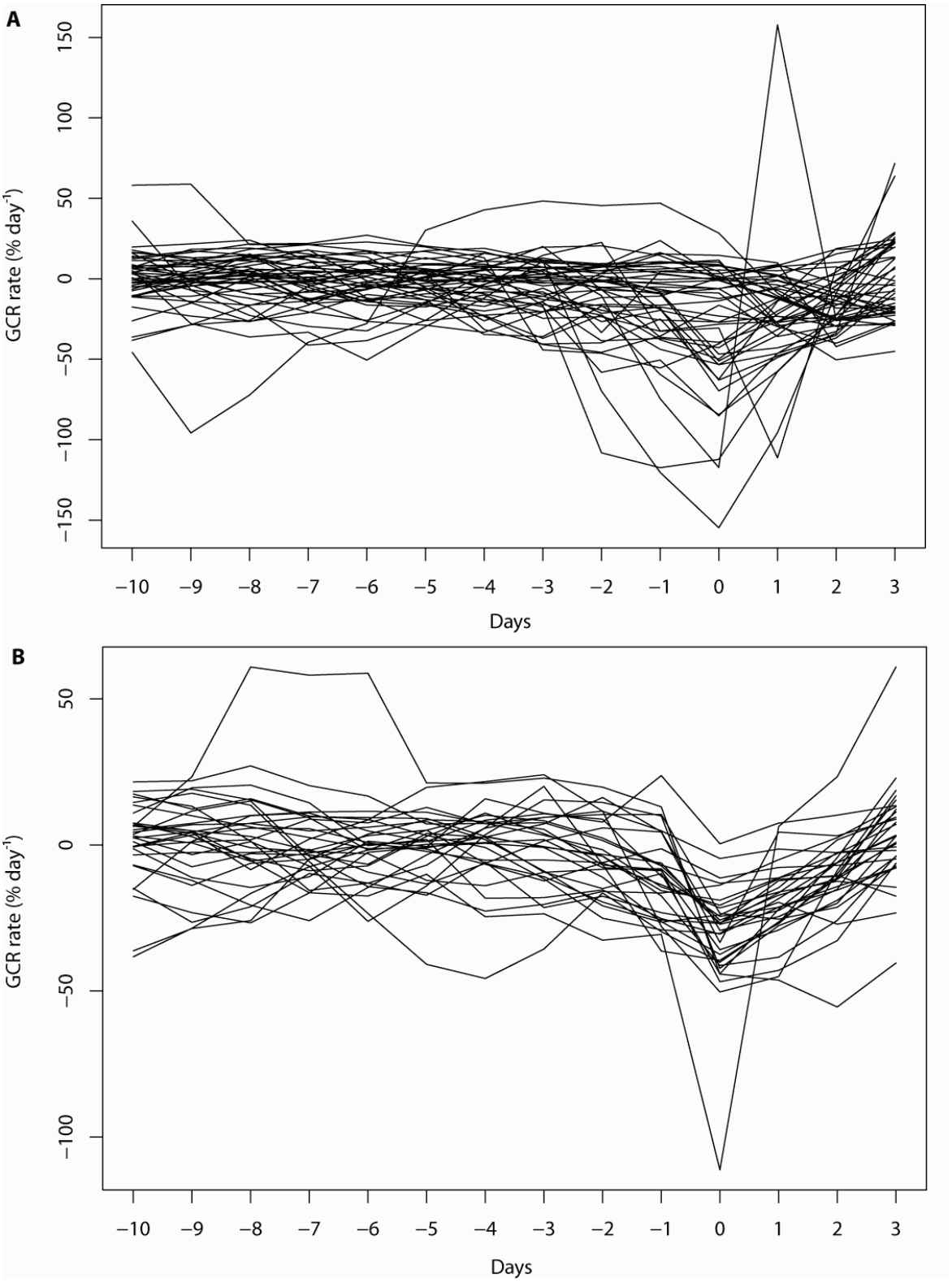

Figure 4.12 Individual rate of GCR flux

The average rate of GCR flux occurring during each individual event in **A)** the original (FD onset) sample and, **B)** the adjusted FD sample. Based on data from Mucmurdo neutron monitor. GCR variations are normalised against the peak to peak variations in the 11-year solar cycle.

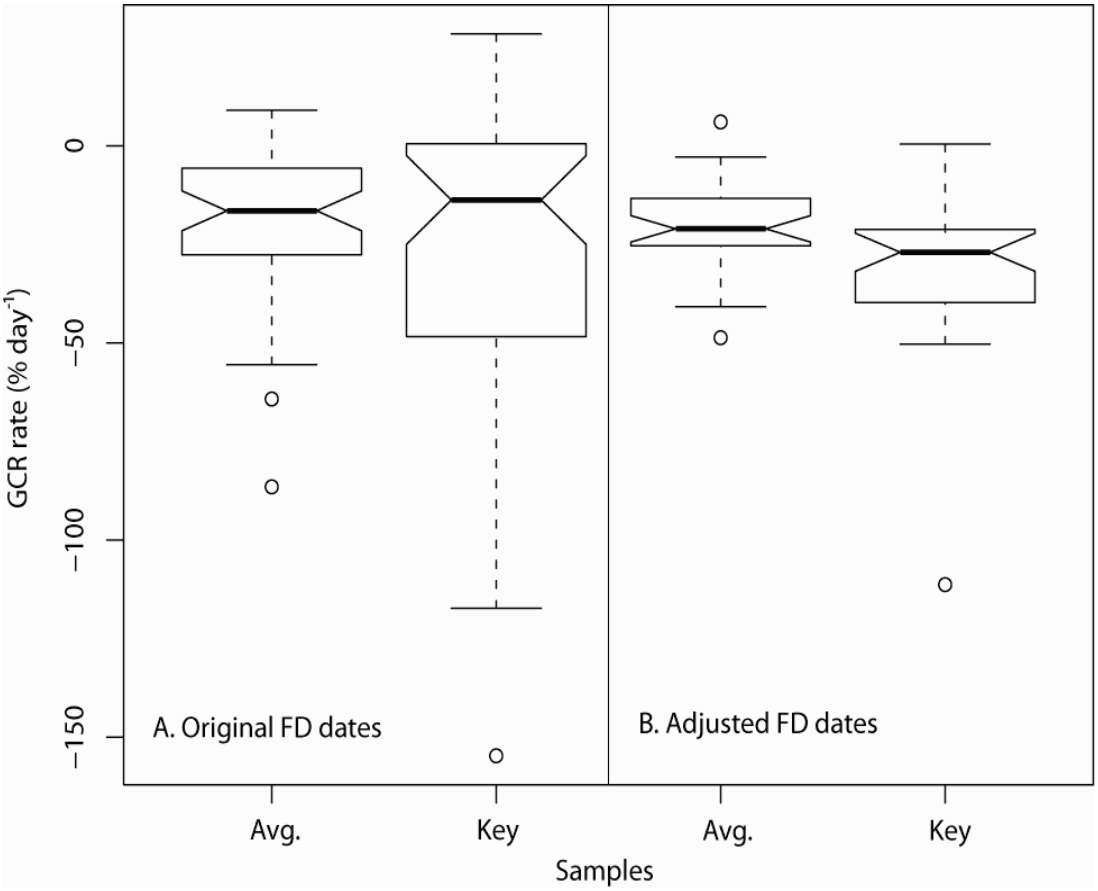

Figure 4.13 Original and adjusted GCR sample distribution

Changes in the sample distribution for the rate of GCR flux, between the key date and its relative averaging period (comprising the average rate of GCR flux on day -5, -4 and -3). **A)** Original (FD onset) sample and, **B)** adjusted FD sample. GCR variations are normalised against the peak to peak variations in the 11-year solar cycle.

Parameter	Data coverage (%)
IMF B_y	23
IMF B_z	47
UV	59
F10.7	66

Table 4.2 Data coverage during the adjusted FD sample

IMF, UV, and F10.7 data coverage over the adjusted FD composite, showing the number of events for which data are available (as a percentage of the sample) (only events for which there is complete coverage over the composite period (-15 to +3 days) are used in the analysis).

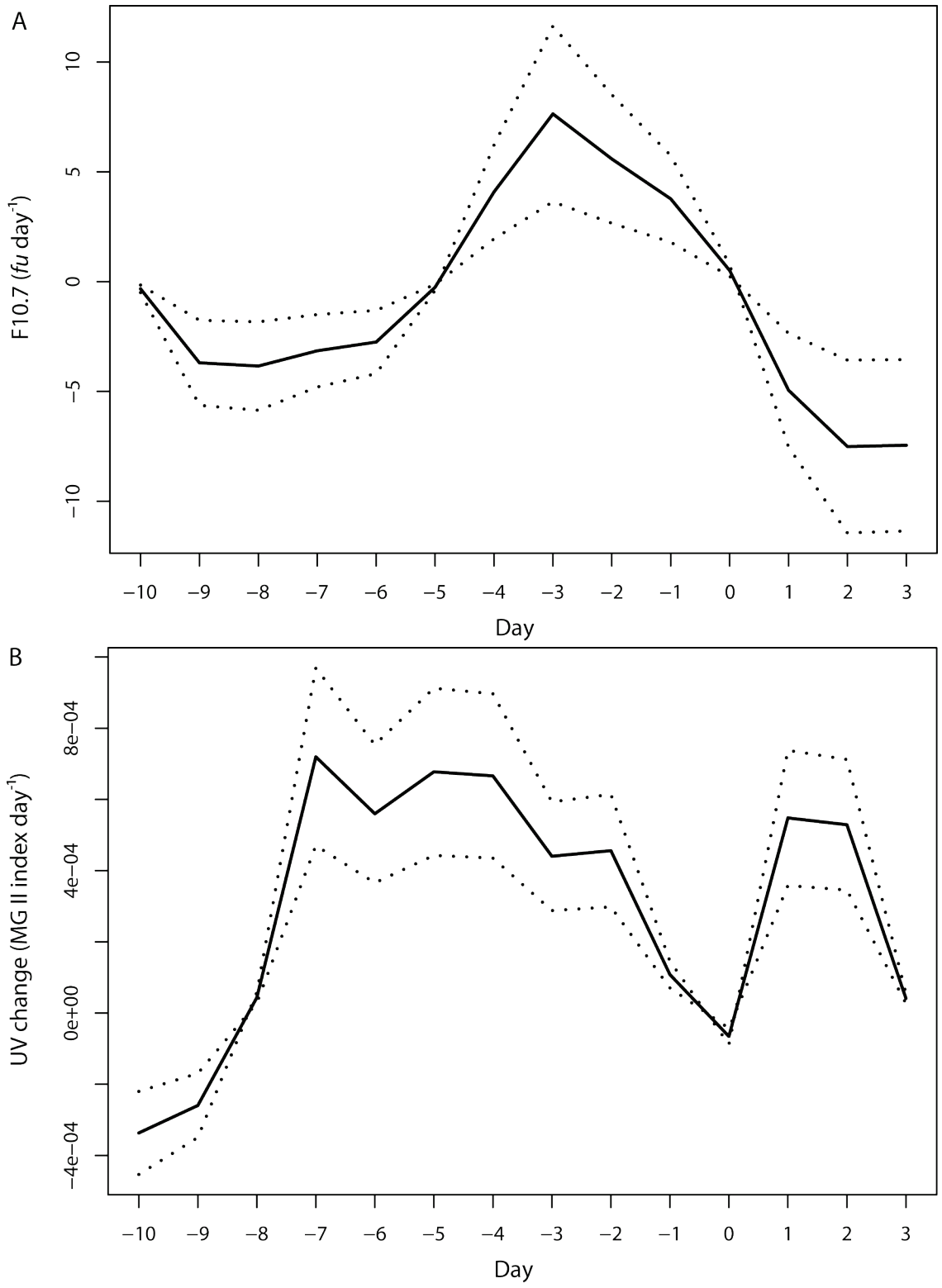

Figure 4.14 Adjusted FD sample solar activity changes

Variations in the mean rate of **A)** F10.7 (10.7 cm 2800 MHz radio flux) and, **B)** UV (MG II index) variations. The 0.95 confidence interval is displayed (dotted line).

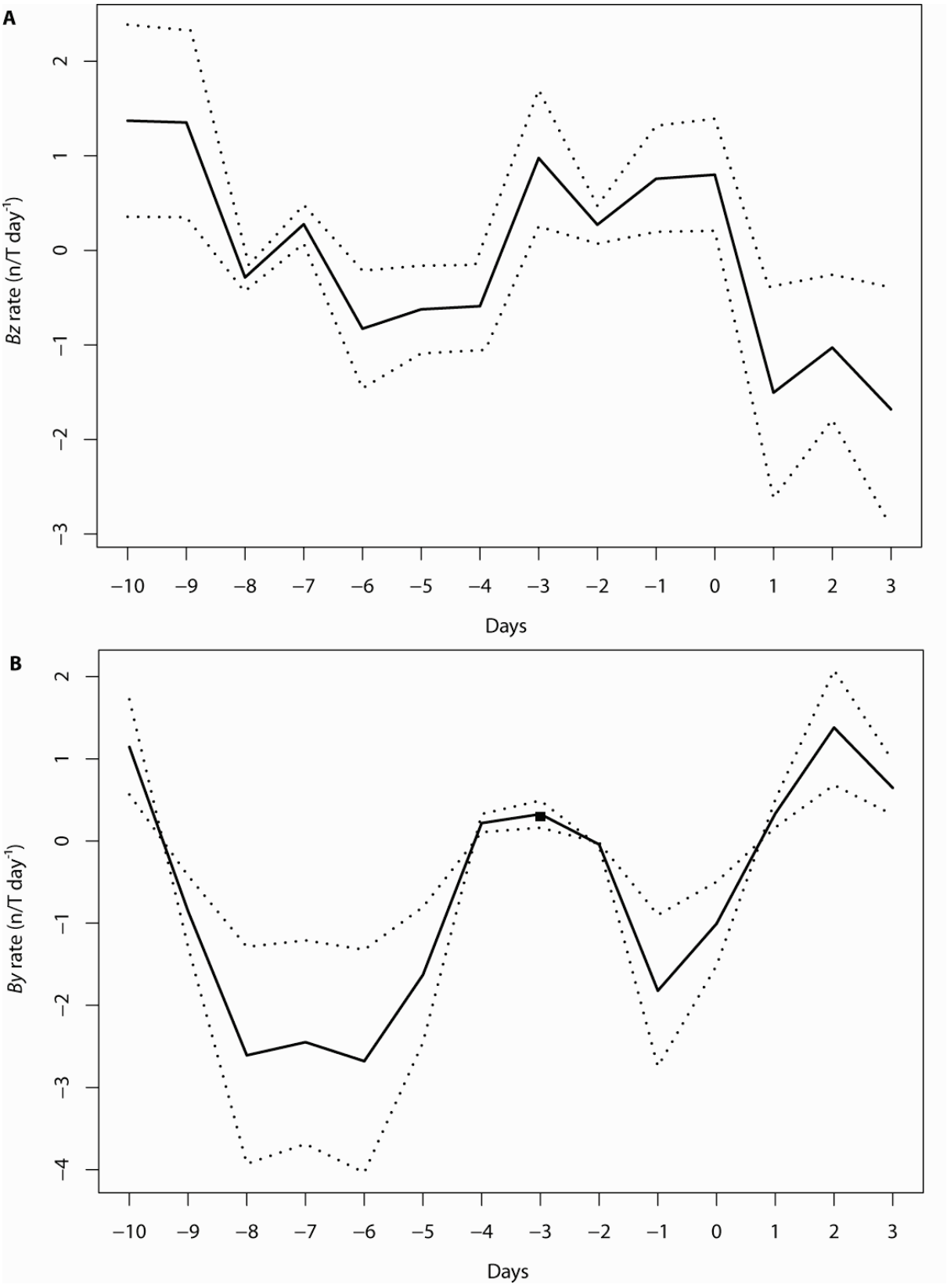

Figure 4.15 Adjusted FD sample solar wind changes

Variations in the average rate of IMF **A)** B_z and **B)** B_y flux occurring over the adjusted FD composite. Statistically significant variations are indicated with markers. Dashed line indicates the 0.95 level confidence interval.

4.3.3 Cloud anomalies observed with adjusted FD composite

Anomalous variations in the rate of cloud cover change are presented over a variety of spatio-temporal domains to identify any statistically significant anomalies that may be occurring over the FD period. A plot of globally-averaged cloud changes occurring between 10 and 1,000 mb over the composite period shows statistically significant decreases in the rate of cloud change (of around -0.8 %) develop after day -3 in the upper troposphere; this decrease persists until the key date of the composite (figure 4.16). In addition, several small significant anomalies are also observed throughout the period.

Latitudinally-averaged cloud cover anomalies occurring between 10 and 180mb over the sample show that the cloud changes are limited to high southern latitude regions and occur most intensely around day -2 of the composite period (figure 4.17). A pressure level/latitude profile of the cloud anomalies on day -2 shows that statistically significant anomalous decreases (of around -3.6 %) are located in the lower stratosphere/upper troposphere region between 70°S and 90°S. A smaller area of statistically significant cloud decrease (of around -1 %) is also observed at mid-tropospheric levels around 50°S (figure 4.18). An analysis of anomalous rates of cloud changes between 10–180 mb, on day -2 of the composite over a latitude/longitude grid, shows the presence of intense regions of locally significant cloud decreases (of up to -16 %) over areas of the Antarctic plateau (figure 4.19). Although these changes are locally intense, their spatial extent is highly limited and they are not found to be field significant.

Similar results have been found as early as 1960's, when Schuurman (1965) and also Schuurman and Oort (1969) demonstrated a detectable influence of SEPs on high latitude pressure changes immediately following solar flares. SEPs arrive at Earth's atmosphere within hours of a flare event, and their effects last for approximately 1 day, whereas IMF disturbances resulting from the same flare activity arrive 3–4 days later (and produces the onset of FD events). Consequently, SEP events may be a good candidate for perturbing Earth's atmosphere at high geomagnetic latitudes prior to FD events producing the observed pressure anomalies.

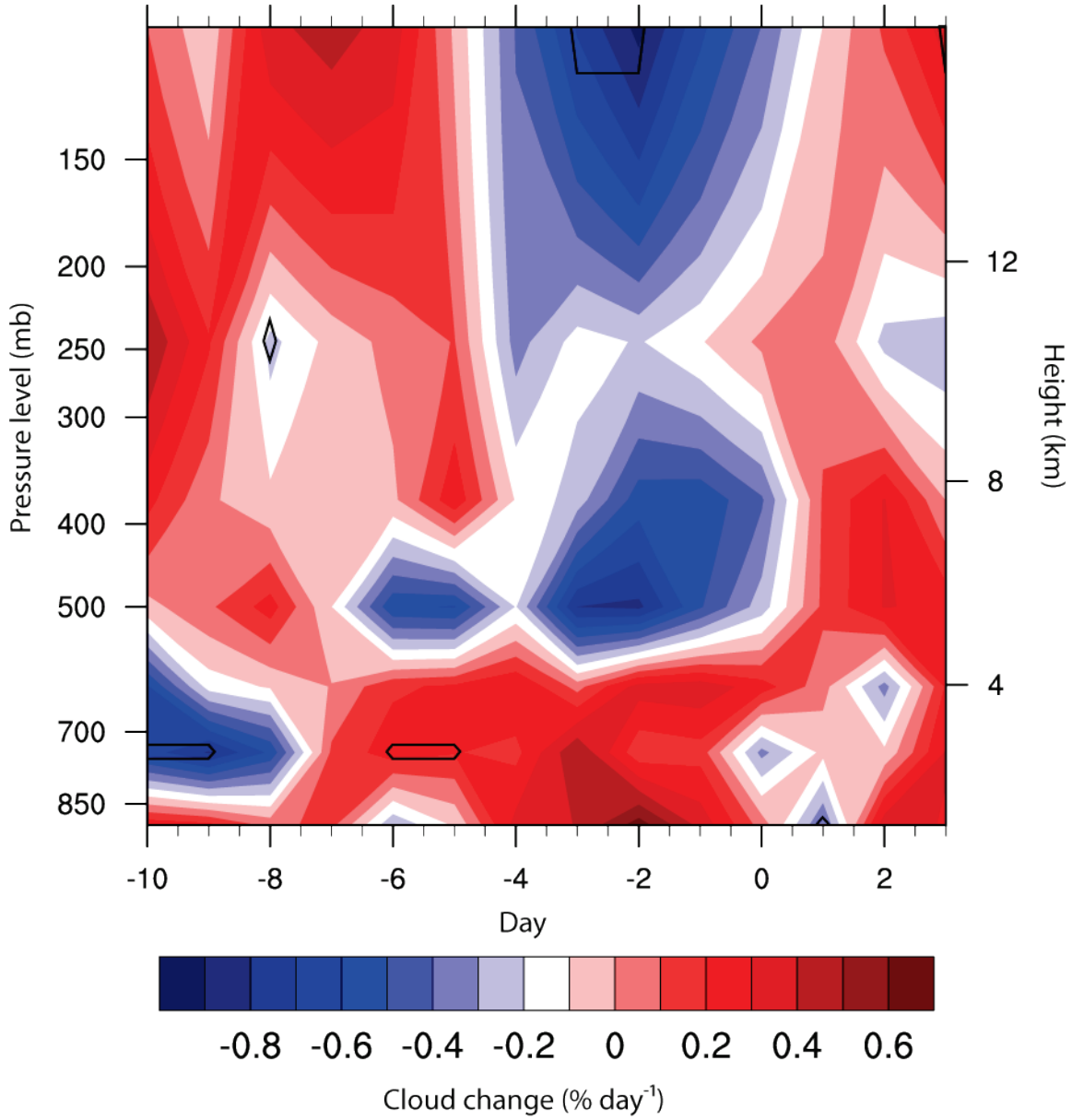

Figure 4.16 Anomalous cloud changes during the adjusted FD sample

Globally-averaged cloud anomalies occurring at pressure levels between 10 and 1,000 mb during the adjusted FD sample. Regions of statistically significant change (above the 0.95 level) are indicated by solid contours.

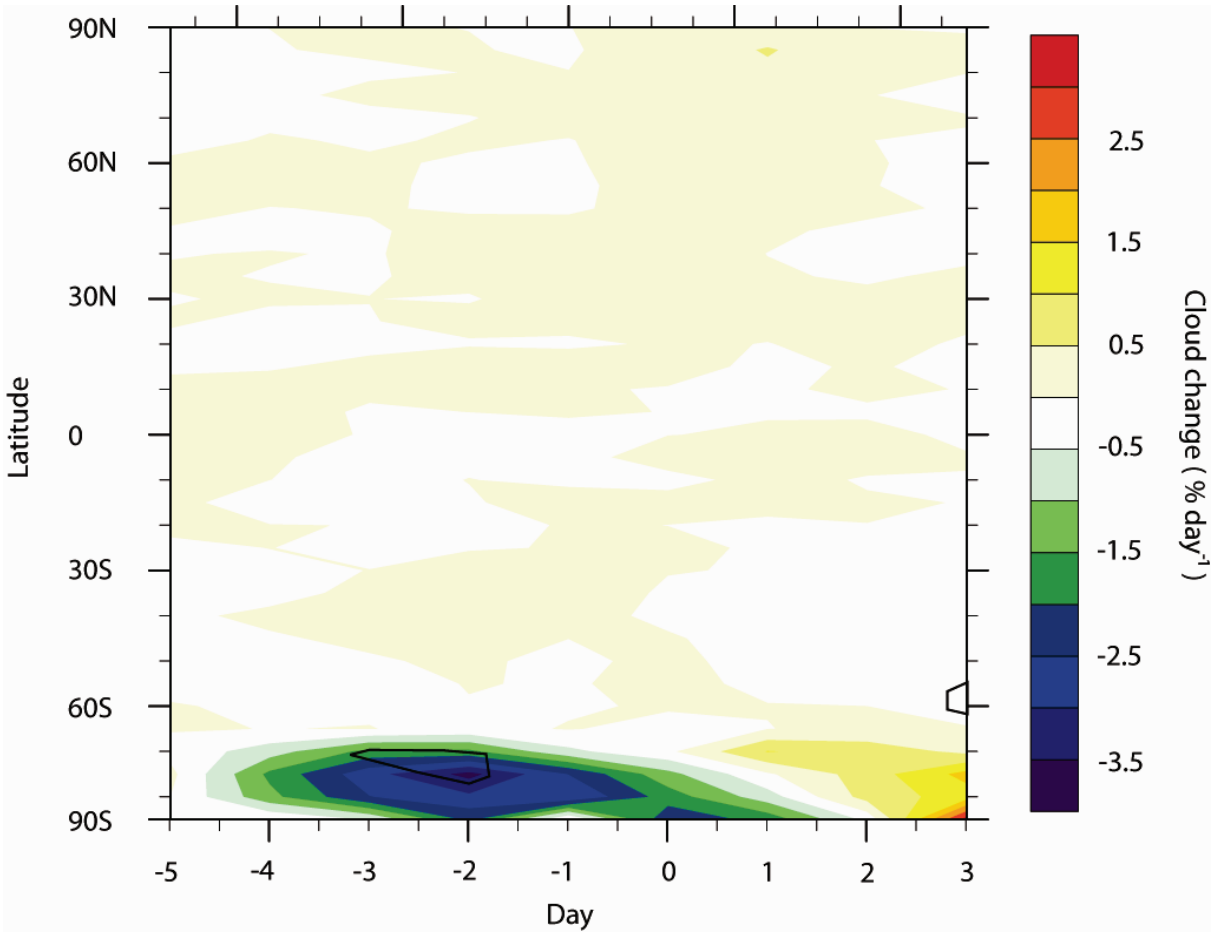

Figure 4.17 Latitude/time adjusted FD sample cloud change

A plot of 10–180 mb, 5° latitudinal mean, anomalous rates of cloud cover change occurring over the adjusted FD composite. Regions of statistically significant change (above the 0.95 level) are indicated by solid contours.

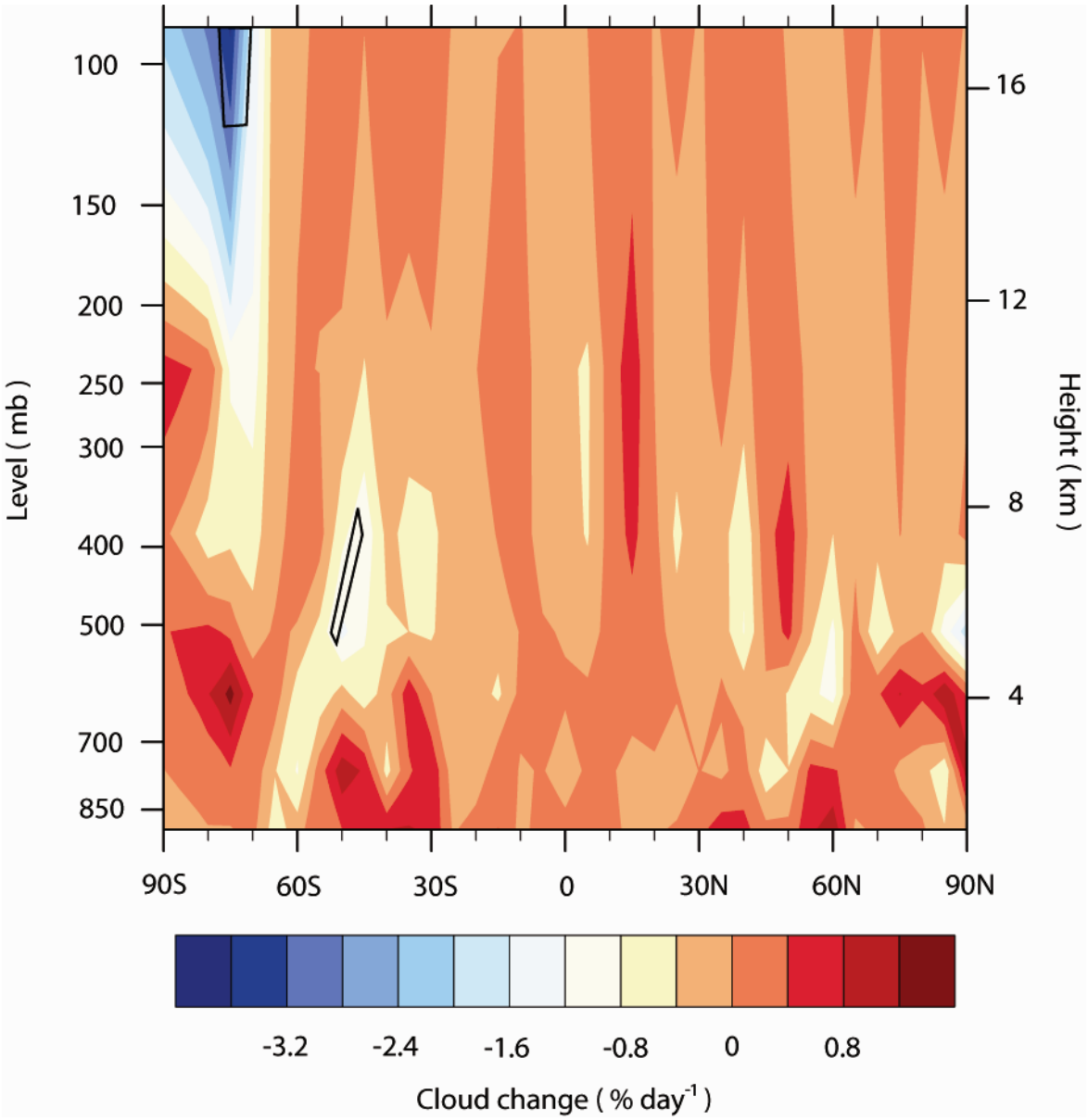

Figure 4.18 Tropospheric profile of adjusted FD sample cloud anomalies

A plot of 5° latitudinal mean, anomalous cloud changes (occurring from 10–1,000 mb) during day -2 of the adjusted FD sample. Regions of statistically significant change (above the 0.95 level) are indicated by solid contours.

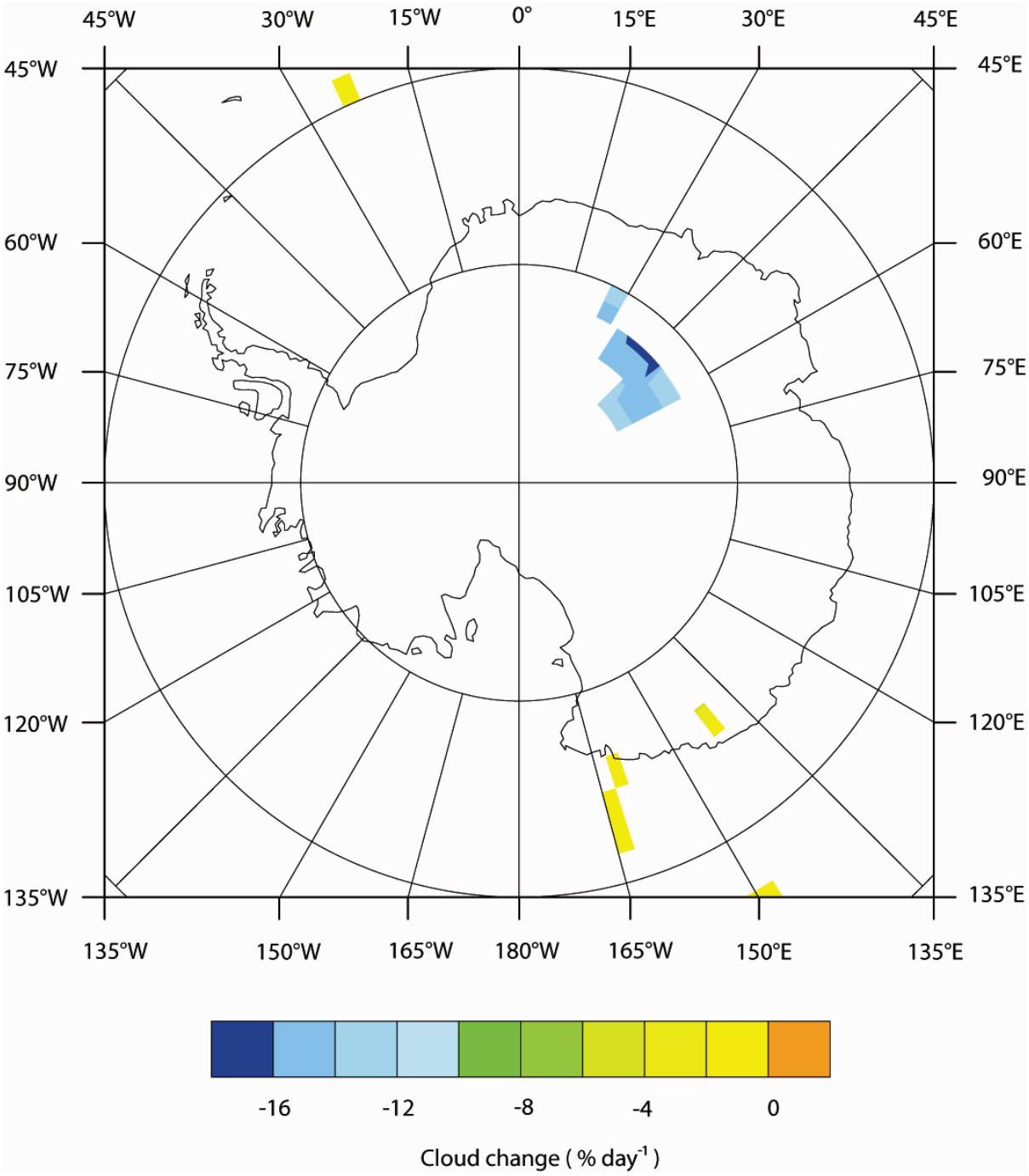

Figure 4.19 Adjusted FD sample Antarctic anomalous cloud change

Locally statistically significant cloud anomalies, occurring at 10–180 mb during day -2 of the adjusted FD sample over the South Pole.

4.3.4 Analysis of FD related cloud changes

The adjusted FD sample has shown indications of an anomalous decrease in the rate of cloud change over the highest ISCCP monitoring level (10–180 mb) over Antarctica. However, these changes are observed to occur two days in advance of the maximal GCR decrease. These findings are broadly similar to the results of TK04, who demonstrate comparable (yet more widespread) anomalies over the Antarctic region at identical pressure levels. The changes identified by TK04 occurred several days after the onset of FD events. Although the timing is different, the similar nature of the anomalies suggests that these may be related cloud changes; the timing conflict may simply be a consequence of the date adjustment applied. Since the cloud changes identified in this work occur during a more isolated GCR signal than those of TK04, the fact that the size and area of the cloud anomalies identified by this work are diminished and occur before the maximal GCR decreases implies that the anomalies may be unrelated to GCR variations. It should be stressed that the anomalies over the Antarctic have been focused upon simply because no other cloud changes suggested the occurrence of any statistically significant anomalies which may be linked to the FD period. In addition, it is known that satellite cloud retrievals are particular problematic for high level clouds over high latitude regions (Rossow and Schiffer, 1999). This issue is of particular relevance to cloud changes detected over the Antarctic plateau (TK04) and consequently, the confidence that can be placed in these results is relatively low.

Troshichev et al. (2008) suggest that cloud cover changes associated with FD events may be causally related to variations in the IMF B_z (north-south) component. The B_z was found to undergo a positive increase around the key date of the composite (figure 4.15); this change suggests a decreased coupling between the IMF and Earth's magnetosphere, which may theoretically result in a decrease in high altitude ionisation and a consequent decrease in cloud cover. However, the B_z variations were not found to be statistically significant above the 0.95 critical level. Furthermore anomalous cloud decreases were found to begin around day -3; during this time, B_z variations of an opposite sign were occurring. This implies B_z changes cannot be responsible for the observed anomalies. Variations in the IMF B_y (east-west) component may also potentially influence cloud changes over the sample, as changes in the B_y are associated with variations in the ionospheric potential at magnetic latitudes greater than 80° (Burns et al., 2007). However, similar to B_z, the B_y component demonstrates an oscillatory behaviour during the anomalous cloud changes, implying no relationship to the cloud decreases. However, it must be noted that the IMF data coverage is limited and consequently any conclusions drawn from this analysis are subject to uncertainty.

4.4 Verifying observed FD related cloud variations

To further test for the presence of a relationship between FD events and cloud changes a secondary composite sample was constructed. This new composite is based around the largest decreases in the rate of GCR flux measured by both Mcmurdo and South Pole neutron monitors (located in Antarctica). This composite is designed to isolate the largest, daily timescale, regional decreases, in atmospheric ionisation over the Antarctic continent. The previously utilised events in the adjusted FD sample were based on neutron monitor decreases detected at Mt. Washington; this neutron monitor is situated at lower latitudes than the Antarctic neutron monitor sites and consequently may be relatively insensitive to lower energy GCR changes experienced over high latitude regions.

Any anomalous cloud changes detected over the new composite will be compared to the previously identified cloud anomalies to determine if similar patterns of change are observed. If similar GCR related processes are influential over both samples then it is logical to assume that similar cloud anomalies should be observed: the presence or absence of such anomalies may provide an indication of GCRs relationship to cloud cover (if any exists).

4.4.1 Constructing a composite of the largest Antarctic GCR decreases

The secondary composite sample (hereafter referred to as the 'Antarctic GCR decrease' (AGD) sample) is constructed from the largest 5 % decreases in the rate of GCR flux measured at Mcmurdo neutron monitor between 1988 and 2006. The events were filtered to remove any dates from the sample which reoccurred within the composite period and any events which occurred within 3 days (±) of a SEP event. In addition, only key dates which were also coincident with the largest 5 % decreases in neutron count rate at the South Pole neutron monitor (90.0°S, 0.0°E) were considered; this ensures that the GCR decrease are widespread over the Antarctic region rather than merely being a localised phenomenon. This treatment results in the generation of a sample of 28 observations (events are listed in table 4.3). Only 6 out of the 28 AGD events were found to be coincident with the adjusted FD events, verifying the assertion made in section 4.4 that largest Antarctic GCR decreases were not necessarily isolated by observing FD events recorded at Mt. Washington neutron monitor.

Event	AGD sample	Event	AGD sample
1	13/02/1989	15	18/02/1999
2	30/12/1989	16	20/06/1999
3	15/03/1991	17	14/12/1999
4	27/04/1991	18	13/02/2000
5	19/08/1991	19	24/05/2000
6	29/01/1992	20	18/09/2000
7	21/02/1992	21	30/10/2000
8	13/07/1992	22	18/12/2001
9	23/08/1992	23	21/10/2002
10	09/09/1992	24	19/11/2002
11	09/10/1992	25	11/04/2003
12	05/11/1992	26	10/01/2004
13	12/04/1997	27	28/12/2004
14	25/10/1997	28	09/05/2005

Table 4.3 List of AGD sample key dates

Dates during which the largest 5 % decreases in the rate of GCR flux at Mcmurdo and South Pole neutron monitors occurred.

4.4.2 AGD sample: GCR, F10.7, UV and IMF variations

The GCR changes occurring over the AGD sample are shown in figure 4.20. These changes show an intense, statistically significant and highly isolated decrease (of approximately -33 %) occurring centred on the key date of the composite. During this period, no statistically significant variations in the IMF B_z or B_y, UV or F10.7 are observed (figure 4.21–4.22). However, sharp decreases centred on the key date, in both the UV and IMF B_y parameters are observed. It must be noted that to a lack of continuous measurements data coverage for the IMF, F10.7 and UV parameters was incomplete over the AGD sample, exact coverage is detailed in table 4.4.

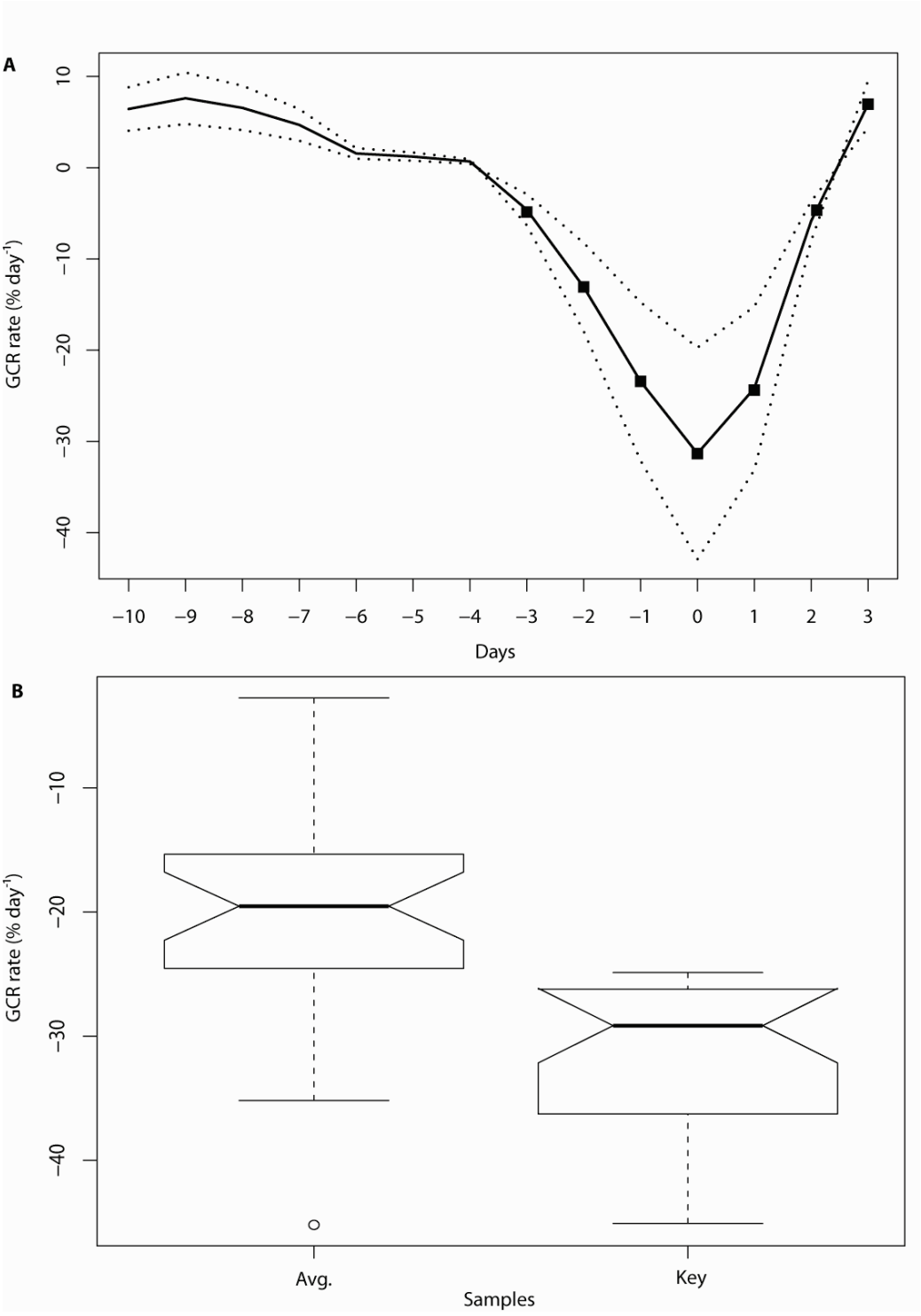

Figure 4.20 Rate of GCR flux during AGD sample

Rate of GCR flux recorded at Mucmurdo, **A**) mean GCR flux with 0.95 level confidence interval displayed (dotted line). Statistically significant changes indicated by markers. **B)** Notched box plots showing sample distribution of key date and relative averaging period (average GCR rate of day -5, -4 and -3). GCR variations are normalised against the peak to peak changes over the 11-year solar cycle.

Parameter	Data coverage (%)
IMF B_y	83
IMF B_z	84
UV	88
F10.7	68

Table 4.4 Data coverage during AGD sample

Data coverage of the: IMF, UV, and F10.7 datasets over the AGD composite. Only sample events with complete coverage over the composite (-15 to 3 days) are used in the sample.

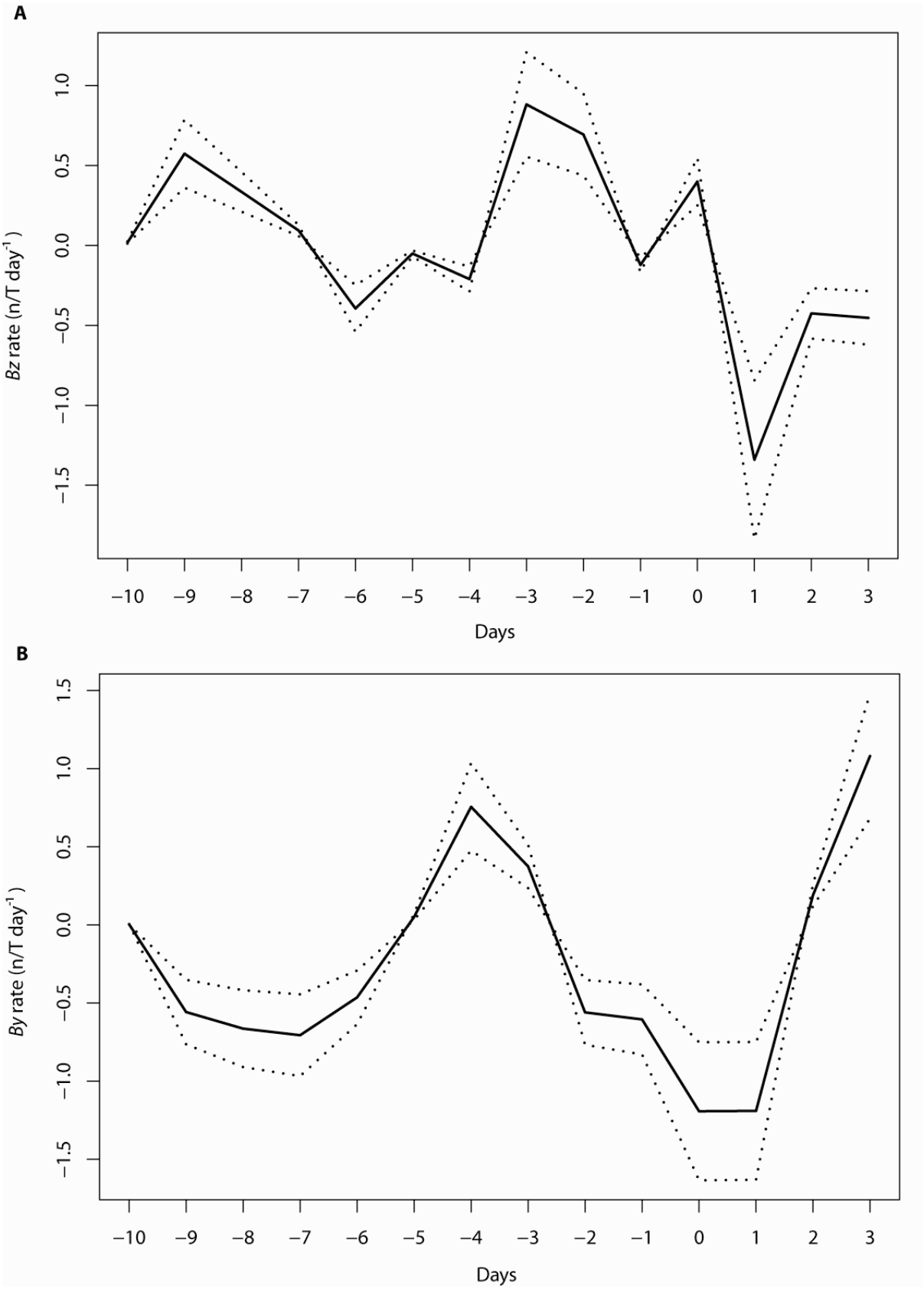

Figure 4.21 AGD sample solar wind changes

Variations in the mean rate of IMF **A)** B_z and, **B)** B_y flux occurring over the AGD composite. Dotted line indicates the 0.95 level confidence interval.

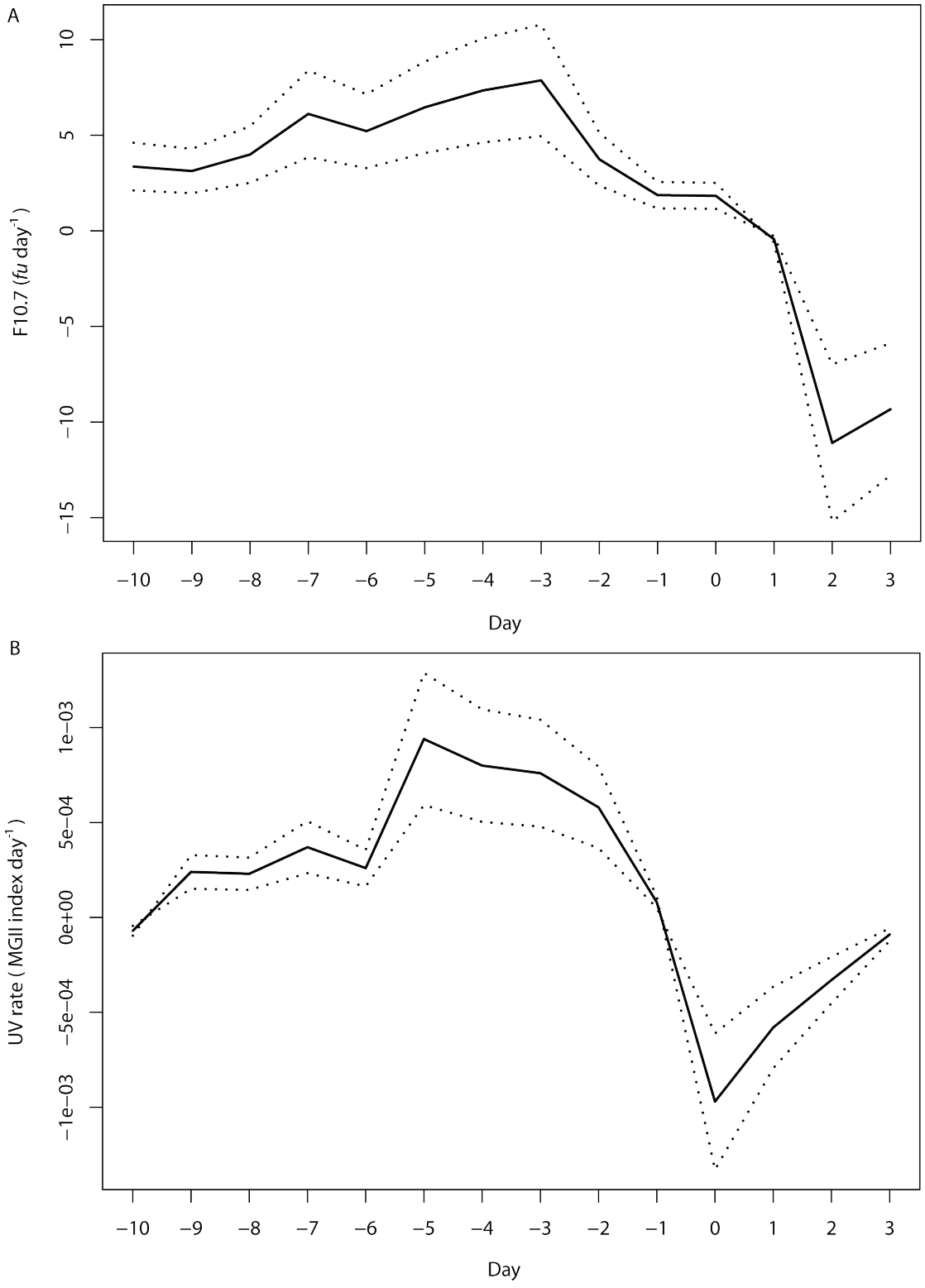

Figure 4.22 AGD sample solar activity changes

Variations in the mean rate of **A)** F10.7 (10.7 cm 2800 MHz radio flux) and, **B)** UV (MG II index) variations. The 0.95 confidence interval is displayed (dotted line).

4.4.3 Analysis of AGD sample cloud change results

Cloud changes occurring between 10 and 180 mb during the AGD sample show that, similar to the adjusted FD sample, anomalous decreases in the rate of cloud change occur over high southern latitudes around day -4 and persist until day 1; however, unlike the adjusted FD sample, these anomalies are not found to be statistically significant above the 0.95 critical level (figure 4.23). A pixel by pixel analysis of anomalous cloud changes occurring at high tropospheric/low stratospheric levels (between 10 and 180 mb) identifies several locally significant cloud decrease (of around -10 %) over a limited regions of the Antarctic plateau on day -2 (figure 4.24). These anomalies do not show field significance at the 0.95 critical level. Although the cloud changes appear to show anomalies which appear comparable to the adjusted FD sample (which may hint at the action of a common process), the lack of any reliable statistical significance over the samples leads to the conclusion that FD-based composites do not provide good evidence of a GCR–cloud link.

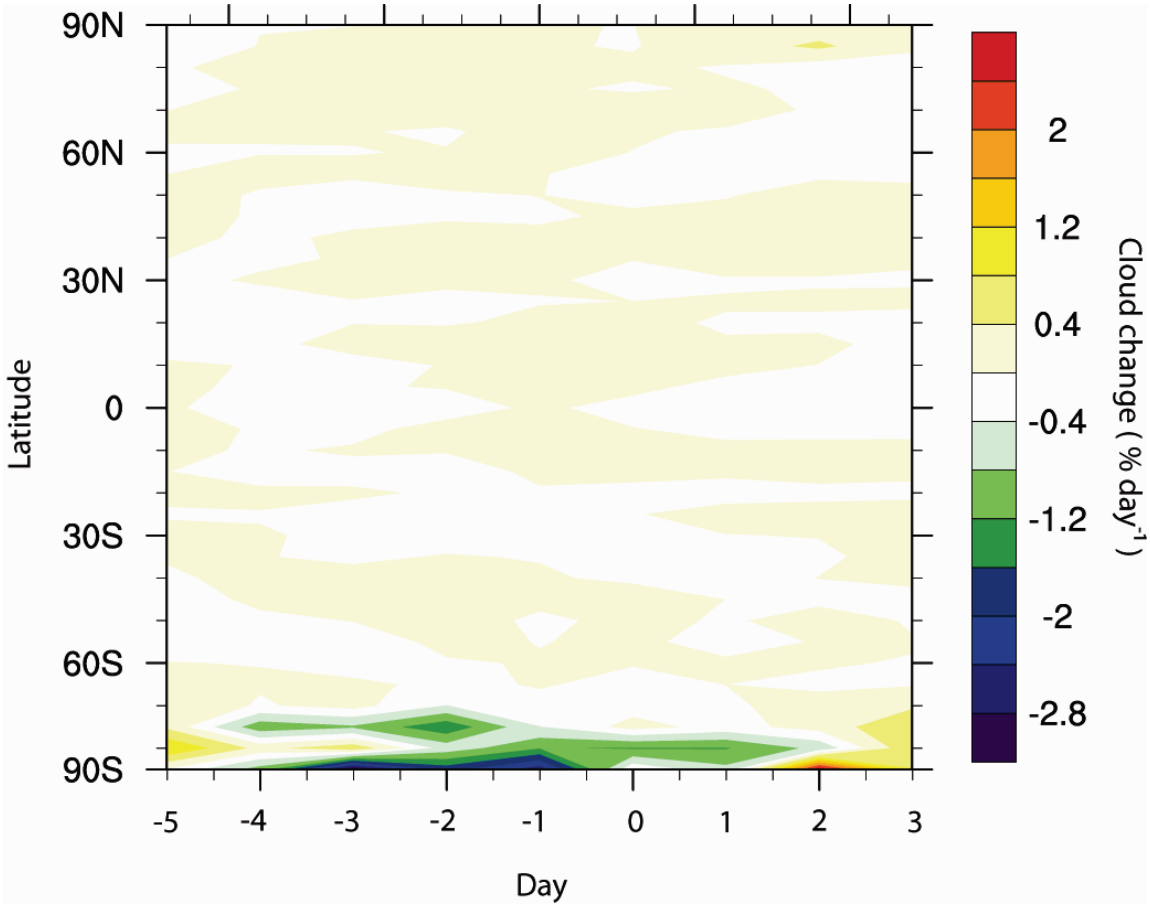

Figure 4.23 Latitude/time AGD cloud change

A plot of 5° latitudinal mean, anomalous rates of cloud change, occurring between 10 to 180 mb over the AGD composite.

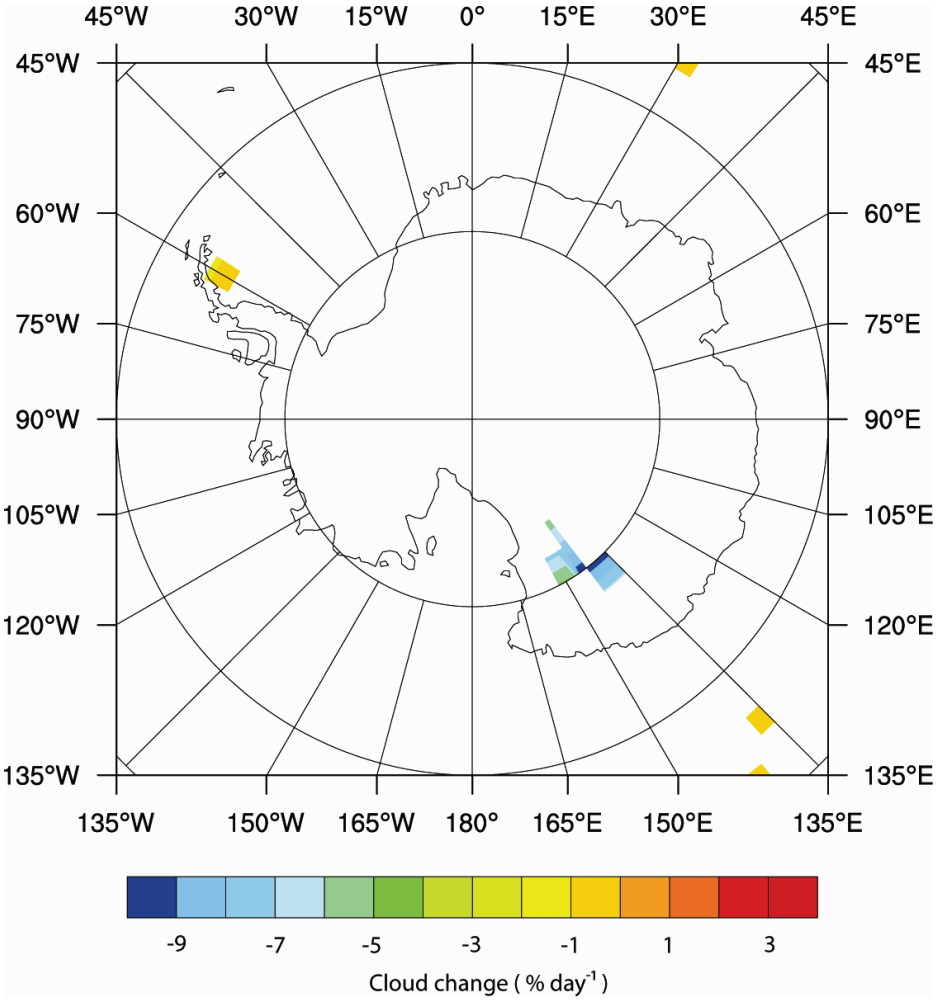

Figure 4.24 AGD sample Antarctic cloud changes

Mean rates of cloud change, occurring between 10 and 180 mb, on day -2 of the AGD sample. Only locally significant changes are displayed.

4.5 Do FD events effectively isolate GCR decreases?

The assumption that sampling based on FD events can provide a unique method of distinguishing the influences of GCR on Earth's environment from solar irradiance changes may require re-examination, as it has been noted that during the extreme solar flare events known as the 'Halloween Storms' (which took place between 28/10/2003 and 04/11/2003) irradiance variations were observed to occur in association with solar flare activity (Woods et al., 2004). This observation implies that FD events may not fully isolate GCR changes from variations in solar activity. TSI is known to increase in white-light flares, but generally there is a poor correlation between TSI and flare activity.

Although the adjusted FD and AGD samples previously discussed in this chapter did not show any statistically significant indications of F10.7 changes over the composite period it may be useful to re-examine the relationship between GCR and F10.7 variations associated with FD events. This may provide further insights in to the often conflicting results of existing FD-based GCR–cloud studies. A composite sample of 269 FD onset events (occurring between 1955 and 2006) is used; these dates are adjusted to the maximal GCR decrease date (in an identical method to the adjusted FD sample). The FD onset events are drawn from several sources, including: NOAA/NGDC's online archives (accessed from http://www.ngdc.noaa.gov/stp /solar/cosmic.html#FDs (last accessed on 25/05/2010)), Todd and Kniveton (2001) and Kristjánsson et al. (2008); the full list of adjusted dates are presented in table 4.5.

The GCR/F10.7 changes observed over this composite are presented in figure 4.25. These results clearly show that, several days prior to the key date GCR decrease F10.7 values show increased activity. This increased state persists for several days, lasting until the maximal GCR decrease, after which time both GCR and F10.7 slowly recover to undisturbed values over a period of approximately one week. A notched box plot of the sample distribution changes occurring both before and during the peak F10.7/GCR variations demonstrates that these changes are statistically significant (figure 4.26). These results confirm that during FD events, both F10.7 and GCR variations undergo related changes; the time lag between peak F10.7/GCR changes is most likely due to the time difference between increased irradiance activity from sunspot/solar flare activity (which travels at the speed of light) and the time it takes the CMEs (travelling at super-sonic speeds) to journey from the Sun to the near-Earth environment.

A scatter plot of the relationship between peak F10.7 and GCR variations shows, that in general, there is not a strong relationship between the two parameters (figure 4.27A). However, a plot of the extreme (top10) largest single day GCR decrease events (measured from Climax Colorado neutron monitor) shows that for high magnitude FD events the strength and significance of the relationship increases dramatically. This indicates that a connection between GCR/F10.7

variations may only be apparent when considering strong FD events. Consequently, this finding is relevant to the results of past FD-based studies, as it is a common practice to sort FD samples by the magnitude of the FD events (as it is assumed that doing so will provide the clearest indications of GCRs effects on climate). These results suggest the opposite may be true and that, in actuality, this approach may be biasing their samples by the inclusion of F10.7 related influences.

These results also offer an additional explanation for the cloud anomalies observed in the adjusted FD, and AGD composite samples presented in this chapter: weak (or non-) significant cloud decreases were detected several days in advance of the maximal GCR decrease during FD events. The timing of these anomalies corresponds to the observed timing of F10.7 variations detected during FD events (figure 4.25). Although no statistically significant F10.7 variations were observed during either the adjusted FD or AGD sample, it is possible that any relationship between F10.7 and these cloud changes is only apparent over a small portion of the events (specifically large FD events) and so overall the signal may be masked by noise. However, to this suggestion it must be stated that theoretically it is most likely that any relationship between climate and irradiance variations would be most readily expressed at low latitudes rather than high latitudes, due to the decreasing angle of incidence of the sun's rays at high latitudes coupled with the fact that during polar night no irradiance variations would be able to influence the sample; this strongly argues against an irradiance influence.

22/09/1956	04/12/1959	07/06/1967	01/11/1972	30/11/1980	06/10/1988	03/04/1998
11/11/1956	25/12/1959	30/10/1967	20/01/1973	20/12/1980	18/12/1988	14/01/1999
26/12/1956	14/01/1960	27/01/1968	15/04/1973	31/01/1981	07/01/1989	10/10/1999
22/01/1957	01/04/1960	07/04/1968	15/05/1973	21/02/1981	13/02/1989	07/02/2000
11/03/1957	01/05/1960	12/06/1968	07/05/1974	27/03/1981	14/03/1989	03/05/2000
18/04/1957	10/05/1960	11/07/1968	07/07/1974	18/05/1981	27/03/1989	24/05/2000
23/06/1957	23/05/1960	21/08/1968	14/09/1974	01/06/1981	11/08/1989	16/07/2000
05/08/1957	29/05/1960	03/10/1968	31/03/1976	26/07/1981	15/08/1989	18/09/2000
30/08/1957	06/06/1960	30/10/1968	14/09/1977	10/08/1981	19/08/1989	27/11/2000
23/09/1957	28/06/1960	17/11/1968	22/09/1977	03/10/1981	28/08/1989	12/04/2001
30/09/1957	15/07/1960	06/12/1968	04/01/1978	14/10/1981	07/09/1989	29/04/2001
23/10/1957	29/08/1960	01/03/1969	30/01/1978	12/11/1981	06/09/1989	28/08/2001
27/11/1957	06/10/1960	17/03/1969	15/02/1978	01/02/1982	19/09/1989	26/09/2001
18/12/1957	25/10/1960	25/03/1969	09/03/1978	12/02/1982	21/10/1989	25/11/2001
18/01/1958	14/11/1960	13/04/1969	11/04/1978	02/03/1982	29/11/1989	30/07/2002
11/02/1958	26/12/1960	28/04/1969	19/04/1978	26/04/1982	22/03/1990	18/11/2002
26/03/1958	14/03/1961	15/05/1969	02/05/1978	10/06/1982	10/04/1990	31/05/2003
30/05/1958	14/04/1961	09/06/1969	29/05/1978	14/07/1982	20/05/1990	20/06/2003
03/07/1958	14/07/1961	28/09/1969	03/06/1978	07/08/1982	01/02/1991	31/10/2003
09/07/1958	14/07/1961	10/11/1969	26/06/1978	07/09/1982	10/03/1991	24/11/2003
18/08/1958	27/07/1961	23/11/1969	14/07/1978	22/09/1982	24/03/1991	10/01/2004
24/08/1958	01/10/1961	30/01/1970	12/11/1978	25/11/1982	26/04/1991	22/01/2004
16/09/1958	29/10/1961	01/04/1970	21/12/1978	10/12/1982	29/05/1991	27/07/2004
02/10/1958	02/12/1961	02/06/1970	20/02/1979	10/01/1983	05/06/1991	08/11/2004
23/10/1958	21/04/1962	19/06/1970	29/03/1979	05/02/1983	13/06/1991	19/01/2005
12/11/1958	03/05/1963	25/07/1970	26/04/1979	13/05/1983	03/07/1991	15/05/2005
16/12/1958	17/09/1963	09/09/1970	08/06/1979	10/06/1983	09/07/1991	17/07/2005
27/01/1959	23/09/1963	07/11/1970	07/07/1979	07/05/1984	19/08/1991	11/09/2005
12/02/1959	30/10/1963	08/11/1970	20/08/1979	29/06/1984	01/11/1991	
26/02/1959	08/10/1965	29/01/1971	12/11/1979	07/09/1984	08/11/1991	
10/04/1959	24/03/1966	16/04/1971	07/02/1980	28/04/1985	27/02/1992	
24/04/1959	31/08/1966	07/10/1971	07/10/1979	09/02/1986	10/05/1992	

Table 4.5 List of Forbush Decrease events

List of FD onset dates taken from various sources, including: NOAA's database (http://www.ngdc.noaa.gov/stp/solar/cosmic.html#FDs), Todd and Kniveton (2004), and Kristjánsson et al. (2008) (n = 269). Original FD onset events were adjusted so as to align day 0 with the maximal GCR reduction below background levels (identical methodology to Laken and Kniveton (2010)).

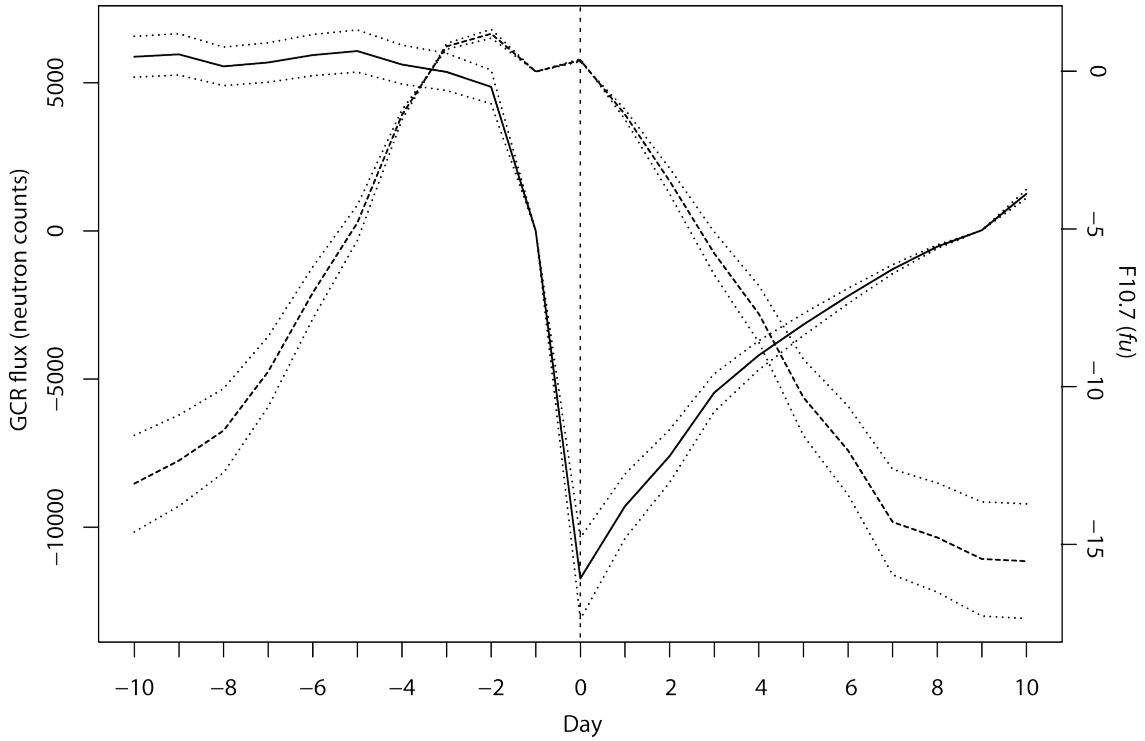

Figure 4.25 Absolute GCR/F10.7 variations during FD events

Mean GCR flux (solid line) and F10.7 (dashed line) variations occurring over a composite of 269 FD events (1955–2005). Day 0 indicates maximal GCR decrease date associated with FD events (highlighted by the vertical dashed line). Dotted line around mean GCR/F10.7 values denotes 0.95 level confidence intervals. GCR data are taken from Climax Colorado neutron monitor (adjusted for barometric pressure variations). F10.7 data are taken from the 10.7cm (2.8 GHz) radio flux, measured from adjusted Pentiction Ottawa. Each event in the composite is normalised against day -1 values for display purposes.

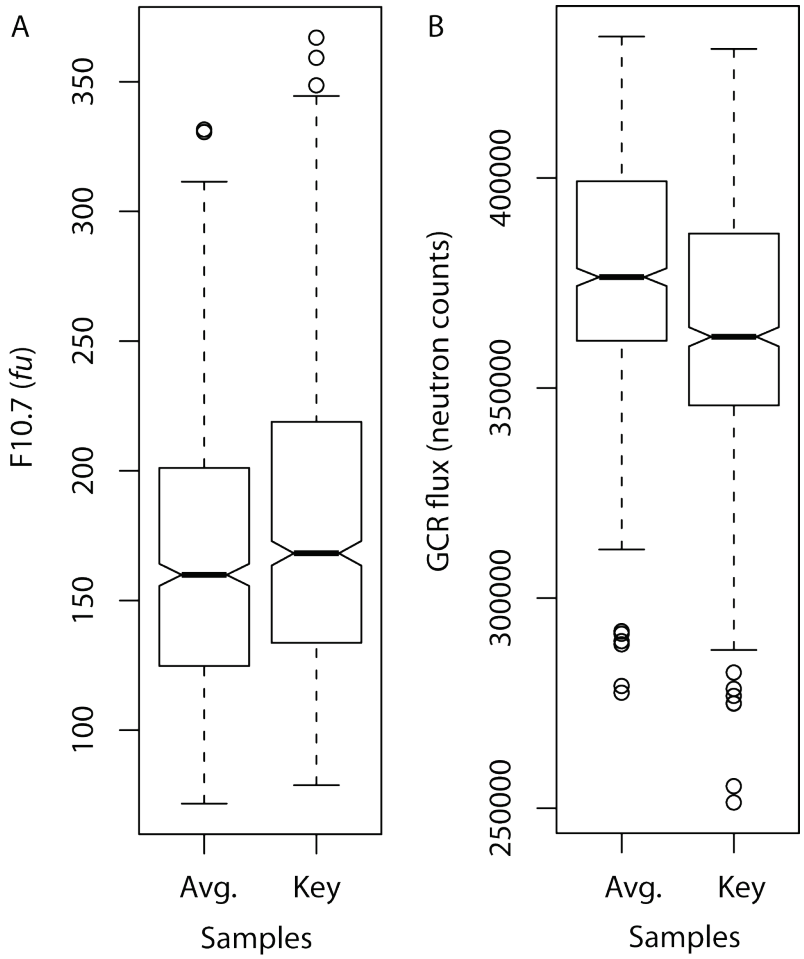

Figure 4.26 F10.7/GCR sample distribution variations during FD events

Absolute **A**) F10.7 and **B)** GCR flux sample distribution changes between an averaging period (Avg.) taken from day -10,-9,-8 (for F10.7) and -5, -4 and -3 (for GCR flux) displayed next to the sample distribution of a key period (Key) of FD-related change on -3,-2,-1 (for F10.7) and day 0,1,2 (for GCR flux). Average and key periods for F10.7/GCR are offset due to lag between responses. Notches on the box plots indicate the 0.95 level confidence interval around the median value, markers indicate outlying data points. GCR data are taken from Climax Colorado neutron monitor (adjusted for barometric pressure variations), F10.7 values are taken from 10.7cm (2.8 GHz) radio flux, from adjusted Pentiction Ottawa data.

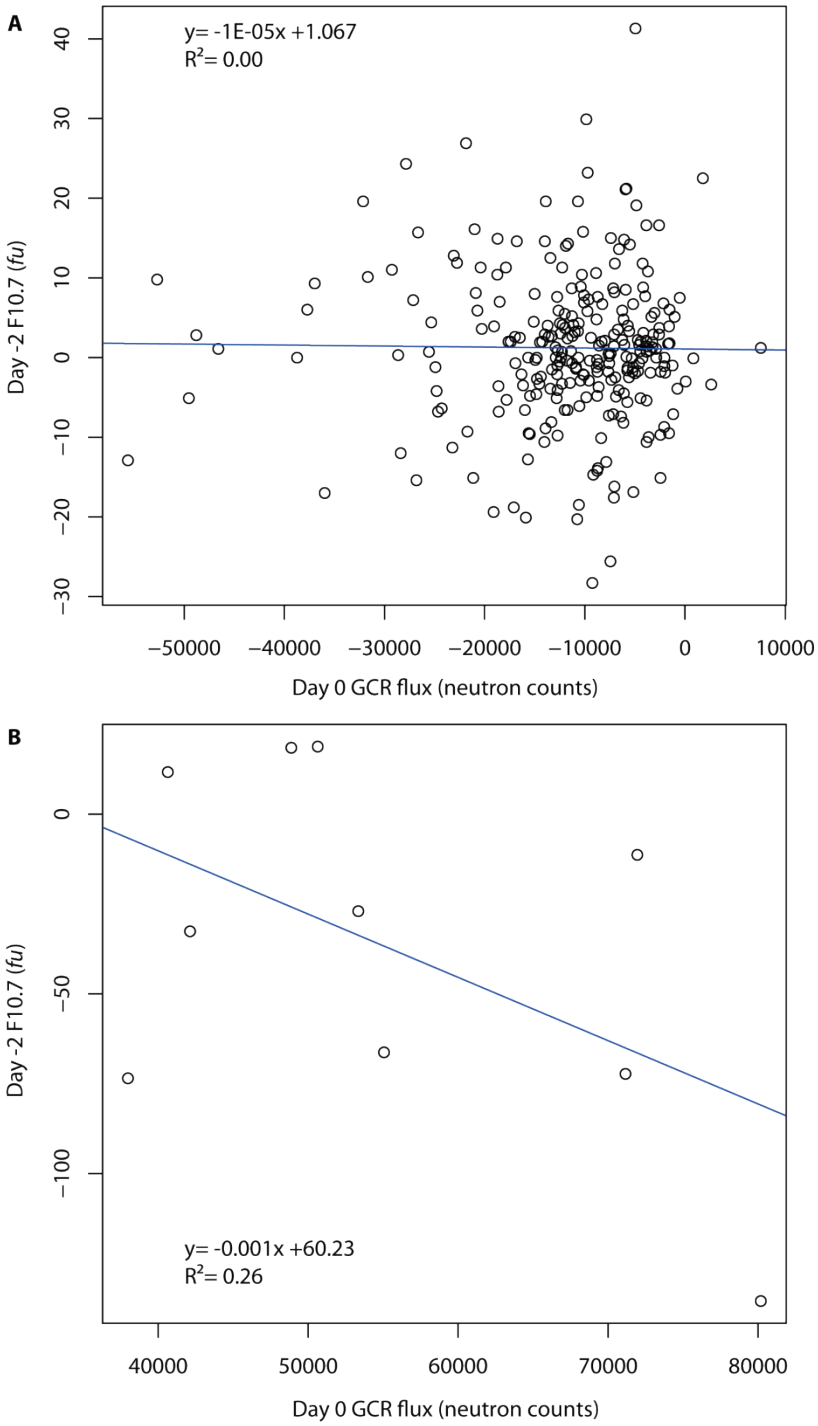

Figure 4.27 F10.7/GCR FD scatter plots

Relationship between the peak F10.7 (day -2) and GCR flux (day 0) changes. Linear regression displayed (blue line), along with regression equation (y) and correlation coefficient (R^2). Plots are shown for **A**) entire sample (n = 269), and **B**) top 10 largest single-day GCR decrease events. Values of F10.7 and GCR are normalised against their respective day -1 values. GCR data are taken from Climax Colorado neutron monitor (adjusted for barometric pressure variations), F10.7 values are taken from 10.7cm (2.8GHz) radio flux from adjusted Pentiction Ottawa data. Dates used are: 14/07/1982, 22/01/1957/ 12/05/1959, 15/02/1978, 05/08/1972, 30/08/1957, 13/06/1991, 21/10/1989, 11/09/2005, 16/07/1959.

4.6 Discussion

Objective 1: *To test for the existence of a relationship between clouds and the GCR flux using a methodological approach based on the composite sampling techniques of past daily timescale GCR studies.*

The composite samples presented in this chapter did not identify a statistically robust relationship between GCR changes and cloud cover and have therefore failed to fulfil objective 1.

The adjusted FD and AGD samples were successful in isolating a high magnitude decrease in the rate of GCR flux to an extent greater than previous studies have achieved. However, despite this confinement, it was found that only a limited number of statistically significant anomalous cloud changes at high tropospheric levels were detected. MC significance testing showed that these anomalies were not field significant. Despite the lack of statistical significance, it is intriguing to note that at a 5° latitudinally-averaged resolution the magnitude and temporal evolution of the cloud anomalies over the two samples was comparable; this may imply the action of a common process. However, due to the lack of reliable statistical significance over the samples, it must be concluded that FD events did not provide robust evidence of a GCR–cloud relationship, but correlated changes in any meteorological parameters are important. It is however vital to state that the observed cloud anomalies were confined to a region where satellite based cloud retrievals are known to be of a questionable quality (Rossow and Schiffer, 1999; Todd and Kniveton, 2004); this strongly limits the confidence that can be placed on any conclusions drawn from these results.

Interestingly, with regard to the cloud changes detected over the Antarctic, the peak in cloud changes observed in both the adjusted FD and AGD samples occurs on day -2 rather than during the maximal GCR decrease on the key date. This result may be interpreted in several ways:

(1) It may indicate there is no relationship between the GCR flux and the observed cloud changes.

(2) It may suggest that the onset of statistically significant GCR decreases is more important than the maximum change.

(3) The cloud anomalies may be more related to irradiance changes found to occur with FD events than to GCR variations.

(4) The cloud detections may be erroneous.

It may be useful to consider the possible GCR–cloud mechanisms which may explain Antarctic cloud decreases during FD events in order to see if there is any theoretical support for the observed cloud changes observed being linked to GCR decreases:

Ion-mediated nucleation: it has been established that atmospheric ions may seed new particles and experimental evidence has suggested that a large ionisation increase over Antarctica related to a particularly intense GLE is linked to a statistically significant increase in sulphate/nitrate aerosol concentrations (Mironova et al., 2008). This evidence may imply that decreases in atmospheric ionisation may similarly result in a reduction of CCN production and theoretically explain a decrease in cloud amount. However, the increased aerosol concentrations observed by Mironova and workers occurred 2 days after the GLE. This time lag suggest that an IMN process is not influencing the cloud changes observed during the adjusted FD or AGD samples described in this chapter, as these cloud changes occur approximately 2 days in advance of the maximal GCR decrease.

Near-cloud effect: it has been hypothesised that a decrease in the J_z of the GEC as a result of decreased GCR flux may reduce the charge accumulation at cloud boundaries. This may affect aerosol scavenging rates of cloud droplets, thereby influencing a range of properties such as cloud lifetimes, droplet concentrations and albedo (Tinsley, 2008). Such a process may be important to supercooled stratus clouds which are a common feature over the Antarctic plateau (Morley et al., 1989). At a local-scale, specific atmospheric responses may rely on a combination of how thunderstorm generation at low latitudes responds to ionisation changes and how the variation in the latitudinal distribution of ionisation balances the local current flow in the GEC (Tinsley, 2008). It has been postulated by Burns et al. (2008) that cloud cover over the Antarctic plateau may increase following a local current increase; therefore a reduction in current may be expected to similarly result in a cloud decrease. However, this process cannot account for the cloud changes being in advance of the maximal GCR decrease.

The fact that FD-based samples have revealed no clear evidence of a significant cloud relationship weakens the hypothesis that GCR changes may affect cloud cover. A possible reason why FD-based studies have failed to identify a significant relationship may come from a consideration of the microphysical mechanisms behind GCR–cloud interactions: in all instances these interactions are strongly second order. That is, they require certain conditions to be met before GCR may influence cloud (i.e. a relationship between GCR–cloud is strongly constrained by environmental precursor conditions). This holds true regardless of the mechanism. For example, for ion-induced processes, precursor aerosols and low concentrations of pre-existing CCNs are essential, whereas, the near-cloud effect requires the presence of stratified cloud layers of appropriate dimensions and droplet sizes to function. Although it may

be expected that over long-timescales or for large datasets a GCR–cloud effect may be detectable regardless of considerations to precursor conditions (as in such instances a sensitive dependence on precursor conditions may merely decrease the signal-to-noise ratio (SNR)), in the context of FD-based composites, initial conditions may be a critical factor determining whether a GCR–cloud response will occur. As the sample sizes are small (and thus a high SNR ratio will greatly impact the results). Considering this, it may be unlikely that evidence of a widespread GCR–cloud relationship may be obtained by an FD sample based approach, as this sampling basis is totally defined by a quasi-random parameter that is external to the climate system (FD events) and such an approach cannot account for a sensitive-dependence upon precursor conditions.

4.7 General summary

An overview of the results of several FD studies were given, these studies have not yet demonstrated a clear GCR–cloud response and instead show inconsistent responses. One recent study has controversially claimed to show a global scale relationship between cloud decreases and FD events. The findings of this study were reanalysed in detail, the results strongly indicate that the conclusions of this study are flawed for several reasons.

In an attempt to improve upon the approaches of existing FD studies and gain a clearer understanding of cloud responses during FD periods, a method of adjustment was applied to a composite of FD onset events which realigned the composite to reflect the date of maximum rate of GCR decrease (this was done as maximal GCR deviations are often offset from FD onset dates by several days). Although this new ‘adjusted’ FD sample showed a significantly more isolated and intense GCR decrease than previously obtained, it did not provide good indications of a GCR–cloud relationship: the only cloud response observed was from locally intense cloud decreases located at the uppermost pressure level of the ISCCP data (10–180 mb) over areas of the Antarctic plateau. An attempt was made to verify these findings, using the construction of a second composite sample based on the largest periods of Antarctic GCR decrease. Although roughly comparable anomalies were detected, these results still did not provide unambiguous statistical evidence of a GCR–cloud relationship. Several potential reasons for this shortcoming were discussed.

Chapter 5 An internal sampling approach

5.1 The need for an internal sampling approach

The previous chapter demonstrated that FD-based composite studies were unable to identify a significant GCR–cloud relationship. This may possibly be due to the limitations associated with FD-based composites, especially those related to: (1) small sample sizes, and (2) the inability to account for a sensitive-dependence upon precursor conditions. With regards to the first issue, the limitation of small sample sizes is a problem inherent to FD-based studies, as there are only a limited number of FD events upon which to base a composite, while the second issue may be critical if a GCR–cloud relationship proves to be a second order phenomenon. Both of these problems may potentially be overcome by constructing samples around a parameter internal to Earth's environment (such as cloud cover); it is this possibility which will be explored in this chapter.

5.1.1 Constructing cloud based samples

A new sampling methodology based around the largest daily timescale variations in the rate of cloud change will now be considered. As in previous sections, this new analysis will continue to use a composite based approach. The samples are based on the daily average rates of cloud change derived from the ISCCP dataset. The cloud data are divided into five distinct sample groups based on regional area, these are: global (equal-area-adjusted 90°N–90°S); tropical latitudes (20°N–20°S); mid-latitudes (60°S–20°S and 20°N–60°S); Arctic latitudes (90°N–60°N); and, Antarctic latitudes (60°S–90°S). Dates with the largest (top 5 %) increases and decreases in the daily rate of cloud change throughout these five aforementioned regions will be selected as key dates for separate composites. Any key dates which were found to recur over the composite period (of -15 to 3 days) or be coincident (within a ±3 day range) of a SEP event were removed from the sample. For each sample, an analysis of the temporal coverage of the neutron monitor data and standard deviations of neutron counts recorded at each individual monitor site are displayed (table 5.1). Any neutron monitor site found to have a standard deviation greater than 1.5x the average standard deviation of the combined neutron monitor data are removed from the final sample: this procedure is designed to minimise the impact of data from monitors found to show abnormally high variability. Stations found to have standard deviations of such values are flagged in red (table 5.1).

An analysis of the distribution of the average standard deviation at each neutron monitor site shows that the sites 'Alma B' (Alma Ata-B) and 'Inuvik' consistently demonstrate an abnormally high variability in comparison to the other neutron monitor sites (figure 5.1). Alma Ata-B is found to be above the threshold standard deviation in each of the ten samples (table 5.1), while Inuvik is found to be above the threshold standard deviation in eight out of the ten samples. Consequently, in the majority of samples, both of these sites are removed from the final composites prior to significance testing.

There were three samples which were found to demonstrate statistically significant changes in the rate of GCR flux on the key date of the composites, these were:

Global increase (GI) sample
Antarctic increases (AI) sample
Mid-latitude decreases (MLD) sample

These three composite samples will now be considered in detail throughout the remainder of this chapter and will be used as the basis for a forthcoming atmospheric analysis and climate modelling experiments in later chapters.

Site	Global increase		Global decrease		Tropic increase		Tropic decrease		Mid Lat. Increase	
	stdev	n(*x*/134)	stdev	n(*x*/114)	stdev	n(*x*/138)	stdev	n(*x*/134)	stdev	n(*x*/133)
Alma Ata-B	4.51	95	4.88	83	4.44	93	3.65	97	3.88	87
Apatity	1.76	132	2.34	113	1.73	135	1.92	132	2.05	131
Climax	1.29	117	1.15	100	1.21	124	1.30	121	1.23	120
Inuvik	3.27	109	2.98	89	2.62	110	3.00	106	3.46	104
Kiel	1.20	129	1.26	106	1.56	131	1.61	130	1.14	127
Magdan	2.25	120	1.74	105	2.01	122	2.14	122	2.26	117
Mcmurdo	1.26	133	1.13	113	1.19	162	1.32	132	1.77	133
Moscow	2.05	134	1.93	114	1.54	138	2.06	134	1.88	133
Newark	1.59	97	1.92	80	1.51	101	1.61	100	1.86	95
South Pole	1.46	93	1.40	77	1.45	97	1.56	96	1.43	90
Thule	1.95	131	1.64	110	1.83	132	1.52	130	1.93	130
Average	2.05		2.03		1.92		1.97		2.08	

Table continued overleaf...

Site	Mid Lat. Decrease		Antarctic Increase		Antarctic Decrease		Arctic Increase		Arctic Decrease	
	stdev	n(*x*/130)	stdev	n(*x*/114)	stdev	n(*x*/115)	stdev	n(*x*/122)	stdev	n(*x*/108)
Alma Ata-B	4.09	93	5.54	78	4.37	79	5.01	92	5.13	79
Apatity	2.17	129	1.76	111	2.25	112	2.30	119	2.52	105
Climax	1.11	117	1.20	104	1.21	101	1.31	110	1.31	96
Inuvik	3.55	107	3.71	89	3.75	89	3.35	95	3.83	81
Kiel	1.43	124	1.14	110	1.39	107	1.19	119	1.37	105
Magadan	2.29	116	2.79	104	1.89	104	1.93	109	2.40	102
Mcmurdo	1.24	128	1.14	113	1.17	111	1.19	120	1.30	107
Moscow	1.59	130	2.20	114	1.54	115	1.84	122	1.81	108
Newark	1.35	91	1.07	87	1.93	83	1.18	88	1.26	102
South Pole	1.36	84	1.37	87	1.49	84	1.51	86	1.53	77
Thule	1.79	129	1.52	114	2.03	113	1.94	118	1.68	106
Average	2.00		2.13		2.09		2.07		2.19	

Table 5.1 Mean standard deviations at each neutron monitor site

Mean rate of GCR flux standard deviations at each neutron monitor site occurring over each individual sample. Standard deviation denoted by 'stdev', units in % day^{-1}. Total potential sample size (n) is stated for each sample at the table header (e.g. potential sample size for mid-latitude decrease sample is 130 observations). Data coverage varies between neutron monitors varies. Sites are highlighted in red if the average standard deviation is greater than 1.5x the average standard deviation of the sample; such sites are not incorporated in to the final sample prior to significance testing.

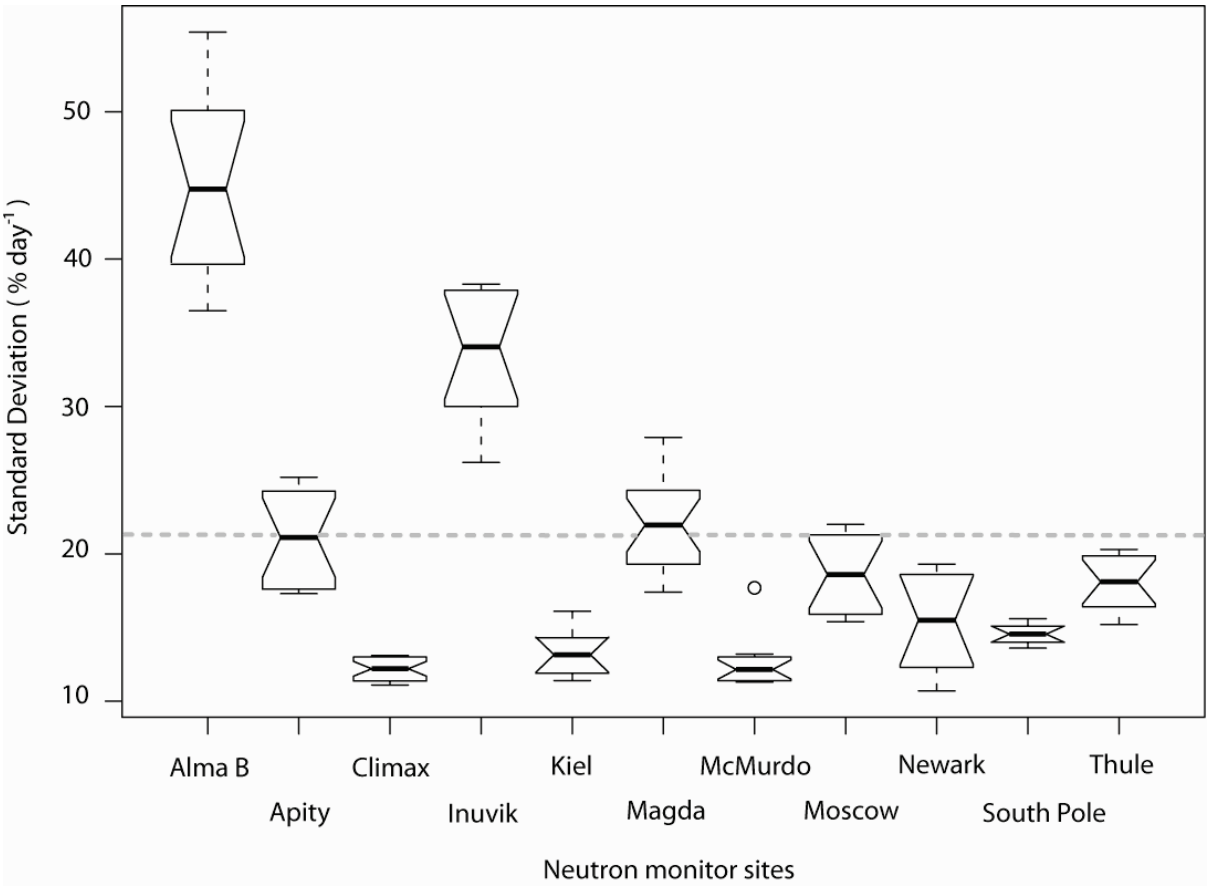

Figure 5.1 Standard deviation at each neutron monitor site

Notched box plots showing the mean standard deviation at each neutron monitor site over all of the composite samples. Standard deviation is calculated as a percentage GCR rate normalised against the peak-to-peak GCR variations over an 11-year solar cycle. Dashed line indicates overall mean standard deviation of the sites.

Region	Increase			Decrease		
	n	sites (*x*/11)	T.Val	n	sites (*x*/11)	T.Val
Globe	134	9	2.99	117	10	1.86
Tropics	138	10	0.83	134	9	-1.23
Mid-Lats.	133	9	-0.91	130	9	3.25
Arctic	122	9	-1.45	108	9	2.01
Antarctic	114	9	3.30	115	9	0.86

Table 5.2 Significance of key date cloud sample GCR variations

Sample size (indicated by 'n'), number of neutron monitor sites used in the composite (indicated by 'sites (*x*/11)') and Students T-value (indicated by 'T.Val') are all displayed for both the largest (top 5 %) increases and decreases in the average daily rates of cloud change (1,000 – 10 mb). Statistically significant samples (above the 0.95 confidence level) are highlighted in yellow. All highlighted changes were found to demonstrate a positive relationship between the rate of GCR flux and cloud cover change.

5.1.2 Seasonal sensitivity of samples

Although the three samples were selected due to the occurrence of statistically significant GCR variations on the key date of the composites, it is possible that the samples may also reflect seasonal variations in cloud formation rates as seasonality is likely to be a strong influence governing changes in the rate of cloud formation over large areas. Logically, a sample which does not contain a seasonal pattern may be more likely to contain a successfully isolated GCR cloud relationship, as variations in the GCR flux have no seasonal component. Whereas, a sample that does display a seasonal component may imply that a GCR–cloud relationship has not been fully isolated from internal climate variability. Alternatively, it is also plausible that seasonal influences may potentially have an impact on GCR-related cloud formation via an effect on precursor conditions.

An analysis of the annual distribution of the key events across the (1) GI sample indicates that the annual distribution of events is random (figure 5.2A); a lack of seasonality in the GI sample is unsurprising, as at a global scale seasonality should not be an influential process. However, the distribution of the AI sample shows peak during the southern hemisphere winter (figure 5.2B), while the MLD sample shows a bimodal distribution, peaking around the times of the

equinoxes (figure 5.2C). The presence of seasonality in the AI and MLD samples may be interpreted in several ways:

1) It may suggest that the AI/MLD samples are causally unconnected to GCR variations, and are instead merely the result of seasonal variability.
2) It may imply that during certain times of the year cloud conditions are more conducive to a GCR–cloud link.
3) It may simply be an artefact of sampling: i.e. the most rapid cloud changes are in periods when both GCR and seasonal changes are acting to alter cloud in a complementary manner, thus producing the most rapid cloud changes over the period.

There is also another potential (but less likely) explanation for the presence of seasonality in the samples: if a GCR–cloud link operates via a GEC related mechanism then it is possible that seasonal variability in the state of the GEC may be influence a GCR–cloud mechanism. It has been suggested that the GEC has both an annual and semi-annual oscillation (Williams, 1994; 2008). The annual oscillation of the GEC is attributed to the asymmetrical distribution of land between the northern and southern hemispheres. The annual variations in air temperature that accompany this asymmetry result in an air-earth current maximum during the northern hemisphere summer. While the proposed semi-annual component of the GEC is related to an enhancement of tropical convection during equinoxial crossings, which has been suggested to increase low latitude lightning activity (Williams, 1994; 2008; Christian et al., 2003). If a GCR–cloud relationship operates via a GEC-related mechanism, GCR-related cloud changes may potentially be enhanced by seasonal variations in the GEC. However, it is most likely that the seasonal component of the samples is more related to simple seasonal variations in the rate of cloud change.

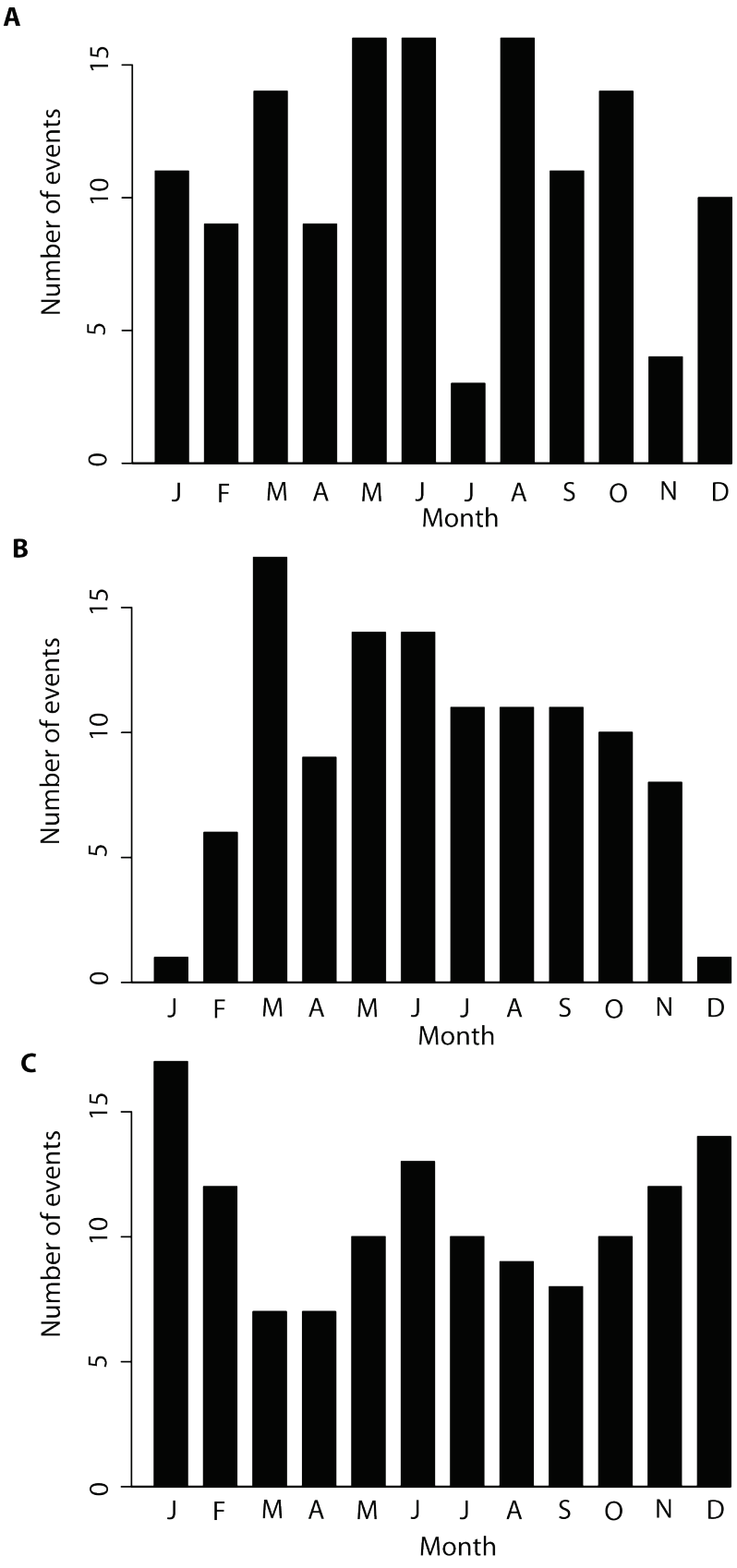

Figure 5.2 Annual distribution of sample events

The distribution of key over the **A)** GI, **B)** AI, and **C)** MLD composites on a month-by-month basis.

5.2 GI sample: GCR, IMF and irradiance variations

The average rate of GCR flux undergoes a sustained increase of approximately 3.3±0.3 % between days -5 to 0 over the GI sample. These changes peak on the key date of the composite period and are found to be statistically significant on days -1 and 0. This suggests that a relationship may exist between increased rates of global cloud change and increases in the rate of GCR flux (figure 5.3).

In contrast to these changes, the IMF B_z and B_y components showed no statistically significant changes over the composite (figure 5.4). Similarly, the UV and F10.7 variations also showed no significant variations and demonstrated no coherent changes with respect to the key date (figure 5.5). It should be noted that the IMF, UV and F10.7 datasets only have partial coverage over the GI sample (specific coverage is detailed in table 5.3). Overall, these results show that a statistically significant co-temporal relationship exists between the largest global increases in the rate of cloud change and increases in the rate of GCR flux which are unconnected to IMF, UV or F10.7 variations.

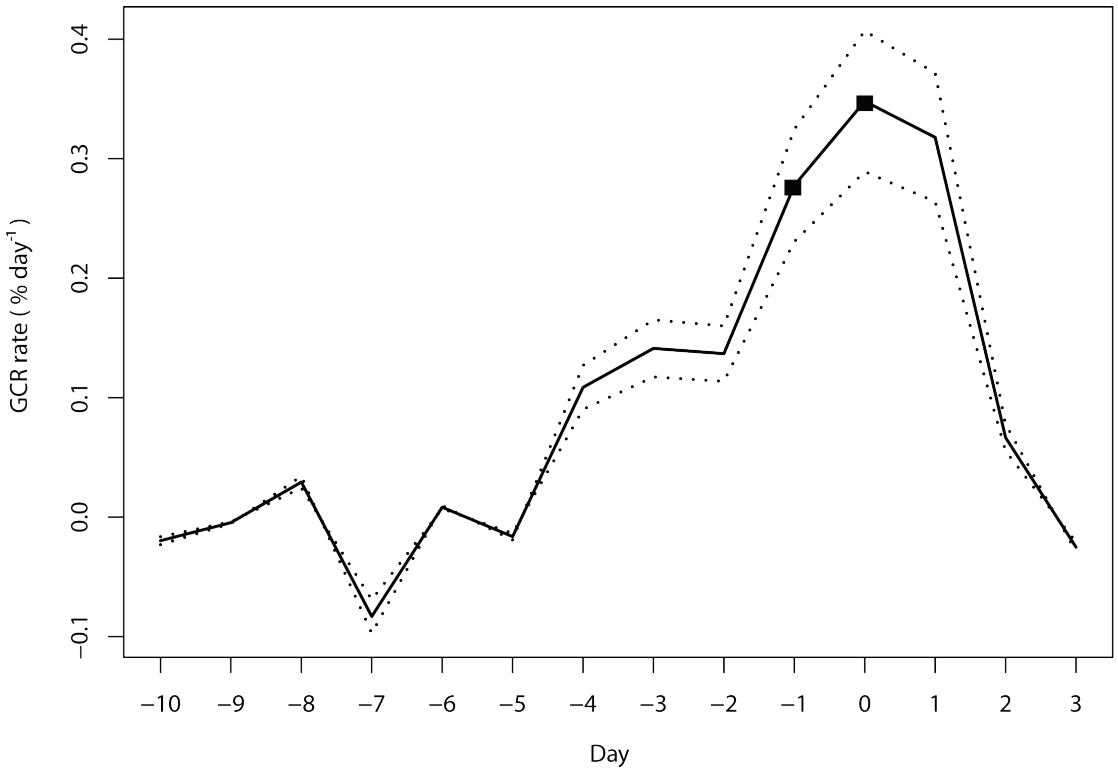

Figure 5.3 GI sample: rate of GCR flux

Rate of GCR flux calculated from daily average neutron counts (based on data from 9 out of 11 neutron monitor sites; see table 5.1 for specific sites included). Units are calculated as a percentage relative to the peak-to-peak variations experienced over an 11-year solar cycle. Statistically significant changes indicated by markers. The confidence interval at the 0.95 level is shown by the dotted lines.

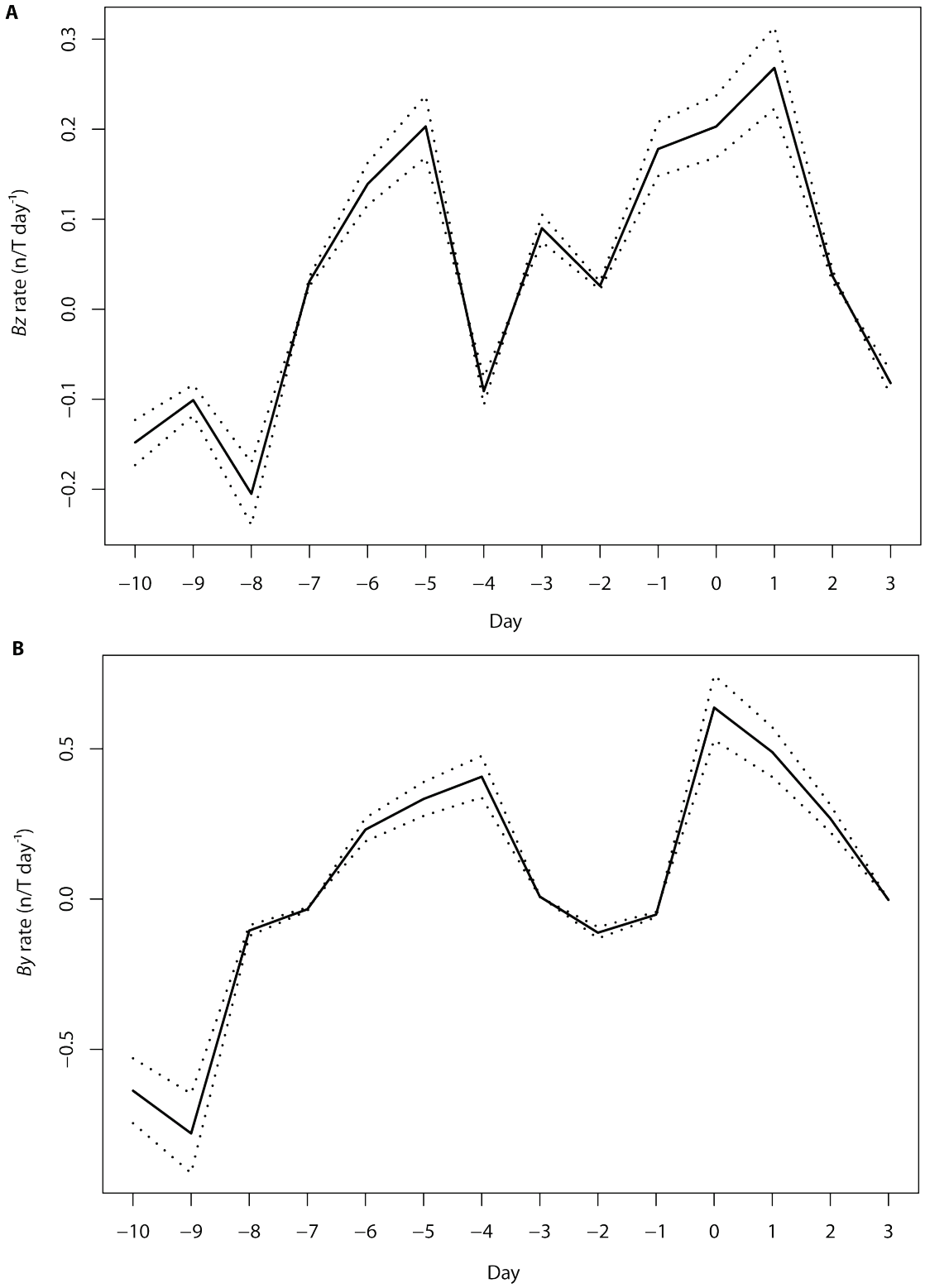

Figure 5.4 GI sample: IMF variations

Average rate of IMF **A)** B_z (north south) and **B)** B_y (east west) components over the GI sample. Dotted lines indicate the 0.95 level confidence interval.

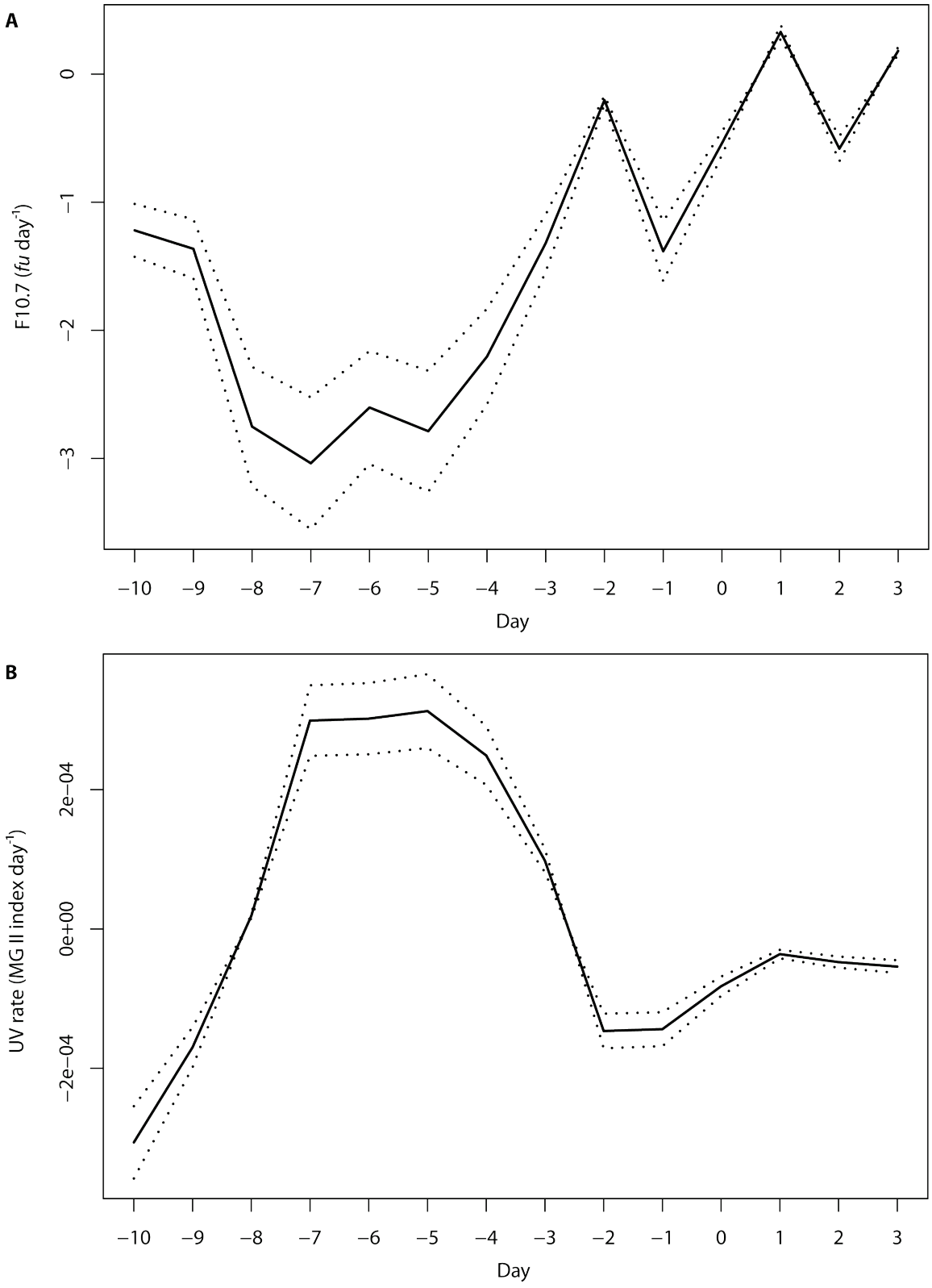

Figure 5.5 GI sample: solar activity variations

Average rate of: **A)** F10.7 (10.7 cm 2.8 GHz radio flux) and, **B)** UV (MG II index) variations over the GI sample. Dotted lines indicates the 0.95 level confidence interval.

Parameter	Data coverage (%)
IMF B_y	87
IMF B_z	84
UV	75
F10.7	44

Table 5.3 GI sample: IMF and solar activity data coverage

IMF, UV and F10.7 temporal coverage over the GI sample, expressed as a percentage.

5.2.1 GI sample: anomalous cloud changes

A plot of the globally-averaged, anomalous cloud changes, occurring across the GI sample shows the presence of large, statistically significant increases beginning around day -2. These anomalies are centred around the key date of the composite and occur throughout the troposphere; these changes reach a maximum intensity of around 3 % on the key date of the composite, at approximately 600 mb. In addition, small negative anomalies (of around -0.4 %) are also evident around day -5 at high pressure levels (figure 5.6).

Extending the analysis, a plot of 5° latitudinally-averaged cloud anomalies reveals that the largest changes are occurring at high latitude regions. The development of these anomalies is found to be symmetrical across both hemispheres (figure 5.7). The cloud changes are found to be widely statistically significant: the anomalous cloud changes appear to extend from high to mid-latitudes, diminishing towards the tropics (figure 5.7).

A latitude/pressure level profile of anomalous rates of cloud change on the key date of the composite shows statically significant Antarctic cloud anomalies which extend from approximately 10–500 mb (roughly from the lower stratosphere/tropopause to the surface of the Antarctic plateau) (figure 5.8). Comparable Arctic anomalies are also evident, located in the mid-troposphere (between 400–800 mb). The Arctic cloud changes appear to be more intense than those over the Antarctic (by approximately 3 %) (figure 5.8).

Locally significant Antarctic cloud changes are observed to be widespread across the continent; the magnitude of the anomalies range between 2.5–22.5 %. In the Arctic, anomalous cloud changes are again found to be slightly more intense, ranging from between 2.5–27.5 %. Both the Arctic and Antarctic cloud changes are found to decrease in magnitude and extent with

decreasing latitude (figure 5.9). Although the anomalies are found to be largest over high latitude regions, smaller anomalies are also observed across the globe. In particular, they appear to be relatively widespread over oceanic regions of the southern hemisphere (figure 5.9).

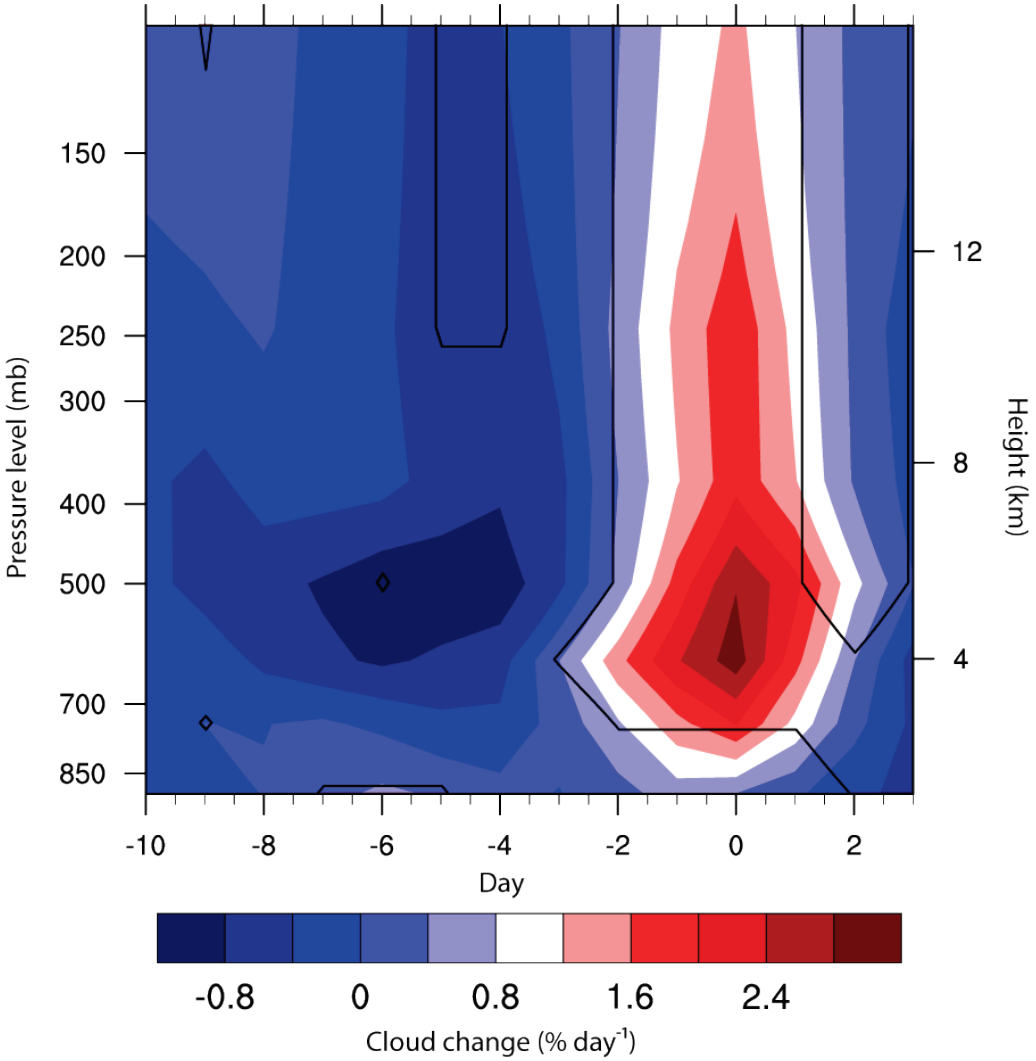

Figure 5.6 GI sample: globally-averaged cloud anomalies

Anomalous cloud changes, occurring across globally-averaged pressure levels as a function of time. Statistically significant changes are indicated by solid contours.

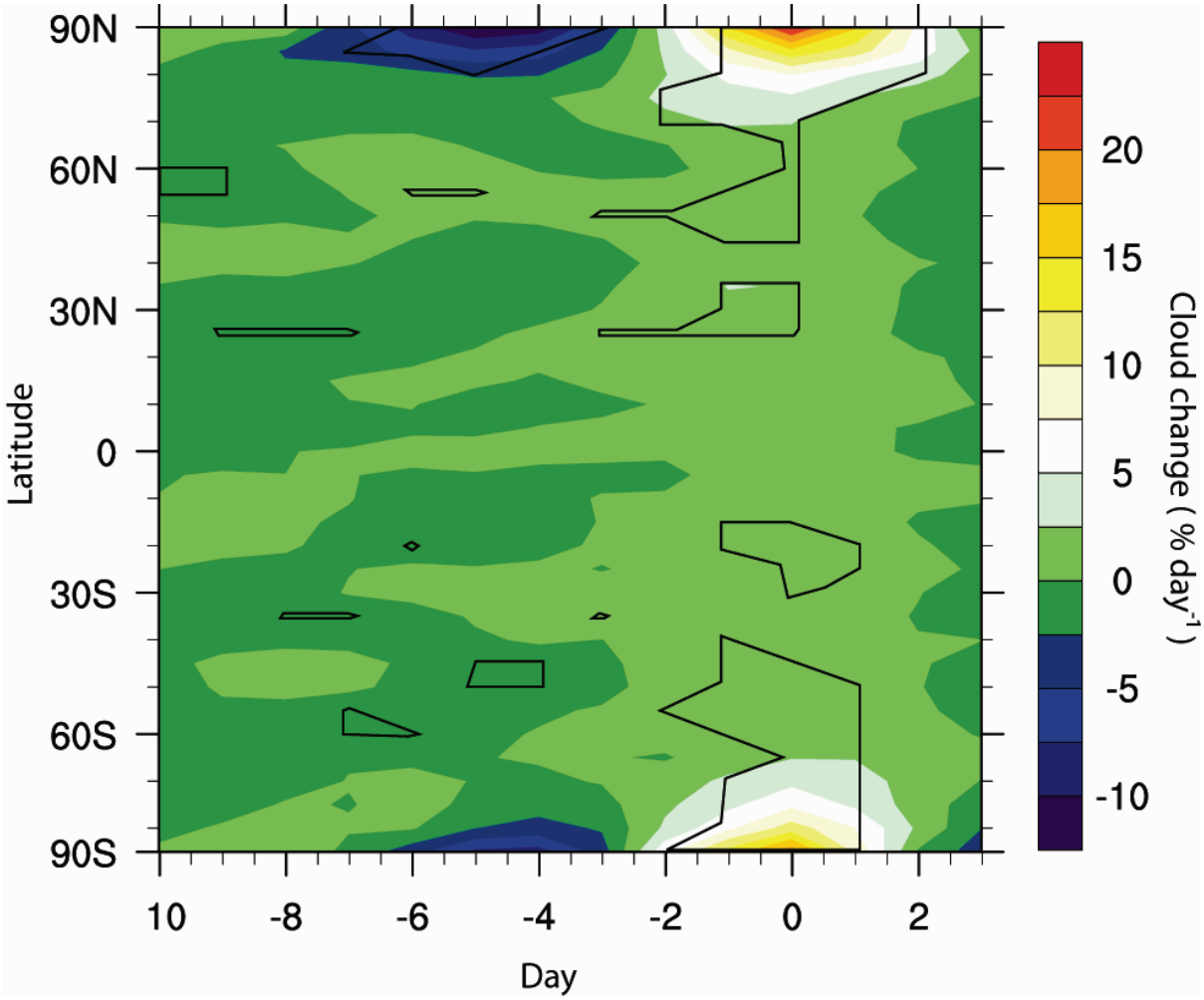

Figure 5.7 GI sample: latitude/time cloud anomalies

A 5° latitudinally-averaged plot of mean anomalous cloud changes (between 10 and 1,000 mb) across the GI composite. Statistically significant changes are indicated by solid contours.

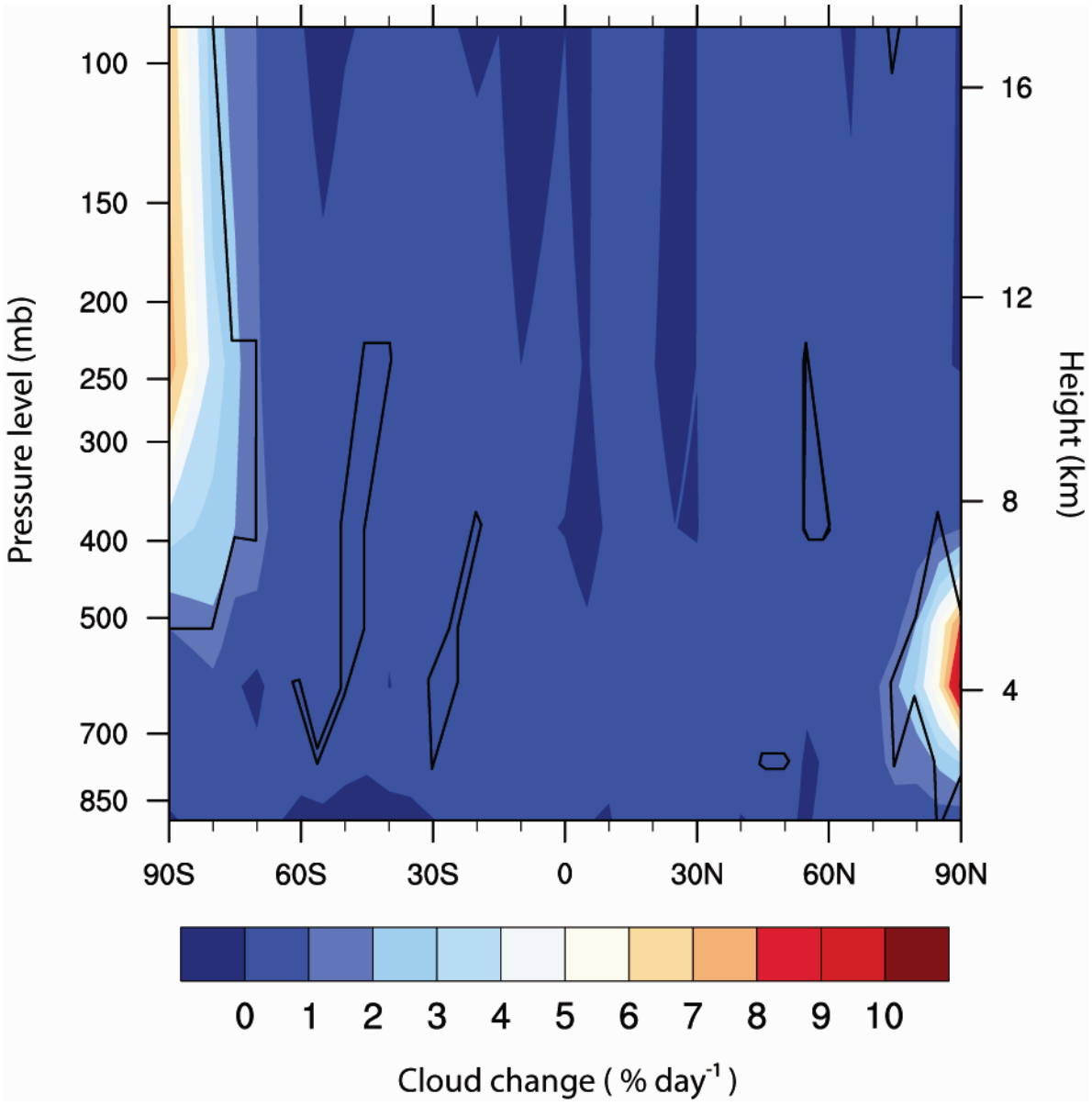

Figure 5.8 GI sample: pressure level/latitude cloud anomalies

A tropospheric profile of 5° latitudinally-averaged anomalous cloud changes occurring on the key date of the sample. Regions of statistically significant changes are indicated by solid contours.

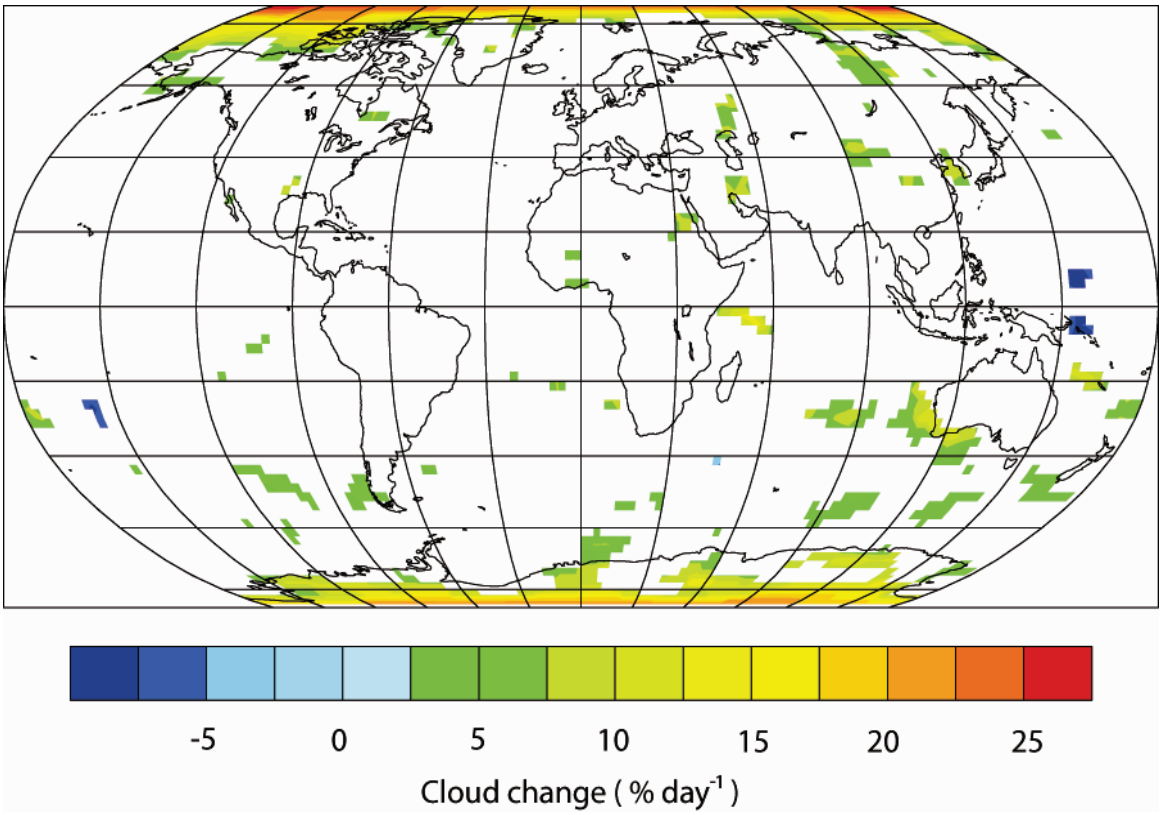

Figure 5.9 GI sample: global cloud anomalies

Robinson projection of anomalous cloud changes (between 10 and 1,000 mb) occurring on the key date of the GI sample. Only locally significant changes are displayed.

5.2.2 GI sample: discussion

Statistically significant increases in the rate of GCR flux were found to develop co-temporally with significant cloud increases over the GI sample; no other solar activity parameter was found to demonstrate any comparable or significant changes over the GI composite period. This finding supports notions of a solar–terrestrial link operating via a connection between the GCR flux and cloud cover.

During the GI sample a significant global average increase in cloud cover of around 3 % was observed; these changes mainly resulted from simultaneous increases in cloud (of around 30 %) over high latitude regions in both hemispheres. The largest magnitude cloud changes were found to occur over regions of the weakest horizontal component of the geomagnetic field, this implies the operation of a process related to variations in atmospheric ionisation. Furthermore, the latitudinally symmetrical pattern and simultaneous development of cloud anomalies across both northern and southern high latitude regions during the composite period provides another

strong indication of a forcing agent external to Earth's environment, as no known internal process could produce such a pattern of variability.

Numerous studies have identified relationships between cloud/atmospheric parameters and the GCR flux/ionisation changes over high latitude regions in the Arctic and Antarctic (e.g. Veretenenko and Pudovkin, 1994; Pudovkin et al., 1996; 1997; Egrova et al., 2000; Mironova and Pudovkin, 2005; Mironova et al., 2008). Such regions may be particularly sensitive to GCR related ionisation changes, as they are undergo relatively large variations in atmospheric ionisation as a result of GCR variations (due to their weak geomagnetic shielding). In addition, high latitude environments have relatively clean and unpolluted atmospheres; this potentially makes clouds over such locations sensitive to small changes in CCN concentrations. The results of the GI sample appear to confirm notions that high latitude regions are sensitive to GCR variations. These results provide highly robust evidence of a link between the GCR flux and cloud cover.

Global scale observations of cloud changes are not well suited to determine detailed information about the microphysical mechanisms responsible for the observed cloud changes. However, aspects of the observed GCR–cloud relationship may provide general indications which may imply the action of a specific GCR–cloud process, for instance: the GI sample shows that cloud and GCR changes develop co-temporal; this suggests that if a causal relationship exists between the GCR and cloud changes, the process involved has a rapid (same-day) response time. The IMN (clean-air) mechanism has a response time which is estimated to range from around 6 hours to several days (Kazil et al., 2008; Mironova et al., 2008), while the GEC (near-cloud) mechanism appears to have a rapid response time (on the timescale of minutes) (Rycroft et al., 2008; Harrison and Ambaum, 2009); this implies that a GEC mechanism is most likely. Further indications of a mechanism may also be drawn from the spatial nature of the cloud changes: while the efficiency of IMN processes varies with latitude due to ion production, it is also additionally constrained by precursor aerosol concentrations. It is predicted that an effect resulting from changes in CCN concentrations due to IMN may show its strongest effects over low-altitude relatively clean marine environments (Kristjánsson and Kristiansen, 2000), whereas, it could be expected that a GEC process may be most influential at locations where atmospheric ionisation changes are strongest. Overall, this implies that if the observed cloud changes are causally related to GCR variations, then it is likely that the responsible mechanism is related to the GEC.

5.3 AI sample: GCR, IMF and irradiance variations

During the AI sample, the rate of GCR flux showed a prolonged decrease (of around -5±0.1 %) between days -9 to -3. These changes were statistically significant on days -5 and -4. After day -3, the rate of GCR flux increased until the key date (recovering by around 3.5±0.1 %) and showed statistical significance on days 0 and 1 (figure 5.10).

The B_z component of the IMF showed no statistically significant variations over the composite, although it did show a negative (southwards) increase around day -4, which was then followed by positive (northwards) changes peaking on the key date, however these anomalies did not show any statistical significance). Similarly, the B_y component underwent a negative (westwards) increase around day -4, after which time positive (eastwards) increases occurred, peaking on day 1 of the composite. The B_y changes were found to be statistically significant on days -4 and 1 (figure 5.11).

Variations in F10.7 and UV over the composite period were found to be non-significant. F10.7 changes showed a prolonged increase from days -10 to 2 (figure 5.12A). Whereas changes in the solar UV component were more variable, lacking in any coherent variations around the key date (figure 5.12B). Temporal coverage of the IMF, UV and F10.7 datasets is detailed in table 5.4. Considering the GCR, IMF and irradiance variations together, these results indicate that only variations in the rate of GCR flux showed a statistically significant change during the key date of the AI sample.

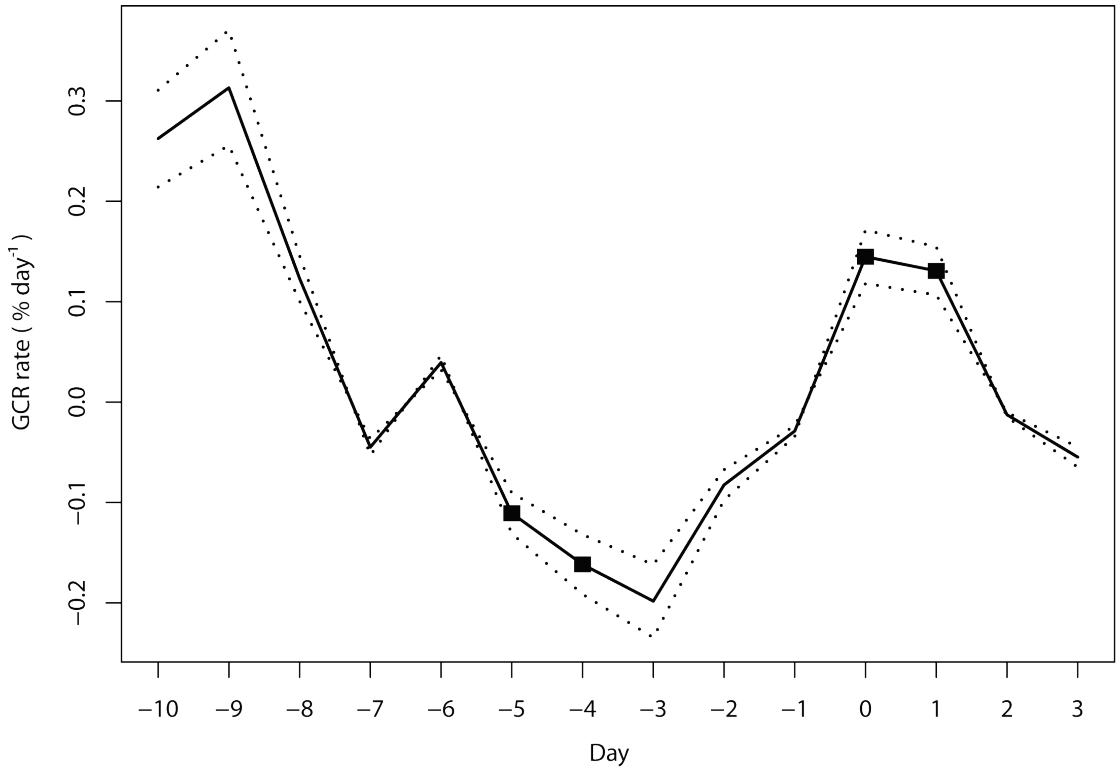

Figure 5.10 AI sample: rate of GCR flux

The rate of GCR flux is calculated from daily average neutron counts (drawn from 9 out of 11 neutron monitor sites, see table 5.1). Units are calculated as a percentage relative to the peak-to-peak variations experienced over an 11-year solar cycle. Statistically significant changes are indicated by markers. The confidence interval at the 0.95 level is shown by the dotted lines.

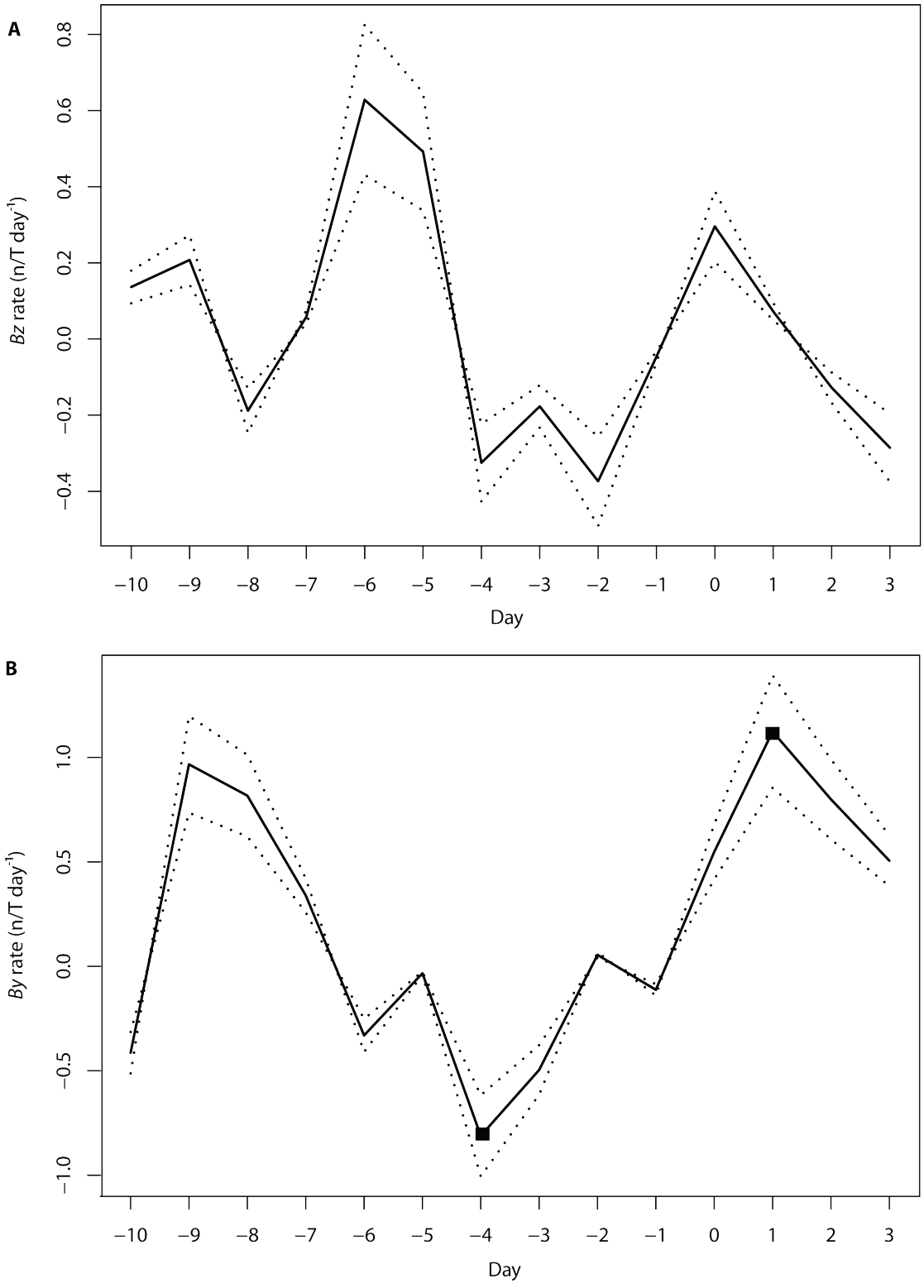

Figure 5.11 AI sample: IMF variations

Average rate of IMF **A)** B_z and **B)** B_y components over the AI sample. Dotted lines indicate the 0.95 confidence interval. Statistically significant changes are indicated by markers.

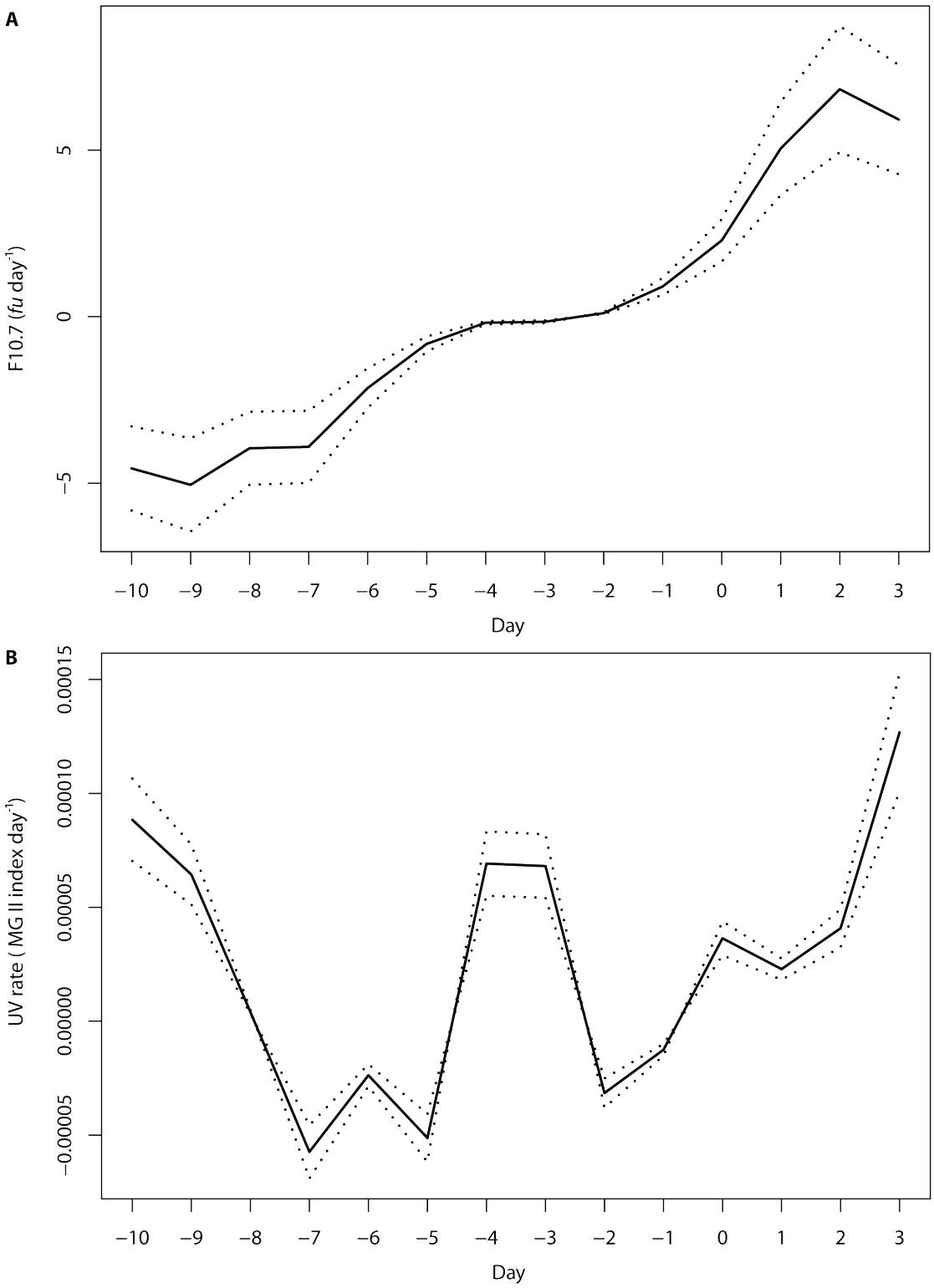

Figure 5.12 AI sample: solar activity variations

Average rate of **A**) F10.7 (10.7 cm 2800 MHz radio flux) and **B)** UV (MG II index) variations over the AI sample. Dotted lines indicate the 0.95 level confidence interval.

Parameter	Data coverage (%)
IMF B_y	59
IMF B_z	34
UV	81
F10.7	44

Table 5.4 AI sample IMF, UV and F10.7 data coverage

Data coverage over the AI sample expressed as a percentage.

5.3.1 AI sample: anomalous cloud changes

A plot of globally-averaged anomalous cloud changes occurring over the sample period shows a statistically significant anomalous decrease in globally-averaged high level cloud cover (of around -0.8 %) occurring between days -6 to -4 (figure 5.13). After day -4, the statistically significant cloud anomalies reverse sign and show a mid- to high level cloud cover increase of 2.4 %, centred around the key date of the composite. Both the decreases and increases in globally significant cloud change show a positive relationship to statistically significant co-temporal anomalous GCR variations.

It appears that the statistically significant average cloud cover anomalies are restricted to high southern latitude regions (figure 5.14). A vertical profile of the anomalous cloud changes during the key date shows that the significant cloud anomalies occur at 90°S–60°S between approximately 10 and 500 mb; this interval roughly spans from the tropopause to the surface of the Antarctic plateau (figure 5.15).

A pixel by pixel analysis of the locally significant anomalous cloud changes on the key date of the composite shows that intense locally significant anomalies are widespread across the Antarctic region. These anomalies are found to be most intense near the interior of the continent (around 38%) and appear to diminish with decreasing latitude. Some positive anomalies (of up to 8 %) are also identified over high latitudes of the South Pacific and around regions of the southern Australian coast (figure 5.16–5.17).

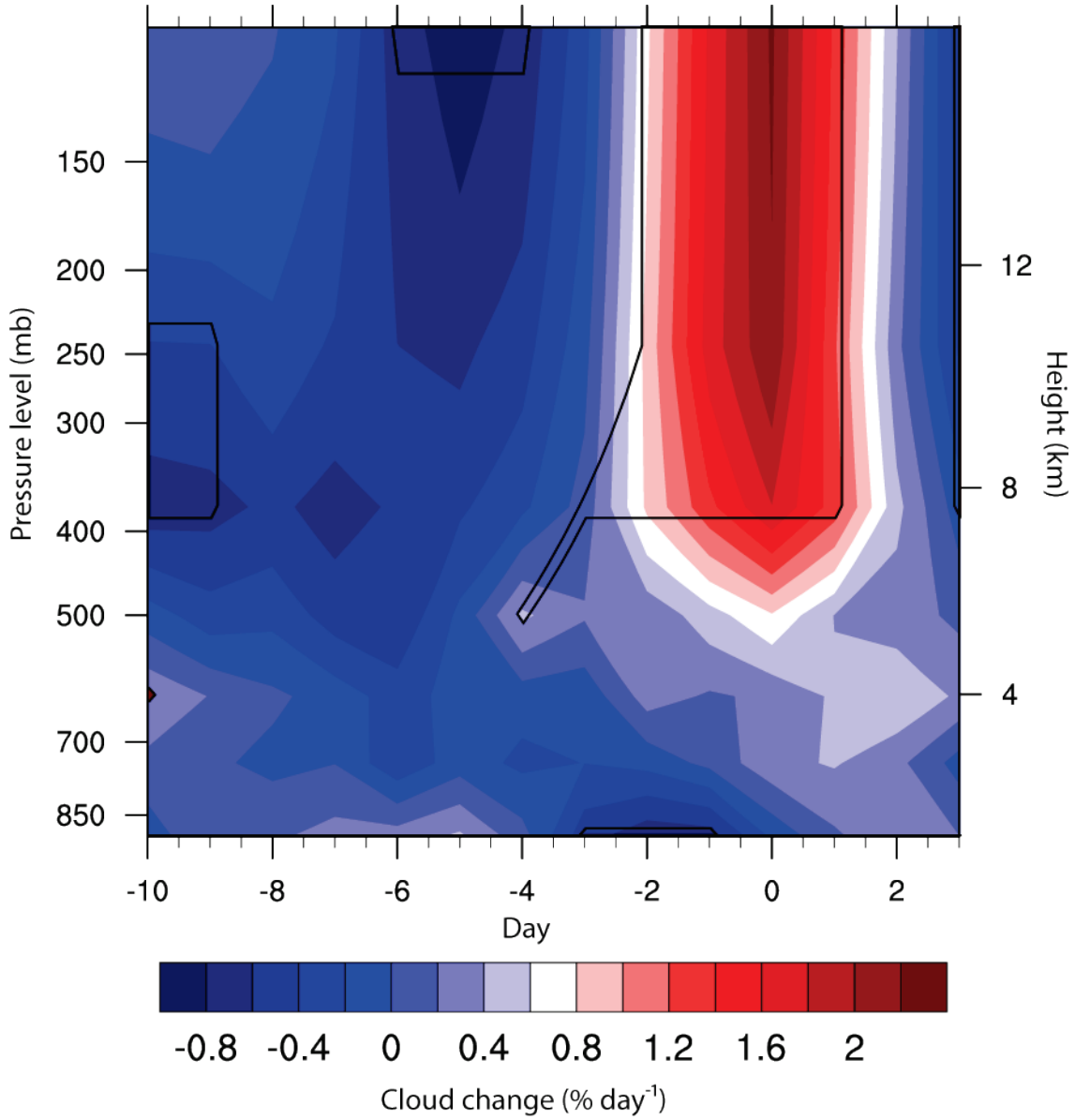

Figure 5.13 AI sample: globally-averaged cloud anomalies

Anomalous cloud changes occurring across globally-averaged pressure levels between 10 and 1,000 mb, as a function of time. Statistically significant changes are indicated by solid contours.

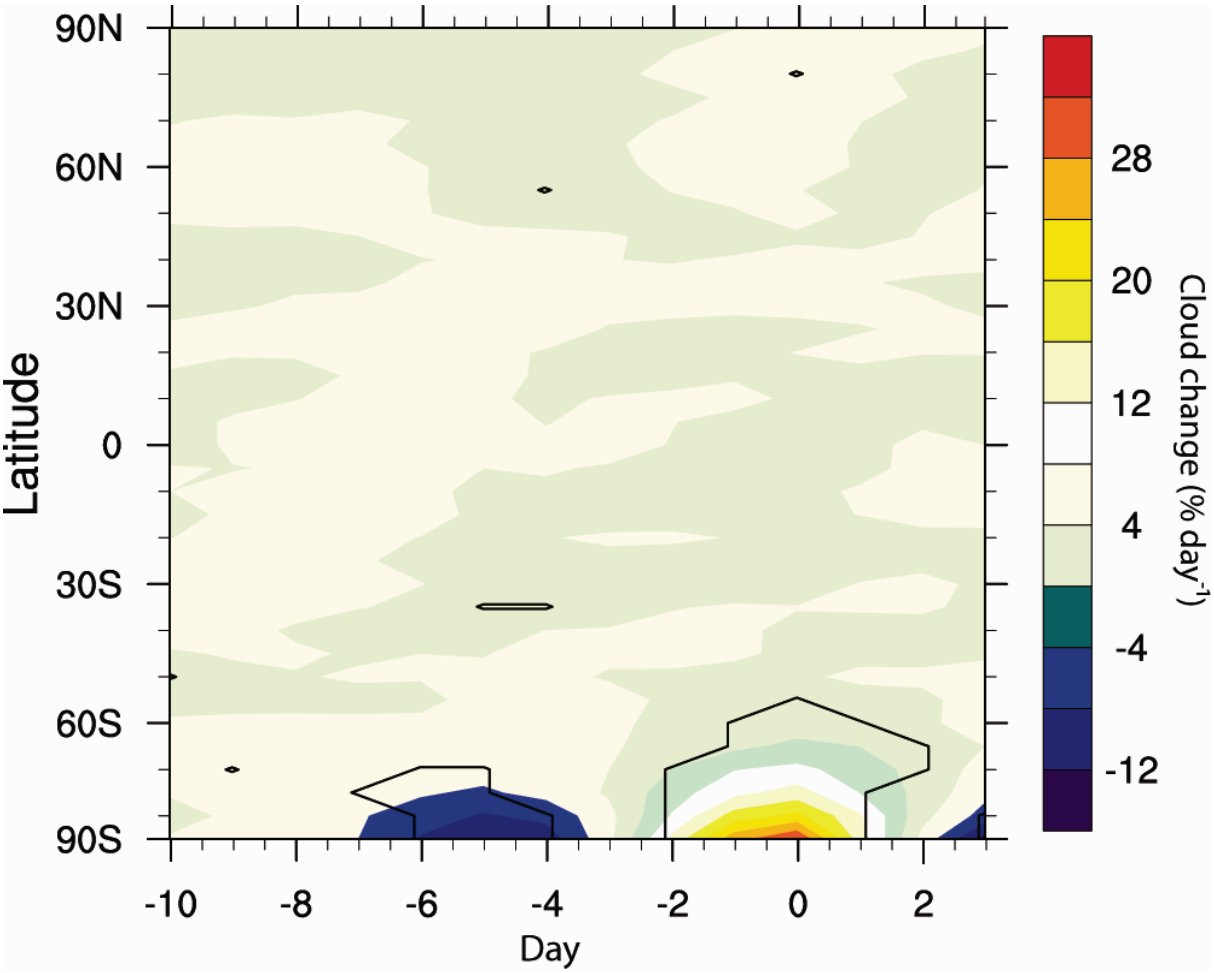

Figure 5.14 AI sample: cloud anomalies (latitude/time)

A plot of 5° latitudinally-averaged anomalous cloud changes (10–1,000 mb) occurring over the composite period. Statistically significant changes are indicated by solid contours.

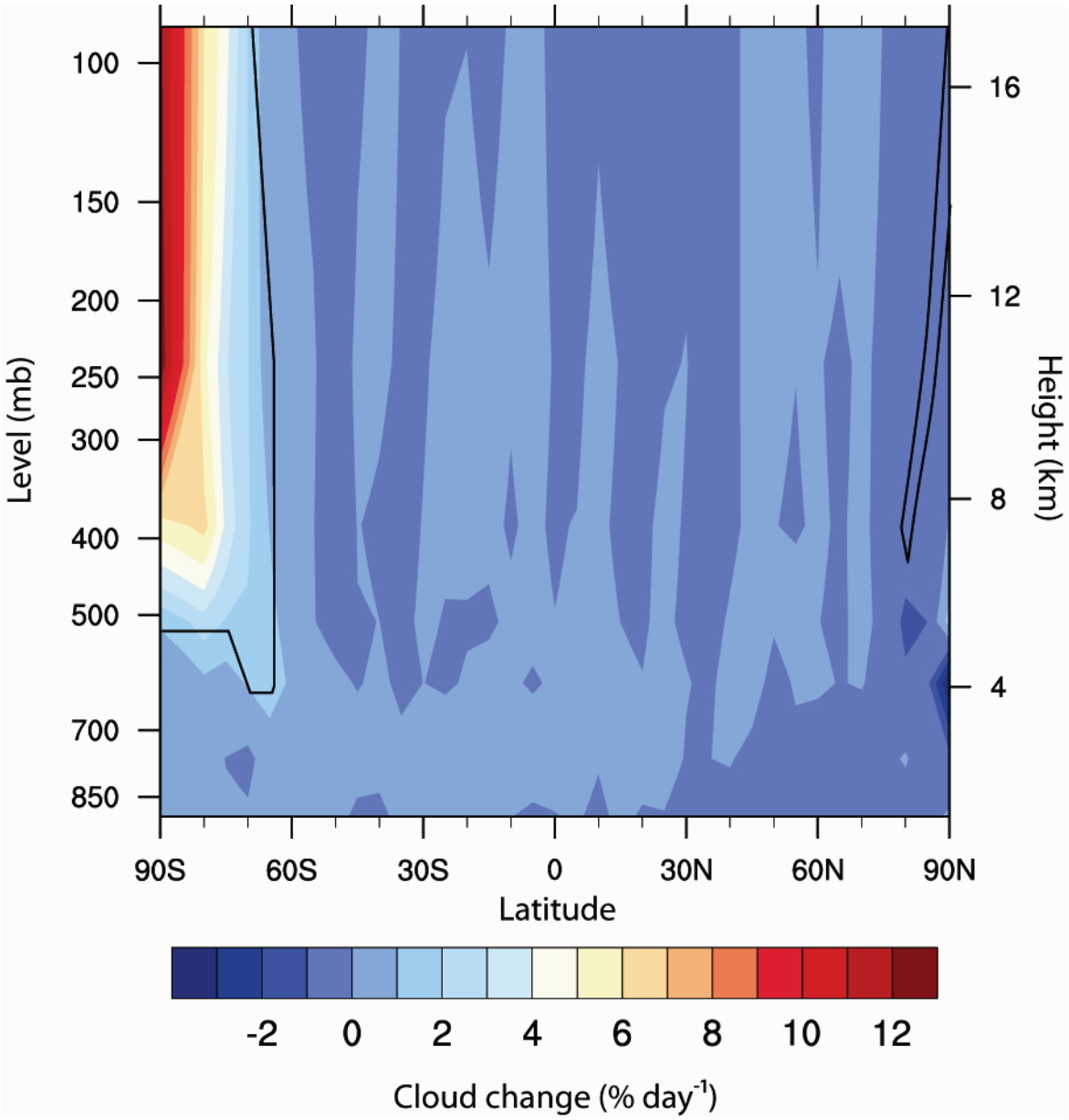

Figure 5.15 AI sample: cloud anomalies (pressure level/latitude)

A vertical profile of 5° latitudinally-averaged anomalous cloud changes (10–1,000 mb) occurring during the key date of the AI sample. Regions of statistically significant changes are indicated by solid contours.

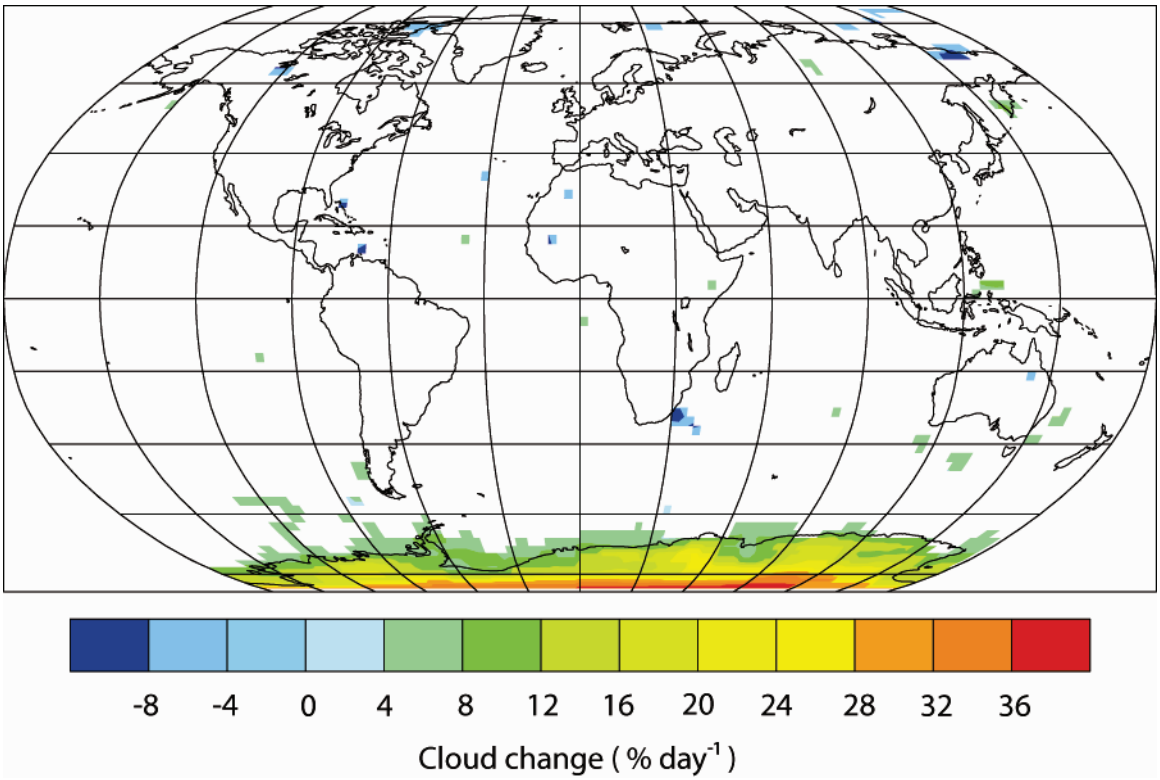

Figure 5.16 AI sample: global cloud anomalies

A Robison projection of anomalous cloud changes (10–1,000 mb) occurring on the key date of the AI sample. Only locally statistically significant changes are displayed.

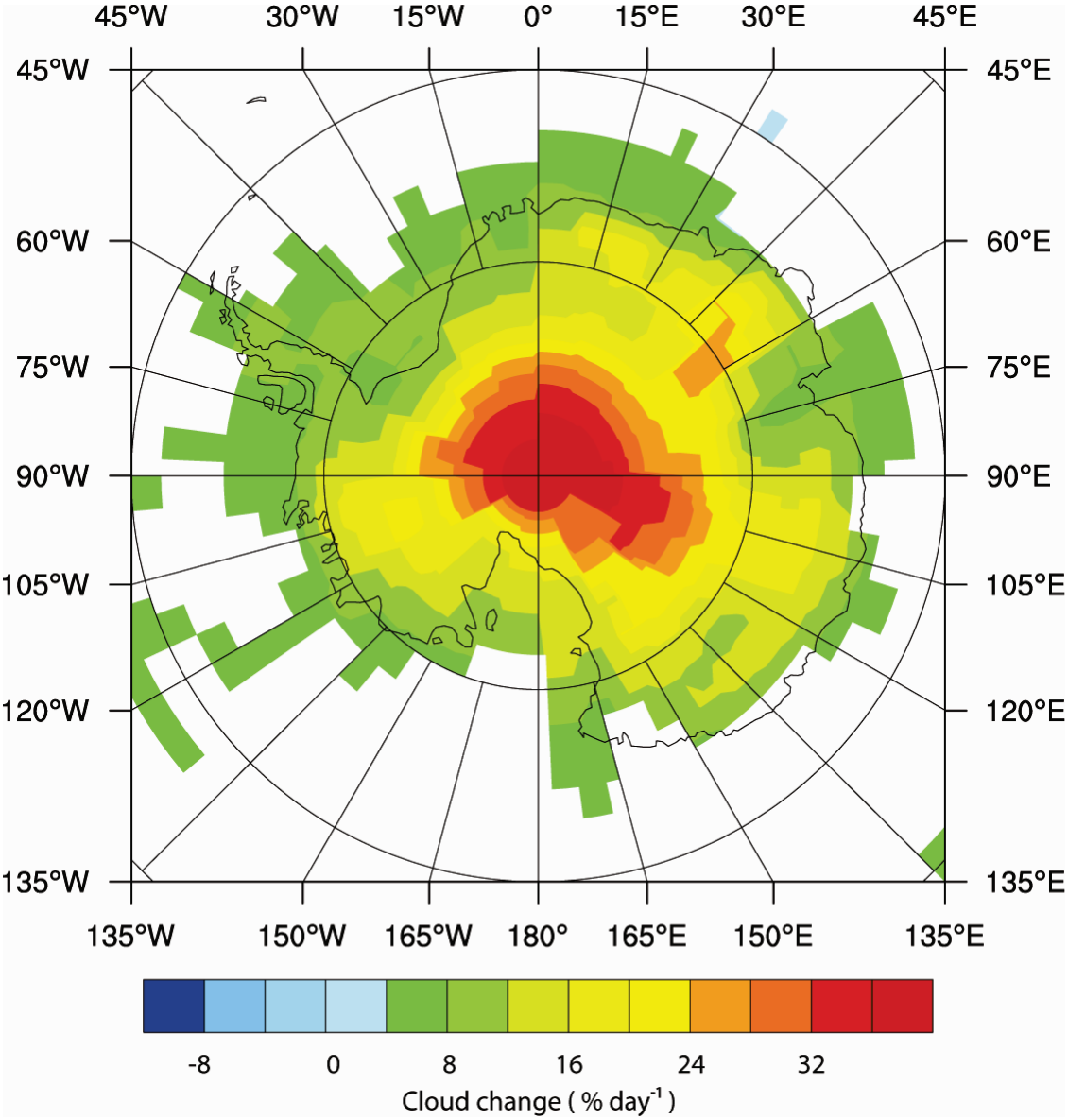

Figure 5.17 AI sample: Antarctic cloud anomalies

A polar stereographic of anomalous cloud changes (10–1,000mb) occurring on the key date of the AI sample. Only locally statistically significant changes are displayed.

5.3.2 AI sample: discussion

The AI sample identifies a statistically significant positive co-temporal relationship between variations in the rate of GCR flux and anomalous cloud changes over the Antarctic region. The previous GI sample showed a comparable relationship between Antarctic cloud and the GCR flux. However, the GI sample also showed corresponding Arctic cloud changes, whereas the AI sample does not. Several possibilities may explain the independent nature of the Antarctic cloud response:

1) There is no causal relationship between the observed cloud changes and the GCR flux.

2) A relationship between the GCR flux and cloud changes is strongly controlled by internal factors. For example, the relative differences in the height of the troposphere over the Antarctic/Arctic regions may be an important factor: low energy GCRs may ionise the upper atmosphere of high latitude regions, if such low energy GCRs are responsible for the observed GCR changes in figure 5.10 it may imply that a GCR related mechanism is unable to influence the relatively low altitude cloud cover over the Arctic region (which is predominately located below 500 mb). Whereas, the Antarctic cloud cover (which occurs between 10 and 500 mb) may be susceptible to modulation by the GCR flux (figure 5.18).

3) GCRs are acting to enhance seasonally high levels of cloud change. It has been observed that the AI sample demonstrates a seasonal distribution (figure 5.2); this may imply that GCRs may merely be acting to enhance natural variability (which in this instance has been isolated over the Antarctic region).

Antarctica has one of the cleanest atmospheres on Earth; this is largely due to consistent and intense circum-polar vortex which effectively isolates the Antarctic troposphere. This feature is not present in the Arctic, which in comparison to Antarctica has an abundance of aerosols. Such differences may also possibly account for varying responses between the northern/southern regions with respect to the same GCR forcing, for example, IMN requires low concentrations of pre-existing CN/CCN (to prevent loss by scavenging) (Carslaw et al., 2002), while changes in local resistivity in the GEC are highly sensitive to local aerosol concentrations (as aerosols scavenge ions and consequently increase atmospheric resistivity) (Harrison, 2004).

As discussed in the context of the GI sample, several authors have reported findings which suggest that high latitude atmospheres may be sensitive to changes in the GCR flux (Veretenko and Pudovkin, 1994; Pudovkin et al., 1996; 1997; Egrova et al., 2000; Mironova and Pudovkin, 2005). The results of the AI sample complement such notions. The same arguments made

during the GI discussion (section 5.2.2) regarding potential microphysical mechanisms responsible for the observed GCR–cloud relationship also applies over this sample: the rapid (same day) response time between GCR–cloud and localised nature to the cloud changes to regions sensitive to large GCR related changes in atmospheric ionisation again suggest the action of a GEC related mechanism.

The changes occurring in the IMF, irradiance and GCR variations occurring during the AI sample may possibly suggest a connection to the approximately 27-day solar (Carrington) rotation. Two pieces of evidence may support this hypothesis: (1) the approximately 12-day coherent increase in irradiance, which may arguably comprise a harmonic of the solar rotation and suggest a long-term change in solar activity is underlying the sample and, (2) statistically significant variations in B_y are seen to occur on day -4 and 1: from trough to peak these changes last approximately 5 days, this period is approximately another harmonic of the Carrington rotations. Furthermore, the B_y increases between day -4 and 1 are preceded by a 6 day decrease of comparable (but opposite) magnitude; *By* changes are often due to quasi-stable oscillations in association with Carrington rotations (or harmonics of this rotation) (Burns et al., 2007). These changes may give a tentative indication that the samples are reflecting short term solar maxima/minima resulting from the influence of Carrington rotations.

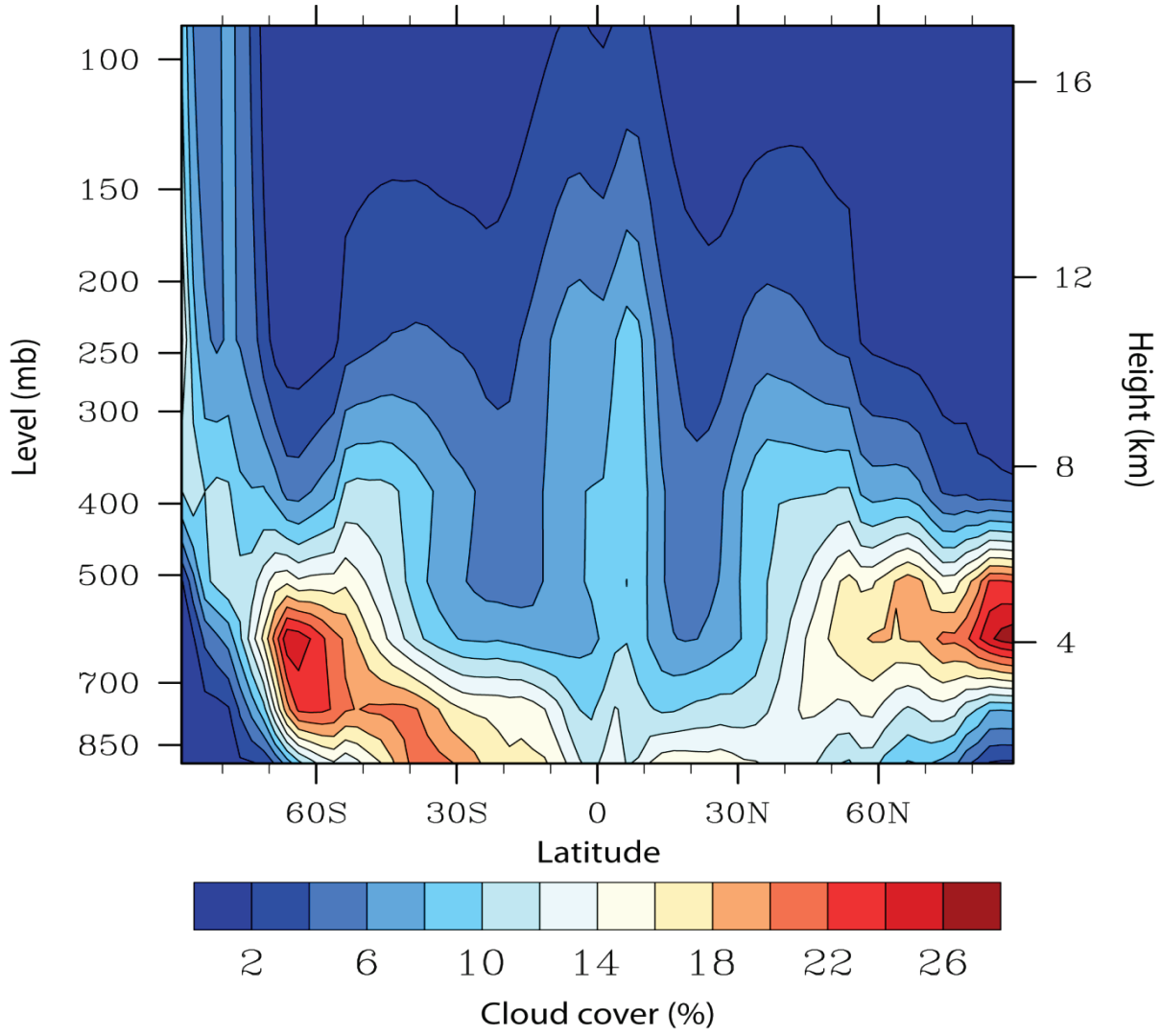

Figure 5.18 ISCCP cloud profile: latitude/height

A 5-year mean vertical profile of 5° latitudinally-averaged cloud cover distribution from ISCCP, using seven layers of IR-retrieved cloud amounts between 10 and 1,000 mb.

5.4 MLD sample: GCR, IMF and irradiance variations

During the MLD sample the rate of GCR flux demonstrated a statistically significant increase of approximately 3.3±0.2 % around day -5, after this time it then underwent a statistically significant decrease of approximately 5±0.1 % centred around the key date of the composite (figure 5.19). Over this period there was an increase in both the B_z and B_y components of the IMF. The B_z showed a sharp (but non-significant) peak of around 0.6 n/T between days -2 and 0, whereas the B_y underwent a more protracted increase, beginning on day -6 and peaking on day -1. The B_y changes were statistically significant on days -4 and -3 (figure 5.20).

F10.7 changes showed a decrease over the composite period of around -1 *fu*. These changes began on day -6 and reached a maximal decrease on day -1, these changes were not found to be statistically significant. The rate of UV output increased on the key date of the composite; however, these changes were not statistically significant (figure 5.21). The temporal coverage of the IMF, F10.7, and UV datasets is detailed in table 5.5.

GCR, IMF B_y and F10.7 variations appear to demonstrate broadly complementary changes over the key date of the composite: while F10.7 and GCR decrease, UV shows an increase in activity. Although the various solar parameters show indications of related variations, only the GCR demonstrates statistically significant changes on the key date of the MLD composite.

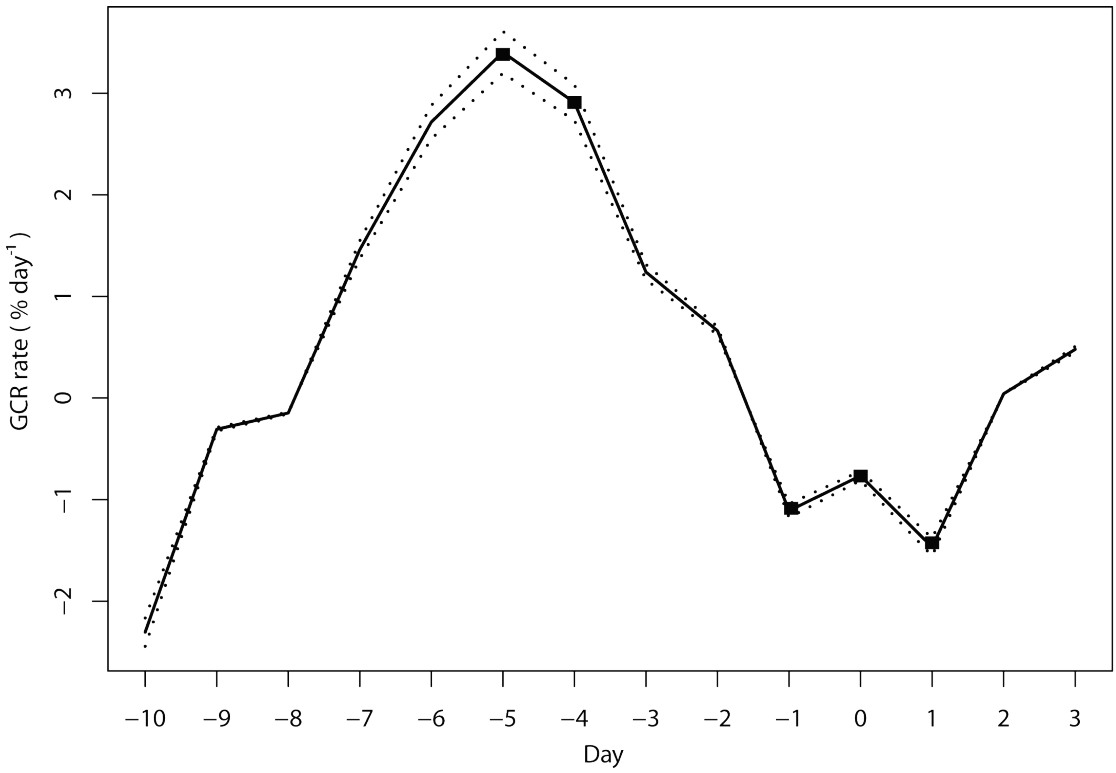

Figure 5.19 MLD sample: rate of GCR flux

Rate of GCR flux calculated from daily average neutron counts (drawn from 9 out of 11 neutron monitor sites, see table 5.1 for specific sites). Units are calculated as a percentage relative to the peak-to-peak variations experienced over an 11-year solar cycle. Statistically significant changes are indicated by markers. The confidence interval at the 0.95 level is shown by the dotted lines.

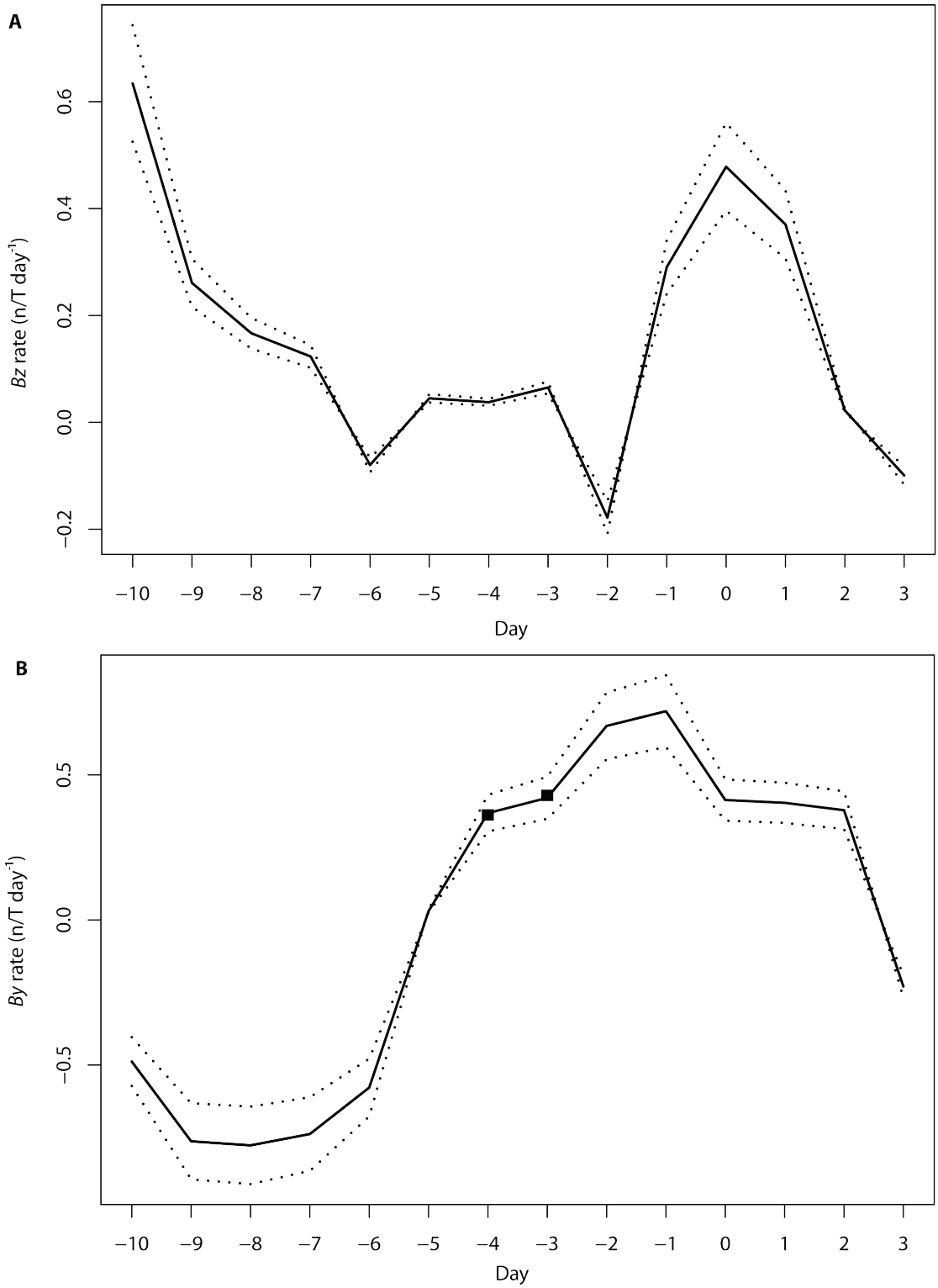

Figure 5.20 MLD sample: IMF variations

Average rate of IMF **A)** B_z and **B)** B_y components over the MLD composite. Dotted lines indicate the 0.95 level confidence interval. Statistically significant changes are indicated by markers.

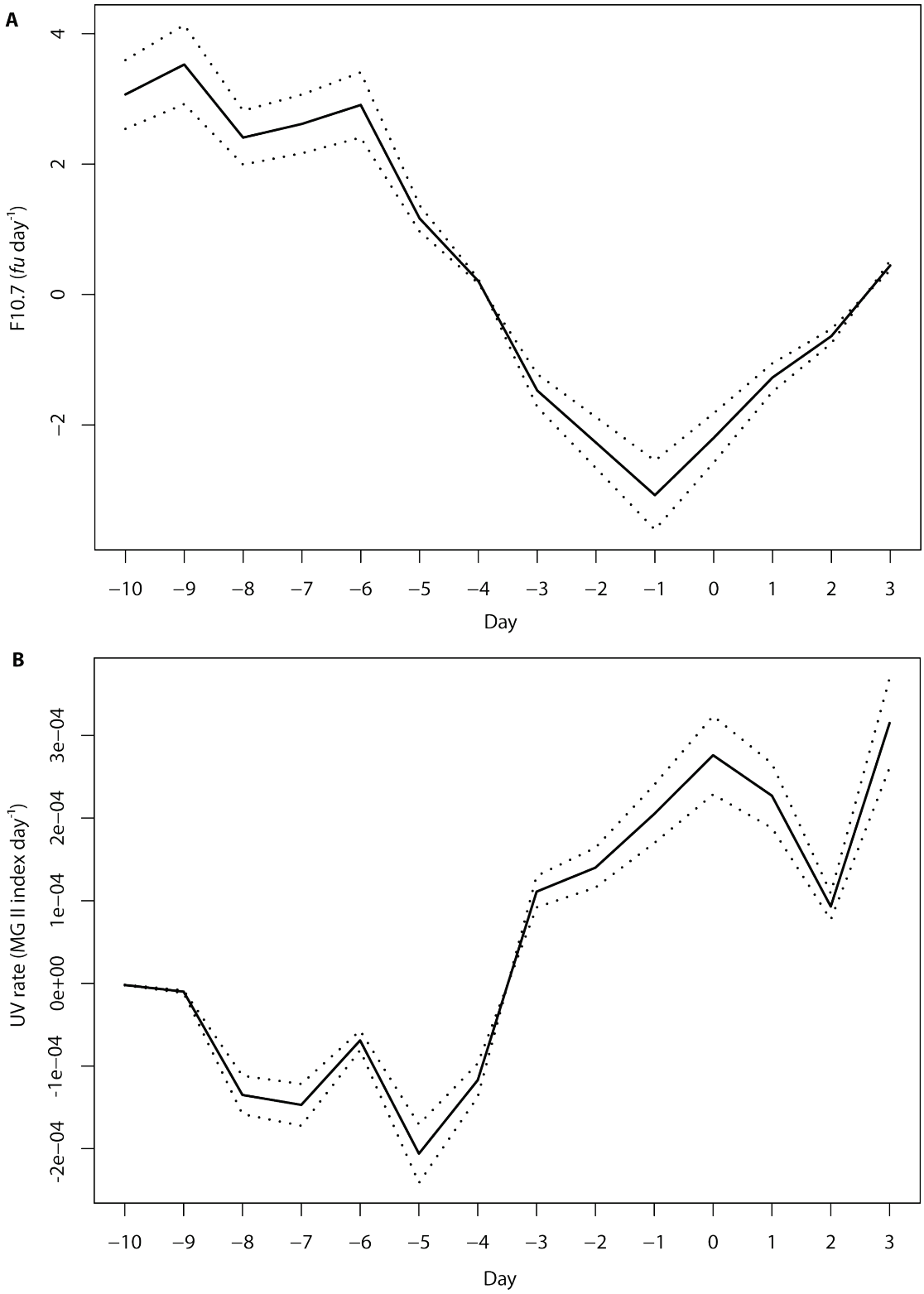

Figure 5.21 MLD sample: solar activity variations

Average rate of **A)** F10.7 (10.7 cm 2.8 GHz radio flux) and **B)** UV (MG II index) variations over the MLD composite. Dotted lines indicate the 0.95 level confidence interval.

Parameter	Data coverage (%)
IMF B_y	59
IMF B_z	42
UV	74
F10.7	42

Table 5.5 MLD sample IMF, UV, and F10.7 data coverage

IMF, UV and F10.7 data coverage over the MLD composite expressed as a percentage.

5.4.1 MLD sample: anomalous cloud changes

A plot of globally-averaged anomalous cloud changes occurring over the MLD composite period shows that statistically significant increases in the rate of cloud change (of approximately 0.6 %) are observed, centred around day -6 at mid-tropospheric levels (figure 5.22). These cloud changes correspond to a statistically significant increase in the rate of GCR flux. After day -2 the cloud anomalies were seen to reverse sign, reaching a maximal decrease on the key date of the composite of around -2 % (figure 5.22); these anomalies were observed to occur primarily at mid- to low tropospheric levels (between 500–1,000 mb) (figure 5.22). The statistically significant increases and decreases in cloud observed on days -6 and 0 show a positively correlated co-temporal relationship to statistically significant variations observed in the rate of GCR flux.

A plot of latitudinally-averaged cloud anomalies occurring over the sample period indicates that the statistically significant anomalies are concentrated at mid-latitude regions and show a remarkably symmetrical pattern of change about the equator. The statistically significant northern hemisphere anomalies ranged between approximately 60°N–20°N and demonstrated a bimodal peak at 50°N and 25°N of around -4 %. On the other hand, the southern hemisphere anomalies occurred between approximately 15°S–60°S and were concentrated around a single centre of activity located at 25°S (where anomalies of up to -5 % were observed). The positive anomalies around day -5 appear to be far more limited in extent and magnitude than the subsequent key date changes (figure 5.23).

A vertical profile of the anomalous cloud changes occurring during the key date of the composite confirmed that statistically significant anomalies were predominately located at mid- to low tropospheric levels (figure 5.24). The most intense cloud changes across both

hemispheres were found to occur at approximately 800 mb. Interestingly, a moderately intense anomalous decrease in cloud is also apparent over high tropospheric (10–180 mb) levels at high southern latitudes; this change is similar to the AGD and adjusted FD samples, however this decrease is not statistically significant (figure 5.24).

A pixel by pixel analysis of the cloud changes occurring on the key date shows locally significant anomalies (of around -12%) that are widespread across the mid-latitudes over both land and sea (figure 5.25). The sign of cloud changes observed on the key date is not found to be unidirectional; several spatially limited but intense areas of locally significant anomalous increases in cloud formation at low latitudes are also observed of up to 10 % (figure 5.25). To understand the detected changes, a plot of all anomalous cloud changes (significant and non-significant) is presented (figure 5.26A) along with the climatology of the key date cloud cover (figure 5.26B). The patterns and positions of the intense low latitude anomalous cloud increases are suggestive of cyclonic activity, indicating that the composite has not been fully successful at isolating atmospheric variability from the sample. However, an area averaged plot of cloud anomalies occurring over the MLD composite period for differing land cover regions over mid-latitude zones (Pacific, Atlantic and land) shows, that on average, all areas demonstrated a comparable pattern of cloud change (figure 5.27).

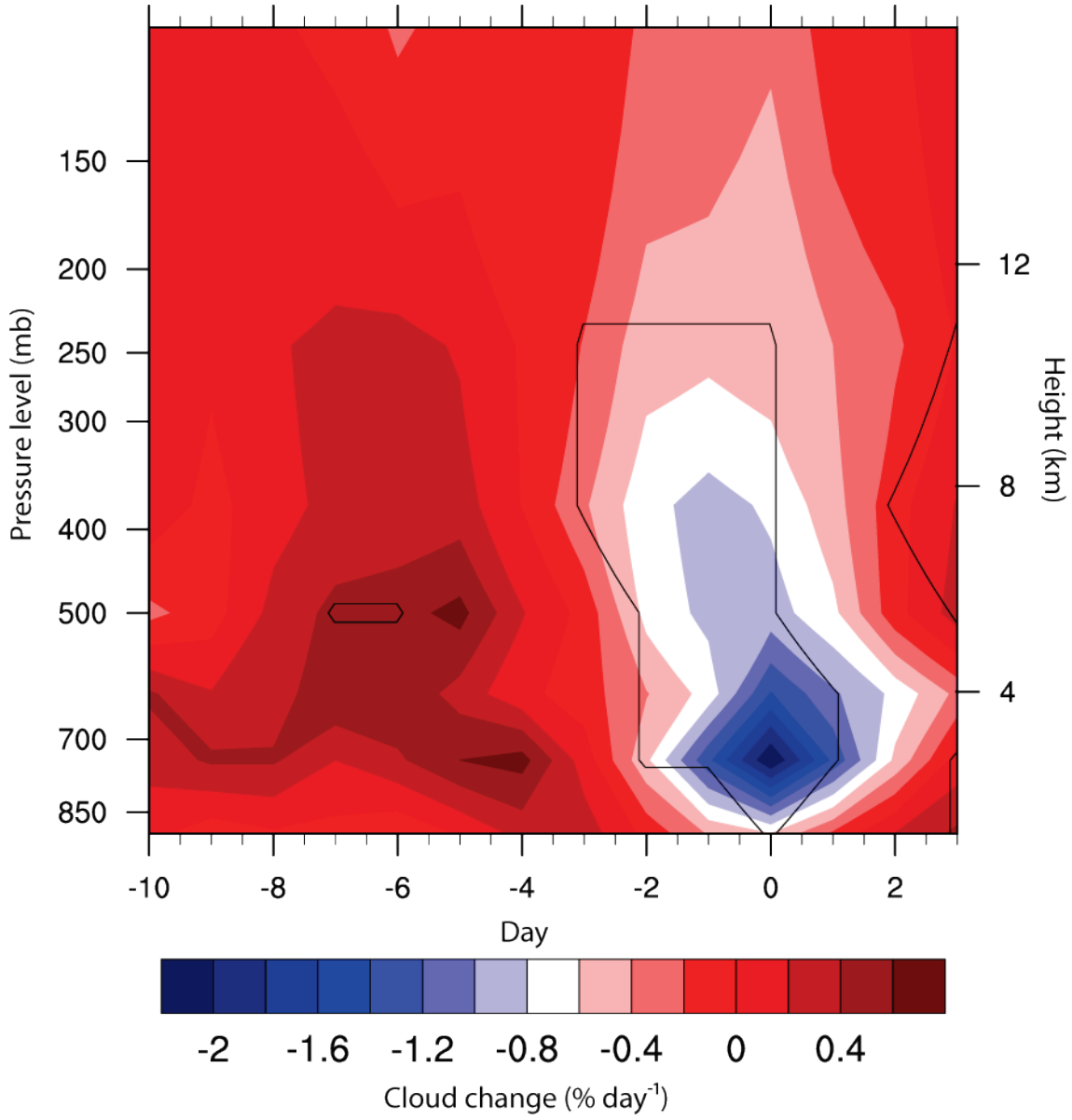

Figure 5.22 MLD sample: globally-averaged cloud anomalies

Anomalous cloud changes, occurring across globally-averaged pressure levels between 10 and 1,000 mb as a function of time. Statistically significant changes are indicated by solid contours.

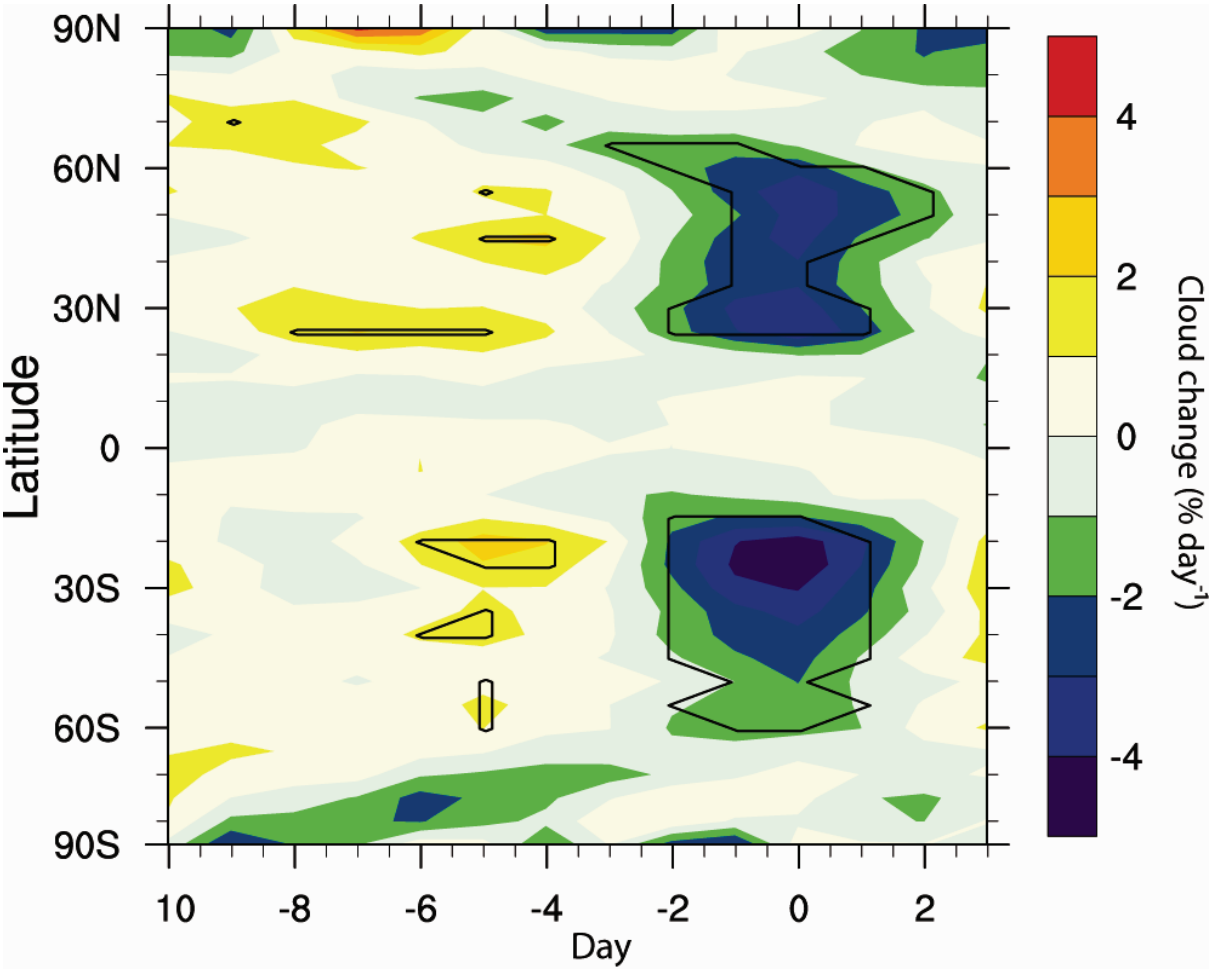

Figure 5.23 MLD sample: latitude/time cloud anomalies

A plot of 5° latitudinally-averaged cloud anomalies (10–1,000 mb) over the composite period. Statistically significant changes are indicated by solid contours.

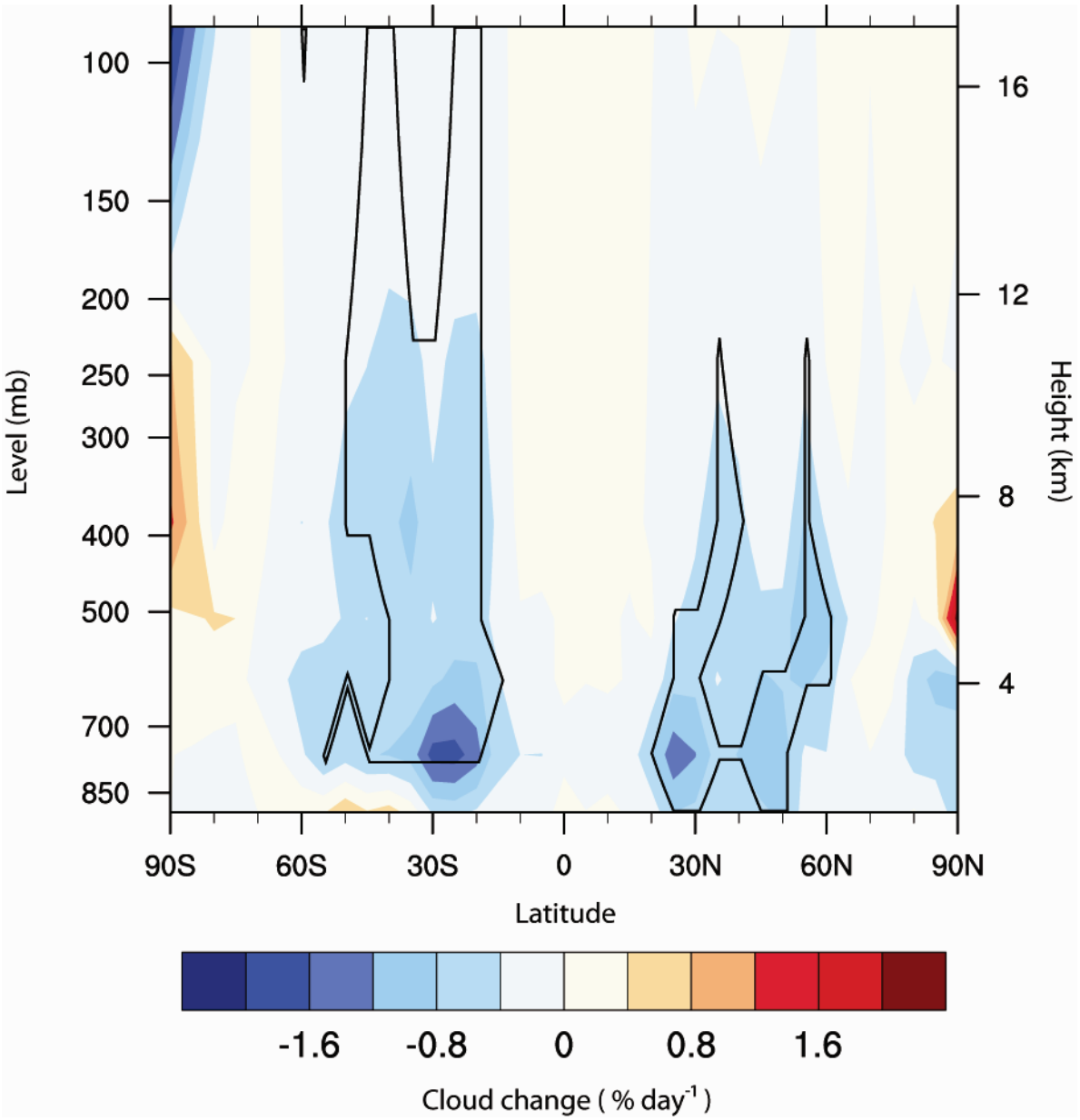

Figure 5.24 MLD sample: pressure level/latitude cloud anomalies

A vertical profile of 5° latitudinally-averaged anomalous cloud changes (10–1,000 mb) occurring on the key date of the MLD sample. Regions of statistically significant changes are indicated by solid contours.

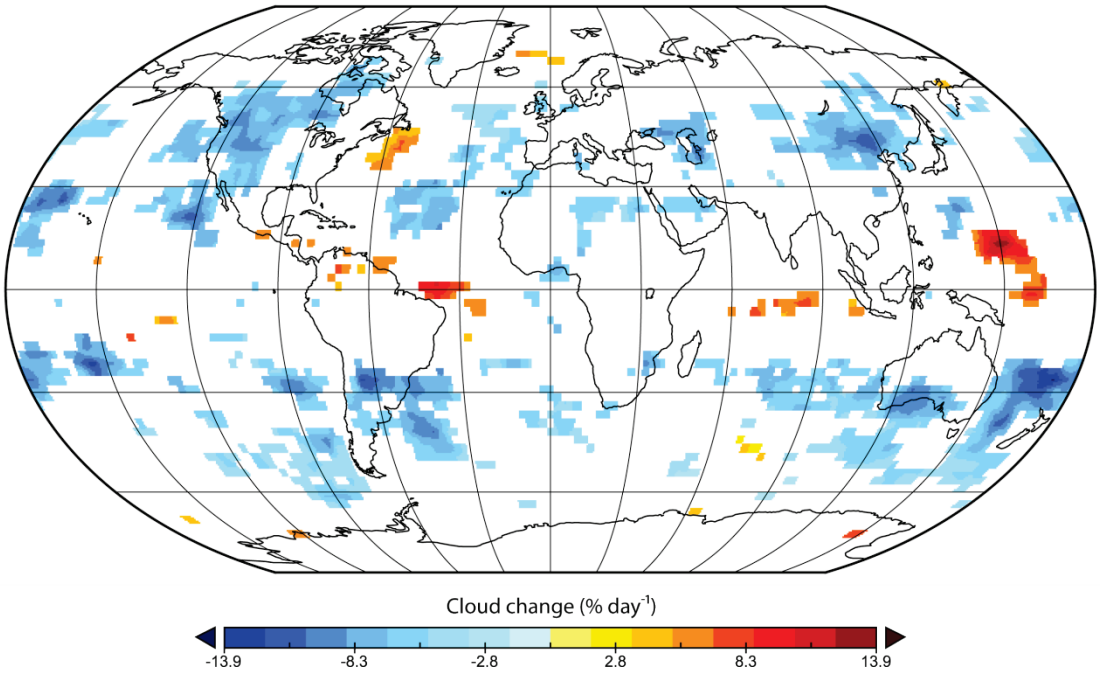

Figure 5.25 MLD sample: locally significant cloud anomalies

A Robinson projection of locally significant anomalous cloud changes (10–1,000 mb) occurring on the key date of the MLD sample.

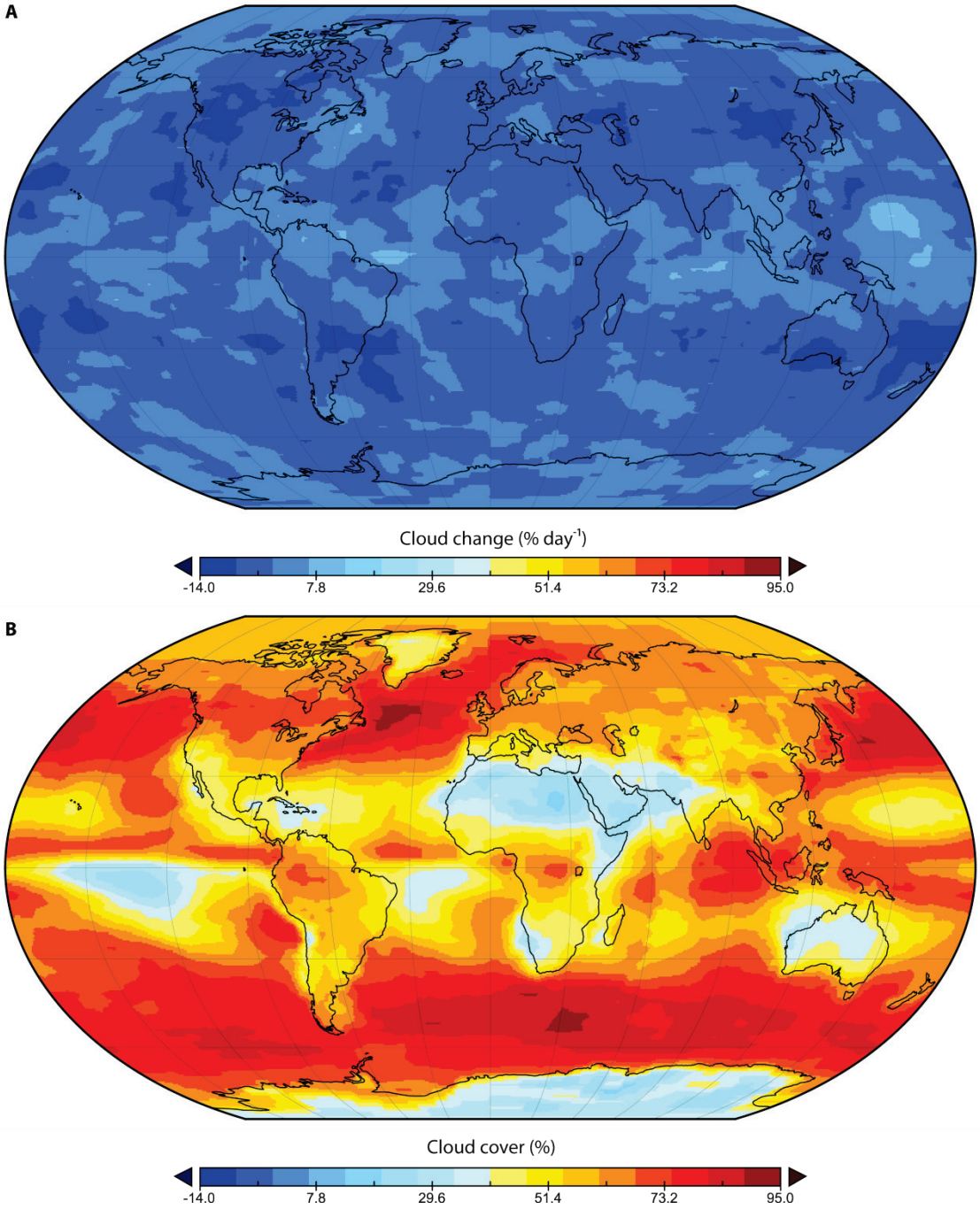

Figure 5.26 MLD sample: global cloud anomalies

A) Robinson projection of mean anomalous cloud changes (10–1,000 mb) occurring on the key date of the MLD sample. All anomalies are displayed regardless of statistical significance. **B**) average cloud cover (10–1,000 mb) on the key date of the MLD composite.

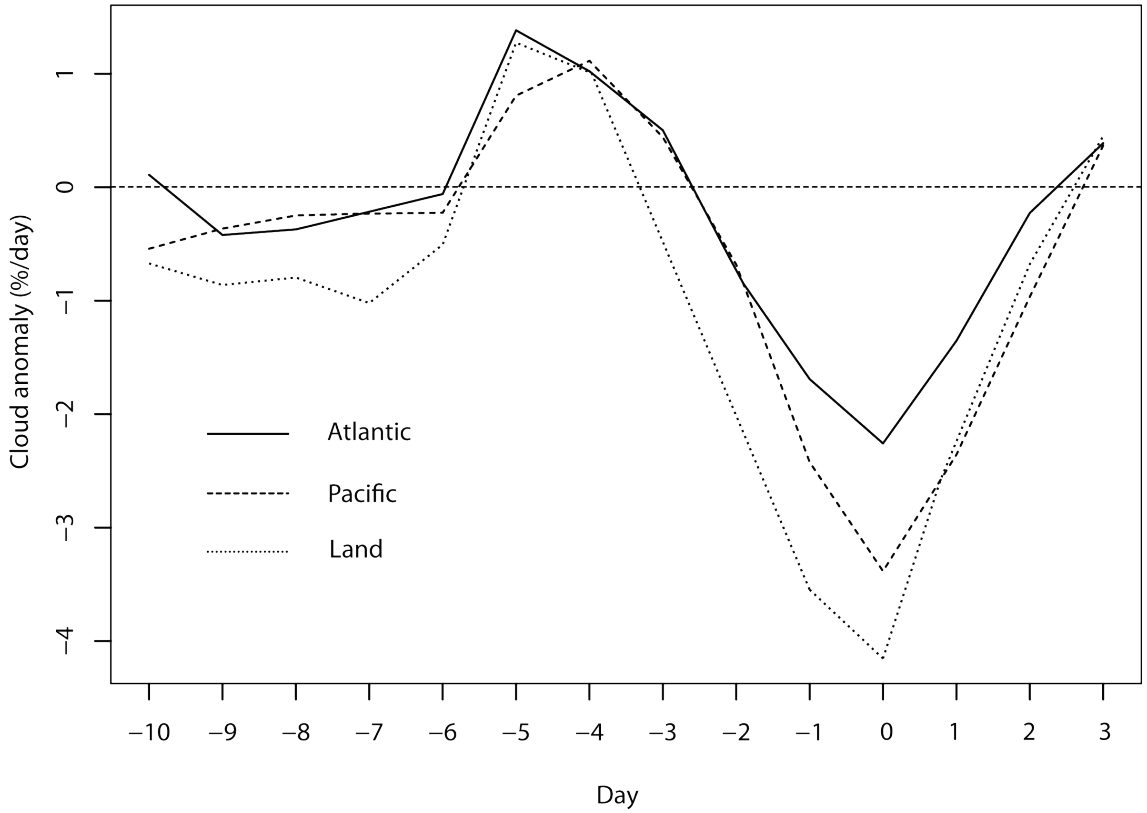

Figure 5.27 MLD sample: Pacific, Atlantic and land area cloud

Area-averaged cloud anomalies in mid-latitude zones over the MLD composite period, for Pacific, Atlantic and land area pixels. Cloud anomalies are calculated between 10 and 1,000 mb.

5.4.2 MLD sample: discussion

In agreement with the previous GI and AI samples, the MLD sample identified a statistically significant positive co-temporal relationship between the rate of GCR flux and cloud anomalies. In this instance, the anomalies were located at mid- to low tropospheric levels over mid-latitude regions. Past studies have suggested the existence of a relationship between mid-latitude regions and the GCR flux, for example: Harrison and Stephenson (2006) identify a small but statistically significant relationship between the GCR flux and the diffuse fraction (DF) measured from UK meteorological sites. While studies by Tinsely and Deen (1991) and Veretenenko et al. (2005) have suggested that GCRs may enhance the activity of mid-latitude cyclones during winter months. In addition, the work by Kniveton and Todd (2001) shows a positive relationship between the GCR flux and precipitation/precipitation efficiency over mid-latitude storm track regions. The locally significant cloud anomalies seen in the MLD sample do not appear to be directly located over storm track regions, in fact several centres of activity are

located in prominent semi-permanent high pressure blocking regions (such as the North American high, and Siberian High).

An analysis of the annual distribution of the MLD sample key dates indicates that the sample has a bimodal nature, peaking at around the time of the solstices. This complements the findings of Tinsley and Deen (1991), who's work indicates that significant decreases in mid-latitude cyclonic activity are correlated with significant reductions in the rate of GCR flux during northern and southern hemisphere winter months. Tinsley and Deen (1991) suggest that the mechanism controlling this relationship is electrofreezing: a GEC related process which influences the growth and development of ice crystals within high level clouds, which in turn are capable of glaciating mid-level clouds in cyclonic systems (via a seeder-feeder process) (Tinsley, 2000).

It is possible that the cloud anomalies shown over the MLD sample may be attributable to a direct IMN effect. A recent study has proposed an interesting mechanistic insight into how IMN may affect cloud changes over sensitive (aerosol impoverished) regions which may be of relevance to the observations presented here: it has been suggested that Rayleigh-Bérnard (RB) convection cell cloud systems (located in the high-pressure return-flow regions of the Hadley cells) may be highly sensitive to changes in cloud condensation nuclei (CCN) (Rosenfeld et al., 2006) and that differences in CCN concentrations may drive a change from closed state to open state RB cells, varying the amount of cloud over mid-latitude regions. As IMN processes are most likely to be significant over aerosol impoverished clean-air oceanic regions (such as those where RB cells are located) (Yu et al., 2008), potential changes in CCN populations by IMN processes over mid-latitude oceanic regions may potentially play a role in regional cloud modulation. Although the response also depends on several factors including: the state of low latitude thunderstorm generators; the local profile of aerosols and radon; and, whether ice or warm-cloud processes are locally dominant. Furthermore, it is theoretically implausible that a GEC mechanism is influencing the observed MLD cloud anomalies for the following reason: after decreases in the GCR flux atmospheric ionisation is reduced; the magnitude of this reduction corresponds to Earth's geomagnetic field strength and is therefore largest at high latitudes weakest at low latitudes (Hays and Roble, 1979). As a consequence of the non-uniform nature of the increased atmospheric resistivity, J_z is diverted from high latitudes to lower latitudes. This results in a decrease in J_z at high latitudes during GCR decreases, but an increase in J_z at low (< 50°) latitudes (Sapkota and Varshneya, 1990, Tinsley and Yu, 2004). Thus during the MLD sample, it is likely that J_z increases are occurring at mid- to low latitudes during the key date of the sample; these changes are of the incorrect sign to account for cloud decreases. A review and discussion of these findings are presented in Laken et al. (2010).

5.5 General discussion

Objective 1: *To test for the existence of a relationship between clouds and the GCR flux using a methodological approach based on the composite sampling techniques of past daily timescale GCR studies.*

The composite methodologies previously utilised in FD-based analysis have been modified to create a sampling regime based on internal (cloud) datasets. From this novel sampling basis, a number of composites have been selected which identify a statistically significant, positive, co-temporal relationship between cloud anomalies and variations in the rate of GCR flux, successfully meeting the requirements of objective 1.

The relationships identified, suggest the occurrence of two seemingly different cloud responses: (1) *A high latitude/mid- to high level cloud response*. For the GI and AI samples the cloud anomalies are found to be largest at high latitude regions; this may imply a connection between the observed anomalous cloud changes and variations in atmospheric ionisation (occurring during changes in the rate of GCR flux); this potentially implies that a GEC related mechanism is responsible for the observed effects. (2) *A mid-latitude/mid-to low-level cloud response*. The MLD sample shows cloud changes occurring at low tropospheric levels over mid-latitude regions in association with changes in the rate of GCR flux. Past studies have suggested that low tropospheric levels may be key areas with regards to the expression of a GCR–cloud link (Marsh and Svensmark, 2000; Pallé et al., 2004a). This effect is thought to be most relevant over clean environments with relatively low abundances of tropospheric aerosols (Kristjánsson and Kristiansen, 2000; Rosenfeld et al., 2006). The identification of statistically significant anomalous cloud changes over mid-latitude/low-level regions may imply an IMN effect (although the inefficacy of this process has been suggested by several studies (Carslaw, 2009)).

Alternatively, decreases in mid-latitude cloud cover may also relate to the GCR flux via microphysical cloud changes mediated by a GEC mechanism. Like-sign charges are conferred upon cloud droplets and aerosol particles at the boundaries of clouds as a result of current flow in the GEC. This produces both long-range repulsive forces (termed electro-anti-scavenging) and short-range attractive forces (termed electro-scavenging). For small cloud droplets with a radius <0.05 μm, electro-anti-scavenging processes dominate. This reduces the collision efficiency below normal levels, resulting in a decrease in the growth of cloud droplets. However, for larger droplets (with a radius >0.05 μm) electro-scavenging processes dominate: the attractive, short-range, electrical image forces increases the collision rates of the cloud droplets. Consequently, the net droplet growth resulting from changes in droplet charging is a function of the droplet size distribution within the clouds. If larger (>0.05 μm radii) droplet

particles dominate the clouds present in the MLD sample, then a reduction in cloud amount may feasibly result from a decrease in electro-scavenging processes which may theoretically occur during a reduction in the rate of GCR flux (Zhou et al., 2009).

While variations in the rate of GCR flux occurring over the FD-based studies in chapter 4 were related FD events, the AI and MLD samples may show indications of a relationship to short term minima/maxima in solar activity connected to the 27-day solar (Carrington) rotation. Indications of this are found in the linked responses of the IMF, UV and F10.7 changes, which may possibly show a harmonic relationship to Carrington rotation periods.

Large and often statistically significant variations in the rate of cloud change of opposite sign appear to occur several days in advance of the key date of each sample. These alternate sign anomalies may simply be a consequence of the sampling approach: essentially, the process of compositing the largest cloud changes may have produced this pattern of change because the dates of most rapid cloud increase (decrease) are likely to follow a lull (increase) in activity. Over most of the samples, both the alternate sign cloud changes and the key date cloud changes are found to develop co-temporally with statistically significant variations in the rate of GCR flux.

The observed variations in the rate of GCR flux occurring during the MLD sample and AI sample are roughly inverse: the MLD sample experiences an increase in the rate of GCR flux around day -5 and is immediately followed by a decrease which persists until the key date, whereas, the AI sample undergoes a significant decrease in the rate of GCR flux at around day -5, followed by an increase in the rate of GCR flux on the key date. However, despite the similar (but inverted) nature of the rate of GCR flux, the centres of statistically significant anomalous cloud activity occur over differing regions. Several possibilities may account for this:

1) The cloud changes are unrelated to changes in the rate of GCR flux.
2) The cloud response is a second order phenomenon. The MLD and AI samples may demonstrate differing underlying conditions as a result of the seasonal distribution identified in the samples. This coupled with the fact that the samples are engineered identify extreme cloud anomalies over specified regions may account for the differing response.

As previously noted, the GI sample appears to be devoid of any apparent seasonal weighting to its distribution. The GCR variations observed over this sample show a clear a statistically significant peak in activity on the key date of the composite; no other solar activity parameter was found to demonstrate a similar change. Over the GI sample the anomalous cloud changes

demonstrate a strongly symmetrical nature of in both hemispheres, with the locally significant cloud anomalies decreasing in magnitude and extent towards low latitudes. These properties provide a strong indication that this sample has indeed identified a robust and reliable indication of the effect of changes in the GCR flux on cloud change. The GI sample indicates variations in cloud cover over regions such as the Arctic may be influenced by changes in the rate of GCR flux. However, significance testing of the largest Arctic cloud changes indicates no statistically significant relationship to GCR (table 5.2). If it is assumed that GCR variations do influence cloud over the Arctic, this situation may illustrate a limit of this method of analysis, as natural variability across the Arctic region may outstrip GCR-enhanced cloud variations, making them undetectable; such a scenario may potentially apply to other regions. This suggests that the internal composite method may be a brute force approach, only able to detect the most apparent signals. Hence it may be wise to consider the GCR–cloud relationships identified by this analysis as merely preliminary, more sensitive approaches that account for internal variability need to be developed to more accurately gauge the nature of a GCR cloud relationship.

Additionally, it should be noted that while the use of the ISCCP data allows for a global scale examination of the GCR–cloud hypothesis, the low spatial resolution of the ISCCP dataset prohibits an analysis of cloud changes at scales where information regarding microphysical mechanisms may be obtained. Therefore, while an analytical approach such as this is useful for validation of the presence of a GCR–cloud connection, it should be used in conjunction with high resolution monitoring of clouds to gain an understanding of the specifics behind GCR–cloud mechanisms.

Another aspect of the methodological approach which warrants discussion concerns the use of rates of change. It is clear that the use of rates has allowed the identification of a GCR–cloud connection. However, it is unclear if this is merely a detection artefact, or if rates changes are related to a GCR–cloud microphysical process. With regards to IMN, it may be argued that rates of change may potentially be involved in microphysical processes in the following manner: it has been proposed that IMN may be an ineffective process because before newly nucleated aerosol particles may accumulate in significant concentrations in the troposphere they will be depleted by CCN scavenging (Carslaw, 2009). However, CCN scavenging can only occur at a finite rate. Consequently, if the rate of aerosol production undergoes a rapid increase, beyond the capacity of CCNs to control the population by scavenging, an accumulation of aerosols may occur. Consider the following scenario: a change in the GCR flux of x % occurs over a given time (t) at a constant rate (scenario A), now consider the same change x % occurs over t x 2 (scenario B). In scenario B the rate of GCR flux is double that of scenario A, although the absolute change is the same; however, in scenario A aerosol nucleation occurs relatively slowly, consequently CCN are more able to maintain aerosol concentrations at a steady level relative to

scenario B by scavenging processes. A similar scenario may be envisaged for GEC mechanisms in relation to the accumulation of space charge at cloud boundaries; with a greater rate of GCR change it may be expected that the accumulation of space charge is more intense (as the charge has less time to dissipate), potentially increase the magnitude of GEC based mechanisms. It is therefore argued that rates of GCR flux are important to GCR–cloud processes.

A major limitation of the cloud analysis involves the reliability of satellite based cloud retrievals over high latitude regions, such detections are problematic as retrieval algorithms essentially differentiate between cloud and surface based on temperature and reflectivity (Rossow and Schiffer, 1999; Todd and Kniveton, 2004). Consequently, over ice covered surfaces clouds are difficult to detect, this problem is further exacerbated during polar night when intense temperature inversions occur. These issues are of relevance as the GI and AI samples highlighted statistically significant cloud anomalies over high latitude regions. Consequently, it would be wrong to place confidence in these results without confirming these findings in alternative datasets: a consideration of this signal validation will be given in the following chapter.

5.6 General summary

It has been speculated that an internal sampling approach may be successful in detecting a GCR–cloud signal, as relationships between GCR and cloud changes may be constrained by preceding atmospheric conditions. This chapter presented the results of such an internal sampling approach and identifies several statistically significant, positive, co-temporal relationships between changes in the rate of GCR flux and cloud anomalies. Over these samples it is possible to distinguish variations in the GCR flux from solar irradiance and IMF changes; the results strongly suggest that no other solar activity parameter may be causally related to the detected cloud anomalies. The spatial and temporal characteristics of the anomalous cloud changes are described in detail and these features are discussed in relation to both previously reported GCR–cloud relationships and potential mechanisms. Overall, these results show the clearest evidence yet presented of a GCR–cloud link. However, it is noted that many of the identified cloud anomalies are located in regions where ISCCP data is known to be subject to retrieval errors.

Chapter 6 Atmospheric Analysis

6.1 An atmospheric perspective

Clouds are capable of exerting a strong influence on climate both directly and indirectly. Direct effects result from modifications to Earth's radiation balance, while indirect effects can result from either dynamic or thermodynamic processes. Many aspects of the interactions between clouds and the climate system are not fully understood and are consequently inadequately incorporated in to climate models (Quante, 2004). As a result, the IPCC indentifies clouds and cloud-related feedbacks as one of the largest sources of uncertainties associated with predicting future climate change (Houghton et al., 2001). This chapter will use NCEP/NCAR reanalysis data in order to determine if any significant atmospheric variations are occurring during the composite samples described in chapters 4 and 5; this analysis will demonstrate the extent to which GCR related cloud changes may interact with the atmosphere. Any anomalous changes detected will be useful for several reasons: (1) they will aid in developing an understanding of the exact nature of a GCR–climate relationship; (2) they will provide a basis upon which to compare the results of subsequent climate model experiments; and (3) they will provide a method of signal triangulation (i.e. detecting atmospheric variations related to observed cloud anomalies will both confirm and validate the presence of the satellite retrieved cloud anomalies). Such an approach is particularly important as satellite cloud retrievals are known to be notoriously erroneous over high latitude regions (Rossow and Schiffer, 1999; Todd and Kniveton, 2004). Consequently, verification of the signal in alternate atmospheric datasets will enable a higher level of confidence to be placed in the results.

6.1.1 Chapter format

The results of the atmospheric analysis will be presented in four sub-sections, each of which will relate to a separate composite sample discussed in previous chapters.

Section 6.2 – Adjusted Forbush decrease (FD) sample
Section 6.3 – Global cloud increase (GI) sample
Section 6.4 – Antarctic cloud increase (AI) sample
Section 6.5 – Mid-latitude cloud decrease (MLD) sample

Within each sub-section a concise presentation, description and analysis of the changes in various atmospheric parameters over the samples will be given. This analysis will be primarily based on the NCEP/NCAR reanalysis data, although samples which have demonstrated the possibility of an Antarctic cloud response will also be supplemented with automatic weather station data from Dome C (located on the Antarctic plateau [77.50 °S, 123.00 °E, 3280 m]), as this provides independent ground-based verification for the reanalysis data over a region where retrievals are arguably the most questionable (Hines et al., 2000; Marshall, 2002). A description of the atmospheric datasets and data handling procedures applied to them has been given in chapter 3.

6.2 Adjusted FD sample: cloud anomalies

To recap the cloud change findings of the adjusted FD sample, no widespread or statistically significant cloud anomalies over the globe were detected. Although, several small locally significant cloud decreases were observed at high southern latitudes over limited regions of the Antarctic plateau the anomalies were not found to be field significant. These anomalies occurred around day -2 of the composite at high (10–180 mb) pressure levels. The timing of these anomalies corresponds to the onset of statistically significant GCR decreases (which begin on day -3 and continue until day 3 of the composite).

6.2.1 Adjusted FD sample: air temperature

During the adjusted FD sample, globally-averaged air temperature anomalies do not demonstrate any statistically significant variations at any pressure level over the sample period (figure 6.1). However, a vertical profile of day -2 air temperature anomalies does show the presence of a statistically significant anomalous decrease of around -0.6 K located around 50°S and an increase of approximately 0.6 K located between 10°S and 10°N. In both instances these anomalies occur at low tropospheric levels (between 950 and 500 mb) (figure 6.2). An examination of the locally significant air temperature changes occurring over the Antarctic region identifies several highly localised anomalous surface level air temperature increases of around 4 K which occur on the Antarctic plateau (figure 6.3).

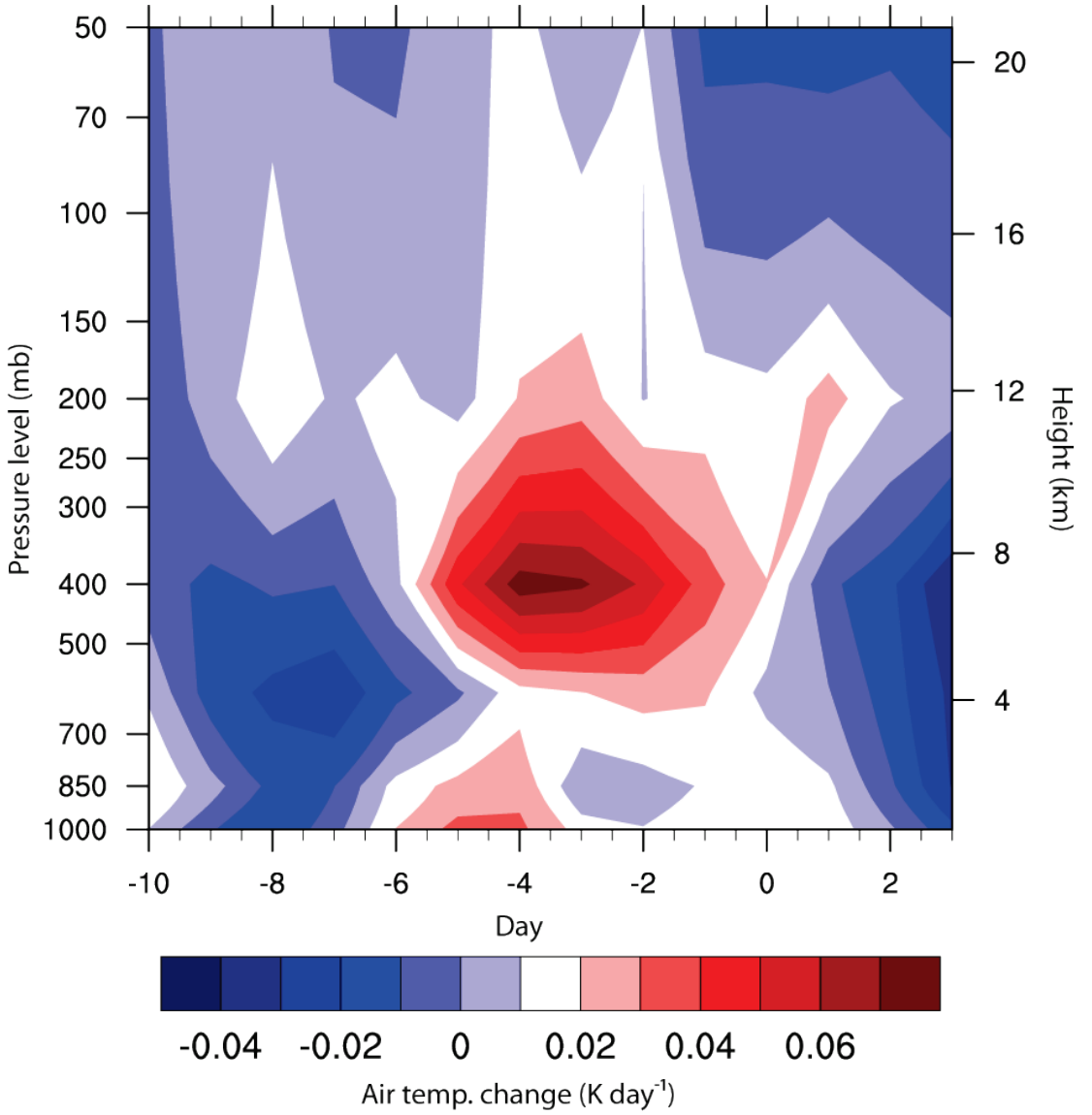

Figure 6.1 Adjusted FD sample: global air temperature anomaly

Globally-averaged anomalous air temperature changes occurring between 50 and 1,000 mb during the adjusted FD sample.

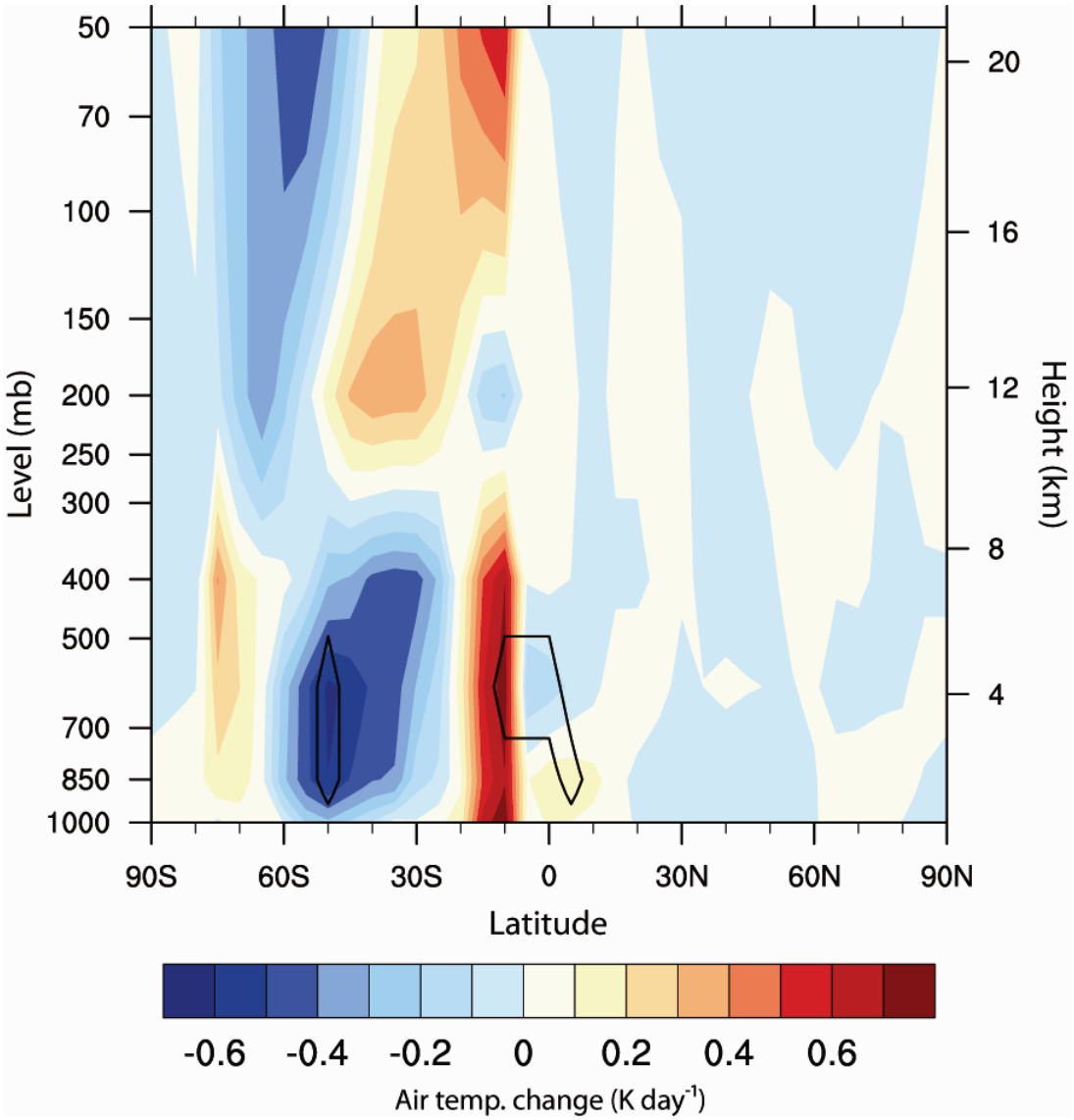

Figure 6.2 Adjusted FD sample: day -2 air temperature anomaly

A plot of 5° latitudinally-averaged air temperature anomalies, occurring on day -2 of the adjusted FD sample. Statistically significant changes are indicated by solid black contours.

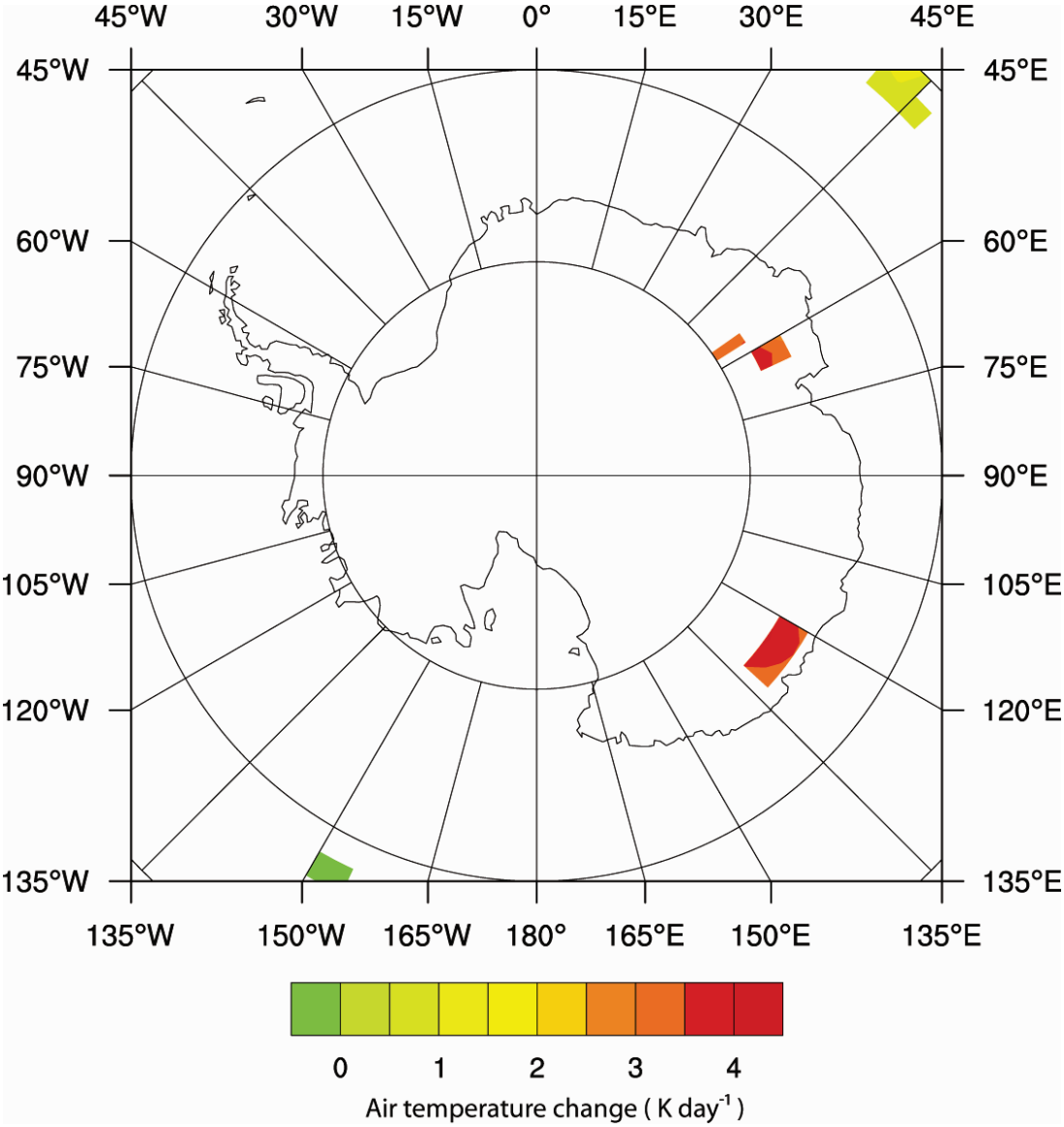

Figure 6.3 Adjusted FD sample: Antarctic air temperature anomaly

Locally significant surface level anomalous air temperature changes, occurring on day -2 of the adjusted FD composite over the Antarctic region.

6.2.2 Adjusted FD sample: pressure

Globally-averaged geopotential height (GPH) anomalies do not demonstrate any statistically significant changes over the sample period (figure 6.4), although latitudinally-averaged GPH anomalies occurring on day -2 did show the presence of statistically significant anomalies located in the southern hemisphere. The sign of the anomaly varies with latitude: at approximately 70°S, GPH increases by approximately 15 m; while between 60°S and 40°S GPH decreases by as much as -30 m; between 30°S and 10°S, GPH increases by as much as 40m. These statistically significant anomalies are found to be most intense at high pressure levels (between 50 and 150 mb) (figure 6.5). Despite the latitudinally-averaged significance, no locally significant pressure anomalies are detected.

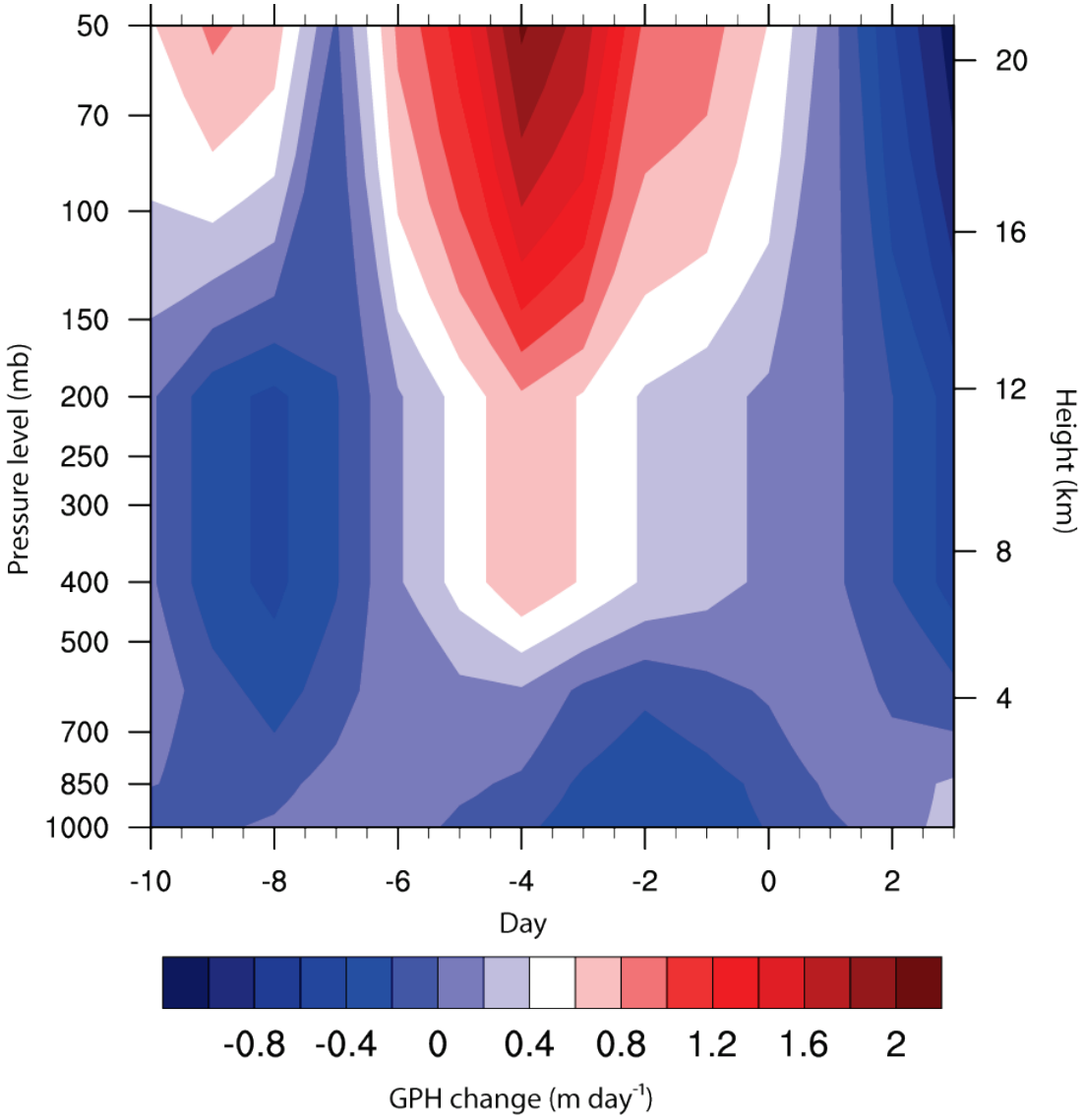

Figure 6.4 Adjusted FD sample: global GPH anomaly

Globally-averaged anomalous GPH changes occurring between 50 and 1,000 mb, during the adjusted FD sample.

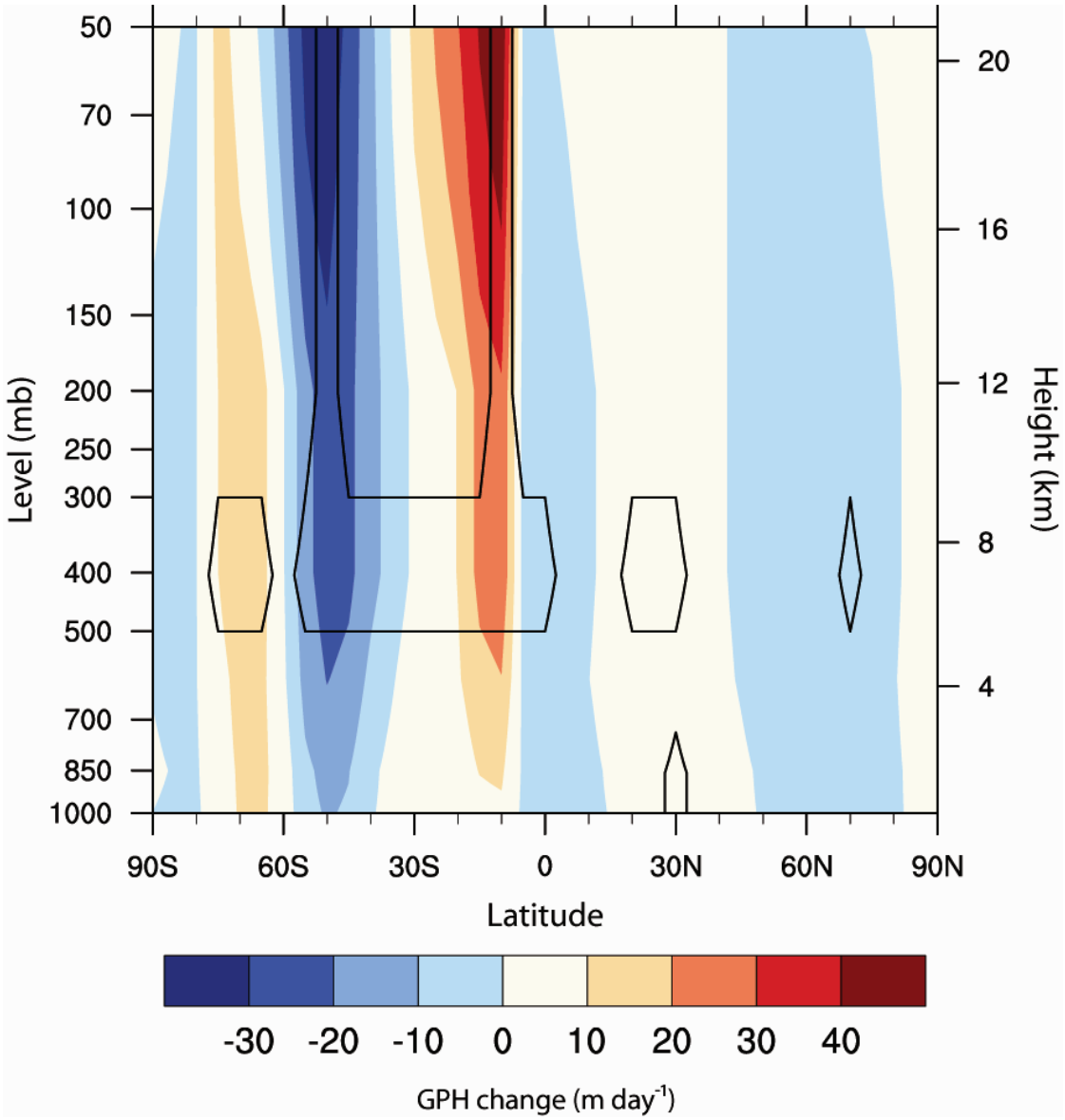

Figure 6.5 Adjusted FD sample: day -2 GPH anomaly

A plot of 5° latitudinally-averaged GPH anomalies, occurring on day -2 of the adjusted FD sample. Statistically significant changes are indicated by solid black contours.

6.2.3 Adjusted FD sample: wind

Globally-averaged wind anomalies do not show any statistically significant zonal or meridional variations over the composite period at any pressure level (figure 6.6). However, latitudinally-averaged anomalies show several small yet statistically significant positive (westerly) zonal anomalies occurring on day -2 of the composite, the most intense of which is located at low tropospheric levels around 40°S with changes of around 0.3 m s^{-1} observed (figure 6.7A). Meridional wind anomalies demonstrate the most widespread statistically significant variations, with two large areas of significant changes in the Southern hemisphere: an increase (indicating enhanced southerly flow) located between 60°S and 40°S, and a decrease (indicating enhanced northerly flow) located between 30°S and 10°S. Although the anomalies extend to surface level, the changes are only statistically significant between 300 and 50 mb (figure 6.7B). The pattern of the meridional anomalies (opposing flows) may suggest the presence of a cyclonic system.

A plot of horizontal vector wind changes on day -2 (figure 6.8) illuminates the findings of figure 6.7 and suggests that a number of changes are occurring, including an easterly intensification of Arctic zonal winds in the upper troposphere, with an associated increase in wind towards the Arctic around the Icelandic and Aleutian low pressure regions, and increased flow from the Arctic to the North Pacific over the easternmost region of Siberia. These anomalies appear to violate the average mean flow patterns (for a ready comparison, the average horizontal vector wind conditions are shown in figure 6.9). Similarly, in the southern hemisphere, vector wind anomalies again appear to violate the mean state; anomalous cyclonic flows around mid-latitude regions appears to be highly disturbed. It is these flows which resulted in the patterns of significant meridional anomalies (figure 6.7B). Furthermore, anomalous northerly winds are observed at peripheral regions of the Antarctic continent around 0° and 140°W and anomalous westerly winds are also observed over Antarctica around 150°E. The extent to which these anomalous circulation patterns may influence regional climate is indicated by figure 6.10; this figure overlays locally significant anomalous surface level air temperature variations with horizontal vector wind over the Antarctic region. The data suggest that the statistically significant air temperature increases of around 4 K (previously presented in figure 6.3) are closely related to anomalous northerly flows, suggesting that the temperature changes may be the result of enhanced lateral advection.

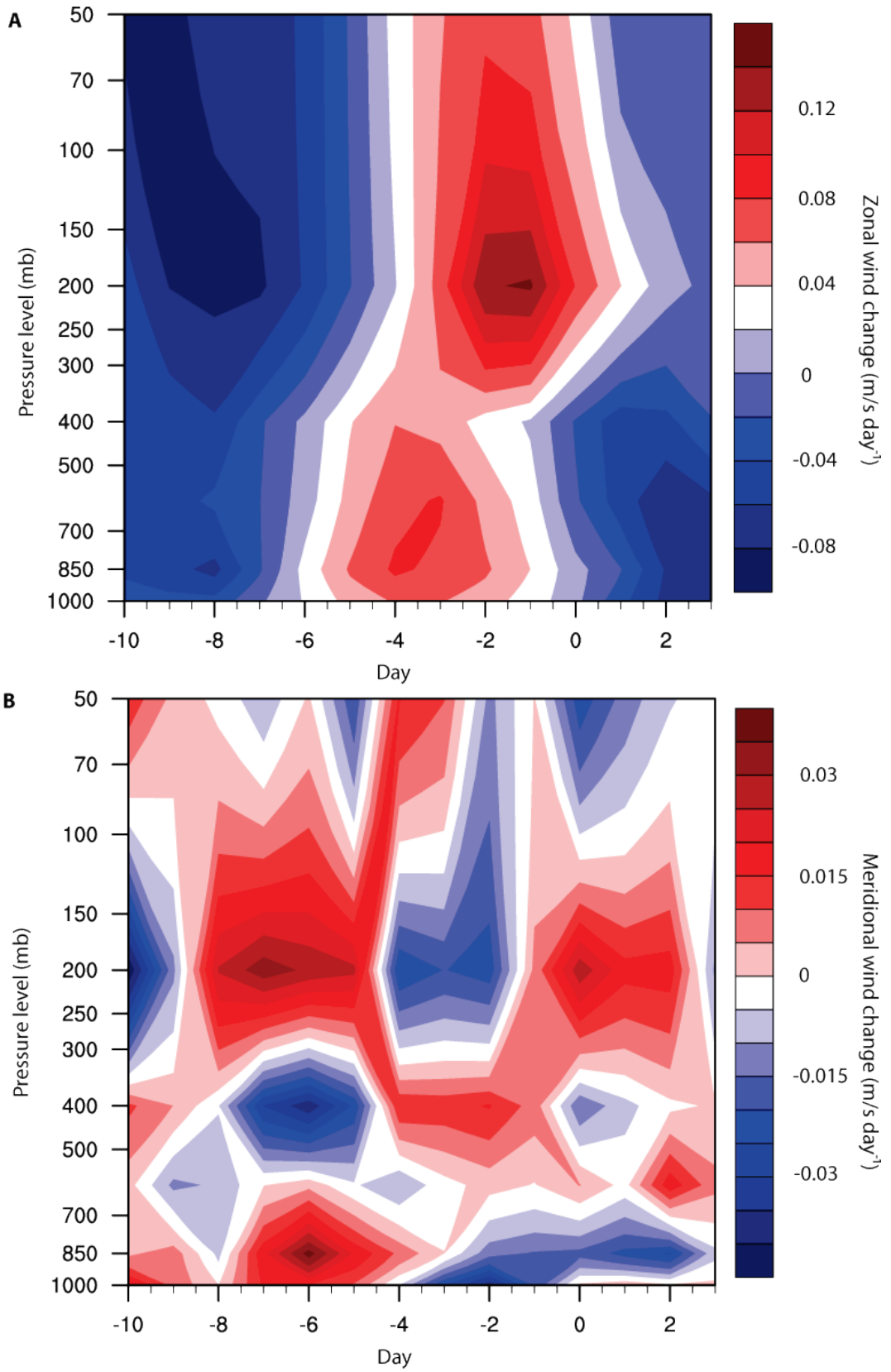

Figure 6.6 Adjusted FD sample: global wind anomaly

Globally-averaged anomalous **A)** zonal and **B)** meridional wind changes, occurring between 50 and 1,000 mb during the adjusted FD sample.

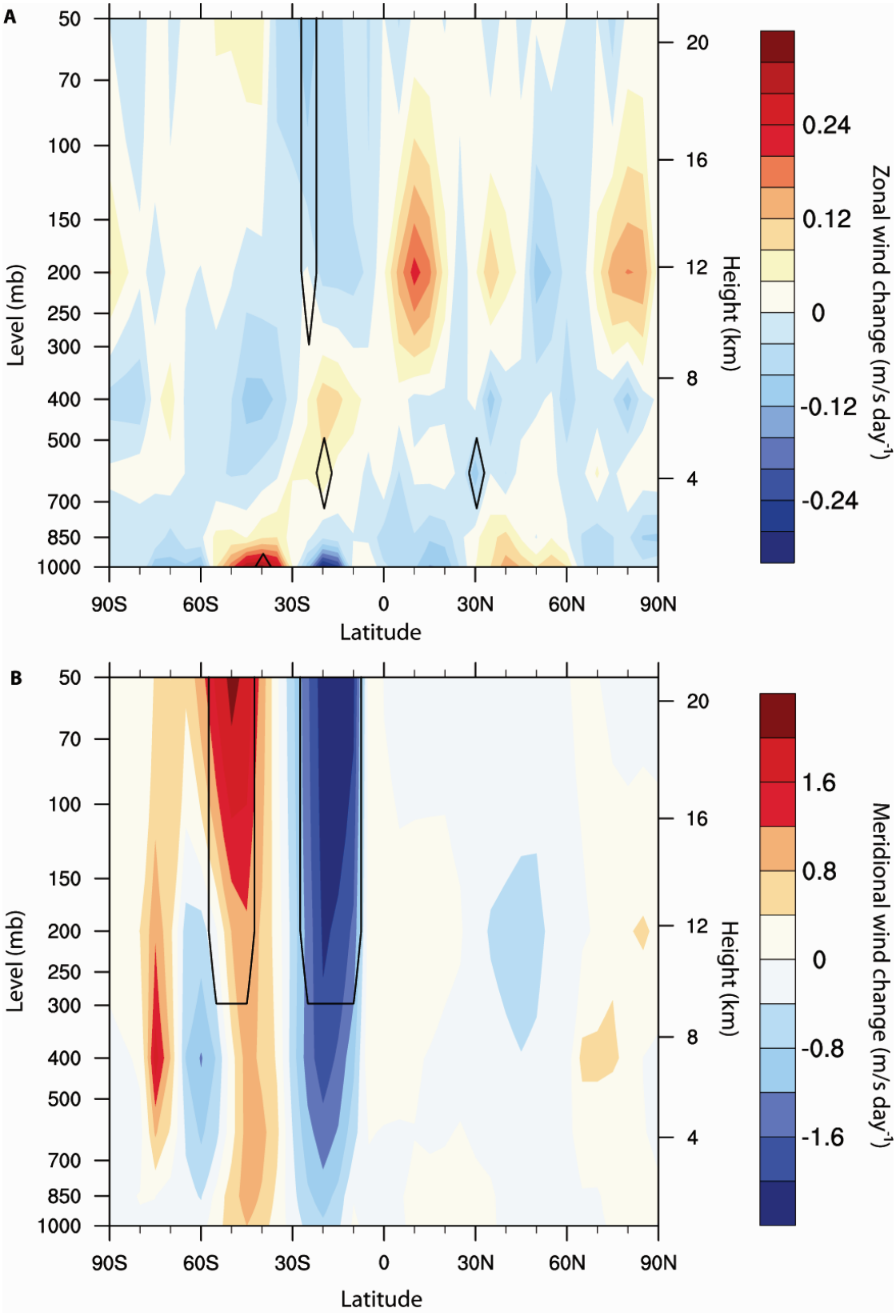

Figure 6.7 Adjusted FD sample: day -2 wind anomaly

A plot of 5° latitudinally-averaged anomalous **A)** zonal and **B)** meridional wind changes, occurring between 50 and 1,000 mb on day -2 of the adjusted FD sample. Statistically significant anomalies are indicated by solid black contours.

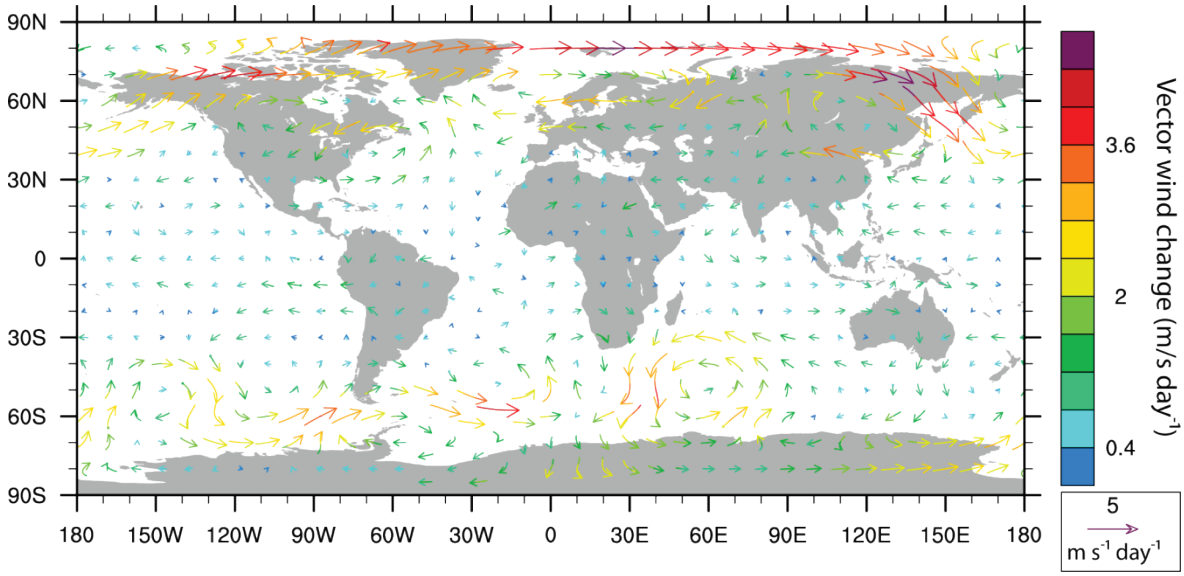

Figure 6.8 Adjusted FD sample: day -2 vector wind anomaly

Horizontal vector wind anomaly on day -2 of the adjusted FD sample at 50 mb.

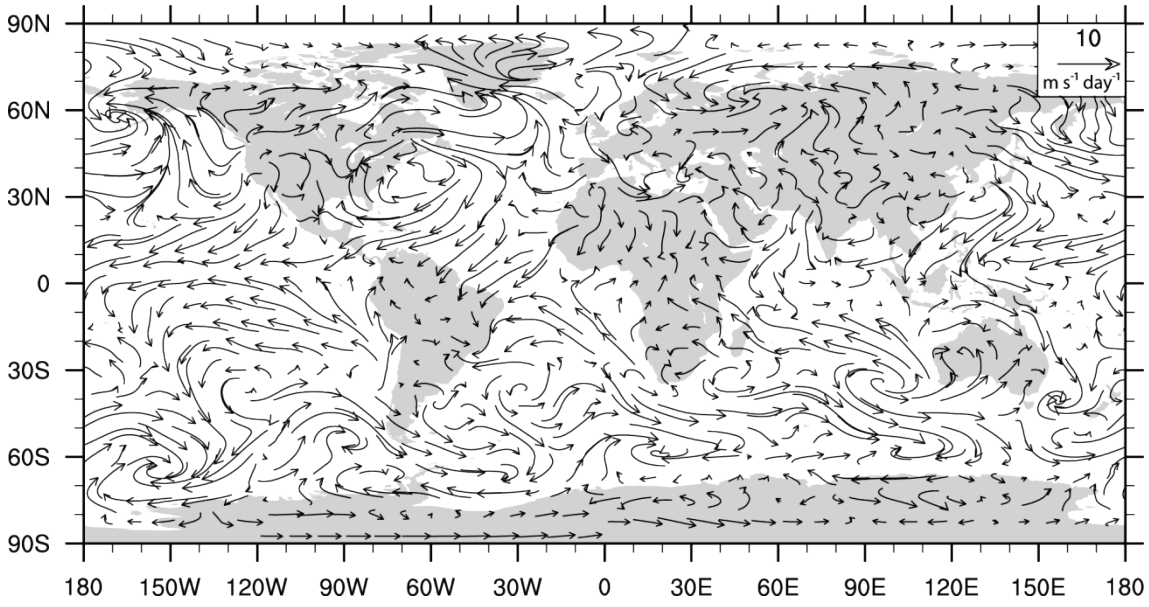

Figure 6.9 Horizontal wind vector mean conditions

Five-year average surface level vector winds. Size of the vectors indicates their magnitude, reference vector of 10 m s^{-1} is shown (top right corner).

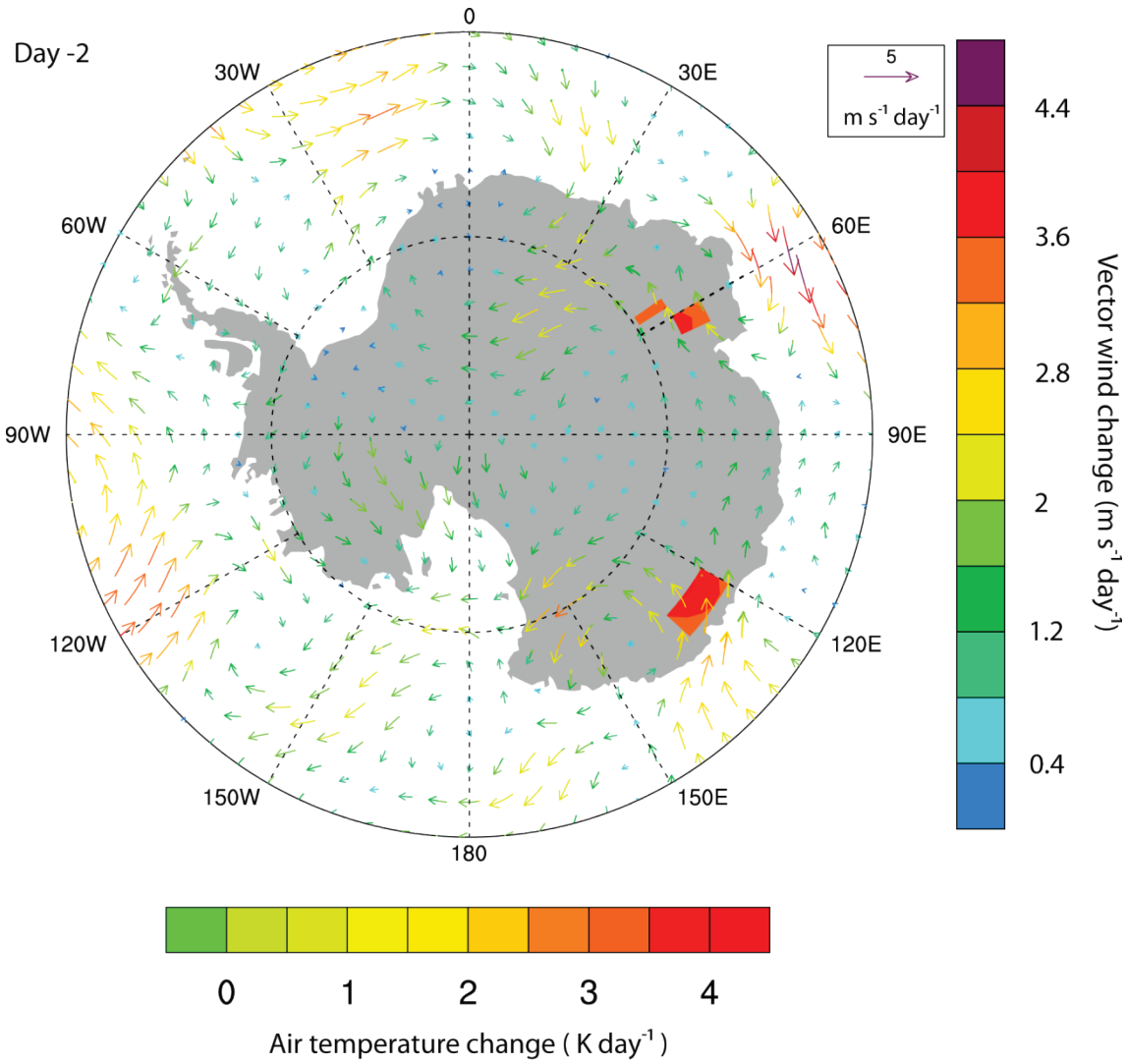

Figure 6.10 Adjusted FD sample: day -2 Antarctic atmospheric disturbance

Day -2 locally significant surface level air temperature anomalies (displayed by filled contours) with anomalous horizontal vector winds overlaid on to a polar stereographic projection of the Antarctic region.

6.2.4 Adjusted FD sample: precipitable water content

To further analyse the atmospheric variations occurring over Antarctica on day -2 of the composite, locally significant anomalous precipitable water content (PW) changes are plotted (figure 6.11). The location of significant PW anomalies correspond to anomalous air temperature/vector wind changes observed in figure 6.10. The spatial correlation of these changes implies that there is a lateral advection of warm and relatively moist air from lower latitudes occurring due to anomalous wind patterns; resulting in increased temperature and precipitation over small areas of Antarctica.

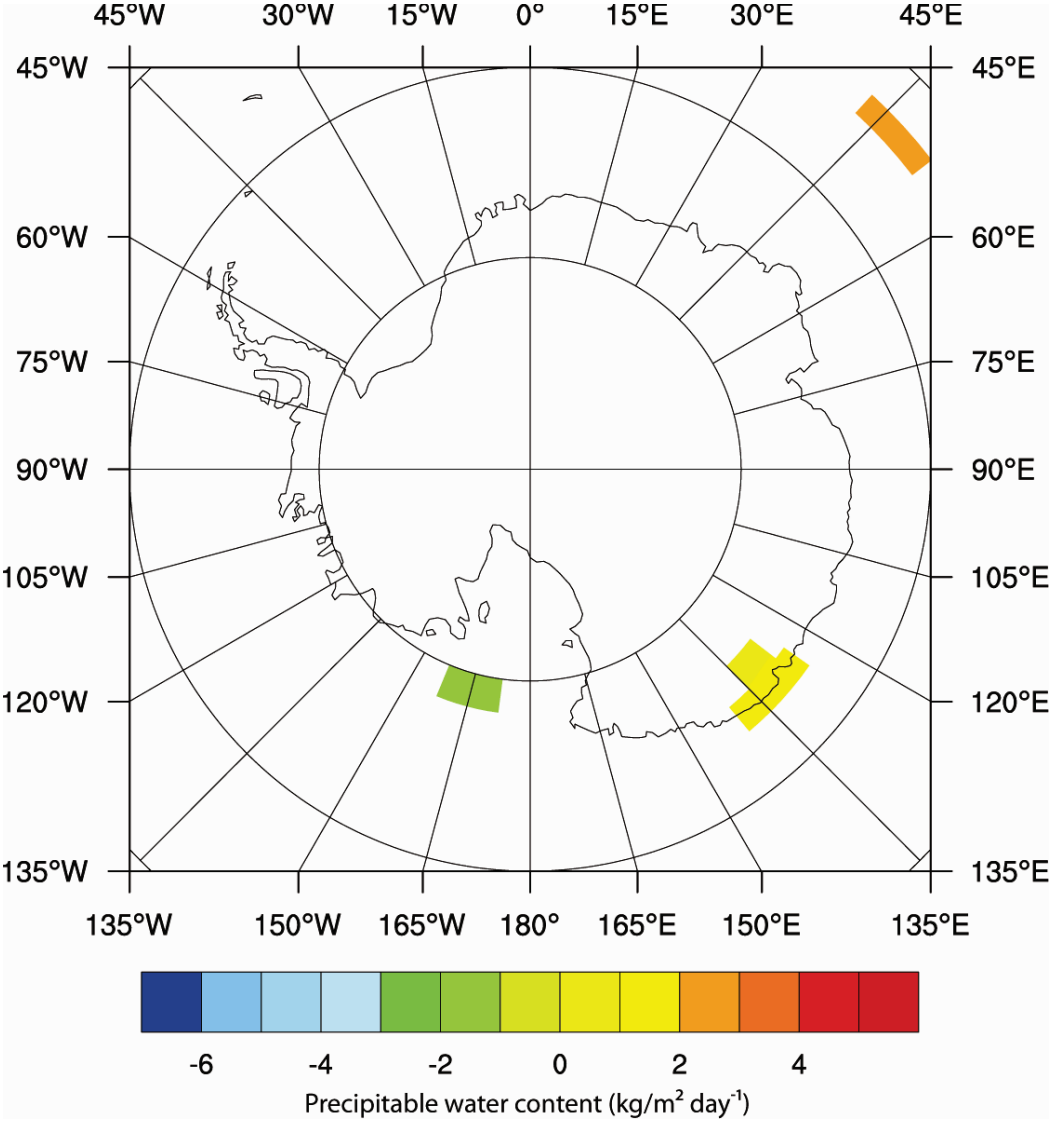

Figure 6.11 Adjusted FD sample: Antarctic precipitable water content

Day -2 locally significant precipitable water content anomaly over the Antarctic region.

6.2.5 Adjusted FD sample: Dome C station data

Automatic weather station (AWS) data from Dome C located on the Antarctic plateau (77.50°S, 123.00°E, 3280m) provides meteorological observations at a 10-minute resolution, from 1984 to the present day. From this dataset, daily averages of air temperature and pressure are constructed; these data are presented here for the adjusted FD sample (figure 6.12).

A statistically significant air temperature increase of approximately 4 K is observed around day -2 of the composite period. Pressure anomalies appear to demonstrate a comparable pattern of variability although, no statistically significant changes are observed. The AWS data support the indications from the NCEP/NCAR reanalysis data that significant anomalous increases in air temperature are observed over limited areas of the Antarctic plateau on day -2 of the composite.

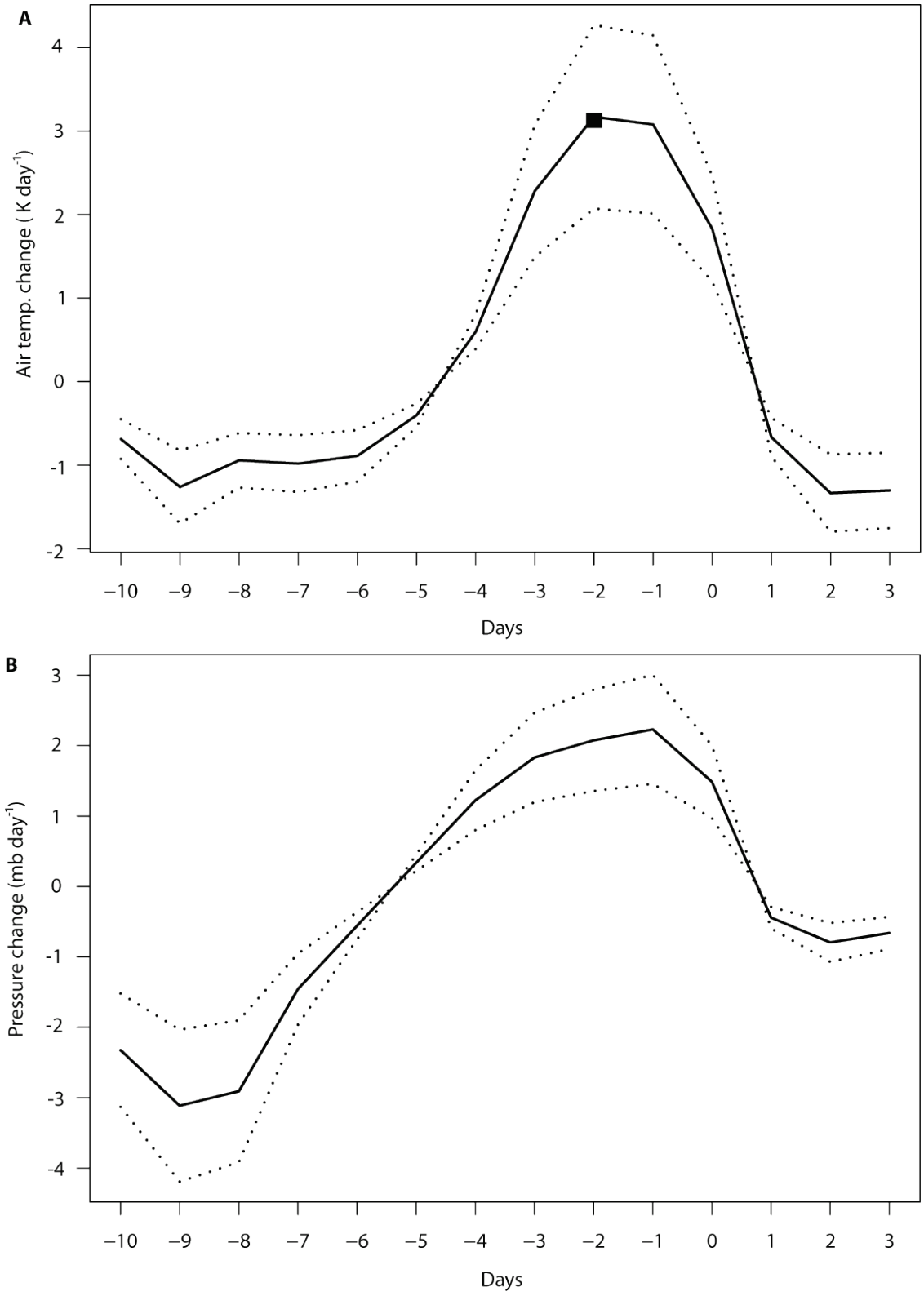

Figure 6.12 Adjusted FD sample: Dome C AWS data

Anomalous **A)** air temperature and **B)** pressure data recorded at the Antarctic plateau Dome C AWS (77.50°S, 123.00°E) during the adjusted FD sample period. Dotted line displays the 0.95 confidence interval, while markers indicate statistically significant anomalies (above the 0.95 critical level).

6.2.6 Adjusted FD sample: analysis and discussion

Generally, the adjusted FD sample demonstrated a low-level of statistical significance; although no significant anomalies were detected at a global scale, some areas of significant atmospheric variability were detected in the southern hemisphere at a latitudinally-averaged scale. The majority of these latitudinally significant atmospheric anomalies were observed on day -2 of the sample, in agreement with the development of locally significant cloud decreases over small areas of the Antarctic plateau. Although the anomalous cloud and temperature/wind changes may be linked via the Antarctic katabatic circulation, it seems unlikely that the cloud anomalies bear a causal relationship to the temperature/wind anomalies. It seems more likely that the upper level Antarctic cloud decreases observed around day -2 might be connected to atmospheric variability rather than a GCR-related process: it is known that the formation and development of cirrus clouds (of which it is possible the clouds in this instance are comprised) are influenced dynamically by gravity waves (Kärcher and Ström, 2003), these are a widespread phenomenon which commonly result from mesoscale atmospheric variability. As widespread atmospheric variability was observed over high Southern latitude ocean regions it may be plausible, that the observed cloud decreases are merely a consequence of dynamic atmospheric variability. Such issues highlight the problems associated with the low signal-to-noise ratio (SNR) of FD-based analysis and again highlights the need to utilise large sample sizes when dealing with such composites.

Both the cloud and air temperature anomalies detected by the adjusted FD composite compare well to the findings of Todd and Kniveton (2001; 2004) (hereafter collectively referred to as TK). The adjusted FD sample is partially based on the dates of TK and consequently may be reflecting similar atmospheric variability. The high level cloud decreases and surface level temperature increases detected by both the adjusted FD sample and TK are not compatible with a contemporary understanding of the impacts of clouds over high latitude ice-covered surfaces; the effect of clouds over such regions should be to promote warming (Stone and Khal, 1991). This implies the temperature changes are not causally related to the cloud anomalies, instead, it is more likely that the temperature (and possibly cloud) changes are the result of mesoscale atmospheric variability detected over the Southern hemisphere circumpolar region. Additionally, further studies should focus on possible solar affects on the katabatic circulation and polar vortex in response to inputs from the IMF or SEP events, as it has been suggested that these factors may be more significant than GCR variations during FD events (Schuurman and Oort, 1969; Troshichev and Janzhura, 2004).

Some research suggests that Antarctic wind anomalies may be linked to FD events and this relationship may influence climate across the Southern hemisphere (Egorova et al., 2000;

Troshichev et al., 2008). However, there is no evidence for a physical process linking the limited upper tropospheric cloud decreases to the anomalous wind flow patterns demonstrated within this sample. A dynamic link between the observed cloud changes, wind patterns and regional atmospheric variability as proposed seems unlikely in this instance due to the small scale and isolated nature of the (upper-level) cloud anomalies relative to the (low-level) tropospheric disturbances. This suggests that the cloud variations are not responsible for driving the anomalous atmospheric variations. Instead, it is more likely that the cloud changes are themselves related to the variations via tropospheric dynamics (such as atmospheric waves producing high level cloud formations).

6.3 GI sample: cloud anomalies

This sample (discussed in section 5.2) appears to provide the most geographically widespread and statistically robust evidence currently found of a GCR–cloud change link. It identified locally significant increases in cloud cover over widespread areas of high latitude regions in both hemispheres. These changes range from approximately 10–25 %, and occurred in conjunction with statistically significant increases in the rate of GCR flux observed at neutron monitor sites across the globe. The results of this sample are perhaps the most compelling evidence yet shown of a GCR–cloud link.

6.3.1 GI sample: air temperature

An examination of globally-averaged air temperature anomalies occurring across the GI composite period indicates that no statistically significant changes (above the 0.95 critical level) are occurring. However, the data show that a negative temperature anomaly (of approximately -0.1 K) develops at low tropospheric levels around the key date of the sample (figure 6.13). A plot of latitudinally-averaged key date air temperature anomalies reveals that a complex range of significant temperature anomalies are occurring. An increase in air temperatures is identified at high southern latitudes in the upper troposphere from 90°S–50°S, located between 50 and 400 mb. At latitudes greater than 50°S the anomaly is located at high tropospheric levels; however, around 50°S it extends throughout the remaining troposphere to sea level. It is at this position where the anomaly shows statistical significance. Additionally, significant decreases in

air temperature are also observed between 35°S and 25°S and 30°N–50°N occurring between 100 and 300 mb and 500–800 mb respectively; the magnitude of these decreases ranges from approximately -0.8 to -2.0 K (figure 6.14). A pixel-by-pixel analysis of anomalous surface level air temperature changes on the key date reveals that only air temperature decreases over the polar regions are locally significant; these decreases are observed in both hemispheres at latitudes greater than 75°N/S. The most intense decreases are around -3 K and are observed over the interior of the Antarctic continent and regions of the Arctic ocean (figure 6.15). Such temperature anomalies are probably responsible for the observed (non-significant) global average low altitude temperature decrease detected around the key date in figure 6.13.

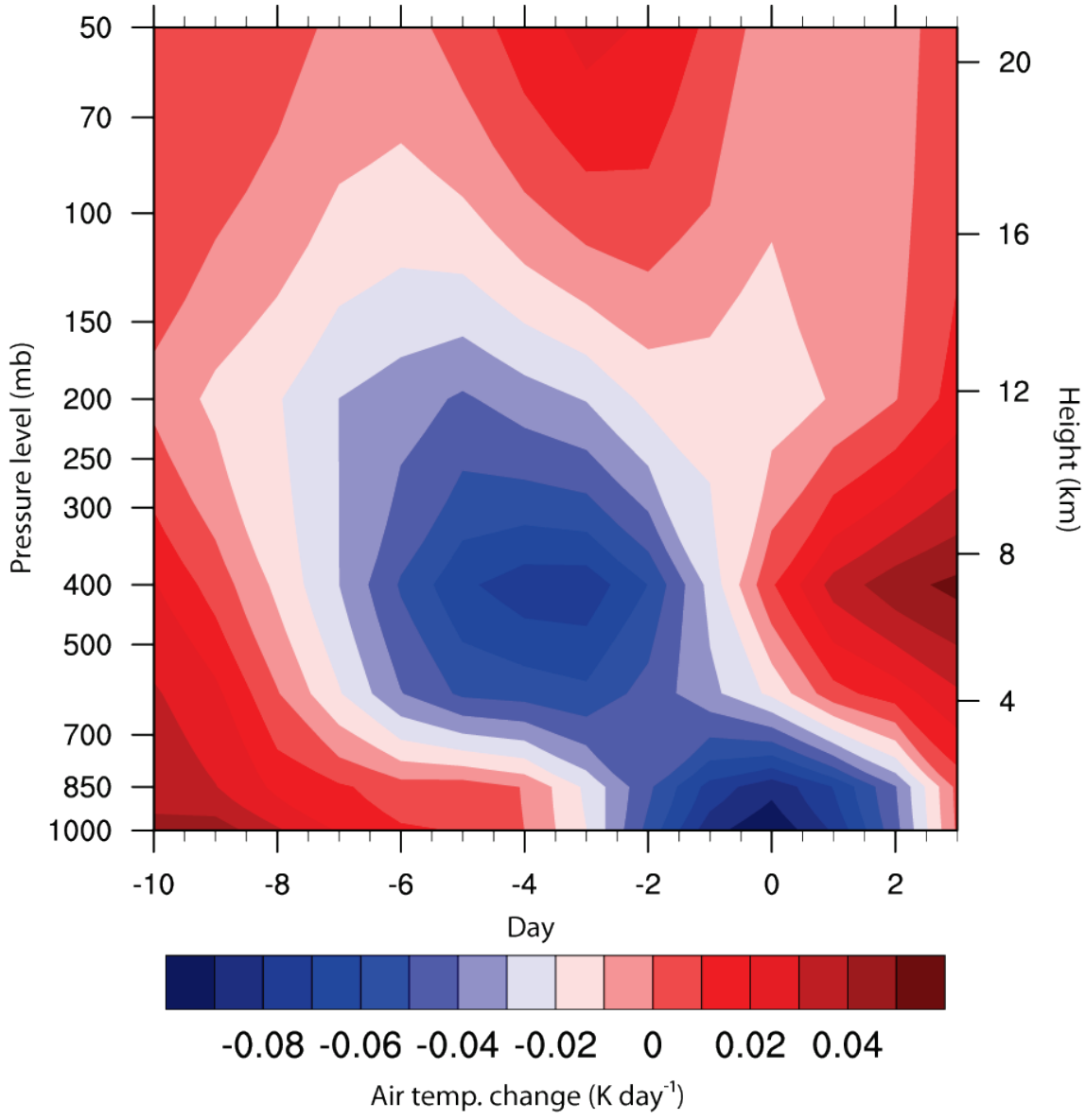

Figure 6.13 GI sample: global air temperature anomaly

Globally-averaged anomalous air temperature changes occurring between 50 and 1,000 mb during the GI sample.

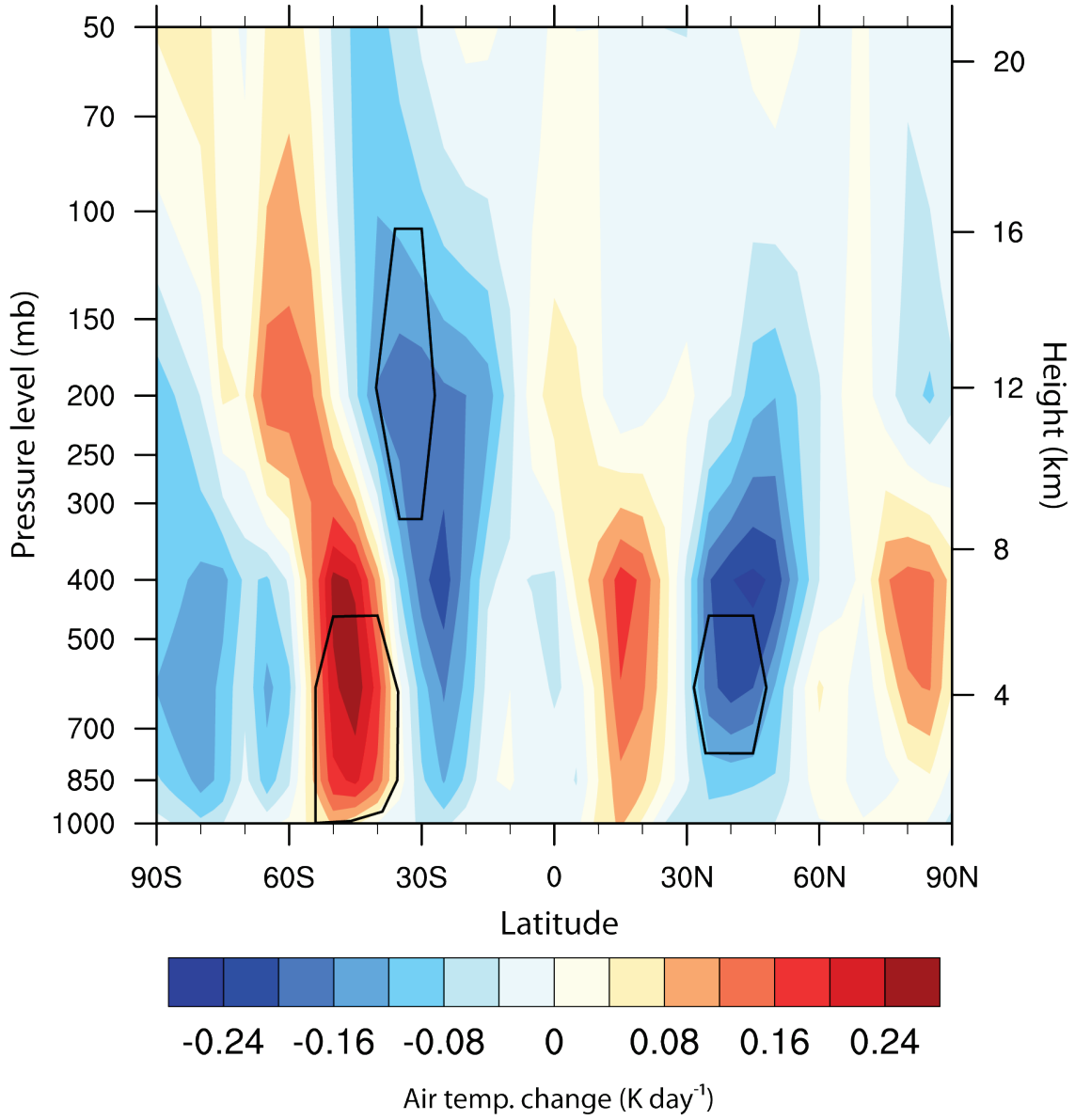

Figure 6.14 GI sample: key date air temperature anomaly

A plot of 5° latitudinally-averaged air temperature anomalies, occurring on the key date of the GI sample. Statistically significant changes are indicated by solid black contours.

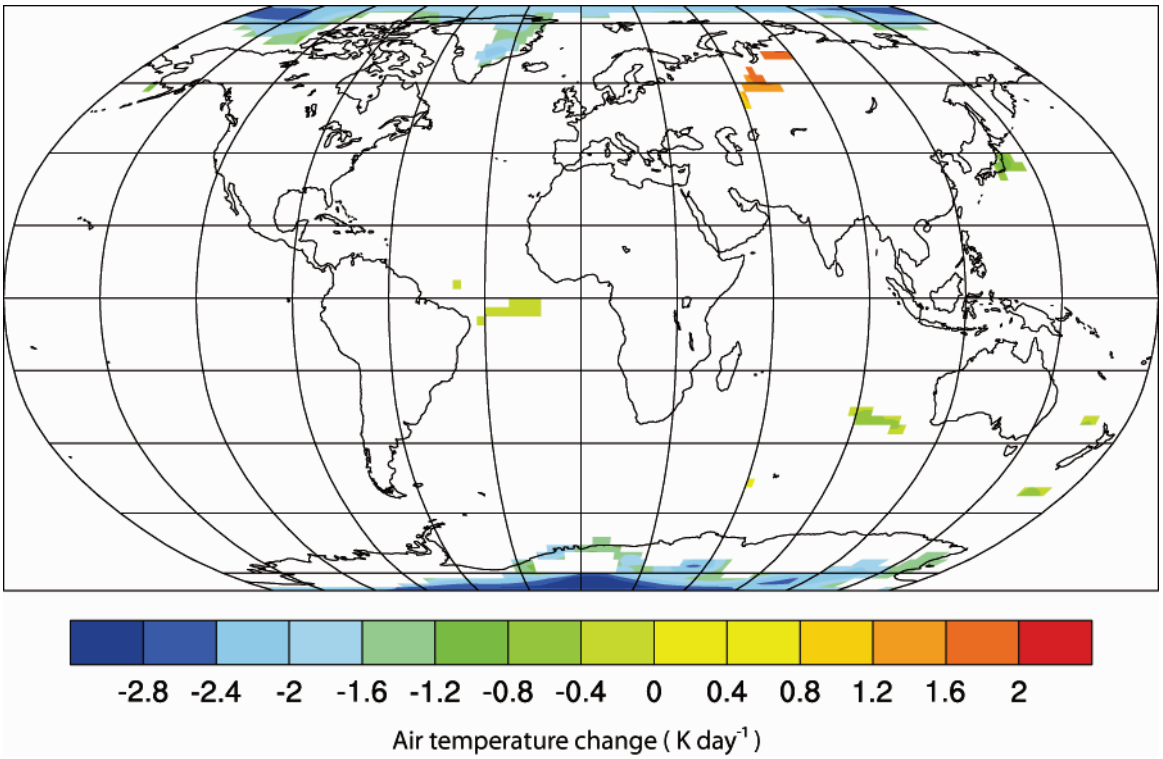

Figure 6.15 GI sample: global air temperature anomaly

Locally significant surface level anomalous air temperature changes occurring on the key date of the GI sample.

6.3.2 GI sample: pressure

Globally-averaged anomalous GPH changes over the sample period show a statistically significant decrease of approximately -1 m occurring between 400 and 200 mb on day -2 (figure 6.16). This anomaly appears to be associated with a widespread GPH decrease occurring at upper to mid- tropospheric levels between days -6 to 0. A latitudinally-averaged plot of key date GPH anomalies indicates that the statistically significant changes occur predominately at mid- tropospheric levels. These changes are most intense in the southern hemisphere, however they also occur to a lesser extent around 0°, 10°N–20°N, 35°N–55°N and 75°N–85°N (figure 6.17). In the southern hemisphere, a GPH decrease of around -5 m is detected between 75°S and 40°S while between 40°S and 20°S an anomalous increase in GPH of around 6m is detected. This pattern of change is similar to that observed in the air temperature data and may suggest the presence of a circulatory anomaly over the southern hemisphere (this idea will be explored further in section 6.3.7).

A pixel-by-pixel analysis of key date, surface level, pressure anomalies identifies a locally significant decrease in pressure (of approximately 300 Pa day^{-1}) centred over the Antarctic plateau. Two additional intense (but spatially limited) areas of significant pressure variations are also observed in the North and South Pacific regions (figure 6.18).

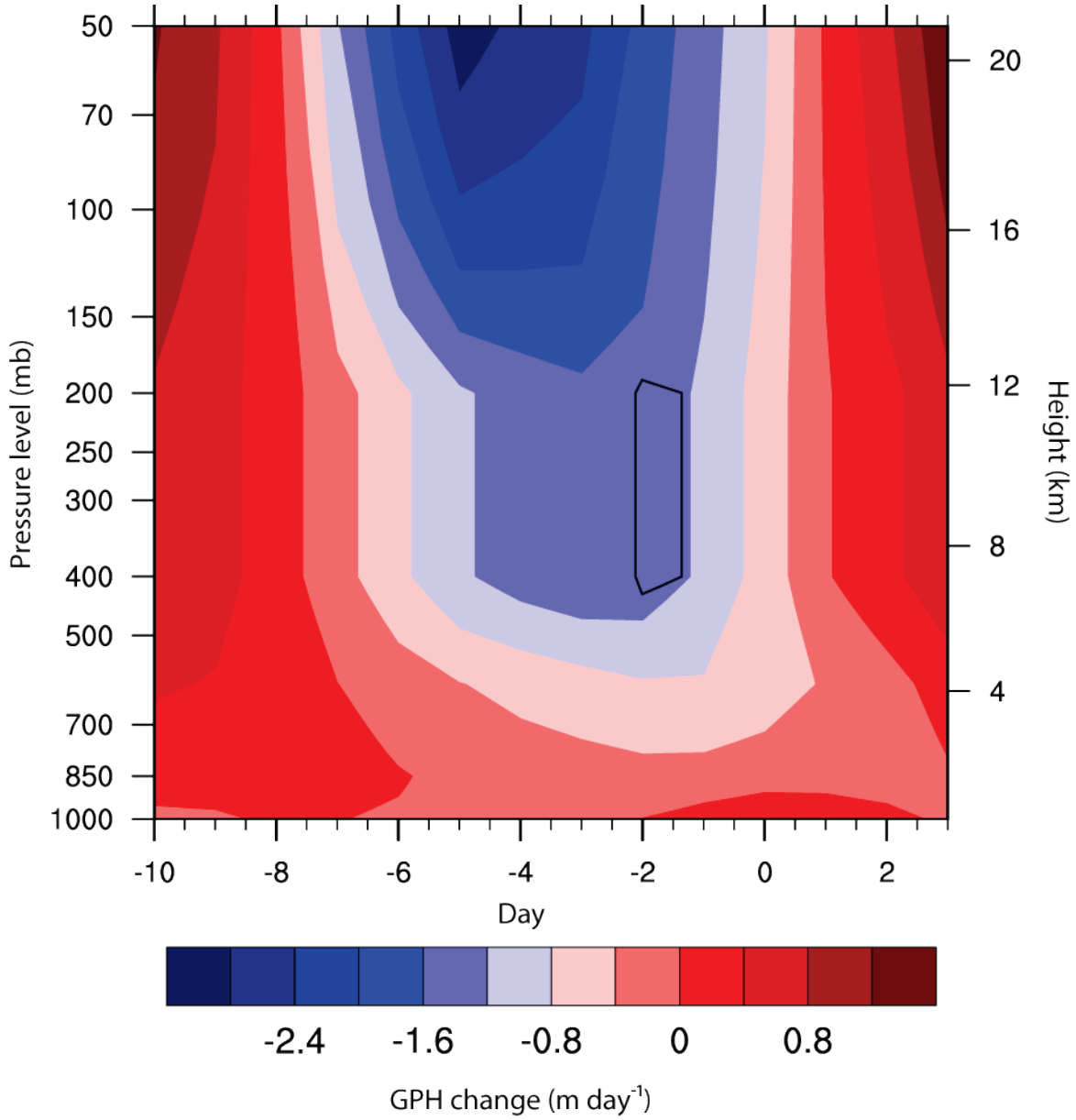

Figure 6.16 GI sample: global GPH anomaly

Globally-averaged anomalous GPH changes occurring between 50 and 1,000 mb during the GI sample. Statistically significant changes are indicated by solid black contours.

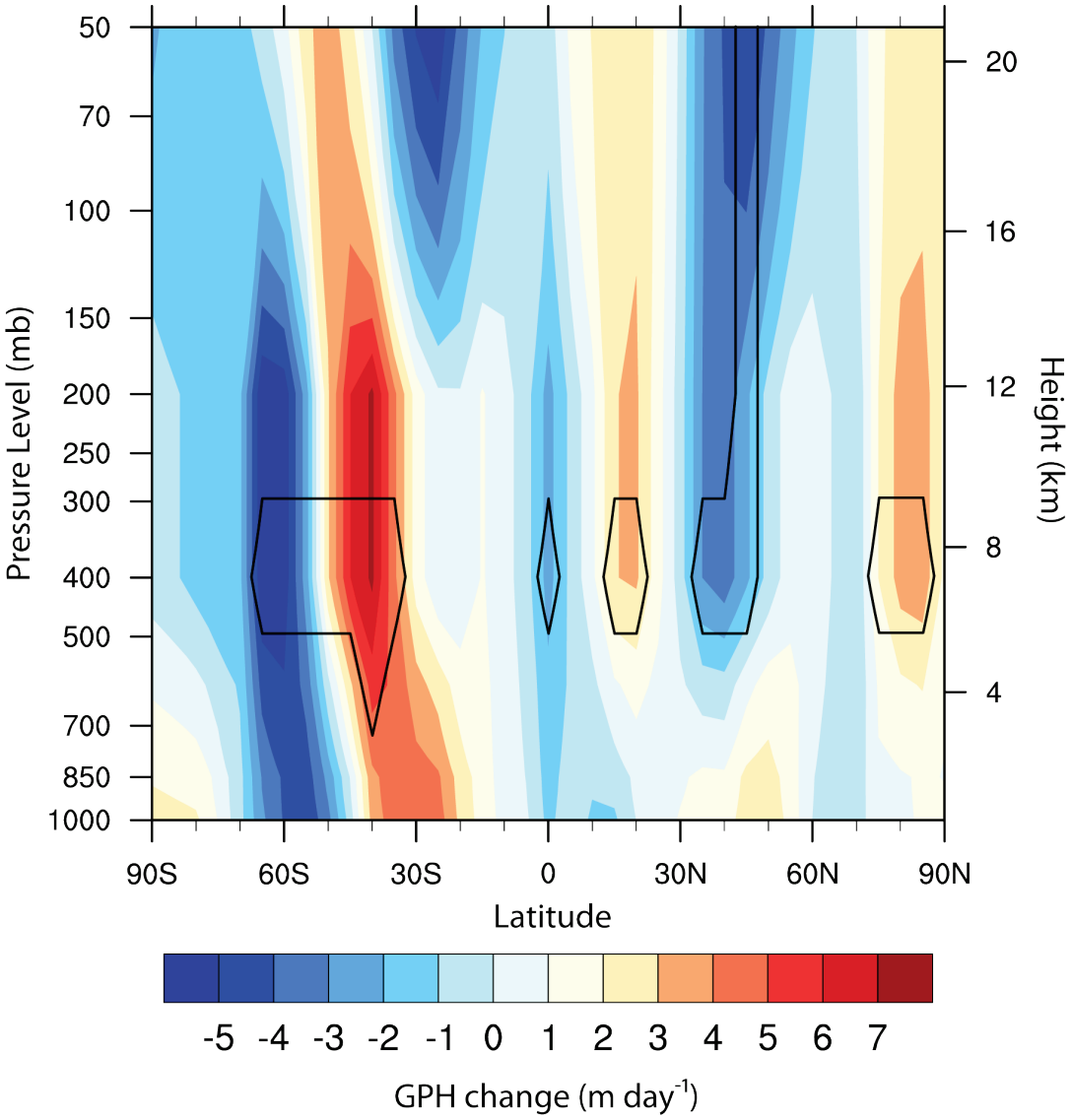

Figure 6.17 GI sample: key date GPH anomaly

A plot of 5° latitudinally-averaged GPH anomalies, occurring on the key date of the GI sample. Statistically significant changes are indicated by solid black contours.

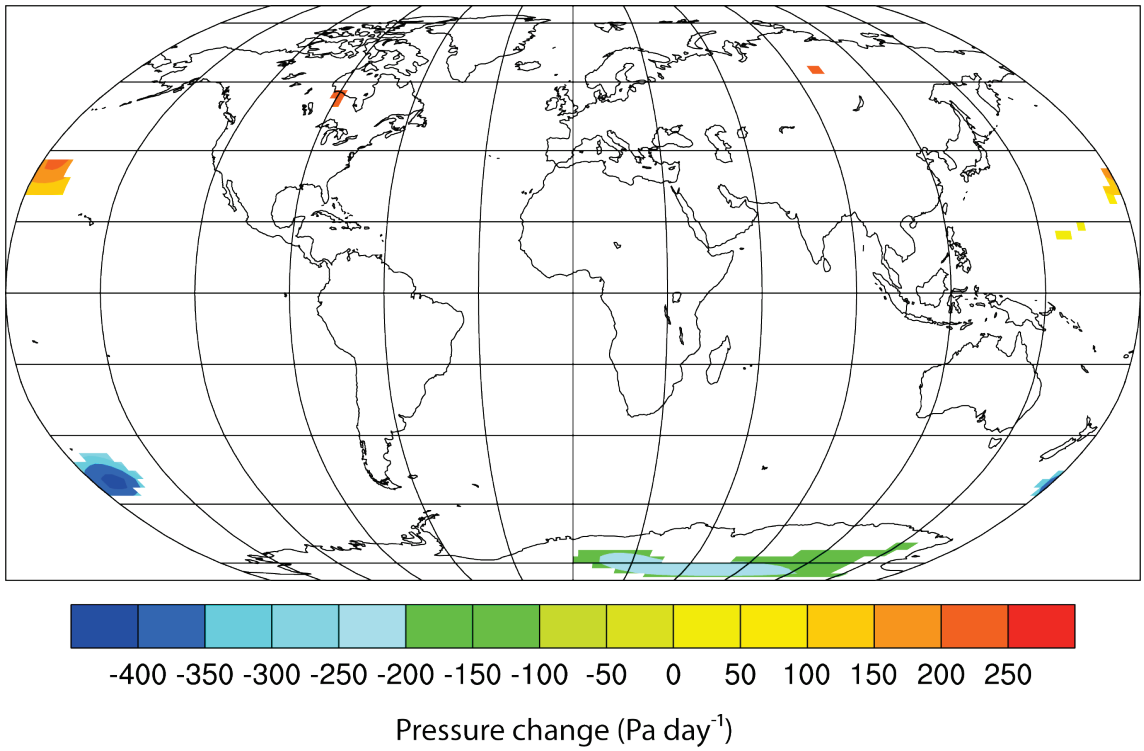

Figure 6.18 GI sample: global pressure anomaly

Locally significant surface level anomalous pressure changes occurring on the key date of the GI sample (units in Pascals).

6.3.4 GI sample: wind

Whilst no statistically significant globally-averaged anomalous zonal or meridional wind changes were observed over the sample period (figure 6.19), zonal wind anomalies do show indications of a coherent positive (westerly) increase (of up to 0.1 m s^{-1} day^{-1}) between days -4 to 2. Latitudinally-averaged zonal wind anomalies show intense, statistically significant, negative (easterly) changes of around -0.12 m s^{-1} day^{-1} at low tropospheric levels (between 1,000 and 700 mb) located at approximately 60°S and 20°N. Non-significant positive (westerly) zonal wind anomalies of up to 0.1 m s^{-1} day^{-1} also occur at higher altitudes directly above both of these negative anomalies (figure 6.20). These westerly zonal anomalies correspond spatially to the locations of the sub-tropical jet streams and may indicate that an intensification of the jet streams is occurring. These changes appear to be responsible for the previously discussed global average positive zonal wind increase around the key date of the composite (figure 6.19). These zonal anomalies are situated directly between statistically significant positive (southerly) and negative (northerly) meridional anomalies (located between 60°S and 30°S and between 5°N

and 50°N); this may indicate a relationship between meridional variability in the low troposphere and the position of the sub-tropical jet streams.

A plot of surface level, horizontal vector wind anomalies on the key date reveals the occurrence of widespread disturbances of around 2 m s^{-1} day^{-1}over regions of the southern hemisphere around 60°S (particularly over the South Pacific) and also, to a lesser extent in areas of the Arctic ocean (around 80°N) (figure 6.21). The disturbed wind flow patterns prevalent over mid-southern latitude regions may indicate that a regional alteration to the polar atmospheric circulation has occurred, since climate variability in this region is dominated by the state of the Antarctic circumpolar flow (Thompson and Solomon, 2002).

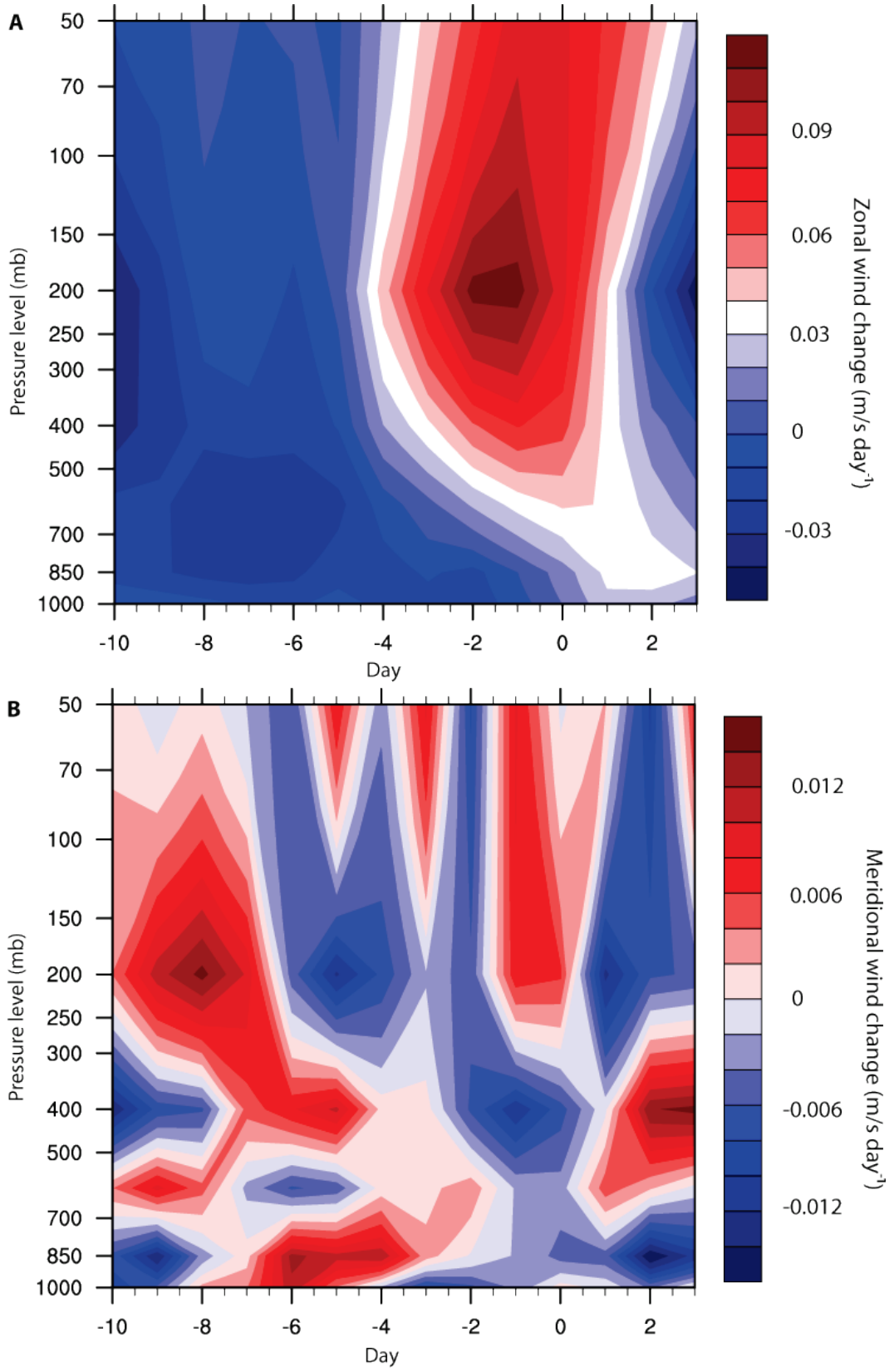

Figure 6.19 GI sample: global wind anomaly

Globally-averaged anomalous **A)** zonal and **B)** meridional wind changes occurring between 50 and 1,000 mb during the GI sample.

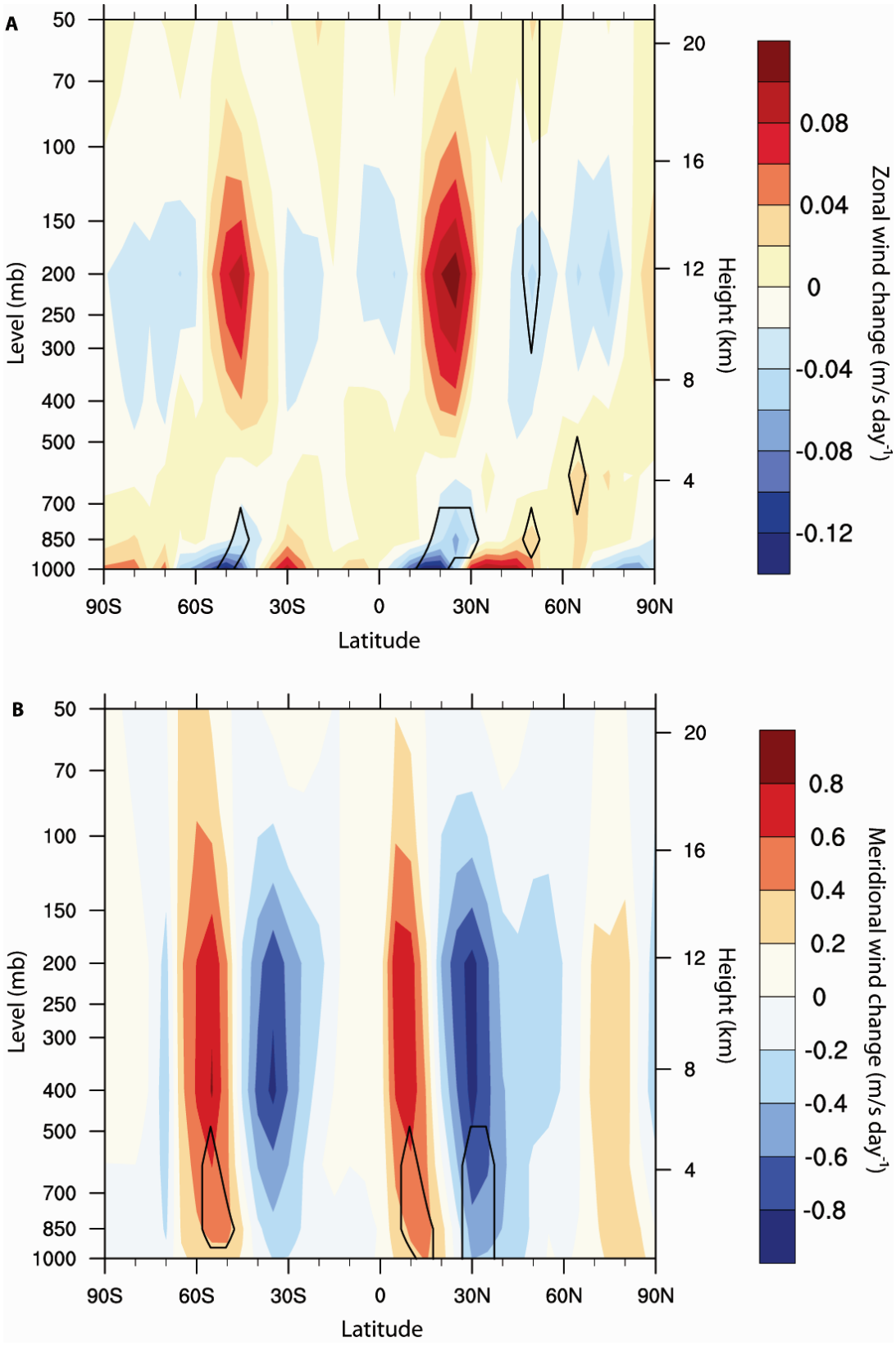

Figure 6.20 GI sample: day -2 wind anomaly

A plot of 5° latitudinally-averaged anomalous **A)** zonal and **B)** meridional wind changes occurring between 50 and 1,000 mb on the key date of the GI sample. Statistically significant anomalies are indicated by solid black contours.

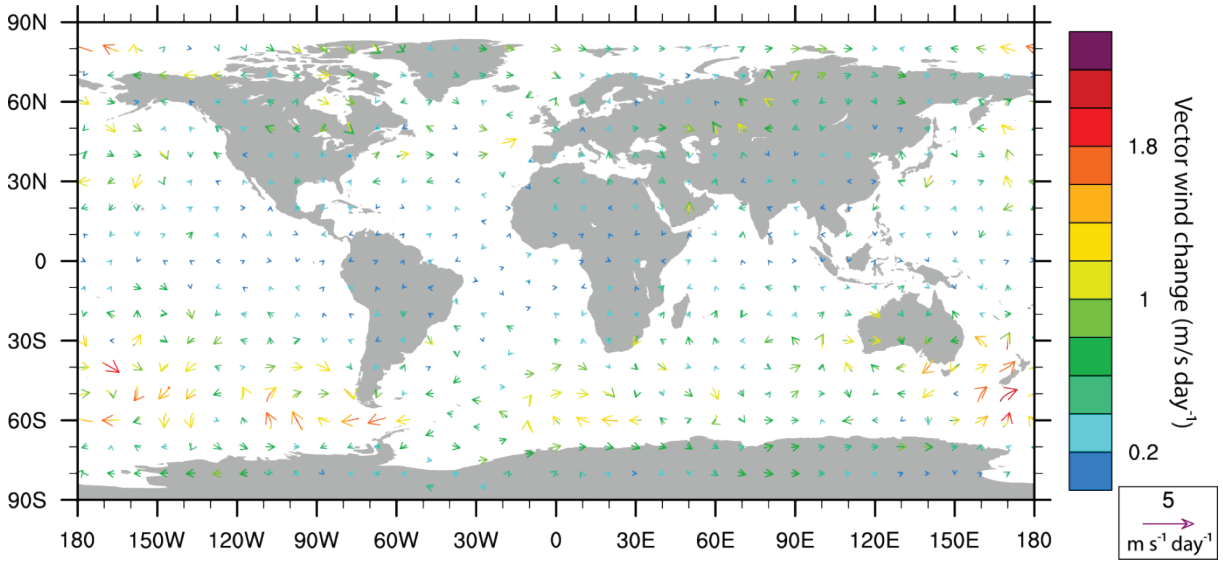

Figure 6.21 GI sample: key date vector wind anomaly

Surface level, horizontal vector wind anomaly on the key date of the GI sample. A 5 m s^{-1} reference vector is displayed on the bottom right hand corner of graph.

6.3.5 GI sample: precipitable water content

A pixel-by-pixel analysis of variations in PW over the key date of the composite indicates locally significant decreases of around -0.8 kg m^2 occurred across high latitude regions in both hemispheres: in the northern hemisphere these decreases primarily occur over Greenland and the Arctic ocean, whereas over the southern hemisphere the decreases primarily occur over the interior of the Antarctic continent (figure 6.22).

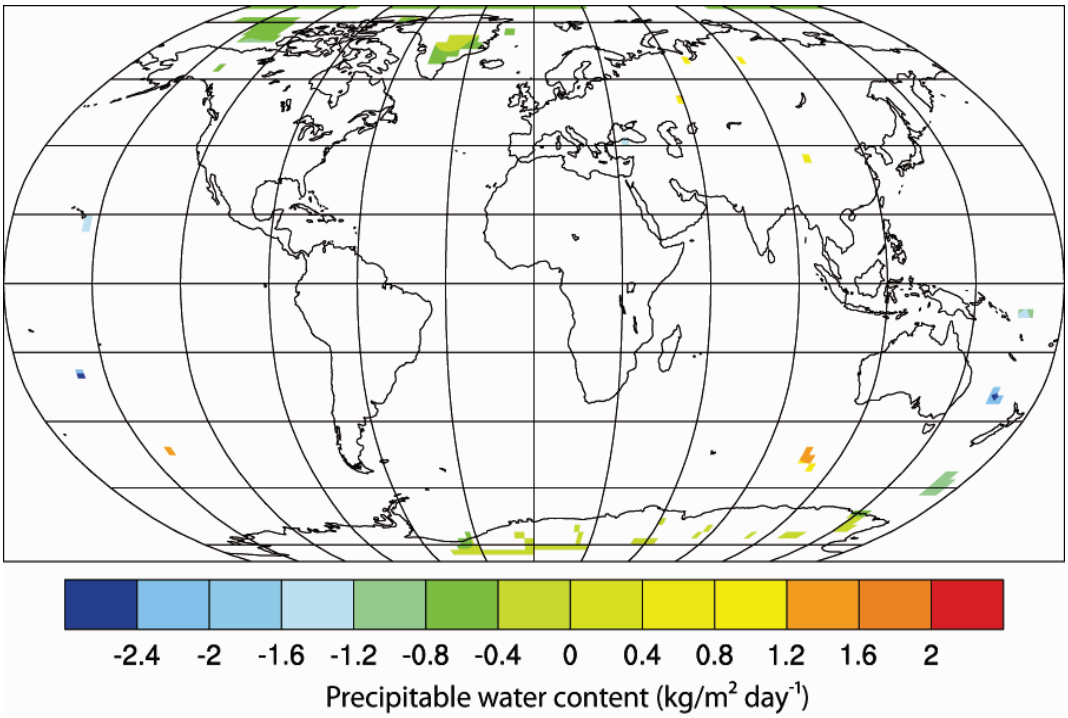

Figure 6.22 GI sample: global precipitable water content anomaly

Locally significant precipitable water content anomaly occurring on the key date of the GI sample.

6.3.6 GI sample: Dome C station AWS data

Dome C AWS data show a statistically significant decrease in anomalous air temperatures on day -6 of around -2 K. Following this decrease, air temperatures recover to an undisturbed state by around day -4, after which time another statistically significant decrease of around -2 K occurs on day 0. A statistically significant decrease in pressure of around -2 mb also occurs on day -1 of the sample (figure 6.23). The pattern of air temperature changes over the GI sample detected at Dome C may possibly be explained by the series of cloud changes observed over the GI composite period. Around day -6, a significant anomalous decrease in cloud cover occurs at polar latitudes, whereas around day 0 a significant anomalous increase in cloud cover occurs. Although these cloud changes are opposing, they may result in air temperature decreases in both instances via different cloud–atmosphere interactions. A direct radiative cloud forcing on day -6 may be capable of resulting in decreased air temperatures, while it may be hypothesised that an indirect dynamic cloud forcing on the key date may also be capable of reducing surface level air temperatures over the Antarctic plateau (this point will be explored further in the following section). Such a change may also offer an explanation for the observed pattern of pressure variability seen at the AWS. However, alternatively these observations may also suggest issued with the ISCCP cloud retrievals (this point will be elaborated upon in the following section).

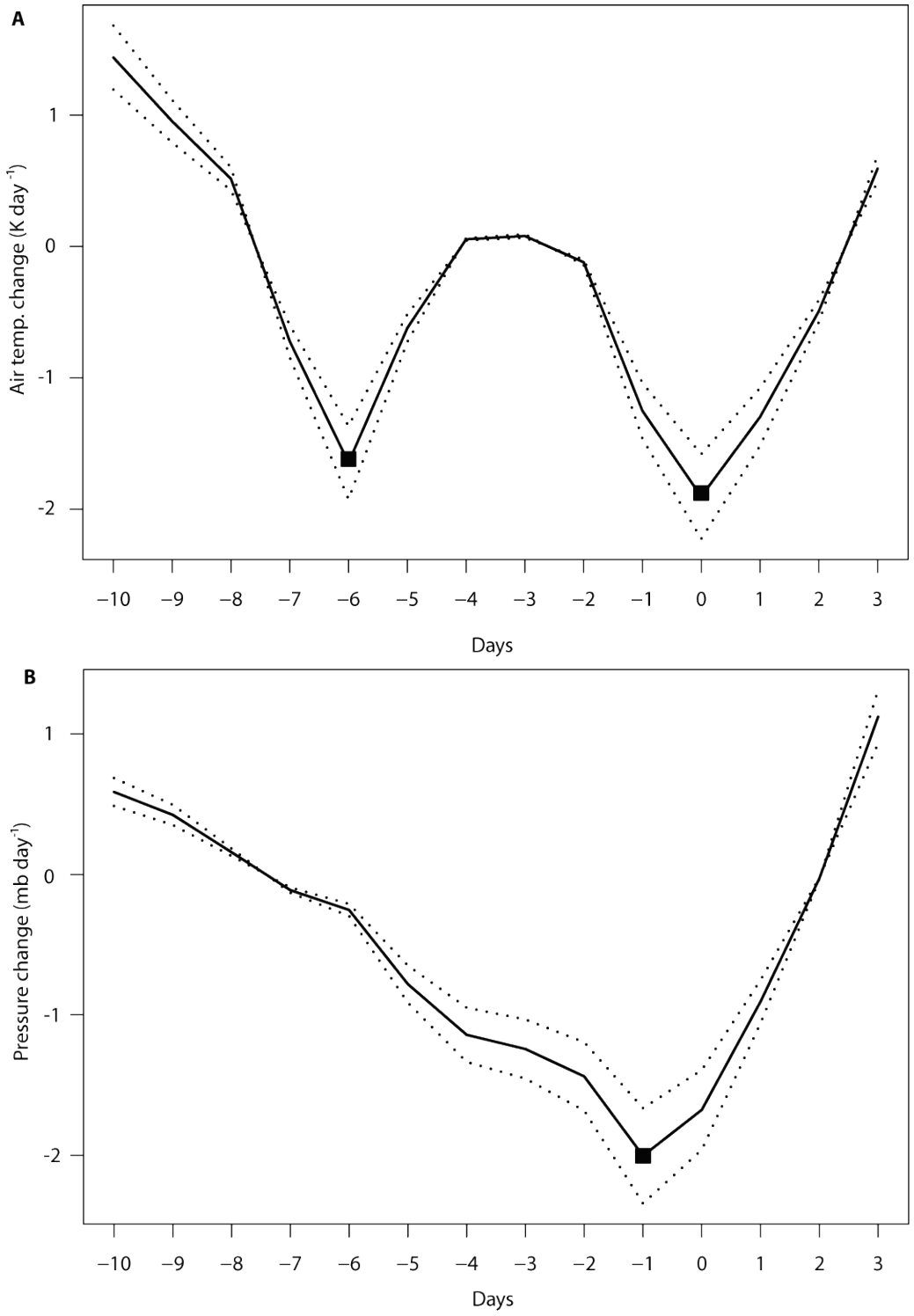

Figure 6.23 GI sample: Dome C AWS data

Anomalous **A)** air temperature and **B)** pressure data recorded at the Antarctic plateau Dome C AWS (77.50°S, 123.00°E) during the GI sample. Dotted lines display the 0.95 level confidence interval, while markers indicate statistically significant anomalies (above the 0.95 critical level).

6.3.7 GI sample: analysis and discussion

The GI sample was based around the top 5 % most rapid increases in cloud cover across the Earth (over an equal-area-adjusted grid) occurring over daily timescales; the global cloud increase signal was found to be the result of cloud changes (of around 25%) at high latitude regions in both hemispheres. An atmospheric analysis identified locally significant temperature, pressure and precipitation changes over comparable regions to the identified polar cloud changes and also showed a number of statistically significant anomalies occurring across a range of lower latitude zones; the implications of these findings will now be discussed.

The surface level air temperature decrease detected over widespread regions of the Arctic and Antarctic are of particular note. Assuming cloud increases are occurring, this anomaly is unexpected, as it is well established that the dominant influence of clouds over high latitude ice covered regions should be to warm the local environment (Stone and Khal, 1991). This suggests several possibilities: (1) the detected cloud increases are false, (2) the cloud–temperature changes are unrelated, or (3) if the cloud–temperature changes are both real and related then it implies the occurrence of a previously unrecognised cloud–climate interaction.

With regards to the first possibility, it is known that both reanalysis and ISCCP data are subject to errors over high latitude regions (Kalnaya et al., 1996; Rossow and Schiffer, 1999). However, the verification of decreased temperatures over Antarctica during the key date by AWS data suggests that the findings of the reanalysis are reliable. The ISCCP detection of cloud relies on temperature and reflectivity, consequently temperature changes over (highly reflective) ice-covered regions may be incorrectly interpreted as cloud changes. These findings may suggest that the cloud detections are artefacts resulting from the air temperature changes themselves (although if this possibility is correct, this raises the question why are the air temperature changes occurring and why do they demonstrate a co-temporal relationship to GCR variations).

The second and third possibility will be tested by the use of GCM based experimentation. With regards to the third possibility, a theory as to how a high latitude temperature decrease might result from cloud increases can be postulated. The surface level temperature anomalies may be the result of an indirect circulatory change over the region (as opposed to a direct radiative forcing), which could be explained by the following scenario:

Step 1 Widespread high latitude increases in high level cloud warm the surrounding air by absorption and re-emission of outgoing LW radiation.

Step 2 Air at high tropospheric levels over the Antarctic plateau normally descends towards surface level in a key component of polar circulation (the polar vortex (PV)), however, the warmed air is less likely to converge towards surface level.

Step 3 The reduction in the descent of air in the PV results in a reduction of surface level temperature. This is because the superposition of constant radiative cooling of surface level air and the adiabatic warming of descending air maintains a quasi-stable thermal equilibrium which can be disrupted by a reduction in the descent of air in the PV (Troshichev and Janzhura, 2004).

Step 4 The PV is crucial to climate across both hemispheres. As air descending in the PV reaches surface level, it undergoes intense radiative cooling and then drains towards lower latitudes in the katabatic wind regime under gravity. As the cold air meets warmer air masses at mid-latitudes, it is deflected eastwards; the constant flow of cold air maintains the cold low pressure system which surrounds high latitude regions (referred to as the circumpolar vortex). Consequently, due to the close association between the PV, katabatic wind regimes, and circumpolar vortices, changes to the system may result in alterations to the circumpolar vortices capable of influencing atmospheric variability at lower latitudes (Parish, 1992).

Step 5 A weakened circumpolar vortex allows the encroachment of relatively warmer lower latitude air masses in to high latitude regions, and a shift in synoptic scale circulatory patterns across the globe.

Tentative evidence supporting this hypothesis can be observed over the sample in both the air temperature and pressure data. The latitudinally average profile of key date air temperatures indicates a warming at high tropospheric levels over southern and northern polar latitudes (figure 6.14). In both hemispheres these air temperature increases approximately relate to the height of the observed cloud cover increases (over the Arctic, cloud cover increases occur at mid-tropospheric levels, whereas over the Antarctic, they occur at high tropospheric levels). Furthermore, the decrease of descending air in the PV should theoretically result in a corresponding decrease in pressure; such a decrease is observed over the Antarctic plateau (figure 6.18).

It has already been established that atmospheric variations over the Antarctic region may indirectly affect climate at lower latitudes across the southern hemisphere (Trenberth, 1980; Mo et al., 1987; Smith and Stearns, 1993). Therefore, it is logical to suggest that the latitudinally-averaged significant anomalies detected at lower latitudes may result from the observed high latitude climate anomalies. This may also provide an indication as to why the latitudinally-averaged anomalies appeared more widespread and intense in the southern hemisphere, since there are large differences between the magnitude, duration, and integrity of polar circulations in the Arctic and Antarctic regions (Waugh and Randel, 1999).

6.4 AI sample: cloud anomalies

The AI sample identified a statistically significant decrease in cloud cover of approximately -10 % between days -6 and -4 and a significant increase in cloud cover of approximately 30 % between days -2 and 1. These changes occurred at mid-to high tropospheric levels and were found to have a positive relationship to co-temporal, statistically significant, variations in the rate of GCR flux.

6.4.1 AI sample: air temperature

During the AI sample, globally-averaged air temperature anomalies did not show any statistically significant changes at any pressure level, although an anomalous decrease in air temperatures (of up to -0.1 K day^{-1}) is observed at low tropospheric levels around the key date of the sample (figure 6.24). Latitudinally-averaged air temperature anomalies occurring on the key date demonstrate regionally significant decrease of around -0.24 K day^{-1} at high southern latitudes (90°S–60°S) at mid-to low tropospheric levels between 500 and 1,000 mb. Other statistically significant air temperature anomalies are also observed on the key date, although these are not as widespread or intense as the 90°S–60°S anomaly. These include several relatively small air temperature decreases of around -0.18 K at 30°S–10°S, 5°N and 30°N–50°N; a low-level air temperature increase of 0.18 K day^{-1} directly adjacent to a significant south pole cooling located around 40°S and, a small upper level (50–300 mb) cooling of around -0.16 K day^{-1} located above the 40°S anomaly (figure 6.25).

A pixel-by-pixel analysis of anomalous surface level air temperature changes on the key date shows that a locally significant cooling of up to -5 K day^{-1} occurs over the interior of the Antarctic continent (figure 6.26); these results are similar to those of the previously discussed GI sample. An anomalous zonal warming of around 0.8 K day^{-1} can be observed in the upper tropospheric levels between 90°S and 60°S (figure 6.25); this is broadly consistent with the previously discussed notion that the large cloud increase observed in this location warms the surrounding air, indirectly resulting in a significant cooling near surface level. This effect may also account for the observed zonally significant anomalies detected at lower latitudes, as a link between Antarctic cloud anomalies and atmospheric variability may influence synoptic-scale climate patterns across the southern hemisphere (as discussed in section 6.3.7).

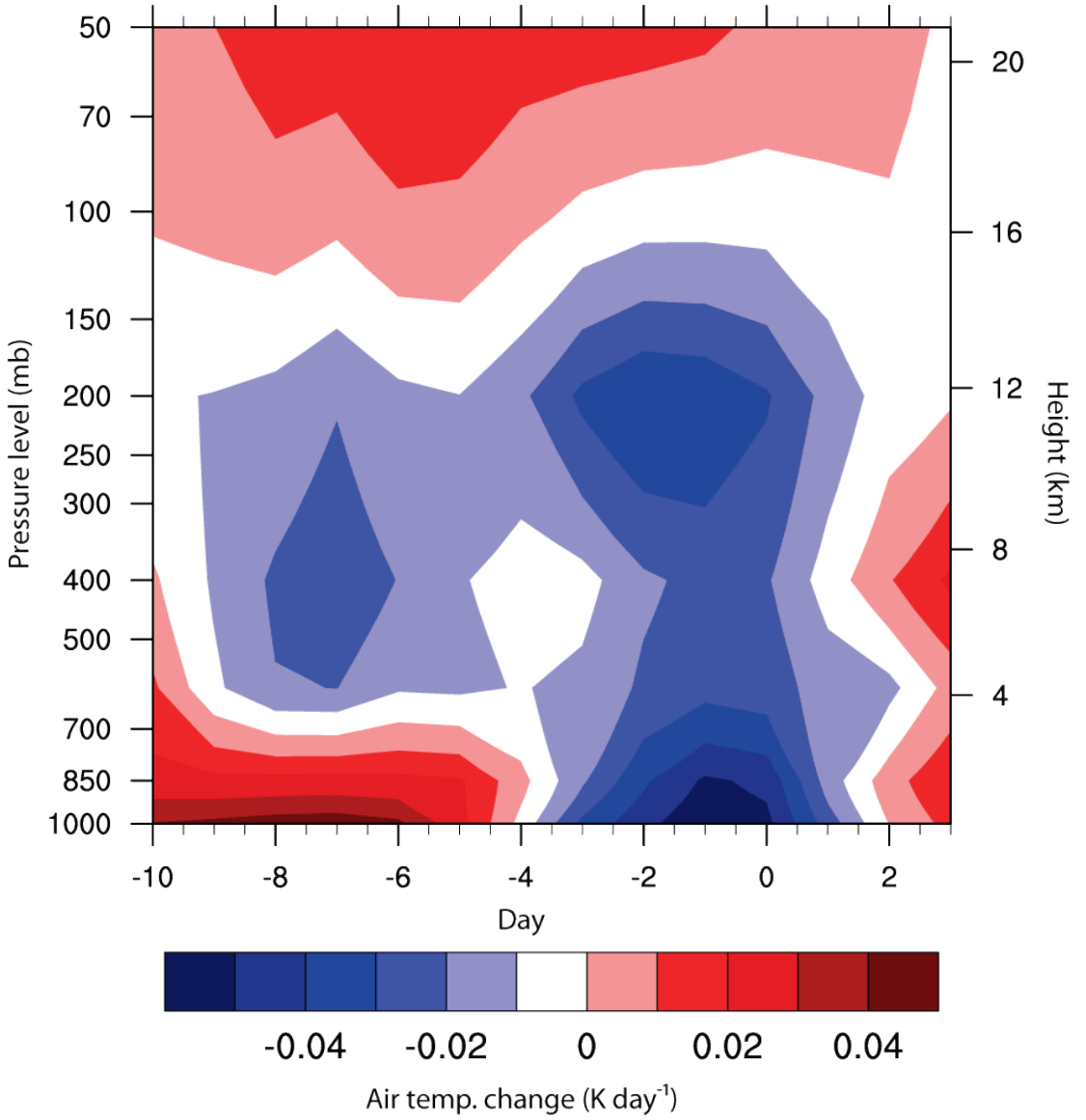

Figure 6.24 AI sample: global air temperature anomaly

Globally-averaged anomalous air temperature changes occurring between 50 and 1,000 mb during the AI sample.

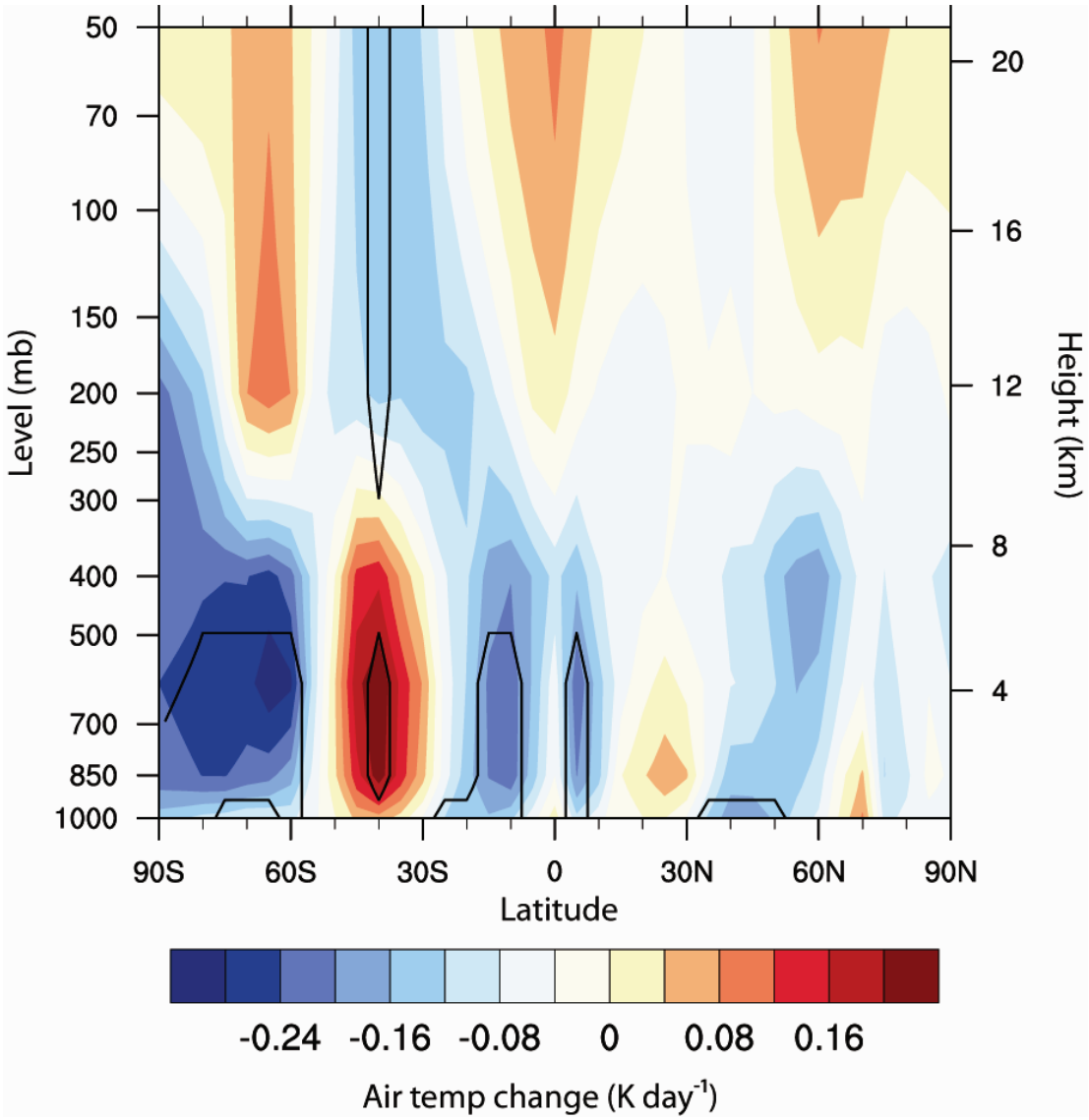

Figure 6.25 AI sample: key date air temperature anomaly

A plot of 5° latitudinally-averaged air temperature anomalies, occurring between 50 and 1,000 mb on the key date of the AI sample. Statistically significant changes are indicated by solid black contours.

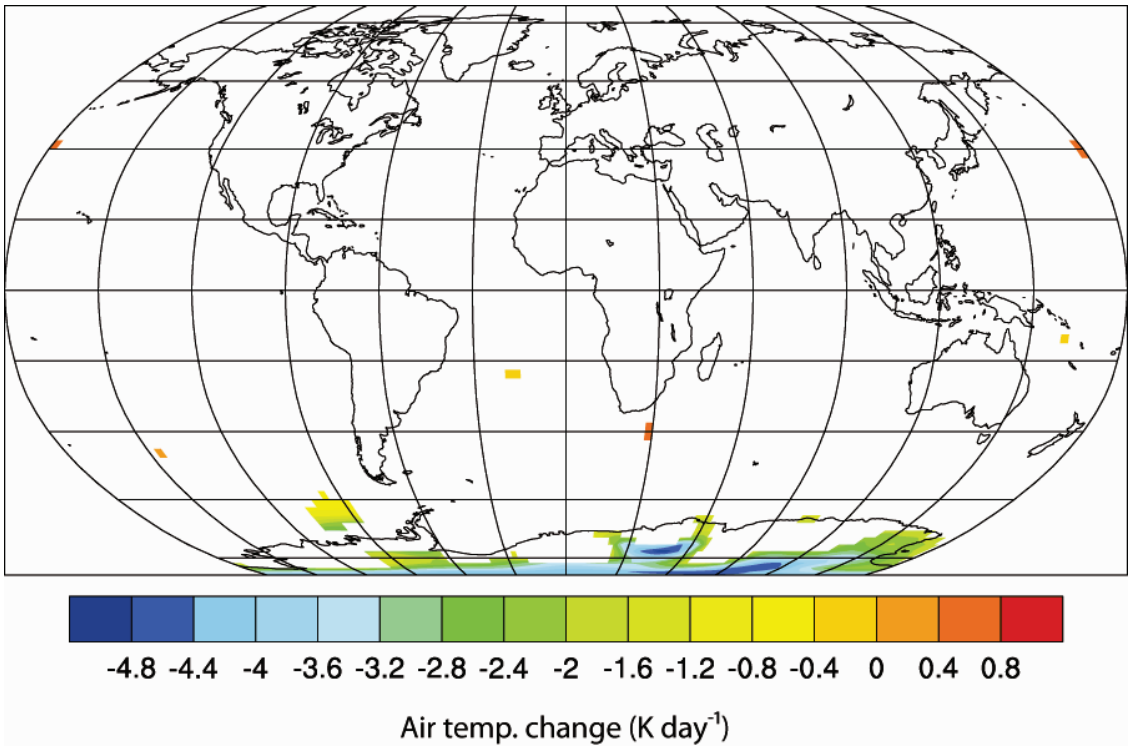

Figure 6.26 AI sample: Antarctic air temperature anomaly

Locally significant surface level anomalous air temperature changes occurring on the key date of the AI sample.

6.4.2 AI sample: pressure

Similar to the previously discussed air temperature anomalies, globally-averaged GPH anomalies occurring over the sample period do not demonstrate any statistically significant changes at any tropospheric level (figure 6.27). However, at a latitudinally-averaged resolution, key date GPH anomalies do show a statistically significant decrease (of around -8 m) occurring between approximately 85°S and 60°S at high to mid-tropospheric levels (figure 6.28). Several other small, but significant GPH anomalies of both positive and negative sign also occur across a range of lower latitude zones around 400 mb. Generally, the strongest and most widespread latitudinally significant GPH anomalies observed are those at high southern latitudes. This supports the theory that atmospheric variability across the Antarctic region may itself be generating the lower latitude anomalies by affecting large-scale circulatory features at lower latitudes.

A pixel-by-pixel plot of surface level pressure anomalies shows an intense, locally significant pressure decrease of approximately -400 Pa day^{-1}, occurring over the interior of the Antarctic

plateau. This change is similar to that observed in the GI sample and may suggest a reduction in the descent of air in the PV has occurred. In addition, a localised but intense pressure decrease of around -500 Pa day^{-1} is also seen off the south-west coast of South America; this particular anomaly may correspond to cyclonic activity in the region (figure 6.29).

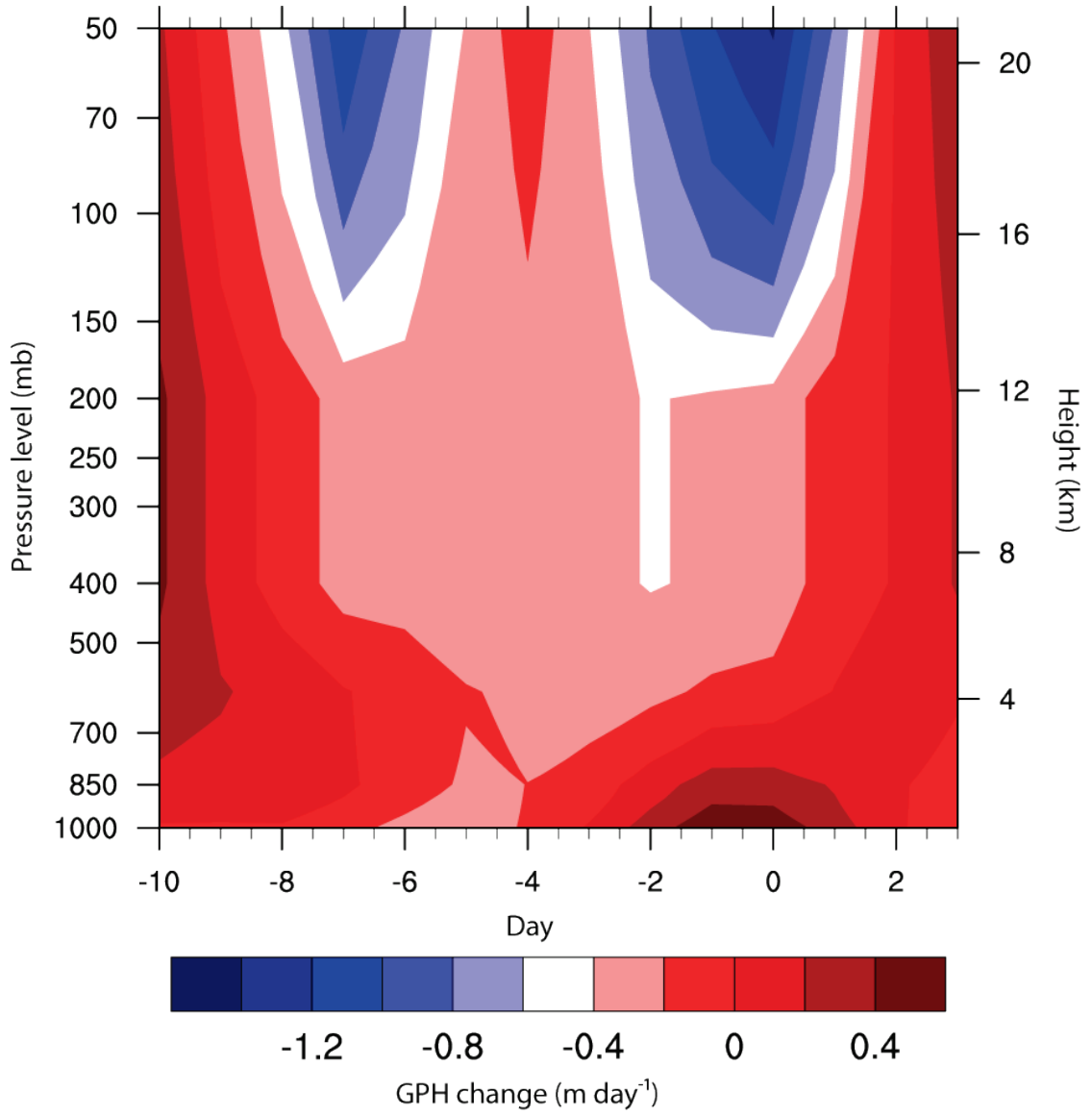

Figure 6.27 AI sample: global GPH anomaly

Globally-averaged anomalous GPH changes occurring between 50 and 1,000 mb during the AI sample.

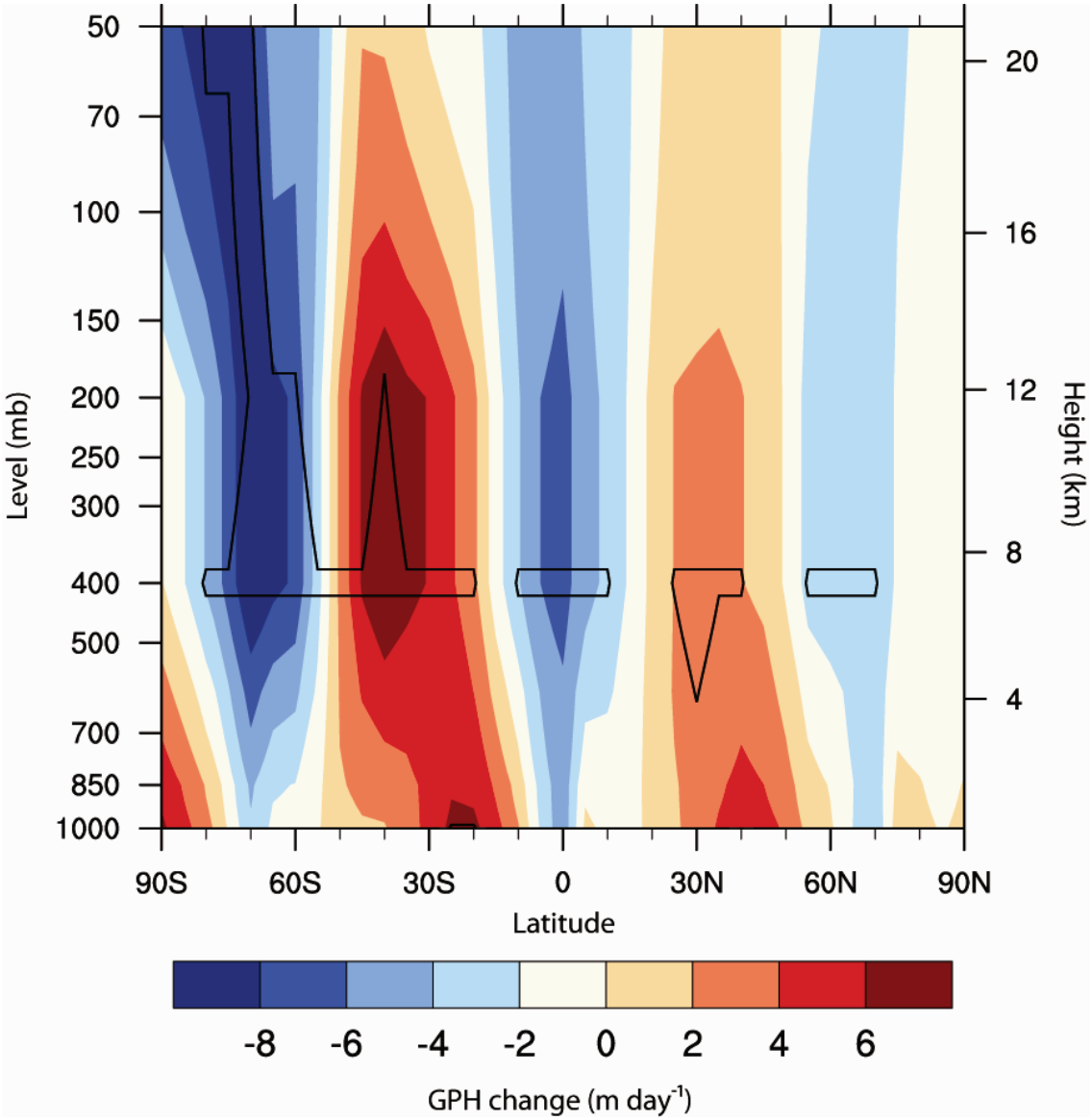

Figure 6.28 AI sample: key date GPH anomaly

A plot of 5° latitudinally-averaged GPH anomalies, occurring between 50 and 1,000 mb on the key date of the AI sample. Statistically significant changes are indicated by solid black contours.

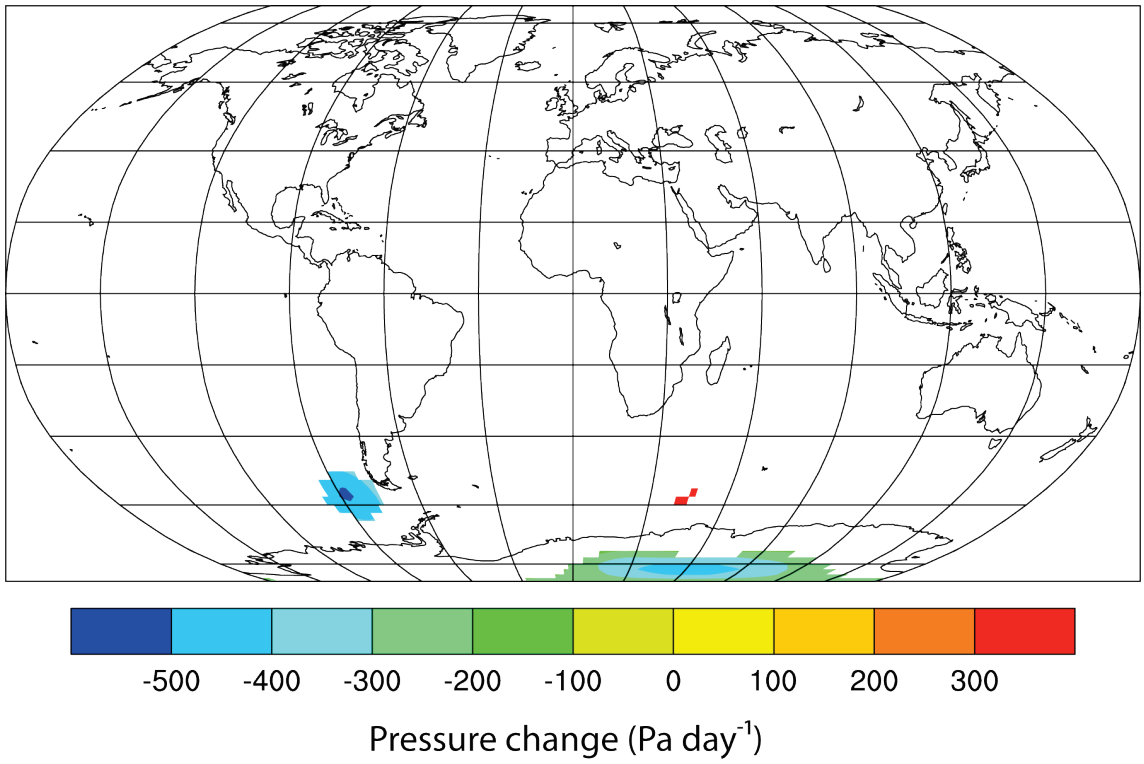

Figure 6.29 AI sample: global pressure anomaly

Locally significant surface level anomalous pressure changes occurring on the key date of the AI sample (units in Pascals).

6.4.3 AI sample: wind

Globally-averaged zonal and meridional wind anomalies show no statistically significant changes at any pressure level, although a coherent positive (westerly) zonal anomaly does appear at upper tropospheric levels between days -5 and 0 (figure 6.30); this pattern of change is similar to that observed in the GI sample. A plot of latitudinally-averaged zonal and meridional anomalies on the key date indicates that whilst these westerly (zonal wind) increases are widespread throughout the upper troposphere, they are largely non-significant (with the exception of one location over the equator). Additionally, a statistically significant easterly (zonal wind) anomaly of approximately 1 ms^{-1} is also observed around 30°S, between 700 and 200 mb (figure 6.31A). In contrast, no statistically significant meridional wind anomalies are identified at any pressure level at a 5° latitudinally-averaged resolution (figure 6.31B).

An examination of the surface level anomalous vector winds occurring on the key date reveals that disturbed flows occur at mid-to high southern latitudes (between 40°S and 90°S). The most intense disturbance observed involves a large scale cyclonic anomaly located off the south-west

coast of South America, with southerly wind speeds of around 2.5 m s^{-1}. This anomaly possesses a spatio-temporal correspondence to a previously discussed locally significant pressure decrease (figure 6.29) and a locally significant surface level air temperature anomaly (figure 6.32). These atmospheric variations suggest the effects of a cyclonic weather system. Separate to the cyclonic anomaly, westerly winds are observed across the interior of the Antarctic plateau (from 0° to 90°E). These data indicate that unusual wind activity is occurring over the Antarctic continent, potentially supporting notions of an indirect cloud–climate interaction operating over this region.

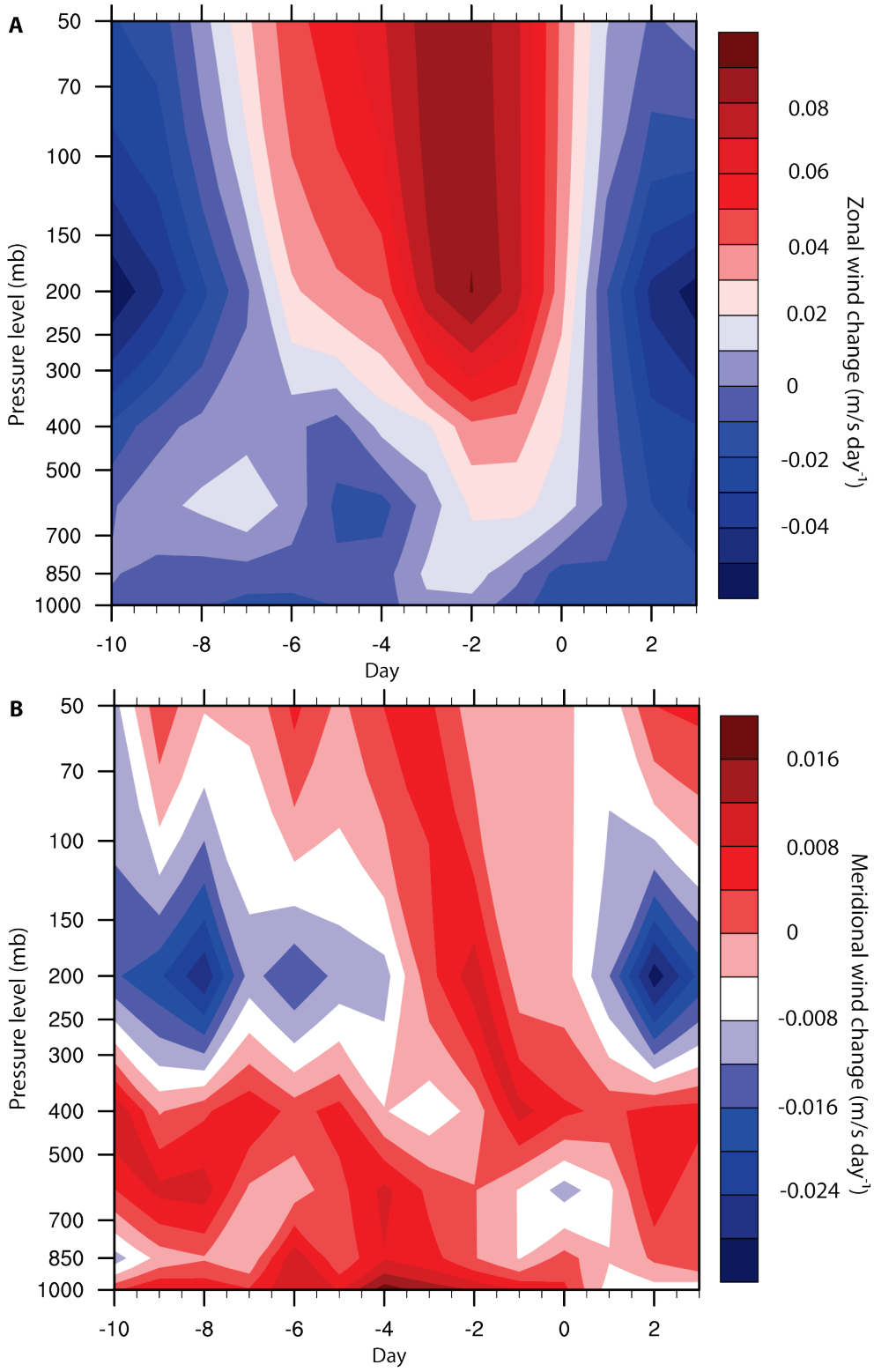

Figure 6.30 AI sample: global wind anomaly

Globally-averaged anomalous **A)** zonal and **B)** meridional wind changes, occurring between 50 and 1,000 mb during the AI sample.

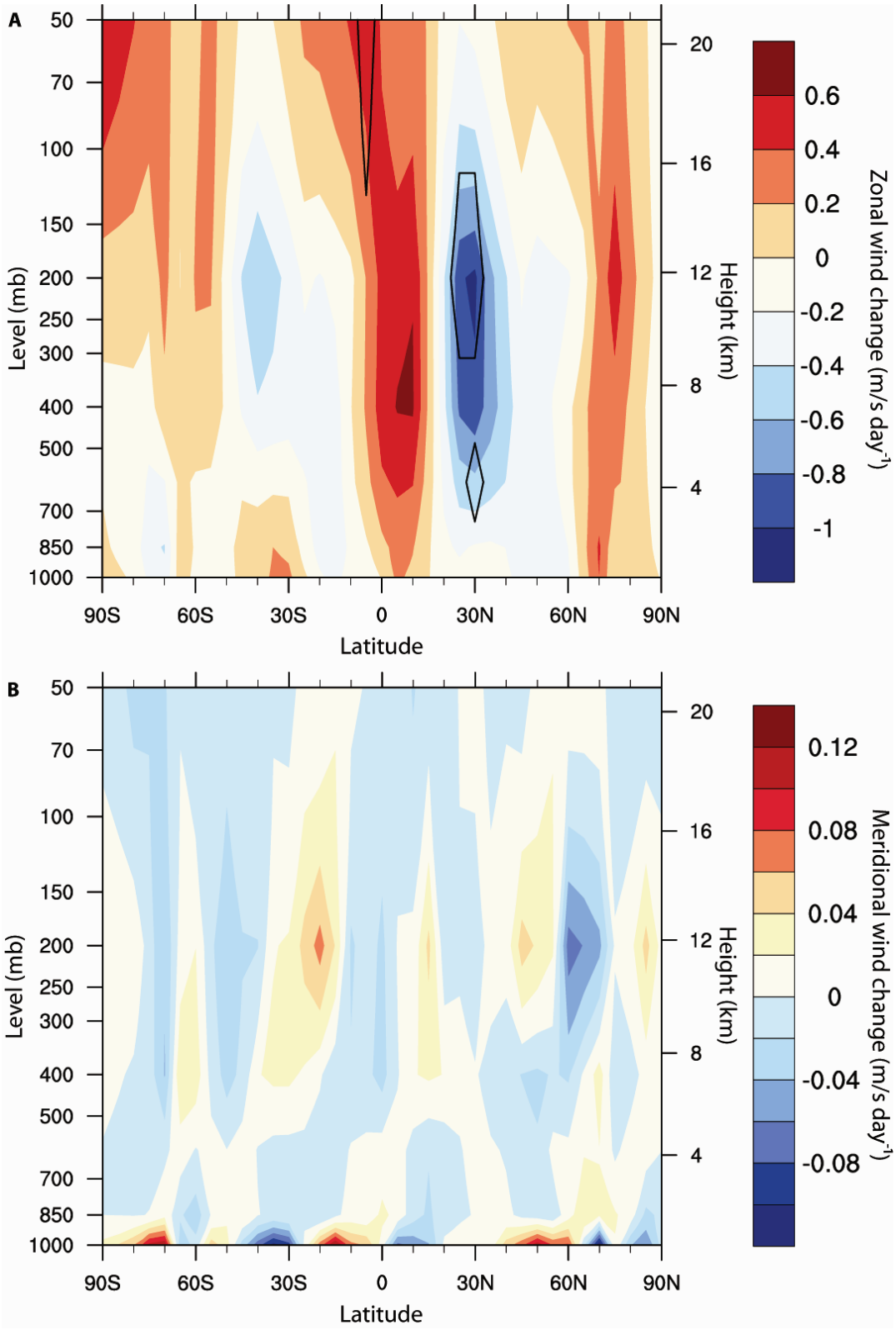

Figure 6.31 AI sample: key date wind anomaly

A plot of 5° latitudinally-averaged anomalous **A)** zonal and **B)** meridional wind changes, occurring between 50 and 1,000 mb on the key date of the AI sample. Statistically significant anomalies are indicated by solid black contours.

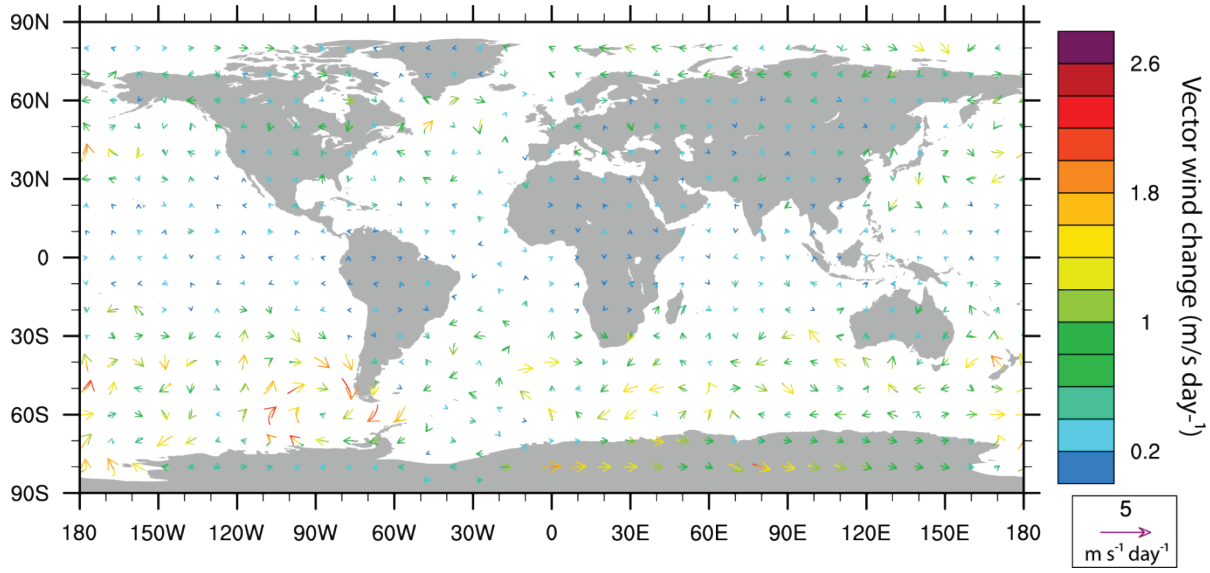

Figure 6.32 AI sample: key date horizontal vector wind anomaly

Surface level horizontal vector wind anomaly on the key date of the AI sample.

6.4.4 AI sample: precipitable water content

A pixel-by-pixel analysis of anomalous key date PW changes over the globe shows that locally significant decreases occur over areas of the eastern Antarctic of around -0.7 kg m^{-2} day^{-1}; this decrease corresponds spatially to locally significant air temperature and pressure anomalies. In addition, an intense decrease of approximately -2.4 kg m^{-2} day^{-1} is also detected off the south-west coast of South America in the same region as a cyclonic weather system (figure 6.33). Several other smaller PW anomalies are also observed, the largest of which is located south of Africa at around 60°S; however, a connection between this anomaly and the various atmospheric changes detected during the AI sample is not readily apparent.

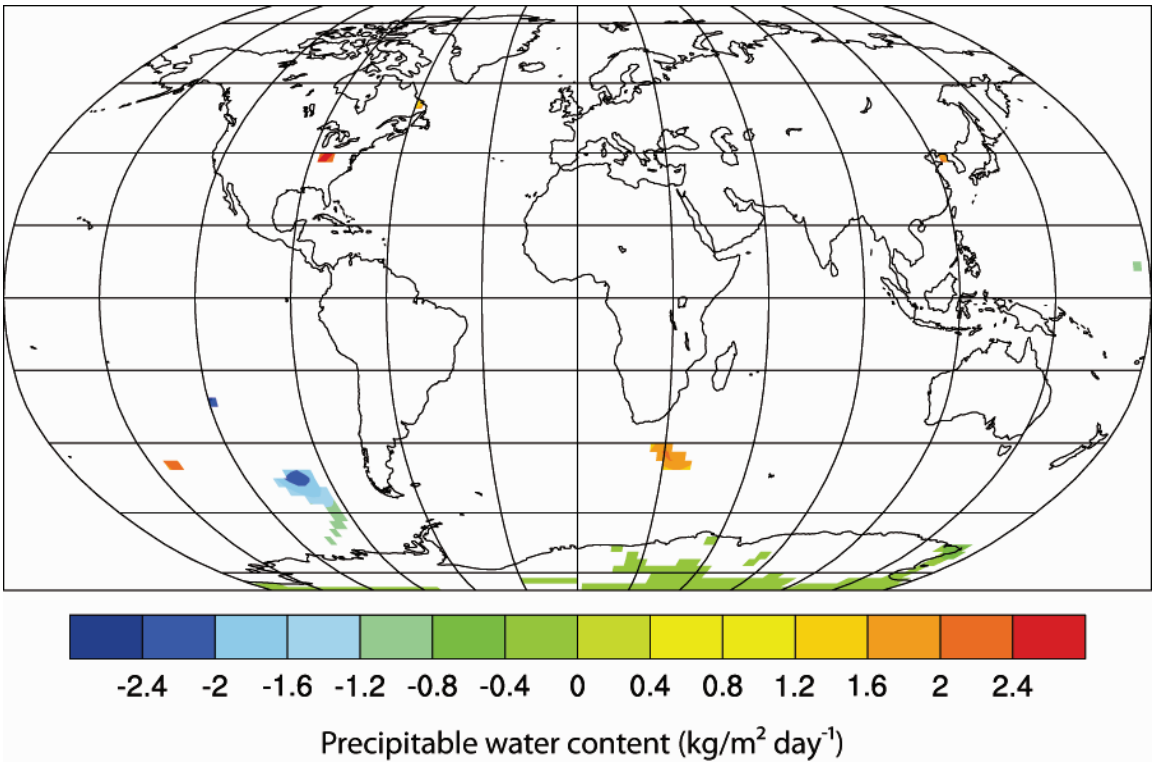

Figure 6.33 AI sample: global precipitable water content anomaly

Key date, locally significant precipitable water content anomaly.

6.4.5 AI sample: Dome C AWS data

AWS data from Dome C show that anomalous decreases in air temperature of approximately -2.3 K occur between days -5 and 0; these changes are found to be statistically significant between days -3 and 0. Similarly, a statistically significant pressure decrease of approximately 6 mb is observed between days -5 and -2 (figure 6.34). These findings are comparable to the NCEP/NCAR reanalysis data, which also showed significant decreases in pressure and air temperature occur over the Antarctic plateau around the key date of the AI sample.

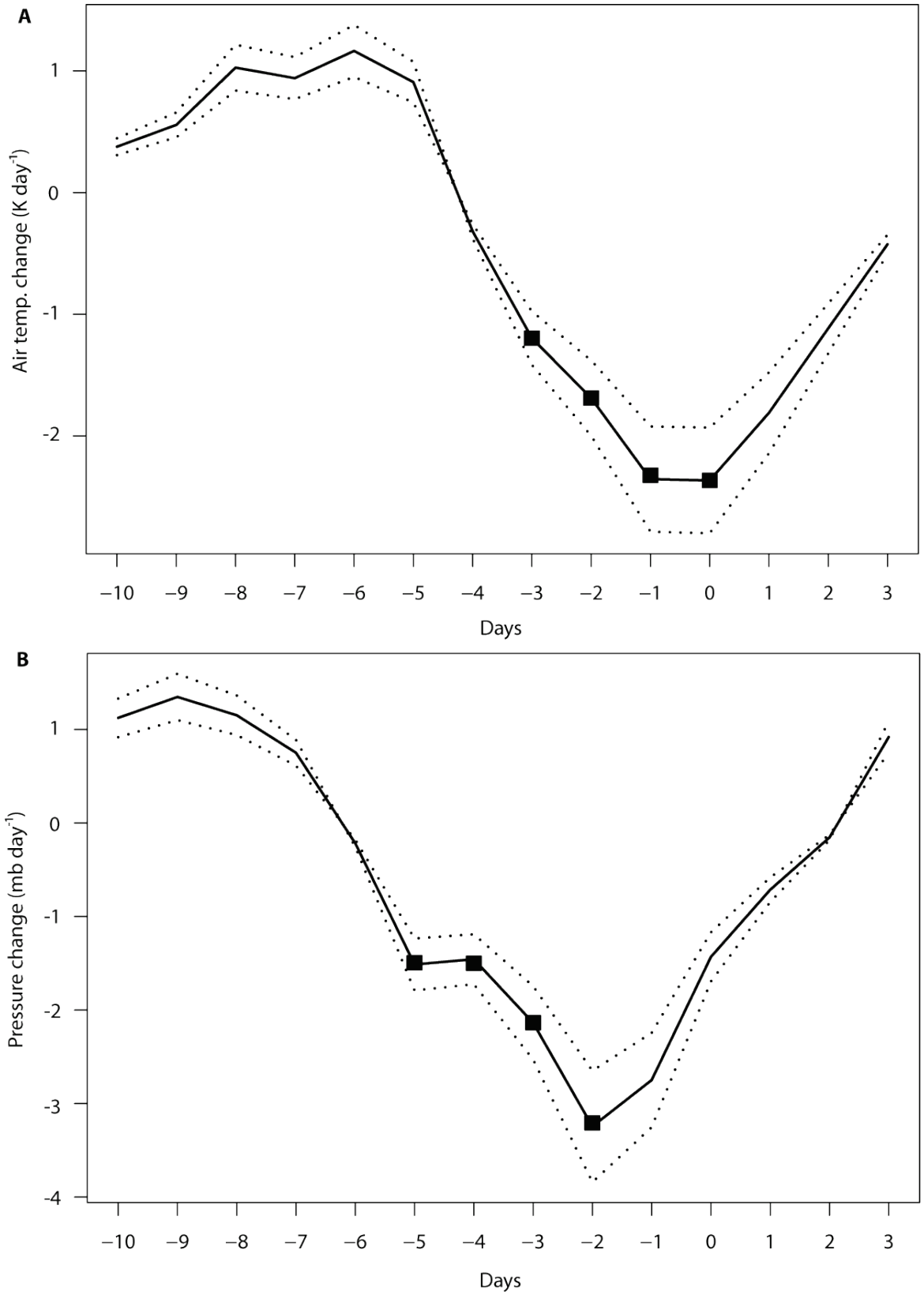

Figure 6.34 AI sample Dome C AWS data

Anomalous **A)** air temperature and **B)** pressure data measured by Dome C AWS (77.50°S, 123.00°E) during the AI sample period. Dotted lines display the 0.95 level confidence interval, while markers indicate statistically significant anomalies (above the 0.95 critical level).

6.4.6 AI sample: analysis and discussion

The AI sample demonstrated a detectable atmospheric response located at high southern latitudes. Statistically significant anomalous activity was found to occur around the key date and around day -6; both of these periods correspond to statistically significant co-temporal variations in the rate of GCR flux and Antarctic cloud cover changes, suggesting a relationship between GCR, cloud and atmospheric anomalies over the Antarctic region comparable to that observed over the GI sample. The pattern of air temperature and pressure variations over the Antarctic continent may provide tentative support for the previously discussed notions of an indirect cloud forcing over polar regions. However, the sample did also show some indications that internal (cyclonic) variability may be influencing the results to some extent.

6.5 MLD sample: cloud anomalies

Over the MLD sample, the rate of GCR flux and cloud changes were found to undergo statistically significant, co-temporal, positively related variations. The rate of GCR flux and mid-latitude cloud change showed a significant increase between days -5 and -4, followed by a significant decrease between days -1 and 1. The largest cloud decreases occurred on the key date at low tropospheric levels (between 700 and 1,000 mb), around 40°–20° (in both hemispheres).

6.5.1 MLD sample: air temperature

Although globally-averaged air temperature anomalies over the MLD sample show no statistically significant changes occurring around the key date at any pressure level (figure 6.35), 5° latitudinally-averaged key date air temperature anomalies do detect a significant increase in air temperature of approximately 0.24 K at low tropospheric levels (between 500 and 900 mb) around 30° in both hemispheres. Additionally, in the southern hemisphere a significant decrease and increase (of approximately 0.24 K) is also detected at 60°S and 90°S respectively (figure 6.36). A pixel-by-pixel analysis of surface level air temperature anomalies indicates that only a limited number of locally significant anomalies are occurring; the largest of which is a temperature increase over North America of around 2 K (figure 6.37). The finding of latitudinally averaged significant temperature changes but no

locally significant changes suggests that mid-latitude temperature changes may be occurring via a regionally diffuse process; if the temperature changes are causally linked to cloud anomalies this may suggest a small but regionally widespread cloud change is occurring.

The dominant effect of a reduction in low cloud cover at mid-latitudes should be to reduce albedo and consequently warm low tropospheric levels (Ramanathan et al., 1989). Latitudinally significant decreases in cloud cover were observed around 30° (north and south); the correlation of these changes to statistically significant temperature increases implies a causal relationship, as such findings are in agreement with the expected temperature forcing resulting from a mid-latitude cloud decrease.

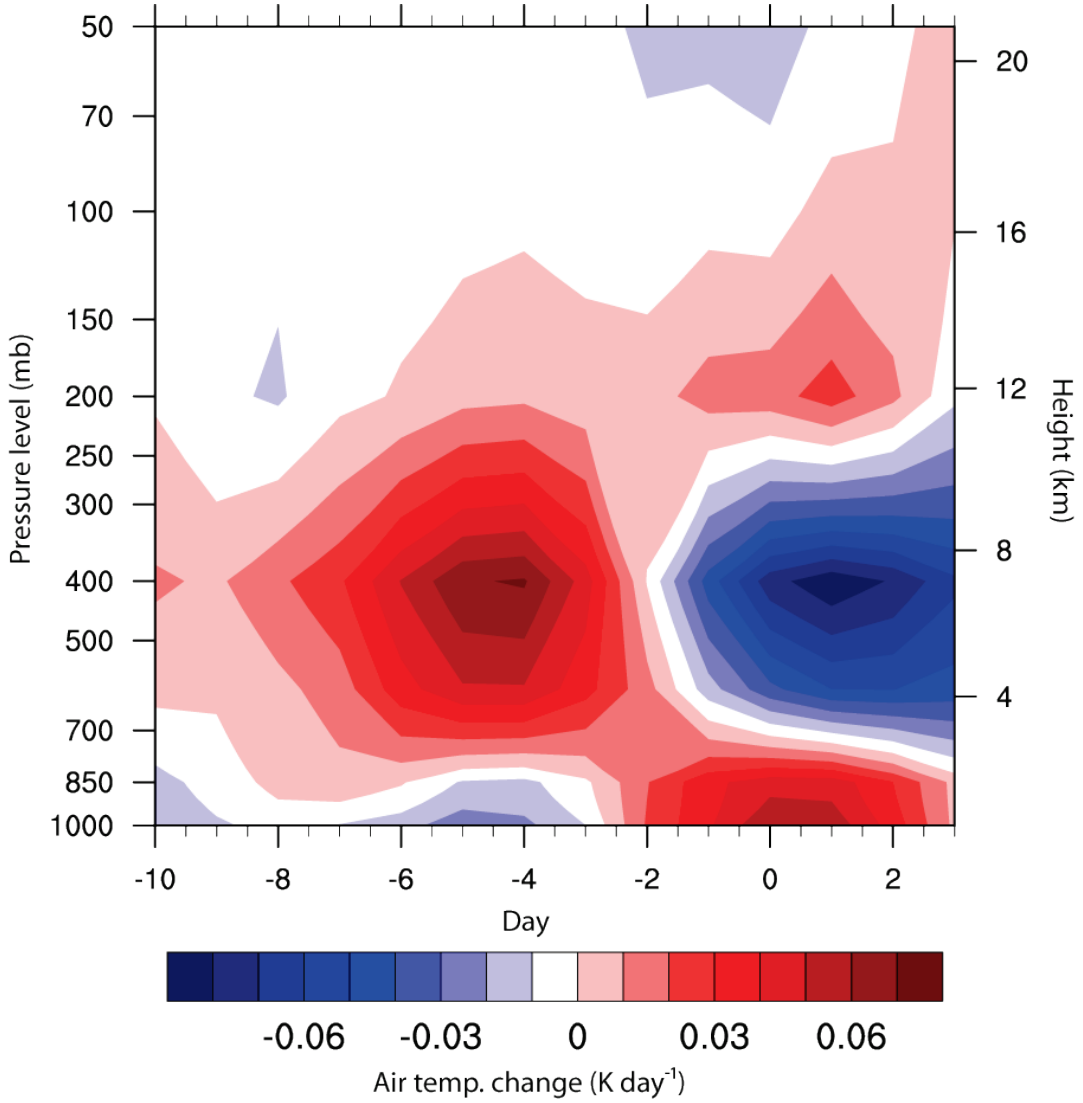

Figure 6.35 MLD sample: global air temperature anomaly

Globally-averaged anomalous air temperature changes occurring between 50 and 1,000 mb during the MLD sample.

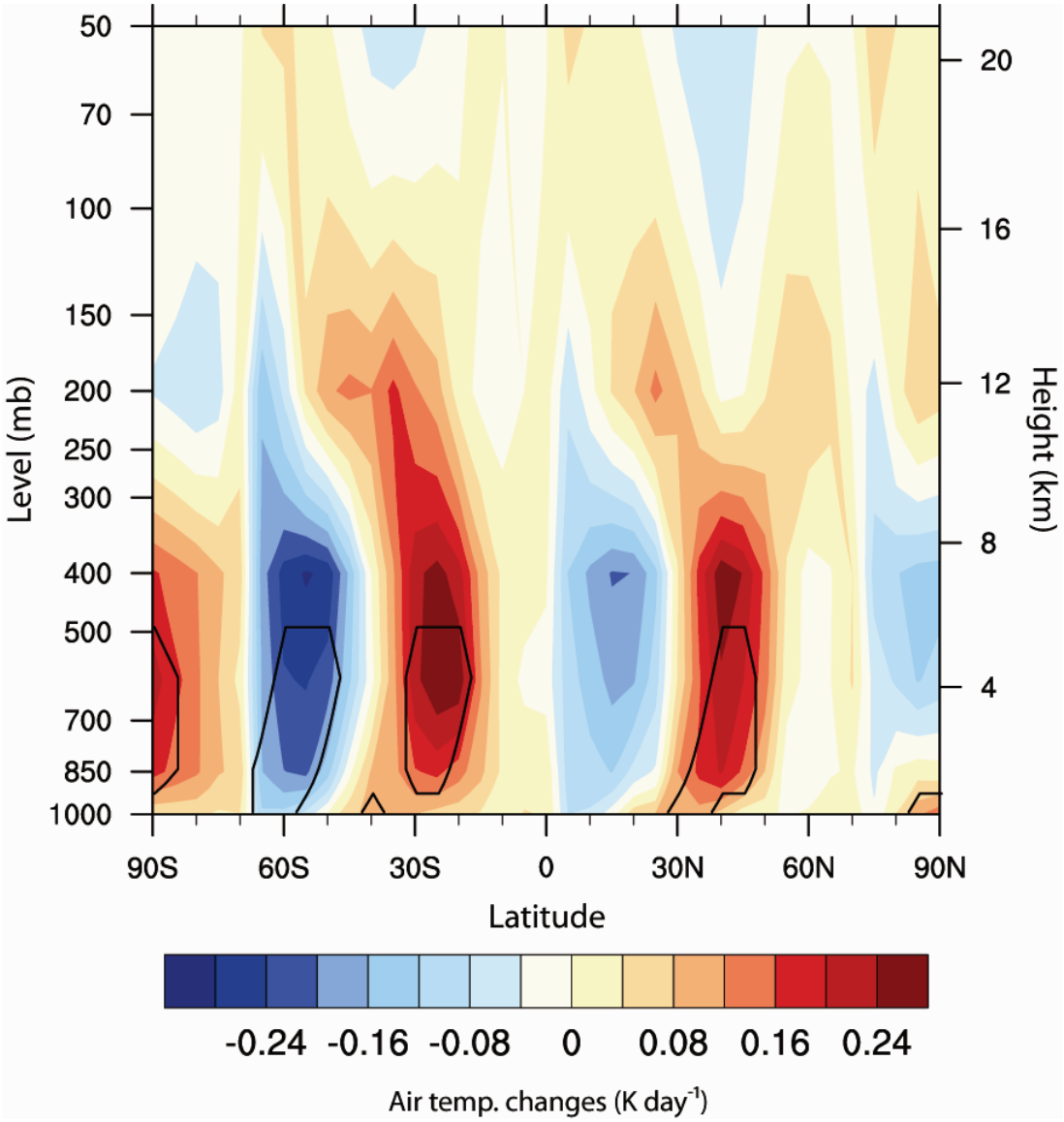

Figure 6.36 MLD sample: key date air temperature anomaly

A plot of 5° latitudinally-averaged air temperature anomalies, occurring between 50 and 1,000 mb on the key date of the MLD sample. Statistically significant changes are indicated by solid black contours.

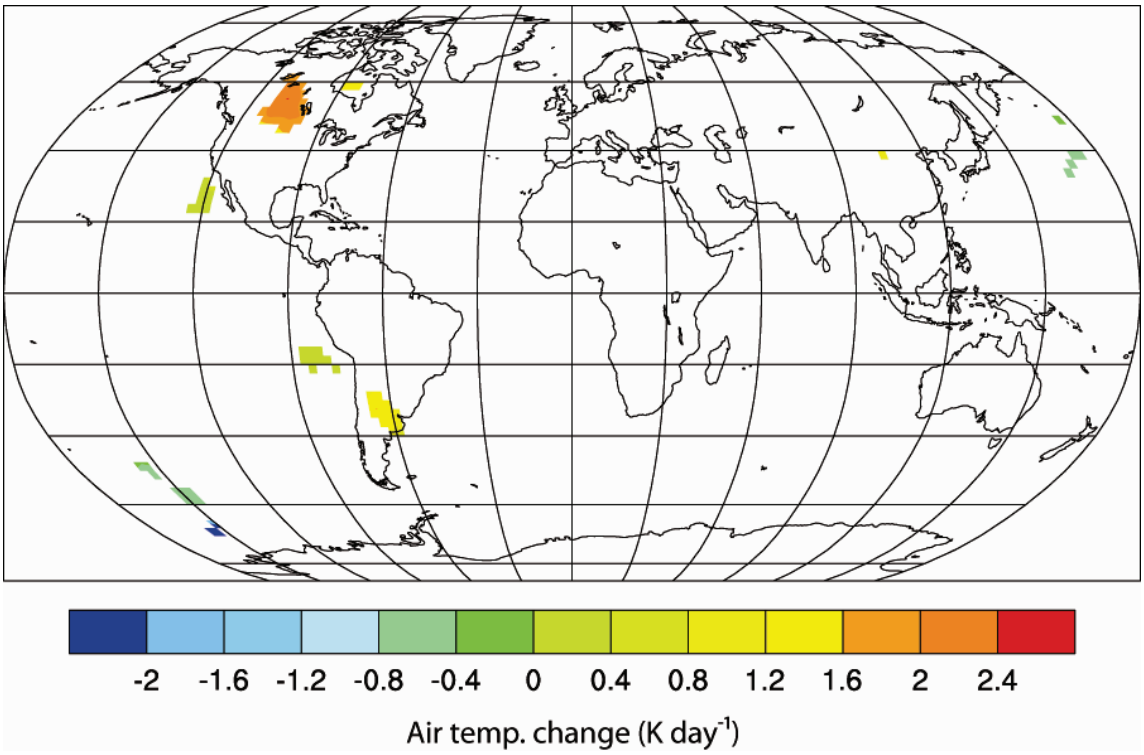

Figure 6.37 MLD sample: global air temperature anomaly

Locally significant surface level anomalous air temperature changes occurring on the key date of the MLD sample.

6.5.2 MLD sample: pressure

Globally-averaged GPH anomalies demonstrate no statistically significant changes over the sample period at any pressure level (figure 6.38). However, 5° latitudinally-averaged anomalous GPH changes on the key date show the occurrence of statistically significant changes across a wide range of latitudinal zones (figure 6.39). These anomalies occur predominately at mid-to high tropospheric levels (between 500 and 50 mb), with the exception of an anomalous increase in near-surface level GPH of around 6 m s^{-1} at 65°S. Positive GPH anomalies of around 6 m s^{-1} occur between the latitude ranges of 90°S–70°S, 30°S–10°S and 30°N–50°N, while negative GPH anomalies of around -7 m s^{-1} occur between the latitude ranges of 60°S–40°S, 10°N–30°N and 60°N–90°N. A pixel-by-pixel analysis of anomalous surface level key date pressure changes indicates that there are virtually no areas of locally significant pressure change over the globe, although anomalous pressure increases of around 280 Pa day^{-1} are detected around areas of the Antarctic continent (figure 6.40).

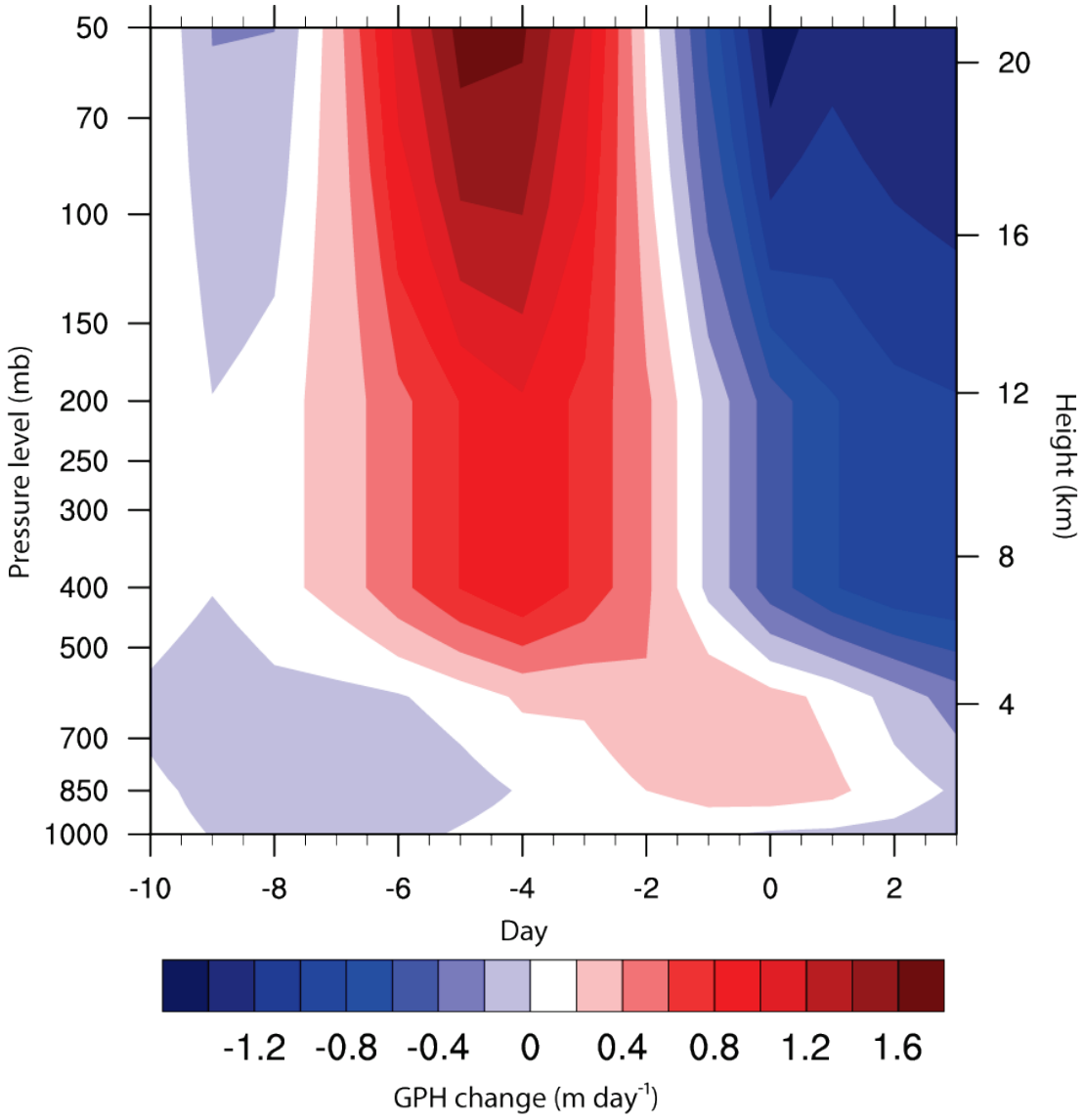

Figure 6.38 MLD sample: global GPH anomaly

Globally-averaged anomalous GPH changes occurring between 50 and 1,000 mb during the MLD sample.

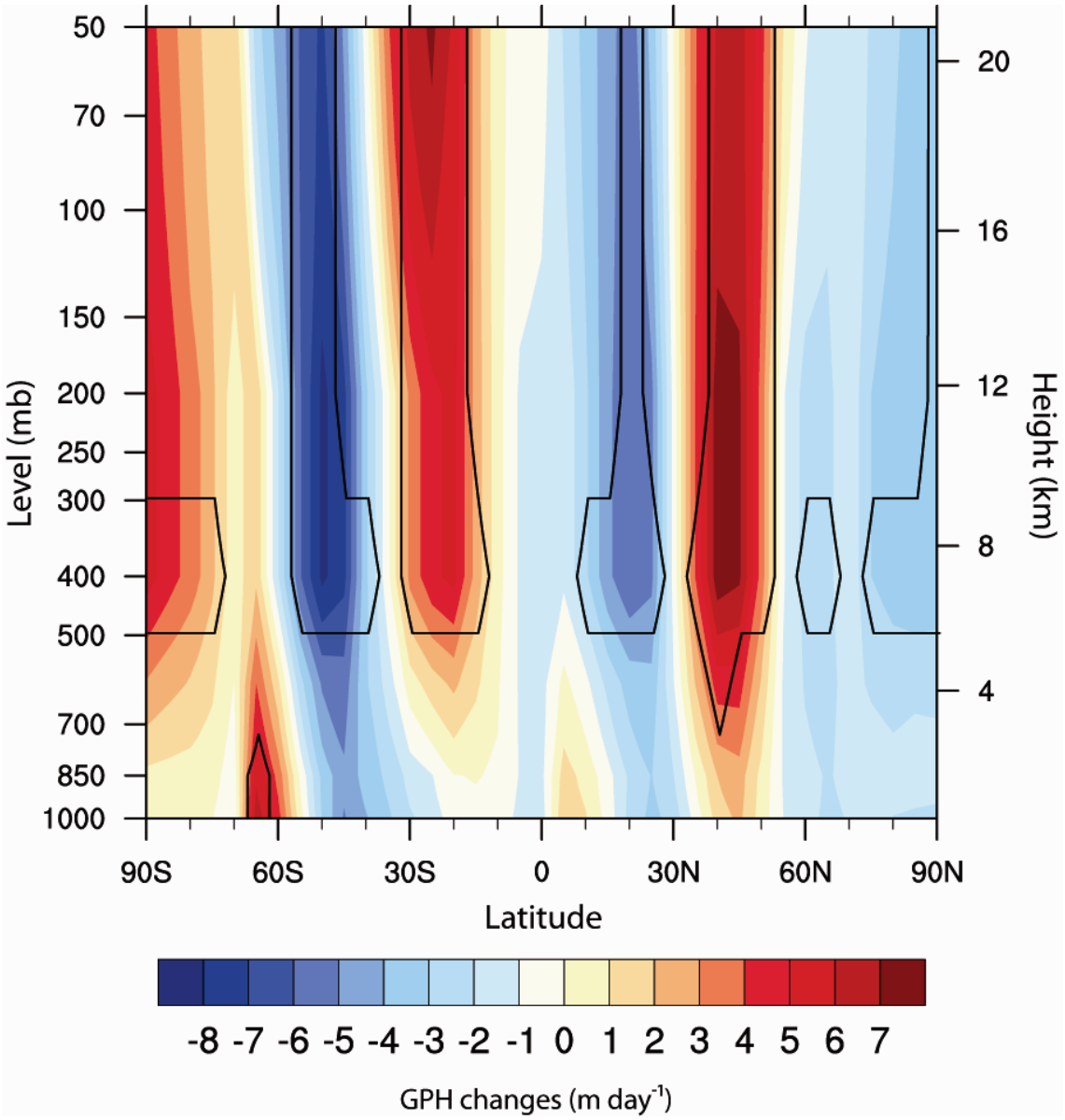

Figure 6.39 MLD sample: key date GPH anomaly

A plot of 5° latitudinally-averaged GPH anomalies, occurring between 50 and 1,000 mb on the key date of the MLD sample. Statistically significant changes are indicated by solid black contours.

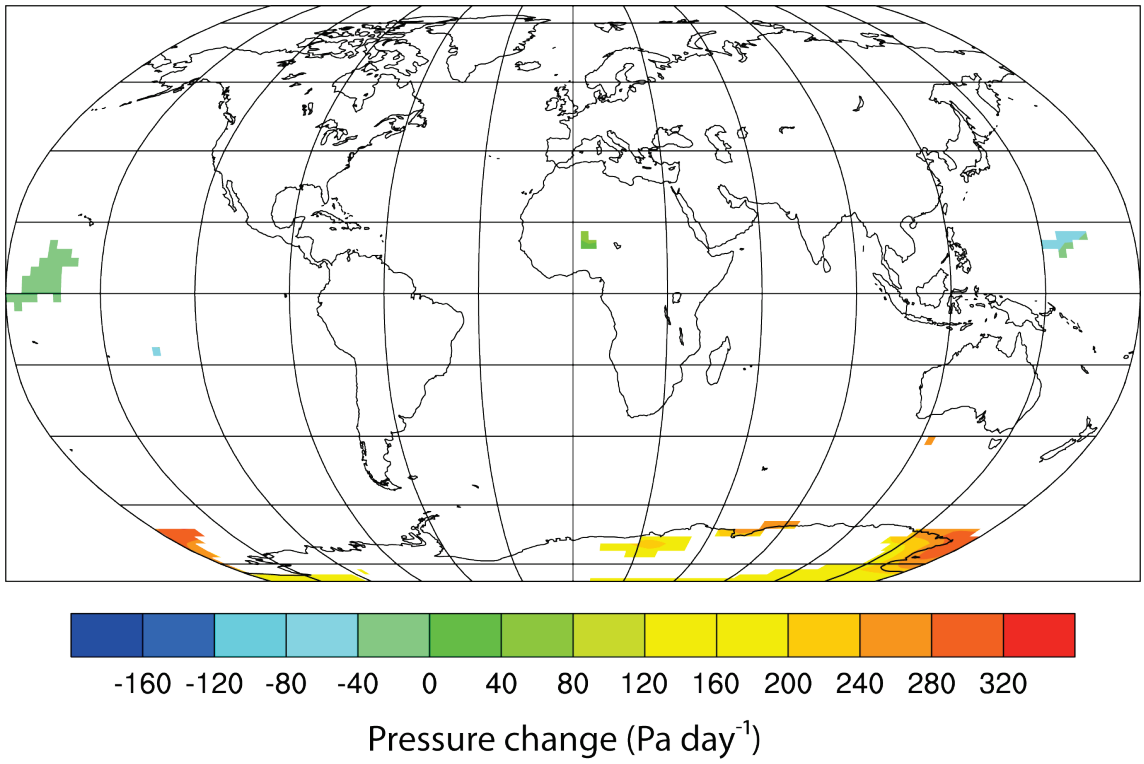

Figure 6.40 MLD sample: global pressure anomaly

Locally significant surface level anomalous pressure changes occurring on the key date of the MLD sample (units in Pascals).

6.5.3 MLD sample: wind

Globally-averaged zonal and meridional anomalous wind changes over the sample period show no statistically significant variations at any pressure level (figure 6.41). However, latitudinally-averaged key date anomalous zonal and meridional changes do demonstrate small regions of statistical significance (figure 6.42); significant positive (westerly) zonal anomalies of around 0.6 m s^{-1} occur at approximately 30°S and 35°N–50°N throughout the troposphere. Additionally, a significant negative (easterly) zonal anomaly of around -0.6 m s^{-1} also occurs between 0° and 10°N (figure 6.42A). Significant positive (southerly) meridional wind anomalies of around 0.75 m s^{-1} are found around the 200 mb level in the same position as the positive zonal anomalies (30°S and 35°N–50°N). Moreover, several localised but significant (positive and negative) meridional anomalies are also detected at low tropospheric levels between 850 and 1,000 mb. The position of these zonal/meridional anomalies (also at 30°S and 35°N–50°N) may be linked to the significant latitudinally average GPH anomalies previously discussed

(figure 6.39); the anomalous wind flow detected may result from the increased pressure difference between these adjacent latitude zones.

A surface level vector plot of anomalous wind flow indicates that disturbances of approximately 2 m s^{-1} day^{-1} are present around mid-to high latitude regions of the southern oceans (40°S–80°S). In contrast, far less anomalous wind activity is observed in the northern hemisphere (figure 6.43).

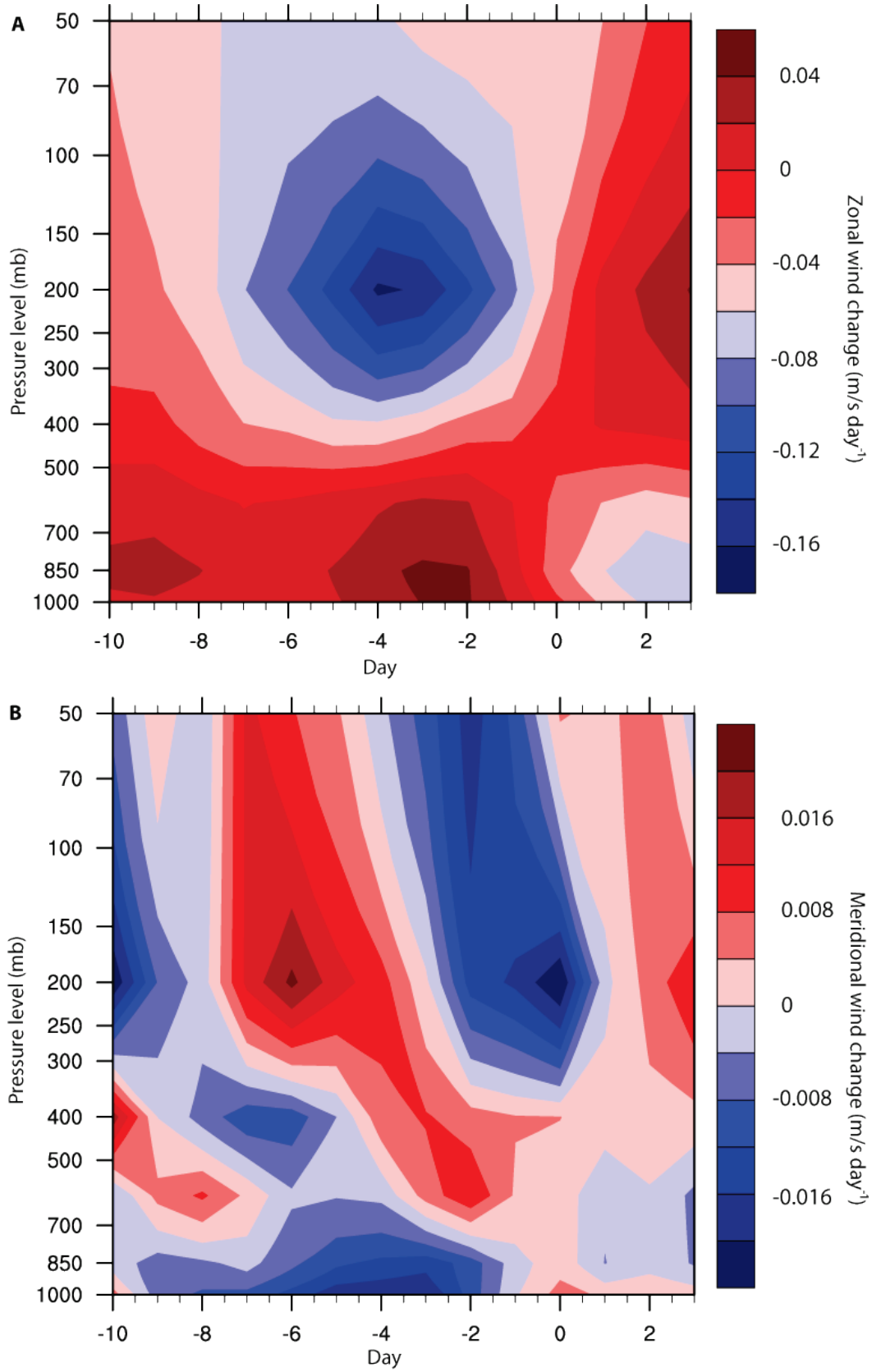

Figure 6.41 MLD sample: global wind anomaly

Globally-averaged anomalous **A)** zonal and **B)** meridional wind changes occurring between 50 and 1,000 mb during the MLD sample.

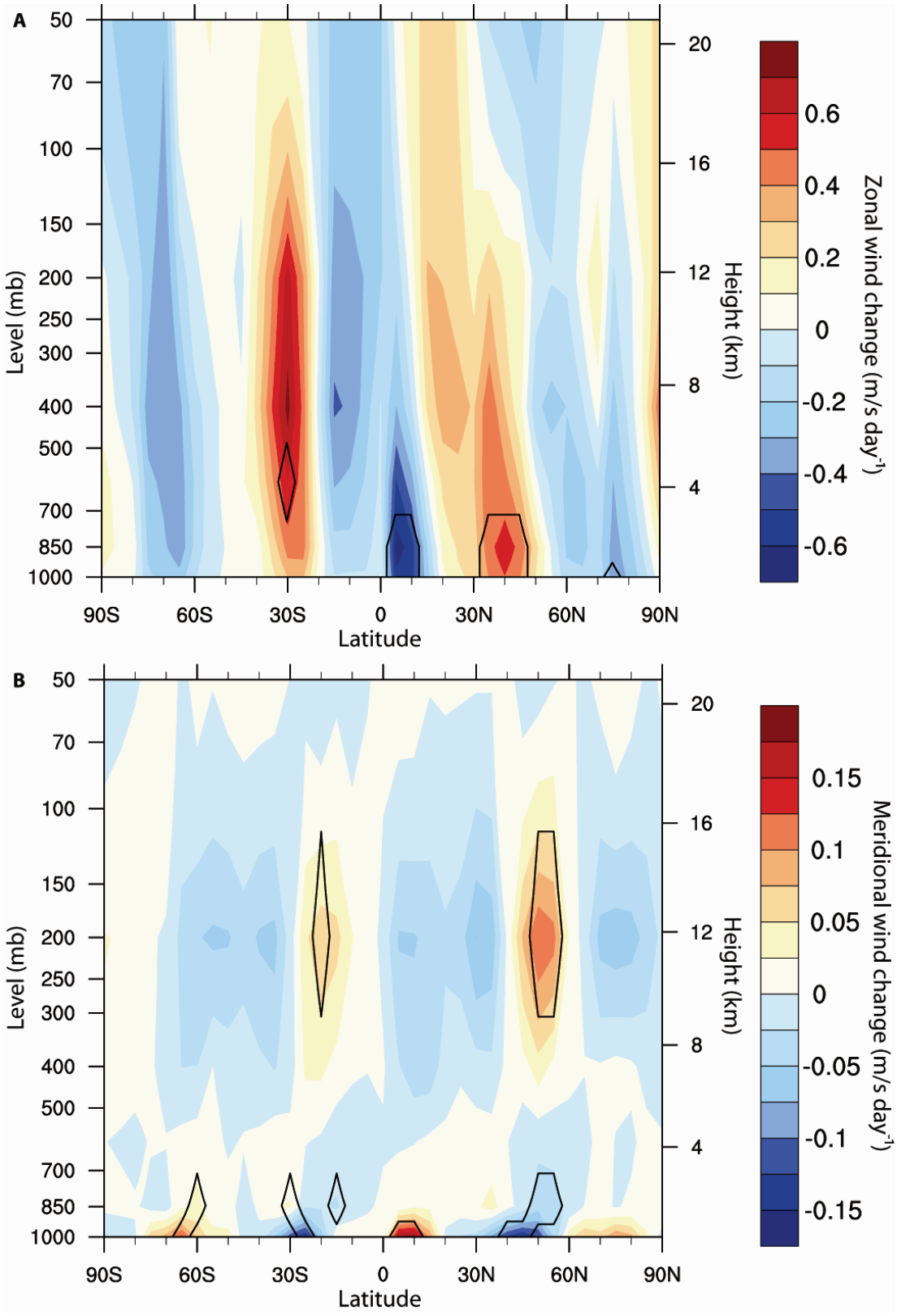

Figure 6.42 MLD sample: key date wind anomaly

A plot of 5° latitudinally-averaged anomalous **A)** zonal and **B)** meridional wind changes occurring between 50 and 1,000 mb on the key date of the MLD sample. Statistically significant anomalies are indicated by solid black contours.

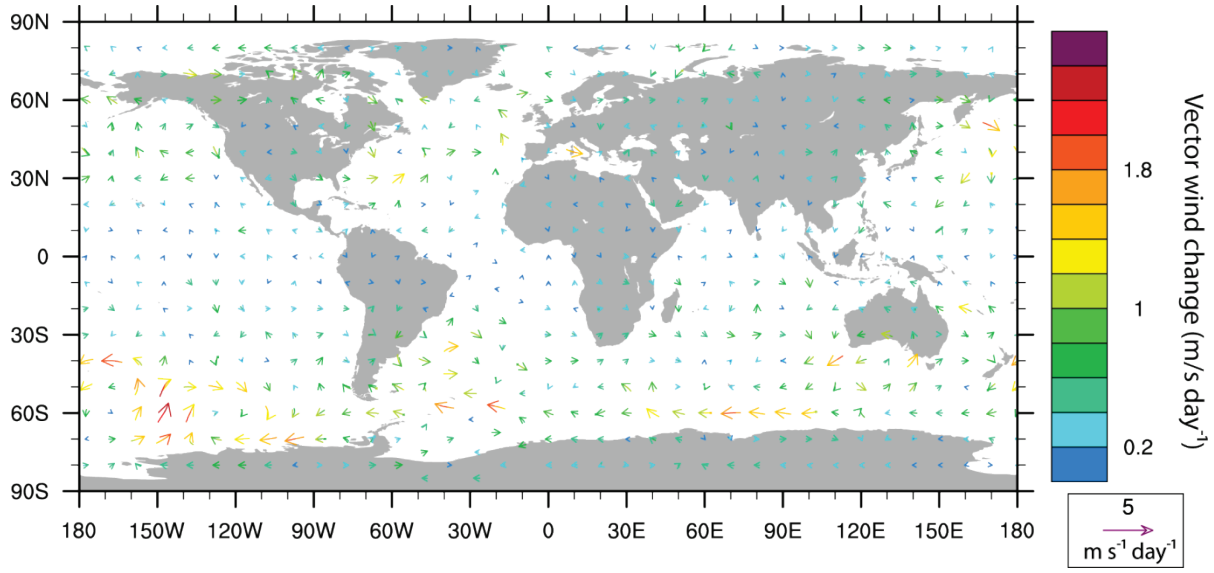

Figure 6.43 MLD sample: key date horizontal vector wind anomaly

Surface level horizontal vector wind anomaly on the key date of the MLD sample.

6.5.4 MLD sample: precipitable water content

Although several small locally significant PW anomalies are observed on the key date, these anomalies do not appear to be anything more than random variability. The appearance of the anomalies suggests that, in general, no locally significant changes are occurring across the globe in response to the mid-latitude cloud decreases (figure 6.44).

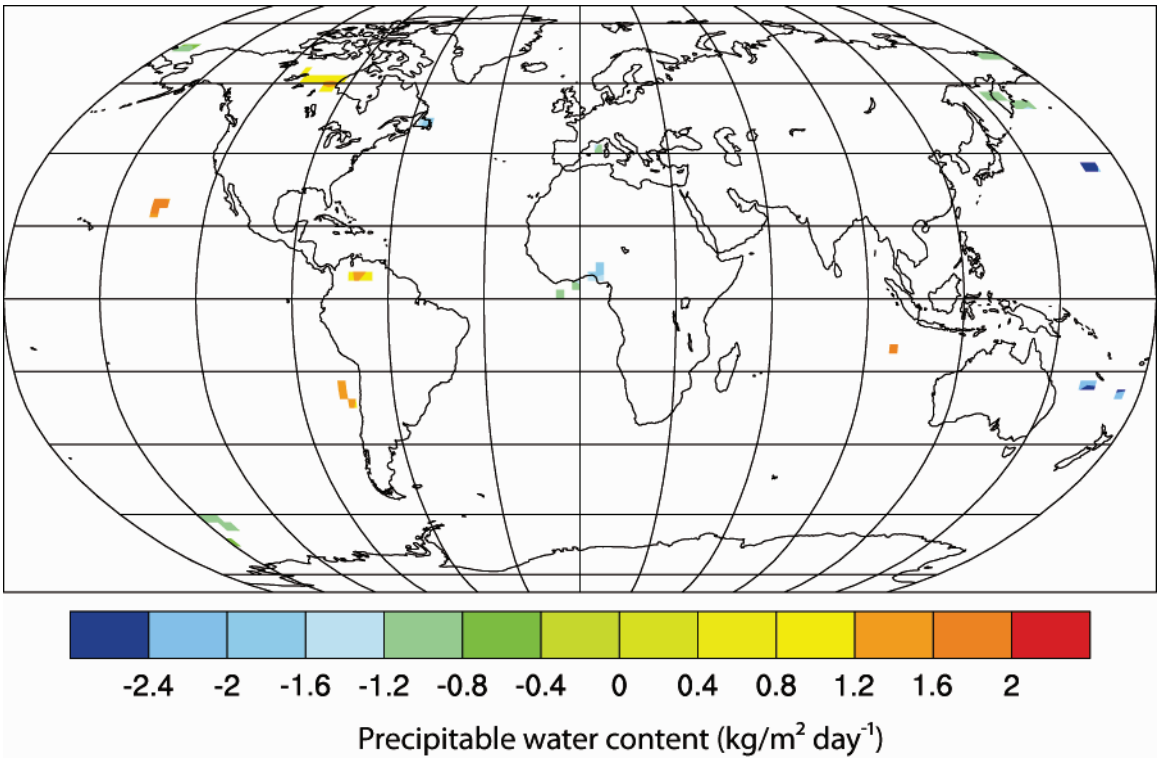

Figure 6.44 MLD sample: global precipitable water content anomaly

Key date locally significant precipitable water content anomaly.

6.5.5 MLD sample: analysis and discussion

The MLD sample robustly indicates that latitudinally significant mid-latitude cloud decreases are accompanied by corresponding latitudinally significant air temperature increases. Such a relationship should be expected following a decrease in mid-to low tropospheric clouds as a consequence of decreased albedo. The detected air temperature anomalies were however not found to be locally significant, which may indicate either: (1) the operation of a small but widespread process occurring throughout the mid-latitude regions; or alternatively, (2) a low

SNR at the individual pixel level, resulting in the capability to detect a statistically significant signal only after an area-averaged approach is applied.

Latitudinally significant GPH anomalies are also observed at subtropical, mid- and polar latitudes, which may suggest a globally widespread climate forcing may be occurring. Although in general there were no observed significant cloud changes occurring at latitudes above or below 30°–60° (N/S), the detected GPH changes outside of these areas may be indirectly related to the detected mid-latitude GCR–cloud relationship.

The GI and AI samples both showed a statistically significant precipitation response which correlated with anomalous temperature/cloud and pressure changes; however, the MLD sample showed no such response. A past study has indicated that, precipitation and precipitation efficiency show statistically significant change over ocean surfaces, of approximately 7–9 % during the 11-year solar cycle at high southern latitudes (between 45°S and 90°S) (Kniveton and Todd, 2001). Most of the cloud changes detected during the MLD sample occur outside of the latitude range highlighted by Kniveton and Todd (2001), implying that observations of precipitation changes may be unlikely. Furthermore, a lack of precipitation decreases may also suggest that the cloud decreases are occurring in cloud systems which do not produce precipitation. As the majority of the detected cloud changes occur at low tropospheric levels (between 600 and 1,000 mb) and do not involve precipitation, it is likely that the clouds are either of a shallow cumulus or stratocumulus variety.

6.6 Vertical velocity evidence of an indirect cloud–climate forcing?

After analysing the GI and AI samples it was speculated that an indirect cloud–climate relationship might be operating. Whereby, increased upper/mid level cloud in the Antarctic/Arctic regions warms the surrounding air and reducing the volume of air descending in the PV. It was suggested that this process may theoretically explain the decreased surface level air temperatures identified during the GI sample (described in section 6.3.7). The validity of this hypothesis can be tested by examining changes in the vertical velocity parameter (omega).

Omega is calculated by combining the effects of vorticity and thermal advection to derive the resulting vertical motion. For reference, a mean of the latitudinally-averaged Arctic (90°N–60°N) and Antarctic (60°S–90°S) omega parameter between 1985 and 2006) is shown in figure 6.45 (positive values indicate descending air, while negative values indicate rising air). The

mean state clearly demonstrates the convergence of air at mid- to low tropospheric levels that occurs over polar regions.

An analysis of the latitudinally-averaged omega anomalies occurring during the GI sample is shown in figure 6.46. This plot indicates that over the Arctic there is a relative reduction in the descent of upper level (100–200 mb) air on the key date of approximately 0.0002 Pa s^{-1} day^{-1}. Whereas, at lower tropospheric levels (200–1,000 mb), there is a relative increase in the rate of descending of air on the key date of the composite of around 0.0008 Pa s^{-1} day^{-1} (figure 6.46A). In Antarctica, the changes in omega are more intense: there is a change from negative to statistically significant positive conditions (at all tropospheric levels), suggesting that on the key date of cloud increase the convergence of air towards the surface level undergoes a relative increase of around 0.0013 Pa s^{-1} day^{-1} (figure 6.46B).

A plot of anomalous omega changes at low (1,000–850 mb), mid- (600–400 mb) and upper (200–100 mb) tropospheric levels shows a different response between the Antarctic an Arctic regions (figure 6.47). In the Antarctic region, omega generally decreases around day -5 and then increases towards the key date. The mid- and low-level anomalies appear to undergo the largest changes: mid-level changes show a statistically significant positive anomaly centred on day -1 of approximately 0.001 Pa s^{-1} day^{-1}, while low-level anomalies also demonstrate a statistically significant positive anomaly of approximately 0.0007 Pa s^{-1} day^{-1} centred on day 1 of the composite. The upper level Antarctic omega anomalies demonstrate a pattern of change comparable to the mid-level anomalies but are relatively weaker (figure 6.47A). The Arctic omega anomalies also indicate the occurrence of a negative anomaly around day -5, followed by a shift towards more positive conditions on the key date. Although the negative anomalies centred on day -5 are of a comparable magnitude to those observed in the Antarctic, the positive anomalies in the Arctic are only around half the magnitude of their Antarctic counterparts. Furthermore, in the Arctic, a mid-level omega response is virtually non-existent, while the upper-level anomaly shows no clear relationship to the key date. The differing magnitude and timing of the response between omega anomalies at the Arctic and Antarctic leads to the conclusion that, although, there may be a response in vertical movement to the cloud anomalies, this response cannot be responsible for producing observed low-level temperature decreases on key date.

A pixel by pixel analysis of omega anomalies supports this conclusion, as it shows that virtually no statistically significant anomalies can be detected over the Arctic or Antarctic regions (figure 6.48–6.49); indicating that the influence of the cloud changes on omega is only observable when observing area-averaged changes. If omega anomalies were responsible for producing the observed locally significant changes in surface level temperature and pressure, then it should be

expected that locally significant omega anomalies of similar spatio-temporal dimensions would be detectable.

Finally, these results show that over both polar regions the opposite sign anomalies to those predicted is occurring: rather than a reduction in the descent of air, an increase in the rate of descent in observed. Consequently, it appears that the hypothesised relationship between the observed cloud increases and air temperature decreases is incorrect. However, it is important to note, when considering these results that the omega reanalysis parameter has been found to be of questionable quality over polar regions, as a result conclusions drawn from this parameter should be treated with caution (Bromwich and Wang, 2005).

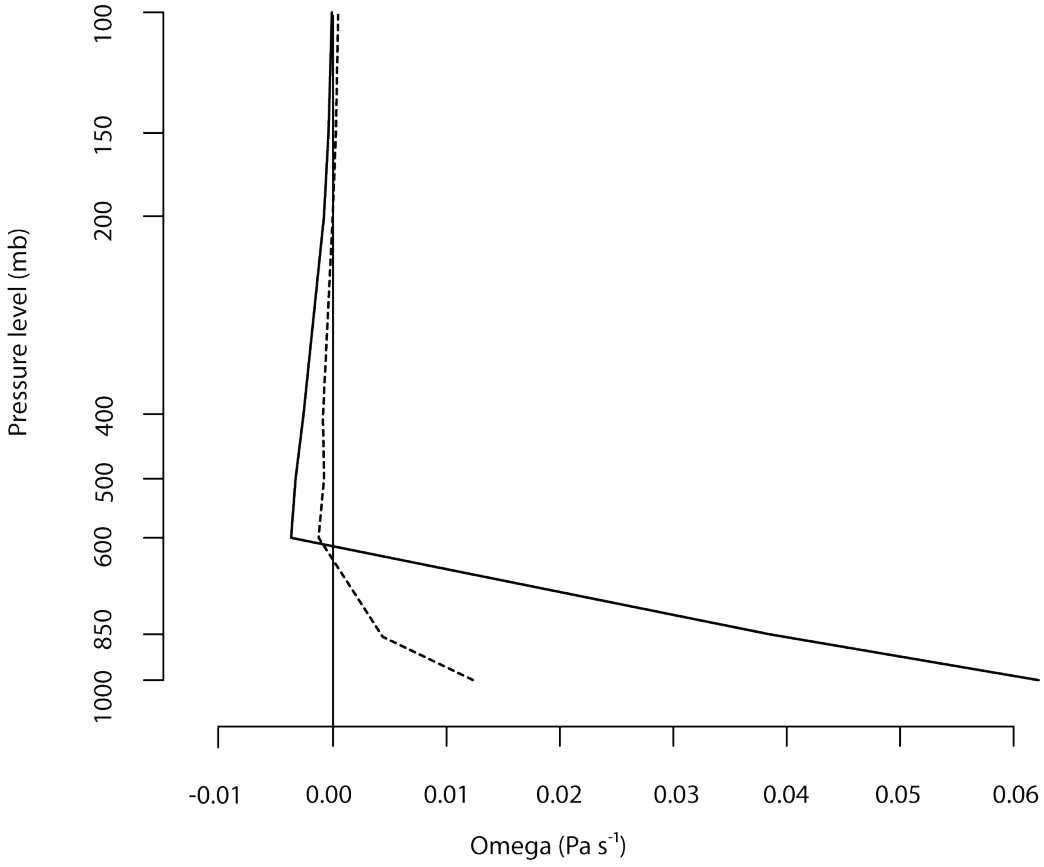

Figure 6.45 Mean omega

A mean of omega between 1985 and 2006, for 90°N–60°N (dashed line) and 60°S–90°S (solid line) between 100 and 1,000 mb.

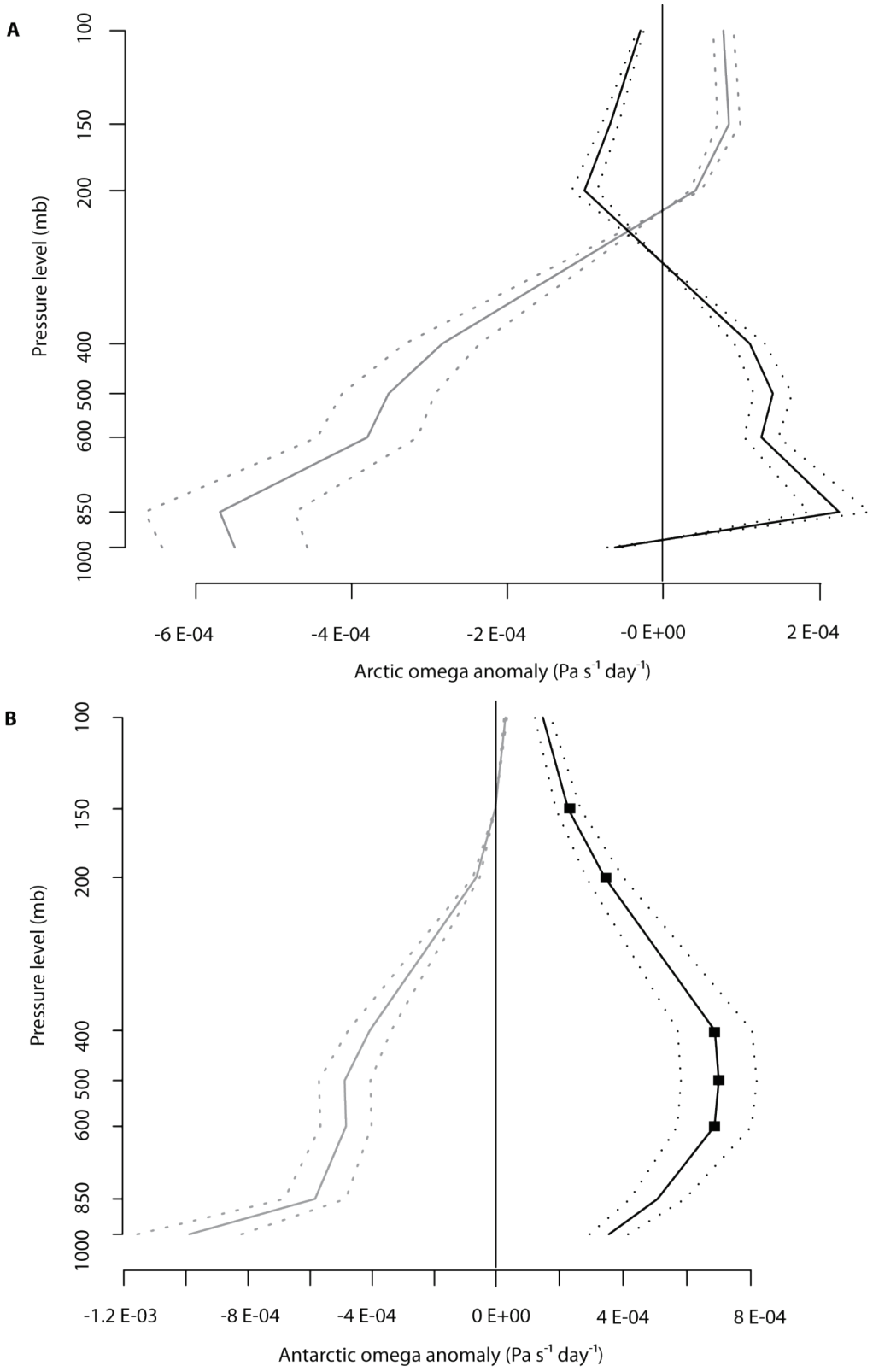

Figure 6.46 GI sample omega anomaly

Latitudinally-averaged omega anomalies occurring over the GI sample during the averaging period (days -5, -4 and -3) (grey line) and key date (black line) over the **A)** Arctic (90°N–60°N) and **B)** Antarctic (60°S–90°S) regions. With the 0.95 level confidence interval shown by the dashed lines and statistically significant changes indicated by markers.

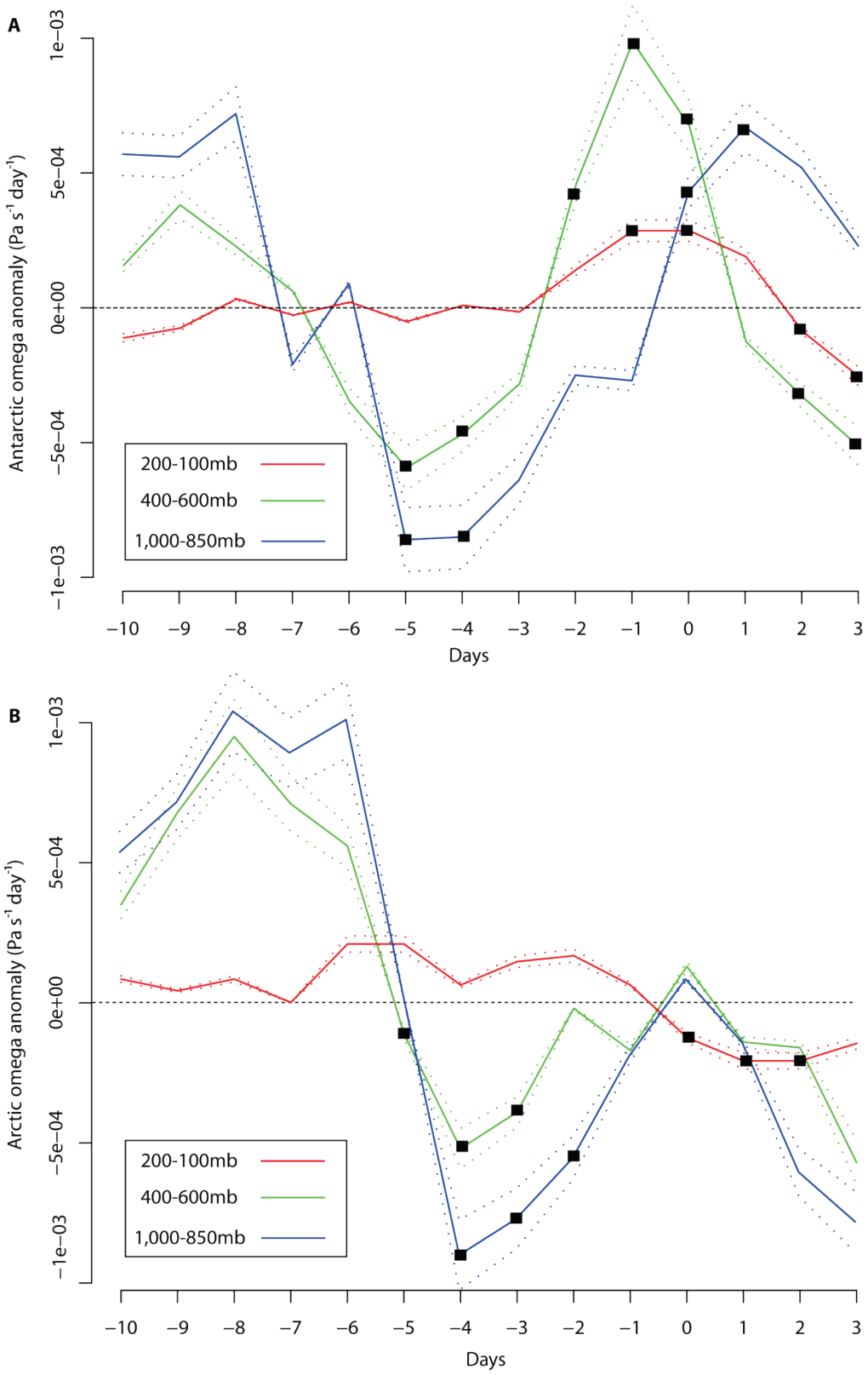

Figure 6.47 Omega anomalies over the GI sample

Upper level (200–100 mb) (red line), mid-level (400–600 mb) and low-level (1,000–850 mb) omega anomalies occurring over the **A)** Antarctic (60°S–90°S) and **B)** Arctic (90°S–60°N) regions during the GI sample period. Dotted lines show the 0.95 level confidence interval, statistically significant changes are indicated by markers.

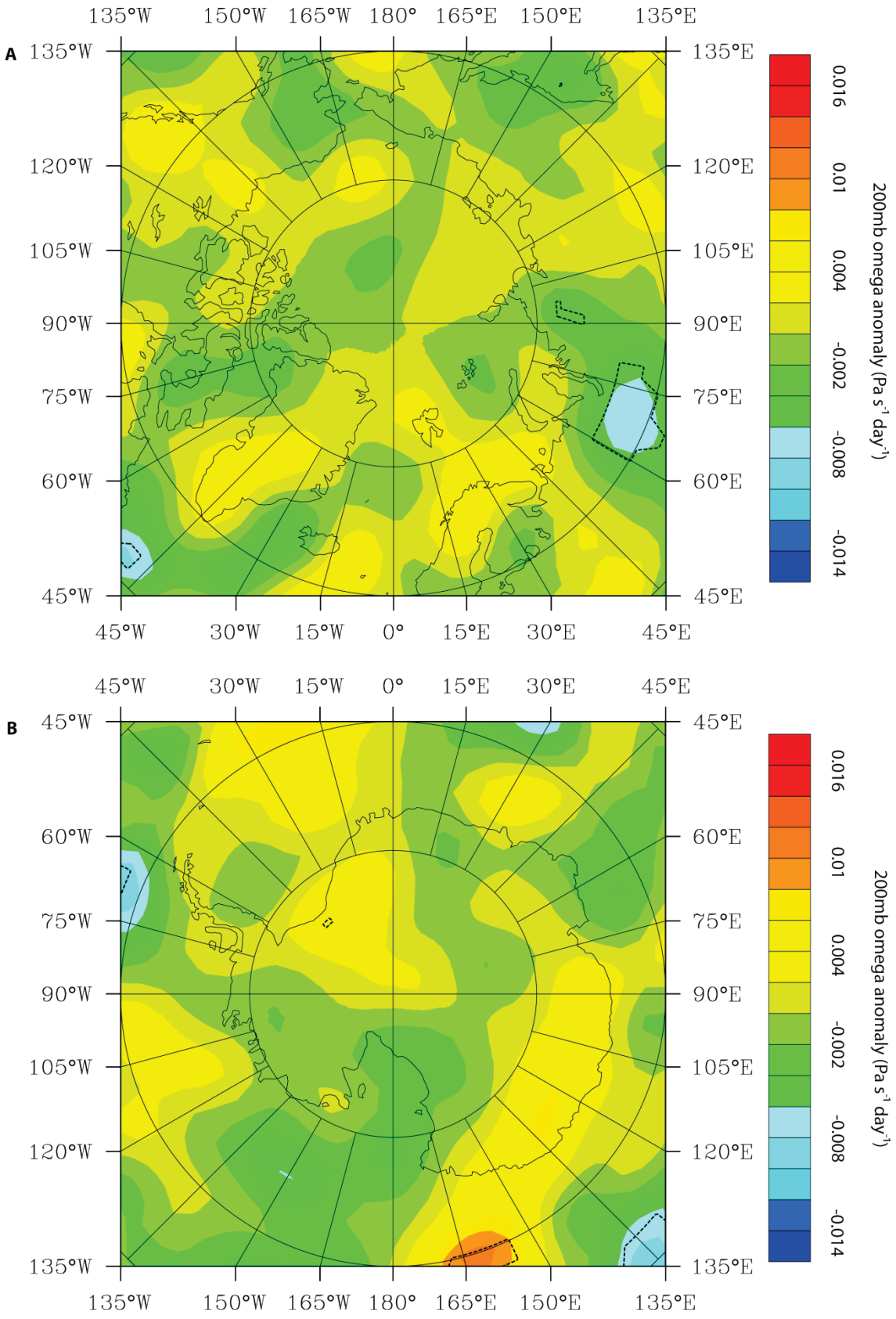

Figure 6.48 Upper level polar region omega anomalies

Anomalous **A)** Arctic region 200 mb and B) Antarctic region 200 mb key date GI sample omega anomalies. Locally significant anomalies indicated by dashed contours.

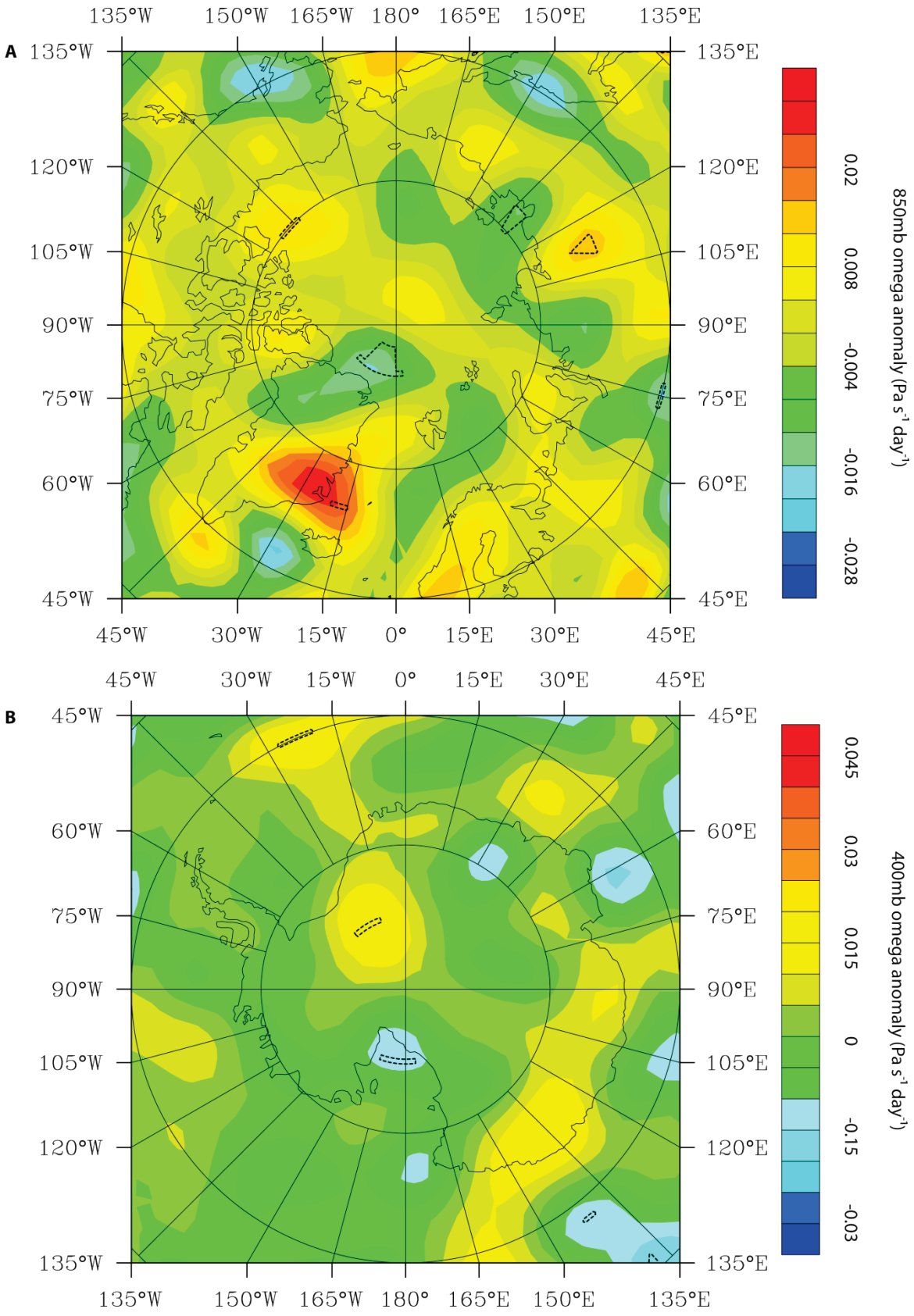

Figure 6.49 Mid- to low-level polar omega anomalies

Anomalous **A)** Arctic region 850 mb and B) Antarctic region 400 mb key date GI sample omega anomalies. Locally significant anomalies indicated by dashed contours.

6.7 General summary

An FD-based analysis did not provide any robust evidence of a GCR–climate relationship, instead, the atmospheric analysis has offered an alternative explanation to account for the upper tropospheric cloud decreases observed over the Antarctic region during the FD sample. Data suggest that internal atmospheric variability occurring around high southern latitude regions may have dynamically influenced cirrus cloud formation and development over Antarctica. Such a proposition weakens the already highly questionable results of the adjusted FD sample. The composite samples constructed from the internal cloud datasets however, yielded more positive results. Most notably, an analysis of these samples suggested that the occurrence of an unexpected high latitude cloud–climate interaction is occurring; whereby, increases in upper-mid tropospheric cloud are accompanied by low-level tropospheric cooling and pressure decreases at high latitude regions.

The negative relationship detected between cloud and high latitude surface temperatures contradicts the contemporary understanding of the radiative impacts of high latitude clouds on climate. Consequently, it was postulated that if the temperature/pressure anomalies are casually related to the detected cloud changes, the cloud–climate interaction may possibly operate indirectly (rather than radiatively), via a disruption to the quasi-stable equilibrium between radiative cooling and adiabatic warming operating over high latitudes under the influence of the PV. However, an analysis of changes in the vertical atmospheric motions over the key date did not support this notion. Alternatively, the temperature variations may be the result of changes in moist convective systems around Antarctica affected by variations in the current flow in the GEC, which may be dynamically linked to changes over the Antarctic continent. However, as the majority of cloud changes were detected over the Antarctic continent itself (rather than in frontal weather systems surrounding circumpolar region) this explanation seems unlikely.

Additionally, a statistically significant temperature/pressure response was also detected over mid-latitude regions. The observed anomalies may potentially be accounted for by changes in the radiative balance over mid-latitude regions as a result of significant cloud cover decreases. This implies that the sample may have successfully identified a robust atmospheric response to GCR related cloud changes.

In the forthcoming chapter, a number of climate model based experiments will be performed in an attempt to replicate the cloud–climate interactions observed in this chapter: the ability of the models to replicate the anomalies based solely on inputted cloud parameters will allow conclusions to be drawn regarding the casual relationship between the atmospheric anomalies to the cloud changes.

Chapter 7 Climate Model Experiments

7.1 Introduction

This chapter presents the findings of several climate model experiments designed to simulate the cloud anomalies described in chapter 5. The aim of these experiments is to determine the relationship of the associated atmospheric changes described in chapter 6 to the cloud anomalies. The rationale behind this approach is that, if atmospheric anomalies similar to observations can be simulated in a GCM by simply modifying cloud, then this may provide a good indication that the cloud changes themselves are responsible for producing the atmospheric anomalies via either radiative or dynamic interactions. When considered together with the statistically significant positive relationship between peak cloud cover changes and variations in the rate of GCR flux (described in chapter 5), such a finding would provide good evidence of a link between GCR, cloud and climate.

7.1.1 Background to GCMs and cloud simulations

One of the primary causes of uncertainty in GCM climate change projections comes from inter-model differences in cloud simulations and cloud–climate feedbacks (Williams et al., 2003; Williams and Tselioudis, 2007; Ogura et al., 2008). Generally, GCMs calculate the location and type of clouds present over an area based on parameters such as relative humidity, vertical velocity and vertical stability. If the air is found to be in a saturated state and vertically stable, then the models will generate stratified clouds or fog, whereas if conditions of saturation and convection occur, then cumulus clouds will be generated. For models with grid scale resolutions of around 100 m, the cloud cover of grid cells can be classified as a binary function (i.e. 1/0, meaning present/absent respectively) (van der Wal, 1998).

This work will utilise HadAM3, the global atmosphere-only version of the climate modelling hierarchy known as the Unified Model (UM), operated by the UK Meteorological Office Hadley Centre (van der Wal, 1998). The UM includes atmosphere-only, ocean-only and coupled components and can be run at either global or regional domains. The GCM experiments in this chapter will be run at the N48 resolution of 2.5° x 3.75°, which equates to an array of 96 x 73 grid cells (east-west/north-south) for a single atmospheric layer. The model has 19 vertical

layers, ranging from 10–1,000mb. Equations are solved at half-hour time steps (48 time steps per day). The equations of the UM's atmospheric prediction scheme are solved for the motion of a fluid on a rotating, near-spherical planet. The scheme is based on hydrostatic primitive equations, meaning that the atmosphere is always in hydrostatic balance with no vertical accelerations. The UM solves the equations using a grid-point scheme on a regular latitude-longitude grid in the horizontal domain and a hybrid scheme in the vertical domain, wherein vertical levels follow the terrain at the surface but change to constant pressure levels aloft (van der Wal, 1998; Williams, 2006).

At the N48 resolution, partial cloud coverage is far more likely than a binary situation. To calculate grid cell cloud cover in HadAM3, the large scale standard cloud parameterisation scheme 1A is used. This calculates both fractional cloud coverage (or non-clear sky fraction) and partitions water content in a grid cell between water vapour and cloud water content, dividing water into solid/liquid phases in accordance with temperature. Such parameterisations only take into account macroscopic processes responsible for the general location of cloud and not localised (sub-grid scale) micro-/nano-scale physical processes of nucleation and droplet growth (Bushell, 1998). The simulation of fractional cloud cover within grid cells is achieved using a statistical parameterisation method (van der Wal, 1998). Fluctuations in the total water content of an individual grid cell is calculated using a method based on probability density functions (PDFs), where the width of the PDF relates to the model's critical relative humidity parameter (Smith, 1990; Smith et al., 1997). As a consequence of this method, the model simulates an unrealistically close relationship between cloud fraction, cloud water contents and relative humidity. A further weakness of the HadAM3 cloud scheme is that it is only semi-prognostic in nature, i.e. for each new time step of the HadAM3 model, cloud is overwritten and re-calculated rather than being updated as a fully prognostic variable would be. However, since the cloud interacts with other schemes of the model, cloud variability is able to influence the evolution of the GCM by affecting other aspects of the model, such as air temperature (Bushell, 1998).

Although many of the problems faced by GCMs attempting to simulate cloud are connected to their inability to simulate sub grid-scale cloud formation processes, it is also known that GCMs (including the HadAM3) encounter additional difficulties with regards to cloud simulations, for example:

(1) *An inability to reproduce cirrus over land*. It is known that the HadAM3 is unable to sufficiently simulate high cloud cover over land. This is a problem faced by most GCMs and appears to result from the lack of a representation of orographic cirrus generated by sub-grid scale orography (Dean et al., 2005). In addition, cirrus simulation

is hampered by improper simulation of tropical thunderstorms: such thunderstorms are responsible for generating widespread cirrus, which are an integral part of the tropical radiation balance. Comparisons of field measurements of ice-phase cloud in thunderstorms to current-generation cloud-resolving models highlighted the models inability to properly simulate ice-phase cloud, and correctly capture the dynamics of thunderstorms responsible for producing tropical cirrus (Wang et al., 2009)

(2) *Issues simulating diurnal cloud variations*. Comparisons of simulated diurnal cloud variations to high resolution tropical cloud data from the European Union Cloud Archive User Service (CLAUS) project has shown that the HadAM3 model struggles to capture the observed phase of the convective diurnal cloud cycle. These problems may be related to fundamental difficulties in the model's physical parameterisations (Yang and Slingo, 2001).

Before performing any experiments with the GCM, it is important to understand more specifically the strengths and weaknesses of the HadAM3's cloud/climate simulations; these will now be assessed.

7.1.2 Validating mean cloud cover

Comparing the mean cloud cover from a 5-year HadAM3 run to 5-years of observed ISCCP D1 IR retrieved cloud cover shows that the HadAM3 is able to broadly simulate synoptic cloud patterns (figure 7.1). In particular, the model appears to reproduce patterns of cloud cover over the South Pacific Ocean, northern Pacific/Atlantic regions and simulate features such as the ICTZ to a good degree. However, the model also appears to underestimate cloud cover over several regions, such as the western coast of North/South America and continental South America, while also overestimating cloud over Antarctica and Greenland.

Comparing simulated and observed cloud cover on a 5° latitudinally-averaged basis suggests that there is a poor agreement between the model and observations (R^2=0.32) (figure 7.2). Furthermore the cloud amount is underestimated by the model over virtually all regions (figure 7.2A): the difference between 5° latitudinally-averaged, observed/modelled mean cloud cover demonstrates a median difference of -12.2 % (the differences range from -29.9 % [at 37°S] to 12.8 % [at 85°S]).

Scatter plots of observed *vs*. modelled cloud amounts show that the ability of the model to simulate realistic cloud conditions decreases with increasing latitude zone (figure 7.3). Correlation coefficients indicate that the model is most effective at reproducing mean cloud cover over the tropics (R^2=0.41), whereas the mid-latitude region demonstrates a correlation coefficient of approximately half the tropical value (R^2=0.28) and polar regions demonstrate the lowest correlation coefficients of all (R^2=0.04).

The GCM's ability to reproduce the vertical structure of mean cloud cover appears to be particularly deficient (figure 7.4). The vertical ISCCP cloud conditions clearly shows key elements which are absent from the GCM simulation. In particular, the model fails to reproduce: (1) upper Antarctic cloud cover; (2) the correct magnitude and height of southern and northern hemisphere mid-latitude cloud cover; (3) mid- to low latitude low-level cloud structures (related to the trade winds); (4) the vertical structure and magnitude of the equatorial convective clouds; and (4) the magnitude, location and vertical structure of Arctic cloud. These issues are highlighted in figure 7.5, which displays the difference between the ISCCP and GCM vertical profiles. Overall, these data indicate that the GCM's simulation of mean cloud cover is rudimentary: over regions where it initially appears that the horizontal, synoptic-scale, tropospheric-averaged cloud conditions have been simulated to a reasonable degree (such as the southern hemisphere oceans), it is found that the vertical simulation of cloud shows major discrepancies relative to observations. Such issues may have a significant impact on the ability of the forthcoming experiments to accurately reproduce observed cloud–climate relationships. These results suggest that for the forthcoming experiments the most meaningful cloud–climate interactions may come from samples where a large-scale area averaging is applied. By extension, this also suggests that, at a local-scale, modelled cloud–climate responses may differ significantly from observations (implying that meaningful results may not be gleaned at high spatial resolutions).

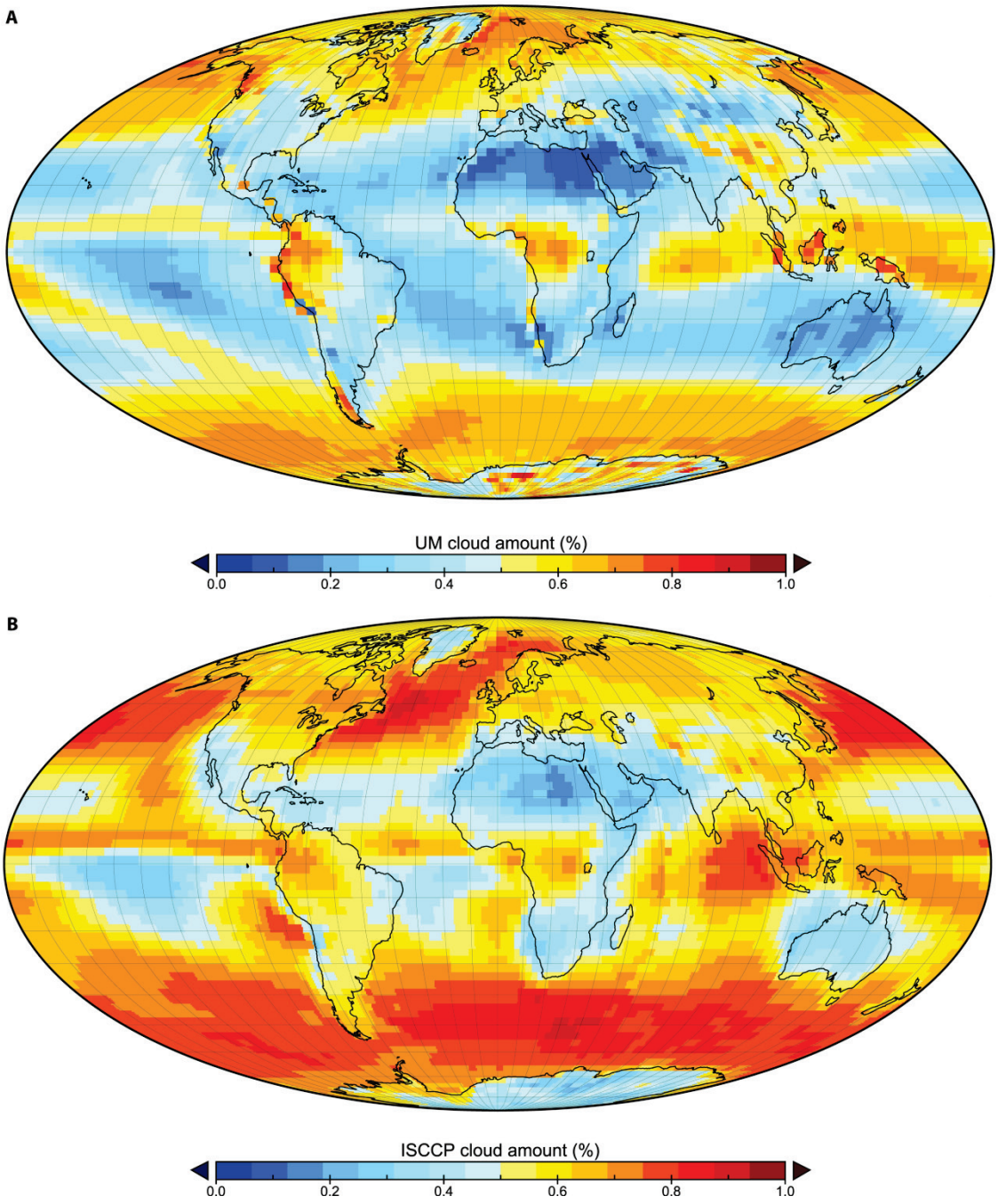

Figure 7.1 Mean observed and modelled cloud cover.

Average cloud cover observed from **A**) a 5-year HadAM3 climate model and **B**) a 5-year period of ISCCP D1 IR observations.

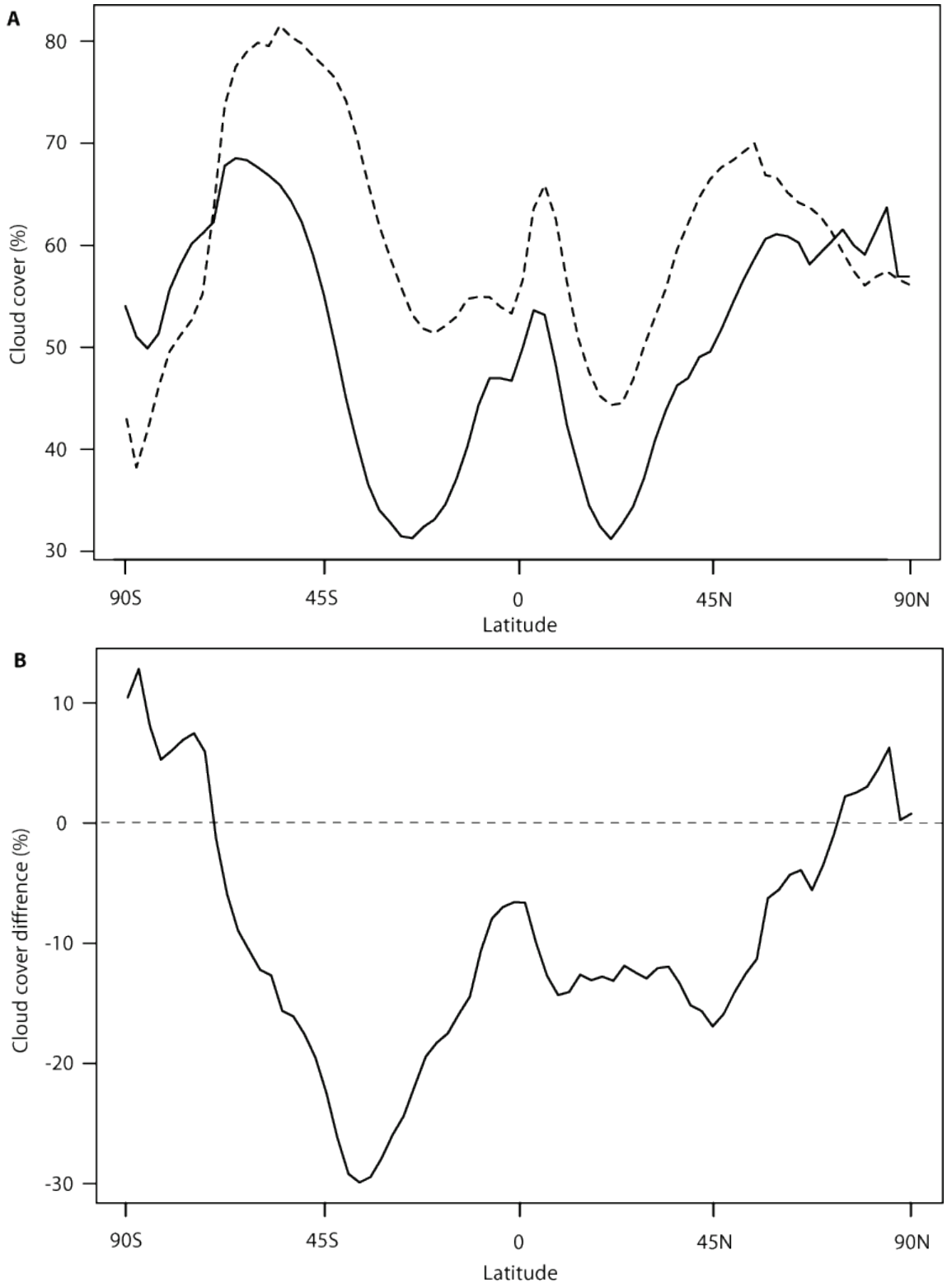

Figure 7.2 Zonal mean cloud cover

Latitudinally-averaged **A)** mean cloud cover from HadAM3 simulations (solid line) and ISCCP observations (dashed line), and **B)** the difference (model subtracted from observation) between modelled and observed cloud cover.

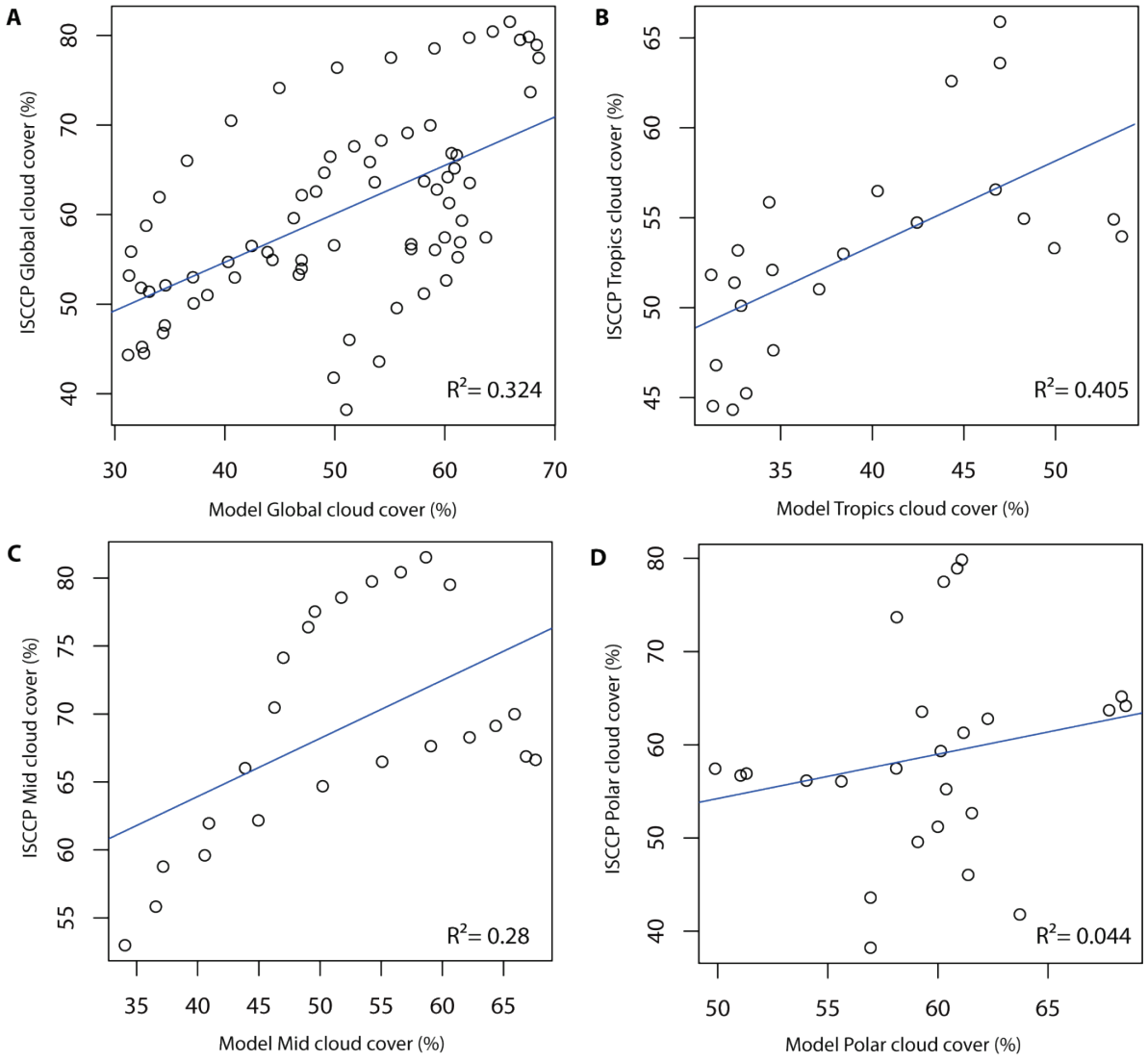

Figure 7.3 Correspondence between zonal mean cloud cover

Latitudinal average mean ISCCP observed cloud cover (*x*-axis) plotted against simulated HadAM3 cloud cover (*y*-axis) at: **A)** global latitudes (90°N–90°S); **B)** tropical latitudes (30°N–30°S); **C)** mid-latitudes (60°N–30°N and 30°S–60°S); **D)** polar latitudes (90°N-60°N and 60°S–90°S). Linear fit (blue line) and correlation coefficients (R^2) are also shown.

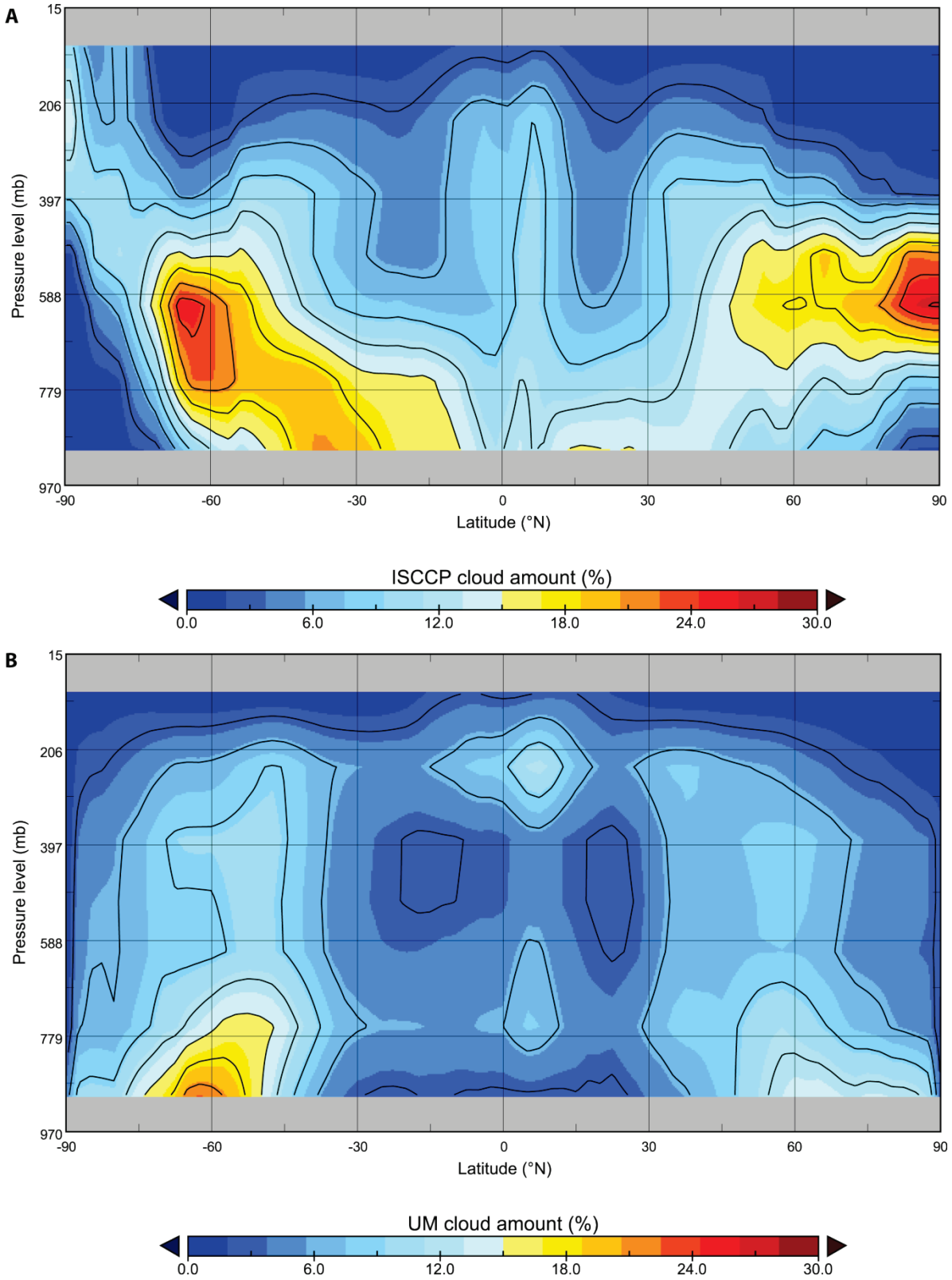

Figure 7.4 Comparing the vertical cloud structure of the GCM to ISCCP

A 5-year mean latitude/height profile of: **A)** the HadAM3, and **B)** ISCCP D1 cloud cover.

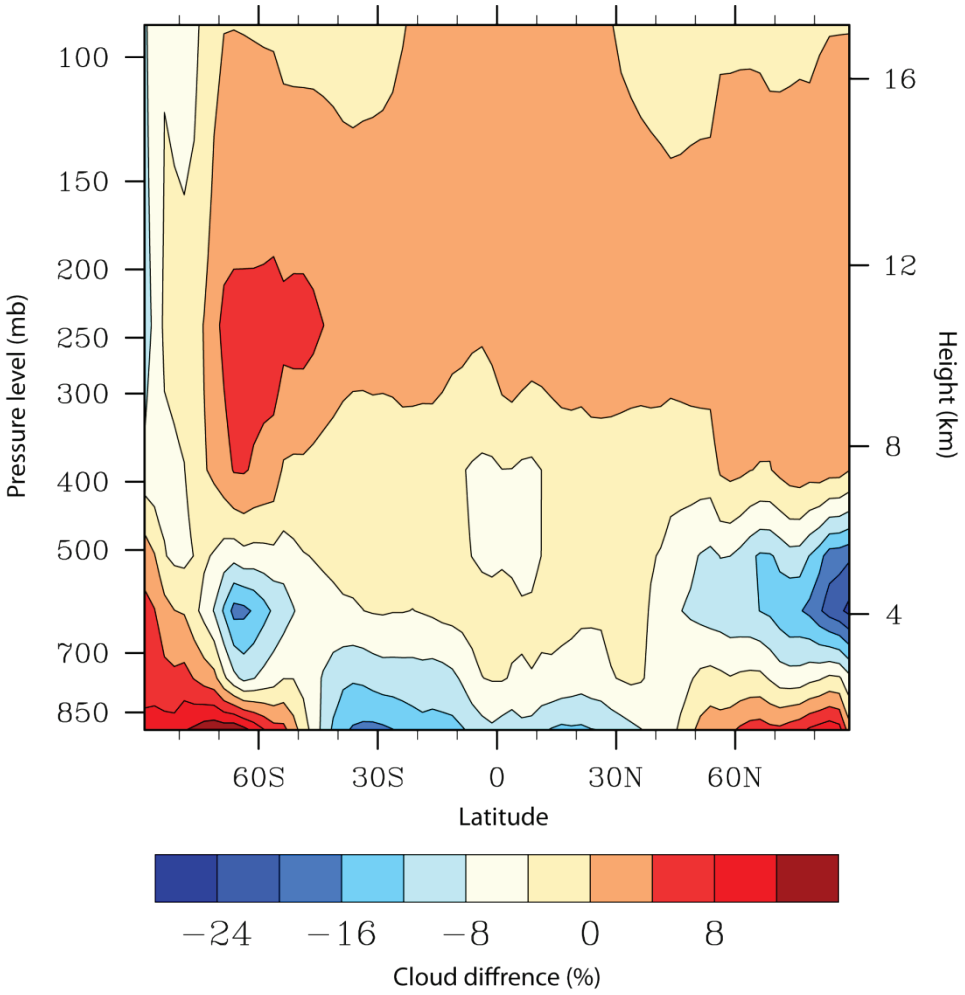

Figure 7.5 Vertical cloud distribution difference

HadAM3 5-year mean latitudinally-averaged cloud cover subtracted from observed (ISCCP) cloud cover (model minus observation). Negative (positive) regions indicate where the GCM has underestimated (overestimated) vertical cloud cover.

7.1.3 Validating model cloud standard deviation

Data from a 5-year HadAM3 control run was used to determine standard deviation cloud amount; this is contrasted against 5 years of observed ISCCP cloud variability. The results indicate a fairly good regional agreement between models and observations. Synoptic-scale features of cloud variability (such as the low variability seen over southern latitude ocean regions) are successfully captured by the model (figure 7.6).

A plot of latitudinally-averaged cloud variability again shows that the model is relatively successful at reproducing the correct magnitude and pattern of cloud variability (R^2=0.41). However, the success of the model varies regionally; the model shows the largest deviations

from observed values over mid-latitude regions, where the model overestimates variability by as much as 6.8 %. Despite this, the model is successful at reproducing the overall pattern of latitudinal variability; for example, the model is able to reproduce a high correlation between variability occurring over 50°S–90°S (R^2=0.97) (figure 7.7).

Scatter plots of observed *vs*. modelled cloud variability divided into tropical, mid-latitude and polar latitude regions, show that the lowest correlation coefficient between observed and modelled cloud variability was found over polar regions (R^2=0.42), while the mid-latitudes showed the highest correlations (R^2=0.78) (figure 7.8).

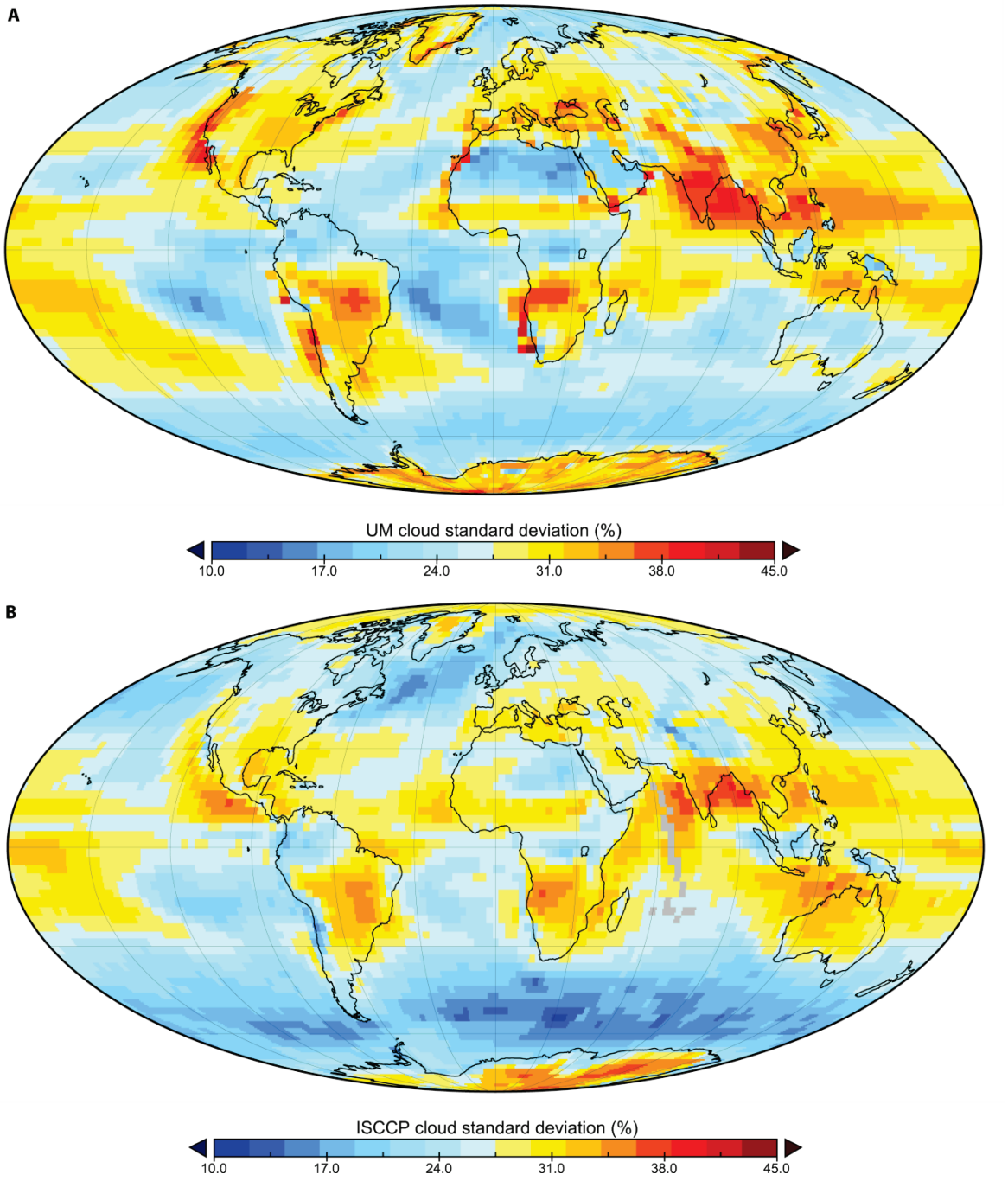

Figure 7.6 Modelled and observed cloud variability

Standard deviation cloud cover observed from **A)** a 5-year HadAM3 climate model, and **B)** a 5-year period of ISCCP D1 IR observations.

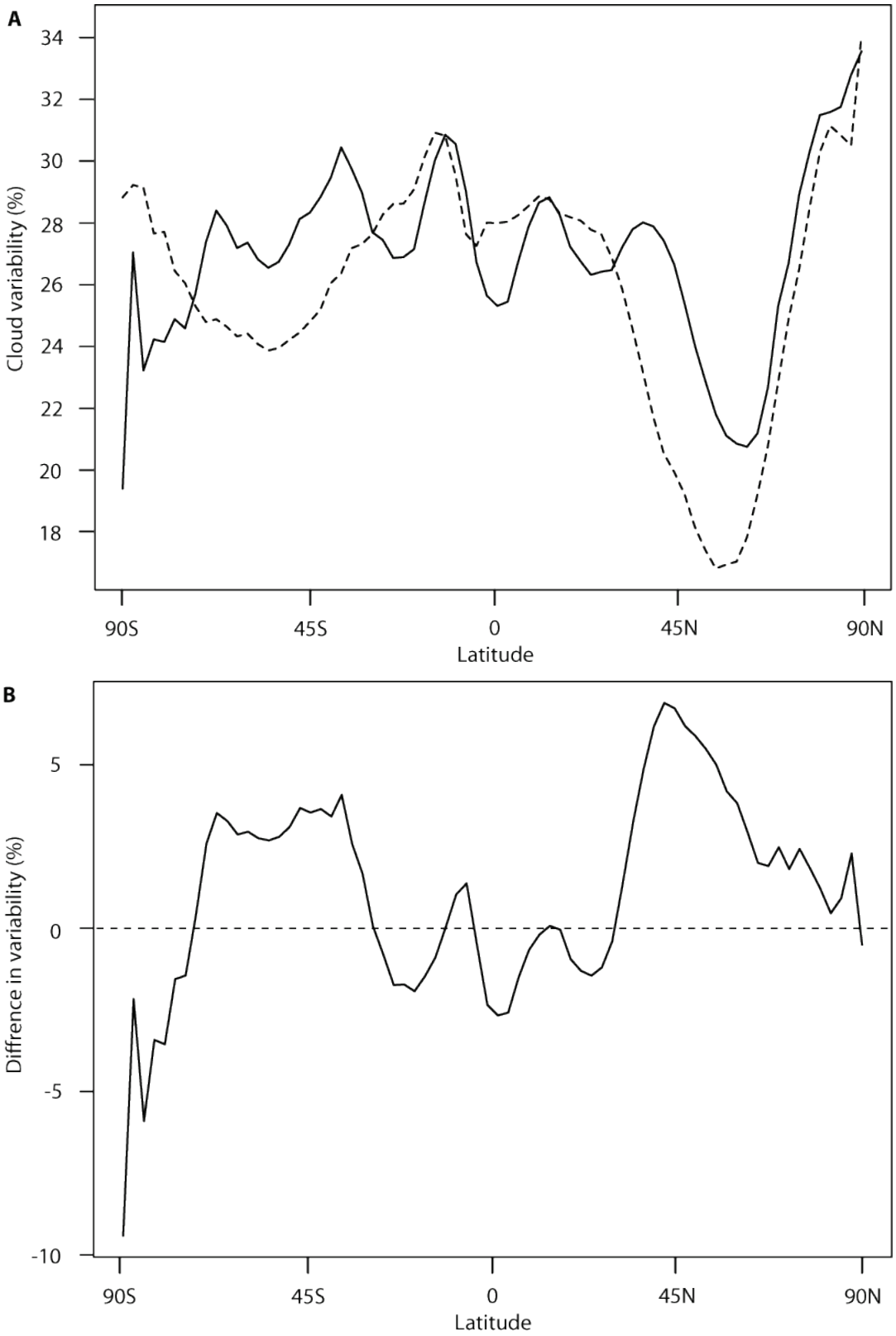

Figure 7.7 Zonal cloud variability

Latitudinally-averaged standard deviation cloud cover, from **A)** HadAM3 simulations (solid line) and ISCCP observations (dashed line), and **B)** the difference between modelled and observed standard deviation cloud cover (model minus observations).

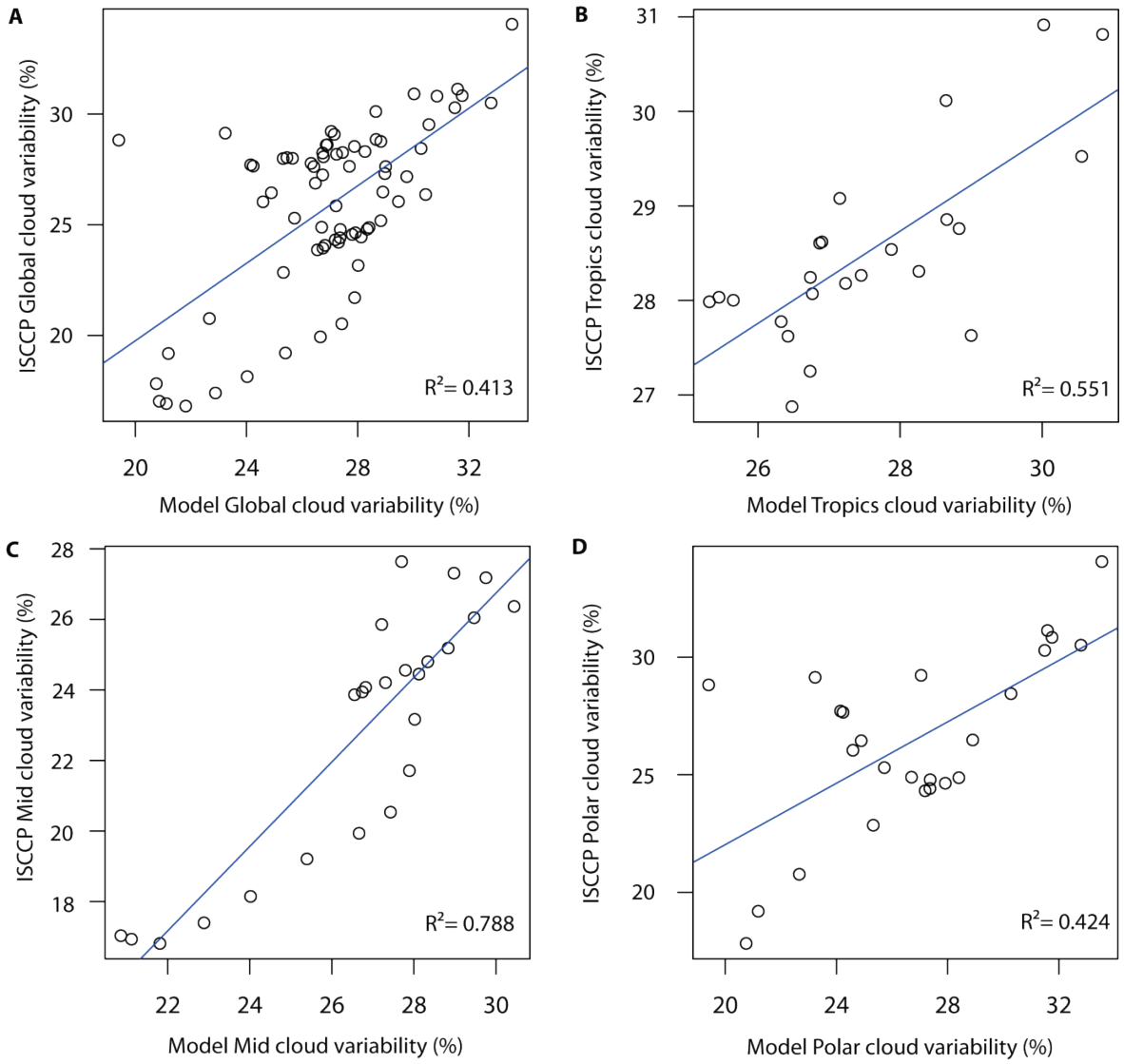

Figure 7.8 Correspondence of zonal cloud standard deviation

Latitudinal average standard deviation ISCCP observed cloud cover (*x*-axis) plotted against simulated HadAM3 cloud cover (*y*-axis) at: **A)** global latitudes (90°N–90°S); **B)** tropical latitudes (30°N–30°S); **C)** mid-latitudes (60°N–30°N and 30°S–60°S); **D)** polar latitudes (90°N–60°N and 60°S–90°S). Linear fit (blue line) and correlation coefficients (R^2) are also shown.

7.1.4 Conclusions on the accuracy of HadAM3 cloud simulations

Although generally the model was able to reproduce the correct sign/synoptic patterns of mean cloud cover and variability, the accuracy of these simulations was found to vary between latitude zones; the poorest correspondence between modelled and observed cloud was found at high latitude regions, whereas the strongest correspondence was found at tropical latitudes.

These results indicate that over most regions of the Earth the HadAM3 model is only able to reproduce cloud conditions to a limited degree. Such a result is typical of GCMs: most models have been found to be capable of reproducing principal cloud regimes, yet commonly struggle to correctly resolve regional cloud features (Williams and Tselioudis, 2007). The poor agreement between observations and the model over the polar regions may prove particularly problematic, as model experiments will require the manipulation of cloud over these regions.

In comparison with other GCMs, however the HadAM3 simulates cloud reasonably well: evidence of this can be seen from the IPCC's inter-model comparisons of outgoing SW radiation over a latitudinally-averaged basis (figure 7.9). This provides a proxy measurement of model cloud differences (as clouds are responsible for around 50% of outgoing SW radiation (IPCC, 2007). The global fully coupled atmosphere-ocean version of the UM (HadCM3) is featured on figure 7.9 integrates the HadAM3 model and the UM ocean-only model (HadOM3). The results of the HadCM3 can be considered to be roughly indicative of the HadAM3 model's performance relative to other GCMs. These data show that the HadCM3 model performs comparatively well in simulating outgoing SW radiation, suggesting that the model is one of the more accurate GCMs with respect to cloud simulations.

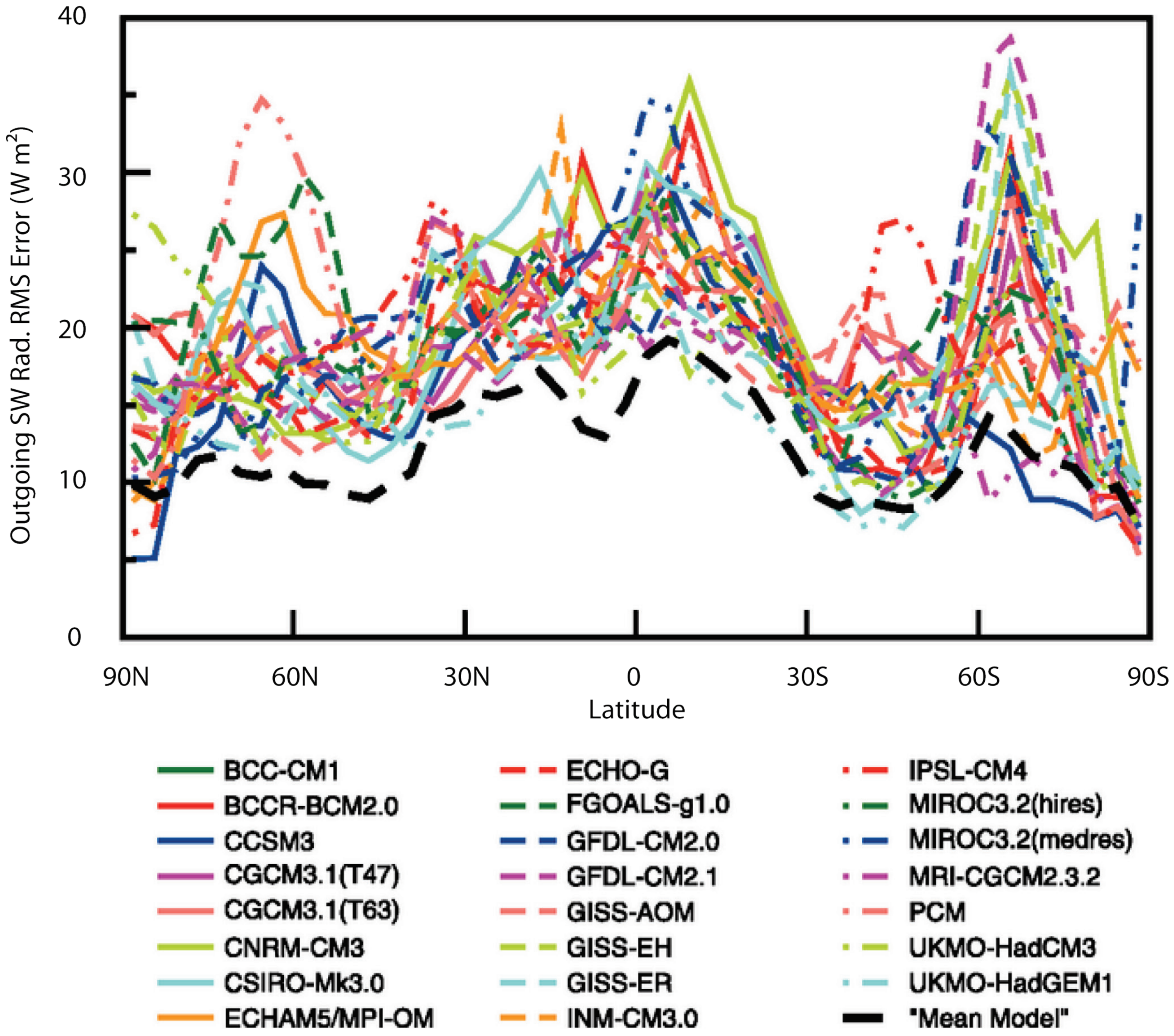

Figure 7.9 Model simulation of outgoing SW/LW radiation

Root-mean-square (RMS) model error as a function of latitude for **A)** SW radiation, and **B)** LW radiation, calculated from multi-year 12-month model climatology against the Earth Radiation Budget Experiment (ERBE) (Barkstrom et al., 1989). The data provide an indirect comparison of the various GCM's abilities to simulate latitudinally-averaged cloud cover. Figure adapted from IPCC AR4 Working Group I: The Physical Science Basis, Chapter 8, figure 8.4.

7.2 Assessing the models ability to simulate regional polar circulation patterns

It is necessary to evaluate the GCM's ability to reproduce circulation patterns over polar regions. This is crucial, since in chapter 6 several samples suggested that large cloud increases at high tropospheric levels over high latitudes may be capable of indirectly affecting climate (possibly via an indirect influence on regional circulation). Consequently, in an attempt to test this hypothesis, it is necessary for the GCM to correctly simulate polar circulation.

To assess the model's ability to simulate polar circulation, three model parameters will be evaluated against observations: (1) the position of the Antarctic polar low pressure system; (2) the wind flow at surface level over Antarctica; and (3) the vertical velocity (omega) of air over the globe and polar regions.

(1) A plot of 5-year mean 200 mb GPH reanalysis data shows a strong region of low pressure over the interior of the Antarctic continent (figure 7.10A). This low pressure region indicates the location of the PV, where upper tropospheric air converges before descending to lower tropospheric levels. Identical data from HadAM3 indicates that the model is capable of correctly reproducing the magnitude of the low pressure region. However, its extent is highly overestimated (figure 7.10B). This suggests that, in order to reproduce the observed reduction in the convergence of air in the PV, it may be necessary to increase the spatial extent of artificially enhanced cloud changes beyond that of the observed cloud anomalies.

(2) After the air has descended from upper tropospheric levels to the surface of the Antarctic continent it undergoes intense radiative cooling. The dense cold air then drains off the continent via the path of least topographic resistance, resulting in a katabatic wind. A plot of five years of averaged 1,000 mb vector wind from NCEP/NCAR reanalysis data clearly shows the drainage patterns of the katabatic wind regime (figure 7.11A). The model is able to broadly replicate these drainage features. However, the wind velocity is found to be approximately 4 m s^{-1} less than the reanalysis data (figure 7.11B). The underestimation of wind speeds may be connected to the overestimated area of the PV observed in figure 7.10B, which may produce less intense wind drainage.

(3) Omega from NCEP/NCAR reanalysis data over a 5-year period is shown at a 5° latitudinally-averaged resolution (figure 7.12A). These data show the patterns of large scale vertical atmospheric motion around the globe. The detail of the data has been largely removed, so as to simply show areas of ascending or descending motion. Broadly, the plot indicates that at tropical and mid-latitudes the air is ascending, while at sub-tropical and polar latitudes the air is descending. A 5-year mean of HadAM3 omega shows that the model is broadly able to reproduce these observed patterns (figure 7.12B). It is important to note that the observed (NCEP/NCAR) omega (shown in figure 7.12A) indicates the presence of ascending air directly over the north and south pole (at low/upper tropospheric levels respectively). Such a situation is physically implausible, since over such regions, air undergoes intense radiative cooling resulting in a strong descending tendency. This suggests that the omega reanalysis data may not be accurate

over these (high latitude) regions. There are comparable precedents in the literature which suggest that reanalysis data may be of questionable quality over high latitude regions (Hines et al., 2000; Smith et al., 2001; Bromwich and Wang. 2005). An analysis of the regionally-averaged vertical omega profile over the north and south polar regions individually shows that at both poles the vertical profile of the modelled omega agrees well with observations (figure 7.13). There are some important differences however. For example, over mid-tropospheric levels of the Arctic region, the HadAM3 and observations disagree on the sign of omega, with the GCM suggesting that air at mid-tropospheric levels shows an ascending tendency (this situation is physically implausible). On the other hand, over Antarctica, HadAM3 is found to produce weaker-than-observed omega values at almost all pressure levels.

From these comparisons, there appears to be a general consensus at the synoptic scale between observations and the GCM over key elements of the climate system. These elements are likely to play an important role in the forthcoming GCM experiments. However, at a local-scale resolution, differences are identified between the HadAM3 and observations in several areas, specifically, the GCM is found to overestimate the area of the PV, underestimate the intensity of the katabatic wind, and produce a weaker vertical motion of air over high latitude regions than observed.

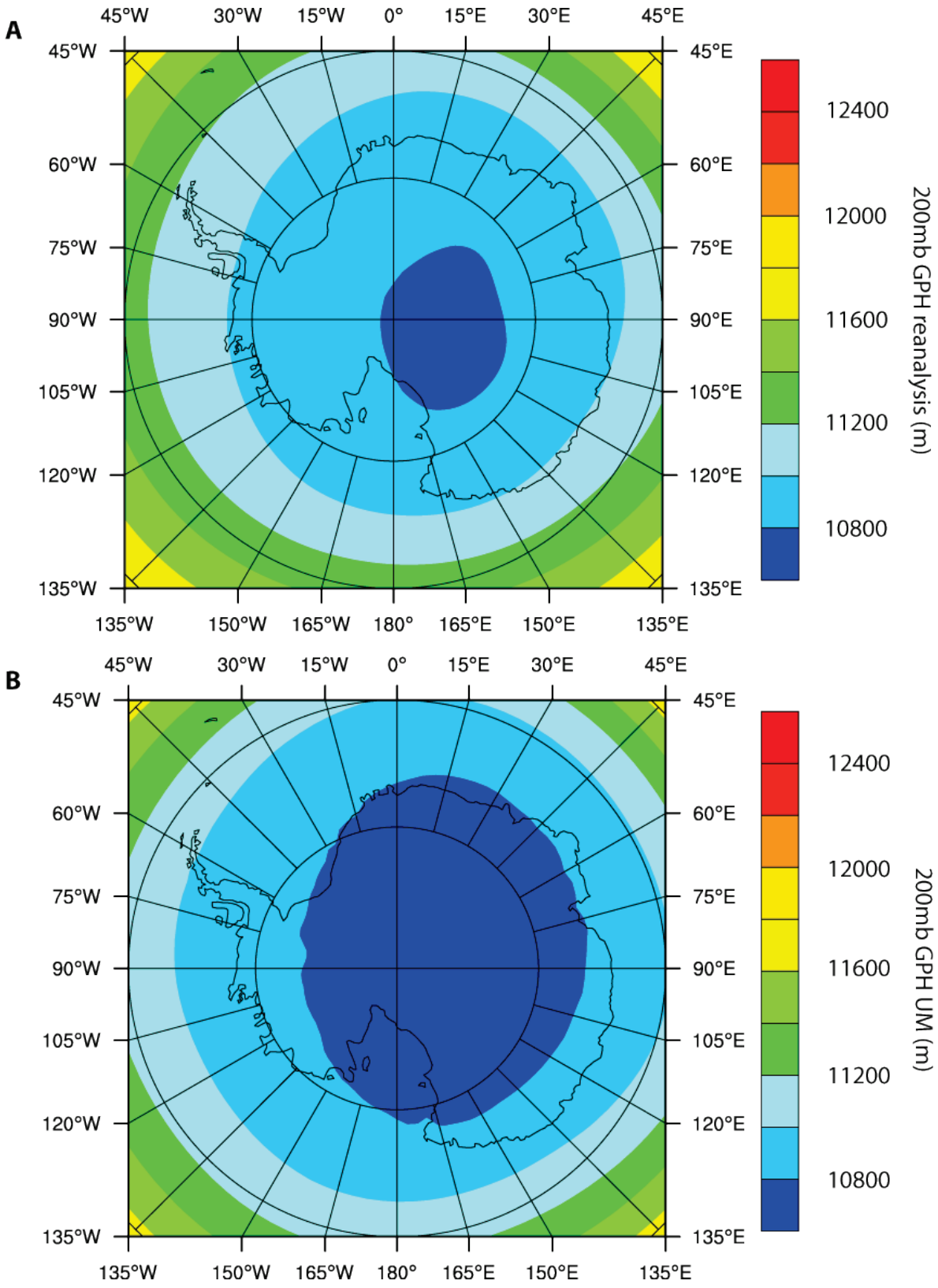

Figure 7.10 Comparison of Antarctic upper tropospheric convergence

A plot of 5-year mean, GPH at 200 mb from **A)** reanalysis data, and **B)** HadAM3 data, indicating the extent of the Antarctic PV.

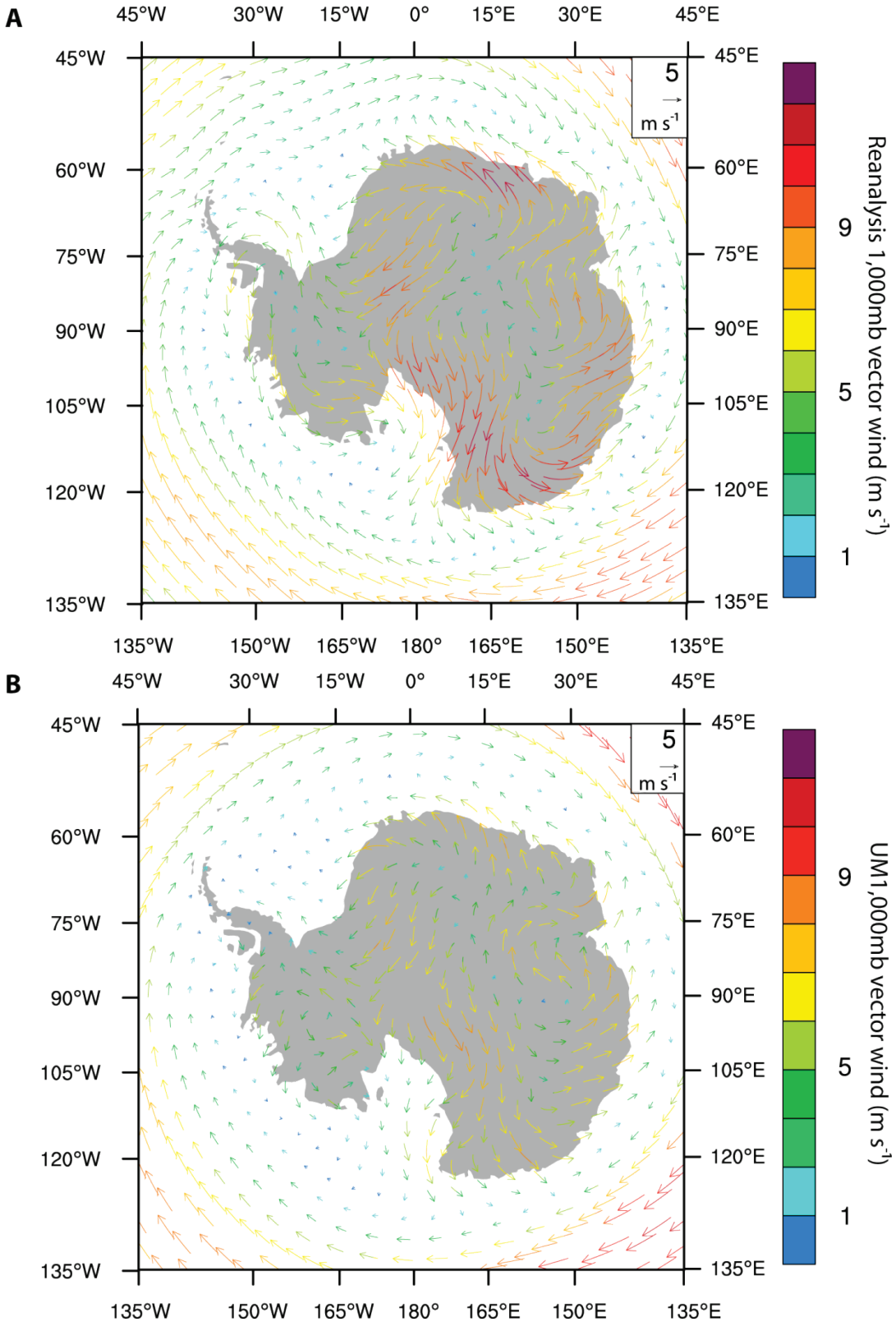

Figure 7.11 Comparison of the Antarctic katabatic wind regime

A plot of 5-year mean vector winds over the Antarctic region from **A)** reanalysis data, and **B)** HadAM3 data at the 1,000 mb level.

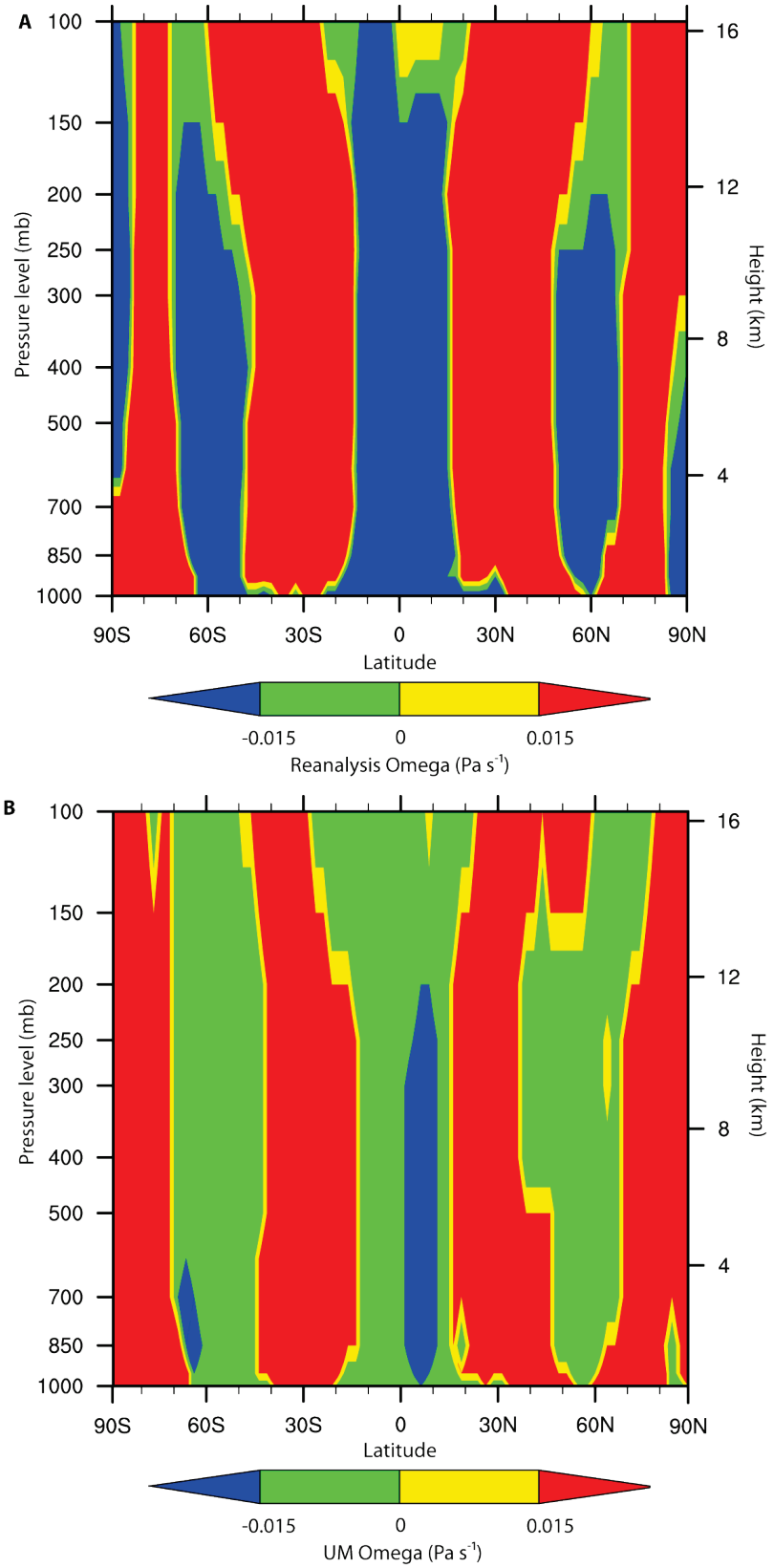

Figure 7.12 Latitudinally-averaged omega

A plot of 5-year mean vertical velocity from **A)** reanalysis data and, **B)** the UM (HadAM3) model (negative values indicate ascending air, positive values indicate descending air) at a 5° latitudinal average resolution.

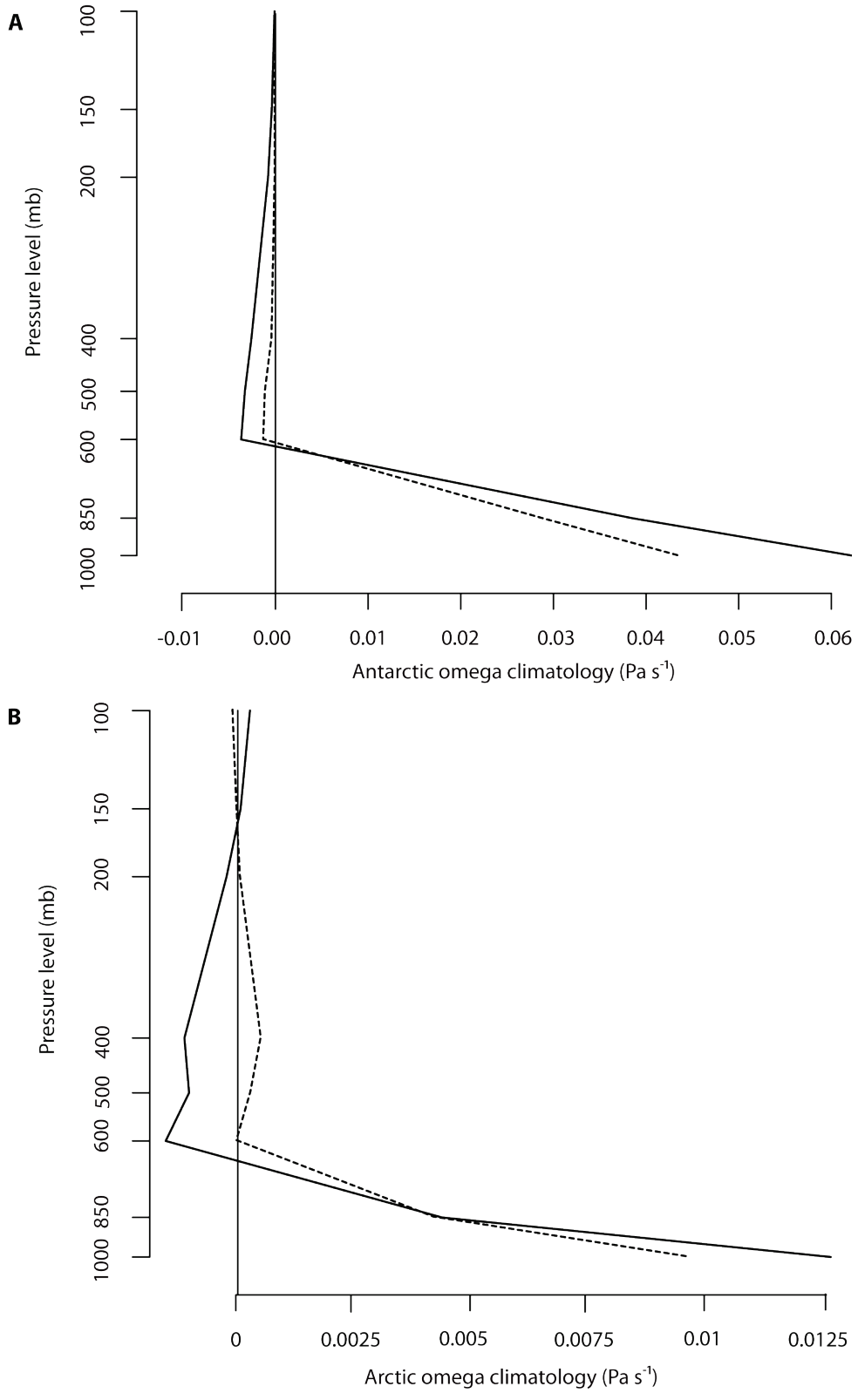

Figure 7.13 Polar region UM *vs*. observed omega

A latitudinally-averaged vertical 5-year mean of **A)** Antarctic (60°S–90°S) and **B)** Arctic (90°N–60°N) regions, for NCEP/NCAR reanalysis data (solid line) and UM data (dashed line). Note differing *x*-axis scales on panel **A** and **B**.

7.3 Description of model experiments

The use of ensembles is common practice when dealing with climate models, since they allow a reduction in the uncertainty which results from natural internal climate variability (Stott and Forest, 2007). The compositing procedures performed throughout this work are essentially a form of an initial-condition ensemble (initial-condition ensembles are ensembles which contain consentient model forcings and physics schemes, but differing initial states). Consequently, the continued use of the composite-based methodology during the forthcoming GCM analysis should preclude the need to perform any additional ensemble approaches. Another issue which warrants consideration is that of climate drift, which may potentially cause spurious trends in GCM results due to the alteration/drift of the mean state of the climate system over time as the model equilibrates. However, as each of the results were based on an ensemble constructed from several separate 5-year runs there was no possibility of climate drift influencing the results (as the timescales used are too short for this effect to be an issue).

In the coming sections, the results of several GCM experiments will be analysed and discussed. These experiments were designed to simulate the observed cloud changes that were identified in earlier chapters. The experiments will mimic the cloud changes of the GI sample (which identified polar cloud anomalies [described in section 5.2.1]) and the MLD sample (which identified mid-latitude cloud anomalies [described in section 5.5.2]). There will be no GCM experiment to relate to FD-based samples (described in section 4.3.3), as no statistically robust cloud–climate interactions were identified under FD sampling regimes. Nor will there be an individual experiment for the AI sample, as the AI results were essentially found to be identical to those of the GI sample and thus an individual treatment should not be required.

The cloud anomalies were inserted into the HadAM3 by directly manipulating the physics of the SW and LW radiation schemes; these radiative changes were inserted directly into the UM code by a modset [FORTRAN code addition], the added code itself (including the explicit points of insertion) are presented in appendix 4 and 5. These modsets forced a repeating sequence of cloud changes every 24 days within the model over two 5-year periods using multiplication (scale) factors derived from observations. Following a one-year spin-up period, the model data were then composited, producing a sample of 120 observations. After compositing, the anomalous rates of change in various model parameters were then calculated from the composite sample in an identical method to that of previous chapters (using equation 3.1). This procedure resulted in the anomaly being calculated for 19 days of the composite period, which directly relates to the -15 to 3 day sampling period used throughout this work (i.e. days of repeating cloud changes occurring once every 24 days were composited, and from these a rate

of change was calculated [using equation 3.1], resulting in 19 days of useful data in the composite).

In this thesis anomalous cloud changes have been calculated using area-averaged rates of change. There has been no specific regard given to the exact origin of the cloud changes at the individual cloud scale, as it is not possible to determine this at the resolution of the ISCCP or NCEP/NCAR reanalysis data. Consequently, it is unclear if the cloud changes are a result of: (1) an increase in the area of existing clouds (figure 7.14A), (2) generation of new clouds (figure 7.14B); or (3) an increase in cloud longevity (figure 7.14C). It is most physically plausible however, that the 1st and 3rd situations are occurring and that GCR variations are modifying existing cloud via an edge-effect, or by altering cloud properties (such as albedo and lifetime). If the 2nd scenario was occurring and cloud cover underwent absolute increases due to GCR variations, then a cloud response following FD events should have been observed.

The use of scale factors within the model experiments assumes scenario 1: cloud cover will be multiplied by a scale factor, resulting in a cloud change which will be directly relative to the original cloud amount. Scenario 2 will not be used within the model, as this would involve forcing cloud changes into locations where the presence of cloud is physically unrealistic (i.e. if the model has determined that cloud should not exist over an area, then it would be physically incorrect to forcibly insert it). Concerning scenario 3, although this is a likely mechanism and one which potentially plays an important role in the observed cloud changes, there is no way to include this scenario within the model due to the semi-prognostic nature of the GCM's cloud scheme (which re-calculates cloud at each time interval). Consequently, only the first of the three cloud change scenarios will be represented within the model. This limitation may result in an under-estimation of modelled anomalies.

The two GCM experiments performed were (1) the Mid-latitude cloud decrease (MLCD) experiment, and (2) the Polar cloud increase (PCI) experiment.

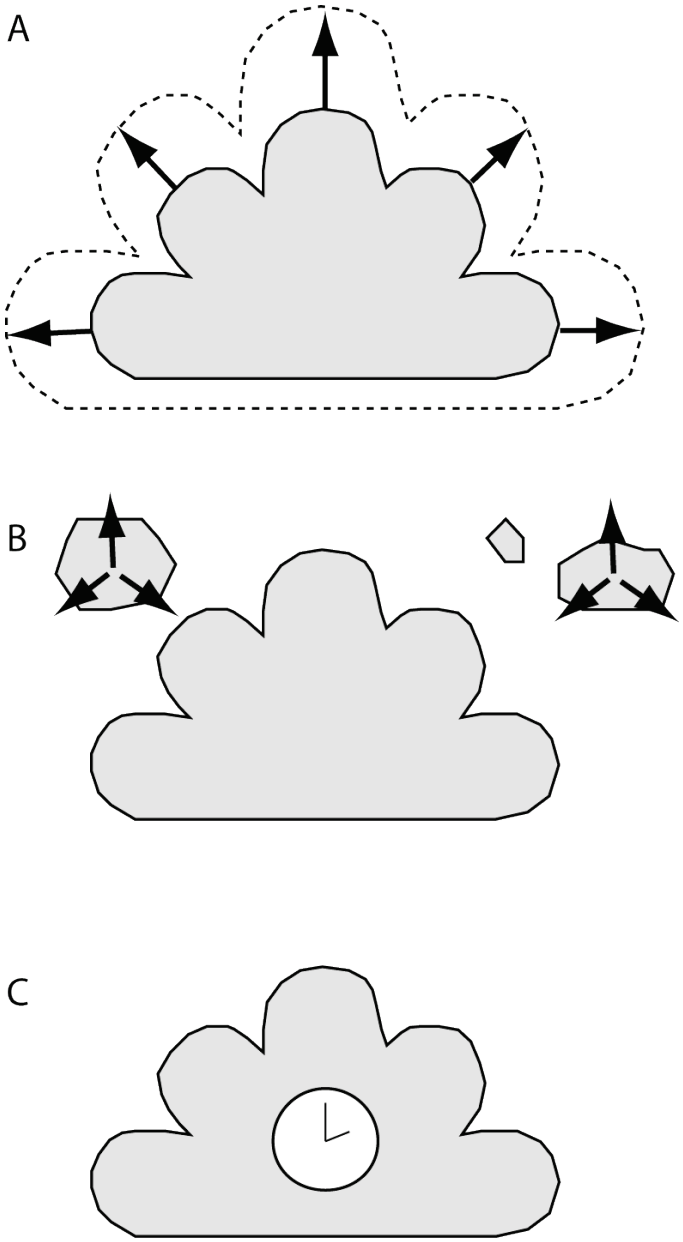

Figure 7.14 Simplified conceptual models of cloud increase

Simple conceptual models of GCR–cloud growth at the scale of individual clouds. These increases result from: **A**) an edge effect (growth at cloud boundaries), a concept supported by GEC theories and observations of the effects of space charge built up at cloud boundaries (Tinsley, 2008; Harrison and Ambaum, 2009); **B**) the growth of new, distinct, cloud bodies, most likely as a result of increased CCN concentrations due to IMN (Yu and Turco, 2001); **C**) increased cloud longevity, due to the effects of the GEC or IMN which may alter cloud properties such as cloud droplet sizes and concentrations (Yu and Turco, 2001; Tinsley, 2008).

7.3.1 MLCD experiment design

The MLCD experiment is based on the pattern of mid-latitude (30°–60°N/S) averaged, statistically significant cloud anomalies described in chapter 6; the regionally-averaged cloud changes associated with this sample are presented below (figure 7.15). The specific cloud forcing scheme applied to the MLCD experiment to simulate these cloud anomalies is detailed in table 7.1.

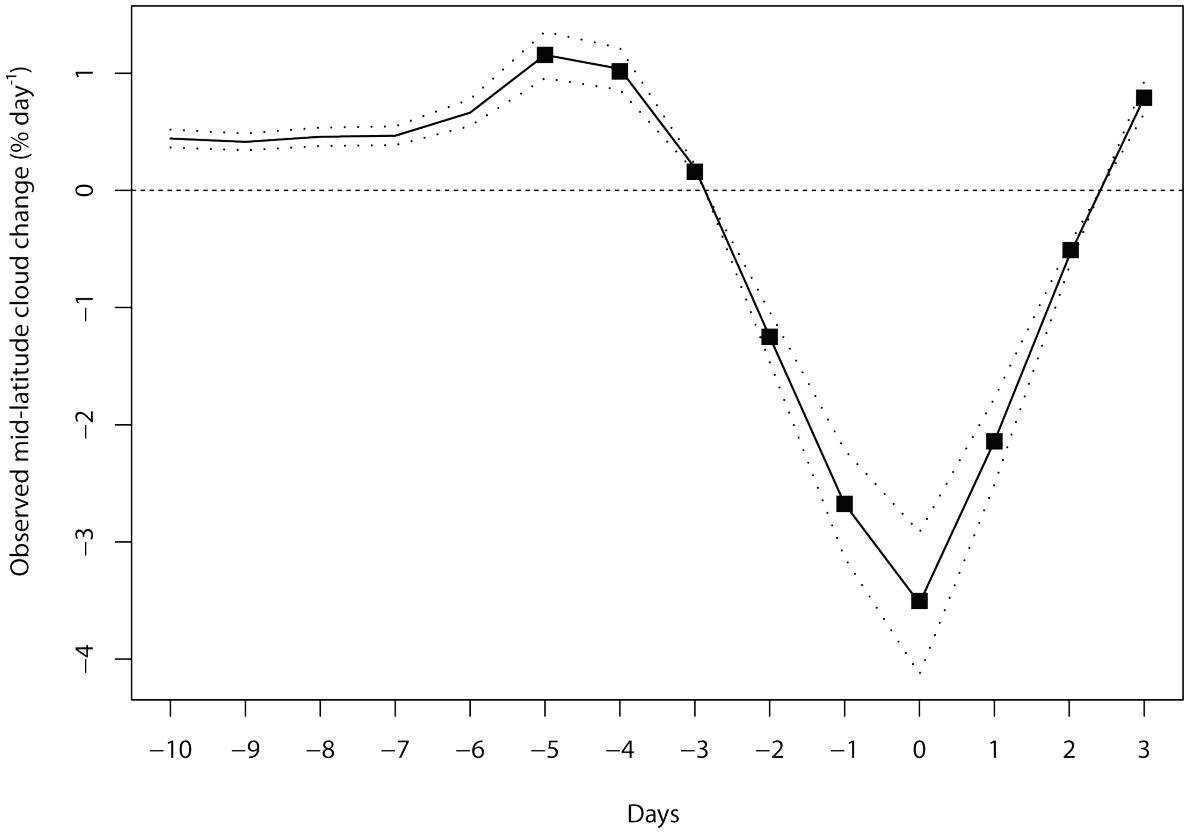

Figure 7.15 Observed mid-latitude cloud changes

Area-averaged mid-latitude cloud changes occurring during the MLCD sample. Dotted lines indicate 0.95 confidence interval, markers indicate statistically significant changes.

Day	Latitude zones (N & S)	Pressure level (mb)	Scale factor
-6	50°–30°	1,013–658	1.04
-5	50°–30°	1,013–658	1.06
-4	50°–30°	1,013–658	1.04
-2	60°–20°	1,013–557	0.97
-1	60°–20°	1,013–557	0.94
0	60°–20°	1,013–557	0.90
1	60°–20°	1,013–557	0.94
2	60°–20°	1,013–557	0.97

Table 7.1 MLCD experiment cloud forcing scheme

Day, latitude zone and height range of the applied cloud forcings. All cloud changes are based on a scale factor applied to the LW and SW model radiation schemes. The scale factor is multiplied against the cloud values of each individual model grid cell. Any changes forced above or below the maximum/minimum cloud amounts are reset to the maximum/minimum values.

The complete annotated FORTRAN code inserted in to the GCM to produce the observed cloud anomalies is presented in Appendix 4 (the method of inserting/modifying the code of the HadAM3 model in this manner is referred to as a modest). A plot of the regionally-averaged mid-latitude cloud changes produced by the modset are presented in figure 7.16. The model output shows that the overall pattern of cloud change over the composite period has been reproduced: increased rates of cloud change have been created between days -6 to -4, which then change sign between days -2 to 1. The magnitude and timing of the anomalies correspond well to observations, although the modelled anomalies are around 0.5 % weaker (with respect to key date anomalies). The spatial extent of the statistically significant modelled anomalies is found to be more limited than those seen in the observed data. A plot of 5° latitudinally-averaged cloud anomalies occurring over the composite period shows that statistically significant anomalous cloud changes develop with comparable magnitude and timing across both hemispheres (figure 7.17). This suggests that the changes to the GCM have effectively reproduced the symmetrical pattern of cloud change observed over the MLD sample. However, there are also a number of unintentional statistically significant anomalies located at high latitudes, which appear throughout the composite period (these are particularly evident in the northern hemisphere). The reason for the existence of such high levels of Arctic region variability are unclear. It is unknown at this stage how such variability may impact the

experiment, although it is probable that it will increase the SNR of the sample. This may complicate the detection of potential cloud–climate signals present in the data. Some attempts were made to overcome this issue. For example, test experiments were performed using composites of doubled sample size, however these samples did not remove the problem and, due to the increase in computational intensiveness which accompanied the doubling of sample sizes, their use continued use for experimentation was unfeasible with regard to computing resources.

A plot of locally significant cloud changes observed on the key date shows that statistically significant anomalies occur over a wide range of locations (including areas outside of mid-latitude regions) (figure 7.18). Approximately 12.2 % of the modelled troposphere demonstrates statistically significant pixels and, of these, 42 % are located within mid-latitude zones. The largest significant anomalous cloud decreases seen within the mid-latitude regions correspond to areas of cyclonic activity (e.g. in the North Atlantic); this suggests that the cloud change created by the modset have disproportionately influenced regions of high storm activity. Experimentally, such a change is unfavourable, as it does not properly reflect the situation seen in the observations, which show no locally significant cloud anomalies over these regions.

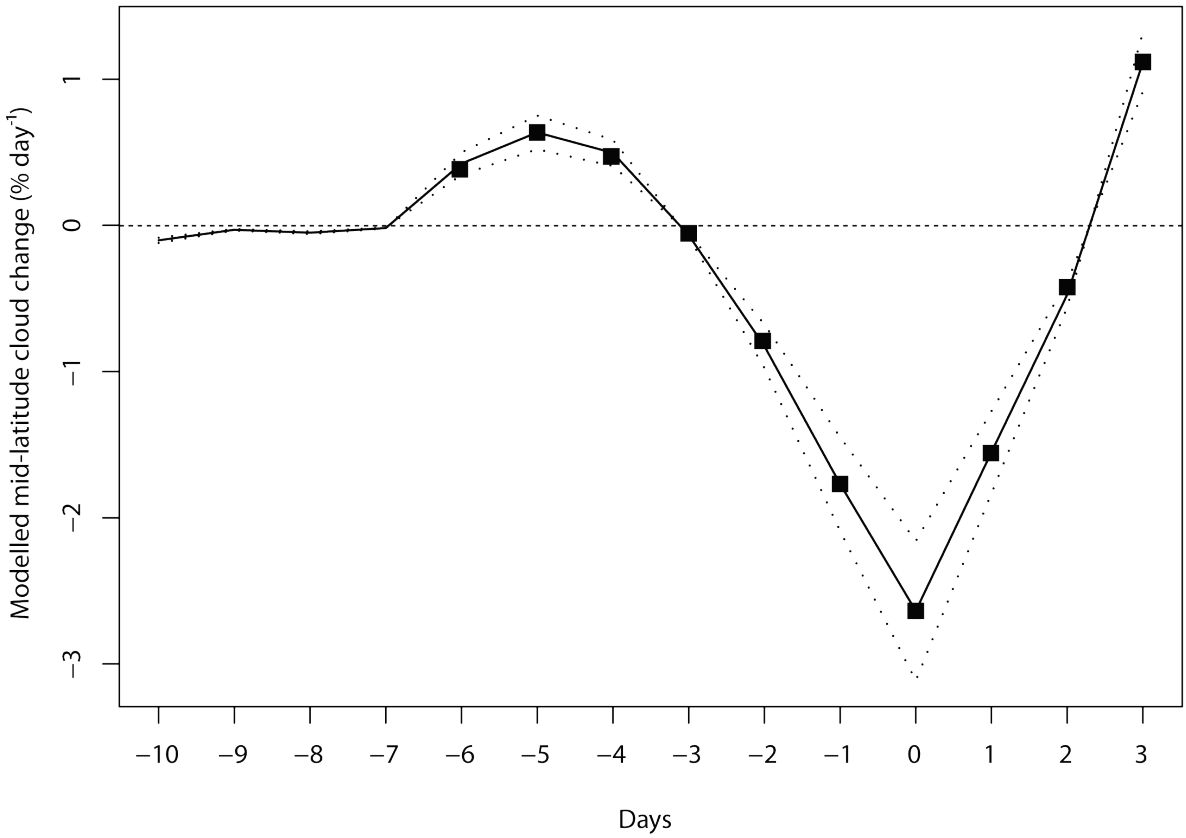

Figure 7.16 Forced MLCD experiment cloud changes

The area-averaged (30°–60° N/S) total cloud changes resulting from the MLCD experiment code changes. The 0.95 level confidence intervals is shown by the dotted lines; days of statistically significant cloud change are indicated by the markers.

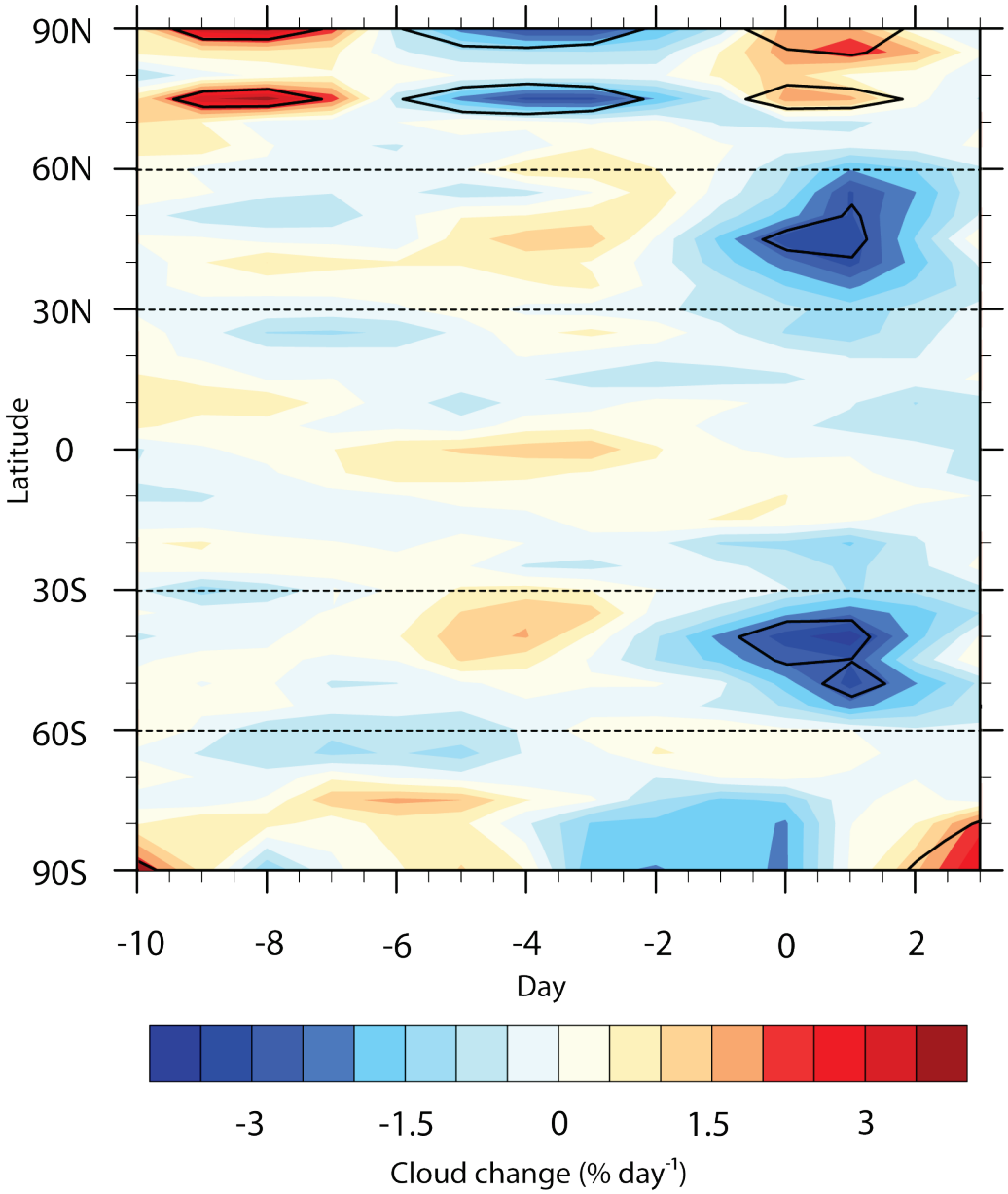

Figure 7.17 Simulated MLCD cloud changes

A plot of 5° latitudinally-averaged cloud cover changes occurring over the composite sample from day -10 to 3. The horizontal dashed lines indicate the mid-latitude zones where cloud changes are intentionally forced. Solid contours show statistically significant anomalies above the 0.95 critical level.

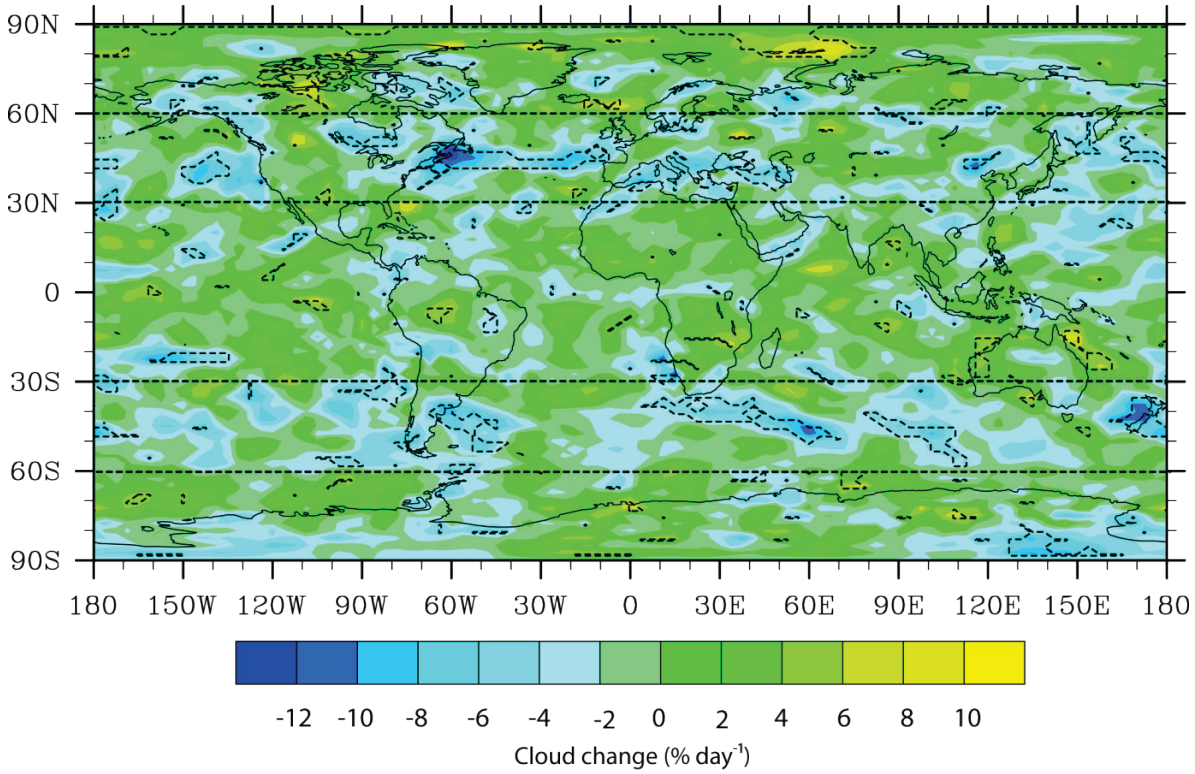

Figure 7.18 Locally significant key date cloud changes

Anomalous key date cloud changes across the globe, with statistical significance overlaid (dashed contours). Dashed solid lines indicate the mid-latitude regions where negative cloud changes are forced. 12.2 % of the total grid shows a statistically significant cloud change, of which 42.0 % is located within mid-latitude zones. Of the statistically significant changes 42.0 % are positive, while 58.0 % are negative.

7.3.2 MLCD experiment results: air temperature

The results of the MLCD experiment show that, although a change between negative/positive anomalies is observed both before and after the key date, no statistically significant air temperature anomalies were produced at a globally-averaged resolution over the composite period (figure 7.19A). A plot of 5° latitudinally-averaged surface level temperature anomalies occurring over the composite period indicates that the regions of largest temperature variability occurred at high latitude zones (figure 7.19B). This implies that the temperature changes observed over the globally-averaged sample is reflecting (unintentional) polar variability as opposed to the desired mid-latitude cloud changes produced by the modset.

During the key date of the composite, no statistically significant air temperature changes were detected at any pressure level (at a 5° latitudinally-averaged resolution) within mid-latitude regions. Overall however, temperature anomalies did appear to be of a positive sign, which may

suggest the influence of cloud decreases on temperature, although these anomalies were of relatively low magnitude (around 0.1 K) (figure 7.20). In comparison, large ($\geq$0.5 K) statistically significant anomalies of both sign were identified over high latitude regions during the key date (figure 7.20); the difference in magnitude between mid-latitude and high latitude temperature variations again implies that, as a global average, a cloud–temperature signal should not be expected from this experiment.

A plot of locally significant surface level air temperature anomalies occurring on the key date finds almost no significant changes identified over any regions; significant anomalies occur over only 3.8 % of the globe (less than the 5 % uncertainty allowed by a 0.95 confidence level T-test) (figure 7.21). Since the cloud changes within mid-latitude regions were found to be relatively localised (figure 7.18), a lack of spatially corresponding temperature anomalies suggests that the forced cloud changes may have only had a small impact on air temperature. The realism of this response is difficult to determine, as locally significant cloud change comparable to those produced in the model did not occur in reality.

Regional averaging of the modelled air temperature response shows far more encouraging results. A negative relationship between forced cloud changes and air temperatures has been reproduced over mid-latitude regions that is highly comparable to observations (figure 7.22). The correlation coefficient between observed cloud and air temperature changes (between day -5 to 3) shows an R^2 value of -0.91, while the correlation coefficient of the forced cloud changes and modelled air temperature response (over the same period) is -0.93, suggesting that the HadAM3 has successfully reproduced the observed cloud/temperature signal at a regional scale. However, it is noted that the modelled air temperature changes lack statistical significance and are only around 25 % of the magnitude of the observed temperature changes. The lack of statistically significant and weaker changes produced by the GCM may be explained in several ways:

(1) *Differences between the observed and modelled significant cloud anomalies*. Locally significant cloud anomalies in the GCM were not found to demonstrate similar characteristics to observed cloud anomalies. Consequently, it is possible that their atmospheric impacts may also diverge from observations.

(2) *Type of cloud changes may not be appropriately captured*. As discussed in 7.3, the types of cloud change occurring at the scale of individual cloud systems may not be fully represented. As a result, differences between observed/modelled effects may potentially arise.

(3) *Cloud–climate interactions may not be fully resolved by the model*. Although the cloud simulations of the HadAM3 are reasonably accurate in relation to other GCMs, modelled cloud and cloud–climate interactions still bear significant inaccuracies.

(4) *Issues of SNR*. A problem of relatively low SNR may be prevalent in the GCM experiments, this problem will be discussed in more detail in 7.3.4.

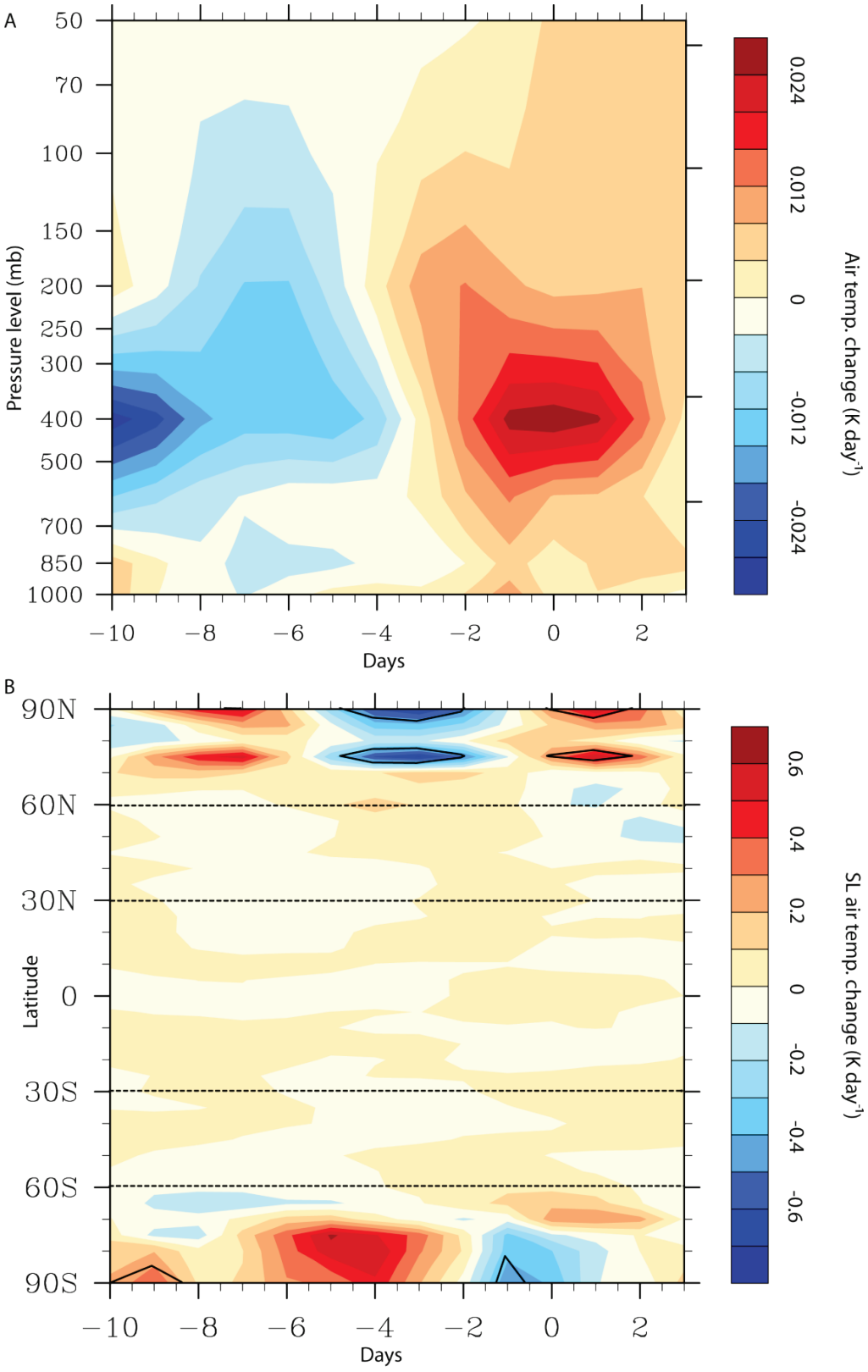

Figure 7.19 MLCD global air temperature anomalies

A) Globally-averaged anomalous air temperatures occurring throughout the troposphere during the composite period, and **B)** 5° latitudinally-averaged surface level air temperature anomalies occurring during the composite period, dashed horizontal line denotes mid-latitude regions. Statistically significant anomalies are indicated by solid black contours.

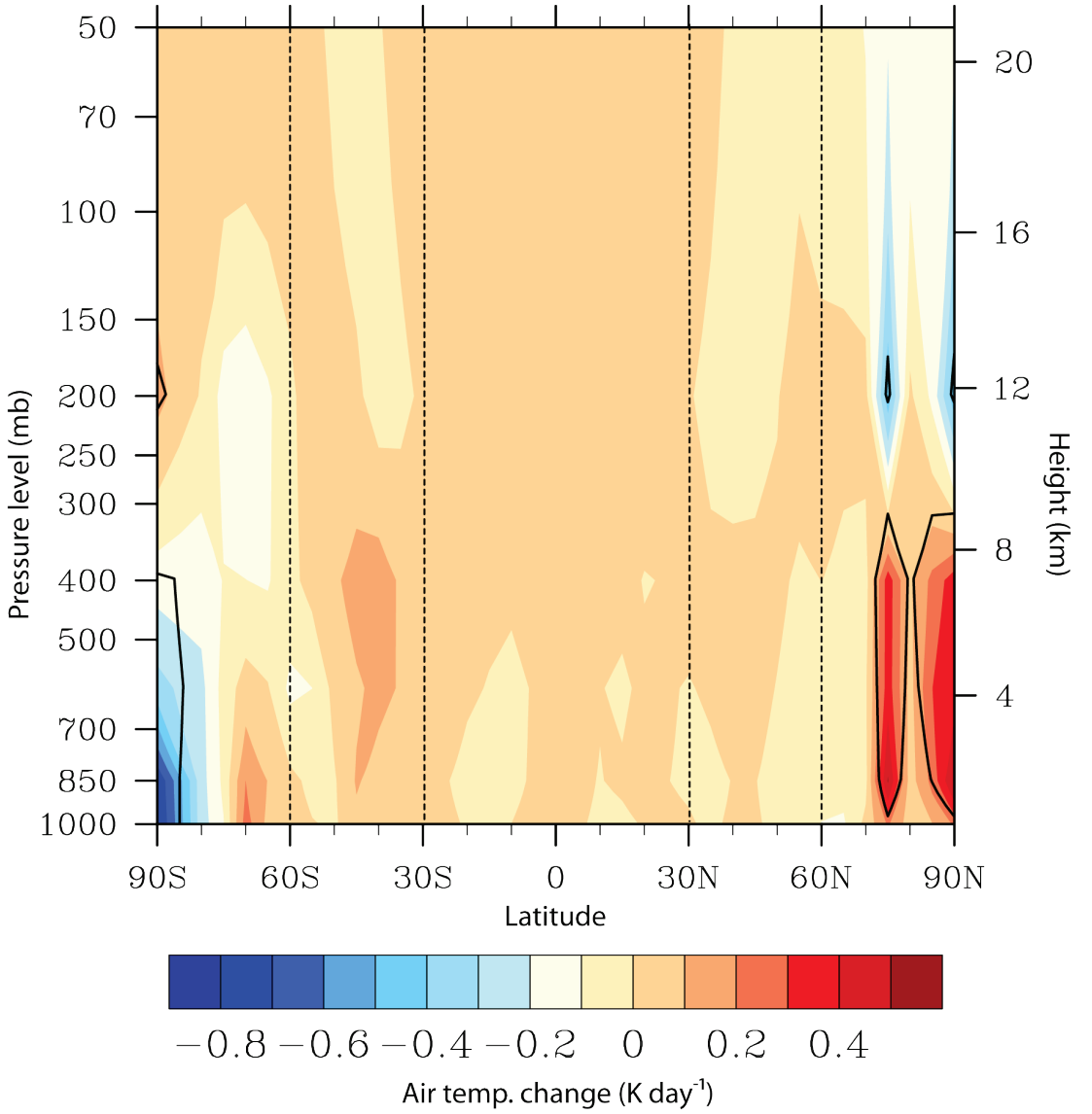

Figure 7.20 Key date modelled air temperature anomalies

A plot of 5° latitudinally-averaged GCM air temperature anomalies occuring on day 0 of the composite. Dashed vertical lines delinate regions of forced cloud changes at mid-latitude regions; solid contours indicate regions of statistical significance.

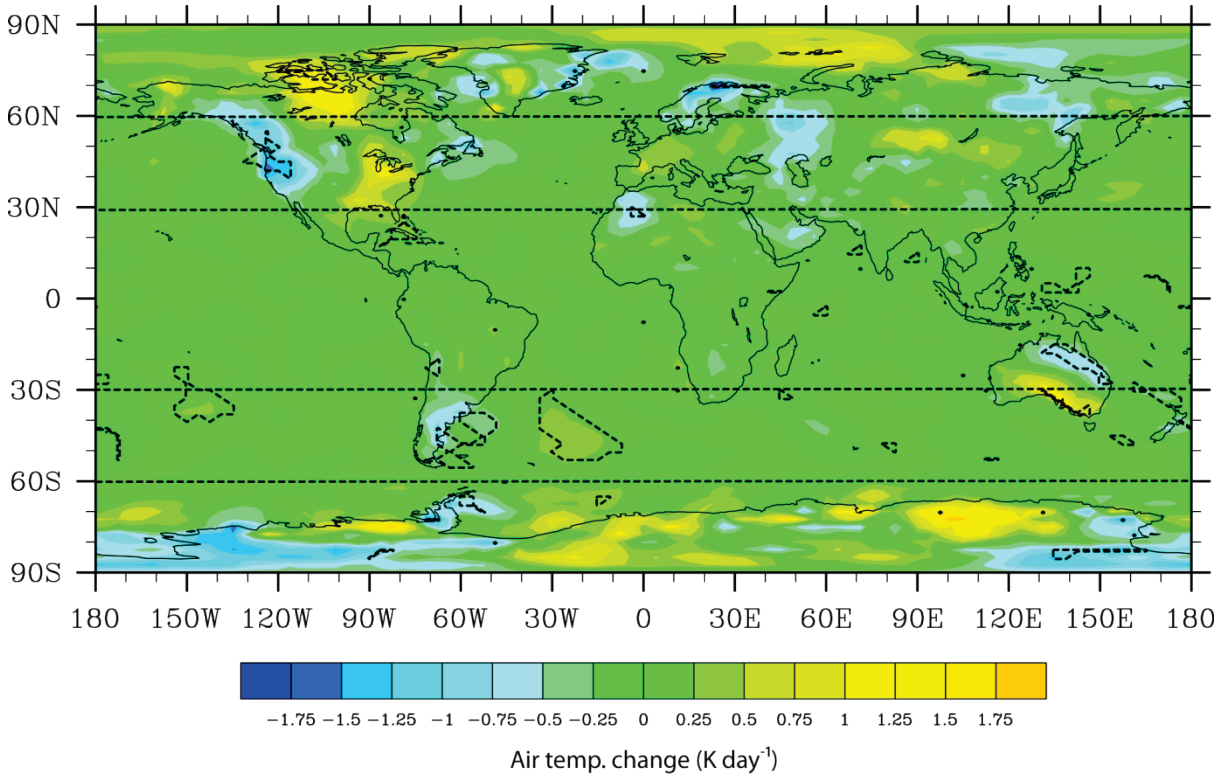

Figure 7.21 Locally significant MLCD air temperature changes

Key date anomalous surface level air temperature changes over the globe. Locally significant anomalies are indicated by dashed contours, dashed lines indicate the mid-latitude regions, wherein negative cloud changes are forced. Locally significant air temperature anomalies were found to occur over 3.8 % of the globe (49.6:50.4 % positive: negative), 53.3 % of the locally signifiant anomalies occur within the mid-latitude regions.

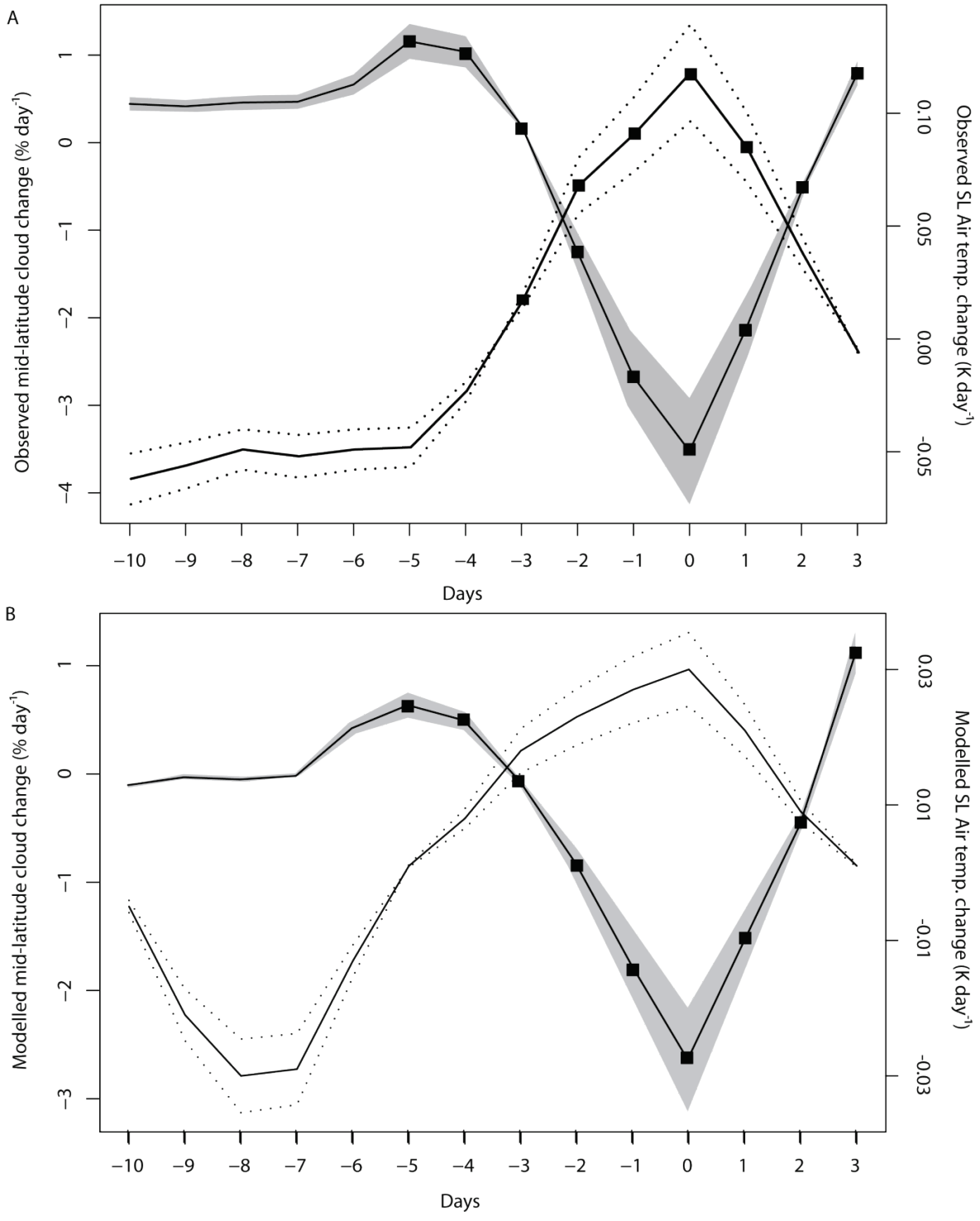

Figure 7.22 Mid-latitude cloud and air temperature anomalies

Solid line shows averaged cloud cover anomaly (between 60° and 30°N/S) (left-hand axis), while dashed line shows the surface level air temperature anomaly (over same region) (right-hand axis). Data are presented for both **A)** the observed (ISCCP and NCEP/NCAR reanalysis), and **B)** the modelled cloud/temperature response. Statistically significant anomalies (above 0.95 level) are indicated by markers, grey shading and dotted lines both indicate the 0.95 level confidence intervals.

7.3.3 MLCD experiment results and analysis: pressure

At a globally-averaged resolution, no statistically significant changes in GPH were identified at any pressure level during the composite period (figure 7.23A). A 5° latitudinally-averaged plot of surface level pressure anomalies over the composite period also shows that, over the mid-latitude regions, no significant pressure anomalies were observed. However, a number of statistically significant anomalies were identified at high latitude regions throughout the composite period (figure 7.23B); the timing and location of these anomalies suggests that they are unconnected to the intentionally forced mid-latitude cloud decreases. These anomalies suggest that unrealistically large variability is produced over high latitude regions.

A 5° plot of latitudinally-averaged anomalous GPH changes on the key date reveals no statistically significant changes over the mid-latitude regions at any pressure level (figure 7.24). Small, but significant, anomalies are apparent over the high latitude regions, but seem to be unrelated to the forced mid-latitude cloud changes. Over the mid-latitude region of the southern hemisphere two relatively large (but non-significant) anomalous GPH changes occur (of -3 and 5 m day^{-1}); however, it is not clear whether these are the result of large (6 m day^{-1}) changes in GPH detected between 90°S–60°S, or the cloud changes produced by the modset.

A plot of surface level pressure anomalies occurring on the key date of the composite reveals the presence of two areas of locally significant pressure decreases within mid-latitude regions (figure 7.25). Confidence in the field significance of this result is low, as locally significant GPH anomalies were found to occur over only 3.0 % of the globe (less than the random 5.0 % expected at a 0.95 confidence level). In addition, the modelled pressure changes failed to show a locally significant increase in surface level pressure around the periphery of the Antarctic continent, as identified in the NCEP/NCAR reanalysis data (figure 6.40); this result is unsurprising given the large atmospheric variability observed at high latitudes during the MLCD experiment.

Theoretically, it should be expected that a decrease in mid-latitude cloud cover should result in increased surface level air temperatures and decreased pressures. So far, globally-averaged and 5° latitudinally-averaged plots have not yet shown indications of a statistically significant pressure response. However, area-averaged, mid-latitude observations of pressure changes during the composite shows a statistically significant surface level decrease of approximately -16 Pa day^{-1}: this decrease begins on day -7 and peaks on day -1 (figure 7.26A). Modelled surface level pressure changes over an identical domain show a comparable pattern of change, with pressure decreases beginning on day -7 and peaking on day -1 (at around -12 Pa day^{-1}) (figure 7.26B). However, it should be noted that the modelled pressure changes failed to demonstrate statistical significance. This result is similar to the air temperature changes of the

MLCD sample, which also only showed changes comparable to observations after area averaging was applied.

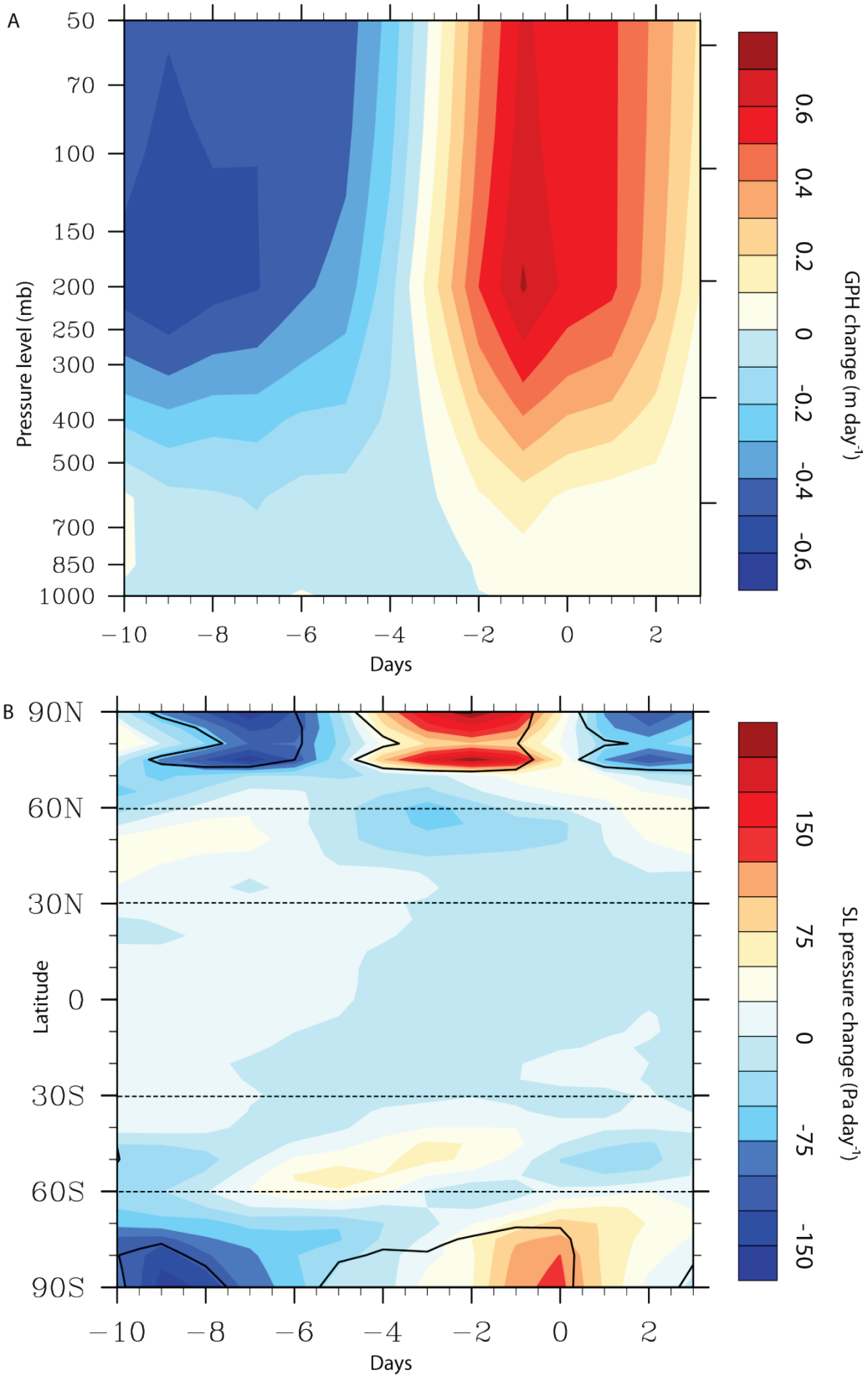

Figure 7.23 MLCD GPH changes over composite period

A) Globally-averaged GPH anomalies occurring throughout the troposphere, and **B)** 5° latitudinally-averaged 1,000 mb GPH anomalies. Solid contours indicate statistically significant anomalies. Horizontal dashed line denotes mid-latitude region wherein negative cloud anomalies are simulated.

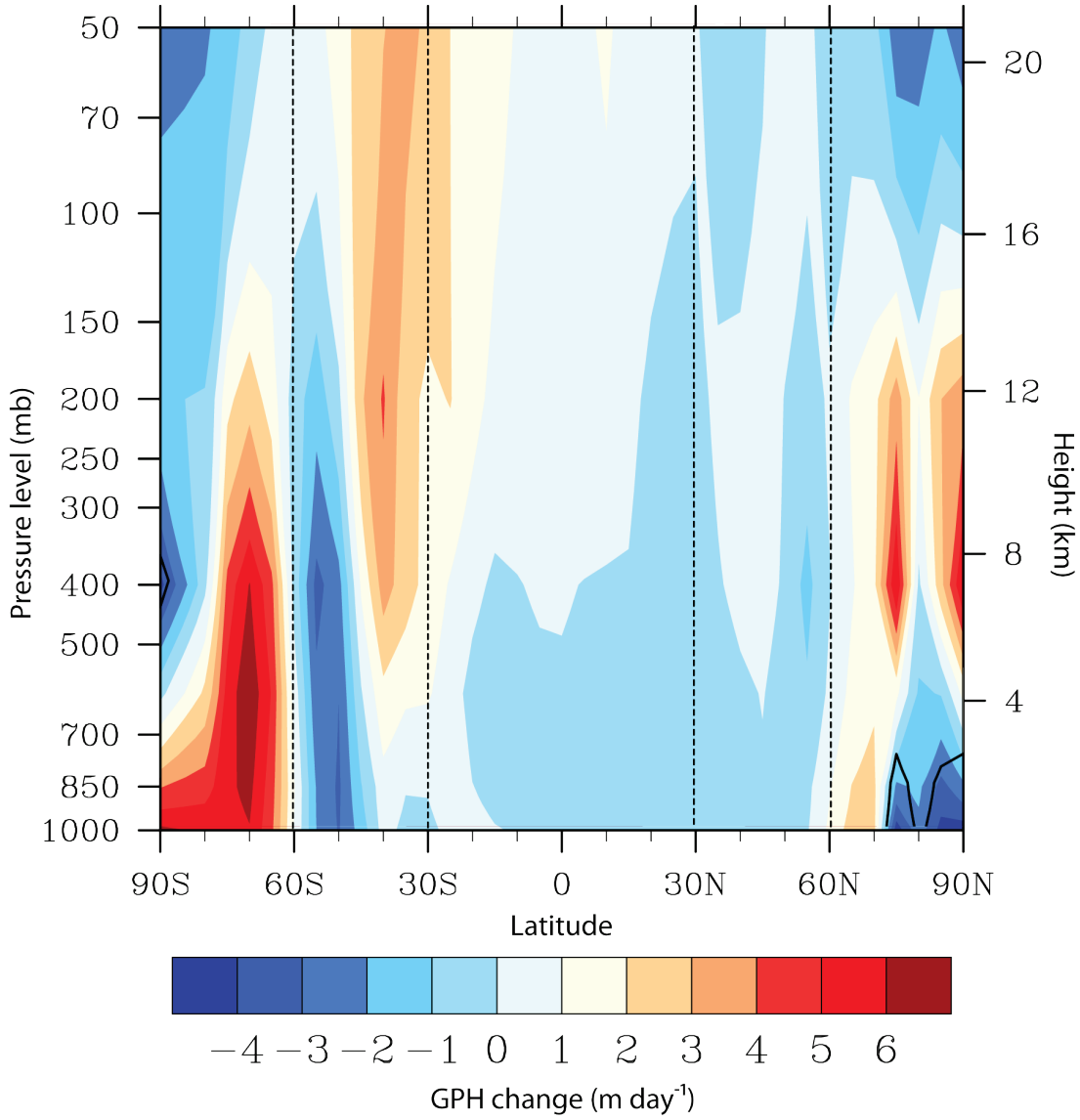

Figure 7.24 Key date GPH changes

A plot of 5° latitudinally-averaged GPH anomalies occurring on the key date of the MLCD composite throughout the troposphere. Vertical dashed lines denote mid-latitude regions, wherein negative cloud changes are simulated.

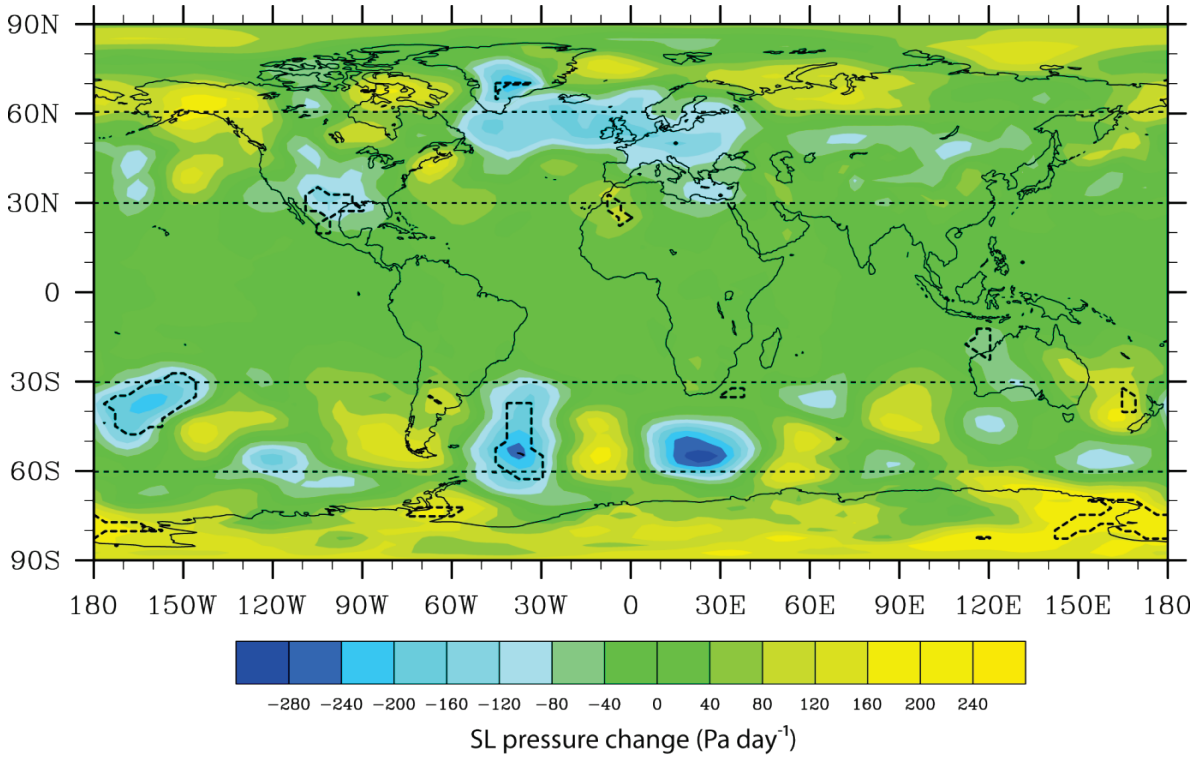

Figure 7.25 Pressure anomalies over the MLCD experiment

Key date anomalous surface level pressure changes over the globe. Locally significant anomalies are indicated by dashed contours; dashed lines indicate the mid-latitude regions, wherein negative cloud changes are forced. Locally significant pressure anomalies were found to occur over 3.0 % of the globe (41.4 : 58.5 % positive : negative); 51.6 % of those anomalies were located within mid-latitude regions.

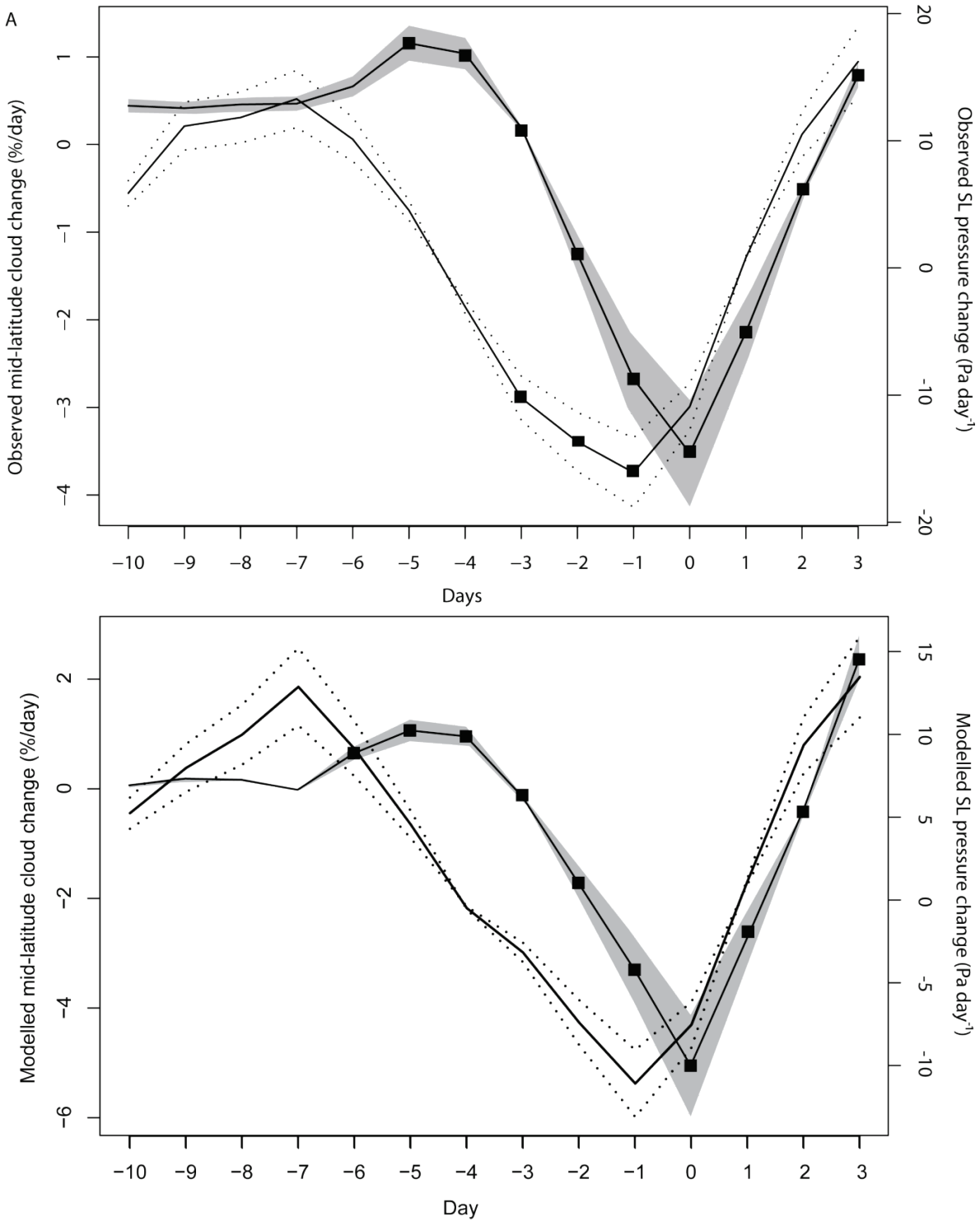

Figure 7.26 Modelled *vs.* observed pressure changes

Averaged cloud cover anomaly (solid lines) (between 60° and 30°N/S) (values plotted on left-hand axis) and mid-latitude surface level pressure anomalies (values plotted on right-hand axis). Data are displayed for both **A)** the observed (ISCCP and NCEP/NCAR reanalysis), and **B)** the modelled cloud/pressure response. Statistically significant anomalies (above 0.95 level) are indicated by markers; grey shading and dotted lines both indicate the 0.95 level confidence intervals. Note differing scales on vertical axes between panels.

7.3.4 MLCD experiment: further analysis

Overall, while the MLCD experiment was unable to reproduce small scale (5° latitudinally-averaged) features detected in the MLD sample (discussed in section 6.5), the experiment was able to successfully capture the observed area-averaged pressure and temperature responses of the mid-latitude regions (although the temperature response was weaker than observed). This is demonstrated in figure 7.27, which compares the area-averaged relationship of the observed/modelled mid-latitude air temperature/pressure anomalies to cloud cover changes over the composite period and shows that, in general, the model was able to appropriately capture a regional cloud–climate response. However, the model underestimates the temperature and pressure response by around 75 % and 31 % respectively. In addition, no detectable 5° latitudinally-averaged changes were identified (contrary to observations) and the temperature/pressure response of the MLCD experiment were not statistically significant.

The fact that the response was only detectable when considering large areas may be explained as follows. The cloud–atmospheric response is a second-order phenomenon: they require the presence of cloud before a cloud change can be applied (i.e. the modset can only change cloud when there is cloud to change). As a consequence, it is likely that there is a large amount of noise present (where noise in this instance simply refers to atmospheric variations unrelated to cloud modifications). Changes at small scales within the mid-latitudes are therefore likely to be partially caused by the modset (if cloud conditions allow) and partially by noise and hence give no overall indications of a signal. Area averaging overcomes this, as it has the effect of increasing the SNR (as over large areas, random noise tends to cancel itself out). As the cloud–climate response only becomes apparent after area averaging, this strongly implies that, at a sub-regional scale, the modelled noise is too great to observe a cloud–atmosphere response (although it is probably present).

This explanation also offers insights into why the temperature/pressure response appeared non-significant and relatively muted compared to observations. The MLD internal sample essentially represents a composite which had been pre-selected by precursor conditions, i.e. the premise of the sample was that ‘if a GCR–cloud connection exists, then it should be distinguishable based on the rapidity of cloud changes’, tests of the MLD sample indicated that this was the case (discussed in chapter 5). Hence, it is logical to assume that if the MLD sample represents rapid cloud changes enhanced by GCR variations, then the conditions required for these changes to have occurred were met and so, in effect the procedure has pre-sorted the sample to minimise noise (where noise relates to natural ‘non-GCR-enhanced’ processes). What this means is that in comparison, the MLCD experiment essentially represents a relatively noisy version of the MLD sample; this may account for the lack of statistical significance and relatively smaller changes

detected. Some further issues regarding the MLCD experiment may lie with the forced cloud decreases themselves; the decreases appear to be concentrated over regions where cloud is formed most frequently and several of these locations are also of cyclonic activity (figure 7.28). For example, an intense cloud decrease (of around -12 %) at 40°S 170°E which coincides with anti-cyclone observations did not show comparable results. The physical effects of decreasing cloud cover within cyclonic systems differs from that implied by the MLD sample; the effect of decreasing cloud in baric systems may have very different (and unintended) climatic consequences, such as the reduction of meridional energy exchange within the model.

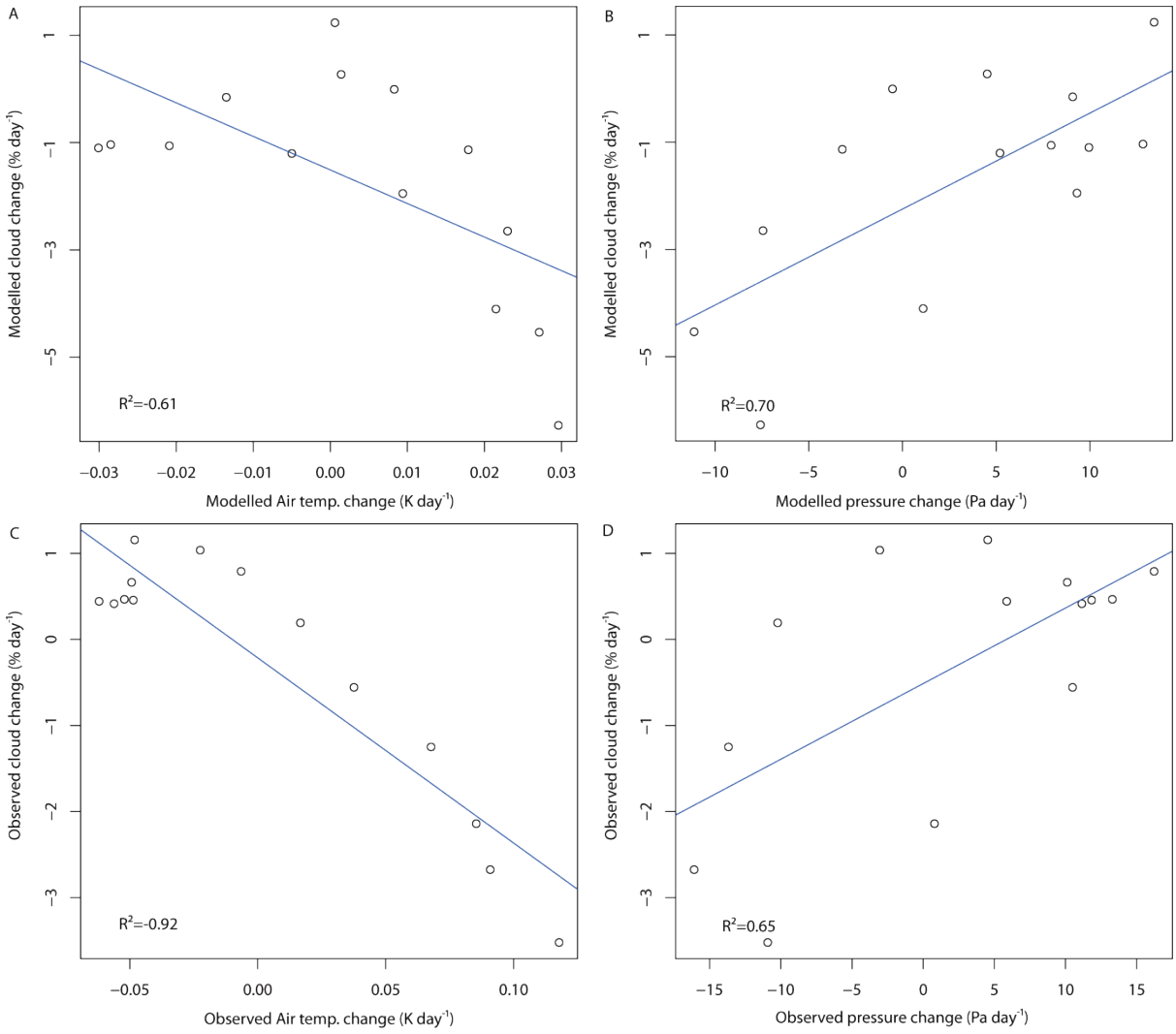

Figure 7.27 Scatter plots of MLCD sample relationships

A) Modelled cloud changes (*y*-axis) and air temperature changes (*x*-axis); **B)** modelled cloud changes (*y*-axis) and pressure changes (*x*-axis); **C)** observed cloud changes (*y*-axis) and air temperature changes (*x*-axis); and **D)** observed cloud changes (*y*-axis) and pressure changes (*x*-axis). Blue lines show linear regressions; the correlation coefficient (R^2) values are also shown on the graphs (the critical value of R^2 with 14 degrees of freedom at the 0.95 level is ±0.50).

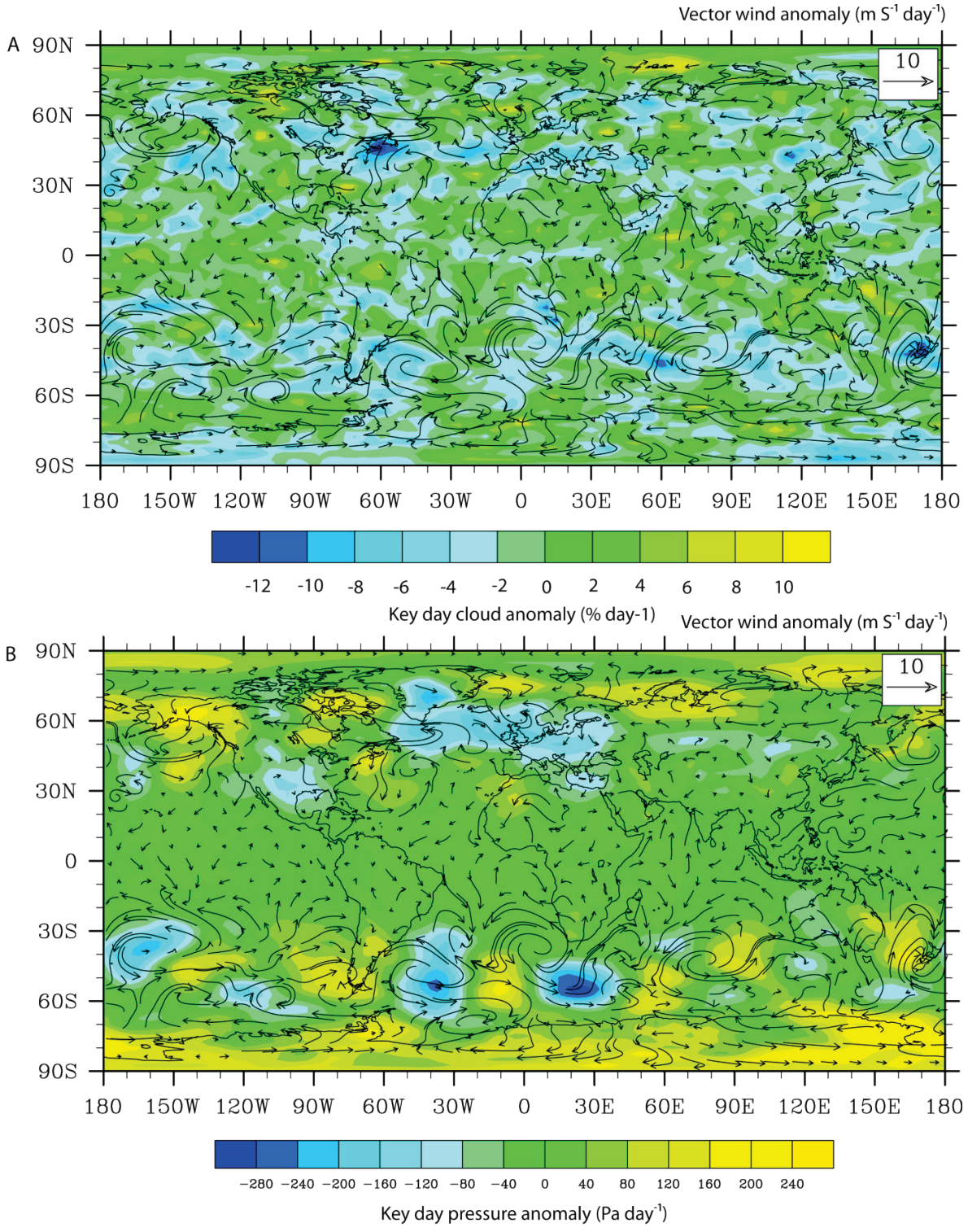

Figure 7.28 MLCD sample cloud/pressure anomalies in relation to vector winds

Anomalous vector wind changes overlaid onto **A)** cloud changes and **B)** surface level pressure anomalies on the key date of the composite.

7.4 PCI experiment: design

The PCI experiment is based on the anomalous cloud changes observed during the GI sample (discussed in section 5.2). These cloud changes were found to be predominately located at high latitudes between 90° and 60°N/S. Vertically, the northern hemisphere cloud anomalies were located at mid-tropospheric levels, whereas the southern hemisphere anomalies were located at mid- to high tropospheric levels. The tropospheric-averaged (ISCCP observed) cloud changes at the polar regions (90°–60°N/S) during the GI sample is shown in figure 7.29. The specific cloud forcing scheme applied during the PCI experiment to reproduce these changes is shown in table 7.2. The complete annotated FORTRAN modset inserted in to the GCM to simulate these anomalies is presented in Appendix 5.

The latitudinally-averaged polar cloud changes produced by the PCI experiment successfully demonstrates a close agreement to observations (figure 7.30). An anomalous cloud decrease of -1.2 % was produced on day -5, after which time anomalous cloud change increased to day 0, peaking at 7.6 %. In comparison, observed cloud changes showed values of -2.8 % and 8.8 % on days -5 and 0 respectively. To illustrate the degree of association between the observed and modelled cloud anomalies, the parameters are presented in a scatter plot (figure 7.31). This figure indicates that a strong agreement between observations and the model has been achieved (quantitatively demonstrated by a statistically significant R^2 value of 0.85). A latitude/time plot of 5° latitudinally-averaged cloud anomalies shows that statistically significant anomalies of approximately 10 % occur around the key date at high latitude regions (90°–60°N/S). This again indicates that the modset was successful in altering polar cloud cover and reproducing observed high latitude cloud anomalies. However, it should be noted that locally these changes were smaller than observed (figure 7.32).

A latitude/longitude plot of the cloud anomalies on the key date of the composite is shown in figure 7.33. This plot confirms the presence of large and significant cloud anomalies at latitudes greater than 60° (N/S) (as suggested by figure 7.32). The widespread nature of the significant polar anomalies is well illustrated by the contrast between the percentages of statistically significant pixels in non-polar/polar regions: 4.2 % of pixels at latitudes lower than 60° are locally significant (less than the 5 % uncertainty range), whereas at latitude greater than 60° (N/S) 76.9 % of pixels show statistically significant changes.

Although the PCI experiment has successfully increased cloud at a regional level, there is considerable local variation to the significant cloud changes. For example, statistically significant anomalies were not produced over large areas of the Arctic Ocean or within the continental region of Antarctica. The lack of significance over such locations may be attributable to the GCM's cloud scheme itself. It was previously noted that the models and

observations differed significantly over polar regions. In particular, the simulation of appropriate cloud amounts at specific pressure levels was observed to be very poor (figure 7.4). In the upper/mid tropospheric levels of the Antarctic/Arctic respectively (locations critical for the experiment), cloud amounts are very poorly reproduced. As a result, the lack of significant cloud anomalies at locations over polar regions may be a direct consequence of the GCM's underestimation of high latitude cloud cover.

Observations from the previous chapter suggested the possibility that an indirect cloud–climate link (operating via changes to polar circulation) may exist. The model's apparent weakness in reproducing the correct vertical structure of polar clouds may ultimately make confirming or refuting this hypothesis impossible and potentially prove to be a critical limitation on the PCI experiment. In light of this, it is important to re-state that the model's weakness in reproducing accurate polar conditions is not a limitation unique to HadAM3, but rather is a widespread issue of GCMs, as polar environments represent geophysical extremes and are consequently difficult to accurately model (CCSP, 2008).

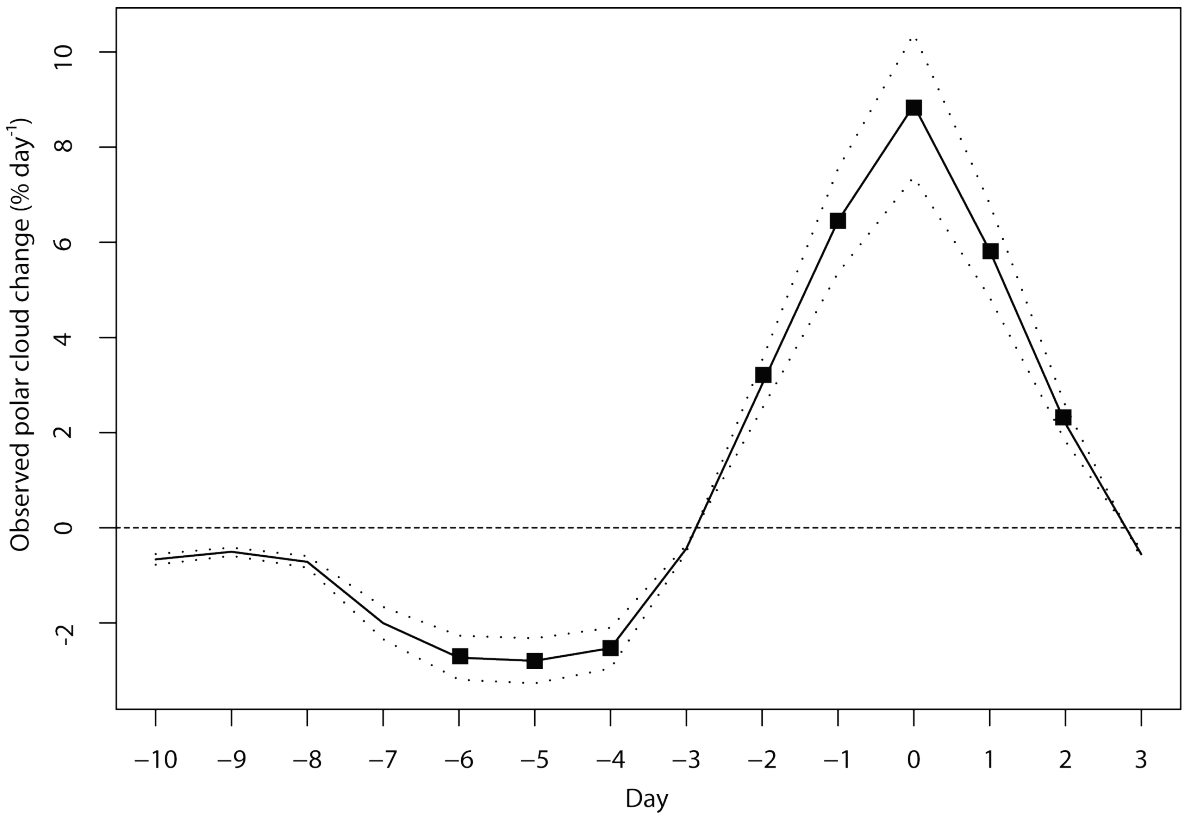

Figure 7.29 Observed high latitude cloud changes

ISCCP cloud changes occurring between 90°–60° (N/S) over the GI internal sample. Dotted lines show the 0.95 level confidence interval; markers indicate statistically significant changes.

Day	Latitude zone	Pressure level (mb)	Scale factor
-6 & -4	60°N–75°N	845–759 & 465–390	0.85
	75°N–90°N	759–465	0.80
	60°S–75°S	658–390	0.85
	75°S–90°S	390–10	0.80
-5	60°N–75°N	845–759 & 465–390	0.80
	75°N–90°N	759–465	0.75
	60°S–75°S	658–390	0.80
	75°S–90°S	390–10	0.75
-2 & 2	60°N–75°N	845–759 & 465–390	1.35
	75°N–90°N	759–465	1.45
	60°S–75°S	658–390	1.35
	75°S–90°S	390–10	1.45
-1 & 1	60°N–75°N	845–759 & 465–390	1.60
	75°N–90°N	759–465	1.75
	60°S–75°S	658–390	1.60
	75°S–90°S	390–10	1.75
0	60°N–75°N	845–759 & 465–390	1.90
	75°N–90°N	759–465	1.99
	60°S–75°S	658–390	1.90
	75°S–90°S	390–10	1.99

Table 7.2 Cloud changes forced during the PCI experiment

The table shows the timing (day), location (latitude zone), altitude (pressure level) and magnitude (scale factor) of the cloud changes inserted in to the GCM to produce the PCI experiment. The scale factor is multiplied against the cloud values of each individual model grid cell. Any cloud change forced above or below the maximum/minimum grid box value is automatically decreased/increased to the maximum/minimum value to prevent model errors. Although the scale factors are based on observations, these values have often been increased as a result of the model being relatively insensitive (i.e. large scale factors are necessary to achieve observed cloud changes as the forced cloud change depends on cloud conditions within the model, which deviate from observations).

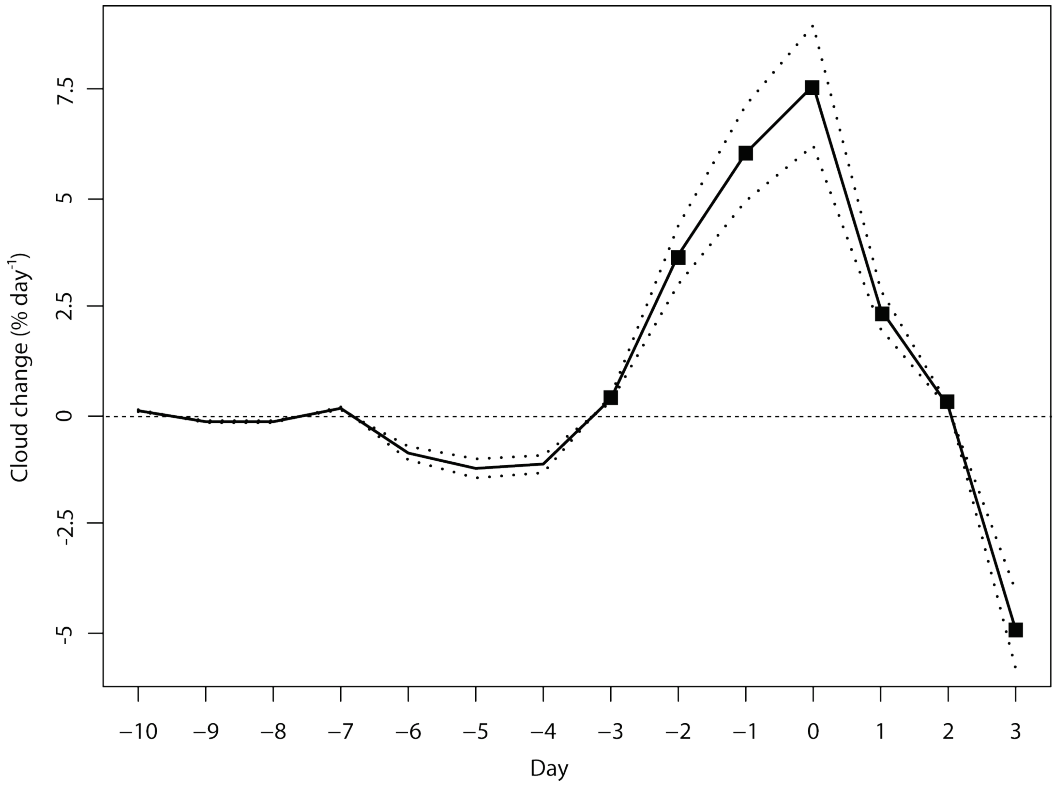

Figure 7.30 Forced PCI experiment cloud changes

Area-averaged PCI experiment cloud changes occurring between 90° and 60°N/S over the composite period. Dashed line shows the 0.95 level confidence interval; statistically significant changes are indicated by markers.

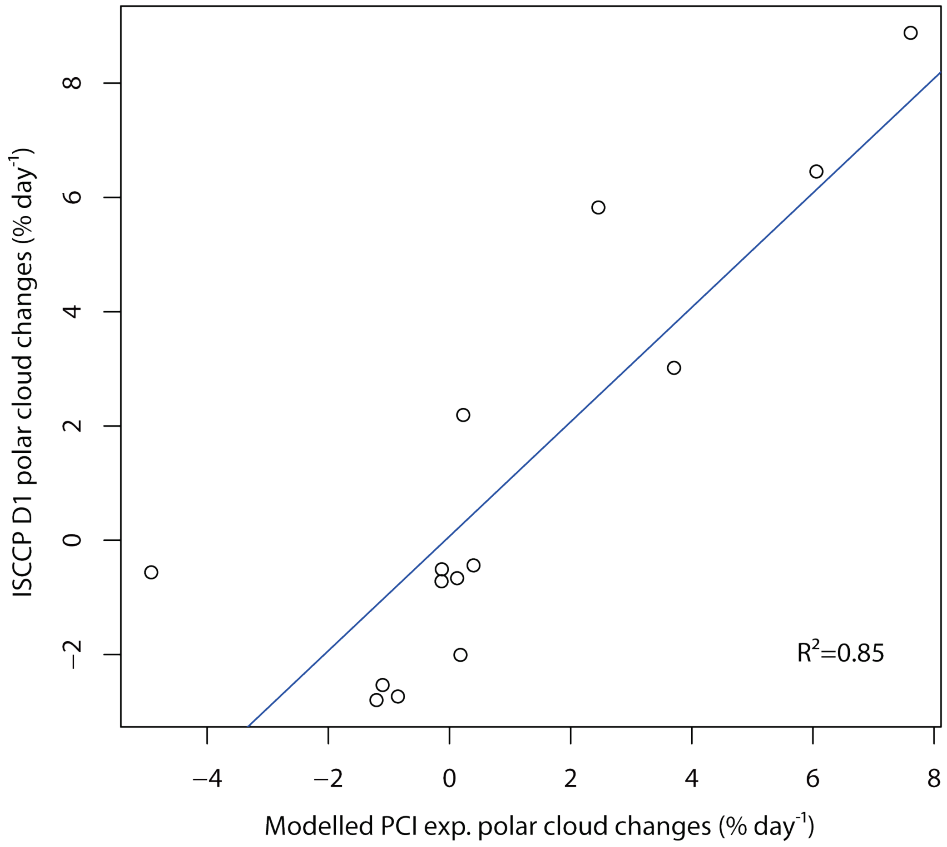

Figure 7.31 Scatter plot of observed *vs.* modelled PCI experiment cloud changes

Observed ISCCP cloud anomalies (*y*-axis) *vs.* modelled cloud anomalies (*x*-axis) over the polar (90°–60° N/S) region, with the line of best fit (blue line) and correlation coefficient (R^2) value displayed.

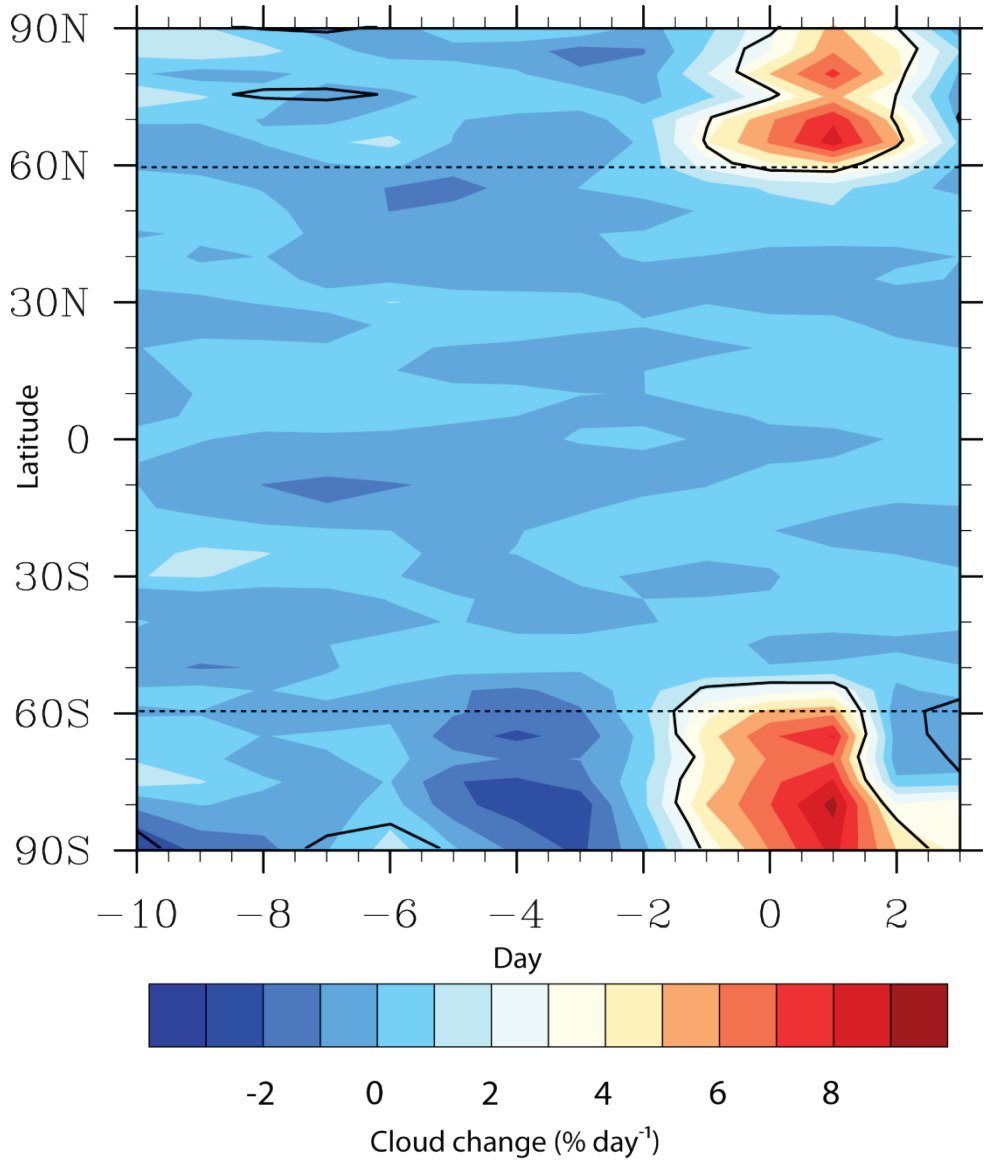

Figure 7.32 PCI experiment cloud changes

Latitude/time tropospheric average cloud changes forced within the GCM. Statistically significant changes at the 0.95 level indicated by the solid contours, dashed line indicates the areas of forced cloud changes (90°–60°N/S); see table 7.2 for exact changes applied to the GCM.

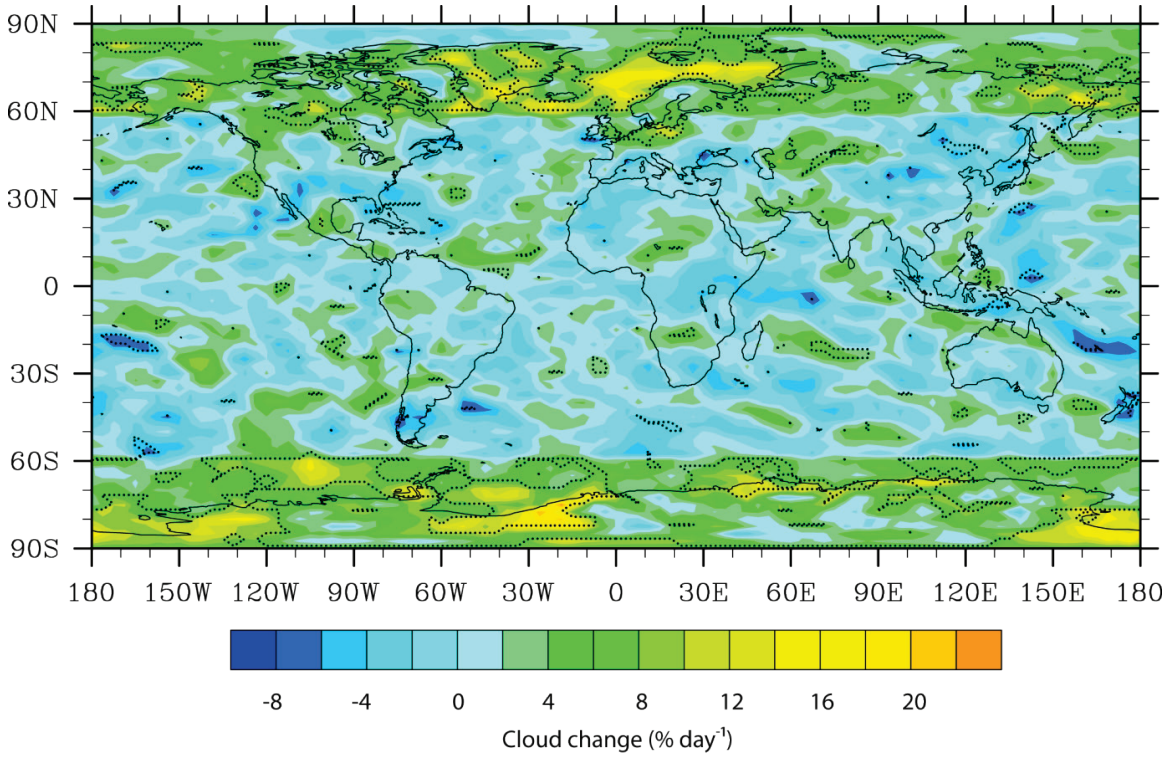

Figure 7.33 PCI experiment key date cloud anomalies

Key date PCI experiment cloud change anomalies; locally statistically significant changes indicated by dotted contours. Outside of polar latitudes (60°N–60°S) only 4.2 % of pixels are locally significant, whereas, within polar latitudes 76.9 % of pixels are locally significant. 100 % of locally significant pixels within polar latitudes are of a positive sign.

7.5.2 PCI experiment results: air temperature

During the PCI experiment, no statistically significant globally-averaged air temperature anomalies were detected at any pressure level over the composite period (figure 7.34A). However, at a latitudinally-averaged resolution, statistically significant surface level air temperature anomalies were found to occur at high latitude regions in both hemispheres across the composite period (figure 7.34B). A 5° latitudinally-averaged vertical profile of the key date air temperature anomalies found the occurrence of a small but significant mid-tropospheric level temperature decrease (of approximately -0.4 K) at high southern latitudes and two small but significant temperature increases (of approximately 0.6 K) at low tropospheric levels (figure 7.35). At a local level, there were virtually no statistically significant anomalies detected during the key date at any location (figure 7.36), although there were several significant decreases (of around -1.6 K) identified over limited areas of the western Antarctic ice sheet.

Overall, the air temperature anomalies appear to occur indiscriminately throughout the composite period at high latitudes; significant anomalies occur with an inconsistent sign in both hemispheres (e.g. around the key date the Arctic demonstrates a significant temperature increase, whilst a significant decrease occurs over the Antarctic). The inconsistency in both the sign and timing of the anomalies strongly suggests that these changes are not due to the forced cloud changes, but instead are probably related to unrealistically high simulations of polar atmospheric variability, similar to those observed during the MLCD experiment (figure 7.19).

A regionally-averaged (60°–90°N/S) plot of observed/modelled cloud and surface level air temperature changes shows that, while observations identified the occurrence of a strong and statistically significant negative relationship between cloud and air temperature, the model produced a relatively weak positive relationship (figure 7.37). Although figure 7.36 demonstrated the existence of locally significant temperature decreases over areas of Antarctica on the key date (which appears to contradict this assertion), the positive temperature response of figure 7.37B is found to occur in both hemispheres simultaneously (figure 7.38). These results indicate that the positive regional air temperature response resulting from the forced cloud changes is only detectable after regional averaging (similar to the findings of the MLCD experiment); this relationship was not detectable at higher spatial resolutions. The results of figures 7.37–7.38 suggest that the forced cloud changes in the PCI experiment did have a weak but widespread effect on temperatures at polar latitudes, but that this effect was contrary to observations. However, the modelled response agrees with the accepted notion that clouds have a warming impact on polar environments (Stone and Khal, 1991). This conflict suggests that either the observations are in error, or an unknown cloud–climate relationship, which cannot be resolved by the GCM, is occurring.

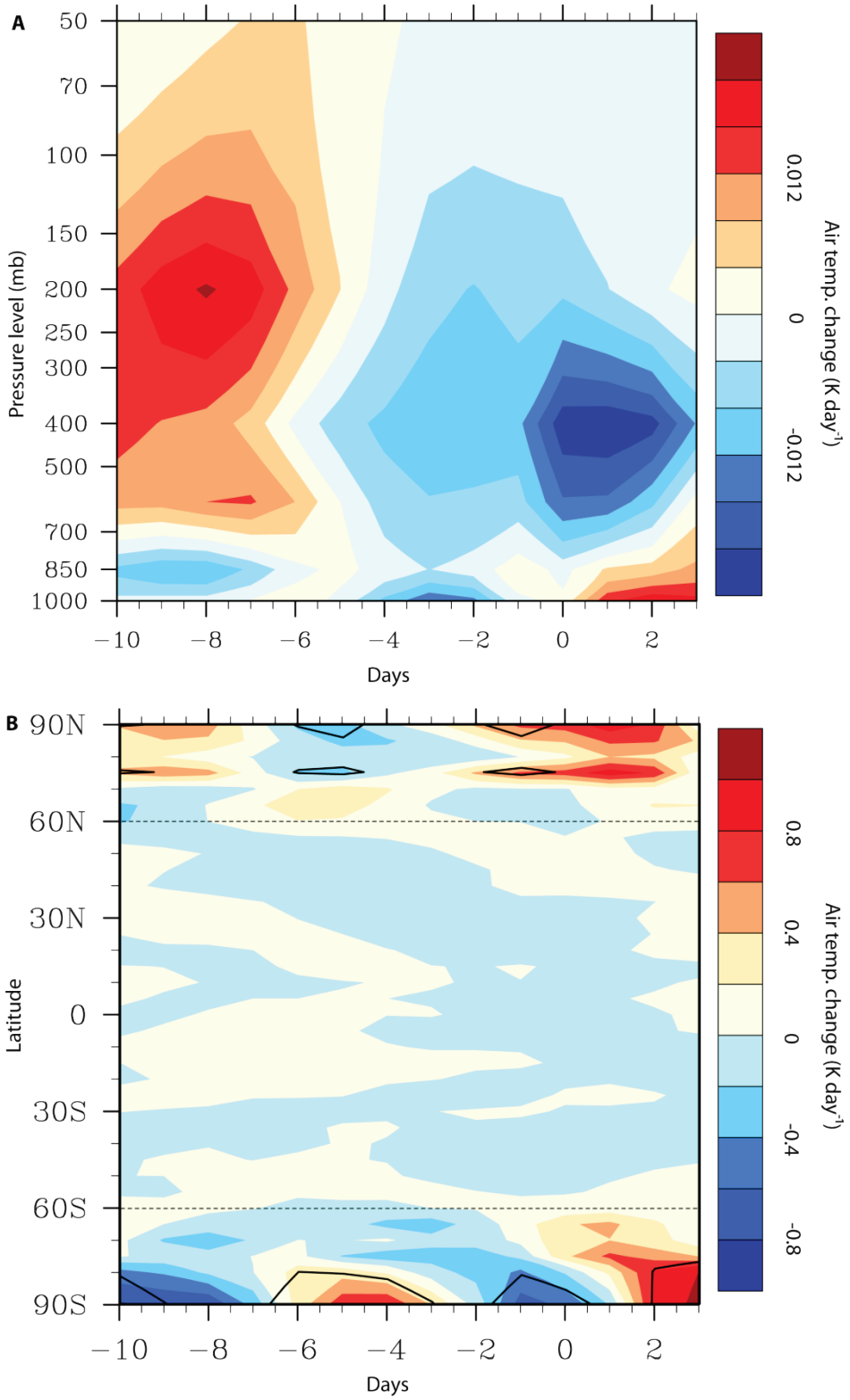

Figure 7.34 Global PCI air temperature anomalies

A) Globally-averaged air temperature anomalies occurring during the composite at different tropospheric levels, and **B)** 5° latitudinally-averaged surface level air temperature anomalies occurring during the composite period as a function of latitude. Statistically significant anomalies are indicated by solid contours; dashed horizontal line shows boundary of polar regions.

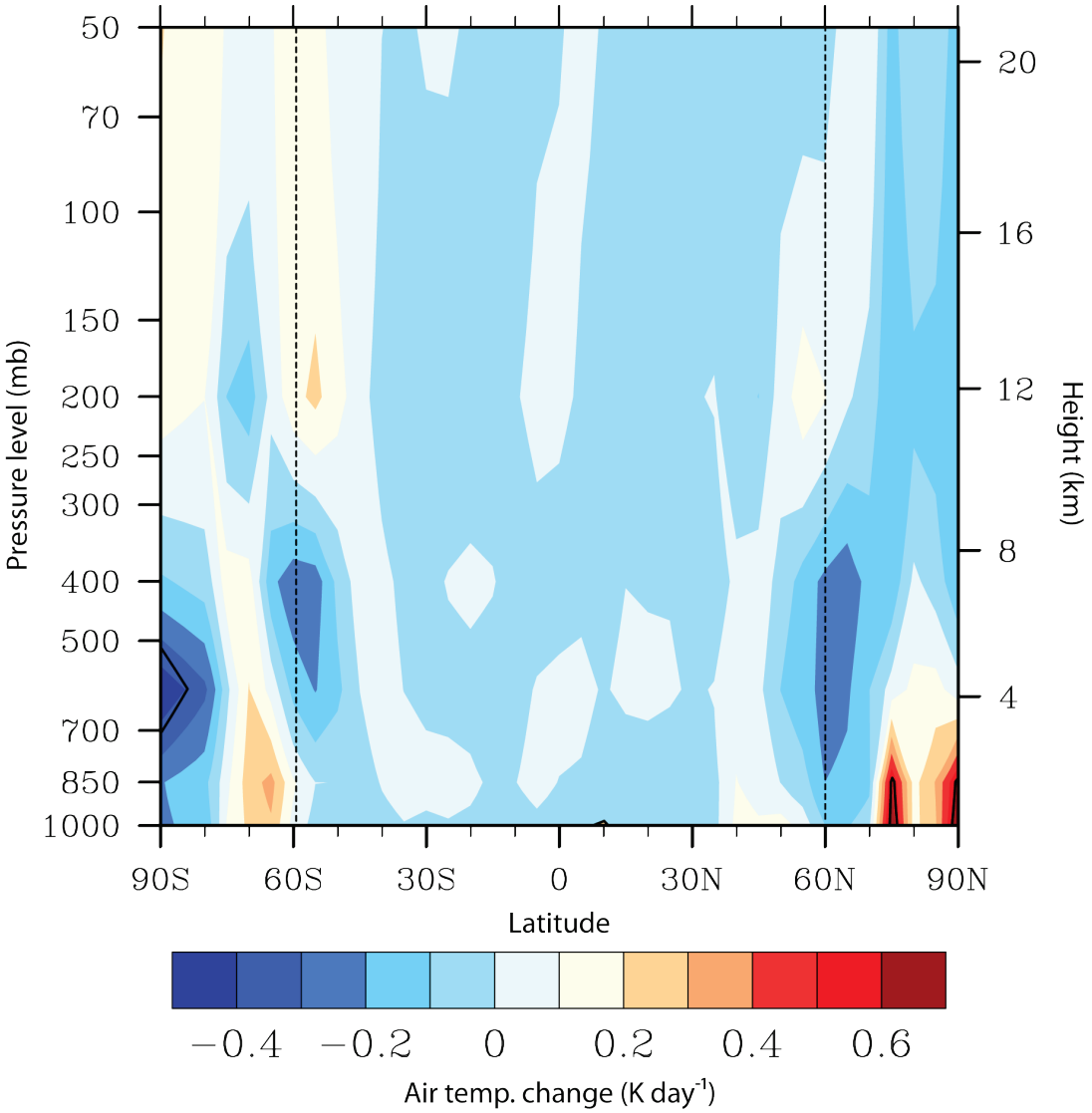

Figure 7.35 Vertical profile of PCI key-date air temperature anomalies

A plot of 5° latitudinally-averaged air temperature anomalies occurring on the key date of cloud change of the PCI experiment. Dashed vertical lines indicate limit of polar regions; solid contours indicate statistically significant anomalies.

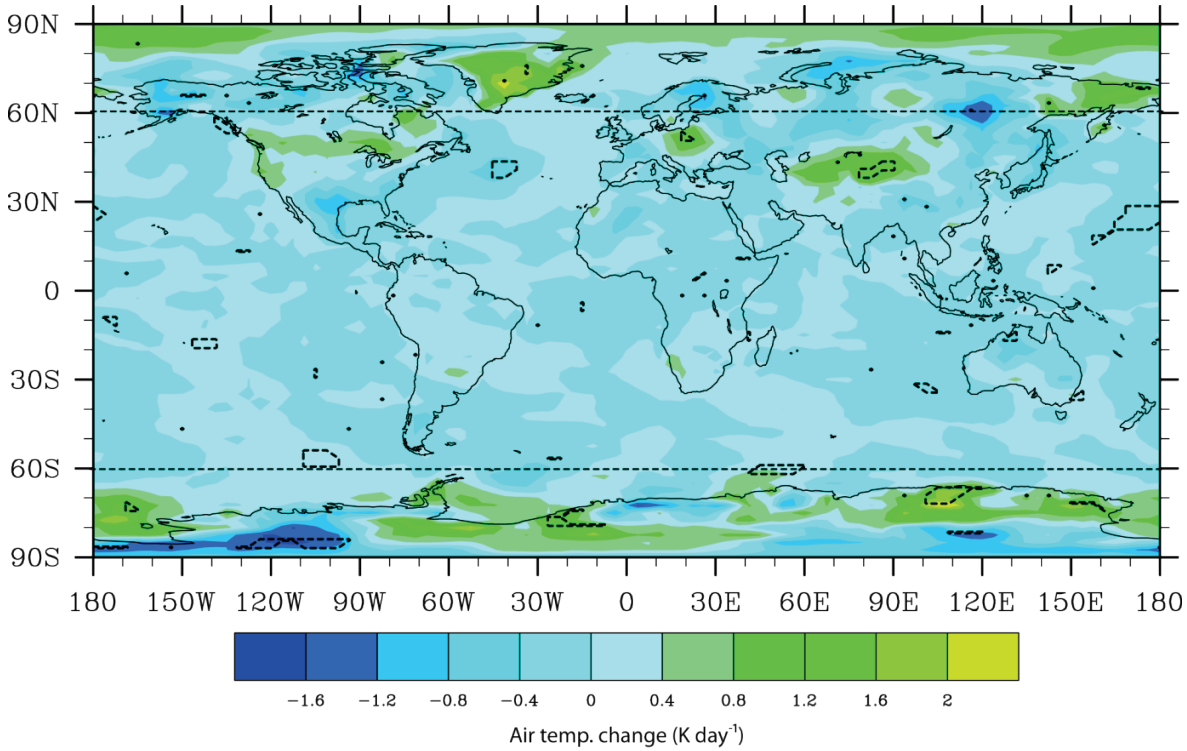

Figure 7.36 Key date air temperature anomalies

Anomalous surface level air temperature changes occurring on the key date of the PCI experiment. Horizontally dashed lines indicate the limits of the polar latitudes; dashed contours indicate regions of statistical significance. 1.6 % of pixels located in non-polar regions (60°N–60°S) are locally significant, while 3.5 % of polar pixels are locally significant. Of the significant polar pixels, 60.6/39.4 % are positive/negative, compared with 36.3/63.7 % positive/negative over non-polar regions.

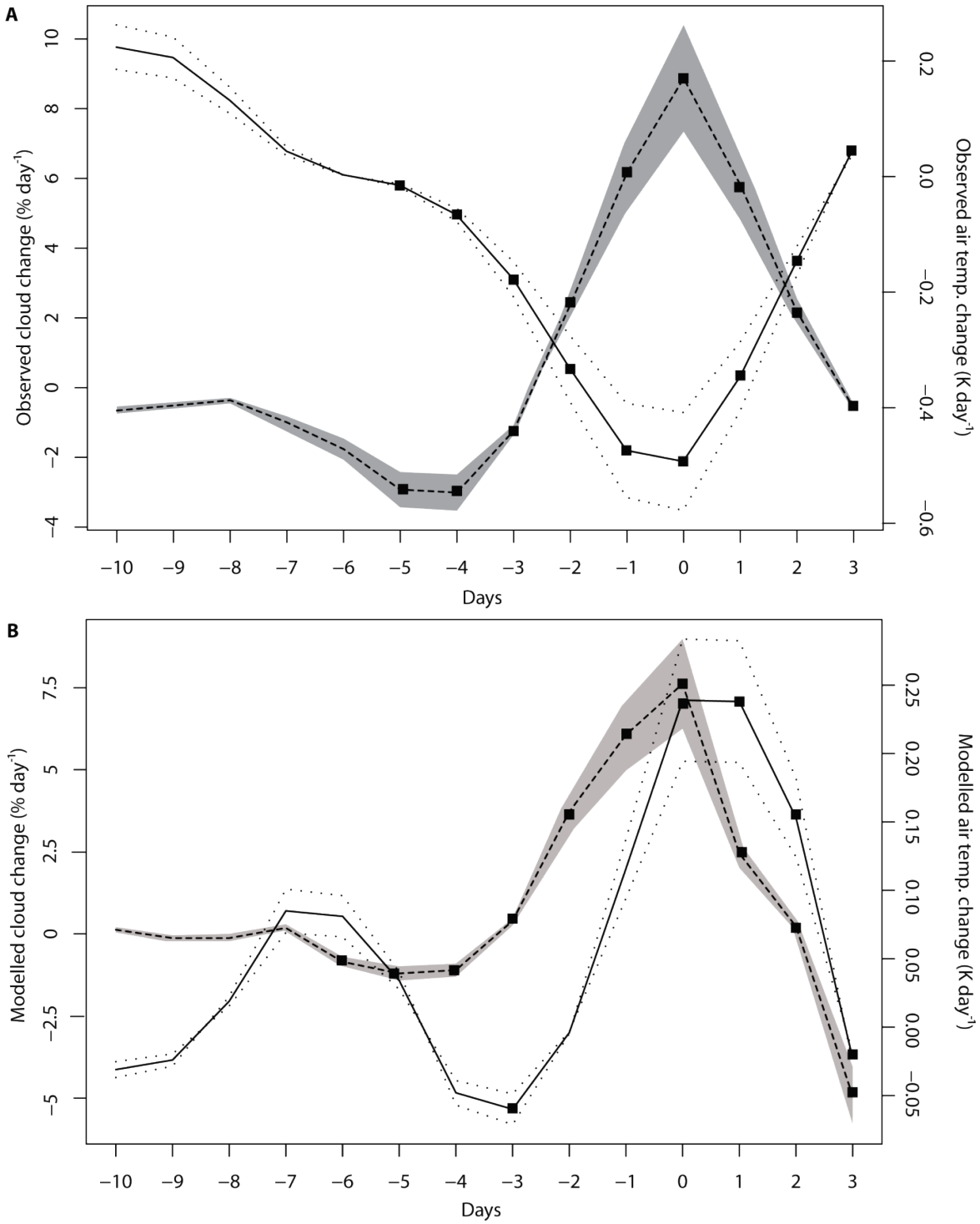

Figure 7.37 Observed and modelled cloud/temperature anomalies

Latitudinally-averaged polar cloud change (solid line) and surface level air temperature (dashed line) anomalies, for both **A)** ISCCP and NCEP/NCAR reanalysis GI sample observations, and **B)** the GCM PCI experiment. The dotted lines/grey shading shows the 0.95 level confidence interval for the air temperature/cloud data respectively. Markers indicate statistically significant changes. Note differing scales on vertical axis of panels.

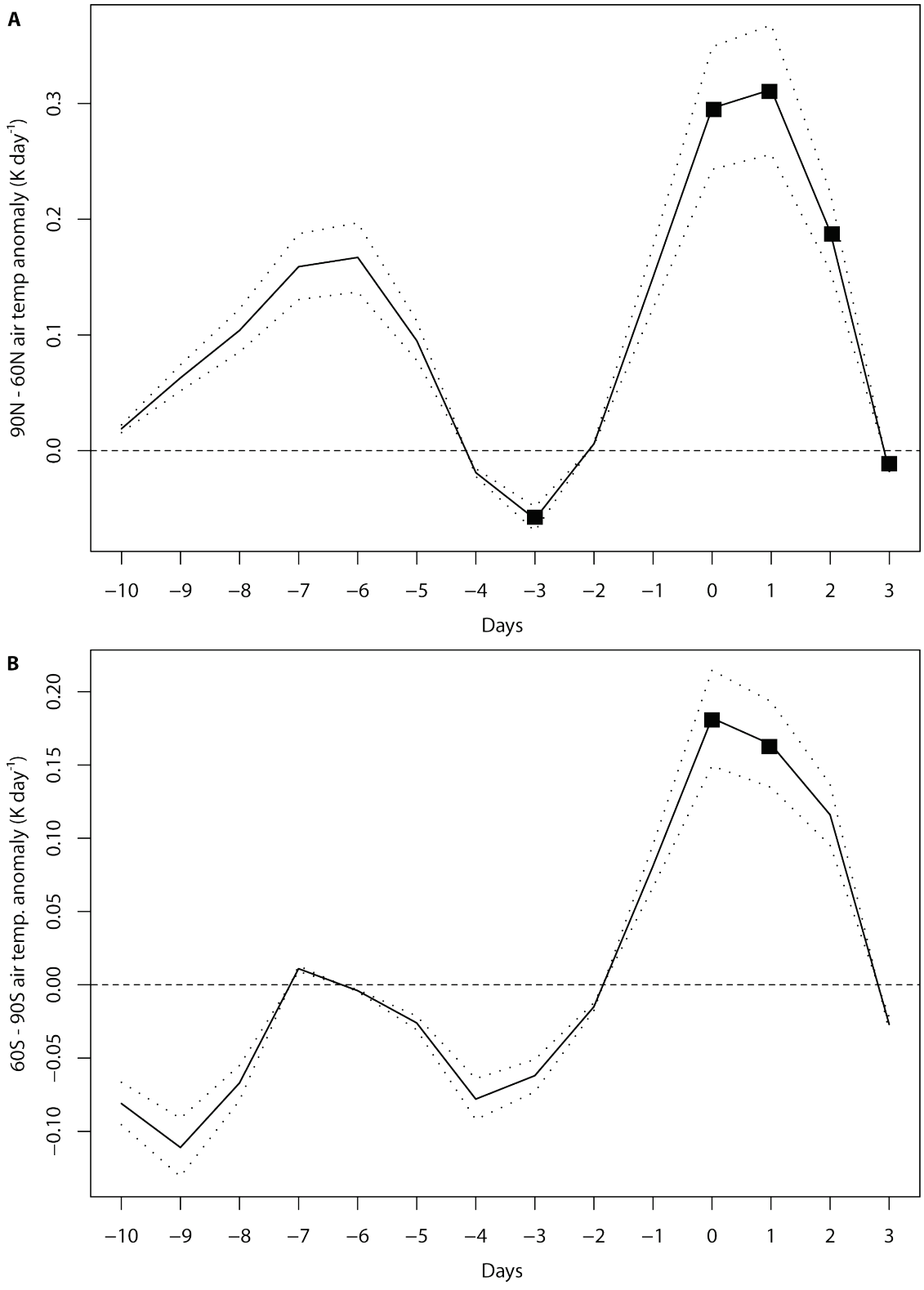

Figure 7.38 PCI experiment Arctic/Antarctic air temperature anomalies

Latitudinally-averaged GCM surface level anomalous air temperatures during the PCI experiment for the **A)** Arctic and **B)** Antarctic regions. Dotted lines indicate the 0.95 level confidence interval; markers indicate statistically significant anomalies.

7.5.3 PCI experiment results: pressure

A globally-averaged plot of GPH anomalies occurring over the PCI composite period shows an increase of approximately 0.5–0.18 m occurring around the key date. These changes are found to be statistically significant at upper tropospheric levels (figure 7.39A). A plot of 5° latitudinally-averaged surface level pressure anomalies shows that a number of statistically significant changes took place during the composite period (figure 7.39B). In general, negative anomalies of around -120 mb occurred at polar latitudes in both hemispheres between days -10 to -4, but between days -4 to 0 these were replaced by stronger positive anomalies of around 200 mb. Several significant anomalies are also identified at mid- and low latitude regions around day -4 and following day 0. The pressure changes occurring during the PCI composite appear to occur slightly out of phase with the forced polar cloud changes.

A latitude/height profile of 5° latitudinally-averaged GPH anomalies occurring on the key date of the PCI experiment show the presence of strong positive anomalies (of approximately 8 m) over high southern latitudes at all tropospheric levels, while strong negative anomalies of around -10 m are identified at mid- to high northern latitudes. In addition, a relatively weak positive mid- to low tropospheric level anomaly (of around 4 m) is also observed at high northern latitudes (figure 7.40). A latitude/longitude plot of key date surface level pressure anomalies indicates that the areas of the largest and most widespread pressure change were over high southern latitudes, which showed intense increases in pressure within the Antarctic continental interior. However, only limited areas within this region were found to demonstrate any local statistical significance (figure 7.41); only 1.6 % of polar pixels were found to be locally significant, while 6.4 % of pixels at non-polar latitudes were significant. The statistically significant pressure anomalies located outside of the polar regions were found in mid-latitude regions of cyclonic activity; this suggests that no direct relationship exists between the anomalies and the forced polar cloud changes.

A regionally-averaged plot of observed/modelled polar cloud and surface level pressure anomalies showed that, during the observed increase in the rate of polar cloud change, a non-significant protracted pressure decrease was occurring (figure 7.42). However, during the PCI experiment a more complex pattern of statistically significant increasing pressure occurs (centred around day -3), followed by a non-significant decrease in pressure (centred around day 0) (figure 7.42). This pattern bears no clear relationship to the observed changes, but it does broadly suggest that broadly the model shows a weak negative relationship between cloud and pressure over the polar regions. The implications of this pressure change in relation to the atmospheric changes occurring during the key date of the PCI experiment will be considered in section 7.5.5.

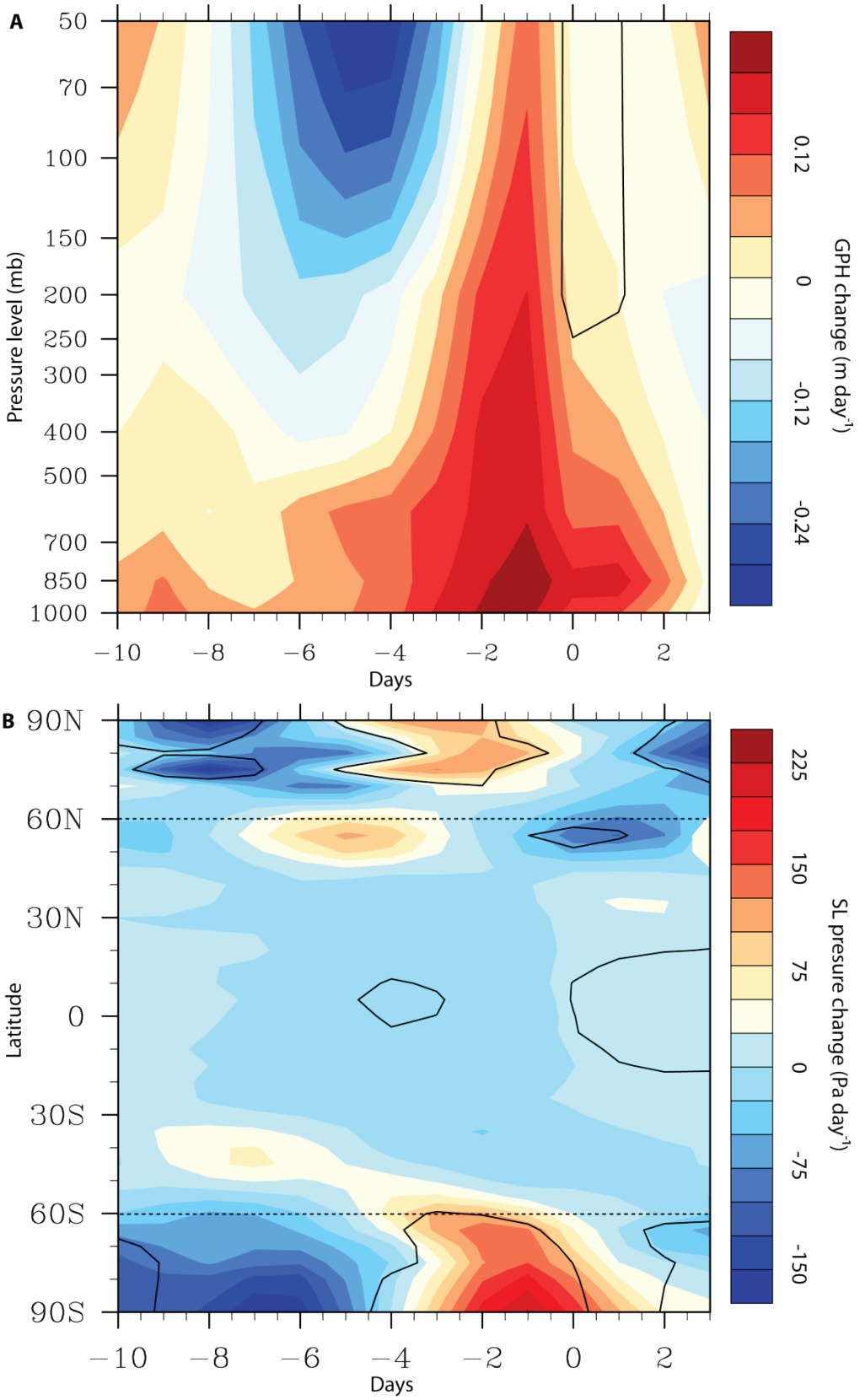

Figure 7.39 PCI experiment pressure anomalies

A) Globally-averaged GPH anomalies at various tropospheric levels, and **B)** surface level pressure anomalies occurring over the PCI composite. Horizontal dashed lines indicate limits of polar regions; solid contours mark regions of statistical significance.

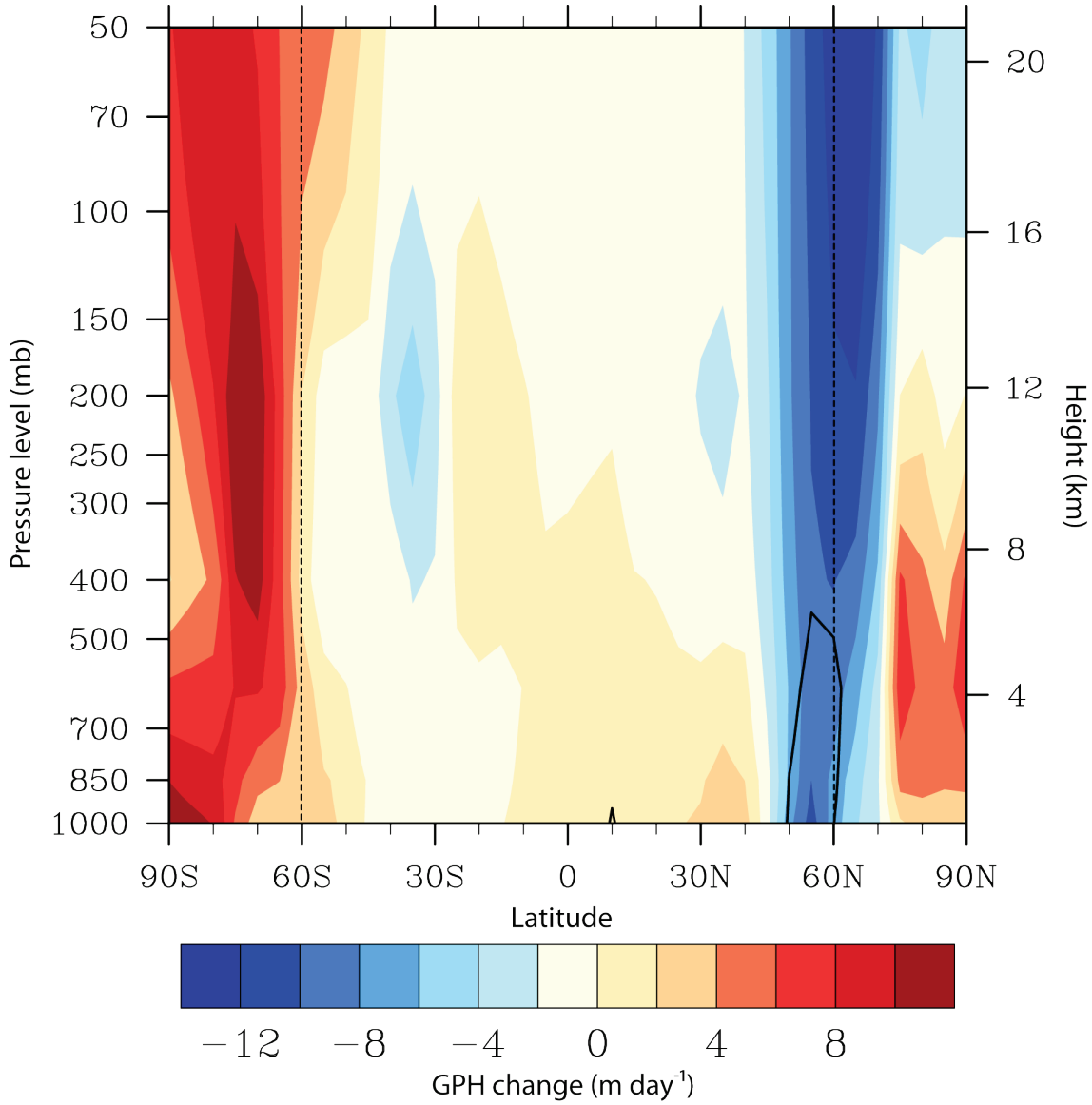

Figure 7.40 PCI experiment key date GPH anomalies

A vertical profile of GPH anomalies occurring on the key date of the PCI experiment. Vertical dashed lines indicate limits of polar regions. Solid contours show areas of statistically significant changes.

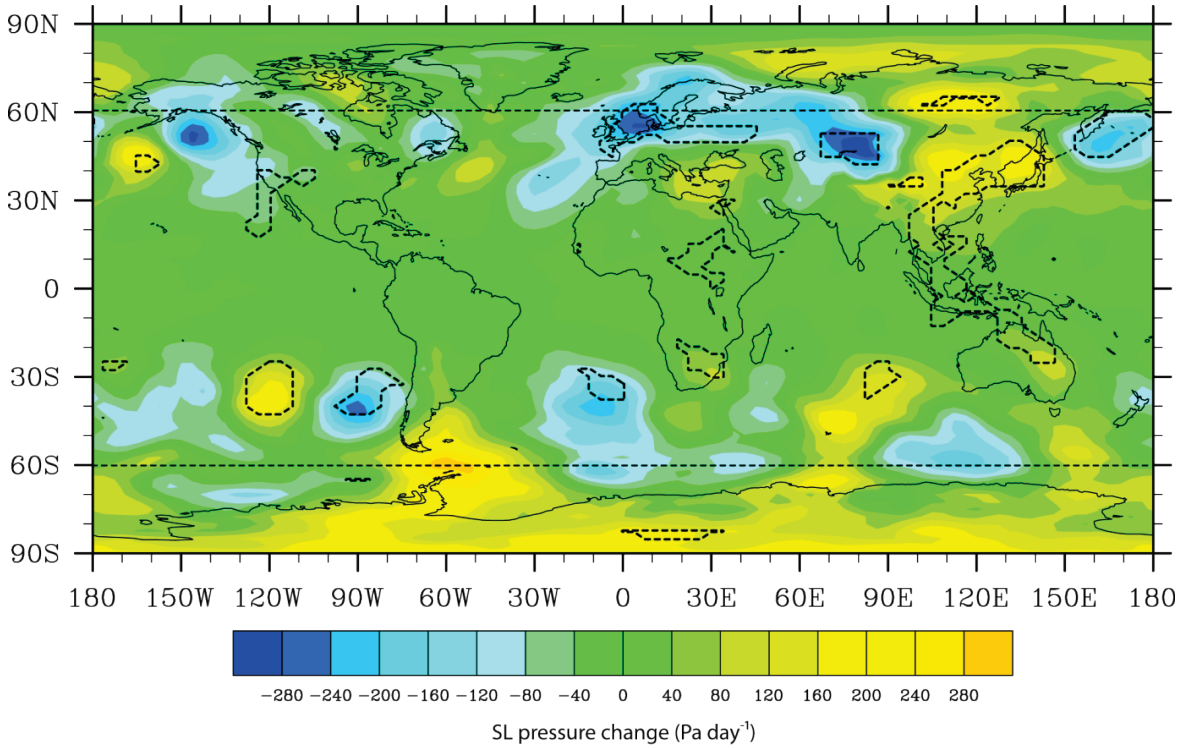

Figure 7.41 Key date PCI experiment pressure anomalies

Anomalous surface level pressure changes occurring on the key date of the PCI experiment. 6.4 % of pixels at non polar (60°N–60°S) latitudes demonstrate local significance, while 1.6 % of polar latitude pixels are locally significant. Of the locally significant polar pixels, 65.0/35.0 % are positive/negative; whereas at non-polar latitudes, 59.6/40.4 % are positive/negative.

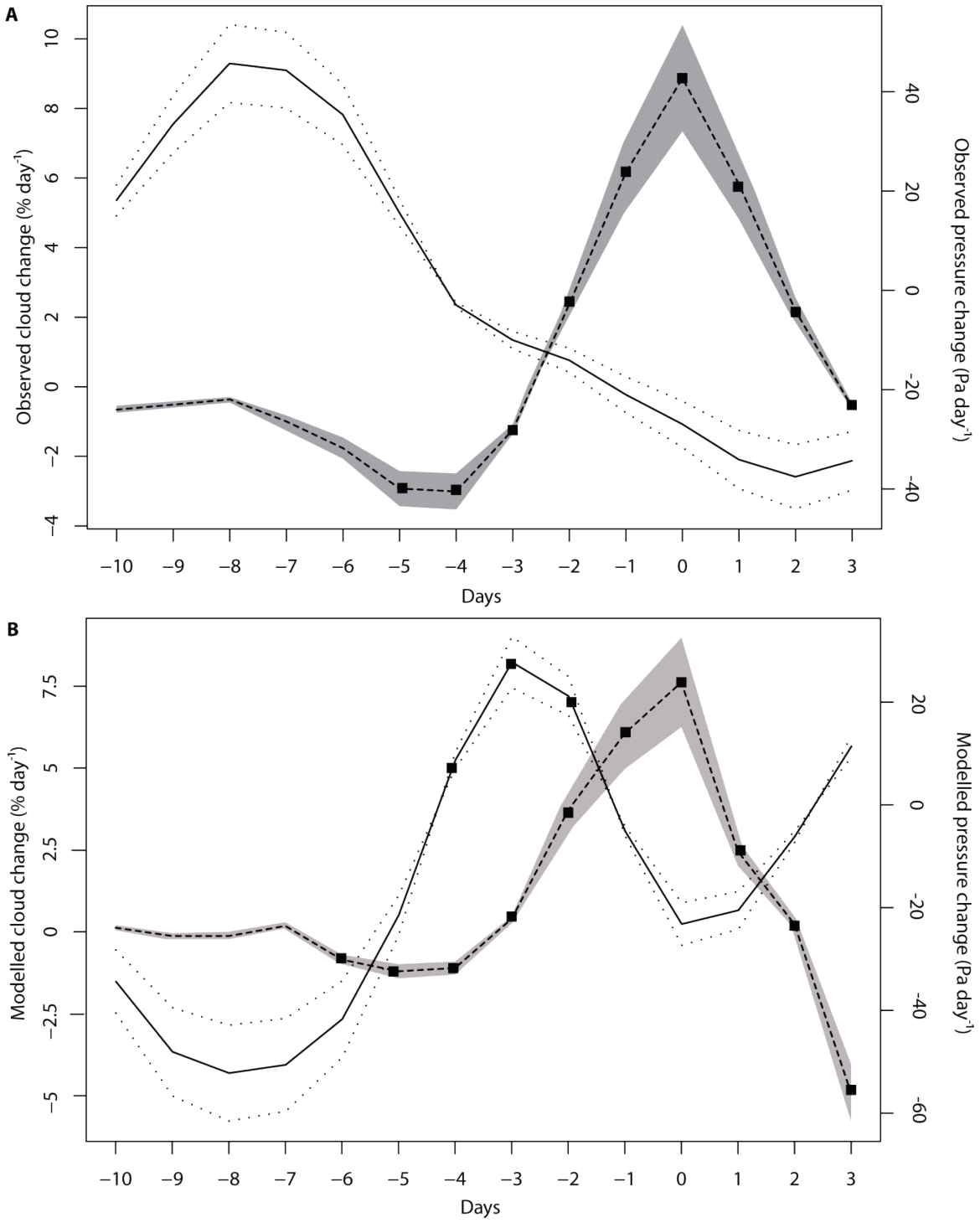

Figure 7.42 Observed and modelled pressure/cloud anomalies

Latitudinally-averaged cloud anomalies (dashed line) and surface level pressure anomalies (solid line) for both **A)** ISCCP and NCEP/NCAR observations, and **B)** the PCI experiment. Dotted lines/grey shading indicates the 0.95 level confidence interval for the mean pressure/cloud anomalies. Markers indicate statistically significant changes. Note differing vertical scales on panels.

7.5.4 PCI experiment: vertical velocity

Observations indicated that during the GI sample there were anomalous changes to the vertical velocity (omega) over polar regions (described in section 6.6). The detected omega anomalies will now be compared to their modelled counterparts from the PCI experiment.

A regionally-averaged (polar) vertical profile of omega anomalies occurring on the key date and its relative averaging period (days -5 to -3) showed that observations identified a negative anomaly of around -0.0002 Pa s^{-1} (i.e. a relative reduction in the descent of air) at upper tropospheric levels (100–200 mb) and a positive anomaly of approximately 0.0008 Pa s^{-1} (i.e. a relative increase in the descent air) over lower-tropospheric levels (400–1,000 mb) (figure 7.43A). It should be noted that these changes were not statistically significant. A comparable but inverse pattern of change was produced in the Arctic by the PCI experiment (figure 7.43B). The modelled omega anomalies were found to be larger than their observed counterparts and demonstrate statistical significance at tropospheric levels below 400 mb.

Over the Antarctic, a relative increase of approximately 0.0012 Pa s^{-1} in the descent of air at all tropospheric levels (relative to the averaging period) is observed. These anomalies are found to be statistically significant between 150 and 600 mb (figure 7.43C). Again, the modelled omega anomalies demonstrate an inverse sign relative to observed values, indicating that an anomalous (but non-significant) decrease of approximately 0.0016 Pa s^{-1} has occurred (figure 7.43D).

Broadly, similar results are found from an analysis of the anomalous changes occurring over the entire composite period (figure 7.44). Although generally there is a similar magnitude and timing of anomalies, with comparable features (such as the weakest changes being located at upper levels and a 1 to 2 day lag between mid- and low-level anomalies over the Antarctic), the modelled omega responses appear to be of inverse sign to observations. This implies either (1) that the model has failed to capture the cloud–climate interaction correctly, or (2) that the NCEP/NCAR reanalysis omega data are incorrect. Consequently, it is difficult to draw firm conclusions. An overview of the observed omega changes in the context of accompanying temperature and pressure changes may provide further clarity, as will a wider discussion of the PCI results.

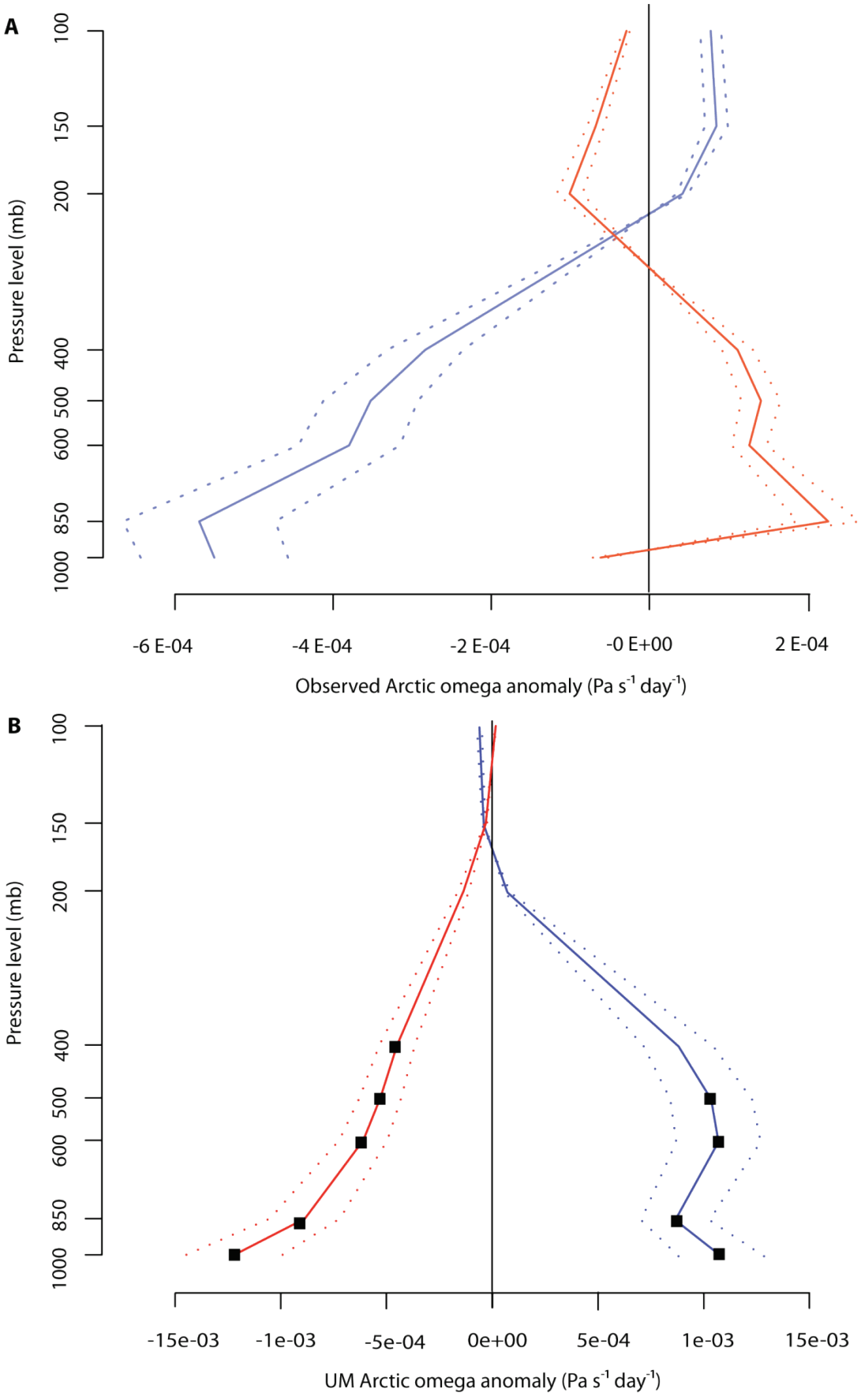

Figure continued overleaf

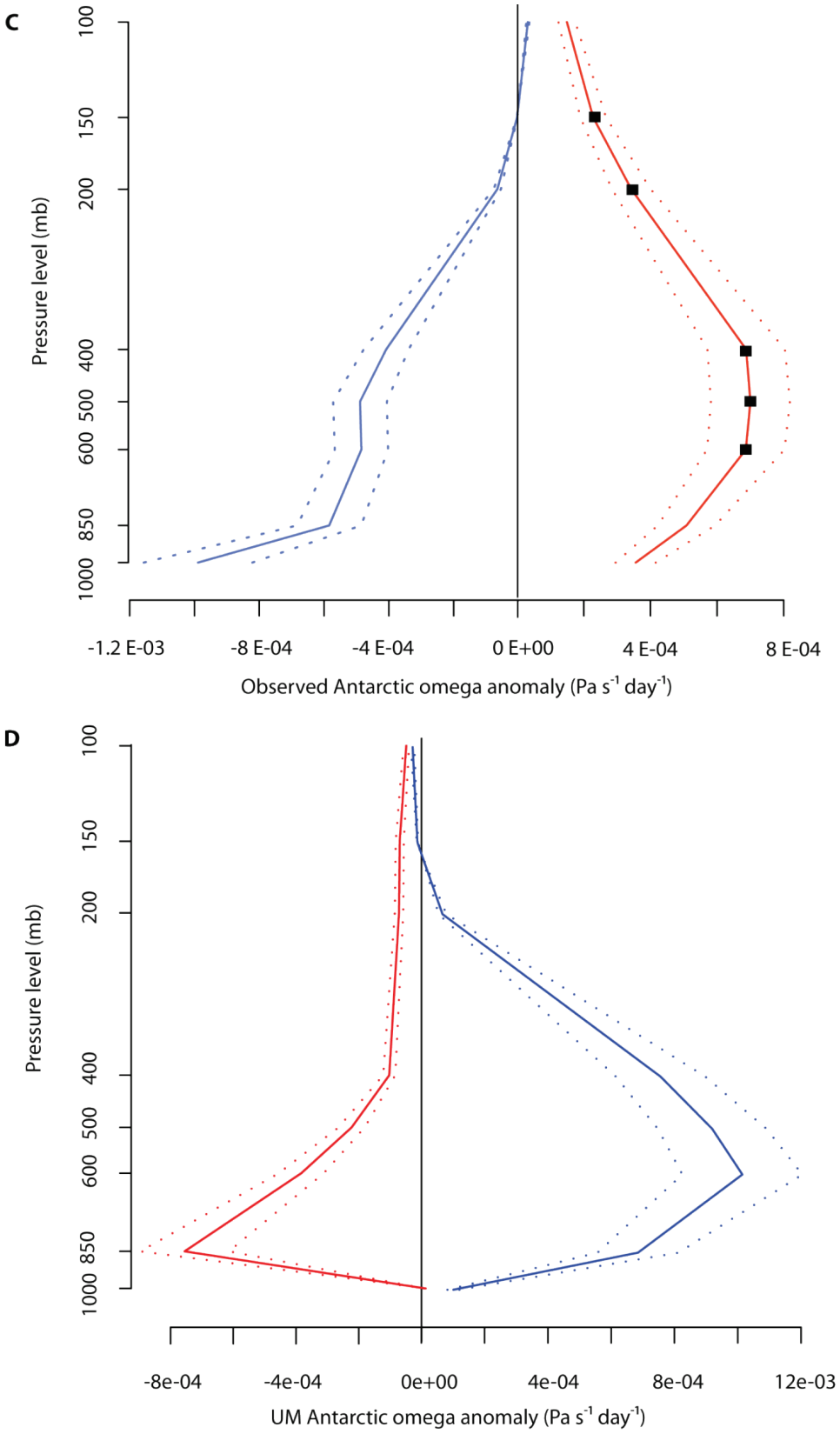

Figure 7.43 Modelled and observed vertical omega profile

Regionally-averaged polar (60°–90°N/S) omega anomaly, during the key date (red line) and relative averaging period (blue line) (day -5, -4 and -3), for GI sample observations and the PCI experiment. Negative/positive values indicate ascending/descending air motion. Note differing scales on vertical axis of panels.

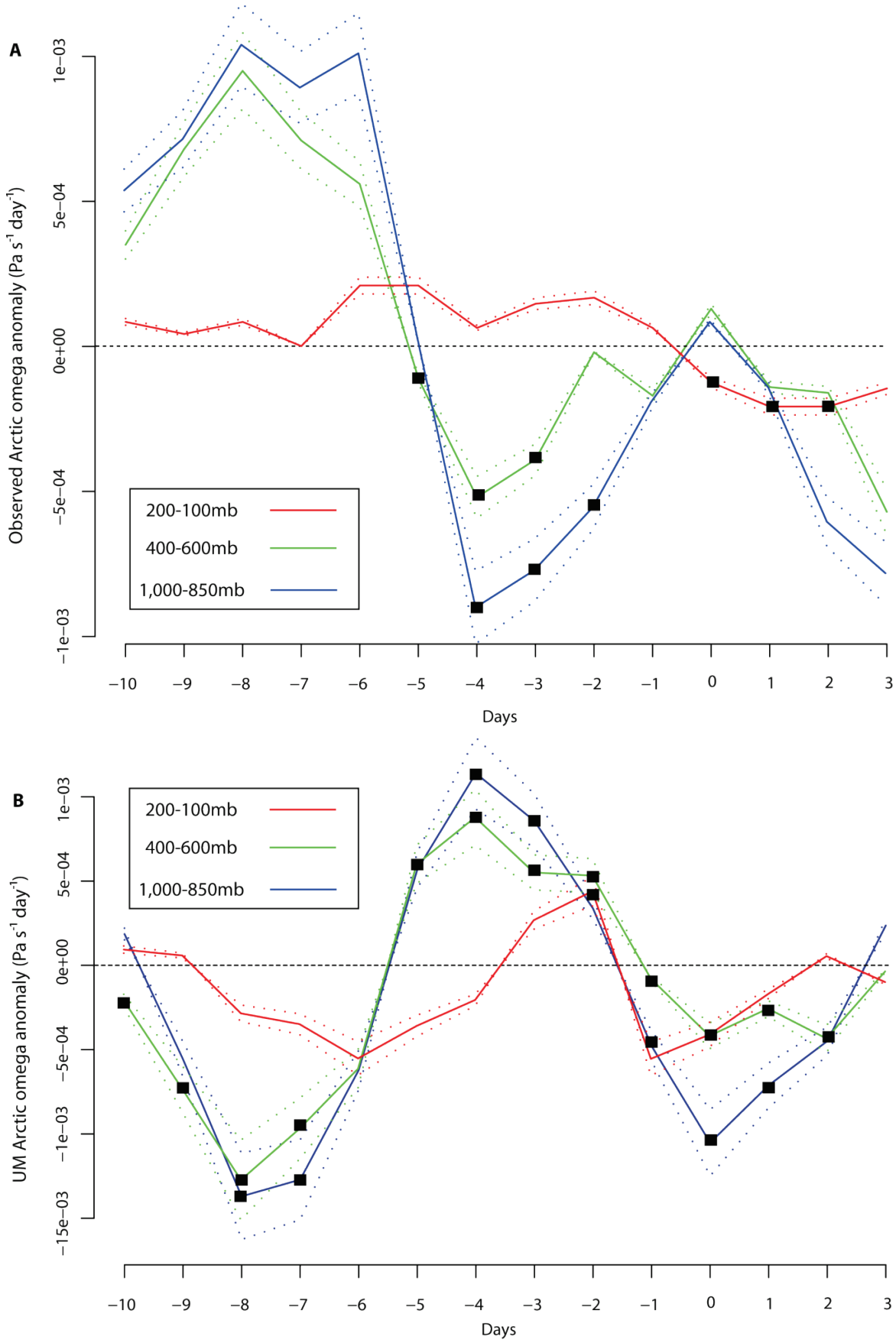

Figure continued overleaf

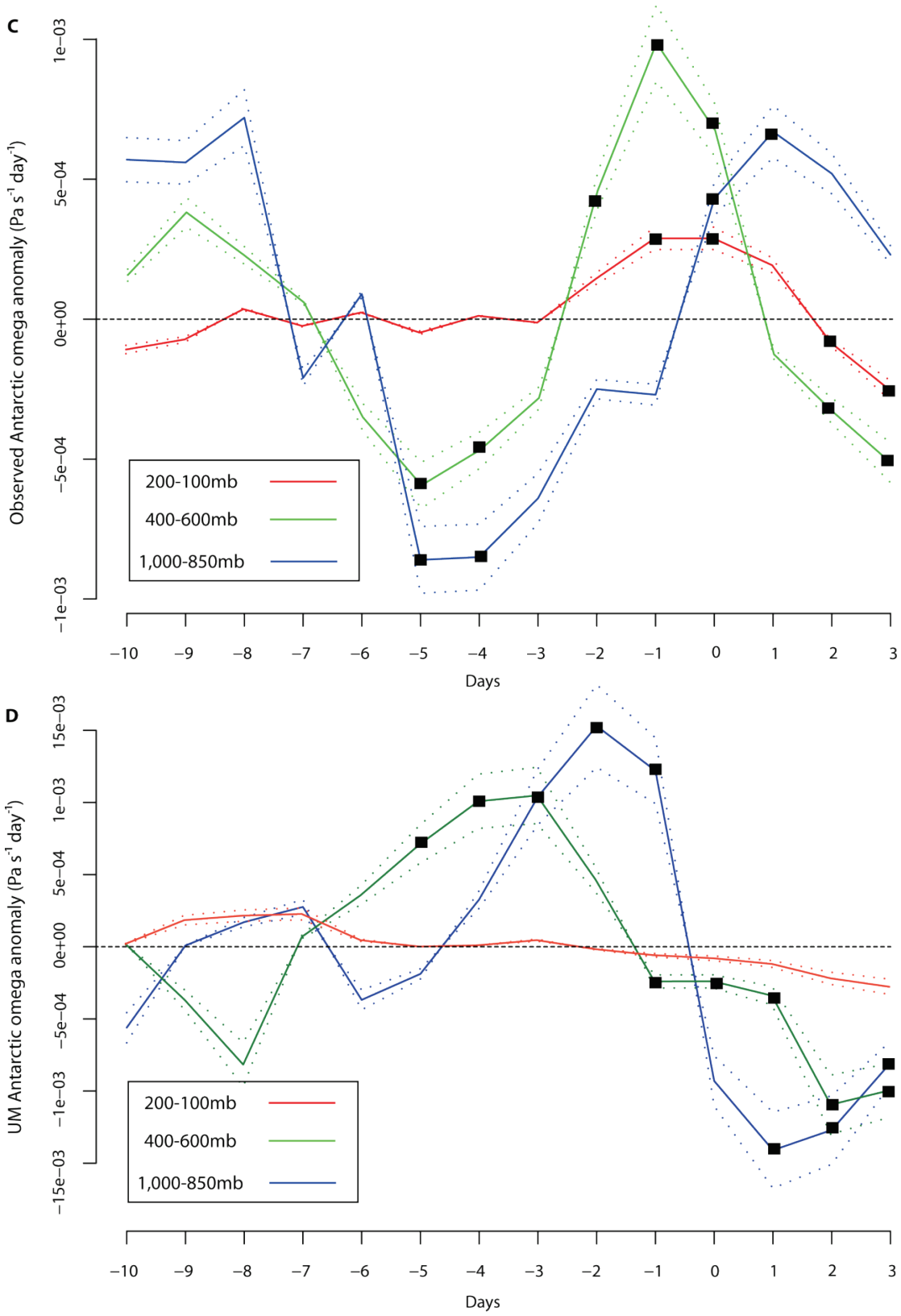

Figure 7.44 Observed and modelled omega anomaly during composite period

Omega anomaly occurring over the Arctic (90°N–60°N) and Antarctic (60°S–90°S) regions during the composite period at: upper (200–100 mb), mid (400–600 mb) and lower (600–1,000 mb) pressure levels. Negative/positive values indicate ascending/descending air motion. Note differing scales on vertical axis of panels.

7.5.5 PCI experiment: further discussion

Overall, while the PCI experiment reproduced the correct timing and magnitude of regional-scale polar cloud changes, the experiment was unable to correctly simulate the observed air temperature, pressure or omega responses detected during the GI internal sample (figure 7.45). Although the simulated relationship between air temperature and cloud was found to be significant (R^2=0.60), the relationship was of inverse sign to that observed. Additionally, the simulated pressure/omega variables were not found to demonstrate a statistically significant relationship to cloud anomalies (R^2=0.03/0.40 respectively).

Observations from chapter 6 unexpectedly indicated that anomalous polar cloud increases were accompanied by significant air temperature decreases; this observation is contrary to contemporary understanding of the impacts of clouds over ice covered surfaces (Stone and Khal, 1991). Consequently, it was hypothesised that this observation was therefore either (1) evidence of a previously unrecognised indirect cloud–climate forcing (described in section 6.3.7), or (2) an indication of a detection error. A successful simulation of a negative relationship between cloud and air temperature would have provided good evidence in support of the first scenario, however, since no such evidence was found it must therefore be concluded that either that the PCI experiment was not sophisticated enough to successfully reproduce the observations, or that the observation of a cloud increase is merely an artefact, possibly resulting from the temperature anomalies themselves. Cloud determinations are performed based on radiative properties, which is a problem over ice covered surfaces as it is difficult for satellites to distinguish between clouds and ice. Consequently, it is possible that changing temperature conditions may be erroneously interpreted as a change in cloud cover or snow cover by the satellites.

Although it is unclear which scenario is correct from these results, an overview of the climatic changes occurring during both the PCI experiment and GI sample may provide more insight. Figure 7.46 presents a summary chart of the cloud, temperature, pressure, and omega anomalies occurring on the key date over the polar regions. The GI sample shows a key date cloud increase accompanied by a relative temperature decrease, pressure decrease and increase in the descent of air (positive omega). Physically, these changes are irreconcilable to cloud increases. It is important to note that the temperature and pressure changes were independently confirmed by measurements from Dome C AWS station (presented in section 6.3.6). The PCI experiment indicates that an increase in polar cloud is accompanied by a rise in temperatures, a decrease in pressure and negative omega values (a relative ascending motion); this chain of events is physically plausible and directly relates to the known impacts of cloud cover increases over high latitude regions (Stone and Khal, 1991).

From this overview it is logical to suggest that the observed cloud (and possibly omega) anomalies may be in error. However, if this line of thinking is continued and the cloud changes are dismissed, then this simply raises the difficult question '*why do temperature changes correlate to changes in the rate of GCR flux?*' Although the cloud increase/temperature decrease scenario is currently inexplicable, it seems unlikely that the observed GCR–temperature connection could be explained without the presence of cloud changes to act as an intermediary, amplifying the effects of GCRs.

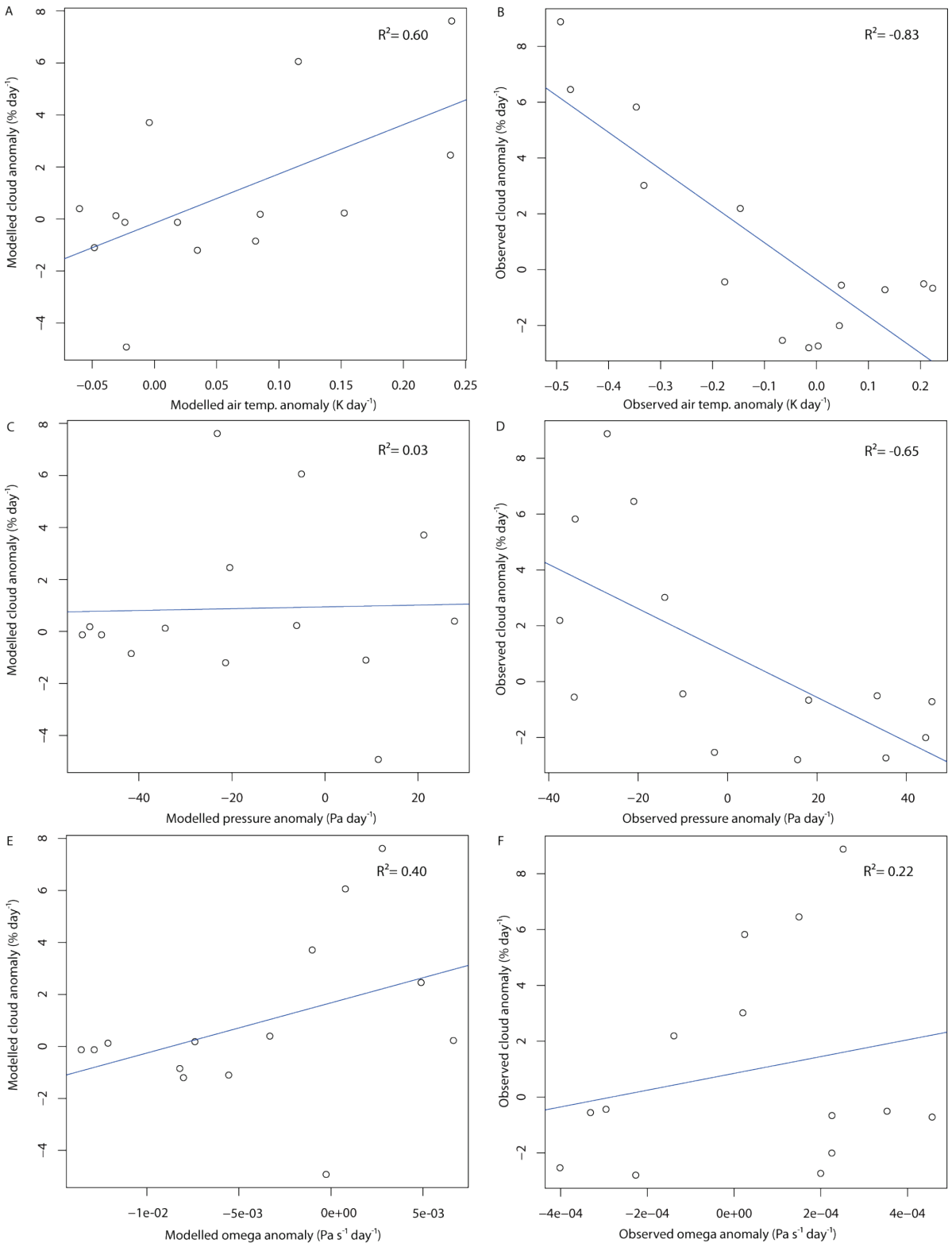

Figure 7.45 Modelled and observed relationships between cloud and climate

Scatter plots showing the relationship between anomalous cloud changes and air temperature, pressure and omega for both observations and models. Linear regression is shown (blue line), as are the correlation coefficients (R^2).

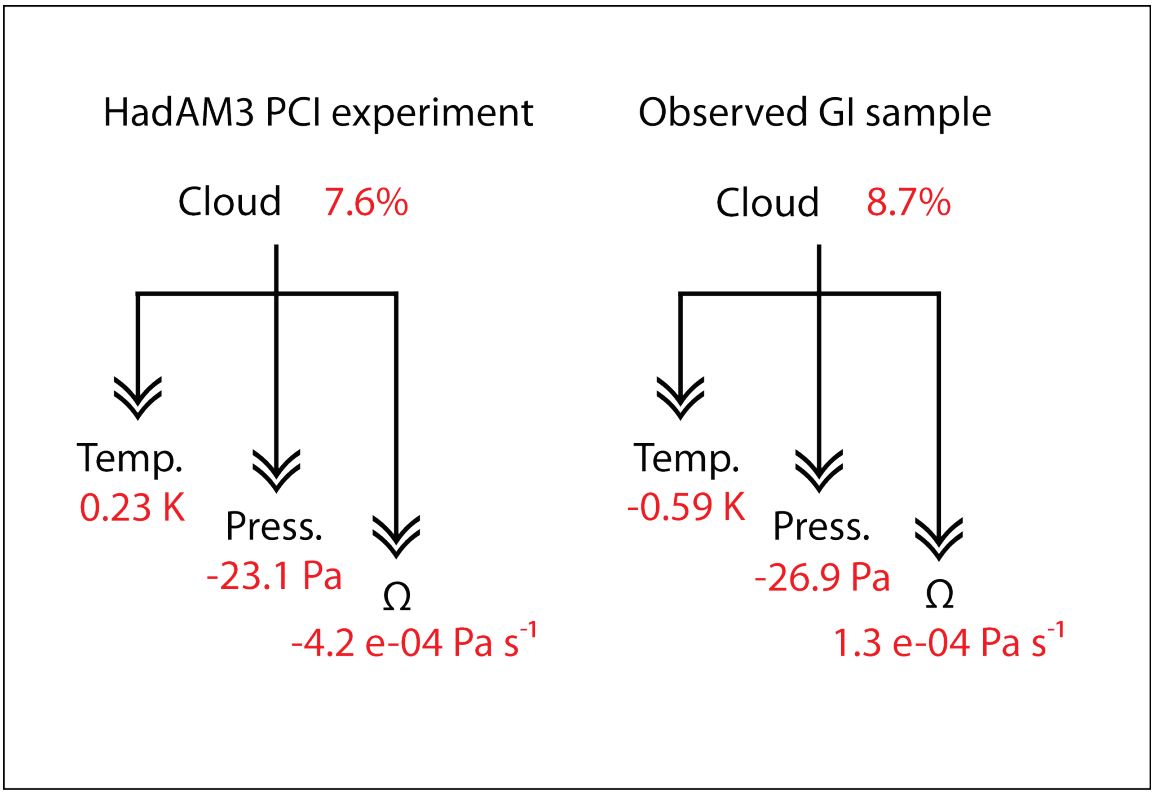

Figure 7.46 Summary chart of PCI experiment key date findings related to GI sample

Summary chart of PCI experiment key date atmospheric changes in relation to the GI internal sample key date changes. Average tropospheric cloud, surface level air temperature (temp.), surface level pressure (press.), and omega (Ω) (where omega values are calculated between 400–600 mb) are all shown. Values for each variable represent key date differential changes (i.e. difference between the key date and a 3-day averaging period beginning on day -5).

7.6 Discussion

7.6.1 Addressing objective 2B

Objective 2B: *Test if the relationship observed between clouds and climate can be reproduced in a GCM.*

Although observations have provided a statistically robust link between changes in the rate of GCR flux and cloud/atmospheric changes it is unclear if the cloud changes are producing the variations, or are merely a product of the atmospheric variations themselves. If the former is true, then it would provide a good indication of a causal link between cloud and climate, whereas if the latter is true, it would instead suggest that the detected cloud anomalies are the result of atmospheric variations; implying no direct link between observed GCR variations and

cloud anomalies. Alternatively, the possibility also exists that the cloud retrievals themselves may be in error.

The two experiments (MLCD and PCI) demonstrated differing results. The MLCD experiment appeared to correctly simulate the pattern of large scale (regionally-averaged) temperature/pressure changes associated with cloud anomalies. Although these temperature/pressure changes were not found to be statistically significant and were only approximately 25 % of observed magnitudes, they provided good indications that cloud anomalies may account for the atmospheric changes observed during the mid-latitude decrease sample (described in chapter 5–6). In contrast to the encouraging MLCD results, the PCI experiment did not produce atmospheric variations in agreement with observations. There are several possible explanations which may account for shortcomings of the MLCD/PCI experiments:

(1) Improper climate simulations within the model may result in differing responses between the model and reality.

(2) The GCM may have an inadequate spatial resolution to resolve cloud–climate relationships, as cloud processes operate at sub-grid scale levels and consequently cloud processes tend to be based around over simplifications and parameterisations that do not accurately capture the behaviour of clouds.

(3) The experiments may be hindered by an incorrect simulation of cloud anomalies at a local level. In other words, although the experiments successfully produced correct cloud anomalies at a regional level, they were generally found to be problematic at higher spatial resolutions. For example, MLCD cloud decreases were incorrectly distributed throughout mid-latitude regions.

(4) The cloud anomalies may bear no causal relationship to observed atmospheric anomalies; therefore their inclusion in the model may be physically unable to produce comparable atmospheric anomalies.

(5) Cloud–climate signals may be obscured/retarded by a high SNR. This is likely to affect both the MLCD and PCI experiments, and probably contributed to the relatively small temperature/pressure responses produced relative to observations (this problem is considered in greater detail in section 7.3.4).

(6) Cloud changes may be lacking from the model experiment as a result of only being able to reproduce relative cloud changes, but not changes in absolute cloud, or cloud longevity (see 7.3.4).

7.7 General summary

The rationale behind performing climate model experiments was to determine if the detected atmospheric anomalies demonstrated in earlier chapters could be causally linked to observed cloud anomalies. In summary, this chapter can be considered in two parts: the first described and evaluated the ability of the HadAM3 GCM to produce realistic cloud and climate simulations required for the experiments, while the second presented the results of two GCM experiments. Regarding the former, the selected GCM was able to broadly simulate synoptic cloud and climate patterns thought necessary to perform the experiments. However, the regional scale details were found to be poor; this limitation is ubiquitous across GCMs. Regarding the latter, the GCM experiments performed were designed to simulate the impacts of a mid-latitude cloud decrease and a polar cloud increase. Results indicated that the GCM was able to simulate the overall temperature and pressure changes associated with a mid-latitude cloud decrease, suggesting that cloud changes are indeed driving atmospheric variations over the sample via an alteration to the radiation balance at mid-latitudes. However, experimentation failed to reproduce the atmospheric anomalies detected with observed polar cloud increases; several reasons for this shortcoming were proposed and discussed.

Chapter 8 Discussion and concluding remarks

8.1 Introduction

This chapter will provide an overview and discussion to the key themes of this thesis. These will chiefly be concerned with addressing: (1) the overall findings of this work in relation to the primary aim of this thesis; (2) how the findings of this work relate to the existing body of literature; (3) the wider significance of the overall findings and conclusions of this work in the context of recent anomalous climate change; (4) the contributions this work has made to advance the field of study and; (5) limitations and potential for future improvements.

8.2 Meeting the overall aim

Aim: *To assess the existence and nature of a daily timescale relationship between the GCR flux and Earth's climate using a combination of remotely sensed atmospheric datasets and GCM experiments.*

Initially, attempts were made to identify a link between the GCR flux and the atmosphere by re-analysing the methods and results of past studies. This involved the composite analysis of satellite-detected cloud cover changes based around daily timescale FD events (primarily those of Todd and Kniveton [2001; 2004], Kristjánsson et al. [2008] and Svensmark et al. [2009]). This approach was one of two methods widely adopted in the literature to test the validity of a GCR–cloud relationship, the other being that of long-term correlation studies (e.g. Svensmark and Friss-Christensen [1997]); this alternative method was ignored due to the numerous limitations associated with it (discussed in section 2.4.5). The re-analysis of FD-based studies did not provide any new or compelling evidence confirming or denying the existence of a GCR–climate relationship (see figure 8.1 for a summary of these findings). Overall, the examination of FD events suggested that there may be anomalous high level cloud decreases occurring over the Antarctic preceding large GCR decreases. However, it seems that these cloud changes may ultimately be more closely related either to irradiance variations or to internal atmospheric variations observed during the composite sample, rather than to changes in the GCR flux.

The lack of a statistically significant GCR–atmosphere relationship present in the FD-based samples prompted the development of a novel sampling procedure (termed internal sampling).

This approach was based on the assumption that if GCR changes are causally related to cloud changes, then GCR-related cloud changes should be distinguishable from background (non-GCR enhanced) cloud variability by the rapidity of the cloud changes. Theoretically, this may be explained by the estimated higher efficiency of electrically-enhanced cloud processes relative to neutral cloud processes (Yu and Turco, 2000; 2001; Tinsley and Yu, 2004).

Several composite samples were constructed using the internal sampling method, which represented the most rapid (top 5%) ISCCP observed cloud changes over a range of different areas during both increases and decreases in the rate of cloud change. Several samples showed that a statistically significant change in the rate of GCR flux occurred during the key dates of these samples (see summary figures 8.2 for an example of the GCR–cloud relationship detected during the GI sample). These changes were distinguishable from variations in solar irradiance and the IMF. When considered together, these samples provided support for notions of a GCR–cloud link operating over daily timescales.

To triangulate and verify the detected GCR–cloud signal, NCEP/NCAR reanalysis datasets were used. These provided atmospheric (air temperature, pressure, wind, precipitation and vertical velocity) data for the internal samples. This analysis revealed that, during increases in global and Antarctic cloud cover, a range of unexpected atmospheric responses were occurring: on the key date, statistically significant cloud increases were accompanied by temperature decreases, pressure decreases and increases in vertical velocity over high latitude regions (see figure 8.3 for a summary of locally significant atmospheric anomalies detected during the GI sample). These changes cannot be accounted for by a conventional understanding of cloud–climate interactions and experiments attempting to simulate these anomalies within a GCM were not successful. This suggests that the cloud–climate relationship observed was either evidence of (1) erroneous satellite/reanalysis changes, or (2) a previously un-described cloud–climate relationship over polar regions. The ambiguity associated with these samples leads to the conclusion that these findings do not currently provide strong evidence of a GCR–climate link over polar regions, although they may highlight an important area upon which to focus future research efforts.

In addition to the GCR–atmospheric anomalies detected over the poles (in the GI/AI internal samples), a statistically significant co-temporal relationship between the rate of GCR flux and cloud anomalies was also identified over mid-latitude regions (figure 8.4). This sample showed associated temperature and pressure responses which suggested a relationship to changes in the radiative balance over mid-latitude regions by clouds (figure 8.5); these findings were verified in a GCM experiment (figure 8.6); indicating that the atmospheric variations observed over the sample period may potentially be casually attributed to changes in cloud cover. This result

provided good evidence of a relationship between GCR, cloud cover and atmospheric responses operating over daily timescales over mid-latitude regions, successfully fulfilling the overall aim of this thesis.

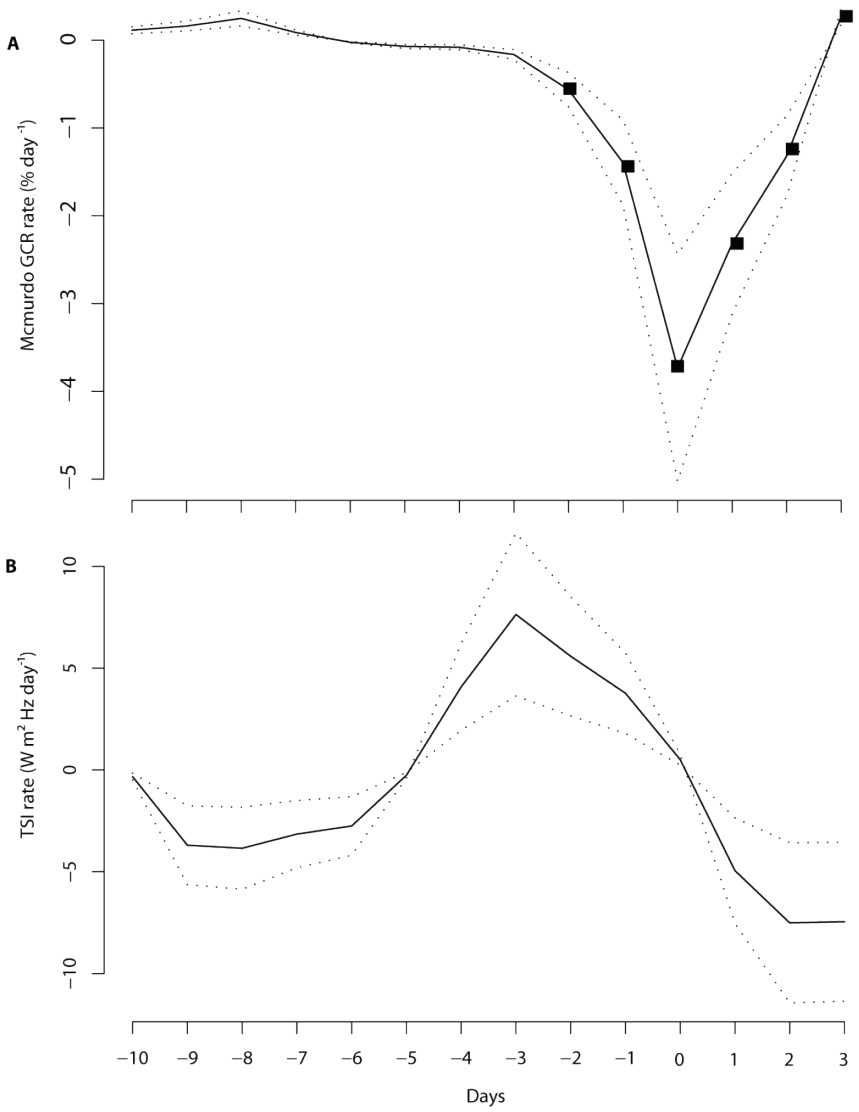

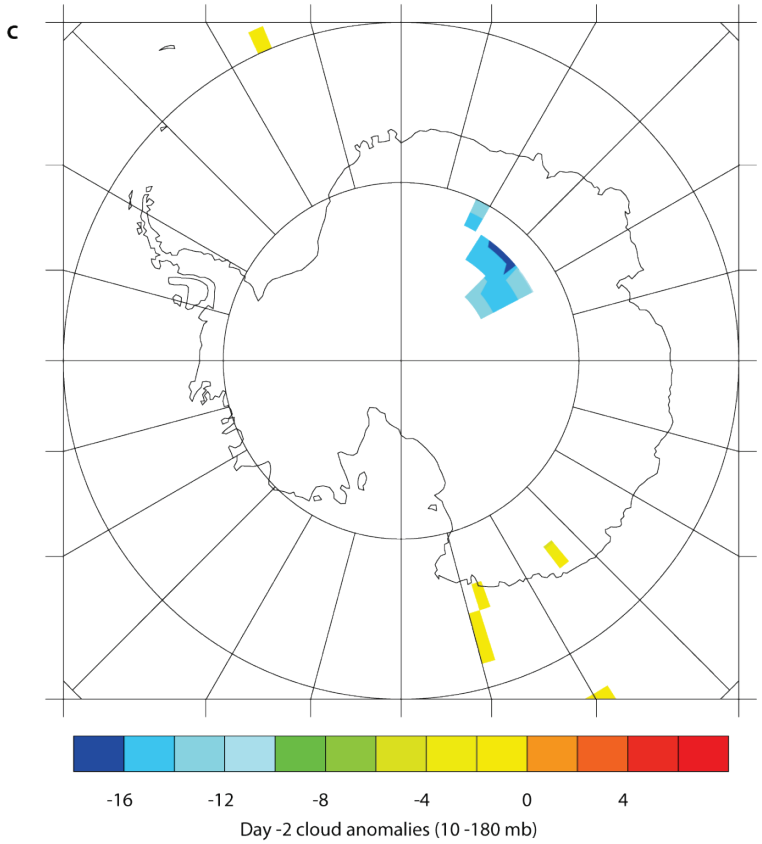

Figure 8.1 FD analysis summary

A summary of **A**) the rate of GCR flux (measured from pressure adjusted Mcmurdo neutron monitor), and **B**) rate of F10.7 change occurring during the adjusted FD sample (discussed in section 4.3.2). Statistically significant anomalies are indicated on line graphs by markers; the dotted lines show the 0.95 level confidence interval. Also shown are the anomalous locally significant cloud changes detected on day -2 of the composite (occurring between 10 and 180 mb).

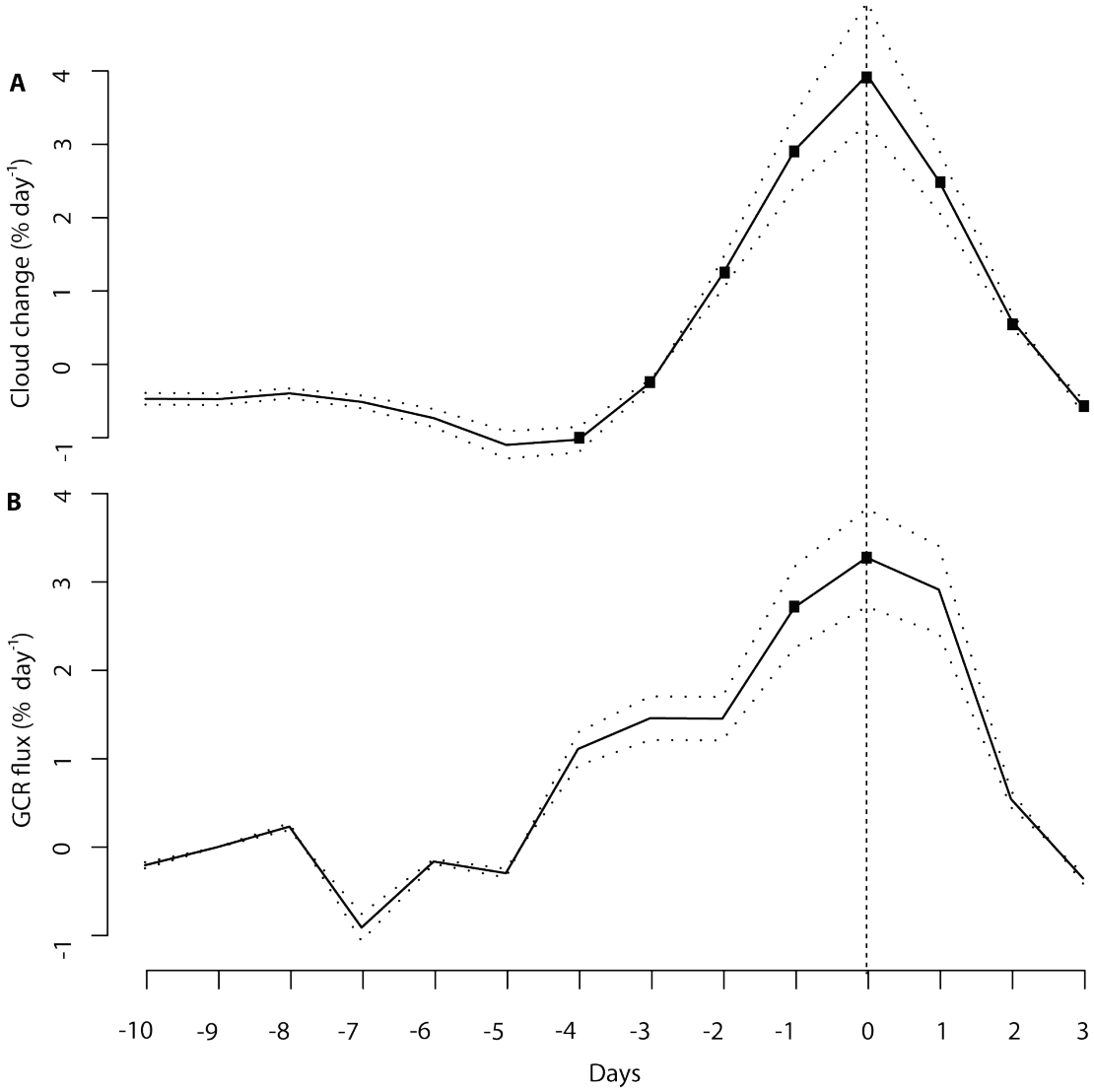

Figure 8.2 GI sample cloud and GCR variations

Changes in the rate of **A**) cloud change (10–1,000 mb) and **B**) GCR flux (changes normalised against peak-to-peak variations experienced over an 11-year solar cycle). Markers indicate statistically significant variations; dotted lines show the 0.95 level confidence intervals. Vertical dashed line indicates key date of cloud change during GI sample.

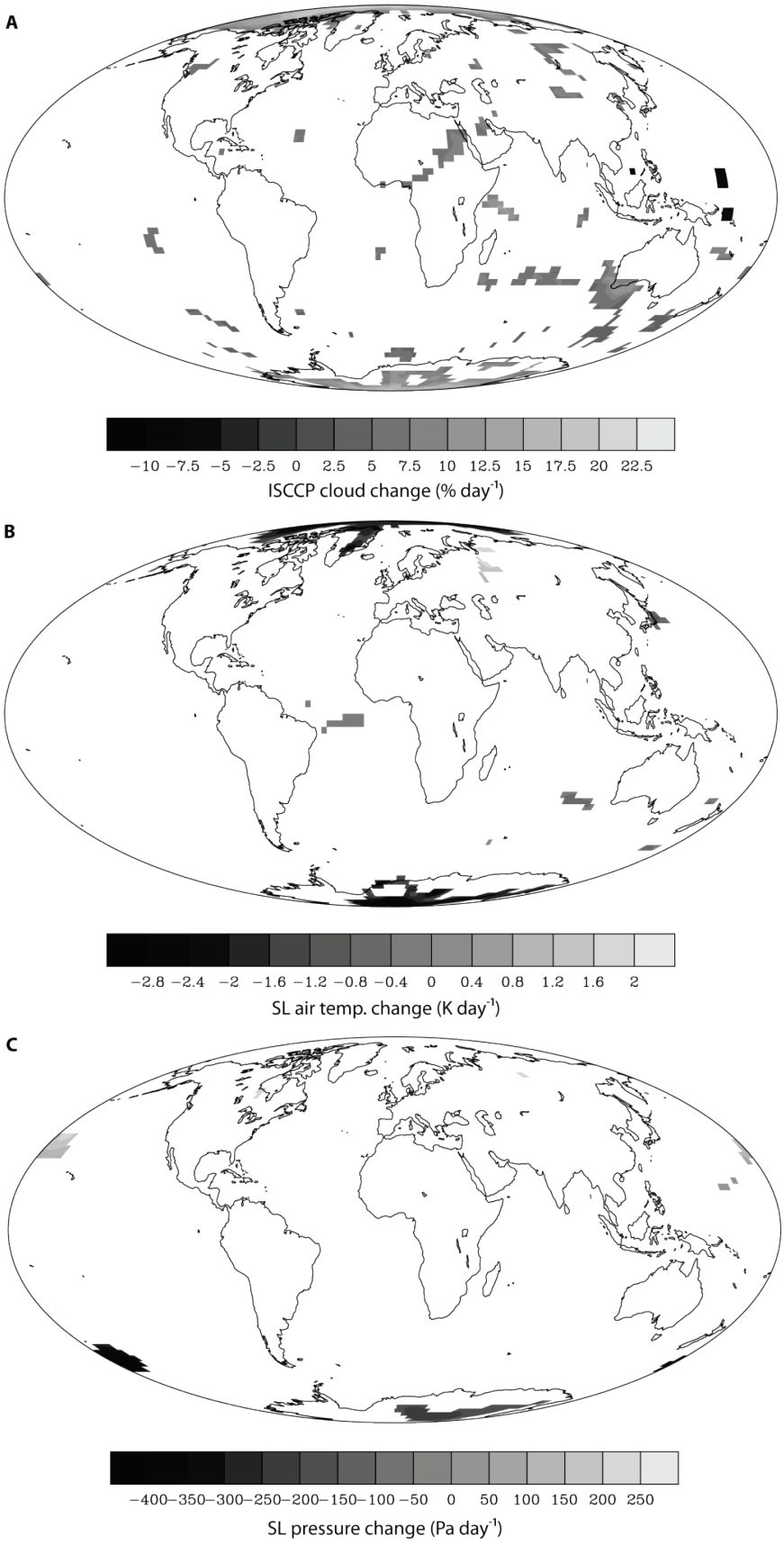

Figure 8.3 Summary of locally significant atmospheric anomalies

Locally significant atmospheric anomalies occurring on the key date of the GI sample.

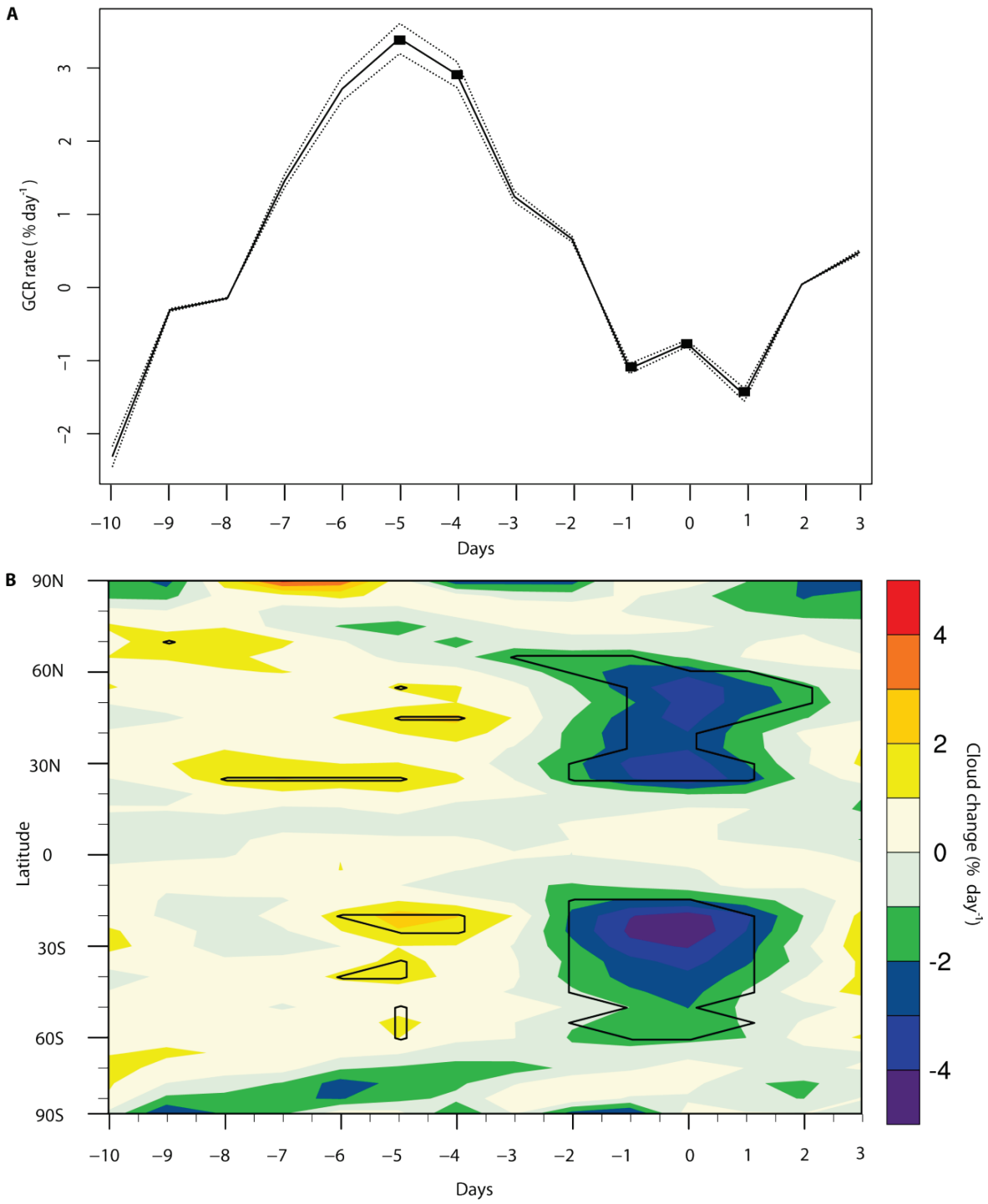

Figure 8.4 MLD sample GCR and cloud changes

Summary of MLD sample rate of **A**) GCR change (normalised against the peak-to-peak variations experienced over an 11-year solar cycle) (statistically significant changes are indicated by markers, dotted lines show the 0.95 level confidence interval), and **B**) 5° latitudinally-averaged cloud changes (10–1,000 mb) occurring over the composite period. Solid lines indicate areas of statistically significant cloud anomalies.

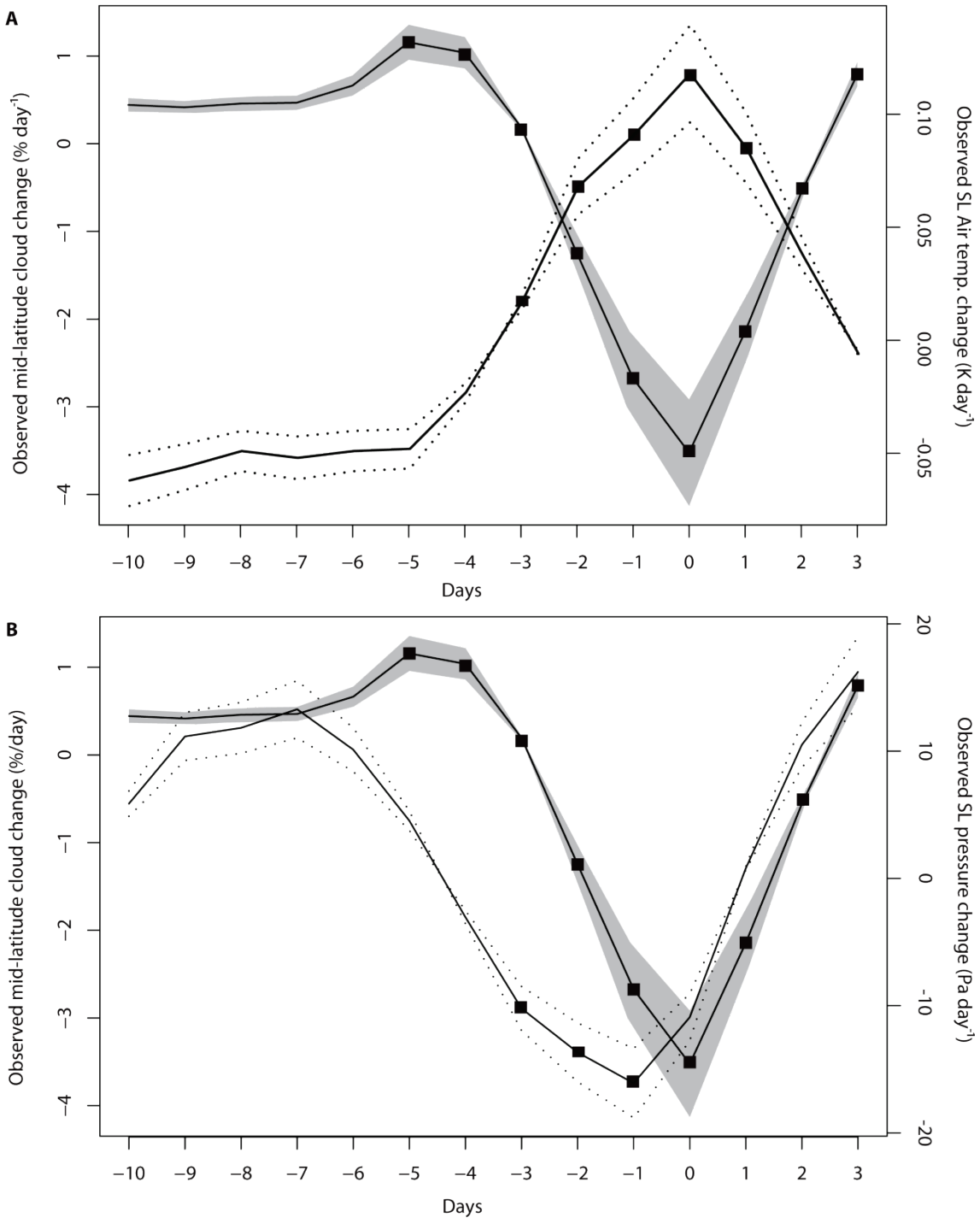

Figure 8.5 Atmospheric changes observed during MLD composite

Summary of cloud (10–1,000 mb), surface level air temperature and surface level pressure changes observed during the MLD composite period. Markers indicate days of statistically significant changes; dotted lines show the 0.95 level confidence interval.

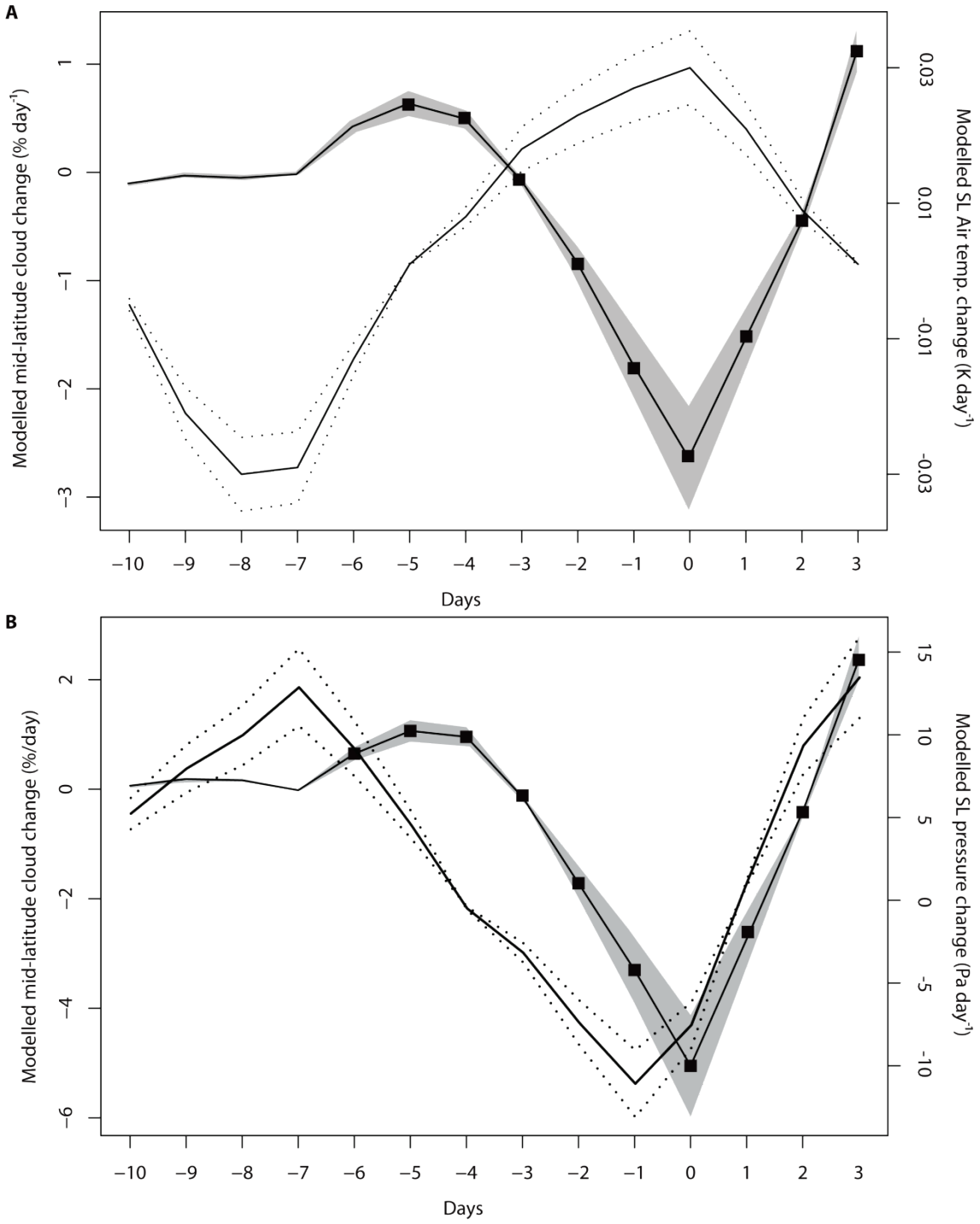

Figure 8.6 Modelled atmospheric changes

Summary of forced cloud changes and resulting modelled surface level air temperature and pressure changes during the MLCD experiment (presented in chapter 7).

8.3 How this work relates to existing studies

8.3.1 FD-based findings

In relation to the findings of past FD-based studies, two distinct lines of research were carried out. The first investigated the claims of Svensmark et al. (2009), who suggested that a significant global cloud change was observed in several datasets (including MODIS and ISCCP) that was causally related to GCR changes during five FD events with a time lag of approximately 6 days. A detailed re-analysis of the MODIS and ISCCP changes occurring during these FD events (performed in section 4.2) found no evidence in support of the claims of SBS (a synthesis of the primary findings and arguments on this topic with regard to MODIS has been given in Laken et al. [2010]). A similar conclusion regarding the findings of SBS was also reached by Calogovich et al. (2010); these researchers used a detailed correlation analysis which examined the relationship between cloud cover changes and modelled atmospheric ionisation changes at 3 hour intervals with a lag time between 0 and 10 days. They concluded that no statistically significant correlation between cloud changes and atmospheric ionisation was found over the events of SBS at any time lag. These findings complement the arguments made in this work that the cloud changes demonstrated by SBS (1) do not show evidence of a response to changes in the GCR flux, and (2) are suggested to operate over mechanistically unfeasible time scales.

The second line of investigation pursued with regards to FD samples relates to the creation of an *adjusted* FD composite. A summary of the results found during this composite is shown in figure 9.1. This sample was based upon the events selected by TK04 and Kristjánsson et al. (2008). The adjusted FD composite was based on a methodological approach adapted from Troshichev et al. (2008), whereby FD onset dates were realigned to reflect the maximal GCR decrease associated with the FD event (as opposed to the FD onset date); this approach allowed the sample to focus on a highly isolated GCR decrease signal (shown in figure 8.1A). However, unlike the study by Troshichev et al. (2008), who used only ground-based visual assessments of cloud changes, satellite retrieved cloud datasets are used in this work. Troshichev and co-workers suggested that, following their sample adjustment, they observed changes in the IMF to be more related to variations in cloud cover than the GCR flux; however, the adjusted FD composite showed no indications of this.

Kristjánsson et al. (2008) found no strong indications of any statistically significant cloud changes over pristine, southern hemisphere, oceanic environments with MODIS data using a composite of FD onset events. Kristjánsson and co-workers chose to focus on such regions, as it has been suggested that these locations may be most likely to provide a clear GCR–cloud signal due to their relatively high sensitivity to changes in tropospheric aerosol concentrations

(Carslaw et al., 20020). The adjusted FD composite showed virtually no statistically significant cloud changes at any location; this finding confirms the results of Kristjánsson et al. (2008). However, the adjusted FD sample did suggest that a cloud change may be occurring over one area: the Antarctic plateau, at high pressure levels (10–180mb) (figure 8.1C). A similar result was also obtained by Todd and Kniveton (2001; 2004). It is important to note that during the adjusted FD composite, the region highlighted as statistically significant represents less than 0.4 % of the total number of ISCCP pixels (counted on days where statistically significant changes in the rate of GCR flux are observed) and, furthermore, that these pixels are located in a region of the atmosphere where cloud detections are known to be highly problematic (Rossow and Schiffer, 1999).

It was suggested that FD events themselves may not isolate variations in the GCR flux from changes in solar irradiance; indications of this were given by Woods et al. (2004). These authors presented the first evidence of variations in solar irradiance during a solar flare event occurring during the unusually intense solar storms, which took place between 28/10/2003 and 04/11/2003 (a period which has since become known as the 'Halloween Storms'). In chapter 4, the results of a detailed statistical analysis of F10.7 variations during 269 FD events was given. These results showed a strong indication that irradiance variations precede GCR decreases during FD events and that this effect was, to an extent, dependent on the magnitude of the individual FD events; these conclusions complement the findings of Woods et al. (2004). The detection of a comparable increase in F10.7 during the adjusted FD sample suggests that irradiance changes may be of relevance to this sample (figure 9.1B).

8.3.2 Internal sampling approach

Although the internal sampling methodology used in chapters 5 and 6 was a novel approach and consequently had no pre-existing counterparts from which a comparative discussion could be based, the samples identified several key features (stated below in italics) which can be evaluated in relation to the existing literature:

A positive co-temporal relationship between GCR and cloud changes. Throughout this work statistically significant GCR changes were found to develop co-temporally with positively related cloud changes. This result is similarly found by studies which have reported theoretical, experimental or observational evidence in favour of a GCR–cloud link (Svensmark and Friis-Christensen, 1997; Marsh and Svensmark, 2000; Kniveton, 2004; Pallé et al., 2004; Harrison

and Stephenson, 2006; Svensmark et al., 2007; Harrison and Ambaum, 2009). Although there is an instance where a negative relationship between the GCR flux and cloud cover changes has been reported (Wang et al., 2006), generally, studies which demonstrate evidence of a significant relationship between the GCR flux and cloud cover suggest a positive relationship.

The samples show an atmospheric response detected across several parameters. Although some studies have shown evidence of localised temperature or pressure variations (e.g. Pudovkin et al., 1996; Egrova et al., 2000), such findings have generally been conspicuous for their lack of evidence of accompanying cloud changes. Most GCR studies have usually presented evidence only of cloud changes rather than atmospheric changes (see references in previous paragraph). In contrast, the internal samples identified in this work clearly demonstrated a statistically significant response in temperature, pressure cloud changes and other atmospheric parameters (figure 8.3 and 8.5). Although several studies have demonstrated changes detected in a single parameter (usually cloud), this work provides evidence of a statistically significant signal present across a range of complementary datasets. A similar approach was taken by Todd and Kniveton (2004), who compared ISCCP detected cloud changes to NCEP/NCAR reanalysis data for surface level air temperature anomalies over the Antarctic region. The use of multiple atmospheric datasets in this work has enabled both signal verification and triangulation and also provided further insights in to the nature of a link between GCR and the atmosphere. Furthermore, it has allowed a GCM model experiment to be performed to validate the hypothesis that cloud changes are likely responsible for producing the observed temperature/pressure variations during the MLD sample (figure 8.6).

No time lag between GCR changes and internal samples atmospheric response. The results of studies involving the effects of GCR on the atmosphere have suggested a wide range of response times, ranging between 6 hours and several days (Pudovkin et al., 1997; Egrova et al., 2000; Kazil et al., 2008; Mironova et al., 2008). In some instances the time lags have been so great (up to 7 days) as to draw criticisms for being physically unconnected to GCR variations (Svensmark et al., 2009; Calogovich et al., 2010). While it is feasible that a response time of around three days exists as a result of aerosol growth times to CCN sizes (Arnold, 2006, 2008), rapid responses on the timescale of minutes have also been observed with changes in the vertical electric field (Harrison and Ambaum, 2009). The absence of a time lag between GCR variations and atmospheric changes observed during the internal samples implies that the mechanism involved does not relate to the growth of CCN over multi-day timescales.

Regional sensitivity to GCR–cloud effects. The internal samples appear to have isolated cloud anomalies with two very distinct characteristics:

(1) The MLD internal sample identified cloud changes at mid- to low tropospheric levels (around 500–1,000 mb) and mid-latitude regions as being sensitive to decreases in the GCR flux. It is possible that these changes are causally related to variations in the GCR flux via IMN processes. The rationale behind this suggestion is that it is understood that variations in atmospheric ion concentrations resulting from changes in the GCR flux are unlikely to produce a spatially uniform cloud response due to differences in their relative abundances. At low latitudes and low tropospheric levels, therefore, the ionisation rate is predicted to be a limiting factor on the formation of new aerosol particles (as there is an abundance of precursor gases from which to form new aerosols, but limited ionisation to facilitate production). At high altitudes and high latitudes however, ion production is far greater and consequently, variations in the GCR flux are predicted to be less likely to constrain aerosol production (instead aerosol production over such regions is limited by the lack of sufficient concentrations of precursor gases from which aerosols may form) (Carslaw et al., 2002; Yu, 2002).

In fact, GCR–cloud studies have suggested that cloud changes may be occurring mostly at low latitudes and low altitudes (Marsh and Svensmark, 2000; Pallé et al., 2004a). In addition to IMN theory and global scale observations, which suggest a GCR–cloud response in low-level/low latitude cloud systems, there has also been some interesting progress in understanding how these changes may function with regards to cloud systems at a local-scale. Rosenfeld et al. (2006) have described the response of marine boundary layer cloud changes to changing CCN concentrations over regions where cloud states transition between a closed cellular convection (total cloud cover), to a CCN-depleted state of open cellular convection (partial cloud cover), to a CCN-starved state of almost no cloud cover. Rosenfeld and co-workers suggest that these cloud systems are sensitive to small changes in aerosol concentrations which may potentially result from GCR-related mechanisms and may influence the transitions between these three cloud states, resulting in large impacts to cloud cover over sensitive (aerosol starved) environments where RB convection governs cloud formation (Rosenfeld et al., 2006).

The MLD sample demonstrated no observable lag time (same day response) between cloud and GCR variations; consequently if GCR is causally related to the observed cloud anomalies, it may be via a rapid (same day) IMN response. Alternatively, a GEC-related mechanism may be responsible: during decreases in the GCR flux, atmospheric ionisation decreases, these changes conform to Earth's horizontal geomagnetic shield strength and consequently atmospheric ionisation decreases are highest at polar latitudes and decrease towards the equator. It has been demonstrated that during decreases in atmospheric conductivity associated with FD events, J_z is diverted away from higher latitude regions towards lower latitudes (Roble and Hays, 1979). Consequently, during GCR decreases, J_z increases at mid- to low latitude regions. It is unclear what influence such changes may have on mid-latitude cloud cover, as the exact effects of such

changes on clouds likely depend on several factors including: cloud microphysics, the dominance of cold cloud/warm cloud processes, cloud type and the state of the thunderstorm generators (Sapkota and Varshneya, 1990; Tinsley and Yu, 2004; Zhou et al., 2009).

(2) The GI/AI samples identified intense cloud anomalies over high latitudes at mid- to high pressure levels. This pattern of cloud change may imply the action of a process that is connected to changes in atmospheric ionisation resulting from GCR variations. This mechanism may possibly operate via GEC pathways: increases in atmospheric conductivity may influence the build of space charge at the boundaries of stratified clouds, potentially resulting in the enhanced scavenging of aerosols by electroscavenging processes. This may alter cloud properties such as cloud droplet concentration, cloud reflectivity and longevity (this mechanism is discussed in detail in section 2.4.2). Evidence of statistically significant cloud changes (of around 13–15 %) detected in the ISCCP D1 dataset have been reported over high latitude regions following extreme increases and decreases in the vertical electric field measured at Vostok, Antarctica (Kniveton et al., 2007). These results give good indications that changes in current flow in the GEC may influence cloud cover over high latitude regions, providing support for a GEC-related explanation for the anomalies observed over the GI/AI samples.

Although only the GI, AI and MLD samples were investigated extensively 10 composite samples were created in total. These composites were based around the largest increases and decreases in the rate of cloud change over a range of area-averaged regions: global (90°N–90°S equal-area-adjusted), tropical (30°N–30°S), mid-latitude (30°–60°N/S), Arctic (90°N–60°N) and Antarctic (60°S–90°S) (discussed in section 5.1.1). It is useful to question why no other samples showed statistically significant relationships to the GCR flux, particularly in regions where it might be expected. For example, the GI sample identified locally significant cloud anomalies over both polar regions, occurring with co-temporal statistically significant increases in the rate of GCR flux. While an examination of the AI sample confirmed the presence of this relationship over Antarctica, the Arctic cloud increase sample did not. This result implies a more general problem with the internal sampling approach presented in this work, namely that the compositing of internal datasets in this method is likely to isolate high variability and thus the samples which identified a statistically significant relationship to the GCR flux are samples where a high SNR allowed for the detection of a relationship. This implies that the internal sampling approach is a brute force method, merely capable of showing the most evident GCR–cloud relationships; it is likely that more exist that remain undetected by this approach.

8.3.3 GCM experiments

A key feature of this work has been the use of GCM experiments in chapter 7, which sought to reproduce observed cloud–atmosphere relationships. The use of GCMs in this manner is comparable to the work of Haigh (1996), who successfully used the ECMWF spectral model developed within the UK Universities Global Atmospheric Modelling Programme (UGAMP) to test the influence that variations in stratospheric ozone have on the climate as a result of changes in UV output during the 11-year solar cycle. The spatial dimensions of the model used by Haigh were similar to those of the HadAM3 model used in chapter 7 (running at 2.8°x2.8° horizontal resolution, with 19 vertical steps). Haigh (1996) ran three experiments of 1,080 days each (excluding spin-up), with each experiment representing a different phase of the solar cycle under different conditions. For comparison, the model experiments performed in chapter 7 ran for a period of 2,880 days each (excluding spin-up). Haigh's experiment identified a stratospheric warming effect in summer months during solar maximum, which produced a shift in patterns of tropospheric variability comparable to observations (although of a smaller magnitude) (Haigh, 1996). A similar result was identified by the MLCD GCM experiment in chapter 7, which also produced anomalies comparable to observations, although again, these anomalies were of a smaller magnitude than observations.

Unlike the MLCD experiment, the PCI experiment was unsuccessful at reproducing observed atmospheric anomalies. Potential reasons for this shortcoming have been previously suggested (see section 7.6.1). Next to reproducing cloud, accurately modelling polar environments is one of the toughest challenges faced by GCMs. These environments are essential for the accurate replication of global climate, yet highly difficult to model due to the range of problematic elements which need to be incorporated in to the model, such as sea ice, seasonally frozen permafrost, seasonal snow cover variations, clear-sky precipitation, highly stable boundary layers and cloud microphysics in clean atmospheres (CCSP, 2008). Consequently, if the shortcomings of the PCI GCM experiment result from model limitations, the use of a different type of model (specifically designed to reproduce polar environments) may be required in future investigations.

8.3.5 The importance of rates

The methodology of selecting large changes in the rate of cloud cover as a basis for composite sampling has allowed the identification of statistically significant GCR–cloud signals. However, it is unclear if the use of rates of change is simply highlighting periods where a relationship is detectable over certain areas, or alternatively, if rates of change are themselves involved in a GCR–cloud mechanisms. It may be postulated that rates of change are influential to GCR processes as follows:

In relation to IMN mechanisms. It has been predicted that changes in IMN over the 11-year solar cycle may only have a small influence on global CCN concentrations and a limited impact on changes in cloud cover (Pierce and Adams, 2009). This is mainly due to aerosol scavenging by pre-existing CCN, which remove aerosol particles before they are able to accumulate in significant concentrations to grow to CN and CCN sizes (Carslaw, 2009). As a result, it is likely that IMN processes are only able to influence cloud cover over areas where CCN concentrations are relatively low, such as over pristine ocean environments (Kristjánsson and Kristiansen, 2000; Rosenfeld et al., 2006). To consider if changes in the rate of GCR flux give a mechanistic advantage over changes in absolute flux it is useful to consider two scenarios. In scenario A, a change in the GCR flux of x % occurs over a given time (t); whereas in scenario B, the same GCR change of x % occurs in half the time ($t½$). Both scenarios have the same absolute GCR change, however scenario B occurs at twice the rate of scenario A. This may generate higher numbers of aerosol particles over shorter timescales, potentially reducing the ability of pre-existing CCN to scavenge enough aerosols to prevent the growth of new CN and CCN particles relative to scenario A. The proposed advantage given by scenario B may also imply that, if IMN processes are responsible for the changes occurring during the MLD sample as a result of changes in the rate of GCR flux, a rapid cloud response is more likely than a protracted response (as the longer the timescales involved, the more scavenging that is able to take place and the less likely IMN may produce a significant/widespread impact on cloud properties).

In relation to electroscavenging mechanisms. It may be speculated that rates of change may also have an advantage over absolute changes in relation to GEC mechanisms. For example, considering changes in atmospheric conductivity resulting from scenarios A and B given above, it may be argued that the higher conductivity changes associated with more rapid atmospheric ionisation (in scenario B) may result in a higher space charge density accumulation at cloud boundaries (as opposed to scenario A, where a lower space charge density would occur, but be maintained over a longer time period). Charges are transferred from air ions to aerosol particles at cloud boundaries and are efficiently entrained within the cloud by electroscavenging processes. Electroscavenging itself depends on the radius of the cloud droplets and the charge of

the aerosol particles (Tinsley et al., 2000; Tinsley and Yu, 2004). Hence, for scenario B, the charging of aerosol particles is likely to be greater than scenario A, implying another mechanistic advantage that rapid GCR variations have over relatively slower changes of equal magnitude. However, it is unknown if a rapid but more intense period of electroscavenging (produced by scenario B) would have greater implications for cloud changes than a weaker but more prolonged period of electroscavenging (produced by scenario A). In addition, over environments such as Antarctica, it is possible that electroscavenging processes may be additionally limited by the relatively low abundance of aerosols (potentially suggesting that scenario B may not produce greater impacts on cloud than scenario A). Further work is needed to better understand the influence of GEC-related processes on cloud cover (Tinsley, 2010).

While it may be possible that rapid GCR changes have a mechanistic advantage over relatively slower changes of a comparable magnitude, this does not necessarily explain why a statistically significant GCR–cloud relationship has been detected via the use of rates of cloud change as a sampling basis instead of absolute cloud amounts. To gain indications of this, it is useful to consider the underlying difference between rates and absolute cloud changes over the course of a year; this is shown in figure 8.7. Absolute cloud values show a peak around Vernal equinox and minimum around the northern hemisphere solstice: constructing a composite sample based on the largest/smallest absolute cloud values would reflect this seasonal variation. However, this spring/summer cloud maximum/minimum is notably absent from the daily rates of cloud change (figure 8.7), this is because although this seasonality results in a large absolute change, it takes place slowly. This implies that composites based around rates of cloud change may be able to distinguish natural (seasonal/periodic) cloud variability (which operates slowly), from GCR related cloud variability, which is predicted to influence the efficiency of cloud forming processes by up to several orders of magnitude (and therefore may potentially occur over relatively rapid timescales) (Clarke et al., 1998; Yu and Turco, 2000, 2001; Laakso et al., 2003; Tinsley and Yu, 2004; Tinsley et al., 2006).

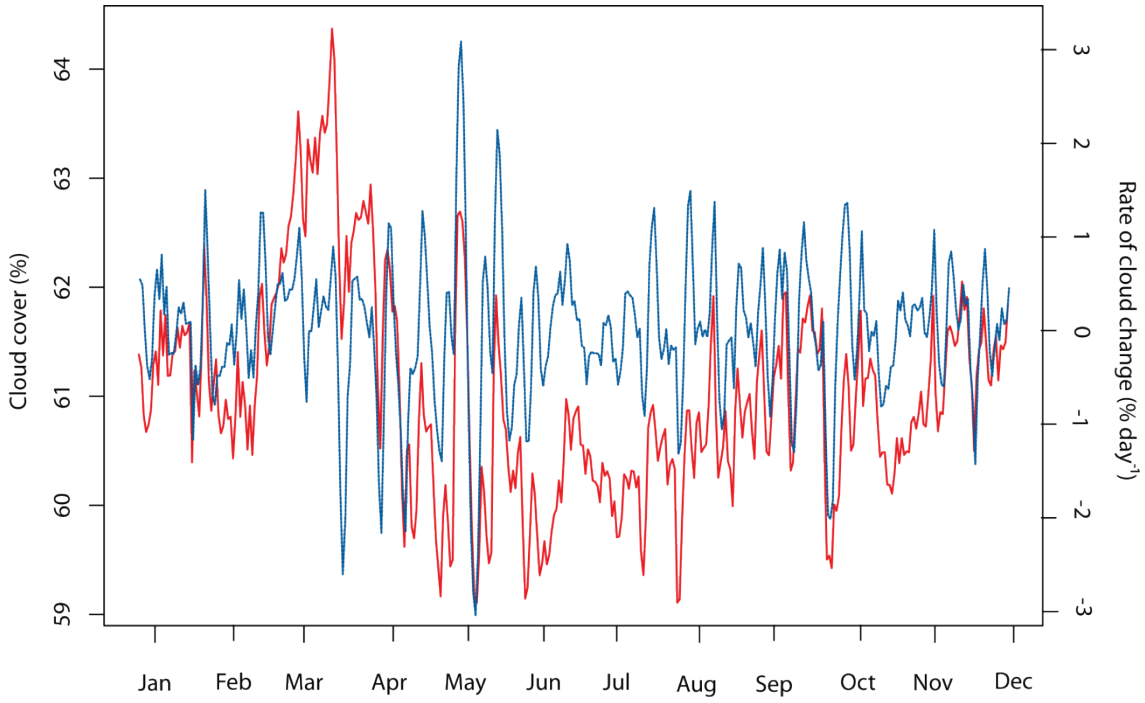

Figure 8.7 Changes in cloud cover and rate of cloud change over a year

Average daily absolute cloud cover (red line) and rate of cloud change (blue line) shown over the course of a year. Values are average daily values between 1988 and 2006 for the ISCCP D1 IR dataset, showing total (10–1,000 mb) cloud cover.

8.4 Overview of main findings and the contribution of this work to the field of study

A brief summary of the main contributions that this work has made to the field of solar-terrestrial studies will now be given:

1) *Provided a reanalysis on the influence of FD events on the atmosphere*. This work has verified the results of some FD studies (Todd and Kniveton, 2001, 2004; Kristjánsson et al, 2008), while questioning the validity of others (Svensmark et al., 2009).

2) *Demonstrates a new method of identifying connections between the GCR flux and cloud cover*. A novel sampling method is presented which successfully identifies statistically robust links between variations in the rate of GCR flux and atmospheric changes operating over daily timescales at mid-latitude regions, which are distinguished from solar irradiance and IMF changes.

3) *Provides evidence of a climatic response to GCR variations*. For perhaps the first time, a clear indication of an atmospheric response to GCRs is given over mid-latitude regions. This relationship is verified in multiple datasets and successfully reproduced by a GCM experiment.

4) *Identifies locations which may prove to be sites of interest for further investigation*. The identification of GCR–atmospheric relationships via the internal sampling methodology identified several regions where GCR–cloud responses appear to be particularly strong (over mid-latitudes and polar latitudes). This identifies regions which may potentially provide useful sites for further study.

5) *Highlights the importance of changing conditions (rate of GCR flux)*. While past studies have focused on the absolute GCR flux, this work has focused instead on the role of changes in the rate of GCR flux. Importantly, differences between the rate/absolute GCR flux may provide indications for the (often) transient nature of observed solar–climate relationships. Rates may also be potentially important with regards to a microphysical GCR–cloud link.

8.5 Limitations and future work

There are many limitations and caveats which have been considered throughout this work and these will not be re-stated here. Instead, this section aims to provide an overview of the limitations relevant to a broader discussion of the work, with specific regard for future areas of improvement.

Individually, both the NCEP/NCAR reanalysis datasets and the ISCCP cloud datasets have associated flaws (particularly with regard to high latitude regions) (Kalnaya et al., 1996; Rossow and Schiffer, 1999). However, the combined use of these datasets along with AWS data aimed to strengthen the confidence that could be placed in the results. Despite this, a clear indication of the nature of the atmospheric changes occurring over the GI/AI samples was not obtained; instead, atmospheric anomalies which appeared to be in conflict were detected. This suggests either an insufficient understanding of the specifics of polar climate, or that there were errors present in the data. Either way, this result highlights a region where further work is necessary. Ideally, a further investigation employing the use of ground based measurements, in conjunction with high-resolution satellite datasets and regional climate models specifically designed to replicate polar climates should be employed to better understand these anomalies.

With regard to the internal sampling methodology, although it has successfully identified robust relationships between the rate of GCR flux and the atmosphere (as set out in the original aims of this thesis) it is important to note that it is essentially a brute force method and, as such, may only be capable of highlighting the most readily apparent relationships. A good example of this is shown by the situation over the Arctic region. When sampling over a global area (using the GI sample), the Arctic is highlighted as a region where anomalous cloud changes are connected to significant GCR changes. However, when sampling over the Arctic region itself, no statistically significant relationship was found. This is likely the result of internal variability outstripping GCR-related variability. Thus, it can be argued that this approach is not a wholly effective basis for compositing to isolate the effects of GCR on the climate. However, there may be ways to refine the approach and potentially provide hitherto unseen details and statistical significance. One such method of approaching this may be to composite samples based on latitudinal symmetry about the equator. The MLD and GI samples both indicated the existence of a very strong symmetrical nature to the detected cloud/temperature anomalies about the equator; from this observation it can be hypothesised that it may be possible to detect a GCR–atmosphere relationship based on latitudinal symmetry. If this is the case then samples composited on this basis may identify a far more isolated GCR–climate signal than obtained by the current internal compositing technique.

Another area where the internal samples perform crudely is with regards to their ability to provide insights in to a mechanism responsible for the cloud changes. In section 7.3, three distinct models of cloud change were outlined, involving: (1) relative changes in cloud amount (from an edge effect) by electroscavenging processes (Tinsley et al., 2000); (2) absolute changes in cloud amount (regardless of pre-existing cloud) by the formation of new CCN particles via IMN (Yu and Turco, 2000); and (3) changes in cloud amount/properties via alterations to the longevity/reflectivity of existing cloud systems via IMN or GEC related mechanisms (Tinsley and Yu, 2004). An understanding of variations in cloud cover from the basis of cloud changes at the individual scale (in conjunction with additional datasets such as aerosol data and vertical current density) may provide good evidence of the specific microphysical mechanisms involved. No such understanding can be gleaned from this current work due to the low spatial resolution of the datasets. An attempt to isolate cloud changes at the scale of individual clouds may itself present many difficulties, as it has been noted that a GCR–atmosphere effect is likely to be a second order phenomenon strongly controlled by precursor conditions. Developing an understanding of these conditions will likely be a crucial element of future studies. Some promising work has already been done in this area, involving direct measurements of clouds and atmospheric electricity variations by Harrison and Ambaum (2009).

In summary, future studies should seek to focus on refining methods of global-scale sampling using a wide range of atmospheric datasets. This approach should be utilised in conjunction with high resolution monitoring of regions deemed to be sensitive to a GCR–climate relationship and local (ground-based) monitoring at the scale of individual cloud systems, while also validating observations against both GCMs and more specialised climate models specifically designed to replicate key environments.

Appendices

Appendix 1 Monte Carlo simulation FORTRAN program

FORTRAN program designed to read in lists of daily average rates of various parameters and randomly generated numbers from which to base 1,000 random samples (of n=100).

> Start of code

```
      PROGRAM MONTE_CARLO_T_CRITS
       parameter  (nobs=100)
       parameter   (sux=7666)
       integer count(1000,100),iday,zcount,cntr,isigprop
       real sum,avrg,i,ix,flux(sux),sample1(100),sample2(100)
       real var1,sdev1,mean1,mean2
       real var2,sd1,sd2,gcr,sighist(1000),ts

c open file containing the GCR data from 1994 to 2004
c read this data into a 1-d array
c opens *.prn file produced in excel of 1000*80 random nos.
        call system('rm shistttest.dat')
        call system ('rm spropttest.dat')
        open(unit=7,file='shistttest.dat',status='new')
        open (unit=8,file='spropttest.dat',status='new')
69      format(I5,F5.2)

       open(unit=1,file='cloud_v7_1.prn',status='old')

20     format(20i8)
       do ix=1,1000
       read(1,20)(count(ix,i),i=1,20)
c      write(*,*)(count(ix,i),i=1,20)
       enddo

       open(unit=2,file='cloud_v7_2.prn',status='old')
       do ix=1,1000
       read(2,21)(count(ix,i+20),i=1,20)
       enddo
21     format(20i8)

       open(unit=3,file='cloud_v7_3.prn',status='old')
22     format(20i8)
       do ix=1,1000
       read(3,22)(count(ix,i+40),i=1,20)
       enddo

       open(unit=4,file='cloud_v7_4.prn',status='old')
       do ix=1,1000
       read(4,23)(count(ix,i+60),i=1,20)
         enddo
23     format(20i8)
```

```
        open (unit=7,file='cloud_v7_5.prn',status='old')
27      format(20i8)
        do ix=1,1000
        read(7,27)(count(ix,i+80),i=1,20)
        enddo

        open(unit=32,file='model_press_mid.prn',status='old')
24      format(f10.6)
      do i=1,sux
      read (32,*)(flux(i))
      enddo

      call system ('rm tvalues.dat')
      open (unit=31,file='tvalues.dat',status='new')

      call system('rm svalues.dat')
      open (unit=33,file='svalues.dat',status='new')

      call system('rm randoms.dat')
      open (unit=34,file='randoms.dat',status='new')

c      read gcr at 100 rand numbers and calculate gcr avg at -5,-4,-3
c      from 100 random numbers
c i=do the run 1000times j=random number samples 1 line,
       cntr=0
c         call system ('rm samples.dat')
c         open(unit=16,file='samples.dat',status='new')
c      write(16,*)count(i,j)

       do i=1,1000
         mean1=0.0
         mean2=0.0
         do j=1,100
          iday=count(i,j)
            write(34,*) count(i,j)
          sample2(j)=flux(iday)
           s0=flux(iday)
c      mean1= averaging period (-5,-4,-3) mean2=average of key dates
           s1=flux(iday-3)
           s2=flux(iday-4)
           s3=flux(iday-5)
           sample1(j)=(s1+s2+s3)/3.0

           mean1=(mean1+sample1(j))
           mean2=(mean2+sample2(j))
         enddo
         mean1=mean1/100.0
         mean2=mean2/100.0

         anom=mean2-mean1
         sd1=0.0
         dev=0.0
           do j=1,100

           dev=sample1(j)-mean1
           dev=dev*dev
           sd1=sd1+dev
         enddo
c variance - sum of dev squared divided by n-1
         sd1=(sd1/99.0)
c        se1=sd1/(sqrt(99.0))
```

```
c  correct var here
           dev2=0.0
               sd2=0.0
          do j=1,100
           dev2=sample2(j)-mean2
           dev2=dev2*dev2
           sd2=sd2+dev2
          enddo

c      T-test below (above calc means/sdev)
           sd2=sd2/99.0
c good var 2
       s=sqrt((sd1/99.0)+(sd2/99.0))

           ts=anom/s
         write (31,*) ts
       enddo

168      continue
       stop
       end
```

Appendix 2 Personal communiqué from Professor William Rossow

Personal communiqué referenced in thesis as (Rossow, 2010). The message is presented below in its original and unedited form (reproduced with permission from Professor William Rossow (NASA Goddard Institute for Space Studies)).

Benjamin, Sorry for the delay but wanted to think about the answer carefully. The main comment about M&S is that they are "adjusting" the observations to fit their hypothesis, which is badly flawed methodology... they have not presented any evidence to invalidate the alternate hypothesis that the quality of the ISCCP record is uniform, instead they are trying only to invalidate the PART of the ISCCP record that disagrees with their hypothesis.

Having said that, their hypothesis is easy to refute but nobody really wants to waste the time doing so. However, I can make four statements and support two of them with publications.

(1) M&S have a fundamental mis-understanding of calibration: they interpret discontinuities in the calibration COEFFICIENT time record as discontinuities in the RADIANCE time record. The whole point of changing coefficients is to remove changes in radiances. We haven't published any updates on calibration since 1997 but you can look at the ISCCP website and the plots of long-term anomalies in cloud optical thickness, together with surface reflectance, for VIS and cloud top temperature, together with surface temperature, for IR to see that there are no radiance discontinuities larger than a few percent. Surface temperature does present some noticeable changes but these have been explained as due to the atmospheric dataset used for retrievals and NOT calibration. The point is we have a complete record of radiances (and there are now some as yet unpublished verifications) that shows no significant discontinuities in the record.

(2) The ISCCP cloud detection algorithm is BY DESIGN almost independent of radiance calibration as explained in Rossow and Garder (1993). TOTAL cloud amount does not depend on calibration. We have done, but not published yet (paper in preparation), the test: changing calibrations (both VIS and IR) by as much as 20% changes TOTAL cloud amount by less than 1% and, since the estimated precision of calibration over the record is about 3% or less, the variation over the record of TOTAL cloud amount due to calibration is no more than 0.1-0.2%. This point undercuts M&S whole argument.

(3) The amounts of ISCCP cloud TYPES depend directly on calibration but in a very specific way. We monitor all of the TYPE time records to watch for such changes. If VIS calibration changes, then the amounts of Cumulus/Cirrus and Stratus/Deep Convection MUST change in the same way for each pair divided by "/" and in opposite ways the two pairs; moreover surface reflectance of land areas and ice sheets MUST change in the same way as Stratus/Deep Convection. If IR calibration changes, then the amounts of Cumulus/Stratus and Cirrus/Deep Convection MUST change in the same way for each pair divided by "/" and in opposite ways for the two pairs; moreover, surface temperature MUST change in the same way as Cumulus/Stratus. Again you can look at the ISCCP

website plots to see that the overall change in TOTAL cloud amount does not reveal coordinated changes of either of these kinds.

(4) If you put the entire ISCCP cloud property record into a radiation code and calculate top-of-atmosphere and surface radiative fluxes, you get results that are very consistent with the long-term ERBE (nonscanner) record and the shorter BSRN record (which does span the supposed discontinuity in the record). In particular, the "global" monthly mean SW reflected anomalies from ERBE (which actually only cover plus-minus 60 degrees of latitude) agree with the calculated ones to within 1 watt per meter squared....so the variations of total cloud cover in ISCCP (together with almost no variation of optical thickness) are confirmed by the agreement with ERBE (see Zhang et al. 2004). This exercise has been done by 3-4 groups, which use different combinations of information from ISCCP. In other words, if the latter half of the ISCCP cloud amount record were in error, we would have noticed a disagreement with ERBE and BSRN.

Rossow, W.B., and L.C. Garder, 1993a: Cloud detection using satellite measurements of infrared and visible radiances for ISCCP. J. Climate, 6, 2341-2369.

Zhang, Y-C., W.B. Rossow, A.A. Lacis, M.I. Mishchenko and V. Oinas, 2004: Calculation of radiative fluxes from the surface to top-of-atmosphere based on ISCCP and other global datasets: Refinements of the radiative transfer model and the input data. J.Geophys. Res., 109, doi 10.1029/2003JD004457 (1-27 + 1-25).

You may have read one paper that purports to show that the ISCCP cloud amount anomalies are artifacts (Evan et al, I think). There are two comments to be made. If this paper were true, then the WHOLE ISCCP record is invalidated which also invalidates M&S hypothesis.... note by the way that right now, ONLY ISCCP of all the long-term cloud records shows the variation that M&S are using (their might be a relevant plot in the last IPCC report) -- they HAVE to believe ONLY ISCCP and ONLY the first part of the record to preserve their hypothesis. We don't know why these datasets disagree, yet.. it is still be investigated... all that can be said at the moment is that the three datasets have very different space-time sampling and differing sensitivity to optically thin clouds.

The second comment is that this paper is not true... it makes the classic mistake of confusing correlation with causation. They show a correlation between the global monthly mean cloud amount anomaly record and changes in satellite viewing geometry but never demonstrate that the effect is large enough to explain the WHOLE signal. I have done an analysis, which I will publish later this year, that shows that, when you remove all locations where viewing angle changes, and re-calculate the anomaly time record, the signal is still present. In other words, the viewing geometry effect distorts a signal already present but does NOT explain most of it.

Hope this helps....

Appendix 3 Note regarding the treatment of ISCCP data in Svensmark *et al.* (2009)

The following two-page note (which appears in its original form including type and formatting errors) regarding the data handling methods employed by Svensmark et al (2009) was received following a personal correspondence with the papers second author, Torsten Bondo, on 21/09/2009.

Data processing related to "Cosmic ray decreases affect atmospheric aerosols and clouds"

Henrik Svensmark, Torsten Bondo and Jacob Svensmark, National Space Institute, Technical University of Denmark, Copenhagen, Denmark

This document describes the data processing related to "Cosmic ray decreases affect atmospheric aerosols and clouds" GEOPHYSICAL RESEARCH LETTERS, VOL. 36, L15101, doi:10.1029/2009GL038429, 2009. Over time we will be responding to the questions we get from other researchers regarding our handling of data and the document may be extended.

ISCCP

For ISCCP we used Low-clouds-D1 3-hourly readings over the oceans below 3.2 km. More specifically we extracted product p28 and p29 (number of IR cloudy pixels from 680-1000mb) and the total number of pixels (p11) and calculated the IR Low clouds over oceans as (p28 + p29)/(p11). The products were extracted using d1read.1var.f downloaded from ISCCP website. We made daily averages over the subtropical/tropical ocean from 40 degrees N to 40 degrees S of only those pixels where all 8 daily values where present for a particular day. Since most counts from the high latitudes area are not included if you require the 8 daily values to be present this makes only a small difference on the signal whether or not you have the high latitudes with. This is shown in Figure 1 where the area of interest is extended to 70 degrees. We decided to use ISCCP only over the ocean due to known problems with ISCCP in determining cloud pixels from over Land.

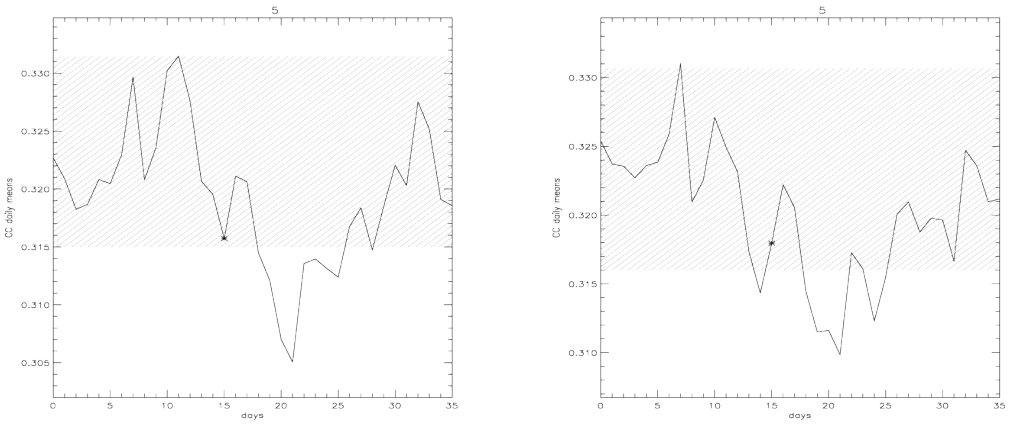

Figure 1: Left) Figure 1 from article only with ISCCP taken from 40N to 40S. Right) the same analysis but extending the area to 70N to 70S

MODIS

MODIS is an infrared and visible passive sensor launched abo ard two American satellites Terra (operating since 2000) and Aqua (oper ating since 2002). A multitude of data can be achieved from http://modis-atmos .gsfc.nasa.gov. Cloud properties on a 1 degree grid can be obtained in daily le vel 3 format already preprocessed and error cleaned. For the present analy sis the MOD 08D 3 Daily Joint Aerosol/Water vapor/Cloud product from Terra i s used since it has the longest data availability. With over 600 geophysica l only the subsets "Cloud _Fraction _Combined and "Cloud _Fraction _Liquid were analyzed. Here we used all pixels over land and ocean. MODIS is a newer algori thm and we feel more confident in their land cloud retrieval. This is som ething we continue to study.

AERONET

For Aeronet an IDL program was developed to compute global aa ngstrom exponent (AE) from daily averages over the FD periods. The global mean of the AE is computed by a mean of all daily stations that return more th an 20 measurements a day as: $\sum_i(\sum_k(ae_{station\ k}/N_k)/N_i$, where N_k must be larger than 20 and i is the stations that have over 20 measurements per day. T his limits the list to around 40 stations but do ensure continuity/stability in the data series and disallows making averages of stations returning single mea surements with stations returning more than 20 measurements. The smallest ava ilable wavelength pair would by intuition express the largest changes during a FD. Therefore the wavelength pair from 340-440 nm is used.

SSMI/I

The present analysis used the liquid water product of SSM/I r eturning daily data from liquid water clouds available since 1987. Here we u sed all pixels over ocean. The hdf data was read into an IDL program and averaged t o daily values during the FD periods. More to come

Appendix 4 MLD experiment annotated FORTRAN 77 modset

Note: Code is designed to run in parallel on a 16 core machine, consequently array dimensions relate to portions of the array tasked to individual processors and not directly to latitude/longitude/vertical components of the array. All latitude and longitude dimensions referred to within the code are calculated as a sine of the latitude/longitude converted to radians.

Any lines of text prefaced with "*/" or "c" are comments within the code.

```
> Start of code
*ID CLOUDCOV
*/-----------------------------------------------------------------
*/ Mod to decrease the cloud area fraction as seen be SW and LW.
*/ This mod uses a latitude and height restriction specific to
*/ observed anomalous cloud over the mid-latitudes.
*/ Code written by Ben Laken (2010) based on code by
*/                          Dominic Kniveton & David Hassell (2005)
*/-----------------------------------------------------------------
*/ *DECLARE = change code in this deck
*DECLARE RAD_CTL1
*/ *I = Insert some code after this line
*I ADB1F400.88
       REAL
     &  AREA_CLOUD_FRACTION_CHANGE(P_FIELDDA,Q_LEVELSDA)
       REAL
     &  CLOUD_FRACTION_CHANGE(P_FIELDDA,Q_LEVELSDA)
          REAL
     &  Z_DAY_NUMBER,W_DAY_NUMBS,X_DAY_NUMBS,ZW_DAY_NUMBS
       INTEGER IW_DAY_NUMBS,ITOP,IANT
       INTEGER ITCLO,IBOUNTI
!  Artificially changed SW+LW Radiation only cloud fraction
*/ *B = Insert some code before this line
*B RAD_CTL1.211
```

```
            CALL UV_TO_P(F3(FIRST_VALID_PT),
     &                SIN_TRUE_LATITUDE(FIRST_VALID_PT+ROW_LENGTH),
     &                U_FIELD-FIRST_VALID_PT+1,
     &                P_FIELD-(FIRST_VALID_PT+ROW_LENGTH)+1,
     &                ROW_LENGTH,upd_P_ROWS+1)
             DO I=FIRST_POINT,LAST_POINT
               SIN_TRUE_LATITUDE(I)=SIN_TRUE_LATITUDE(I)*0.5/OMEGA
           END DO
c            DO I=FIRST_POINT,LAST_POINT
c           write(*,*)'Bens Lat(new): ',I,SIN_TRUE_LATITUDE(I)
c         ENDDO
            IF ( H_SECT(1) .EQ. '02B' ) THEN
             Z_DAY_NUMBER=REAL(I_DAY_NUMBER)
            ELSE
             Z_DAY_NUMBER=REAL(PREVIOUS_TIME(7))
           write(*,*)'Ben Day num',PREVIOUS_TIME(7)
            ENDIF
            W_DAY_NUMBS=Z_DAY_NUMBER/24.0
          IW_DAY_NUMBS=INT(W_DAY_NUMBS)
          write(*,*)'Ben Wday/IWday',W_DAY_NUMBS,IW_DAY_NUMBS
         ZW_DAY_NUMBS=REAL(IW_DAY_NUMBS)
         X_DAY_NUMBS=ZW_DAY_NUMBS-W_DAY_NUMBS
         X_DAY_NUMBS=(X_DAY_NUMBS)*(-1.0)
         write(*,*)'Ben Xday-numbs:',X_DAY_NUMBS
             ITCLO=NINT((REAL(Q_LEVELSDA))/3.0)
             IBOUNTI=Q_LEVELSDA-ITCLO
c cant get the x_day numbs exactly due to lack of precision, need to
c use IF statements to isolate the days I want to change, due to
precision of    c HECTOR, need to calculate days based on number
ranges (as cant identify day num  c specifically...)
c change (day -6)
        IF(X_DAY_NUMBS.GT.0.57. AND.X_DAY_NUMBS.LT.0.59) THEN
c If within a certain timeframe increase cloud...
          write(*,*)'Changing day -6 cloud ',X_DAY_NUMBS
```

```
          DO I=1,P_FIELDDA
            DO J=1, Q_LEVELSDA
c...level and lat restriction
            IF(SIN_TRUE_LATITUDE(I).LT.0.76.AND.SIN_TRUE_LATITUDE(I).
     &        GT.0.5.AND.J.GE.1.AND.J.LE.7.OR.SIN_TRUE_LATITUDE(I).
     &        GT.-0.76.AND.SIN_TRUE_LATITUDE(I).LT.-0.5.AND.J.GE.1.
     &        AND.J.LE.7)THEN
         AREA_CLOUD_FRACTION_CHANGE(I,J)=AREA_CLOUD_FRACTION(I,J)*1.04
         CLOUD_FRACTION_CHANGE(I,J)=CLOUD_FRACTION(I,J)*1.04
c  ..if cloud is inc. beyond max then set to 100%...
         IF(AREA_CLOUD_FRACTION_CHANGE(I,J).GT.1.0)THEN
            AREA_CLOUD_FRACTION_CHANGE(I,J)=1.0
         ENDIF
         IF(CLOUD_FRACTION_CHANGE(I,J).GT.1.0)THEN
            CLOUD_FRACTION_CHANGE(I,J)=1.0
         ENDIF
c...below else-endif for lat/level restriction
         ELSE
         CLOUD_FRACTION_CHANGE(I,J)=CLOUD_FRACTION(I,J)
         AREA_CLOUD_FRACTION_CHANGE(I,J)=AREA_CLOUD_FRACTION(I,J)
               ENDIF
            END DO
          END DO
c change (day -5)
        Else IF(X_DAY_NUMBS.GT.0.60. AND.X_DAY_NUMBS.LT.0.64) THEN
c If within a certain timeframe increase cloud...
          write(*,*)'Changing day -5 cloud ',X_DAY_NUMBS
          DO I=1,P_FIELDDA
            DO J=1, Q_LEVELSDA
c...level and lat restriction
            IF(SIN_TRUE_LATITUDE(I).LT.0.76.AND.SIN_TRUE_LATITUDE(I).
     &        GT.0.5.AND.J.GE.1.AND.J.LE.7.OR.SIN_TRUE_LATITUDE(I).
     &        GT.-0.76.AND.SIN_TRUE_LATITUDE(I).LT.-0.5.AND.J.GE.1.
```

```
     &         AND.J.LE.7)THEN
          AREA_CLOUD_FRACTION_CHANGE(I,J)=AREA_CLOUD_FRACTION(I,J)*1.06
          CLOUD_FRACTION_CHANGE(I,J)=CLOUD_FRACTION(I,J)*1.06
c  ..if cloud is dec. beyond min then set to 0...
          IF(AREA_CLOUD_FRACTION_CHANGE(I,J).GT.1.0)THEN
             AREA_CLOUD_FRACTION_CHANGE(I,J)=1.0
          ENDIF
          IF(CLOUD_FRACTION_CHANGE(I,J).GT.1.0)THEN
             CLOUD_FRACTION_CHANGE(I,J)=1.0
          ENDIF
c...below else-endif for lat/level restriction
          ELSE
          CLOUD_FRACTION_CHANGE(I,J)=CLOUD_FRACTION(I,J)
          AREA_CLOUD_FRACTION_CHANGE(I,J)=AREA_CLOUD_FRACTION(I,J)
               ENDIF
             END DO
           END DO
c change (day -4)
        ELSE IF(X_DAY_NUMBS.GT.0.65. AND.X_DAY_NUMBS.LT.0.68) THEN
c If within a certain timeframe increase cloud...
           write(*,*)'Changing day -4 cloud ',X_DAY_NUMBS
           DO I=1,P_FIELDDA
             DO J=1, Q_LEVELSDA
c...level and lat restriction
             IF(SIN_TRUE_LATITUDE(I).LT.0.76.AND.SIN_TRUE_LATITUDE(I).
     &         GT.0.5.AND.J.GE.1.AND.J.LE.7.OR.SIN_TRUE_LATITUDE(I).
     &         GT.-0.76.AND.SIN_TRUE_LATITUDE(I).LT.-0.5.AND.J.GE.1.
     &         AND.J.LE.7)THEN
          AREA_CLOUD_FRACTION_CHANGE(I,J)=AREA_CLOUD_FRACTION(I,J)*1.04
          CLOUD_FRACTION_CHANGE(I,J)=CLOUD_FRACTION(I,J)*1.04
c  ..if cloud is inc. beyond max then set to 100%...
          IF(AREA_CLOUD_FRACTION_CHANGE(I,J).GT.1.0)THEN
             AREA_CLOUD_FRACTION_CHANGE(I,J)=1.0
```

```
          ENDIF
          IF(CLOUD_FRACTION_CHANGE(I,J).GT.1.0)THEN
             CLOUD_FRACTION_CHANGE(I,J)=1.0
          ENDIF
c...below else-endif for lat/level restriction
           ELSE
          CLOUD_FRACTION_CHANGE(I,J)=CLOUD_FRACTION(I,J)
          AREA_CLOUD_FRACTION_CHANGE(I,J)=AREA_CLOUD_FRACTION(I,J)
                ENDIF
             END DO
           END DO
c change (day -2)
        ELSE IF(X_DAY_NUMBS.GT.0.72. AND.X_DAY_NUMBS.LT.0.77) THEN
c If within a certain timeframe increase cloud...
           write(*,*)'Changing day -2 cloud ',X_DAY_NUMBS
           DO I=1,P_FIELDDA
             DO J=1, Q_LEVELSDA
c...level and lat restriction
             IF(SIN_TRUE_LATITUDE(I).LT.0.86.AND.SIN_TRUE_LATITUDE(I).
     &         GT.0.34.AND.J.GE.1.AND.J.LE.8.OR.SIN_TRUE_LATITUDE(I).
     &         GT.-0.86.AND.SIN_TRUE_LATITUDE(I).LT.-0.34.AND.J.GE.1.
     &         AND.J.LE.8)THEN
          AREA_CLOUD_FRACTION_CHANGE(I,J)=AREA_CLOUD_FRACTION(I,J)*0.97
          CLOUD_FRACTION_CHANGE(I,J)=CLOUD_FRACTION(I,J)*0.97
         IF(AREA_CLOUD_FRACTION_CHANGE(I,J).LT.0.0)THEN
c          If cloud change is o.t.t. back it down
             AREA_CLOUD_FRACTION_CHANGE(I,J)=0.0
          ENDIF
          IF(CLOUD_FRACTION_CHANGE(I,J).LT.0.0)THEN
             CLOUD_FRACTION_CHANGE(I,J)=0.0
          ENDIF
c...below else-endif for lat/level restriction
            ELSE
```

```
          CLOUD_FRACTION_CHANGE(I,J)=CLOUD_FRACTION(I,J)
          AREA_CLOUD_FRACTION_CHANGE(I,J)=AREA_CLOUD_FRACTION(I,J)

          ENDIF
             END DO
           END DO
c change (day -1)
        ELSE IF(X_DAY_NUMBS.GT.0.77.AND.X_DAY_NUMBS.LT.0.81) THEN
c If within a certain timeframe increase cloud...
           write(*,*)'Changing day -1 cloud ',X_DAY_NUMBS
           DO I=1,P_FIELDDA
             DO J=1, Q_LEVELSDA
c...level and lat restriction
             IF(SIN_TRUE_LATITUDE(I).LT.0.86.AND.SIN_TRUE_LATITUDE(I).
     &         GT.0.34.AND.J.GE.1.AND.J.LE.8.OR.SIN_TRUE_LATITUDE(I).
     &         GT.-0.86.AND.SIN_TRUE_LATITUDE(I).LT.-0.34.AND.J.GE.1.
     &         AND.J.LE.8)THEN
          AREA_CLOUD_FRACTION_CHANGE(I,J)=AREA_CLOUD_FRACTION(I,J)*0.94
          CLOUD_FRACTION_CHANGE(I,J)=CLOUD_FRACTION(I,J)*0.94
c  ..if cloud is inc. beyond max then amp it down...
          IF(AREA_CLOUD_FRACTION_CHANGE(I,J).LT.0.0)THEN
             AREA_CLOUD_FRACTION_CHANGE(I,J)=0.0
          ENDIF
          IF(CLOUD_FRACTION_CHANGE(I,J).LT.0.0)THEN
             CLOUD_FRACTION_CHANGE(I,J)=0.0
          ENDIF
c...below else-endif for lat/level restriction
            ELSE
          CLOUD_FRACTION_CHANGE(I,J)=CLOUD_FRACTION(I,J)
          AREA_CLOUD_FRACTION_CHANGE(I,J)=AREA_CLOUD_FRACTION(I,J)

          ENDIF
             END DO
           END DO
```

```
c change (day 0)
        ELSE IF(X_DAY_NUMBS.GT.0.81.AND.X_DAY_NUMBS.LT.0.85) THEN
c If within a certain timeframe increase cloud...
          write(*,*)'Changing day 0 cloud ',X_DAY_NUMBS
          DO I=1,P_FIELDDA
            DO J=1, Q_LEVELSDA
c...level and lat restriction
            IF(SIN_TRUE_LATITUDE(I).LT.0.86.AND.SIN_TRUE_LATITUDE(I).
     &        GT.0.34.AND.J.GE.1.AND.J.LE.8.OR.SIN_TRUE_LATITUDE(I).
     &        GT.-0.86.AND.SIN_TRUE_LATITUDE(I).LT.-0.34.AND.J.GE.1.
     &        AND.J.LE.8)THEN
          AREA_CLOUD_FRACTION_CHANGE(I,J)=AREA_CLOUD_FRACTION(I,J)*0.90
          CLOUD_FRACTION_CHANGE(I,J)=CLOUD_FRACTION(I,J)*0.90
c  ..if cloud is inc. beyond max then amp it down...
          IF(AREA_CLOUD_FRACTION_CHANGE(I,J).LT.0.0)THEN
             AREA_CLOUD_FRACTION_CHANGE(I,J)=0.0
          ENDIF
          IF(CLOUD_FRACTION_CHANGE(I,J).LT.0.0)THEN
             CLOUD_FRACTION_CHANGE(I,J)=0.0
          ENDIF
c...below else-endif for lat/level restriction
            ELSE
          CLOUD_FRACTION_CHANGE(I,J)=CLOUD_FRACTION(I,J)
          AREA_CLOUD_FRACTION_CHANGE(I,J)=AREA_CLOUD_FRACTION(I,J)

          ENDIF
             END DO
           END DO
c change (day +1)
        ELSE IF(X_DAY_NUMBS.GT.0.86.AND.X_DAY_NUMBS.LT.0.89) THEN
c If within a certain timeframe increase cloud...
          write(*,*)'Changing day +1 cloud ',X_DAY_NUMBS
          DO I=1,P_FIELDDA
```

```
            DO J=1, Q_LEVELSDA
c...level and lat restriction
            IF(SIN_TRUE_LATITUDE(I).LT.0.86.AND.SIN_TRUE_LATITUDE(I).
     &        GT.0.34.AND.J.GE.1.AND.J.LE.8.OR.SIN_TRUE_LATITUDE(I).
     &        GT.-0.86.AND.SIN_TRUE_LATITUDE(I).LT.-0.34.AND.J.GE.1.
     &        AND.J.LE.8)THEN
          AREA_CLOUD_FRACTION_CHANGE(I,J)=AREA_CLOUD_FRACTION(I,J)*0.94
          CLOUD_FRACTION_CHANGE(I,J)=CLOUD_FRACTION(I,J)*0.94
c  ..if cloud is inc. beyond max then amp it down...
          IF(AREA_CLOUD_FRACTION_CHANGE(I,J).LT.0.0)THEN
             AREA_CLOUD_FRACTION_CHANGE(I,J)=0.0
          ENDIF
          IF(CLOUD_FRACTION_CHANGE(I,J).LT.0.0)THEN
             CLOUD_FRACTION_CHANGE(I,J)=0.0
          ENDIF
c...below else-endif for lat/level restriction
            ELSE
          CLOUD_FRACTION_CHANGE(I,J)=CLOUD_FRACTION(I,J)
          AREA_CLOUD_FRACTION_CHANGE(I,J)=AREA_CLOUD_FRACTION(I,J)

          ENDIF
             END DO
           END DO
c change (day +2)
        ELSE IF(X_DAY_NUMBS.GT.0.90.AND.X_DAY_NUMBS.LT.0.93) THEN
c If within a certain timeframe increase cloud...
           write(*,*)'Changing day +2 cloud ',X_DAY_NUMBS
           DO I=1,P_FIELDDA
             DO J=1, Q_LEVELSDA
c...level and lat restriction
            IF(SIN_TRUE_LATITUDE(I).LT.0.86.AND.SIN_TRUE_LATITUDE(I).
     &        GT.0.34.AND.J.GE.1.AND.J.LE.8.OR.SIN_TRUE_LATITUDE(I).
     &        GT.-0.86.AND.SIN_TRUE_LATITUDE(I).LT.-0.34.AND.J.GE.1.
```

```
     &         AND.J.LE.8)THEN
          AREA_CLOUD_FRACTION_CHANGE(I,J)=AREA_CLOUD_FRACTION(I,J)*0.97
          CLOUD_FRACTION_CHANGE(I,J)=CLOUD_FRACTION(I,J)*0.97
c  ..if cloud is inc. beyond max then amp it down...
          IF(AREA_CLOUD_FRACTION_CHANGE(I,J).LT.0.0)THEN
             AREA_CLOUD_FRACTION_CHANGE(I,J)=0.0
          ENDIF
          IF(CLOUD_FRACTION_CHANGE(I,J).LT.0.0)THEN
             CLOUD_FRACTION_CHANGE(I,J)=0.0
          ENDIF
c...below else-endif for lat/level restriction
            ELSE
          CLOUD_FRACTION_CHANGE(I,J)=CLOUD_FRACTION(I,J)
          AREA_CLOUD_FRACTION_CHANGE(I,J)=AREA_CLOUD_FRACTION(I,J)

          ENDIF
             END DO
           END DO
           ELSE
c...if outside either timeframe make cloud equal to norm cloud.
           write(*,*)'A non C.change day',X_DAY_NUMBS
           DO I=1,P_FIELDDA
             DO J=1, Q_LEVELSDA
           AREA_CLOUD_FRACTION_CHANGE(I,J)=AREA_CLOUD_FRACTION(I,J)
          CLOUD_FRACTION_CHANGE(I,J)=CLOUD_FRACTION(I,J)
             END DO
           END DO
           ENDIF
*/ *D = Replace code with this line to remove original call Sin_t..
*D APBBF401.9
*D APBBF401.10
*D APBBF401.11
*D APBBF401.12
```

```
*D APBBF401.13
*D APBBF401.14
*D RAD_CTL1.258
*D RAD_CTL1.259
*D RAD_CTL1.260
*/ *D = Replace the following lines (or range of lines) with some code
*D RAD_CTL1.416
*/ Change call to SWRAD
     &     D1(JPSTAR+JS),AKH,BKH,CLOUD_FRACTION_CHANGE(FIRST_POINT,1),
*D AWI1F403.322
*/ Change call to SWRAD
     &    D1(JPSTAR+JS),AKH,BKH,CLOUD_FRACTION_CHANGE(FIRST_POINT,1),
*D ASK1F405.269
*/ Change call to R2_SWRAD
     &        AREA_CLOUD_FRACTION_CHANGE(FIRST_POINT,1),
*D ADB1F400.174
*/ Change call to R2_SWRAD
     &        CLOUD_FRACTION_CHANGE(FIRST_POINT,1),
*D ASK1F405.270
*/ change call to CALL SWDKDI
     &    AREA_CLOUD_FRACTION_CHANGE(START_POINT_NO_HALO,1),
*D ADB1F400.258
*/ Change call to LWRAD
     &        CLOUD_FRACTION_CHANGE(FP_LOCAL(I),1),
*D ASK1F405.272
*/ Change call to R2_LWRAD
     &        AREA_CLOUD_FRACTION_CHANGE(FP_LOCAL(I),1),
*D ADB1F400.316
*/ Change call to R2_LWRAD
     &        CLOUD_FRACTION_CHANGE(FP_LOCAL(I),1),
*/ -- End of Mod -
```

Appendix 5 Polar increase experiment annotated Fortran 77 modset

Note: Code is designed to run in parallel on a 16 core machine, consequently array dimensions relate to portions of the array tasked to individual processors and not directly to latitude/longitude/vertical components of the array. All latitude and longitude dimensions referred to within the code are calculated as a sine of the latitude/longitude converted to radians.

Any lines of text prefaced with "*/" or "c" are comments within the code.

```
 > START OF CODE

*ID CLOUDCOV

*/-----------------------------------------------------------------------
-----------------------------------------------------------------------
---------

*/ Mod to decrease the cloud area fraction as seen be SW and LW.  This
mod uses a latitude and height restriction */specific to   observed
anomalous cloud over Arctic/Antarctic. This is the final version
modified on 10/01/2010.

*/ This decreases cloud on day -6 to -4 (by around -15%) over poles
and increases cloud on day -2 to +2

*/(by around +30%) over poles. changes cloud between 60-90 N/S,
between 759-557mb (Npole) and

*/ 228-10mb (Spole).Different scale change (higher 75-90)

*/-----------------------------------------------------------------------
-----------------------------------------------------------------------
----------

*/ *DECLARE = change code in this deck

*DECLARE RAD_CTL1

*/ *I = Insert some code after this line

*I ADB1F400.88

       REAL

     &  AREA_CLOUD_FRACTION_CHANGE(P_FIELDDA,Q_LEVELSDA)

       REAL

     &  CLOUD_FRACTION_CHANGE(P_FIELDDA,Q_LEVELSDA)

          REAL

     &  Z_DAY_NUMBER,W_DAY_NUMBS,X_DAY_NUMBS,ZW_DAY_NUMBS

       INTEGER IW_DAY_NUMBS,ITOP,IANT

       INTEGER ITCLO,IBOUNTI
```

```
!  Artificially changed SW+LW Radiation only cloud fraction
*/ *B = Insert some code before this line
*B RAD_CTL1.211
            CALL UV_TO_P(F3(FIRST_VALID_PT),
     &                SIN_TRUE_LATITUDE(FIRST_VALID_PT+ROW_LENGTH),
     &                U_FIELD-FIRST_VALID_PT+1,
     &                P_FIELD-(FIRST_VALID_PT+ROW_LENGTH)+1,
     &                ROW_LENGTH,upd_P_ROWS+1)


             DO I=FIRST_POINT,LAST_POINT
               SIN_TRUE_LATITUDE(I)=SIN_TRUE_LATITUDE(I)*0.5/OMEGA
           END DO
           IF ( H_SECT(1) .EQ. '02B' ) THEN
            Z_DAY_NUMBER=REAL(I_DAY_NUMBER)
           ELSE
            Z_DAY_NUMBER=REAL(PREVIOUS_TIME(7))
          write(*,*)'Ben Day num',PREVIOUS_TIME(7)
           ENDIF
           W_DAY_NUMBS=Z_DAY_NUMBER/24.0
         IW_DAY_NUMBS=INT(W_DAY_NUMBS)
         write(*,*)'Ben Wday/IWday',W_DAY_NUMBS,IW_DAY_NUMBS
        ZW_DAY_NUMBS=REAL(IW_DAY_NUMBS)
        X_DAY_NUMBS=ZW_DAY_NUMBS-W_DAY_NUMBS
        X_DAY_NUMBS=(X_DAY_NUMBS)*(-1.0)
        write(*,*)'Ben Xday-numbs:',X_DAY_NUMBS
            ITCLO=NINT((REAL(Q_LEVELSDA))/3.0)
            IBOUNTI=Q_LEVELSDA-ITCLO
c cant get the x-day numbs exactly due to lack of precision, need to
use IF statements to isolate the days I want to
c change (day -6)
        IF(X_DAY_NUMBS.GT.0.57. AND.X_DAY_NUMBS.LT.0.59) THEN
c If within a certain timeframe increase cloud...
          write(*,*)'Changing day -6 cloud ',X_DAY_NUMBS
```

```
          DO I=1,P_FIELDDA
            DO J=1, Q_LEVELSDA
c...level and lat restriction
            IF(SIN_TRUE_LATITUDE(I).GT.0.86.AND.J.GE.4.AND.J.LE.9.
     &        OR.SIN_TRUE_LATITUDE(I).LT.-0.86.AND.J.GE.6.AND.J.
     &        LE.19)THEN
         AREA_CLOUD_FRACTION_CHANGE(I,J)=AREA_CLOUD_FRACTION(I,J)*0.85
         CLOUD_FRACTION_CHANGE(I,J)=CLOUD_FRACTION(I,J)*0.85
c  ..if cloud is dec. beyond min then set to 0...
         IF(AREA_CLOUD_FRACTION_CHANGE(I,J).LT.0.0)THEN
            AREA_CLOUD_FRACTION_CHANGE(I,J)=0.0
         ENDIF
         IF(CLOUD_FRACTION_CHANGE(I,J).LT.0.0)THEN
            CLOUD_FRACTION_CHANGE(I,J)=0.0
         ENDIF
c Below is a second lat/level restriction nested within the first
            IF(SIN_TRUE_LATITUDE(I).GT.0.96.AND.J.GE.6.AND.J.LE.8.
     &        OR.SIN_TRUE_LATITUDE(I).LT.-0.96.AND.J.GE.9.AND.J.
     &        LE.19)THEN
         AREA_CLOUD_FRACTION_CHANGE(I,J)=AREA_CLOUD_FRACTION(I,J)*0.80
         CLOUD_FRACTION_CHANGE(I,J)=CLOUD_FRACTION(I,J)*0.80
c  ..if cloud is dec. beyond min then set to 0...
         IF(AREA_CLOUD_FRACTION_CHANGE(I,J).LT.0.0)THEN
            AREA_CLOUD_FRACTION_CHANGE(I,J)=0.0
         ENDIF
         IF(CLOUD_FRACTION_CHANGE(I,J).LT.0.0)THEN
            CLOUD_FRACTION_CHANGE(I,J)=0.0
         ENDIF
         ENDIF
c...below else-endif for lat/level restriction
         ELSE
         CLOUD_FRACTION_CHANGE(I,J)=CLOUD_FRACTION(I,J)
```

```
          AREA_CLOUD_FRACTION_CHANGE(I,J)=AREA_CLOUD_FRACTION(I,J)

          ENDIF
             END DO
           END DO
c
c change (day -5)
        ELSE IF(X_DAY_NUMBS.GT.0.61. AND.X_DAY_NUMBS.LT.0.64) THEN
c If within a certain timeframe increase cloud...
           write(*,*)'Changing day -5 cloud ',X_DAY_NUMBS
           DO I=1,P_FIELDDA
             DO J=1, Q_LEVELSDA
c...level and lat restriction
             IF(SIN_TRUE_LATITUDE(I).GT.0.86.AND.J.GE.4.AND.J.LE.9.
     &         OR.SIN_TRUE_LATITUDE(I).LT.-0.86.AND.J.GE.6.AND.J.
     &         LE.19)THEN
          AREA_CLOUD_FRACTION_CHANGE(I,J)=AREA_CLOUD_FRACTION(I,J)*0.80
          CLOUD_FRACTION_CHANGE(I,J)=CLOUD_FRACTION(I,J)*0.80
c  ..if cloud is dec. beyond min then set to 0...
          IF(AREA_CLOUD_FRACTION_CHANGE(I,J).LT.0.0)THEN
             AREA_CLOUD_FRACTION_CHANGE(I,J)=0.0
          ENDIF
          IF(CLOUD_FRACTION_CHANGE(I,J).LT.0.0)THEN
             CLOUD_FRACTION_CHANGE(I,J)=0.0
          ENDIF
c a second nested latitude/level restriction
             IF(SIN_TRUE_LATITUDE(I).GT.0.96.AND.J.GE.6.AND.J.LE.8.
     &         OR.SIN_TRUE_LATITUDE(I).LT.-0.96.AND.J.GE.9.AND.J.
     &         LE.19)THEN
          AREA_CLOUD_FRACTION_CHANGE(I,J)=AREA_CLOUD_FRACTION(I,J)*0.75
          CLOUD_FRACTION_CHANGE(I,J)=CLOUD_FRACTION(I,J)*0.75
c  ..if cloud is dec. beyond min then set to 0...
          IF(AREA_CLOUD_FRACTION_CHANGE(I,J).LT.0.0)THEN
```

```
            AREA_CLOUD_FRACTION_CHANGE(I,J)=0.0
          ENDIF
          IF(CLOUD_FRACTION_CHANGE(I,J).LT.0.0)THEN
            CLOUD_FRACTION_CHANGE(I,J)=0.0
          ENDIF
          ENDIF
c...below else-endif for lat/level restriction
           ELSE
          CLOUD_FRACTION_CHANGE(I,J)=CLOUD_FRACTION(I,J)
          AREA_CLOUD_FRACTION_CHANGE(I,J)=AREA_CLOUD_FRACTION(I,J)

          ENDIF
            END DO
           END DO
c
c change (day -4)
        ELSE IF(X_DAY_NUMBS.GT.0.64. AND.X_DAY_NUMBS.LT.0.68) THEN
c If within a certain timeframe increase cloud...
           write(*,*)'Changing day -4 cloud ',X_DAY_NUMBS
           DO I=1,P_FIELDDA
             DO J=1, Q_LEVELSDA
c...level and lat restriction
             IF(SIN_TRUE_LATITUDE(I).GT.0.86.AND.J.GE.4.AND.J.LE.9.
     &         OR.SIN_TRUE_LATITUDE(I).LT.-0.86.AND.J.GE.6.AND.J.
     &         LE.19)THEN
          AREA_CLOUD_FRACTION_CHANGE(I,J)=AREA_CLOUD_FRACTION(I,J)*0.85
          CLOUD_FRACTION_CHANGE(I,J)=CLOUD_FRACTION(I,J)*0.85
c  ..if cloud is dec. beyond min then set to 0...
          IF(AREA_CLOUD_FRACTION_CHANGE(I,J).LT.0.0)THEN
            AREA_CLOUD_FRACTION_CHANGE(I,J)=0.0
          ENDIF
          IF(CLOUD_FRACTION_CHANGE(I,J).LT.0.0)THEN
            CLOUD_FRACTION_CHANGE(I,J)=0.0
```

```
         ENDIF
c second nested latitude/height restriction
            IF(SIN_TRUE_LATITUDE(I).GT.0.96.AND.J.GE.6.AND.J.LE.8.
     &        OR.SIN_TRUE_LATITUDE(I).LT.-0.96.AND.J.GE.9.AND.J.
     &        LE.19)THEN
         AREA_CLOUD_FRACTION_CHANGE(I,J)=AREA_CLOUD_FRACTION(I,J)*0.80
         CLOUD_FRACTION_CHANGE(I,J)=CLOUD_FRACTION(I,J)*0.80
c  ..if cloud is dec. beyond min then set to 0...
         IF(AREA_CLOUD_FRACTION_CHANGE(I,J).LT.0.0)THEN
            AREA_CLOUD_FRACTION_CHANGE(I,J)=0.0
         ENDIF
         IF(CLOUD_FRACTION_CHANGE(I,J).LT.0.0)THEN
            CLOUD_FRACTION_CHANGE(I,J)=0.0
         ENDIF
         ENDIF
c...below else-endif for lat/level restriction
           ELSE
         CLOUD_FRACTION_CHANGE(I,J)=CLOUD_FRACTION(I,J)
         AREA_CLOUD_FRACTION_CHANGE(I,J)=AREA_CLOUD_FRACTION(I,J)

         ENDIF
            END DO
          END DO
c  Now cloud changes become positive (from day -6 to -4 negative)
c change (day -2)
        ELSE IF(X_DAY_NUMBS.GT.0.74.AND.X_DAY_NUMBS.LT.0.77) THEN
c If within a certain timeframe increase cloud...
          write(*,*)'Changing day -2 cloud ',X_DAY_NUMBS
          DO I=1,P_FIELDDA
            DO J=1, Q_LEVELSDA
c...level and lat restriction
            IF(SIN_TRUE_LATITUDE(I).GT.0.86.AND.J.GE.4.AND.J.LE.9.
     &        OR.SIN_TRUE_LATITUDE(I).LT.-0.86.AND.J.GE.6.AND.J.
```

```
     &        LE.19)THEN
          AREA_CLOUD_FRACTION_CHANGE(I,J)=AREA_CLOUD_FRACTION(I,J)*1.35
          CLOUD_FRACTION_CHANGE(I,J)=CLOUD_FRACTION(I,J)*1.35
c  ..if cloud is inc. beyond max then amp it down...
          IF(AREA_CLOUD_FRACTION_CHANGE(I,J).GT.1.0)THEN
c          write(*,*)'BENS CLOUD IS O.T.T!',I,J
             AREA_CLOUD_FRACTION_CHANGE(I,J)=1.0
          ENDIF
          IF(CLOUD_FRACTION_CHANGE(I,J).GT.1.0)THEN
             CLOUD_FRACTION_CHANGE(I,J)=1.0
          ENDIF
c second lat/height restriction nested below
             IF(SIN_TRUE_LATITUDE(I).GT.0.96.AND.J.GE.6.AND.J.LE.8.
     &         OR.SIN_TRUE_LATITUDE(I).LT.-0.96.AND.J.GE.9.AND.J.
     &         LE.19)THEN
          AREA_CLOUD_FRACTION_CHANGE(I,J)=AREA_CLOUD_FRACTION(I,J)*1.45
          CLOUD_FRACTION_CHANGE(I,J)=CLOUD_FRACTION(I,J)*1.45
c  ..if cloud is inc. beyond max then amp it down...
          IF(AREA_CLOUD_FRACTION_CHANGE(I,J).GT.1.0)THEN
c          write(*,*)'BENS CLOUD IS O.T.T!',I,J
             AREA_CLOUD_FRACTION_CHANGE(I,J)=1.0
          ENDIF
          IF(CLOUD_FRACTION_CHANGE(I,J).GT.1.0)THEN
             CLOUD_FRACTION_CHANGE(I,J)=1.0
          ENDIF
          ENDIF
c...below else-endif for lat/level restriction
            ELSE
          CLOUD_FRACTION_CHANGE(I,J)=CLOUD_FRACTION(I,J)
          AREA_CLOUD_FRACTION_CHANGE(I,J)=AREA_CLOUD_FRACTION(I,J)

          ENDIF
             END DO
```

```
          END DO
c change (day -1)
        ELSE IF(X_DAY_NUMBS.GT.0.78.AND.X_DAY_NUMBS.LT.0.80) THEN
c If within a certain timeframe increase cloud...
          write(*,*)'Changing day -1 cloud ',X_DAY_NUMBS
          DO I=1,P_FIELDDA
            DO J=1, Q_LEVELSDA
c...level and lat restriction
            IF(SIN_TRUE_LATITUDE(I).GT.0.86.AND.J.GE.4.AND.J.LE.9.
     &        OR.SIN_TRUE_LATITUDE(I).LT.-0.86.AND.J.GE.6.AND.J.
     &        LE.19)THEN
          AREA_CLOUD_FRACTION_CHANGE(I,J)=AREA_CLOUD_FRACTION(I,J)*1.60
          CLOUD_FRACTION_CHANGE(I,J)=CLOUD_FRACTION(I,J)*1.60
c  ..if cloud is inc. beyond max then amp it down...
          IF(AREA_CLOUD_FRACTION_CHANGE(I,J).GT.1.0)THEN
             AREA_CLOUD_FRACTION_CHANGE(I,J)=1.0
          ENDIF
          IF(CLOUD_FRACTION_CHANGE(I,J).GT.1.0)THEN
             CLOUD_FRACTION_CHANGE(I,J)=1.0
          ENDIF
c second nested latitude/height restriction below
             IF(SIN_TRUE_LATITUDE(I).GT.0.96.AND.J.GE.6.AND.J.LE.8.
     &        OR.SIN_TRUE_LATITUDE(I).LT.-0.96.AND.J.GE.9.AND.J.
     &        LE.19)THEN
          AREA_CLOUD_FRACTION_CHANGE(I,J)=AREA_CLOUD_FRACTION(I,J)*1.75
          CLOUD_FRACTION_CHANGE(I,J)=CLOUD_FRACTION(I,J)*1.75
c  ..if cloud is inc. beyond max then amp it down...
          IF(AREA_CLOUD_FRACTION_CHANGE(I,J).GT.1.0)THEN
             AREA_CLOUD_FRACTION_CHANGE(I,J)=1.0
          ENDIF
          IF(CLOUD_FRACTION_CHANGE(I,J).GT.1.0)THEN
             CLOUD_FRACTION_CHANGE(I,J)=1.0
          ENDIF
```

```
         ENDIF
c...below else-endif for lat/level restriction
           ELSE
         CLOUD_FRACTION_CHANGE(I,J)=CLOUD_FRACTION(I,J)
         AREA_CLOUD_FRACTION_CHANGE(I,J)=AREA_CLOUD_FRACTION(I,J)

         ENDIF
            END DO
          END DO
c
c change (day 0)
        ELSE IF(X_DAY_NUMBS.GT.0.81.AND.X_DAY_NUMBS.LT.0.84) THEN
c If within a certain timeframe increase cloud...
          write(*,*)'Changing day 0 cloud ',X_DAY_NUMBS
          DO I=1,P_FIELDDA
            DO J=1, Q_LEVELSDA
c...level and lat restriction
            IF(SIN_TRUE_LATITUDE(I).GT.0.86.AND.J.GE.4.AND.J.LE.9.
     &        OR.SIN_TRUE_LATITUDE(I).LT.-0.86.AND.J.GE.6.AND.J.
     &        LE.19)THEN
         AREA_CLOUD_FRACTION_CHANGE(I,J)=AREA_CLOUD_FRACTION(I,J)*1.90
         CLOUD_FRACTION_CHANGE(I,J)=CLOUD_FRACTION(I,J)*1.90
c  ..if cloud is inc. beyond max then amp it down...
         IF(AREA_CLOUD_FRACTION_CHANGE(I,J).GT.1.0)THEN
            AREA_CLOUD_FRACTION_CHANGE(I,J)=1.0
         ENDIF
         IF(CLOUD_FRACTION_CHANGE(I,J).GT.1.0)THEN
            CLOUD_FRACTION_CHANGE(I,J)=1.0
         ENDIF
c second nested lat/height restriction below
            IF(SIN_TRUE_LATITUDE(I).GT.0.96.AND.J.GE.6.AND.J.LE.8.
     &        OR.SIN_TRUE_LATITUDE(I).LT.-0.96.AND.J.GE.9.AND.J.
     &        LE.19)THEN
```

```
          AREA_CLOUD_FRACTION_CHANGE(I,J)=AREA_CLOUD_FRACTION(I,J)*1.99
          CLOUD_FRACTION_CHANGE(I,J)=CLOUD_FRACTION(I,J)*1.99
c  ..if cloud is inc. beyond max then amp it down...
          IF(AREA_CLOUD_FRACTION_CHANGE(I,J).GT.1.0)THEN
             AREA_CLOUD_FRACTION_CHANGE(I,J)=1.0
          ENDIF
          IF(CLOUD_FRACTION_CHANGE(I,J).GT.1.0)THEN
             CLOUD_FRACTION_CHANGE(I,J)=1.0
          ENDIF
          ENDIF
c...below else-endif for lat/level restriction
            ELSE
          CLOUD_FRACTION_CHANGE(I,J)=CLOUD_FRACTION(I,J)
          AREA_CLOUD_FRACTION_CHANGE(I,J)=AREA_CLOUD_FRACTION(I,J)

          ENDIF
             END DO
           END DO
c change (day +1)
        ELSE IF(X_DAY_NUMBS.GT.0.86.AND.X_DAY_NUMBS.LT.0.89) THEN
c If within a certain timeframe increase cloud...
           write(*,*)'Changing day +1 cloud ',X_DAY_NUMBS
           DO I=1,P_FIELDDA
             DO J=1, Q_LEVELSDA
c...level and lat restriction
             IF(SIN_TRUE_LATITUDE(I).GT.0.86.AND.J.GE.4.AND.J.LE.9.
     &         OR.SIN_TRUE_LATITUDE(I).LT.-0.86.AND.J.GE.13.AND.J.
     &         LE.19)THEN
          AREA_CLOUD_FRACTION_CHANGE(I,J)=AREA_CLOUD_FRACTION(I,J)*1.60
          CLOUD_FRACTION_CHANGE(I,J)=CLOUD_FRACTION(I,J)*1.60
c  ..if cloud is inc. beyond max then amp it down...
          IF(AREA_CLOUD_FRACTION_CHANGE(I,J).GT.1.0)THEN
             AREA_CLOUD_FRACTION_CHANGE(I,J)=1.0
```

```
          ENDIF
          IF(CLOUD_FRACTION_CHANGE(I,J).GT.1.0)THEN
             CLOUD_FRACTION_CHANGE(I,J)=1.0
          ENDIF
c second nested lat/height restriction below
             IF(SIN_TRUE_LATITUDE(I).GT.0.96.AND.J.GE.6.AND.J.LE.8.
     &         OR.SIN_TRUE_LATITUDE(I).LT.-0.96.AND.J.GE.9.AND.J.
     &         LE.19)THEN
          AREA_CLOUD_FRACTION_CHANGE(I,J)=AREA_CLOUD_FRACTION(I,J)*1.75
          CLOUD_FRACTION_CHANGE(I,J)=CLOUD_FRACTION(I,J)*1.75
c  ..if cloud is inc. beyond max then amp it down...
          IF(AREA_CLOUD_FRACTION_CHANGE(I,J).GT.1.0)THEN
             AREA_CLOUD_FRACTION_CHANGE(I,J)=1.0
          ENDIF
          IF(CLOUD_FRACTION_CHANGE(I,J).GT.1.0)THEN
             CLOUD_FRACTION_CHANGE(I,J)=1.0
          ENDIF
          ENDIF
c...below else-endif for lat/level restriction
            ELSE
          CLOUD_FRACTION_CHANGE(I,J)=CLOUD_FRACTION(I,J)
          AREA_CLOUD_FRACTION_CHANGE(I,J)=AREA_CLOUD_FRACTION(I,J)

          ENDIF
             END DO
           END DO
c
c change (day +2)
         ELSE IF(X_DAY_NUMBS.GT.0.90.AND.X_DAY_NUMBS.LT.0.94) THEN
c If within a certain timeframe increase cloud...
           write(*,*)'Changing day +2 cloud ',X_DAY_NUMBS
           DO I=1,P_FIELDDA
             DO J=1, Q_LEVELSDA
```

```
c...level and lat restriction
            IF(SIN_TRUE_LATITUDE(I).GT.0.86.AND.J.GE.4.AND.J.LE.9.
     &        OR.SIN_TRUE_LATITUDE(I).LT.-0.86.AND.J.GE.6.AND.J.
     &        LE.19)THEN
          AREA_CLOUD_FRACTION_CHANGE(I,J)=AREA_CLOUD_FRACTION(I,J)*1.30
          CLOUD_FRACTION_CHANGE(I,J)=CLOUD_FRACTION(I,J)*1.30
c  ..if cloud is inc. beyond max then amp it down...
          IF(AREA_CLOUD_FRACTION_CHANGE(I,J).GT.1.0)THEN
             AREA_CLOUD_FRACTION_CHANGE(I,J)=1.0
          ENDIF
          IF(CLOUD_FRACTION_CHANGE(I,J).GT.1.0)THEN
             CLOUD_FRACTION_CHANGE(I,J)=1.0
          ENDIF
c second nested lat/height restriction
             IF(SIN_TRUE_LATITUDE(I).GT.0.96.AND.J.GE.6.AND.J.LE.8.
     &        OR.SIN_TRUE_LATITUDE(I).LT.-0.96.AND.J.GE.9.AND.J.
     &        LE.19)THEN
          AREA_CLOUD_FRACTION_CHANGE(I,J)=AREA_CLOUD_FRACTION(I,J)*1.45
          CLOUD_FRACTION_CHANGE(I,J)=CLOUD_FRACTION(I,J)*1.45
c  ..if cloud is inc. beyond max then amp it down...
          IF(AREA_CLOUD_FRACTION_CHANGE(I,J).GT.1.0)THEN
             AREA_CLOUD_FRACTION_CHANGE(I,J)=1.0
          ENDIF
          IF(CLOUD_FRACTION_CHANGE(I,J).GT.1.0)THEN
             CLOUD_FRACTION_CHANGE(I,J)=1.0
          ENDIF
          ENDIF
c...below else-endif for lat/level restriction
            ELSE
          CLOUD_FRACTION_CHANGE(I,J)=CLOUD_FRACTION(I,J)
          AREA_CLOUD_FRACTION_CHANGE(I,J)=AREA_CLOUD_FRACTION(I,J)

          ENDIF
```

```
            END DO
          END DO
          ELSE
c...if outside either timeframe make cloud equal to norm cloud.
          write(*,*)'A non C.change day',X_DAY_NUMBS
          DO I=1,P_FIELDDA
            DO J=1, Q_LEVELSDA
          AREA_CLOUD_FRACTION_CHANGE(I,J)=AREA_CLOUD_FRACTION(I,J)
         CLOUD_FRACTION_CHANGE(I,J)=CLOUD_FRACTION(I,J)
            END DO
          END DO
          ENDIF
*/ *D = Replace code with this line to remove original call Sin_t..
*D APBBF401.9
*D APBBF401.10
*D APBBF401.11
*D APBBF401.12
*D APBBF401.13
*D APBBF401.14
*D RAD_CTL1.258
*D RAD_CTL1.259
*D RAD_CTL1.260
*/ *D = Replace the following lines (or range of lines) with some code
*D RAD_CTL1.416
*/ Change call to SWRAD
     &     D1(JPSTAR+JS),AKH,BKH,CLOUD_FRACTION_CHANGE(FIRST_POINT,1),
*D AWI1F403.322
*/ Change call to SWRAD
     &    D1(JPSTAR+JS),AKH,BKH,CLOUD_FRACTION_CHANGE(FIRST_POINT,1),
*D ASK1F405.269
*/ Change call to R2_SWRAD
     &        AREA_CLOUD_FRACTION_CHANGE(FIRST_POINT,1),
*D ADB1F400.174
```

```
*/ Change call to R2_SWRAD
     &        CLOUD_FRACTION_CHANGE(FIRST_POINT,1),
*D ASK1F405.270
*/ change call to CALL SWDKDI
     &    AREA_CLOUD_FRACTION_CHANGE(START_POINT_NO_HALO,1),
*D ADB1F400.258
*/ Change call to LWRAD
     &        CLOUD_FRACTION_CHANGE(FP_LOCAL(I),1),
*D ASK1F405.272
*/ Change call to R2_LWRAD
     &        AREA_CLOUD_FRACTION_CHANGE(FP_LOCAL(I),1),
*D ADB1F400.316
*/ Change call to R2_LWRAD
     &        CLOUD_FRACTION_CHANGE(FP_LOCAL(I),1),
*/ -- End of Mod --
```

Appendix 6 Personal communiqué from Professor Brian Tinsley

Personal communiqué referenced in thesis as (Tinsley, 2010). The message is presented below in its original and unedited form (reproduced with permission from Professor Brian Tinsley (Department of Physics, University of Texas, Dallas)).

Concerning the CMAS mechanism (Charge Modulation of Aerosol Scavenging)which has also been called the 'near cloud mechanism', the reduced ionization during a Forbush decrease reduces Jz, but if the shape of the vertical profile of potential remains the same with a constant ionospheric potential, then the electric field gradients at the gradients of conductivity will not change, and the equilibrium space charge will not change. But the aerosol particles and the droplets take tens of minutes to hours to charge, and this is comparable with the dynamic timescale of cloud development. Because the rate of charging increases with increasing ion concentration, this will affect the amount of CMAS. However, the ionospheric potential will change somewhat as the Forbush decrease affects the thunderstorm generators, and the shape of the vertical profile changes somewhat. So my summary is that we don't have good enough analytical theory or models to say what should happen according to theory in a rapid onset Forbush decrease, let alone the difference between a rapid onset and a slow onset one.

Brian A Tinsley, Professor
MS WT15, Center for Space Sciences
University of Texas at Dallas
800 W Campbell Rd.,
Richardson, TX, 75080-3021, USA
Ph.: 972 883 2838
e-mail: Tinsley@UTDallas.edu
http://www.utdallas.edu/physics/faculty/tinsley.html

References

Arnold, F. (2006). 'Atmospheric aerosols and cloud condensation nuclei formation: a possible influence of cosmic rays?' *Space Science Reviews*. **125**: 169–186

Arnold, F. (2008). 'Atmospheric ions and aerosol formation'. *Space Science Reviews*. **137**: 225–239

CCSP (2008). '*Climate Models: An Assessment of Strengths and Limitations.'* A Report by the U.S. Climate Change Science Program and the Subcommittee on Global Change Research [Bader D.C., C. Covey, W.J. Gutowski Jr., I.M. Held, K.E. Kunkel, R.L. Miller, R.T. Tokmakian & M.H. Zhang (Authors)]. Department of Energy, Office of Biological and Environmental Research, Washington, D.C., USA, 124 pp

Barkstrom, B. R., Harrison, E., Smith, G., Green, R., Kibler, J., Cess, R. & TEAM, A.T.E.S. (1989). 'Earth Radiation Budget Experiment (ERBE) archival and April 1985 results'. *Bulletin of the American Meteorological Society*. **70**: 1254–1262

Bazilevskaya, G.A. & Svirzhevskaya, A.K. (1998). 'On the stratospheric measurements of cosmic rays'. *Space Science Reviews*. **85**: 431–521

Beard, K. V., Ochs, H. T. & Twohy, C. H. (2004). 'Aircraft measurements of high average charges on cloud drops in layer clouds'. *Geophysical Research Letters*. **31**: L14111

Berezhko, E.G. (2008). 'Cosmic ray acceleration by supernova shocks'. *Advances in Space Research*. **41**: 429–441

Bering, E.A., Few, A.A. & Benbrook, J.R. (1999). 'The global electric circuit'. *Physics Today*. **51**: 24–30

Bond, G.C. & Lotti, R. (1995). 'Iceberg discharges into the North Atlantic on millennial time scales during the last glaciation'. *Science*. **267**: 1005–1010

Bond, G., Kromer, B., Beer, J., Muscheler, R., Evans, M.N., Showers, W., Hoffmann, S., Lotti-Bond, R., Hajdas, I. & Bonani, G. (2001). 'Persistent solar influence on North Atlantic climate during the Holocene'. *Science*. **294**: 2130–2136

Bond, G., Showers, W., Cheseby, M., Lotti, R., Almasi, P., Demenocal, P., Priore, P., Cullen, H., Hajdas, I. & Bonani, G. (1997). 'A pervasive millennial-scale cycle in North Atlantic Holocene and glacial climates'. *Science*. **278**: 1257–1266

Boy, M., Kazil, J., Lovejoy, E.R., Guenther, A. & Kulmala, M. (2008). 'Relevance of ion-induced nucleation of sulphuric acid and water in the lower troposphere over the boreal forest at northern latitudes'. *Atmospheric Research*. **90**: 151–158

Broecker, W.S. (2001). 'Was the medieval warm period global?' *Science*. **291**: 1497–1499

Bromwich, D.H. & Wang, S.H. (2005). 'Evaluation of the NCEP–NCAR and ECMWF 15- and 40-yr reanalyses using rawinsonde data from two independent Arctic field experiments'. *Monthly Weather Review*. **133**: 3562–3578

Burns, G.B., Tinsley, B.A., Frank-Kamenetsky, A.V. & Bering, E.A. (2007). 'Interplanetary magnetic field and atmospheric electric circuit influences on ground-level pressure at Vostok'. *Journal of Geophysical Research - Atmospheres*. **112**: D04103

Bushell, A.C. (1998). *Unified Model User Guide*. Version 4.4. The Meteorological Office, Reading, UK: 192pp

Butler, C.J., Garcia-Suarez, A. & Pallé, E. (2008). 'Trends and cycles in long Irish meteorological series'. *Biology & Environment: Proceedings of the Royal Irish Academy*. **107**: 157–165

Calogovic, J., Albert, C., Arnold, F., Beer, J., Desorgher, L. & Flueckiger, E. O. (2010). 'Sudden cosmic ray decreases: no change of global cloud cover'. *Geophysical Research Letters*. **37**: L03802

Camp, C.D. & Tung, K.K. (2007). 'Surface warming by the solar cycle as revealed by the composite mean difference projection'. *Geophysical Research Letters*. **34**: L14703

Campbell, G. (2004). 'View angle dependence of cloudiness and the trend in ISCCP cloudiness'. In *13th Conference on Satellite Meteorology and Oceanography*. Norfolk. American Meteorological Society

Campbell, G. (2006). 'Diurnal and angular variability of cloud detection: consistency between polar and geosynchronous ISCCP products'. In *14th Conference on Satellite Meteorology and Oceanography. Florida*

Carslaw, K. (2009). 'Cosmic rays, clouds and climate'. *Nature*. **460**: 332–333

Carslaw, K.S., Harrison, R.G. & Kirkby, J. (2002). 'Cosmic rays, clouds, and climate'. *Science*. **298**: 1732–1737

Charlson, R.J., Lovelock, J.E., Andreae, M.O. & Warren, S.G. (1987). 'Oceanic phytoplankton, atmospheric sulphur, cloud albedo and climate'. *Nature*. **326**: 655–661

Chen, J., Wan, G., Zhang, D. D., Chen, Z., Xu, J., Xiaot, T. & Huang, R. (2005). 'The 'Little Ice Age' recorded by sediment chemistry in Lake Erhai, southwest China'. *The Holocene*. **15:** 925–931

Christian, H.J., Blakeslee, R.J., Boccippio, D.J., Boeck, W.L., Buechler, D.E., Driscoll, K.T., Goodman, S.J., Hall, J.M., Koshak, W.J., Mach, D.M. & Stewart, M. (2003). 'Global frequency and distribution of lightning as observed from space by the Optical Transient Detector'. *Journal of Geophysical Research*. **108**: ACL4.1-4.15

Clarke, A.D., Davis, D., Kapustin, V.N., Eisele, F.L., Chen, G., Paluch, I., Lenschow, D., Bandy, A.R., Thornton, D., Moore, K., Mauldin, L., Tanner, D.J., Litchy, M., Carroll, M.A., Collins, J. & Albercook, G. (1998). 'Particle nucleation in the tropical boundary layer and its coupling to marine sulfur sources'. *Science*. **282**: 89–92

Costa, E., Dunbar, R.B., Kryc, K.A., Mucciarone, D.A., Brachfeld, S., Roark, E.B., Manley, P.L., Murray, R.W. & Leventer, A. (2007). 'Solar forcing and El Niño-Southern Oscillation (ENSO) influences on productivity cycles interpreted from a late-Holocene high-resolution marine sediment record, Adélie drift, East Antarctic margin'. *U.S. Geological Survey and The National Academies*. USGS OF-2007–1047

Coughlin, K. & Tung, K.K. (2004). 'Eleven-year solar cycle signal throughout the lower atmosphere'. *Journal of Geophysical Research*. **109**: D21105.1-7

Courtillot, V., Gallet, Y., Le Mouël, J.L., Fluteau, F., Genevey, A. (2007). 'Are there connections between the Earth's magnetic field and climate?' *Earth and Planetary Science Letters*. **235**: 328–339

Dahl-Jensen, D., Mosegaard, K., Gundestrup, N., Clow, G.D., Johnsen, S.J., Hansen, A.W. & Balling, N. (1998). 'Past temperatures directly from the Greenland ice sheet'. *Science.* **282**: 268–271

Dean, S.M., Lawrence, B.N., Grainger, R.G. & Heuff, D.N. (2005). 'Orographic cloud in a GCM: the missing cirrus'. *Climate Dynamics*. **24**: 771–780

Dengel, S., Aeby, D. & Grace, J. (2009). 'A relationship between galactic cosmic radiation and tree rings'. *New Phytologist.* **184:** 545–551

Douglass, D.H. & Clader, B.D. (2002). 'Climate sensitivity of the Earth to solar irradiance'. *Geophysical Research Letters.* **29**: 33.1-4

Duplissy, J., Enghoff, M., Aplin, L., Arnold, F., Aufmhoff, H., Avngaard, M., Baltensperger, U., Bondo, T., Bingham, R., Carslaw, K., Curtis, J., David, A., Fastrup, B., Gagné, S., Hahn, F., Harrison, R.G., Kellet, B., Kirkby, J., Kulmala, M., Laakso, L., Laaksonen, A., Lillestol, E., Lockwood, M., Mäkelä, J., Makhmutov, V., Marsh, N., Nieminen, T., Onnela, A., Pedersen, E., Pedersen, J., Polny, J., Reichl, U., Seinfeld, J., Siplä, M., Stozhkov, Y., Stratmann, F., Svensmark, H., Svensmark, J., Veenhof, R., Viisanen, Y., Wagner, P., Wehrle, G., Weingartner, E., Wex, H., Wihelmsson, M. & Winkler, P. (2010). 'Results from the CERN pilot CLOUD experiment'. *Atmospheric Chemistry and Physics*. **10**: 1635–1647

Eddy, J.A. (1976). 'The Maunder minimum'. *Science*. **192**: 1189–1202

Egrova, L.V., Vovk, V.Y. & Troshichev, O.A. (2000). 'Influence of variations of the cosmic rays on atmospheric pressure and temperature in the Southern geomagnetic pole region'. *Journal of Atmospheric and Solar-Terrestrial Physics*. **62**: 955–966

Egrova, L., Vovk, V.Y. & Troshichev, O. (2000). 'Influence of variations of the cosmic rays on atmospheric pressure and temperature in the southern geomagnetic pole region'. *Journal of Atmospheric and Solar-Terrestrial Physics*. **62**: 955–966

Ermakov, V.I., Bazilevskaya, G.A., Pokrevsky, P.E. & Stozhkov, Y.I. (1997). 'Ion balance equation in the atmosphere'. *Journal of Geophysical Research.* **102**: 23413–23420

Evan, A.T., Heidinger, A.K. & Vimont, D.J. (2007). 'Arguments against a physical long-term trend in global ISCCP cloud amounts'. *Geophysical Research Letters.* **34**: L04701

Fabrikant, I.I. (2007). 'Dissociative electron attachment on surfaces and in bulk media'. *Physical Review Letters*. **76**: 012902-1-012914

Farrar, P.D. (2000). 'Are cosmic rays influencing oceanic cloud coverage – or is it only El Niño?' *Climatic Change*. **47**: 7–15

Fleitmann, D., Burns, S.J., Mudelsee, M., Neff, U., Kramers, J., Mangini, A. & Matte, A. (2003). 'Holocene forcing of the Indian monsoon recorded in a stalagmite from southern Oman'. *Science*. **300**: 1737–1739

Floyd, L.E., Prinz, D.K., Crane, P.C. & Herring, L.C. (2002). 'Solar cycle UV irradiance variation during cycles 22 and 23'. *Advances in Space Research*. **29**: 1957–1962

Floyd, L., Rottman, R., Deland, M. & Pap, J. (2003). '11 years of solar UV irradiance measurements from UARS'. In *Solar Variability as an Input to the Earth's Environment. International Solar Cycle Studies (ISCS) Symposium.* **535**: 195–203

Flueckiger, E., Bűtikofer, R., Moser, M. & Desorgher, L. (2005). 'The cosmic ray ground level enhancement during the Forbush decrease in January 2005'. In Proceedings of the 29th International Cosmic Ray Conference [Acharya, B.S., Gupta, S., Jagadeesan, P., Jain, A., Karthikeyan, S., Morris, S. & Tonwar, S. (eds.)]. Tata Institute of Fundamental Research. Mumbai

Forbush, S.E. (1993). '*Cosmic rays, the sun and geomagnetism: the works of Scott E. Forbush'.[Van Allen, J.A. (eds.)]*. American Geophysical Union. Washington, D.C., 472pp

Foukal, P., North, G. & Wigley, T. (2004). 'A stellar view on solar variations and climate'. *Science*. **306**: 68–69

Friis-Christensen, E. & Lassen, K. (1991). 'Length of the solar cycle–an indicator of solar activity closely associated with climate'. *Science.* **254**: 698–700

Fröhlich, C. (2006). 'Solar irradiance variability since 1978: revision of the PMOD composite during solar cycle 21'. *Space Science Reviews*. **125**: 53–65

Garcin, Y., Williamson, D., Bergonzini, L., Radakovitch, O., Vincens, A., Buchet, G., Guiot, J., Brewer, S., Mathe, P.E. & Majule, A. (2007). 'Solar and anthropogenic imprints on Lake Masoko (southern Tanzania) during the last 500 years'. *Journal of Paleolimnology*. **37**: 475–490

Gleckler, P.J., Taylor, K.E. & Doutriaux, C. (2008). 'Performance metrics for climate models'. *Journal of Geophysical Research*. **113**: D01604

Gleeson, L.J. & Axford, W.I. (1968). 'Solar modulation of galactic cosmic rays'. *Astrophysical Journal*. **154**: 1011–1026

Gleisner, H., Thejll, P., Stendel, M., Kaas, E. & Machenhauer, B. (2005). 'Solar signals in tropospheric re-analysis data: comparing NCEP/NCAR and ERA40'. *Journal of Atmospheric and Solar-Terrestrial Physics*. **67**: 785–791

Gray, L.J, Haigh, J.D. & Harrison, R.G., (2005). 'The influence of solar changes on the Earth's climate'. *Hadley Centre Technical Note*. 62

Griffiths, R.F., Latham, J. & Myers, V. (1974). 'The ionic conductivity of electrified clouds'. *Quarterly Journal of the Royal Meteorological Society.* **100**: 181–190

Grousset, F.E., Pujol, C.E., Labeyrie, L., Auffret, G. & Boelaert, A. (2000). 'Were the North Atlantic Heinrich events triggered by the behaviour of the European ice sheets?' *Geology*. **28**: 123–126

Grün, E., Gustafson, B.E., Mann, I., Baguhl, M., Morfill, G.E., Staubach, P., Taylor, A. & Zook, H.A. (1994). 'Interstellar dust in the heliosphere'. *Astronomy and Astrophysics*. **286**: 915–924

Gupta, A.K., Anderson, D.M. & Overpeck, J.T. (2003). 'Abrupt changes in the Asian southwest monsoon during the Holocene and their links to the North Atlantic Ocean'. *Nature*. **421**: 354–357

Haigh, J. (1996). 'The impact of solar variability on climate'. *Science*. **272**: 981–984

Haigh, J.D. (2003). 'The effects of solar variability on the Earth's climate'. *Philosophical Transactions of the Royal Society of London Series A-Mathematical Physical and Engineering Sciences*. **361**: 95–111

Haigh, J.D. (2007). 'The Sun and the Earth's climate'. *Living Reviews in Solar Physics*. **4**: 2 http://www.livingreviews.org/lrsp-2007-2 (assessed on 01/12/2009)

Haigh, J. & Blackburn, M. (2006). 'Solar influences on dynamical coupling between the stratosphere and troposphere'. *Space Science Reviews*. **125**: 331–344

Harrison, R.G. (2004). 'The global atmospheric electrical circuit and climate'. *Surveys in Geophysics*. **25**: 441–484

Harrison, R.G. & Ambaum, M.H.P. (2009). 'Observed atmospheric electricity effect on clouds'. *Environmental Research Letters*. **4**: 014003

Harrison, R.G. & Carslaw, K.S. (2003). 'Ion-aerosol-cloud processes in the lower atmosphere'. *Reviews of Geophysics*. **41**: 1012

Hatton, A.D. (2002). 'Influence of photochemistry on the marine biogeochemical cycle of dimethylsulphide in the northern North Sea'. *Deep Sea Research Part II: Topical Studies in Oceanography*. **49**: 3039–3052

Hatzianastassiou, N., Matsoukas, C., Fotiadi, A., Pavlakis, K.G., Drakakis, E., Hatzidimitriou, D. & Vardavas, I. (2005). 'Global distribution of Earth's surface shortwave radiation budget'. *Atmospheric Chemistry and Physics Discussions.* **5**: 4545–4597

Hays, P.B. & Roble, R.G. (1979). 'A quasi-static model of global atmospheric electricity. 1. The lower atmosphere'. *Journal of Geophysical Research*. **84**: 3291–3305

Hefu, Y. & Kirst, G.O. (1997). 'Effect of UV radiation on DMSP content and DMS formation of Phaeocystis'. *Polar Biology*. **18**: 402–409

Heinrich, H. (1988). 'Origin and consequences of cyclic ice rafting in the northeast Atlantic ocean during the past 130,000 years'. *Quaternary Research.* **29:** 142–152

Herman, J.R. & Goldberg, R.A. (1978). *Sun, Weather and Climate,* Dover Pubns, Washington D.C., 372pp

Herschel, W. (1801). 'Observations tending to investigate the nature of the Sun, in order to find the causes and symptoms of its variable emission of light and heat'. *Philosphical Transactions of the Royal Society*. **91**: 261–331

Hines, K.M., Bromwich, D.H. & Marshall, G.J. (2000). 'Artificial surface pressure trends in the NCEP–NCAR Reanalysis over the Southern Ocean and Antarctica'. *Journal of Climate*. **13**: 3940–3952

Hodell, D.A., Brenner, M., Curtis, J.H., Medina-González, R., Can, E.I.C., Albornaz-Pat, A. & Guilderson, T.P. (2005). 'Climate change on the Yucatan peninsula during the Little Ice Age'. *Quaternary Research.* **63**: 109–121

Horrak, U., Salm, J. & Tammeth, H. (1998). 'Bursts of intermediate ions in atmospheric air'. *Journal of Geophysical Research*. **103**: 13909–13916

Hoyt, D.V. & Schatten, K.H. (1993). 'A discussion of plausible solar irradiance variations, 1700-1992'. *American Geophysical Union*. **98**: 18895–18906

IPCC (2001). *Climate Change 2001: The Scientific Basis.* [Houghton, J.T., Ding, Y., Griggs, D.J., Nouger, M., Linden, van der Linden, P.J., Dai, X., Maskell, K., & Johnson, C.A. (eds.)] Contributions of Working Group I to the Third Assessment Report of the Intergovernmental Panel on Climate Change. Cambridge University Press: Cambridge

IPCC (2007). Summary for policy makers. In: Climate Change 2007: The Physical Science Basis. Contribution of working Group I to the Fourth Assessment Report of the Intergovernmental Panel on Climate Change [Solomon, S., Qin, D., Manning, M., Chen, Z., Marquis, M., Averyt, K.B., Tignor, M. & Miller H.L. (eds.)]. Cambridge University Press: Cambridge

Iida, K., Stolzenburg, M., McMurry, P. & Smith, J. (2008). 'Estimating nanoparticle growth rates from size-dependent charged fractions: analysis of new particle formation events in Mexico City'. *Journal of Geophysical Research*. **113**: D05207

Jacobwitz, H., Stowe, L., Ohring, G., Heidinger, A., Knapp, K. & Nalli, N. (2003). 'The Advanced Very High Resolution Radiometer Pathfinder Atmosphere (PATMOS) climate dataset: a resource for climate research'. *Bulletin of the American Meteorological Society*. **84**: 785–793

Jaecker-Voirol, A. & Mirabel, P. (1989). 'Heteromolecular nucleation in the sulfuric acid-water system'. *Atmospheric Environment*. **23**: 2053–2057

Jirikowich, J. L. & Pallé, E. (1994). 'The medieval solar activity maximum'. *Climate Change*. **26**: 309–316

Kalnay, E., Kanamitsu, M., Kistler, R., Collins, W., Deaven, D., Gandin, L., Iredella, M., Saha, S., White, G., Woollen, J., Zhu, Y., Leetmaa, A., Reynolds, R., Chelliah, M., Ebisuzaki, W., Higgins, W., Janowiak, J., Mo, K.C., Ropelewski, C., Wang, J., Jenne, R. & Joseph, D. (1996). 'The NCEP/NCAR 40-Year Reanalysis Project'. *Bulletin of the American Meteorological Society.* **77**: 437–471

Kanamitsu, M., Kistler, R.E. & Reynolds, R.W. (1997). 'NCEP/NCAR reanalysis and the use of satellite data'. *Advances in Space Research*. **19**: 481–489

Kärcher, B. & Ström, J. (2003). 'The roles of dynamical variability and aerosols in cirrus cloud formation'. *Atmospheric Chemistry and Physics*. **3**: 823–838

Kastkina, E., Shumilov, O., Lukina, N.V., Krapiec, M. & Jacoby, G. (2006). 'Stardust component in tree rings'. *Dendochronologia*. **24**: 131–135

Kazil, J., Harrison, R.G. & Lovejoy, N. (2008). 'Tropospheric new particle formation and the role of ions'. *Space Science Reviews*. **137**: 241–255

Kazil, J., Lovejoy, E.R., Barth, M.C., O'Brien, K. (2006). 'Aerosol nucleation over oceans and the role of galactic cosmic rays'. *Atmospheric Chemistry and Physics*. **6**: 4905–4924

Kiendler, A. & Arnold, F. (2002). 'Unambiguous identification and measurement of sulfuric acid cluster chemiions in aircraft jet engine exhaust'. *Atmospheric Environment*. **36**: 1757–1761

Kirkby, J. (2007). 'Cosmic rays and climate'. *Surveys in Geophysics*. **28**: 333–375

Knapp, K. (2008). 'Calibration assessment of ISCCP geostationary infrared observations using HIRS'. *Journal of Atmospheric and Oceanic Technology*. **25**: 183–195

Kniveton, D.R. (2004). 'Precipitation, cloud cover and Forbush decreases in galactic cosmic rays'. *Journal of Atmospheric and Solar-Terrestrial Physics*. **66**: 1135–1142

Kniveton, D.R. & Todd, M.C. (2001). 'On the relationship of cosmic ray flux and precipitation'. *Geophysical Research Letters*. **28**: 1527–1530

Kniveton, D.R., Tinsley, B.A., Burns, G., Bering, E.A. & Troshichev, O.A. (2007). 'Variations in global cloud cover and the fair-weather vertical electric field'. *Journal of Atmospheric and Solar-Terrestrial Physics*. **70**: 1633–1642

Kniveton, D.R., Todd, M.C., Sciare, J. & Mihalopoulos, N. (2003). 'Variability of atmospheric dimethylsulphide over the southern Indian ocean due to changes in ultraviolet radiation'. *Global Biogeochemical Cycles*. **17**: 7.1–7.6

Kristjánsson, J.E. & Kristiansen, J. (2000). 'Is there a cosmic ray signal in recent variations in global cloudiness and cloud radiative forcing?' *Journal of Geophysical Research-Atmospheres*. **105**: 11851–11863

Kristjansson, J.E., Stjern, C.W., Stordal, F., Færaa, A.M., Myhre, G. & Jonasson, K. (2008). 'Cosmic rays, cloud condensation nuclei and clouds – a reassessment using MODIS data'. *Atmospheric Chemistry and Physics*. **8**: 7373–7387

Krivova, N.A., Balmacedal, L. & Solanki, S.K. (2007). 'Reconstruction of solar total irradiance since 1700 from the surface magnetic flux'. *Astronomy and Astrophysics*. **467:** 335–346

Krivova, N.A., Solanki, S.K. & Floyd, L. (2006). 'Reconstruction of solar UV irradiance in cycle 23'. *Astronomy and Astrophysics*. **452**: 631–639

Krivova, N.A., Solanki, S.K., Wenzler, T. & Podlipnik, B. (2009). 'Reconstruction of solar UV irradinace since 1974'. *Journal of Geophysical Research.* **114**: D00104

Krüger, H. & Grün, E. (2008). 'Interstellar dust inside and outside the heliosphere'. *Space Science Reviews*. **143**: 347–356

Kulamla, M., Riipinen, I., Nieminen, T., Hulkkonen, M., Sogacheva, L., Manninen, H., Paasonen, P., Petäjä, T., Dal Maso, M.D., Aalto, P., Viljanen, A., Usoskin, I., Vainio, R., Mirme, S., Mirme, A., Minikin, A., Petzold, A., Hõrrak, U., Plabß-Dülmer, C., Birmili, W. & Kerminen, V.M. (2009). 'Atmospheric data over a solar cycle: no connection between galactic cosmic rays and new particle formation'. *Atmospheric Chemistry and Physics*. **10**: 1885–1898

Kulmala, M., Vehkamaki, H., Petaja, T., Dal Maso, M., Lauri, A., Kerminen, V.M., Birmili, W. & Mcmurry, P.H. (2004). 'Formation and growth rates of ultrafine atmospheric particles: a review of observations'. *Aerosol Science*. **35**: 143–176

Laakso, L., Kulmala, M. & Lehtinen, K.E.J. (2003). 'Effect of condensation rate enhancement factor on 3-nm (diameter) particle formation in binary ion-induced and homogeneous nucleation'. *Journal of Geophysical Research*. **108**: 4574–4580

Laakso, L.J., Mäkelä, J.M., Pirjola, L., Kulmala, M. (2002). 'Model studies on ion-induced nucleation in the atmosphere'. *Journal of Geophysical Research–Atmospheres*. **107**: AAC5.1-9

Labitzke, K., Austin, J., Butchart, N., Knight, J., Takahashi, M., Nakamoto, M., Nagashima, T., Haigh, J. & Williams, V. (2002). 'The global signal of the 11-year solar cycle in the stratosphere: observations and models'. *Journal of Atmospheric and Solar-Terrestrial Physics*. **64**: 203–210

Laken, B.A. & Kniveton, D.R. (2010). 'Forbush decreases and Antarctic cloud anomalies in the upper troposphere'. *Journal of Atmospheric and Solar-Terrestrial Physics*. In press

Laken, B.A., Wolfendale, A. & Kniveton, D.R. (2009). 'Cosmic ray decreases and changes in the liquid water cloud fraction over the oceans'. *Geophysical Research Letters*. **36**: L23803

Laken, B.A., Kniveton, D.R. & Frogley, M.R. (2010). 'Cosmic rays linked to rapid mid-latitude cloud changes'. *Atmospheric Chemistry and Physics Discussions*. **10**: 18235–18253

Lam, M. & Rodger, A. (2002). 'The effect of Forbush decreases on tropospheric parameters over South Pole'. *Journal of Atmospheric and Solar-Terrestrial Physics*. **64**: 41–45

Landgraf, M., Augustsson, K., Grün, E. & Gustafson, B.A.S. (1999). 'Deflection of the local interstellar dust flow by solar radiation pressure'. *Science*. **286:** 2319–2322

Laut, P. (2003). 'Solar activity and terrestrial climate: an analysis of some purported correlations'. *Journal of Atmospheric and Solar-Terrestrial Physics*. **65**: 801–812

Lean, J. (1987). 'Solar ultraviolet irradiance variations: A review'. *Journal of Geophysical Research.* **92**: 839–868

Lean, J. (2005). 'Living with a variable sun'. *Physics Today,* **58**: 32–38

Lee, R.B., Gibson, M.A., Wilson, R.S. & Thomas, S. (1995). Long-term total solar irradiance variability during sunspot cycle 22. *Journal of Geophysical Research.* **100**: 1667–1675

Leventer, A., Domack, E.W., Ishman, S.E., Brachfeld, S., Mcclennen, C.E. & Manley, P. (1996). 'Productivity cycles of 200-300 years in the Antarctic Peninsula region: understanding linkages among the sun, atmosphere, oceans, sea ice and biota'. *GSA Bulletin*. **108**: 1626–1644

Lindell, M.J., Graneli, W. & Tranvik, L.J. (1995). 'Enhanced bacterial growth in response to photochemical transformation of dissolved organic matter'. *Limnology and Oceanography*. **40**: 195–199

Lockwood, G.W., Stamper, R. & Wild, M.N. (1999). 'A doubling of the sun's coronal magnetic field during the last 100 years'. *Nature*. **399**: 437–439

Lockwood, M. & Fröhlich, C. (2008). 'Recent oppositely directed trends in solar climate forcings and the global mean surface air temperature. II. Different reconstructions of the total solar irradiance variation and dependence on response time scale'. *Proceedings of the Royal Society A-Mathematical Physical and Engineering Sciences*. **464**: 1367–1385

Loon, H.V., Meehl, G.A. & Arblaster, J.M. (2004). 'A decadal solar effect in the tropics in July–August'. *Journal of Atmospheric and Solar-Terrestrial Physics*. **66**: 1767–1778

Lu, Q.B. (2009). 'Correlation between cosmic rays and ozone depletion'. *Physical Review Letters*. **102**: 1180501–1180504

Lu, Q.B. (2010). 'Cosmic-ray-driven electron-induced reactions of halogenated molecules adsorbed on ice surfaces: implications for atmospheric ozone depletion and global climate change'. *Physics Reports*. **487**: 141–167

Lu, Q.B. & MadleyY, T.E. (1999). 'Giant enhancement of electron-induced dissociation of chlorofluorocarbons coadsorbed with water or ammonia ices: implications for atmospheric ozone depletion'. *Journal of Chemical Physics,* **111**: 2861–2865

Lu, Q.B. & Sanche, L. (2001). 'Effects of cosmic rays on atmospheric chlorofluorocarbon dissociation and ozone depletion'. *Physical Review Letters*. **87**: 078501–078505

MacAyeal, D.R. (1993).' Binge/purge oscillations of the Laurentide ice sheet as a cause of the North Atlantic's Heinrich events'. *Paleoceanography*. **8**: 775–784

Mann, M.E., Bradley, R.S. & Hughes, M.K. (1999). 'Northern hemisphere temperatures during the past millennium: inferences, uncertainties, and limitations'. *Geophysical Research Letters*. **26**: 759–762

Markson, R. (1978). 'Solar modulation of atmospheric electrification and possible implication for the sun-weather relationship'. *Nature*. **273**: 103–109

Markson, R. (1981). 'Modulation of the Earth's electric field by cosmic radiation'. *Nature*. **291**: 304–308

Marsh, N.D. & Svensmark, H. (2000). 'Low cloud properties influenced by cosmic rays'. *Physical Review Letters*. **85**: 5004–5007

Marsh, N.D. & Svensmark, H. (2003). 'Galactic cosmic ray and El Niño–Southern Oscillation trends in International Satellite Cloud Climatology Project D2 low-cloud properties'. *Journal of Geophysical Research*. **108**: 4195

Marshall, G.J. (2002). 'Trends in Antarctic geopotential height and temperature: a comparison between radiosonde and NCEP–NCAR reanalysis data'. *Journal of Climate*. **15**: 659–674

Maso, M.D., Kulmala, M., Riipinen, I., Wagner, R., Hussein, T., Aalot, P. & Lehtinen, K. (2005). 'Formation and growth of fresh atmospheric aerosols: eight years of aerosol size distribution data from SMEAR II, Hyytiälä, Finland'. *Boreal Environment Research*. **10**: 323–336

Mironova, I.A., Desorgher, L., Usoskin, I.G., Fluckiger, E.O. & Butikofer, R. (2008). 'Variations of aerosol optical properties during the extreme solar event in January 2005'. *Geophysical Research Letters*. **35**: L18610

Mironova, I.A. & Pudovkin, M.I. (2005). 'Increase in the aerosol content of the lower atmosphere after the solar proton flares in January and August 2002 according to data of lidar observations in Europe'. *Geomagnetism and Aeronomy*. **45**: 221–226

Mo, K.C., Pfaendtner, J. & Kalnay, E. (1987). 'A GCM study on the maintenance of the June 1982 blocking in the southern hemisphere'. *Journal of Atmospheric Sciences*. **44**: 1123–1142

Moberg, A., Sonechkin, D.M., Holmgren, K., Datsenko, N.M. & Karlen, W. (2005). 'Highly variable northern hemisphere temperatures reconstructed from low and high resolution proxy data'. *Nature*. **433**: 613–618

Morley, B.M., Uthe, E.E. & William, V. (1989). 'Airborne lidar observations of clouds in the Antarctic troposphere'. *Geophysical Research Letters*. **16**: 491–494

Müller, R. (2003). 'Impact of cosmic rays on stratospheric chlorine chemistry and ozone depletion'. *Physical Review Letters*. **91**: 058502–058506

Nadykto, A.B. & Yu, F. (2003). 'Uptake of neutral polar vapour molecules by charged clusters/particles: enhancement due to dipole-charge interaction'. *Journal of Geophysical Research*. **108**: 4717–4724

Neff, U., Burns, G., Mangini, A., Mudelsee, M., Fleitmann, D. & Matter, A. (2001). 'Strong coherence between solar variability and the monsoon in Oman between 9 and 6kyr ago'. *Nature*. **411**: 290–293

Nicoll, K.A. & Harrison, R.G. (2009). 'A lightweight balloon-carried cloud charge sensor'. *Review of Scientific Instruments*. **80**: 014501–014505

Norris, J.R. (2000). 'What can cloud observations tell us about climate variability?' *Space Science Reviews*. **94**: 375–380

Ogura, T., Emori, S., Webb, M.J., Tsushima, Y., Yokohata, T., Ouchi, A.A. & Kimoto, M. (2008). 'Towards understanding cloud response in atmospheric GCMs: the use of tendency diagnostics'. *Journal of the Meteorological Society of Japan*. **86**: 69–79

Pallé, E. (2005). 'Possible satellite perspective effects on the reported correlations between solar activity and clouds'. *Geophysical Research Letters*. **32**: L03802

Pallé, E. & Butler, C.J. (2000). 'The influence of cosmic rays on terrestrial cloud and global warming'. *Astronomy & Geophysics*. **41**: 18–22

Pallé, E. & Butler, C.J. (2001). 'Sunshine records from Ireland: cloud factors and possible links to solar activity and cosmic rays'. *International Journal of Climatology*. **21**: 709–729

Pallé, E., Butler, C.J. & O'Brien, K. (2004a). 'The possible connection between ionization in the atmosphere by cosmic rays and low level clouds'. *Journal of Atmospheric and Solar-Terrestrial Physics*. **66**: 1779–1790

Pallé, E., Goode, P.R., Montanes-Rodruguez, P. & Koonin, S.E. (2004b). 'Changes in Earth's reflectance over the past two decades'. *Science*. **304**: 1299–1301

Parish, T.R. (1992). 'On the role of Antarctic katabatic winds in forcing large-scale tropospheric motions'. *Journal of Atmospheric Sciences*. **49**: 1374–1385

Parish, T.R. & Bromwich, D.H. (1991). 'Continental-scale simulation of the Antarctic katabatic wind regime'. *Journal of Climate*. **4**: 135–146

Pierce, J.R. & Adams, P.J. (2007). 'Efficiency of CCN formation from ultrafine particles'. *Atmospheric Chemistry and Physics*. **7**: 1367–1379

Pierce, J.R. & Adams, P.J. (2009). 'Can cosmic rays affect cloud condensation nuclei by altering new particle formation rates?' *Geophysical Research Letters*. **36**: L09820

Pinker, R.T., Zhang, J.W. & Dutton, E.G. (2005). 'Do satellites detect trends in surface solar radiation?' *Science*. **308**: 850–854

Polissar, P.J., Abbott, M.B., Wolfe, A.P., Bezada, M., Rull, V. & Bradley, R.S. (2006). 'Solar modulation of Little Ice Age climate in the tropical Andes.' *Proceedings of the National Academy of Sciences of the United States of America*. **103**: 8937–8942

Pudovkin, M.I. & Veretenko, S.V. (1995). 'Cloudiness decreases associated with Forbush decreases of galactic cosmic rays'. *Journal of Atmospheric and Solar-Terrestrial Physics*. **75**: 1349–1355

Pudovkin, M.I., Veretenenko, S.V., Pellinen, R. & Kyrö, E. (1996). 'Cosmic ray variation effects in the temperature of the high-latitudinal atmosphere'. *Advances in Space Research*. **17**: 165–168

Pudovkin, M.I., Veretenenko, S.V., Pellinen, R. & Kyrö, E. (1997). 'Meteorological characteristic changes in the high-latitudinal atmosphere associated with Forbush decreases of the galactic cosmic rays'. *Advances in Space Research*. **20**: 1169–1172

Quante, M. (2004). 'The role of clouds in climate system'. *Journal de Physique IV France*. **121**: 61–86

Ramanathan, V., Cess, R.D., Harrison, E.F., Minnis, P., Barkstrom, B.R., Ahmad, E. & Hartmann, D. (1989). 'Cloud-radiative forcing and climate: results from the Earth Radiation Budget Experiment'. *Science*. **243**: 57–63

Ramanathan, V. & Inamdar, A.K. (2006). 'The radiative forcing due to clouds and water vapor'. In *Frontiers of Climate Modelling* [Kiehl, J.T. & Ramanathan, V. (eds.)]. Cambridge University Press: Cambridge. 381pp

Roble, R.G. (1991). 'On modelling component processes in the Earth's global electric circuit'. *Journal of Atmospheric and Solar-Terrestrial Physics*. **53**: 831–847

Roble, R.G. & Hays, P.B. (1979). 'A quasi-static model of global atmospheric electricity, II'. *Journal of Geophysical Research*. **84**: 3291–3305

Rogers, R.R. & Yau, M.K. (1989). *A Short Course in Cloud Physics*. Pergamon Press: Exeter. 304pp

Rosenfeld, D., Kaufman, Y. & Koren, I. (2006). 'Switching cloud cover and dynamical regimes from open to closed Bernard cells in response to the suppression of precipitation by aerosols'. *Atmospheric Chemistry and Physics*. **6**: 2503–2511

Rossow, W. (2010). '*Personal communiqué*'. Presented in Appendix 2.

Rossow, W.B. & Schiffer, R.A. (1999). 'Advances in understanding clouds from ISCCP'. *Bulletin of the American Meteorological Society,* **80**: 2261–2287

Rossow, W., Walker, A.W., Beuschel, D.E. & Roiter, M.D. (1996). 'ISCCP Documentation of New Cloud Datasets'. *World Meteorological Organisation Technical Document.* **737**: 115pp

Rossow, W.B., Walker, A.W. & Garder, L.C. (1993). 'Comparison of ISCCP and other cloud amounts'. *Journal of Climate*. **6**: 2394–2418

Russell, J.M. & Johnson, T.C. (2005). 'Late Holocene climate change in the North Atlantic and equatorial Africa: millennial-scale ITCZ migration'. *Geophysical Research Letters*. **32**: L17705

Rutledge, S.A. & Hobbs, P.V. (1983). 'The mesoscale and microscale structure and organization of clouds and precipitation in midlatitude cyclones. VIII: a model for the "seeder-feeder" process in warm-frontal rainbands'. *Journal of the Atmospheric Sciences*. **40**: 1185–1206

Rycroft, M.J., Harrison, R.G. & Nicoll, K.A. (2008). 'An overview of Earth's global electric circuit and atmospheric conductivity'. *Space Science Reviews*. **137**: 85–105

Rycroft, M.J., Israelsson, S. & Price, C. (2000). 'The global atmospheric electric circuit, solar activity and climate change'. *Journal of Atmospheric and Solar-Terrestrial Physics*. **62**: 1563–1576

Sapkota, B.K. & Varshneya, N.C. (1990). 'On the global atmospheric electrical circuit'. *Journal of Atmospheric and Terrestrial Physics*. **52**: 1563–1576

Scafetta, N. & West, B.J. (2005). 'Estimated solar contribution to the global surface warming using the ACRIM TSI satellite composite'. *Geophysical Research Letters*. **32**: L18713

Schuurman, C.J.E. (1965). 'Influence of solar flare particles on the general circulation of the atmosphere.' *Nature*. **205**: 167–168

Schuurman, C.J.E. & Oort, A.H. (1969). 'A statistical study of pressure changes in the troposphere and lower stratosphere after strong solar flares.' *Pure and Applied Geophysics*. **75**: 233–246

Shapiro, S.S. & Wilk, M.B. (1965). 'An analysis of variance test for normality (complete samples)'. *Biometrika.* **52**: 591–611

Shindell, D., Rind, D., Balachandran, N., Lean, J. & Lonergan, P. (1999). 'Solar cycle variability, ozone, and climate'. *Science*. **284**: 305–308

Siingh, D., Gopalakrishnan, V., Singh, R., Kamra, A.K., Singh, S., Pant, V., Singh, R. & Singh, A. (2006). 'The atmospheric global electric circuit: an overview'. *Atmospheric Research*. **84**: 91–110

Simpson, J.A. (1957). 'Cosmic-radiation neutron intensity monitor'. *Annals of the International Geophysical Year*. **4**: 351–373

Simpson, J.A. (1983). 'Elemental and isotopic composition of the galactic cosmic-rays'. *Annual Review of Nuclear and Particle Science*. **33**: 323–381

Slezak, D., Brugger, A. & Herndl, G.J. (2001). 'Impact of solar radiation on the biological removal of dimethylsulfoniopropionate and dimethylsulfide in marine surface waters'. *Aquatic Microbial Ecology*. **25**: 87–97

Smart, D.F., Shea, M.A. & Lifton, N. (2008). 'Evolution of geomagnetic cutoff rigidities on short-and long-term time scales'. *American Geophysical Union, Spring Meeting 2008*. GP53A-03

Smith, R.N.B. (1990). 'A scheme for predicting layer clouds and their water contents in a General Circulation Model'. *The Quarterly Journal of the Royal Meteorological Society*. **116**: 435–460

Smith, S.R. & Stearns, C.R. (1993). 'Antarctic pressure and temperature anomalies surrounding the minimum in the Southern Oscillation Index'. *Journal of Geophysical Research*. **98**: 13071–13083

Smith, R.N.B., Gregory, D., Wilson, C. & Bushell, A.C. (1997). 'Calculation of Specific humidity and Large-scale cloud'. *Unified Model Documentation Paper 30*. The Meteorological Office: Reading

Smith, S.R., Legler, D.M. & Verzone, K.V. (2001). 'Quantifying uncertainties in NCEP reanalyses using high-quality research vessel observations'. *Journal of Climate*. **14**: 4062–4072

Solanki, S.K. & Krivova, N.A. (2003). 'Can solar variability explain global warming since 1970?' *Journal of Geophysical Research*. **108**: 1087–1091

Solanki, S.K., Usoskin, I., Kromer, B., Schussler, M. & Beer, J. (2004). 'Unusual activity of the sun during recent decades compared to the previous 11,000 years'. *Nature*. **431**: 1084–1087

Solovyev, V.S. & Kozlov, V.I. (2009). 'Influence of cosmic ray variations on cloudiness distribution over Northern Asia'. *Russian Physics Journal*. **52**: 127–131

Soon, W. & Baliunas, S. (2003). 'Proxy climatic and environmental changes of the past 1000 years'. *Climate Research*. **23**: 89–110

Spracklen, D.V., Carslaw, K.S., Kulmala, M., Kerminen, V., Sihto, S., Riipinen, I., Merikanto, J., Mann, G.W., Chipperfield, M.P., Wiedensohler, A., Birmili, W. & Lihavainen, H. (2008). 'Contribution of particle formation to global cloud condensation nuclei concentrations'. *Geophysical Research Letters*. **35**: L06808

Stone, R.S. & Khal, J.D. (1991). 'Variations in boundary layer properties associated with clouds and transient weather disturbances at the south pole during winter'. *Journal of Geophysical Research*. **96**: 5137–5144

Stott, P.A. & Forest, C.E. (2007). 'Ensemble climate predictions using climate models and observational constraints'. *Proceedings of the Royal Society A–Mathematical Physical and Engineering Sciences*. **365**: 2029–2052

Stozhkov, Y.I. (2003). 'The role of cosmic rays in the atmospheric processes'. *Journal of Physics G–Nuclear and Particle Physics*. **29**: 913–923

Svensmark, H. (1998). 'Influence of cosmic rays on Earth's climate'. *Physical Review Letters.* **81**: 5027–5030

Svensmark, H. (2000). 'Cosmic rays and Earth's climate'. *Space Science Reviews*. **93**: 175–185

Svensmark, H. (2007). 'Cosmoclimatology: a new theory emerges'. *Astronomy & Geophysics*. **48**: 18–24

Svensmark, H. & Friis-Christensen, E. (1997). 'Variation of cosmic ray flux and global cloud coverage–a missing link in solar-climate relationships'. *Journal of Atmospheric and Solar-Terrestrial Physics*. **59**: 1225–1232

Svensmark, H., Bondo, T. & Svensmark, J. (2009). 'Cosmic ray decreases affect atmospheric aerosols and clouds'. *Geophysical Research Letters.* **36**: L15101

Svensmark, H., Pedersen, J., Marsh, N., Enghoff, M. & Uggerhoj, U. (2007). 'Experimental evidence for the role of ions in particle nucleation under atmospheric conditions'. *Proceedings of the Royal Society A–Mathematical Physical and Engineering Sciences*. **463**: 385–396

Tachikawa, H. & Abe, S. (2007). 'Reaction dynamics following electron capture of chlorofluorocarbon adsorbed on water cluster: A direct density functional theory molecular dynamics study'. *Journal of Chemical Physics*. **126**: 194310

Thompson, D.W.J. & Solomon, S. (2002). 'Interpretation of recent southern hemisphere climate change'. *Science*. **296**: 895–899

Tinsley, B.A. (2000). 'Influence of solar wind on the global electric circuit, and inferred effects on cloud microphysics, temperature, and dynamics in the troposphere'. *Space Science Reviews*. **94**: 231–258

Tinsley, B.A. (2008). 'The global atmospheric electric circuit and its effects on cloud microphysics'. *Reports on Progress in Physics*. **71**: 066801

Tinsley, B.A. (2010). *Personal communiqué*. Presented in Appendix 6

Tinsley, B.A. & Deen, G.W. (1991). 'Apparent tropospheric response to MeV-GeV particle flux variations: a connection via electrofreezing of supercooled water in high-level clouds?' *Journal of Geophysical Research*. **96**: 2283–2296

Tinsley, B.A. & Heelis, R.A. (1993). 'Correlations of atmospheric dynamics with solar-activity: evidence for a connection via the solar-wind, atmospheric electricity, and cloud microphysics'. *Journal of Geophysical Research-Atmospheres*. **98**: 10375–10384

Tinsley, B.A., Burns, G.B. & Zhou, L. (2007). 'The role of the global electric circuit in solar and internal forcing of clouds and climate'. *Advances in Space Research*. **40**: 1126–1139

Tinsley, B.A. & Yu, F. (2004). 'Atmospheric ionization and clouds as links between solar activity'. *Geophysical Monograph*. **141**: 321–339

Tinsley, B.A. & Zhou, L.M. (2006). 'Initial results of a global circuit model with variable stratospheric and tropospheric aerosols'. *Journal of Geophysical Research-Atmospheres*. **111:** D16205

Tinsley, B.A., Rohrbaugh, R.P. & Hei, M. (2001). 'Electroscavenging in clouds with broad droplet size distributions and weak electrification'. *Atmospheric Research*. **59**: 115–135

Tinsley, B.A., Rohrbaugh, R.P., Hei, M. & Beard, K.V. (2000). 'Effects of image charges on the scavenging of aerosol particles by cloud droplets and on droplet charging and possible ice nucleation processes'. *Journal of the Atmospheric Sciences*. **57**: 2118–2134

Tinsley, B.A., Zhou, L.M. & Plemmons, A. (2006). 'Changes in scavenging of particles by droplets due to weak electrification in clouds'. *Atmospheric Research*. **79**: 266–295

Todd, M.C. & Kniveton, D.R. (2001). 'Changes in cloud cover associated with Forbush decreases of galactic cosmic rays'. *Journal of Geophysical Research-Atmospheres*. **106**: 32031–32041

Todd, M.C. & Kniveton, D.R. (2004). 'Short-term variability in satellite-derived cloud cover and galactic cosmic rays: an update'. *Journal of Atmospheric and Solar-Terrestrial Physics*. **66**: 1205–1211

Trenbeth, K.E. (1980). 'Planetary waves at 500mb in the southern hemisphere'. *Monthly Weather Review*. **108**: 1378–1389

Troshichev, O.A. & Janzhura, A. (2004). 'Temperature alterations on the Antarctic ice sheet initiated by the disturbed solar wind'. *Journal of Atmospheric and Solar-Terrestrial Physics*. **66**: 1159–1172

Troshichev, O., Egrova, L., Janzhura, A. & Vovk, V.Y. (2005). 'Influence of the disturbed solar wind on atmospheric processes in Antarctica and El-Nino Southern Oscillation (ENSO)'. *Memorie della Societa Astronomica Italiana*. **76**: 890–898

Troshichev, O., Vovk, V.Y. & Egrova, L. (2008). 'IMF-associated cloudiness above near-pole station Vostok: impact on wind regime in winter Antarctica'. *Journal of Atmospheric and Solar-Terrestrial Physics*. **70**: 1289–1300

Tung, K.K. & Camp, C.D. (2008). 'Solar cycle warming at the Earth's surface in NCEP and ERA-40 data: a linear discriminant analysis'. *Journal of Geophysical Research*. **113**: D05114

Usoskin, I., Tylka, A., Kovaltsov, G. & Dietrich, W. (2009). 'Ionization effect of strong solar particle events: Low-middle atmosphere'. In *Proceedings of the 31st ICRC*. University of Łódź. Łódź, Poland

Vallero, D. (2008). *Fundamentals of Air Pollution* 4th Ed., London, Academic Press: 968pp

van der Wal, A. (1998). 'The Unified Model'. *Unified Model Users Guide*. Version 2. The Meteorological Office: Reading. 192pp

Veizer, J. (2005). 'Celestial climate driver: a perspective from four billion years of the carbon cycle'. *Geoscience Canada*. **32**: 13–28

Veretenenko, S. & Pudovkin, M. (1995). 'The galactic cosmic ray Forbush decrease effects on total cloudiness variations'. *Geomagnetism and Aeronomy (English Translation)*. **34**: 463–468

Veretenko, S.V. & Pudovkin, M.I. (1994). 'Effects of Forbush decrease of galactic cosmic rays in variations of general cloudiness'. *Geomagnetizm I Aeronomiya*. **34**: 38–44

Veretenenko, S.V. & Pudovkin, M.I. (1997). 'Cosmic ray variation influence on the total radiation fluxes in the lower atmosphere'. *Coupling and Energetics in the Stratosphere-Mesosphere-Thermosphere-Ionosphere System*. **20**: 1173–1176

Veretenenko, S.V. & Thejil, P. (2004). 'Effects of energetic solar proton events on the cyclone development in the North Atlantic'. *Journal of Atmospheric and Solar-Terrestrial Physics*. **66**: 393–405

Veretenenko, S.V., Dergachev, V.A. & Dmitriyev, P.B. (2005). 'Long-term variations of the surface pressure in the North Atlantic and possible association with solar activity and galactic cosmic rays'. *Advances in Space Research*. **35**: 484–490

Veretenenko, S.V., Dergachev, V.A. & Dmitriev, P.B. (2007). 'Effect of solar activity and cosmic-ray variations on the position of the Arctic front in the North Atlantic'. *Bulletin of the Russian Academy of Sciences: Physics*. **71**: 1010–1013

Viereck, R.A. & Puga, L.C. (1999). 'The NOAA Mg II core-to-wing solar index: construction of a 20-year time series of chromospheric variability from multiple satellites'. *Journal of Geophysical Research*. **104**: 9995–10005

Wallace, J.M. & Hobbs, P.V. (1977). '*Atmospheric Science: An Introductory Survey'*. Academic Press Ltd: Orlando. 504pp

Wang, M.J., He, L.P. & Jia, H.Y. (2006). 'Cloudiness variation observed at Yangbajing during Forbush decrease of galactic cosmic rays'. *High Energy Physics and Nuclear Physics–Chinese Edition*. **30**: 75–78

Wang, Y.J., Cheng, H., Edwards, R.L., He, Y.Q., Kong, X.G., An, Z.S., Wu, J.Y., Kelly, M.J., Dykoski, C.A. & Li, X.D. (2005). 'The Holocene Asian monsoon: links to solar changes and North Atlantic climate'. *Science*. **308**: 854–857

Wang, Y., Long, C.N., Leung, L.R., Dudhia, J., McFarlane, S.A., Mather, J.H., Ghan, S.J. & Liu, X. (2009). 'Evaluating regional cloud-permitting simulations of the WFR model for the tropical warm pool international cloud experiment (TWP-ICE), Darwin, 2006'. *Journal of Geophysical Research*. **114**: D21203

Waugh, D.W. & Randel, W.J. (1999). 'Climatology of Arctic and Antarctic polar vortices using elliptical diagnostics'. *Journal of the Atmospheric Sciences*. **56**: 1594–1613

Weber, R.J., McMurry, P.H., Tanner, D.J., Eisele, F.L., Kreidenweis, S.M., Schilawski, R.D. & Baugmgardner, D. (1998). 'A study of new particle formation and growth involving biogenic and trace gas species measured during ACE 1'. *Journal of Geophysical Research*. **103**: 16385–16396

Wenzler, T., Solanki, S.K., Krivova, N.A. & Fröhlich, C. (2006). 'Reconstruction of solar irradiance variations in cycles 21-23 based on surface magnetic fields'. *Astronomy and Astrophysics*. **460**: 583–595

Williams, C. (2006). '*Rainfall Variability and Extremes over Southern Africa*'. PhD thesis. University of Sussex: Brighton. 237pp

Williams, E.R. (1994). 'Global circuit response to seasonal variations in global surface air temperature'. *Monthly Weather Review*. **122**: 1917–1929

Williams, E.R. (1996). 'Current budget of the atmospheric electric global circuit – comment'. *Journal of Geophysical Research–Atmospheres*. **101**: 17029–17031

Williams, E.R. (2008). 'The global electrical circuit: a review'. *Atmospheric Research*. **91**: 140–152

Williams, K.D. & Tselioudis, G. (2007). 'GCM intercomparison of global cloud regimes: present-day evaluation and climate change response'. *Climate Dynamics*. **29**: 231–250

Williams, K.D., Ringer, M.A. & Senior, C.A. (2003). 'Evaluating the cloud response to climate change and current climate variability'. *Climate Dynamics*. **20**: 705–721

Willson, R.C. & Mordvinov, A.V. (2003). 'Secular total solar irradiance trend during solar cycles 21-23'. *Geophysical Research Letters*. **30**: 1199–1202

Willson, R.C., Gulkis, S., Janssen, M., Hudson, H.S. & Chapman, G.A. (1981). 'Observation of solar irradiance variability'. *Science*. **211**: 700–702

Wilson, C.T.R. (1920). 'Investigations on lightning discharges and on the electric field of thunderstorms'. *Philosophical Transactions of the Royal Society of London Series A, Containing Papers of a Mathematical or Physical Character*. **221**: 73–115

Woods, T.N., Eparvier, F.G., Fontenla, J., Harder, J., Kopp, G., Mcclintock, W.E., Rottman, G., Smiley, B. & Snow, M. (2004). 'Solar irradiance variability during the October 2003 solar storm period'. *Geophysical Research Letters*. **31**: L10802

Wylie, D., Jackson, D., Menzel, P. & Bates, J. (2005). 'Trends in global cloud cover in two decades of HIRS observations'. *Journal of Climate*. **18**: 3021–3031

Yamanouchi, T. & Shudou, Y. (2007). 'Trends in cloud amount and radiative fluxes at Syowa Station, Antarctica'. *Polar Science*. **1**: 17–23

Yang, G.Y. & Slingo, J. (2001). 'The diurnal cycle in the Tropics'. *Monthly Weather Review*. **129**: 784–801

Yu, F. (2002). 'Altitude variations of cosmic ray induced production of aerosols: implications for global cloudiness and climate'. *Journal of Geophysical Research*. **107**: 1118

Yu, F. & Turco, R. (2008). 'What controls particle formation in Boreal Forests?' In *American Geophysical Union*. Fall Meeting: AC12C-07

Yu, F. & Turco, R.P. (2000). 'Ultrafine aerosol formation via ion-mediated nucleation'. *Geophysical Research Letters*. **27**: 883–886

Yu, F. & Turco, R.P. (2001). 'From molecular clusters to nanoparticles: role of ambient ionization in tropospheric aerosol formation'. *Journal of Geophysical Research*. **106**: 4949–4814

Yu, F., Wang, Z. & Turco, R. (2008). 'Ion-mediated nucleation as an important global source of tropospheric aerosols'. *Atmospheric Chemistry and Physics*. **8**: 2537–2554

Zhou, L., Tinsley, B.A. & Plemmons, A. (2009). ‘ Scavenging in weakly electrified and subsaturated clouds, treating aerosols and droplets as conducting spheres’. *Journal of Geophysical Research*. **114**: D18201